kj-ceramics31.changwon.ac.kr

The 31st International Korea-Japan Seminar on Ceramics

November 26(Wed.) - 29(Sat.), 2014

CECO(Changwon Exhibition Covention Center), Korea

Organized by

- Organizing Committee of the 31st International Korea-Japan Seminar on Ceramics
- Executive Committee of the 31st International Korea-Janpan Seminar on Ceramics

Sponsors

Gyeongnam
Changwon
The Korean Ceramic Society
Changwon National University
Chungnam National University
Kyungnam University
Engineering Research Center for Integrated Mechatronics Materials and Components
KIET Engineering Research Center for Integrated Mechatronics Materials and Components
KOCERA Korea Ceramic Association
KCC Corporation
T.H. ELEMA ENG. CO.,LTD.
Korea Tourism Organization

KJ-Ceramics 31

Program & Abstract

The 31st International Korea-Japan Seminar on Ceramics

November 26th – 29th, 2014

Changwon Exhibition Convention Center(CECO),
Changwon, Gyeongnam, Korea

http://kj-ceramics31.changwon.ac.kr/

CONTENTS

Welcome Message 3
General Information 4
Conference Venue 5
Committees 6
Sponsors 13
On-site Registration Guideline 14
Presentation Guideline 15
Exhibition 16
Social Programs 17
Program at a Glance 18
Detailed Program 19
Scientific Program
- Invited & Oral Presentation 21
- Poster Presentation 54
Abstracts
- Plenary Presentation 71
- Invited Presentation 75
- Oral Presentation 176
- Poster Presentation 267
Author Index 374

Welcome Message

The 31st International Korea-Japan Seminar on Ceramics, Changwon, Korea, is expected to be very successful, because of the large number of participants and presentations which is the largest since the very first Korea-Japan meetings. This may suggest that the meeting is getting more attractive and productive among ceramists in both countries.

Due to the increased interests and demands from both countries, local organizing committee decided to open more sessions to cover from traditional and structural ceramics to functional and high-end technologies. During the meeting, we are going to have approximately 300 presentations (200 oral and 100 poster presentations). We believe that the meeting will provide a good chance for the participants to understand more on the specific topics, as well as to socialize each others. Especially, young scientists and students from both countries are encouraged to participate actively.

We expect to see every one of you in Changwon, soon.

Byong Ho Kim
Korea University
Chairman, Organizing Committee

Myong-Ho Kim
Changwon National University
Chairman, Local Organizing Committee

General Information

Date	November 26 (Wed) ~ 29 (Sat), 2014
Venue	Changwon Exhibition Convention Center (CECO)
Official Language	English
Organized by	· Organizing Committee of the 31st International Korea-Japan Seminar on Ceramics · Executive Committee of the 31st International Korea-Japan Seminar on Ceramics
Seminar Topics	· Synthesis, Raw Materials & Advanced powder processing · Thermoelectrics · Thin Films & Layers · Nano-particles & Nano-structured Materials · Fuel cells and Batteries · Electronic Ceramics · Structural Ceramics & Refractory Materials · Glass & Opto-Electronic Materials · Biomaterials · Sensor Materials · Electric Field assisted Sintering (PAS,SPS and Related Processing Techiques) · Piezoelectric Materials, Devices & Applications · Lead-free Piezoelectrics · Computational Ceramic Science and Engineering · Ceramics Culture and Education · LED and Display Materials · Advanced Coating for Gas Turbines
Contact Information	KJ-Ceramics 31 Secretariat Tel : +82-55-212-1337, Fax : +82-55-212-1331 E-mail : kj-ceramics31@changwon.ac.kr Website: http://kj-ceramics31.changwon.ac.kr/

Locations and Hour of Conference Function Rooms

Function	Location	Nov. 26 (Wed)	Nov. 27 (Thu)	Nov. 28 (Fri)
Registration Desk	Convention Hall Lobby (3F)	14:00-18:00	08:00-18:00	08:00-16:00
Internet Lounge	Convention Hall Lobby (3F)	14:00-18:00	08:00-18:00	08:00-16:00
Poster Session	Convention Hall Lobby (3F)	-	12:00~13:30	12:00~13:30
Exhibition	Convention Hall Lobby (3F)	14:00-17:30	09:00-17:30	09:00-16:00

Conference Venue

▶ 3F

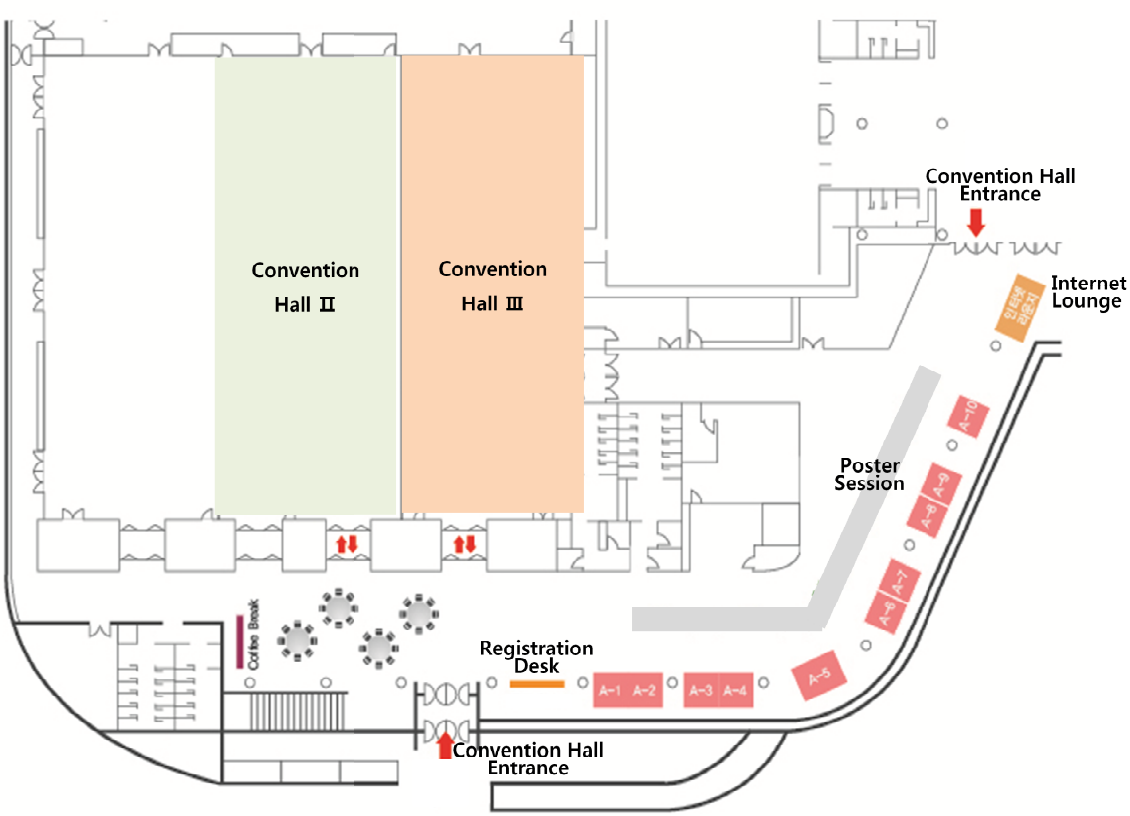

▶ 6F

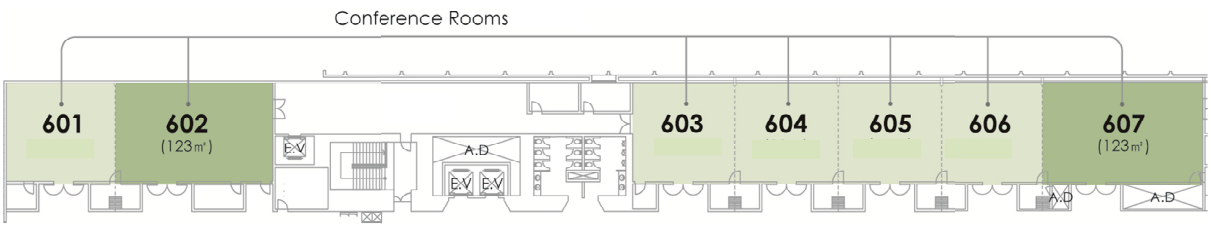

Committees

Organizing Committee (Korean Side)

Honorary Chairman

Byong Sik JEON	Korea Ceramic Association, Honorary President

Chairman

Byong Ho KIM	Korea University, Professor Emeritus

Vice Chairman

Hyung Sun KIM	Inha University, Professor, Chairman of Executive Committee

Members of Committee

Tae Hyun CHOI	Ministry of Trade, Industry and Energy, Director General for Materials and Components Industries
Min KIM	Korea Institute of Ceramic Engineering & Technology, President
Dae Soon LIM	Korea University, Professor The Korean Ceramic Society, President
Jae Soo SHIN	Korea Ceramic Association, President
Young Jo LEE	Korea Fine Ceramic Association, President
Hai Doo KIM	Korea Institute of Material Science, Principal Researcher President of The Korean Union Chemical Science & Technology Societies
Hyeong Joon KIM	Seoul National University, Professor, Vice President of The Korean Ceramic Society
Gi Tae JOO	Seoul National University of Science and Technology, Professor
Suk Joong KANG	Korea Academy Institute of Science and Technology, Professor
Byung Ha LEE	Myongji University, Professor
Jong HEO	Pohang University of Science & Technology, Professor
Myong-Ho KIM	Changwon National University, Professor
Byung Sei JUN	Kyungnam University, Professor
Suk Young KIM	Youngnam University, Professor
Sang Kuk WOO	Korea Institute of Energy Research, Senior Researcher

Hyung Ho PARK	Yonsei University, Professor
Jeong Joo KIM	Kyungpook National University, Professor
Byung Eun PARK	University of Seoul, Professor
Hyung Tae KIM	Korea Institute of Ceramic Engineering and Technology, Director of Icheon Branch
Sang Yeup PARK	Gangneung-Wonju National University, Professor
Ik Jin KIM	Hanseo University, Professor
Soon Gil YOON	Chungnam National University, Professor
Kwang Bo SHIM	Hanyang University, Professor
Moo Kyung KIM	Korea Ceramic Association, Consultant
Jun Young LEE	Korea Ceramic Association, Executive Director
Jong Oh BYUN	KCC Corp., Yeoju Plant, Senior Managing Director
Jae Hyun KIM	Korea Research Institute of Chemical Technology, President
Wung Yong CHOO	Research Institute of Industrial Science & Technology, President
Sang Il JOON	Tong Yang Cement Co., Ltd., President
Won Kyu PARK	Samsung Corning Precision Materials Co., Ltd., President
Hwa Il LEE	Chosun Refractory Co., Ltd., President
Yoon Ho LEE	Ssangyong Cement Industrial Co., Ltd., President
Yong Ju KIM	Haengnam Chinaware Co., Ltd., President
Young Shin KIM	Hankook Chinaware Co., Ltd., President

Advisors

Kee Dong NAM	Korea Ceramic Association, Honorary President
Kee Hyong KIM	Korea Ceramics Culture Society, President
Ee Young HA	Daewon Trading Co. Ltd, Advisor
Sung Do JANG	Korea Fine Ceramics Association, Advisor
Soon Ja PARK	Seoul National University, Professor Emeritus
Jong Min LEE	Korea Institute of Ceramic Engineering and Technology, Consultant

Organizing Committee (Japanese Side)

Chairman

Tetsuya KAMEYAMA	National Institute of Advanced Industrial and Science Technology, Researcher Emeritus

Vice Chairman

Motohiro TORIYAMA	National Institute of Advanced Industrial and Science Technology, Chubu Center, Director

Members of Committee

Tetsuhiko KOBAYASHI	National Institute of Advanced Industrial and Science Technology, Kansai Center, Director
Koh HARADA	National Institute of Advanced Industrial and Science Technology, Tohoku Center, Director
Masanobu WATANABE	National Institute of Advanced Industrial and Science Technology, Kyushu Center, Director
Osamu NAKAMURA	National Institute of Advanced Industrial and Science Technology, Chugoku Center, Director
Masanobu AWANO	National Institute of Advanced Industrial and Science Technology, Divisonal Director
Mamoru NAKAMURA	National Institute of Advanced Industrial and Science Technology, Divisonal Director
Eiji MUROMACHI	National Institute for Materials Science, Executive Board
Hajime HANEDA	National Institute for Materials Science, Executive Manager
Sakae TANEMURA	Nagoya Technology University, Professor
Masasuke TAKATA	Japan Fine Ceramics Center, Director
Shigeyuki KIMURA	The Society of Non-Traditional Technology, Board Chairman
Osamu NAITO	Japan Fine Ceramics Association, Managing Director
Jun AKEDO	National Institute of Advanced Industrial and Science Technology, Executive Chief Researcher
Junji NISHII	Hokkaido University, Professor
Masato KAKIHANA	Tohoku University, Professor
Tohru SEKINO	Osaka University, Professor
Kiyoshi OKADA	Tokyo Institute of Technology, Vice President
Masaru MIYAYAMA	The University of Tokyo, Professor
Junichi TATAMI	Yokohama National University, Professor

Takashi YAMAMOTO	National Defense Academy of Japan, Professor
Hisao SUZUKI	Shizuoka University, Professor
Toshio OGAWA	Shizuoka Institute of Science and Technology, Professor
Kunihito KOUMOTO	Nagoya University, Professor
Shinobu HASHIMOTO	Nagoya Technology University, Associate Professor
Koichi NIIHARA	Nagaoka University of Technology, President
Nobuhito IMANAKA	Osaka University, Professor
Yoko SUYAMA	Shimane University, Professor
Akiyoshi OSAKA	Okayama University, Professor Emeritus
Kei INUMARU	Hiroshima University, Professor
Junichi HOJO	Kyushu University, Professor Emeritus
Yasuo UCHIYAMA	Nagasaki University, Professor Emeritus
Yoshihiro HIRATA	Kagoshima University, Professor
Takanori WATARI	Saga University, Professor
Hiroaki KATSUKI	Saga Ceramics Research Laboratory, Researcher Emeritus
Mitsuyoshi NAGANO	Nippon Tungsten Co.,Ltd., Director
Masahiko OKUYAMA	NGK Spark Plug Co., Ltd., Executive Officer
Hiroshi TAKAGI	Murata Mfg. Co., Ltd., Executive Advisor
Norio KITAMURA	KF Group, President
Hiroshi ITAHARA	Toyota Central R&D Labs., Inc, Senior Researcher
Shinji KAWASAKI	NGK Insulators, Ltd., Basic Technology Laboratory, Director

Advisor

Akio KATO	Professor Emeritus, Former Chiarperson

Executive Committee (Korean Side)

General Chair

Hyung Sun KIM	Inha University, Professor

Members of Committee

Sang Yeup PARK	Gangneung-Wonju National University, Professor

Soon Gil YOON	Chungnam National University, Professor
Ik Jin KIM	Hanseo University, Professor
Suk Young KIM	Yeungnam University, Professor
Myong-Ho KIM	Changwon National University, Professor
Sahn NAHM	Korea University, Professor
Jong Hee KIM	Korea Institute of Ceramic Engineering and Technology, Principal Researcher
Hyung Tae KIM	Korea Institute of Ceramic Engineering and Technology, Director of Incheon Branch
Hyung Ho PARK	Yonsei University, Professor
Jun Young LEE	Korean Ceramic Association, Executive Director
Moo Kyung KIM	Korean Ceramic Association, Advisor

Local Organizing Committee (Korean Side)

Chairman

Myong-Ho KIM	Changwon National University, Professor

Members of Committee

Byung Sei JUN	Kyungnam National University, Professor
Hai-Doo KIM	Korea Institute of Materials Science, Senior Researcher
Nam Kyun KIM	Korea Electrotechnology Research Institute
Sang Su KIM	Changwon National University, Professor
Kyu Hong HWANG	Gyeongsang National University, Professor
Dong-Sik BAE	Changwon National University, Professor
Hyo Tae KIM	Korea Institute of Ceramic Engineering & Technology, Senior Researcher
Tae Kwon SONG	Changwon National University, Professor
Won-Jeong KIM	Changwon National University, Professor
Il-Won KIM	Ulsan University, Professor
Hui Suk YUN	Korea Institute of Materials Science, Senior Researcher

Program Committee

Synthesis, Raw Materials & Advanced powder processing (SY)	• Dong-Sik Bae / Changwon National University
Thermoelectrics (TE)	• Won-Seon Seo / Korea Institute of Ceramic Engineering and Technology • Soonil Lee / Korea Institute of Ceramic Engineering and Technology • Takashi Teranishi / Okayama University
Thin Films & Layers (TF)	• Soon-Gil Yoon / Chungnam National University Kazumi Kato / Advanced Industrial Science and Technology
Nano-particles & Nano-structured Materials (NA)	• Chang Yeol Kim / Korea Institute of Ceramic Engineering and Technology • Sekino Tohru / Osaka University • Hayashi Yamato / Tohoku University • Nakayama Tadachika / Nagaoka University of Technology
Structual Ceramics & Re-fractory materials (ST)	• Hyung Tae Kim / Korea Institute of Ceramic Engineering and Technology • Seongwon Kim / Korea Institute of Ceramic Engineering and Technology • Hai-Doo Kim / Korea Institute of Materials Science • Junichi Tatami / Yokohama National University
Fuel cells and Batteries (FU)	• Hyeong-Tae Lim / Changwon National University • Youngsik Kim / Ulsan National Institute of Science and Technology • Nobuhito Imanaka / Osaka University
Electronic Ceramics (EL)	• Eung Soo Kim / Kyonggi University • Ji Won Choi / Korea Institute of Science and Technology • Hisao Suzuki / Shizuoka University • Hitoshi Ohsato / Nagoya Institute of Technology
Glass & Opto-Electronic Materials (GL)	• Jong Heo / Pohang University of Science and Technology • Yong Gyu Choi / Korea Aerospace University • Hirokazu Masai / Kyoto University • Junji Nishii / Hokaido University
Biomaterials (BI)	• Byong Taek Lee / Soon Chun Hyang University • Hui Suk Yun / Korea Institute of Materials Science
Sensor Materials (SE)	• Jong-Heun Lee / Korea University • Kengo Shimanoe / Kyushu University
Electric Field Assisted Sin-tering (PAS, SPS and Relat-ed Processing Techniques) (EF)	• Young Hwan Han / Yeungnam University • Toshiyuki Nishimura / National Institute for Materials Science • Koji Morita / National Institute for Materials Science

Piezoelectric Device & Application (PI)	• Sahn Nahm / Korea University • Jungho Ryu / Korea Institute of Materials Science • Takeshi Morita / University of Tokyo
Lead-free Piezoelectrics (LP)	• Ho-Yong Lee / Sunmoon University • Wook Jo / Ulsan National Institute of Science and Technology • Satoshi Wada / University of Yamanashi • Hajime Nagata / Tokyo University of Science
Computational Ceramic Science and Engineering (CO)	• Kyoon Choi / Korea Institute of Ceramic Engineering and Technology • Tamio Oguchi / Osaka University
Ceramics Culture and Education (CE)	• Woo Seok Cho / Korea Institute of Ceramic Engineering and Technology • Junichi Hojo / Kyushu University
LED and Display Materials (LD)	• Hyun-Suk Kim / Chungnam National University • In-Hwan Lee / Chonbuk National University • Yasushi Nanishi / Ritsumeikan University
Advanced Coating for Gas Turbines (AD)	• Yeon-Gil Jung / Changwon National University • Byung-Koog Jang / National Institute for Materials Science

Sponsors

■ **Gyeongnam**
경상남도 www.gsnd.net

■ **Changwon**
창원시 www.changwon.go.kr

■ **The Korean Ceramic Society**
(사)한국세라믹학회 www.kcers.or.kr

■ **Changwon National University**
창원대학교 www.changwon.ac.kr

■ **Chungnam National University**
충남대학교 www.cnu.ac.kr

■ **Kyungnam University**
경남대학교 www.kyungnam.ac.kr

■ **Engineering Research Center for Integrated Mechatronics Materials and Components**
창원대학교 메카트로닉스 융합부품소재 연구센터 www.changwon.ac.kr

■ **Korea Institute of Ceramic Engineering and Technology**
한국세라믹기술원 www.kicet.re.kr

■ **Korea Ceramic Association**
한국세라믹총협회 www.kocera.or.kr

■ **KCC**
KCC www.kccworld.co.kr

■ **T.H. ELEMA ENG. CO., LTD.**
㈜태화에레마 thelema.co.kr/main.asp

■ **Korea Tourism Organization**
한국관광공사 kto.visitkorea.or.kr

On-site Registration Guideline

■ Date : November 26(Wed) ~ 28(Fri), 2014

■ Time

November 26(Wed)	14:00~18:00
November 27(Thu)	08:00~18:00
November 28(Fri)	08:00~16:00

■ Venue : 3rd Floor of CECO, Convention Hall Lobby)

■ **Registration Fee**

Category	Pre-Registration Fee (Registered by Nov. 14, 2014)	On-site Registration Fee
Regular	350,000 KRW	380,000 KRW
Student	120,000 KRW	150,000 KRW
Banquet	50,000 KRW	60,000 KRW

※ Students registrants must purchase banquet coupon at the registration desk to participate in the banquet.

■ **Registration Fee includes,**

For Regular Registrants	Admission to All Technical Sessions, Conference Program Book, 2 coupons for Lunch, Coffee Breaks, and Welcome Party, Banquet
For Student Registrants	Admission to All Technical Sessions, Conference Program Book, 2 coupons for Lunch and Coffee Breaks

■ **How to Register and Pay**

- Pre-Registrants : Please show your business card or ID card with credit card or cash to the staff at early registration desk.
- On-site Registrants : Fill in the on-site registration form at the fill-up desk first and submit the form with the registration fee at on-site registration desk.
- Conference program book, name tag with lunch coupons, and the receipt for registration will be provided after completing your registration process.

■ **Payment Policy**

- Registration fee should be paid by credit card or cash in KRW(Korean Won).
- In case of foreign credit card, only Visa, Master, JCB, AMEX card should be used.

Presentation Guideline

■ Oral Presentations

The time allotted to each plenary speaker is 45 minutes (35~40 minutes for presentation and 5~10 minutes for discussion) and to each invited speaker is mostly 25 minutes (20 minutes for presentation and 5 minutes for discussion). General oral presenters will mostly be provided with 12 minustes for the presentation including discussion time.

All session rooms will be equipped with a beam projector, a laptop computer and a screen. Presenters should test their presentations on the designated computers before their sessions start. Presenters may bring their own laptop computers to use. The laptops in oral session rooms are not equipped with audio sound system.

■ Poster Presentations

The poster sessions will be held on November 27th(Thu.) and 28th(Fri.) at the convention hall lobby (3F), Changwon Convention Exhibition Center(CECO). Poster stands and tapes for mounting will be provided at registration desk. The displayable area is approximately 79cm(W) x 146cm(H) and holds about 16 A4-size papers. A sign designating your poster board number(Ex: SY-P01) will be provided and positioned in the upper left-hand corner of the board. The boards for poster presentations will be arranged in numerical order listed in the final program.

There are two poster sessions, POSTER I, POSTER II during the seminar. Posters should be displayed during the designated hours. Posters should be removed from 16:30 to 17:00 of each poster session.

Please note that KJ-Ceramics 31 assumes no responsibility for materials that may be left behind, lost, stolen, or damaged. Please also be reminded that each poster presentation must have at least one author presenting during the session. Posters that are not posted on time will be treated as "No-show's", and such papers will be rejected without review.

Exhibition

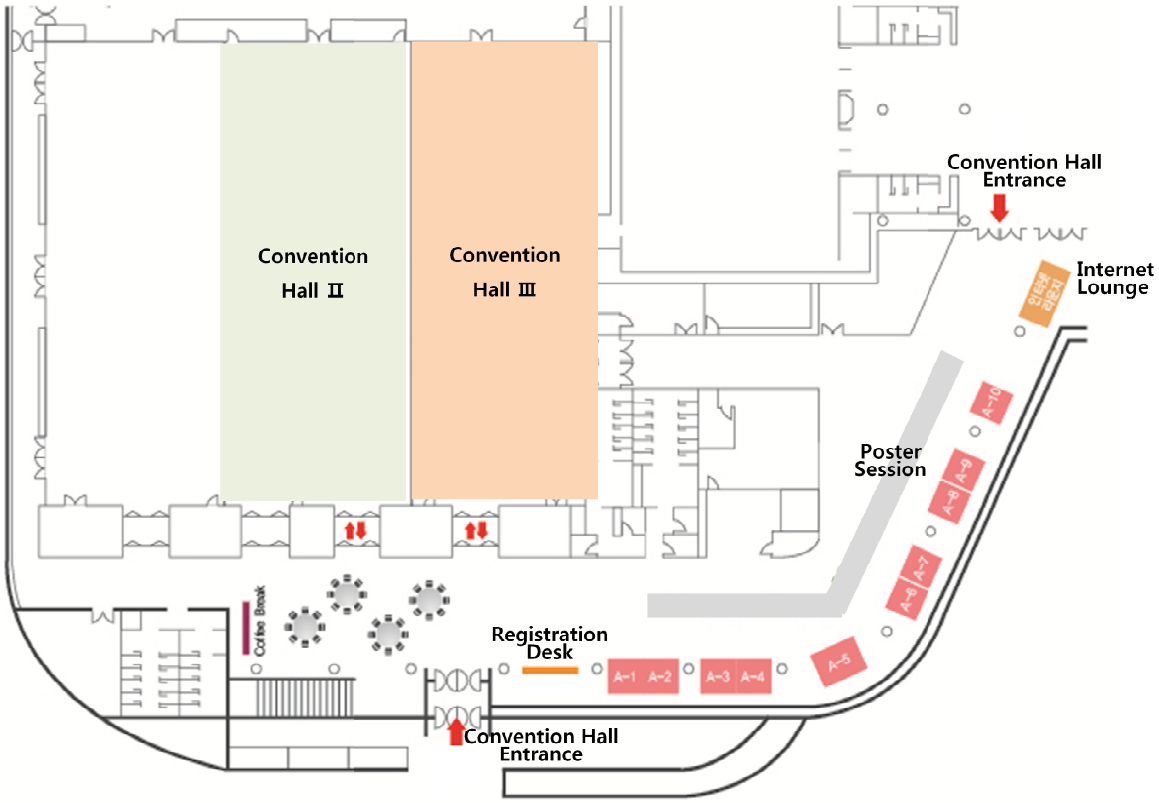

Booth No.	Exhibitor Name
A-1	Engineering Research Center for Integrated Materials and Components, Changwon National University
A-2	Basic Research Lab for UV2IR Nano Optoelectronic Devices
A-3, 4	Kyungnam University Kaolin RIS Agency
A-5	Alfa Aesar Korea
A-6	Ecopia corp
A-7	KCMC
A-8	PI Korea
A-9	Soletek Trading Co., Ltd.
A-10	EURO Industries Co., Ltd.

Social Programs

■ Welcome Party

Date	November 26 (Wed), 2014
Time	18:00 - 20:00
Venue	Grand Ballroom(2F), Hanlim Pullman Hotel (Next to CECO)
Program	Refreshments & Networking

■ Banquet

Date	November 27 (Thu), 2014
Time	18:00 - 20:00
Venue	Convention Hall 2, CECO
Program	Dinner, Short Performance & Networking

■ Excursion

Date	November 29 (Sat), 2014
Time	09:00 - 17:00
Course	Haeinsa Temple
Price	KRW 30,000 (Only cash available)

* Excursion slots should be reserved with advance payment of the fee and will be allocated on a first-come first-serve basis.
* The bus will leave at 09:00 sharp in front of Hanlim Pullman Hotel lobby(1F).

Program at a Glance

<table>
<tr><th>Time/Date</th><th>Nov. 26 (Wed)</th><th>Nov. 27(Thu)</th><th>Nov. 28(Fri)</th><th>Nov. 29 (Sat)</th></tr>
<tr><td>08:00~08:30</td><td rowspan="15"></td><td colspan="2">Registration
(Convention Hall Lobby)</td><td rowspan="15"></td></tr>
<tr><td>08:30~09:00</td><td colspan="2">Registration
(Convention Hall Lobby)</td></tr>
<tr><td>09:00~09:30</td><td colspan="2">Opening Ceremony
(Convention Hall 3)</td><td rowspan="15">Excursion</td></tr>
<tr><td>09:30~10:00</td><td colspan="2">Plenary Lecture 1 (Con-vention Hall 3)</td><td rowspan="2">Plenary Lecture 2~3
(Convention Hall 3)</td></tr>
<tr><td>10:00~10:30</td><td colspan="2" rowspan="2">Photo Time &
Coffee Break</td></tr>
<tr><td>10:30~11:00</td><td>Coffee Break</td></tr>
<tr><td>11:00~11:30</td><td colspan="2" rowspan="2">Oral Session 1
(Rm. 601~606)</td><td rowspan="2">Oral Session 5
(Rm. 601~606)</td></tr>
<tr><td>11:30~12:00</td></tr>
<tr><td>12:00~12:30</td><td colspan="2" rowspan="3">Lunch &
Poster Session</td><td rowspan="3">Lunch &
Poster Session</td></tr>
<tr><td>12:30~13:00</td></tr>
<tr><td>13:00~13:30</td></tr>
<tr><td>13:30~14:00</td><td rowspan="3">Oral Session 2
(Rm. 601~606)</td><td rowspan="3">Executive Committee Meeting
(Rm. 607)</td><td rowspan="3">Oral Session 6
(Rm. 601~606)</td></tr>
<tr><td>14:00~14:30</td></tr>
<tr><td>14:30~15:00</td><td>Coffee Break</td><td>Coffee Break</td></tr>
<tr><td>15:00~15:30</td><td rowspan="7">City Tour</td><td colspan="2" rowspan="2">Oral Session 3
(Rm. 601~606)</td><td rowspan="2">Oral Session 7
(Rm. 601~606)</td></tr>
<tr><td>15:30~16:00</td></tr>
<tr><td>16:00~16:30</td><td colspan="2">Coffee Break</td><td>Coffee Break</td></tr>
<tr><td>16:30~17:00</td><td colspan="2" rowspan="3">Oral Session 4
(Rm. 601~606)</td><td rowspan="3">Oral Session 8
(Rm. 601~606)</td></tr>
<tr><td>17:00~17:30</td></tr>
<tr><td>17:30~18:00</td></tr>
<tr><td>18:00~18:30</td><td rowspan="4">Welcome Party
(Pullman Hotel Grand Ball-room)</td><td colspan="2" rowspan="4">Banquet
(Convention Hall 2)</td><td>Closing Ceremony
(Rm. 602)</td><td rowspan="4"></td></tr>
<tr><td>18:30~19:00</td><td rowspan="3"></td></tr>
<tr><td>19:00~19:30</td></tr>
<tr><td>19:30~20:00</td></tr>
</table>

Detailed Program

■ November 27(Thu), 2014

<table>
<tr><th>Time</th><th colspan="6">Program</th></tr>
<tr><td>08:00~08:30</td><td colspan="6" rowspan="2">Registration
(Convention Hall Lobby)</td></tr>
<tr><td>08:30~09:00</td></tr>
<tr><td>09:00~09:30</td><td colspan="6">Opening Ceremony (Convention Hall 3)</td></tr>
<tr><td>09:30~10:00</td><td colspan="6" rowspan="2">Plenary Lecture 1 (09:30~10:15/Convention Hall 3)</td></tr>
<tr><td>10:00~10:30</td></tr>
<tr><td></td><td colspan="6">Photo Time (Convention Hall Lobby)</td></tr>
<tr><td>10:30~11:00</td><td colspan="6">Coffee Break (Convention Hall Lobby)</td></tr>
<tr><td>11:00~11:30</td><td rowspan="2">-</td><td>PI-I
(Rm.602)</td><td>GL-I
(Rm.603)</td><td>TE-I
(Rm.604)</td><td>LD-I
(Rm.605)</td><td>SE-I
(Rm.606)</td></tr>
<tr><td>11:30~12:00</td></tr>
<tr><td>12:00~12:30</td><td colspan="6" rowspan="3">Lunch & Poster Session
(FU, PI, GL, SY, TE, LD, AD, SE, BI)</td></tr>
<tr><td>12:30~13:00</td></tr>
<tr><td>13:00~13:30</td></tr>
<tr><td>13:30~14:00</td><td rowspan="2">FU-I
(Rm.601)</td><td rowspan="2">PI-II
(Rm.602)</td><td rowspan="2">GL-II
(Rm.603)</td><td rowspan="2">TE-II
(Rm.604)</td><td rowspan="2">LD-II
(Rm.605)</td><td rowspan="2">BI-I
(Rm.606)</td></tr>
<tr><td>14:00~14:30</td></tr>
<tr><td>14:30~15:00</td><td colspan="6">Coffee Break</td></tr>
<tr><td>15:00~15:30</td><td rowspan="2">ST-I
(Rm.601)</td><td rowspan="2">PI-III
(Rm.602)</td><td rowspan="2">SY-I
(Rm.603)</td><td rowspan="2">TE-III
(Rm.604)</td><td rowspan="2">AD-I
(Rm.605)</td><td rowspan="2">BI-II
(Rm.606)</td></tr>
<tr><td>15:30~16:00</td></tr>
<tr><td>16:00~16:30</td><td colspan="6">Coffee Break</td></tr>
<tr><td>16:30~17:00</td><td rowspan="2">ST-II
(Rm.601)</td><td rowspan="2">LP-I
(Rm.602)</td><td rowspan="2">SY-II
(Rm.603)</td><td rowspan="2">TF-I
(Rm.604)</td><td rowspan="2">AD-II
(Rm.605)</td><td rowspan="2">EL-I
(Rm.606)</td></tr>
<tr><td>17:00~17:30</td></tr>
<tr><td>17:30~18:00</td><td colspan="6" rowspan="4">Banquet
(Convention Hall-2F)</td></tr>
<tr><td>18:00~18:30</td></tr>
<tr><td>18:30~19:00</td></tr>
<tr><td>19:00~19:30</td></tr>
<tr><td>19:30~20:00</td><td colspan="6"></td></tr>
</table>

Code	Category	Code	Category
FU	Fuel cells and batteries	PI	Piezoelectric Materials, Devices & Applications
GL	Glass & Opto-Electronic Materials	SY	Synthesis, Raw Materials & Advanced powder processing
TE	Thermoelectrics	LD	LED and Display Materials
AD	Advanced Coating for Gas Turbines	SE	Sensor materials
BI	Biomaterials		

■ November 28(Fri), 2014

<table>
<tr><th>Time</th><th colspan="6">Program</th></tr>
<tr><td>08:00~08:30</td><td colspan="6" rowspan="2">Registration
(Convention Hall Lobby)</td></tr>
<tr><td>08:30~09:00</td></tr>
<tr><td>09:00~09:30</td><td colspan="6" rowspan="2">Plenary Lecture 2 (09:00~09:45/Convention Hall 3)</td></tr>
<tr><td rowspan="2">09:30~10:00</td></tr>
<tr><td>10:00~10:30</td><td colspan="6">Plenary Lecture 3 (09:45~10:30/Convention Hall 3)</td></tr>
<tr><td rowspan="2">10:30~11:00</td><td colspan="6">Coffee Break</td></tr>
<tr><td rowspan="3">EL-II
(Rm.601)</td><td rowspan="3">LP-II
(Rm.602)</td><td rowspan="3">NA-I
(Rm.603)</td><td rowspan="3">ST-III
(Rm.604)</td><td rowspan="3">LD-III
(Rm.605)</td><td rowspan="3">CE-I
(Rm.606)</td></tr>
<tr><td>11:00~11:30</td></tr>
<tr><td>11:30~12:00</td></tr>
<tr><td>12:00~12:30</td><td colspan="6" rowspan="3">Lunch & Poster Session
(EL, TF, NA, EF, LP, CO, CE, ST)</td></tr>
<tr><td>12:30~13:00</td></tr>
<tr><td>13:00~13:30</td></tr>
<tr><td>13:30~14:00</td><td rowspan="3">EL-III
(Rm.601)</td><td rowspan="3">LP-III
(Rm.602)</td><td rowspan="3">NA-II
(Rm.603)</td><td rowspan="3">ST-IV
(Rm.604)</td><td rowspan="3">LD-IV
(Rm.605)</td><td rowspan="3">CE-II
(Rm.606)</td></tr>
<tr><td>14:00~14:30</td></tr>
<tr><td rowspan="2">14:30~15:00</td></tr>
<tr><td colspan="6">Coffee Break</td></tr>
<tr><td>15:00~15:30</td><td rowspan="3">FU-II
(Rm.601)</td><td rowspan="3">LP-IV
(Rm.602)</td><td rowspan="3">NA-III
(Rm.603)</td><td rowspan="3">ST-V
(Rm.604)</td><td rowspan="3">EF-I
(Rm.605)</td><td rowspan="5">CE-III
(Rm.606)</td></tr>
<tr><td>15:30~16:00</td></tr>
<tr><td rowspan="2">16:00~16:30</td></tr>
<tr><td colspan="5">Coffee Break</td></tr>
<tr><td>16:30~17:00</td><td rowspan="3">FU-III
(Rm.601)</td><td rowspan="3">LP-V
(Rm.602)</td><td rowspan="3">TF-II
(Rm.603)</td><td rowspan="3">CO-I
(Rm.604)</td><td rowspan="3">EF-II
(Rm.605)</td></tr>
<tr><td>17:00~17:30</td><td rowspan="2"></td></tr>
<tr><td>17:30~18:00</td></tr>
<tr><td>18:00~18:30</td><td colspan="6">Closing Ceremony (Rm.602)</td></tr>
</table>

Code	Category	Code	Category
EL	Electronic Ceramics	TF	Thin Films & Layers
NA	Nano-particles & Nano-structured Materials	EF	Electric Field assisted Sintering (PAS,SPS and Related Processing Techiques)
LP	Lead-free Piezoelectrics	CO	Computational Ceramic Science and Engi-neering
CE	Ceramics Culture and Education	ST	Structural Ceramics & Refractory Materials

Scientific Program

Scientific Program

- Oral Sessions -

November 27 (Thu), 2014

Opening Ceremony (09:00~09:30) – Convention Hall 3(3F)

Plenary Lecture 1 **Convention Hall 3 (3F)**

Chair : Nam-Kyun Kim(KERI)

PL-01 09:00~09:45

Silicon Carbide Power Semiconductor and Electronic Devices

Hyeong Joon KIM

(Seoul National University, Korea)

Photo Time & Coffee Break (10:15~10:45) – Convention Hall Lobby(3F)

Oral Session 1 [10:45-12:10]

PI-I | **Piezoelectric Device & Application** | **Rm. 602 (6F)**

Chair(K): Hongsoo Choi (Daegu Gyeongbuk Institute of Science and Technology)

Chair(J): Isaku Kanno (Kobe University)

PI-I01 10:45~11:05

Energy Harvesting Devices by Piezoelectric Ceramics

Toshio OGAWA[1], *Hiroshi AKAISHI*[2]

([1]Shizuoka Institute of Science and Technology, Japan, [2]Plus Comfort Co., Ltd., Japan)

PI-I02 11:05~11:25

Piezoelectric Energy Harvesting for Wearable and Implantable Applications

Miso KIM

(Korea Research Institute of Standards and Science, Korea)

PI-O01 11:25~11:37

PZT-PZNN Ceramics for Energy Harvesting and Multilayer Actuator Applications

Joon HUR, ***Dae-hyeon KIM****, In-Tae SEO, Sahn NAHN*

(Korea University, Korea)

PI-O02 11:37~11:49

Mechanical Energy Harvesters Utilizing (001) Textured PZT Films on Flexible Metal Foils

Hong Goo YEO*, Charles B. YEAGER, Thomas N. JACKSON, Christopher RAHN, Xiaokun MA, Susan TROLIER-MCKINSTRY*

(The Pennsylvania State University, USA)

PI-O03 11:49~12:01

Exceptionally High Magnetoelectric Characteristics in Laser Annealed PZT Thick Films on Magnetostrictive Metglas Foil

Haribabu PALNEEDI[1,2], *Ju-Eun KANG*[2], *Deepam MAURYA*[3], *Shashank PRIYA*[3], *Suk-Joong L. KANG*[1*], *and Jungho RYU*[2]
([1]*Korea Advanced Institute of Science and Technology (KAIST), Korea,* [2]*Korea Institute of Materials Science (KIMS), Korea,* [3]*Virginia Tech., USA)*

GL-I | Glass & Opto-Electronic Materials | Rm. 603 (6F)

Chair(K): Yong Gyu Choi (Korea Aerospace University)
Chair(J): Atsunobu Masuno (The University of Tokyo)

GL-I01 10:45~11:10

Glass materials for white LED color converters

Woon Jin CHUNG[1], *Hyun-A PARK*[1], *Karam HAN*[1], *Sang Hun LEE*[1], *Won Bin IM*[2], *Jong HEO*[3]
([1]*Kongju National University, Korea,* [2]*Chonnam National University, Korea*
[3]*Pohang University of Science and Technology (POSTECH), Korea)*

GL-O01 11:10~11:22

DC voltage application to alkali containing oxide glass

Junji NISHII, *T. MISAWA and H. KAIJU*
(Hokkaido University, Japan)

GL-O02 11:22~11:34

Potassium ion migration between non-contacted glass plates using corona discharge treatment in H_2 atmosphere

Keiga KAWAGUCHI, *Hideo KAIJU, Junji NISHII*
(Hokkaido University, Japan)

GL-O03 11:34~11:46

Recent Progress in Laser Patterning of Functional Crystals with High Orientation in Glasses

Takayuki KOMATSU, *Tsuyoshi HONMA, Kenji SHINOZAKI*
(Nagaoka University of Technology, Japan)

GL-O04 11:46~11:58

Fabrication of Sn^{2+}-doped Phosphate Glasses for Phosphor Applications

Hirokazu MASAI[1], *Toshiro TANIMOTO*[1], *Shun OKUMURA*[1], *Kentaro TERAMURA*[1], *Syuji MATSUMOTO*[2], *Takayuki YANAGIDA*[3], *Yomei TOKUDA*[1], *Toshinobu YOKO*[1]
([1]*Kyoto University, Japan,* [2]*Asahi Glass Co., Ltd.,Japan,* [3]*Kyushu Institute of Technology, Japan)*

GL-O05 11:58~12:10
Accumulation of Lanthanide Ions inside the Crystalline Phases in Vitustie Glass-Ceramics Wasteforms
Miae KIM[1], *Jayhyok SONG*[2], *Jong HEO*[1]
([1]Pohang University of Science and Technology(POSTECH), Korea, [2]Samsung SDI, Korea)

TE-I Thermoelectrics Rm. 604 (6F)

Chair(K): Soonil Lee (Korea Institute of Ceramic Engeneering and Technology)
Chair(J): Yoshiaki Kinemuchi (AIST)

TE-I01 10:45~11:10
N-type Oxide Thermoelectric Materials Having Spin/Orbital Correlations
Tetsuji OKUDA
(Kagoshima University, Japan)

TE-I02 11:10~11:35
Thermoelectric properties of thick film elements fabricated by aerosol deposition method
Yuichi NAKAMURA, *Mitsuteru INOUE*
(Toyohashi University of Technology, Japan)

TE-O01 11:35~11:47
Thermoelectric Properties of Titanium Doped Zinc Oxide Thin Films Deposited by Co-Sputtering method
Venkatraju.JELLA, *Soon-Gil YOON*
(Chungnam National University, Korea)

TE-O02 11:47~11:59
Thermoelectric Properties of Bulk $Bi_2Mg_{2/3}Nb_{4/3}O_7$-Bi (BMNO-Bi) Composite and BMNO-Bi Composite Thin Films
Ji-Ho EOM[1], *San-Kwon LEE*[2], *Soon-Gil YOON*[1]
([1]Chungnam National University, Korea, [2]Chung-Ang University, Korea)

LD-I LED and Display Materials Rm. 605 (6F)

Chair(K): In-Hwan Lee (Chonbuk National University)
Chair(J): Motoaki Iwaya (Meijo University)

LD-I01 10:45~11:10
New Approach to Fabricate Green, Red and IR Light Sources Based on Nitride Semiconductors by DERI Method
Y. NANISHI[1], *T.YAMAGUCHI*[2] *and T.ARAKI*[1]
([1]Ritsumeikan University, Japan, [2]Kogakuin University, Japan)

LD-I02 11:10~11:35

GaN Electronic Devices and Their Applications

Jae Kyoung MUN[1,2]*, *Woojin CHANG*[1], *Sang Choon KO*[1], *Eun Soo NAM*[3]
(ETRI, Korea, Univ. of Sci. & Tech.(UST), Korea)

LD-O01 11:35~11:47

Optical properties of $Ag@SiO_2$ nanoparticles embedded nanopillar LED structures

Kang-Bin BAE, *Jin-Hyeon YUN, Han-Su CHO and In-Hwan LEE*
(Chonbuk National University, Korea)

LD-O02 11:47~11:59

A Novel technology for fabrication of AlGaN/GaN HFETs using by photosensitive polyimide IMD layer

Seung Kyu OH[1], *Hwa Young KO*[2], *Taehoon JANG*[2], *Joon Seop KWAK*[1]*
([1]Sunchon National University, Korea, [2]LG Electronics, Korea)

LD-O03 11:59~12:11

Enhanced optical output power of InGaN/GaN blue LED embedded with SiO_2 nanopaticles

Hansu CHO[1], *Kyeongseob KWON*[1], *Myeongji DONG*[1], *Kangbin BAE*[1], *Taehoon CHUNG*[2], *Jonghyeob BAEK*[2], *Inhwan LEE*[1]*
([1]Chonbuk National University, Korea, [2]Korea Photonics Technology Institute, Korea)

SE-I | Sensor Materials | Rm. 606 (6F)

Chair(K): Jong-Heun Lee (Korea University)
Chair(J): Kengo Shimanoe (Kyushu University)

SE-I01 10:45~11:10

Catalytic combustion type gas sensor of FIGARO engineering

Junji OMORI, *Kazuya SHINNISHI, Tatsuya TANIHIRA, Kazunari KANEYASU*
(Figaro Engineering , Japan)

SE-I02 11:10~11:35

Development of Oxide Semiconductor Gas Sensors for High Sensitivity under Humid Condition

Kengo SHIMANOE[1], *Nan MA*[1], *Miyuki SASAKI*[1], *Koichi SUEMATSU*[2], *Masayoshi YUASA*[1]
([1]Kyushu University, Japan, [2]Fukuoka Industrial Technology Center, Japan)

SE-I03 11:35~12:00

Metal oxide thin films with highly ordered nanostructures for high performance gas sensors

Ho Won JANG
(Seoul National University, Korea)

SE-O01 12:00~12:12
Catalyst-loaded oxide semiconductor yolk-shell nanostructures for gas sensor applications
Ji-Wook YOON[1], *Young Jun HONG*[2], *Yun Chan KANG*[1], *Jong-Heun LEE*[1]
([1]Korea University, Korea, [2]Konkuk University, Korea)

Lunch Break & Poster Session I (12:10~13:30) – Convention Hall Lobby (3F)

Oral Session 2 [13:30-14:55]

FU-I	Fuel cells and Batteries	Rm. 601 (6F)

Chair(K): Hyung-Tae Lim (Changwon National University)
Chair(J): Naoaki Yabuuchi (Tokyo Denki University)

FU-I01 13:30~13:55
Pure Mg^{2+} Ion Conducting Solid Electrolyte Having NASICON-type Structure
Nobuhito IMANAKA, *Megumi YAMANE, Shinji TAMURA*
(Osaka University, Japan)

FU-I02 13:55~14:20
Solid Oxide Electrolysis Cell (SOEC) Technology for Hydrogen Production
Kyung Joong YOON, *Jongsup HONG, Hyoungchul KIM Hae-Ryoung KIM, Ji-Won SON, Jong-Ho LEE, Byung-Kook KIM, Hae-June JE*
(Korea Institute of Science and Technology, Korea)

FU-I03 14:20~14:45
Lithium-Excess High-Capacity Electrode Materials with 4d-Transition Metals for Rechargeable Lithium Batteries
Naoaki YABUUCHI
(Tokyo Denki University, Japan)

PI-II	Piezoelectric Device & Application	Rm. 602 (6F)

Chair(K): Miso Kim (Korea Research Institute of Standards and Science)
Chair(J): Takeshi Morita (Tokyo University)

PI-I03 13:30~13:50
Piezoelectric MEMS devices for artificial cochlea and ultrasonic cell stimulation
Hongshoo CHOI
(Daegu Gyeongbuk Institute of Science and Technology(DGIST), Korea)

PI-I04 13:50~14:10
Piezoelectric thin films and their MEMS applications

Isaku KANNO
(Kobe University, Japan)

PI-O04 14:10~14:22

High Temperature Nano-grained PbTiO3 Thick Film by Aerosol-Deposition

Jungho RYU[1], *Si-Young CHOI[1], Susan TROLIER-McKINSTRY[2], Hongsoo CHOI[3], Shashank PRIYA[4], Jong-Woo KIM[1], Woon-Ha YOON[1], Jong-Jin CHOI[1], Dong-Soo PARK[1], Cheol-Woo AHN[1], Byung-Dong HAHN[1], Dae-Yong JEONG[5]*
([1]Korea Institute of Materials Science (KIMS), Korea, [2]The Pennsylvania State University, USA, [3]Daegu Gyeongbuk Institute of Science and Technology (DGIST), Korea, [4]Virginia Tech, USA, [5]Inha University, Korea)

PI-O05 14:22~14:34

Prototype of a Micro Piezoelectric Ultrasonic Motor

Tomoaki MASHIMO
(Toyohashi University of Technology, Japan)

PI-O06 14:34~14:46

Piezoelectric Multi-layer Ceramics for Haptic Actuator

In-Tae SEO, *Joon HUR, Jong-Hyun KIM, Tae-Ho LEE, Sahn NAHM*
(Korea University, Korea)

GL-II | Glass & Opto-Electronic Materials | Rm. 603 (6F)

Chair(K): Woonjin Chung (Kongju National University)
Chair(J): Hirokazu Masai (Kyoto University)

GL-I02 13:30~13:55

Functional oxide glasses prepared by a levitation technique

Atsunobu MASUNO
(The University of Tokyo, Japan)

GL-O06 13:55~14:07

Kinetics of PbS Quantum Dots Precipitation on Nd^{3+}-O Clusters

J. HEO[1], *Won Ji PARK[1], Woon Jin CHUNG[2]*
([1]Pohang University of Science and Technology (POSTECH), Korea, [2]Kongju National University, Korea)

GL-O07 14:07~14:19

Luminescence and Absorption Properties of PbS Quantum Dots in Glasses

Won Ji PARK, *Mi Ae KIM, Jong HEO*
(Pohang University of Science and Technology (POSTECH), Korea)

GL-O08 14:19~14:31

Influence of composition on near-infrared luminescence of $BaSn_xO_3$

Yosuke OHYA[1], *Yuichiro KUROKI[2], Tomoichiro OKAMOTO[1]*, Masasuke TAKATA[3]*
([1]Nagaoka University of Technology, Japan, [2]Salesian polytechnic, Japan, [3]Japan Fine Ce-

ramics Center, Japan)

GL-O09 14:31~14:43
In-Situ XAFS Study of Amorphous $Ge_{50}Se_{50}$ Film under DC Electric Field
Sang Yeol SHIN[1], *Roman GOLOVCHAK*[2], *Byung-ki CHEONG*[3], *Himanshu JAIN*[4], *Yong Gyu CHOI*[1]
[1]*Korea Aerospace University, Korea,* [2]*Austin Peay State University, USA,* [3]*Korea Institute of Science and Technology (KIST), Korea,* [4]*Lehigh University, USA)*

GL-O10 14:43~14:55
Improved Luminous Efficacy by Enhancing Transmittance of Phosphor-in-Glass
Yurian KIM, *Sunil KIM, Hyungsun KIM*
(Inha University, Korea)

TE-II | Thermoelectrics | Rm. 604 (6F)

Chair(K): Kyu hyoung Lee (Kangwon National University)
Chair(J): Tetsuji Okuda (Kagoshima University)

TE-I03 13:30~13:55
A study on thermoelectric properties of perovskite-type oxides
Hiroshi NAKATSUGAWA, *Masaki KUBOTA, Takanori YAMAMOTO, Yosuke WATANABE*
(Yokohama National University, Japan)

TE-I04 13:55~14:20
Oxygen Defect Application for Oxide Thermoelectrics
Soonil LEE
(Korea Institute of Ceramic Engineering and Technology(KICET), Korea)

TE-I05 14:20~14:45
How can we boost thermoelectric properties of oxides by nano?
Yoshiaki KINEMUCHI
(National Institute of Advanced Industrial Science and Technology (AIST), Japan)

LD-II | LED and Display Materials | Rm. 605 (6F)

Chair(K): In-Hwan Lee (Chonbuk National University)
Chair(J): Yasushi Nanishi (Ritsumeikan University)

LD-I03 13:30~13:55
Towards Performance Enhancement of InGaN/GaN LED by Exploring Localized Surface Plasmons
In-Hwan LEE
(Chonbuk National University, Korea)

LD-I04 13:55~14:20

***In situ* XRD analysis of GaInN/GaN heterostructure grown on GaN underlying layer with different dislocation density**
***Motoaki IWAYA*[1]**, *Koji ISHIHARA[1], Taiji YAMAMOTO[1], Daisuke IIDA[1], Yasunari KONDO[1], Hiroyuki MATSUBARA[1], Tetsuya TAKEUCHI[1], Satoshi KAMIYAMA[1], and Isamu AKASAKI[1,2]*
([1]Meijo University, Japan, [2]Nagoya University, Japan)

LD-I05 14:20~14:45
High Mobility and Highly Stable Aluminum-doped Indium Zinc Tin Oxide Thin-Film Transistors Compatible with Back-Channel Etch Process
***Sung Haeng CHO*[1]**, *Sang-Hee Ko PARK[2], Hee-Ok KIM[1], Oh-Sang KWON[1], Eun-Sook PARK[1], Min Ki RYU[1], Sun Kwon LIM[3] and Chi-Sun HWANG[1]*
([1] Electronics and Telecommunications Research Institute (ETRI), Korea, [2]Korea Advanced Institute of Science and Technology (KAIST), Korea, [3]Heesung Metal Ltd., Korea)

LD-O04 14:45~14:57
Deposition of nanoparticles on substrate for layer-by-layer assembly
Myeong-Ji DONG, *In-Hwan LEE*
(Chonbuk National University, Korea)

BI-I | Biomaterials | Rm. 606 (6F)

Chair(K): Byong Taek Lee (Soonchunhyang University)
Chair(J): Il Young Kim (Nagoya University)

BI-I01 13:30~13:55
GRAPE® technology: in vitro and in vivo evaluations
***K. UETSUKI*[1]**, *T. KURAMOTO[1], S. HAYAKAWA[2], A. OSAKA[2]*
([1] Nakashima Medical Co., Japan, [2]Okayama University, Japan)

BI-O01 13:55~14:07
The Relevance of Biological Nutrients to the Prevention and Treatment of Osteoporosis
Garima TRIPATHI, *Hui Suk YUN*
(Korea Institute of Materials Science(KIMS), Korea)

BI-O02 14:07~14:19
Behaviour of Human Stem Cell on HA-TCP Composites
Indu BAJPAI, *Duk Yeon KIM, Jung Kyong-JIN, Soyoung YANG, In-Hwan SONG, Sukyoung KIM*
(Yeungnam University, Gyeongsan, Korea)

BI-O03 14:19~14:31
Fabrication of Core shell scaffolds by simultaneous extrusion of ceramic and hydrogel for bone tissue engineering
***Naren RAJA*[1, 2]**, *Jongman LEE[2], Hui-suk YUN[1, 2]*
([1]Korea University of Science and Technology, Korea, [2]Korea Institute of Materials Science,

Korea)

BI-O04 14:31~14:43
Tissue engineered regeneration of completely transected femur using modified hydroxyapatite porous scaffold
Thuy Ba Linh NGUYEN, *Dong Woo JANG, Young Ki MIN and Byong Taek LEE*
(Soonchunhyang University, Korea)

BI-O05 14:43~14:55
Characterization of Multiwalled Carbon Nanotube-Reinforced Hydroxyapatite Composites Consolidated by Spark Plasma Sintering
Duk-Yeon KIM[1], *Young-Hwan HAN[1], Sungsil JUNG[2], Sukyoung KIM[1]*
([1]Yeungnam University, Korea, [2]Pohang Techno Park, Korea)

Break Time (14:55~15:00)

Oral Session 3 [15:00-16:15]

ST-I	Structual Ceramics & Refractory Materials	Rm. 601 (6F)

Chair(K): Hai-Doo Kim (KIMS)
Chair(J): Junichi Tatami (Yokohama National University)

ST-I01 15:00~15:30
Effect of Additive Composition on Thermal Conductivity of Liquid-Phase Sintered Silicon Carbide Ceramics
Young-Wook KIM
(University of Seoul, Korea)

ST-O01 15:30~15:50
Fabrication of Si_3N_4 ceramics by post-reaction sintering using Si-Y_2O_3-Al_2O_3 nanocomposite particles prepared by mechanical treatment
Kwangjin JEONG[1], *Motoyuki IIJIMA[1], Takuma TAKAHASHI[2] Junichi TATAMI[1*]*
([1]Yokohama National University, Japan, [2]Kanagawa Academy of Science and Technology, Japan)

ST-O02 15:50~16:10
Analysis of High Temperature Stability of White Amorphous Si–O–C(–H) Ceramics in Terms of Structure Evolution and Photoluminescence Degradation
Masaki NARISAWA[1], *Guangyu MA[1], Hiroki HOKAZONO[1], Seiji WATASE[2], Kimihiro MATSUKAWA[2] and Akihiro IWASE[1]*
[1]Graduate School of Engineering, Osaka Prefecture University, 1-1 Gakuen-Cho, Naka-Ku, Sakai, Osaka599-8531, Japan[2]Osaka Municipal Technical Research Institute, 1-6-50, Morinomiya, Joto-ku, Osaka 536-8553, Japan)

PI-III	Piezoelectric Device & Application	Rm. 602 (6F)

Chair(K): In-tae Seo (Korea University)
Chair(J): Tomoaki Mashimo (Toyohashi University of Technology)

PI-I05 15:00~15:20
Resonant-type Smooth Impact Drive Mechanism (R-SIDM)
Takeshi MORITA
(The University of Tokyo, Japan)

PI-I06 15:20~15:40
Piezoelectric, ferroelectric and structural properties of $BiFeO_3$-$BaTiO_3$ electroceramics
Myang Hwan LEE, Da Jeong KIM, Jin Su PARK, ***Tae Kwon SONG***
(Changwon National University, Korea)

PI-O07 15:40~15:52
Enhancement of Multiferroic Properties in Nano-heterostructured Multilayer Bismuth Ferrite Thin Films
V. Annapu REDDY[1,2]*, and R. NATH[1]*
([1]Korea Institute of Materials Science (KIMS), Korea, [2]Indian Institute of Technology Roorkee, India)

PI-O08 15:52~16:04
Effects of Na excess on dielectric and electrical properties of $(Na_{0.53+x}K_{0.47})(Nb_{0.55}Ta_{0.45})O_3$ ceramics
M. S. KIM*, J. S. KIM, T. K. SONG, W. J. KIM, M. H. KIM*
(Changwon National University, Korea)

SY-I	Synthesis, Raw Materials & Advanced Powder Processing	Rm. 603 (6F)

Chair(K): Dong Sik Bae (Changwon National University)
Chair(J): Koichiro Tsuzuku (Gunma University)

SY-I01 15:00~15:25
Novel Environmentally Friendly (Bi, Ca, Zn, La)VO_4 Yellow Pigments
Toshiyuki MASUI, *Wendusu, Taihei HONDA, Nobuhito IMANAKA*
(Osaka University, Japan)

SY-I02 15:25~15:50
Novel Low Temperature Synthesis Method of Ceramic Oxide Materials
Kenji TODA*[1], Tatsuro KANEKO[1], Kazuyoshi UEMATSU[1], Tadashi ISHIGAKI[1], Sun Woog KIM[1], Mineo SATO[1], Junko KOIDE[2] , Masako TODA[2] , Yoshiaki KUDO[2]*
([1]Niigata University, Japan , [2]N-Luminescence Corporation, Japan)

SY-O01 15:50~16:05
Sintering and Thermal properties of the Glass/Al_2O_3 Composites for the Substrate of Supercapacitor
Tae-Ho LEE, *Dae-Hyeon KIM, In-Tae SEO, Sahn NAHM*
(Korea University, Korea)

SY-O02 16:05~16:20
Electronic Spectra of Tourmaline Treated by Heat and Electron Beam Irradiation
Apichate MANEEWONG[1, 2, 3], *Beak Seok SEONG*[1, 2], *Jeong Seog KIM*[4]
([1]Korean University of Science & Technology, Korea, [2]Korea Atomic Energy Research Institute, Korea, [3]Thailand Institute of Nuclear Technology,Thailand, [4]Hoseo University, Korea)

SY-O03 16:20~16:35
Synthesis and Characterization of the Spinel System Inorganic-Pigment by a Reverse Micelle Processing
Jeong Hun SON, *Dong Sik BAE*
(Changwon National University, Korea)

TE-III | Thermoelectrics | Rm. 604 (6F)

Chair(K): Soonil Lee (Korea Institute of Ceramic Engeneering and Technology)
Chair(J): Yuichi Nakamura (Toyohashi University of Technology)

TE-I06 15:00~15:25
Thermoelectric Properties of Doped n-type $Cu_{0.008}Bi_2Te_{2.7}Se_{0.3}$
Kyu Hyoung LEE[1], *Sung Wng KIM*[2,3]
([1]Kangwon National University, Korea, [2]Sungkyunkwan University, Korea, [3]Sungkyunkwan University, Korea)

TE-I07 15:25~15:50
One alternative way to high thermoelectric performance: the intrinsically low thermal conductivity
Li-Dong ZHAO
(Beihang University, China)

AD-I | Advanced Coating for Gas Turbines | Rm. 605 (6F)

Chair(K): Yoonsuk Oh (KICET)
Chair(J): Shunkichi Ueno (Nihon University)

AD-I01 15:00~15:25
Thermal Properties of Y_2O_3 doped ZrO_2 Thermal Barrier Coatings
Byung-Koog JANG[1], *Seongwon KIM*[2], *Yoon-Suk OH*[2], *Hyung-Tae KIM*[2]
([1]National Institute for Materials Science, Japan, [2]Korea Institute of Ceramic Engineering and Technology, Korea)

AD-I02 15:25~15:50
Mechanical Behavior of Thermal Barrier Coatings after Thermal Shock using Spherical Indentation Analysis
Kee Sung LEE[1], *Dong Heon Lee*[2]
([1]Kookmin University, Korea)

AD-I03 15:50~16:15
Effects of Feedstock Species in Top Coat on Thermal Durability of Thermal Barrier Coatings in Cyclic Thermal Exposure
Sang-Won MYOUNG[1], *Zhe LU*[1], *Qi-Zheng CUI*[1], *Je-Hyun LEE*[1], *Yeon-Gil JUNG*[1*], *Ungyu PAIK*[2], *Byung-Koog JANG*[3]
([1]Changwon National University, Korea, [2]Hanyang University, Korea, [3]National Institute for Materials Science(NIMS), Japan)

BI-II Biomaterials Rm. 606 (6F)

Chair(K): Hui Suk YUN (Korea Institute of Materials Science)
Chair(J): K. Uetsuki (Nakashima Medical Co)

BI-I02 15:00~15:25
Development and evaluation of novel hybrid systems of ceramic and polymer for bone tissue regeneration
Byong Taek LEE
(Soonchunhyang University, Korea)

BI-O06 15:25~15:37
Effect of Ag_2O substitution on solubility and structure of CaO-P_2O_5-Nb_2O_5 glasses
Sungho LEE[1], *Hirotaka MAEDA*[1], *Akiko OBATA*[1], *Kyosuke UEDA*[2], *Takayuki NARUSHIMA*[2], *Toshihiro KASUGA*[1]
([1]Nagoya Institute of Technology, Japan, [2]Tohoku University, Japan)

BI-O07 15:37~15:49
Synthesis of Bioglass Ceramic Using Commercial Water Glasses for Plasma Spray Coating on Dental Implants
Jaehui JEON, *Sukyoung KIM*
(Yeungnam University, Korea)

BI-O08 15:49~16:01
The influence of calcium chloride ($CaCl_2$) concentration on apatite precipitation of surface-modified cobalt-chromium (Co-Cr) alloys in a simulated body fluid
Chao LIU, *Toshiki MIYAZAKI and Yuki SHIROSAKI*
(Kyushu Institute of Technology, Japan)

BI-O09 16:01~16:13
Response of human osteoblast-like cells to different surface modified titanium al-

loys
J. M. ZHAO, *K. H. HWANG*
(Gyeongsang National University, Korea)

BI-O10 16:13~16:25
Morphology of hydroxyapatite prepared from single crystals of calcium compounds
Ill Yong KIM, *Koichi KIKUTA, Chikara OHTSUKI*
(Nagoya University, Japan)

Coffee Break (16:15~16:30)

Oral Session 4 [16:30-18:00]

ST-II	Structual Ceramics & Refractory Materials	Rm. 601 (6F)

Chair(K): Hai-Doo Kim (KIMS)
Chair(J): Junichi Tatami (Yokohama National University)

ST-O03 16:30~16:50
Carbon Nanotubes Grown on Cobalt Supported Zeolite-Porous Ceramics
Jung Gyu PARK[1], *Wei ZHAO*[2], *Sangram MAZUMDER*[1], *and Ik Jin KIM*[1]
([1]Hanseo University, Korea, [2]Yeungnam University, Korea)

ST-O04 16:50~17:10
Co-dispersion system of ZrB2-SiC in non-aqueous solvent
Jin Soon HAN, *Sung Bok WEE, Gye Seok AN, Jae Seok CHOI, Hyun Cheol OH, Sung Churl CHOI*
(Hanyang University, Korea)

ST-O05 17:10~17:30
Slow Crack Growth Behavior of Yttrium Oxide from Static/dynamic Fatigue and Double Torsion Tests
Sung-Min LEE[1], *Amit SHYAM*[2], *and Hua-Tay LIN*[2]
([1]Korea Institute of Ceramic Engineering and Technology(KICET), Korea, [2]Oak Ridge National Laboratory, USA)

ST-I02 17:30~18:00
Stochastic Model on Granule Collapse during Cold Isostatic Pressing
Kouichi YASUDA[1], *Satoshi TANAKA*[2], *Makio NAITO*[1]
([1] Tokyo Institute of Technology, Japan, [2]Nagaoka University of Technology, Japan, [3]Osaka University, Japan)

LP-I	Lead-free Piezoelectrics	Rm. 602 (6F)

Chair(K): Jae-Shin Lee (University of Ulsan)
Chair(J): Satoshi Wada (University of Yamanashi)

LP-I02 16:30~16:55
"Lead-free" Piezoelectric Single Crystals Fabricated by Solid-State Crystal Growth (SSCG) Method:Development and Application
*Sung-Min LEE[1], Dong-Ho KIM[1], Jong-Yeb LEE[1], Hyun-Taek OH[1], **Ho-Yong LEE**[1,2]*
([1]Ceracomp Co., Ltd., Korea, [2]Sunmoon University, Korea)

LP-I03 16:55~17:20
Fabrication and characterization of epitaxial KNN films
***Feng CHEN**[1], Yuanhang LI[1], Wenbin WU[1], Ke WANG[2], Jing-Feng LI[2], Shunyi LI[3] and Adreas KLEIN[3]*
([1]Chinese Academy of Science, China, [2]Tsinghua University, China, [3]Technische Universität Darmstadt,Germany)

LP-I04 17:20~17:45
Synthesis of NaNbO3-BaTiO3 Lead-free Piezoelectric Ceramics using Submicron-sized Starting Materials
Rintaro AOYAGI
(Nagoya Institute of Technology, Japan)

LP-O01 17:45~17:57
Effect of Firing Temperature and DC Poling on Acoustic Wave Velocities in Barium Titanate Piezoelectric Ceramics
***Taiki IKEGAYA**, Toshio OGAWA*
(Shizuoka Institute of Science and Technology, Japan)

LP-O02 17:57~18:09
Electric properties of unmodified $BiFeO_3$-$BaTiO_3$ ceramics system by using tape casting method
***Dajeong KIM**[1], Myanghwan LEE[1], Jinsu PARK[1], Myong-Ho KIM[1], Taekwon SONG[1*]*
Dalhyun DO[2], Ho-Yong LEE[3]
([1]Changwon Nat'l Univ., Korea, [2]Keimyung Univ., Korea, [3]Ceracomp Co., Ltd., Korea)

SY-II	Synthesis, Raw Materials & Advanced powder processing	Rm. 603 (6F)

Chair(K): Dong Sik Bae (Changwon National University)
Chair(J): Kenji Toda (Niigata University)

SY-I03 16:35~17:00
Novel Oxide Phosphor Materials Synthesized by Melt Synthesis Method
***Sun Woog KIM**, Takuya HASEGAWA, Yukari KAWANO, Hiroko NAKAGAWA, Tadashi ISHIGAKI, Kenji TODA, Kazuyoshi UEMATSU, Mineo SATO*
([1]Niigata University, Japan)

SY-O04 17:00~17:15
Synthesis and tribological characteristics of silicon carbide-derived carbon layer synthesized from different α- and β-SiC polytypes
Yoon-Soo CHUN, *Min-Gun JEONG, Dae-Soon LIM*
(Korea University, Korea)

TF-I | Thin Films & Layers | Rm. 604 (6F)

Chair(K): Jaeyeong Heo (Chonnam National University)
Chair(J): Hiromitsu Kozuka (Kansai University)

TF-I01 16:30~16:55
Domain Structure Change with Temperature in (100)/(001)- oriented Epitaxial $PbTiO_3$ Films Grown on $KTaO_3$ Films
Hiroshi FUNAKUBO[1], *Takaaki NAKASHIMA*[1], *Daichi ICHINOSE*[1], *Yoshitaka EHARA*[1], *Takao SHIMIZU*[1], *Takeshi KOBAYASHI*[2], *and Tomoaki YAMADA*[3, 4]
([1]Tokyo Institute of Technology, Japan, [2]National Institute of Advanced Industrial Science and Technology (AIST), Japan, [3]Nagoya University, Japan, [4]Japan Science and Technology Agency, Japan)

TF-I02 16:55~17:20
Stress Evolution in Sol-Gel-Derived Thin Films
Hiromitsu KOZUKA
(Kansai University, Japan)

TF-I03 17:20~17:45
Atomic Layer Deposition of Multicomponent Oxides for Photovoltaic Applications
Jaeyeong HEO
(Chonnam National University, Korea)

TF-O01 17:45~17:57
Perovskite manganite based hetero-junction structure for cross-point arrays of ReRAM
Hong-Sub LEE, *Yoon Kwang LEE, Hyung-Ho PARK*
(Yonsei University, Korea)

AD-II | Advanced Coating for Gas Turbines | Rm. 605 (6F)

Chair(K): Kee Sung Lee (Kookmin University)
Chair(J): Byung-Koog Jang (National Institute for Materials Science)

AD-I04 16:30~16:55
Microstructure Design and Thermal Durability of Thermal Barrier Coatings with Layered Structure
Yeon-Gil JUNG

(Changwon National University,Korea)

AD-I05 16:55~17:20

Development of Oxides Eutectic EBC for Silicon Nitride Ceramics

Shunkichi UENO
(Nihon University, Japan)

AD-O01 17:20~17:35

Change in Characteristics of $(La_{1-x}Gd_x)_2Zr_2O_7$ TBCs Fabricated by Suspension Plasma Spray after Heat Treatment

Byung-Koog JANG*, Seongwon KIM[2], Yoon-Suk OH[2], Hyung-Tae KIM[2]*
([1] National Institute for Materials Science, Japan, [2] Korea Institute of Ceramic Engineering and Technology, Korea)

AD-I06 17:35~18:00

Growth behavior of YSZ thermal barrier coatings based on the substrate condition and heat treatment by electron beam evaporation method

Chanyoung Park[1,3], Yoonsoo Han[1], Seongwon Kim[1], Sungmin Lee[1], Hyungtae Kim[1], Byungkoog Jang[2], Daesoon Lim[3], and ***Yoonsuk Oh[1]***
([1]Korea Institute of Ceramic Engineering and Technology(KICET), Korea, [2]National Institute for Materials Science(NIMS), Japan , [3]Korea University, Korea)

EL-I Electronic Ceramics Rm. 606 (6F)

Chair(K): Chae Il Cheon (Hoseo University)
Chair(J): Hitoshi Ohsato (Nagoya Industrial Science Research)

EL-I01 16:30~16:55

Effect of Processing Method on Low-temperature Crystallization of Ionconductive Cubic $Li_7La_3Zr_2O_{12}$ Nanoparticles

Hisao SUZUKI[1]*, Mamoru SENNA[1, 2], Naonori SAKAMOTO[1], Naoki WAKIYA[1],*
([1]Shizuoka University, Japan, [2]Keio University, Japan)

EL-I02 16:55~17:20

Dielectric Relaxation in $BiFeO_3$-based Ceramics

Chae Il CHEON[1]*, Jin Hong CHOI[1], Jeong Seog KIM[1], Wook JO[2]*
([1]Hoseo University, Korea, [2]Ulsan National Institute of Science and Technology(UNIST), Korea)

EL-I03 17:20~17:45

Investigation of the interaction between the dispersant molecule and the surface of $BaCO_3$ particle

Koichiro TSUZUKU*, Takeshi YAMANOBE*
(Gunma University, Japan)

EL-O01 17:45~17:57

Fabrication and Characterization of Wrinkle-Free Monolayer

Graphene using the Ti/Glass Substrates
Byeong-Ju PARK *and Soon-Gil YOON*
(Chungnam National University, Korea)

EL-O02 17:57~18:09
Indialite Glass Ceramic Substrates for Millimeterwave Applications
Hitoshi OHSATO[1,2], *Akinori KAN[3], Jeong-Seog KIM[4], Isao. KAGOMIYA[5]*
([1]Nagoya Industrial Science Research Institute, Japan, [2]Nagoya Institute of Technology, Japan, [3]Meijo University, Japan , [4]Hoseo University, Korea, [5]Nagoya Institute of Technology, Japan)

EL-O03 18:09~18:21
Effects of Mg and/or Ti-site substitution on Microwave Dielectric Properties of $MgTiO_3$-based Ceramics
Hyun Jin JO, *Eung Soo KIM*
(Kyonggi University, Korea)

Banquet (18:00~20:00) – Convention Hall 2 (3F)

- Oral Sessions -

November 28 (Fri), 2014

Plenary Lecture 2~3 — Convention Hall 3 (3F)

Chair : Jaeho Jeon (KIMS)

PL-02 09:00~09:45

Niobate-based lead-free piezoelectric ceramics: from fundamental towards application

Jing-Feng LI, *Ke WANG, Fang-Zhou YAO, Li-Qian CHENG and Fang-Yuan ZHU*
(School of Materials Science and Engineering, Tsinghua University, China)

Chair : Won Jeong Kim (Changwon National University)

PL-03 09:45~10:30

Hot Spot Phenomenon of Ceramics and its Application

Masasuke TAKATA
(Japan Fine Ceramics Center (JFCC))

Coffee Break (10:30~10:45)

Oral Session 5 [10:45-12:30]

EL-II Electronic Ceramics — Rm. 601 (6F)

Chair(K): Jong-Sook Lee (Chonnam National University)
Chair(J): Nobuyasu Adachi (Nagoya Institute of Technology)

EL-I04 10:45~11:10

Preparation of Bismuth Gallium Iron Garnet on glass substrate by MOD Technique

Nobuyasu ADACHI, *Saeko FUJIUCHI, Yusaku KIBA, Toshitaka Ota*
(Nagoya Institute of Technology, Japan)

EL-I05 11:10~11:35

Thin film Electrodes for All-solid-state Microbatteries

Ji-Won CHOI[1,2] *and Haena YIM*[1]
([1]Korea Institute of Science and Technology(KIST), Korea, [2]University of Science and Technology, Korea)

EL-I06 11:35~12:00

Preparation of the Sol-gel derived Metal Oxide Electrode

Tomoya OHNO[1], *Takeshi MATSUDA*[1], *Naonori SAKAMOTO*[2], *Naoki WAKIYA*[2], *Hisao*

SUZUKI[2]
(Kitami Institute of Technology, Japan, [2]Shizuoka University, Japan)

EL-O04 12:00~12:12
Microstructure and Electrical Properties of $TiNbO_5$ and Ti_5NbO_{14} Thin Films grown by Electrophoretic Method
Mir IM, *Sang-Hyo KWEON, Sahn NAHM*
(Korea University, Korea)

EL-O05 12:12~12:24
Effect of oxide electrode and synthesis conditions on electrical properties of CSD-derived $Pb(Mg_{1/3}Nb_{2/3})O_3$-$PbTiO_3$ thin films
Takashi ARAI[1], *Tomoya OHNO[2], Takeshi MATSUDA[2], Naonori SAKAMOTO[1], Naoki WAKIYA[1], and Hisao SUZUKI[1]*
([1]Shizuoka University Japan, [2]Kitami Institute of Technology, Japan)

LP-II | Lead-free Piezoelectrics | Rm. 602 (6F)

Chair(K): Wook Jo (Ulsan National Institute of Science and Technology)
Chair(J): Wataru Sakamoto (Nagoya University)

LP-I05 10:45~11:10
Phase Transition and Effect of Poling Temperature on Piezoelectricity of $CaZrO_3$-Modified (K, Na)NbO_3-Based Lead-Free Ceramics
Ke WANG, *Fang-Zhou YAO and Jing-Feng LI*
(Tsinghua University, China)

LP-I06 11:10~11:35
Piezoelectric Properties Of $(Bi_{0.5}Na_{0.5})TiO_3$-$BaTiO_3$-Based Lead-Free Ceramics And Its Application To Ultrasonic Cleaner
Tonshaku TOU, *Yuki HAMAGUTI, Yuichi MAIDA*
(Electronics Co., Ltd., Japan)

LP-O03 11:35~11:47
Evaluation of single crystal growth behaviour of $(K_{0.5}Na_{0.5})NbO_3$-$SrTiO_3$ lead free piezoelectric ceramics grown by the solid state crystal growth (SSCG) method
Muhammad Umer FAROOQ *and John G. FISHER*
(Chonnam National University, Korea)

LP-O04 11:47~11:59
Piezoelectric properties of Lead-free $0.5Ba(Ti_{0.8}Zr_{0.2})O_3$-$0.5(Ba_{0.7}Ca_{0.3})TiO_3$ epitaxial thin films grown onto Si (001) substrate by Pulsed Laser Deposition for Energy Harvesting Applications
Jae-Ryong LIM, *TRAN Mhan Trung, and Soon-Gil YOON*
(Chungnam National University, Korea)

NA-I | Nano-particles & Nano-structured Materials | Rm. 603 (6F)

Chair(K): Chang-Yeoul Kim (KICET)
Chair(J): Yamamoto Hayashi (Tohoku University)

NA-I01 10:45~11:10

Synthesis and 3D Characterization of Barium-Ferrite Hybrid System with Highly Regulated Structures

Tadachika NAKAYAMA[1], *Hong-Baek CHO*[1], *Masanao KANNO*[1], *Shaifulazuar Bin ROZALI*[2], *Tadafumi ADSCHIRI*[3], *Hisayuki SUEMATSU*[1], *Tsuneo SUZUKI*[1], *Koichi NIIHARA*[1]
([1]Nagaoka University of Technology, Japan, [2]University Malaya, Malaysia, [3]Tohoku University, Japan)

NA-I02 11:10~11:35

Fabrication of a Ni/MgO Nanocomposite Catalyst by Exolution

Yesol LIM, Jong Seol YOON, ***Haejin HWANG***
(Inha University, Korea)

NA-O01 11:35~11:47

The New Methodologies for the Synthesis of Nano Precipitated Calcium Carbonates

THENEPALLI Thriveni, ***CHILAKALA. Ramakrishna****, Ji-Whan AHN*
(Korea Institute of Geoscience and Mineral Resources(KIGAM), Korea)

NA-O02 11:47~11:59

Enzyme-mimetic Activity of Ce-doped Titanate Nanosheets

Kai KAMADA*, Hisanori KOBAYASHI, Taro UEDA, Takeo HYODO, Yasuhiro SHIMIZU
(Nagasaki University)

ST-III | Structual Ceramics & Refractory Materials | Rm. 604 (6F)

Chair(K): Sangwhan Park (KIST)
Chair(J): Satoshi Tanaka (Nagaoka University of Technology)

ST-O06 11:00~11:20

Transparent $MgAl_2O_4$ Spinel Fabricated by Sinter-HIP process

Ha-Neul KIM*, Jin-Myung KIM, Jae-Woong KO, Young-Jo PARK, and Hai-Doo KIM*
(Korea Institute of Materials Science(KIMS), Korea)

ST-O07 11:20~11:40

Common Ceramics for Refrigeration: Be Cool Be Environmental Friendly

M. S. ANWAR*, Bon Heun KOO*
(Changwon National University, Korea)

ST-O08 11:40~12:00

Ceramic membrane for water treatment using diatomite based natural materials

In-Hyuck SONG[1], *Jang-Hoon HA*[1], *Byungseo BAE*[1], *Young-Wook KIM*[2]

([1]Korea Institute of Materials Science(KIMS), Korea, [2]The University of Seoul, Korea)

ST-O09 12:00~12:20

Characteristics of Zirconate-based Oxides for Thermal Barrier Coatings (TBCs)

Seongwon KIM[1], *Chang-Sup KWON[1], Yoon-Suk OH[1], Sung-Min LEE[1], Hyung-Tae KIM[1], and Byung-Koog JANG[2]*
([1]Korea Institute of Ceramic Engineering and Technology(KICET), Korea, [2]National Institute of Materials Science(NIMS), Japan)

LD-III | LED and Display Materials | Rm. 605 (6F)

Chair(K): Hyun-Suk Kim (Chungnam National University)
Chair(J): Hiroshi Fujioka (the University of Tokyo)

LD-I06 10:45~11:10

Zinc-Tin Oxide Thin Film Transistors based on atmospheric processes

Hye Ji JEON, Jae Yoon BAE, and ***Jin-Seong PARK***
(Hanyang University, Korea)

LD-I07 11:10~11:35

Electrical stability of multilayer MoS_2 field effect transistor under negative bias stress at various temperatures

Suk YANG, Solah PARK, Sukjin JANG, Hojoong KIM, and ***Jang-Yeon KWON***
(Yonsei University, Korea)

LD-O05 11:35~11:47

Electrical characteristics of low damage sputtered ITO Ohmic contact to p-GaN

Yu-Jung CHA, *Yu Lim LEE, Tae Kyoung KIM, Seung Kyu OH and Joon Seop KWAK*
(Sunchon National University, Korea)

CE-I | Ceramics Culture and Education | Rm. 606 (6F)

Chair(K): Kyusung Han (KICET)
Chair(J): Natsuki Hosoya (Yamaguchi Prefectural Industrial Technology Institute)

CE-I01 10:45~11:10

Technological Innovation in Ceramics:History of Pottery to Ceramic Industries

Junichi HOJO
(Kyushu University, Japan)

CE-I02 11:10~11:35

Applying the Social Network Service in Ceramic Culture and Education

Jongup CHUN
(Induk University, Korea)

CE-I03 11:35~12:00

Johjima roof tile's past, present and future
Naotaka SAKAMOTO
(Fukuoka Industrial Technology Center, Japan)

Lunch Break & Poster Session II(12:10~13:30) – Convention Hall Lobby(3F)

Oral Session 6 [13:30-14:57]

EL-III | Electronic Ceramics | Rm. 601 (6F)

Chair(K): Eung Soo Kim (Kyonggi University)
Chair(J): Hisao Suzuki (Shizuoka University)

EL-I07 13:30~13:55
AC characterization of electroceramics: Issues and way out
Jong-Sook LEE
(Chonnam National University, Korea)

EL-I08 13:55~14:20
Thermally Stimulated Depolarization Current Analysis for the Dielectric Phenomena of $BaTiO_3$-based Multi Layer Ceramic Capacitor
***Seok-Hyun YOON**, Jae-Sung PARK, Chang-Hoon KIM, and Doo-Young KIM*
(Samsung Electro-Mechanics Co. Ltd., Korea)

EL-O06 14:20~14:32
Dielectric Properties and Microstructure Control of $(Ba_{0.7}Sr_{0.25}Ca_{0.05})(Ti_{0.9}Zr_{0.1})O_3$ Ceramics
***Young Jun EOH** and Eung Soo KIM*
(Kyonggi University, Korea)

EL-O07 14:32~14:44
Microstructure and Microwave Dielectric Properties of $Zn_{1.8}SiO_{3.8}$ Ceramics Prepared by Two-Step Sintering
***Hong Jun AHN**, Young Jun EOH, Eung Soo KIM*
(Kyonggi University, Korea)

LP-III | Lead-free Piezoelectrics | Rm. 602 (6F)

Chair(K): Soon-Jong Jeong (KERI)
Chair(J): Hiroyuki Shimizu (Taiyo Yuden Co., Ltd.)

LP-I07 13:30~13:55
Piezoelectric Enhancement of Lead-free Piezoelectrics with Nano/macro Complex-domain Configurations for Piezo-frontier

***Satoshi WADA*[1]**, *Ryo IIZUKA[1], Shintaro UENO[1], Kouichi NAKASHIMA[1], Chikako MORIYOSHI[2], Yoshihiro KUROIWA[2]*
([1]University of Yamanashi, Japan, [2]Hiroshima University, Japan)

LP-I08 13:55~14:20

Enhanced Strain Properties of Relaxor Matrix Ferroelectric Composites in Bi-Based Lead-Free Piezoelectric Ceramics

***Jae-Shin LEE*[1]**, *Chang-Won AHN[1], Soon-Jong JEONG[2], Jing-Feng LI[3], and Wook JO[4]*
([1]University of Ulsan, Korea, [2]Korea Electrotechnology Research Institute(KERI), Korea, [3]Tsinghua University, China, [4]Ulsan National Institute of Science and Technology(UNIST), Korea)

LP-I09 14:20~14:45

Giant Electrostrain in Textured $Bi_{0.5}(Na,K)_{0.5}TiO_3$–based Ceramics

***Chang Won AHN*[1]**, *Si-Young CHOI[2], Gang Ho CHOI[1], Aman ULLAH,[1] Dae-Soo LEE[3], Soon-Jong JEONG[3], Ki Bong JANG[4], Jae-Shin LEE[5], and Ill Won KIM[1]*
([1]University of Ulsan, Korea, [2]Korea Institute of Materials Science(KIMS), Korea, [3]Korea Electrotechnology Research Institute(KERI), Korea, [4]Samjeon Co. Ltd., Korea, [5]University of Ulsan, Korea)

LP-O05 14:45~14:57

Performance Stabilized Lead-free Piezoelectric Ceramics: (Li, Na, K)(Nb, Ta)O_3 Modified by $BaZrO_3$

***Fangyuan ZHU**, Ke Wang and Jing-Feng LI*
(Tsinghua University, China)

NA-II | Nano-particles & Nano-structured Materials | Rm. 603 (6F)

Chair(K): Hae Jin Hwang (Inha University)
Chair(J):Hong-Baek Cho (Nagasaki University of Technology)

NA-I03 13:30~13:55

Synthesis of Magnetite Nanoparticles and Their Surface Modification For Hyper-thermia Application

Chang-Yeoul KIM
(Korea Institute of Ceramic Engineering &Technology(KICET), Korea)

NA-I04 13:55~14:20

Eco-fabrication of Metal nanoparticle related Materials by Ultrasonic and Microwave Reactors

Yamato HAYASHI
(Tohoku University, Japan)

NA-O03 14:20~14:32

Solid state dye sensitized solar cell using TiO_2 blocking layer deposited by atomic layer deposition

***Yun-Jeong KIM**, Tung-Duong THANH, Soon-Gil YOON*

(Chungnam National University, Korea)

NA-O04 14:32~14:44

Three-Dimensional Structural control of insulating BN assembles in Polymer-nanocomposites

Hong-Baek CHO, *Tadachika NAKAYAMA, Hisayuki SUEMATSU, Tsuneo SUZUKI, Weihua JIANG and Koichi NIIHARA*
(Nagaoka University of Technology, Japan)

ST-IV | Structual Ceramics & Refractory Materials | Rm. 604 (6F)

Chair(K): Young-Wook Kim (The University of Seoul)
Chair(J): Kouichi Yasuda (Tokyo Institute of Technology)

ST-I03 13:30~14:00

High Temperature Oxidation Kinetics of Ultra-High Temperature Ceramics

Young-Hoon SEONG[1, 2], Changyeon BAEK[1], and ***Do Kyung KIM***[1]
([1]Korea Advanced Institute of Science and Technology (KAIST), Korea, [2]Korea Institute of Energy Research(KIER), Korea)

ST-O10 14:00~14:20

Sintering of transparent polycrystalline Y_2O_3 by using graphite vacuum furnace

Young-Jo PARK, *Lin GAN, Mi-Jeung PARK, Jin-Myung KIM, Haneul KIM, Jae-Woong KO, Hai-Doo KIM*
(Korea Institute of Materials Science(KIMS), Korea)

ST-O11 14:20~14:40

Measurement of Local Fracture Toughness of Soda-lime Glass and Si_3N_4 Ceramics Using Microcantilever Beam Specimens

Junichi TATAMI[1], *Masaki KATAYAMA[1], Motoyuki IIJIMA[1], Tsukaho YAHAGI[2] and Takuma TAKAHASHI[2]*
([1] Yokohama National University, Japan , [2]Kanagawa Academy of Science and Technology, Japan)

LD-IV | LED and Display Materials | Rm. 605 (6F)

Chair(K): Joon Seop Kwak (Sunchon National University)
Chair(J): Yasushi Nanishi (Ritsumeikan University)

LD-I08 13:30~13:55

Transparent Display using Quantum Dot LED & Solution-based Oxide TFT

Min Suk OH
(Korea Electronics Technology Institute(KETI), Korea)

LD-I09 13:55~14:20

Feasibility of Large Area Devices Based on Group III Nitrides
***H. FUJIOKA*[1,2]**, *K. UENO[1], A. KOBAYASHI[1], and J.OHTA[1]*
([1]University of Tokyo, Japan, [2]JST-CREST,, Japan)

LD-I10 14:20~14:45
Carrier transport phenomena in sputtered ITO ohmic contacts to p-GaN
Joon Seop KWAK
(Sunchon National University, Korea)

LD-O06 14:45~14:57
Optical properties of modified light-emitting diodes structures using localized surface plasmons
***Jin-Hyeon YUN**, Han-Su CHO, Kang-Bin BAE, Myeong-Ji DONG, In-Hwan LEE*
(Chonbuk National University, Korea)

CE-II	Ceramics Culture and Education	Rm. 606 (6F)

Chair(K): Ung-Soo Kim (KICET)
Chair(J): Naotaka Sakamoto (Fukuoka Industrial Technology Center)

CE-I04 13:30~13:55
Effect of *Onggi* on Fermentation Characteristics of Korean Traditional Soy Sauce, *Ganjang*
Misook KIM
(Dankook University, Korea)

CE-I05 13:55~14:20
Construction of Ceramic Color Database and its recent improvement
***Toyohiko SUGIYAMA**, Masayoshi OHASHI, Keiji KUSUMOTO*
(National Institute of Advanced Industrial Science and Technology, Japan)

CE-I06 14:20~14:45
Quantitative Phase Analysis of Porcelain Raw Materials Using X-ray Diffraction Method
***Seung-Joo KIM*[1]**, *Jaegyeom KIM[1], Jong-Young KIM[2]*
([1]Ajou University, Korea, [2]Korea Institute of Ceramic Engineering and Technology(KICET), Korea)

Break Time (14:45~15:00)

Oral Session 7 [15:00-16:30]

FU-II	Fuel cells and Batteries	Rm. 601 (6F)

Chair(K): Jong-Jin Choi (KIMS)
Chair(J): Nobuhito Imanaka (Osaka University)

FU-I04 15:00~15:25
All-solid-state lithium ion battery by utilizing oxide-based solid electrolyte
Byoungwoo KANG
(Pohang University of Science and Technology(POSTECH), Korea)

FU-I05 15:25~15:50
Preparation and Characterization of Fast Ion Conducting Solid State Electrolytes for the Solid State Li-ion Battery
Inseok SEO[1], *Steve W. MARTIN[2]*
([1]POSCO Global R&D Center, Korea, [2]Iowa State University, USA)

FU-O01 15:50~16:02
Decomposition of Carbon Monoxide and Carbon Dioxide Using Cathode-Supported Dense Yttria-Stabilized Zirconia Electrolyte Cell
Taro SHIMONOSONO, *Mana UENO, Yoshihiro HIRATA, Soichiro SAMESHIMA*
(Kagoshima University, Japan)

LP-IV | Lead-free Piezoelectrics | Rm. 602 (6F)

Chair(K): Ke Wang (Tsinghua University)
Chair(J): Rintaro Aoyagi (Nagoya Institute of Technology)

LP-I10 15:00~15:25
Electric Field Induced Antiferroelectric - Ferroelectric Phase Transition on $NaNbO_3$-Based Lead-Free Ceramics
Hiroyuki SHIMIZU[1,2], *Youichi MIZUNO[1], Clive RANDALL[2]*
([1]Taiyo Yuden Co. Ltd.,Japan, [2]The Pennsylvania State University, USA)

LP-I11 15:25~15:50
Electromechanical Properties of $0.94Bi_{0.5}(Na_{0.75}K_{0.25})_{0.5}TiO_3$-$0.06BiAlO_3$ / $Bi_{0.5}(Na_{0.8}K_{0.2})_{0.5}TiO_3$ ceramic composite
Soon-Jong JEONG, *Min-Soo KIM, Seok-Myung JANG*
(Korea Electrotechnology Research Institute, Koreea)

LP-I12 15:50~16:15
Giant Electric-Field-Induced Strain and Coupling Mechanisms of Relaxor-Ferroelectric Lead-Free Ceramic Composites
Haibo ZHANG[1], *Qi ZHANG[2], Wook JO[3] Shenglin JIANG[1]*
([1]Huazhong University of Science and Technology, China, [2]The University of New South Wales, Australia, [3]Ulsan National Institute of Science and Technology(UNIST), Korea)

NA-III | Nano-particles & Nano-structured Materials | Rm. 603 (6F)

Chair(K) : Bum Sung Kim (KITECH)
Chair(J): Yamamoto Hayashi (Tohoku University)

NA-I05
Withdrawal

NA-I06 15:00~15:25
The increased optical transmission of the glass substrate coated with SnO_2 nanorod film using nano-aerosol spray pyrolysis deposition
Jeong-Wook LEE[1], Sung-Hwan PARK[2], and ***Doh-Hyung RIU[1,2]***
([1]Seoul National University of Science and Technology, Korea, [2]SolarCeramic Co., Korea)

NA-O05 15:25~15:37
Synthesis and characterization of novel semiconducting Si-based nanocomposites with slit-like nanopores
Hiroshi ITAHARA*, Song-Yul OH, Haruo IMAGAWA*
(Toyota Central Research & Development Labs., Inc., Japan)

ST-V | Structual Ceramics & Refractory Materials | Rm. 604 (6F)

Chair(K): Do-kyung Kim (KAIST)
Chair(J): Masaki Narisawa (Osaka Prefecture University)

ST-I04 15:00~15:30
Evaluation of internal defects and their coarsening during sintering in alumina ceramics system
Satoshi TANAKA[1] *, Tsuyohi HONDO[1] , Kouichi YASUDA[2]*
([1]Nagaoka Univeristy of Technology, Japan, [2]Tokyo Institute of Technology, Japan)

ST-O12 15:30~15:50
Synthesis of Meso-Macro Porous β-SiC by a Direct Reaction between Metallic Si and Carbon
Sang Whan PARK*, Mi-Rae YOUM, Sung-Il YUN*
(Korea Institute of Science and Technology(KIST), Korea)

ST-O13 15:50~16:10
Effect of grain size on properties of porous alumina for support substrates of permselective ceramic membranes
Sawao HONDA[1]*, Gaetan GRABARSKI[2], Yusuke DAIKO[1], Shinobu HASHIMOTO[1], Benoit NAIT-ALI[2], David S. SMITH[2], Yuji IWAMOTO[1]*
([1]Nagoya Institute of Technology, Japan, [2]Center Europeen de la Ceramique, France)

ST-O14 16:10~16:30
Erosion Resistance and Degradation of Various SiC/SiC Composites
Min-Soo SUH*, Se-Young KIM, In-Sub HAN, Sang-Kuk WOO*
(Korea Institute of Energy Research (KIER), Korea)

EF-I	Electric Field Assisted Sintering (PAS, SPS and Related Processing Techniques)	Rm. 605 (6F)

Chair(K): Young-Hwan Han (Yeungnam University)
Chair(J): Tetsuo Uchikoshi (National Institute for Materials Science)

EF-I01 15:00~15:25
Densification of Undoped Yttria by Means of Flash-sintering
Hidehiro YOSHIDA[1], *Yoshio SAKKA*[1], *Takahisa YAMAMOTO*[2], *Jean-Marie LEBRUN*[3], *Rishi RAJ*[3]
([1]*National Institute for Materials Science(NIMS), Japan,* [2]*Nagoya University, Japan,* [3]*University of Colorado at Boulder, USA)*

EF-I02 15:25~15:50
Influence of Carbon Nanotubes on Phase Transformation (*t - m*) of Spark Plasma Sintered ZrO_2
Young-Hwan HAN
(Yeungnam University, Korea)

EF-I03 15:50~16:15
Spark-Plasma-Sintering (SPS) of Transparent $MgAl_2O_4$ Spinel
Koji MORITA[1], *Byung-Nam KIM*[1], *Hidehiro YOSHIDA*[1], *Keijiro HIRAGA*[2], *Yoshio SAKKA*[1]
([1]*National Institute for Materials Science(NIMS), Japan,* [2]*Kitami Institute of Technology, Japan)*

CE-III	Ceramics Culture and Education	Rm. 606 (6F)

Chair(K): Woo-Seok Cho (KICET)
Chair(J): Toyohiko Sugiyama (National Institute of Advanced Industrial Science and Technology)

CE-I07 15:00~15:25
Role of Kogaratsu Research and Exchange Association on the Coming Progress of Karatsu Ware
Hiroaki KATSUKI[1] , *Masahito MINAMIMORI*[2], *Yasumoto KAJIHARA*[3]
([1]*Saga Ceramics Research Laboratory, Japan,* [2]*Ryujin Gama, Japan,* [3]*Ohtani Thobou Handou Gama, Japan)*

CE-O01 15:25~15:40
Synthesis and characterization of glazed ceramic ink for ink-jet printing
Kyu-Sung HAN, *Ji-Hyeon LEE, Jin-Ho KIM, Kwang-Taek HWANG, Woo-Seok CHO*
(Korea Institute of Ceramic Engineering and Technology, Korea)

CE-I08 15:40~16:05
Trend of Research and Development for Environmentally Benign Ceramic Technology in Gifu Tono Region

Tetsuya KAMEYAMA[1] *and Seizo OBATA*[2]
([1]National Institute of Advanced Industrial Science and Technology, Japan, [2]Gifu Prefectural Ceramics Research Institute, Japan)

CE-O02 16:05~16:20
Comparative Study on the Celadon Color Spectrum between Goryeo and China
Hyunggoo NO[1], *Ung Soo KIM*[2], *Woo Seok CHO*[3]
(Ceramicware Team, KICET, Korea)

CE-I09 16:20~16:45
Investigation for Materials of Old Porcelain Wares in Houhoku-town
Natsuki HOSOYA[1], *Akira MIKUNI*[1], *Yoshinori MIYATA*[2]
([1]Yamaguchi Prefectural Industrial Technology Institute, [2]IKKEI-gama, Japan)

CE-O03 16:45~17:00
The skill of Traditional Clay Pot Making in Kgatleng District
Tae-Chun KANG, *Sung-Jae CHOI*
(Korea National University of Cultural Heritage, Korea)

Coffee Break (16:15~16:30)

Oral Session 8 [16:30-18:22]

FU-III	Fuel cells and Batteries	Rm. 601 (6F)

Chair(K): Youngsik Kim (UNIST)
Chair(J): Nobuhito Imanaka (Osaka University)

FU-I06 16:30~16:55
Solid Oxide Fuel Cells based on the Low Temperature Ceramic Coating Process
Jong-Jin CHOI, *Dong-Soo PARK*
(Korea Institute of Materials Science(KIMS), Korea)

FU-O02 16:55~17:07
Preparation and electrochemical properties of $Li_{1.3}Ti_{1.7}Al_{0.3}(PO_4)_3$ solid electrolyte for Li ion batteries by sol-gel process
Seoung Soo LEE[1], *Hyun Woo KIM*[2], *Jing LI*[1], *Yeon-Gil JUNG*[1*], *Youngsik KIM*[2]
([1]Changwon National University, Korea, [2]Ulsan National Institute of Science and Technology(UNIST), Korea)

LP-V	Lead-free Piezoelectrics	Rm. 602 (6F)

Chair(K): Chang Won Ahn (University of Ulsan)
Chair(J): Tonshaku Tou (Honda Electronics Co., Ltd.)

LP-I13 16:30~16:55

Processing and Characterization of Reduction-Resistant Lead-Free Piezoelectric (Ba,Ca)TiO_3 Ceramics and Their Grain Growth Control
Wataru SAKAMOTO[1], *Hiroki ICHIKAWA*[1], *Yoshikazu AKIYAMA*[2], *Toshinobu YOGO*[1]
([1]Nagoya University, Japan, [2]Ricoh Co., Ltd., Japan)

LP-I14 16:55~17:20
Regarding electric-field-induced transition between ferroelectric and relaxor
Wook JO
(Ulsan National Institute of Science and Technology(UNIST), Korea)

LP-O06 17:20~17:32
Enhanced Low-Field Strain in Lead-Free Ferroelectric-Relaxor Composite Ceramics
Thi Hinh DINH[1], *Chang-Ho YOON*[1], *Jin-Kyu KANG*[1], *Young-Hwan HONG*[1],*Mohammad Reza BAFANDEH*[2], *and Jae-Shin LEE*[1]*
([1]University of Ulsan, Korea, [2]University of Kashan, Iran)

LP-O07 17:32~17:44
Ferroelectric and Piezoelectric response of lead-free $Bi_{0.5}Na_{0.5}TiO_3$-BaTiO-$BaZrO_3$ ceramics
Jamil Ur RAHMAN, *Ali HUSSAIN, Adnan MAQBOOL, Rizwan Ahmed MALIK, Tae Kwon SONG, Won Jong KIM and Myong Ho KIM*
(Changwon National University, Korea)

LP-I15 17:44~18:05
Fabrication of Textured $Na_{0.5}Bi_{0.5}TiO_3$–$BaZrO_3$ Ceramics by Tape Casting Technique
Ali HUSSAIN, *Rizwan-Ahmed MALIK, Jin-Soo KIM, Myong-Ho KIM, Tae-Kwon SONG and Won-Jeong KIM*
(Changwon National University, Korea)

TF-II | Thin Films & Layers | Rm. 603 (6F)

Chair(K): Soon-Gil Yoon (Chungnam National University)
Chair(J): Hiroshi Funakubo (Tokyo Institute of Technology)

TF-I04 16:30~16:55
Enhanced transparency, mechanical durability, and antibacterial activity of zinc nanoparticles on glass substrate
Hyung-Jin CHOI and ***Soon-Gil YOON***
(Chungnam National University, Korea)

TF-O02 16:55~17:07
TiO_2 blocking layer grown by nanocluster deposition for improved perovskite solar cell performance
Thanh Tung DUONG *and Soon-Gil YOON*

(Chungnam National University, Korea)

TF-O03 17:07~17:19

Fabrication and field emission properties of nanostructuralized diamond films

Chunyuan LU[1], *Qi DONG*[1], *Kelimu TULUGAN*[2], *Yeong Min PARK*[1], *Dae Woo KIM*[1], *Jeong Wan KIM*[1], *Tae Gyu KIM*[1]
([1]Pusan National University, Korea, [2]Gyeongsang National University, Korea)

TF-O04 17:19~17:31

Effect of Surface Modification of Boron-doped Diamond Electrode on Electro-chemical Degradation of Organic Dyes in Wastewater

Choong-hyun LEE, *Ji-yoon BAK, Dae-soon LIM*
(Korea University, Korea)

TF-O05 17:31~17:43

Epitaxial growth and the electric/magnetic properties of magneto-electric Cr_2O_3 thin film

Takeshi YOKOTA, *Izuna TSUBOI, Manabu GOMI*
(Nagoya Institute of Technology, Japan)

CO-I | Computational Ceramic Science and Engineering | Rm. 604 (6F)

Chair(K): Seungwu Han (Seoul National University)
Chair(J): Nakeshi Nishimatsu (Tohoku University)

CO-I01 16:30~16:55

Multi-scale computational design of active components for Li-ion batteries

Joonhee KANG[1], *Hyejin LEE*[1], *Byoungwoo KANG*[2], *Habin CHUNG*[2], ***Byungchan HAN***[1]
([1]Daegu Gyeongbuk Institute of Science & Technology(DGIST), Korea, [2]Pohang University of Science and Technology(POSTECH), Korea)

CO-I02 16:55~17:20

First-Principles Study of Piezoelectricity in AlN-based Materials

Hiroyoshi MOMIDA[1], *Akihiko TESHIGAHARA*[2], *Tamio OGUCHI*[1]
([1]Osaka University, Japan, [2]DENSO CORPORATION, Japan)

CO-I03 17:20~17:45

Molecular dynamics simulations of caloric effects in ferroelectrics

Takeshi NISHIMATSU
(Tohoku University, Japan)

CO-I04 17:45~18:10

Strategy for high-throughput *ab initio* screening of functional ceramic materials

Kanghoon YIM[1], *Joohee LEE*[1], *Kyuhyun LEE*[1], *Yong YOUN*[1], *Ho-Hyun NAHM*[1,2], ***Seungwu HAN***[1]
([1]Seoul National University, Korea, [2]Institute for Basic Science (IBS), Korea)

CO-O01 18:10~18:22

Application of CFD Simulation in the SiC-CVD Process

Kyoon CHOI[1], *J.-W. SEO*[1,2], *Y.-S. Hahn*[1], *J.-H. Lee*[2]
([1]Korea Institute of Ceramic Engineering & Technology (KICET), Korea, [2]Korea University, Korea)

EF-II	Electric Field Assisted Sintering (PAS, SPS and Related Processing Techniques)	Rm. 605 (6F)

Chair(K): Young-Hwan Han (Yeungnam University)
Chair(J): Koji Morita (National Institute for Materials Science)

EF-I04 16:30~16:55

Low-Temperature Spark Plasma Sintering of Transparent Alumina and Unusual Grain Growth

Byung-Nam KIM
(National Institute for Materials Science(NIMS), Japan)

EF-I05 16:55~17:20

Spark plasma sintering temperature effects on the microstructure and magnetic properties of carbon nanotube/NiZn ferrite composites

Xiaobing ZHOU[1], *Young-Hwan HAN*[2], *Jaehyung LEE*[2], *Qing HUANG*[1]
([1]Ningbo Institute of Materials Technology and Engineering, China, [2]Yeungnam University, Korea)

EF-I06 17:20~17:45

Milliwave Sintering of Silicon Carbide with Carbon additives

Tetsuo UCHIKOSHI, *Tohru S. SUZUKI*[*], *Hidehiko TANAKA, Toshiyuki NISHIMURA, Yoshio SAKKA*
(National Institute for Materials Science, Japan)

Closing Remarks (18:00~18:10) – Rm. 602 (6F)

- Poster Sessions -

November 27 (Thu), 2014

[Time : 12:00 – 13:30 / Venue : Convention Hall Lobby]

SY-P Synthesis, Raw Materials & Advanced Powder Processing

SY-P01
The Pulsed laser assisted synthesis of Tm^{3+} doped $CaMoO_4$ colloidal nanocrystals and its upconversion luminescence
Jung-Il LEE, *Joon HWANG, Chang Woo HONG, Jeong Ho RYU*
(Korea National University of Transportation, Korea)

SY-P02
Continuous Production of Monodisperse Silica Particles Using Tubular Reactor
Young-Sang CHO
(Korea Polytechnic University, Korea)

SY-P03
Catalytic Liquid-phase Oxidation of Acetaldehyde over a Pt/CeO_2-ZrO_2-SnO_2/γ-Alumina Catalyst
Pil-Gyu CHOI, *Takanobu OHNO, Nashito FUKUHARA, Toshiyuki MASUI, Nobuhito IMANAKA*
(Osaka University, Japan)

SY-P04
Synthesis of Hydroxyapatite Using Room-temperature Reaction between Egg Shell and Phosphoric Acid
Tae Sung KANG, *Mircea Cristian PANTILIMON, Sang-Jin LEE*
(Mokpo National University, Korea)

SY-P05
Fabrication of WO_3 from UP-Cycled Ammonium ParaTungstate (APT)
Jun-Ki Chung, *Sung-Jin Kim, Jin-Ho On, Sang-Yeup Park*
(Gangneung-Wonju National University)

TE-P Thermoelectrics

TE-P01
Thermoelectric Properties of Ceramic Oxide $Sr_{1-x}La_xTiO_3$
Iqbal MAHMUD, *Man-Soon YOON, Il-Ho KIM, Dong-Seob KIM, Soo-Young SONG, Moon-Kwan CHOI, Soon-Chul UR**
(Korea National University of Transportation, Korea)

TE-P02
Characterization of stacking faults and thermoelectrical properties of $Mo_{1-x}Ta_xSe_2$
Jaegyeom KIM, *Jong-Hyeon PARK, Seung-Joo KIM*
(Ajou University, Korea)

TE-P03
Improvement of power-factor deviation in a spark-plasma-sintered polycrystalline for doped *n*-type $Bi_2Te_{2.7}Se_{0.3}$ thermoelectric materials
Soon-Mok CHOI[1], *Kyu Hyoung LEE*[2], *Young Soo LIM*[3], *Won-Seon SEO*[3], *Soonil LEE*[3]
([1]Koreatech Co., Korea, [2]Kangwon National University, Korea, [3]Korea Institute of Ceramic Engineering and Technology(KICET), Korea)

TE-P04
Thermoelectric Properties of Chalcogenide based Composite Thin Films
Ji-Eun HONG *and Soon-Gil YOON*
(Chungnam National University, Korea)

TE-P05
Thermoelectric Properties of ZnO based composite thin films
Jin-A KIM, *Soon-Gil YOON*
(Chungnam National University, Korea)

FU-P Fuel cells and Batteries

FU-P01
$Er_{0.4}Bi_{1.6}O_3$ Electrolyte for Intermediate-Temperature Solid Oxide Fuel Cell
Ji-Na JEUNG, *Soon-Gil YOON*
(Chungnam National University, Korea)

FU-P02
Fabrication and characterization of spherical $Li_3V_2(PO_4)_3$/C cathode material by hydrothermal method
Jung-In MOON[1], *Eun-Young KIM*[2], *Chang-Sam KIM*[2], *Jeong-Hwan SONG*[1,*]
([1]PaiChai University, Korea, [2]Korea Institute of Science and Technology(KIST), Korea)

FU-P03
Sintering Behavior and Electrical Properties of Gd-doped Ceria with the Addition of Li Salt
Jung-A LEE, *Joon-Hyung LEE, Young-Woo HEO and Jeong-Joo KIM*
(Kyungpook National University, Korea)

FU-P04
Degradation Study of Yttria Doped Barium Cerate (BCY) Electrolyte in Protonic Ceramic Fuel Cells under Various Test Conditions

Mi Young PARK, *Myung Geun JUNG, Young Jin KIM, Hyung-Tae LIM*
(Changwon National University, Korea)

FU-P05
Performance of sulfide based all-solid-state lithium secondary batteries with Li-Si alloy anode
Joo Sung JIN, *Hye Won PARK, Hyung-Tae LIM*
(Changwon National University, Korea)

FU-P06
Fabrication of reduced graphene oxide single layer coated TiO_2 nanorod/FTO electrode for solar hydrogen evolution
Hyun KIM, *Sang Won PARK, Gi Wook LEE, Bee Lyong YANG*
(Kumoh National Institute of Technology, Korea)

FU-P07
Effects of graphene single layer on TiO_2 nanorod/FTO electrode for solar hydrogen evolution
Hyun KIM, *Jin Seok CHOI, Sang Won PARK, Gi Wook LEE, Sung Jin AN, Bee Lyong YANG*
(Kumoh National Institute of Technology, Korea)

FU-P08
A Study of photo-corrosion free CuO photo-catalyst by passivation layers for solar hydrogen evolution
Hyun KIM, *Sang Won PARK, Gi Wook LEE, Bee Lyong YANG*
(Kumoh National Institute of Technology, Korea)

FU-P09
Preparation and Characterization of Fast Ion Conducting Solid State Electrolytes for the Solid State Li-ion Battery
Inseok SEO[1], *Steve W. MARTIN*[2]
([1]POSCO Global R&D Center, Korea, [2]Iowa State University, USA)

GL-P Glass & Opto-Electronic Materials

GL-P01
Synthesis and luminescence property of $Li_{1.11}Ta_{0.89}Ti_{0.11}O_3$: Eu^{3+}, Sm^{3+} red phosphor
Hiromi NAKANO[1], *Syohei FURUYA*[1], *Suzuya YAMADA*[2]
([1]Toyohashi University of Technology, Japan, [2]Denki Kagaku Kogyo K.K., Japan)

GL-P02
Synthesis and luminescence property of RE^{3+}doped $Li_{1.11}(Ta_{1-z}Nb_z)_{0.89}Ti_{0.11}O_3$ ($0 \le z \le 1.0$, *RE*: Sm, Dy, Tm or Er) phosphor
Syohei FURUYA[1], *Hiromi NAKANO*[1], *Hiroyuki HAYASHI*[2], *Suzuya YAMADA*[3]

([1]Toyohashi University of Technology, Japan, [2] KRI, Inc., Japan, [3] Denki Kagaku Kogyo K.K., Japan)

GL-P03

The contributions of flaw healing effect and ion-exchange to the strength improvement of glass-infiltrated alumina

Dong-Hwan KIM[1,3], *Jee-hun MAENG[1], Seong-Jai CHO[2], Sung-Churl CHOI[3], Hyeong-Jun KIM[1]*
([1]Korea Institute of Ceramic Engineering & Technology(KICET), Korea, [2]Korea Research Institute of Standards and Science(KRISS), Korea, [3]Hanyang University, Korea)

GL-P04

Micro-crack Healing on Glass Using Chemically Strengthening

Dong-Hwan KIM[1,2], *Jee-hun MAENG[1], Sung-Min LEE[1], Sung-Churl CHOI[2], Hyeong-Jun KIM[1]*
([1]Korea Institute of Ceramic Engineering & Technology(KICET), Korea, [2]Hanyang University, Korea)

GL-P05

Improved Thermal Stability of Phosphor in Glass Varying Glass to Phosphor Mixing Ratio

Hyun-A PARK[1], *Sang Heon LEE[1], Won Bin IM[2], and Woon Jin CHUNG[1]*
([1]Kongju National University, Korea, [2]Chonnam National University, Korea)

GL-P06

Oxyfluoride glass ceramic doped with Eu^{2+}/Eu^{3+} for 400nm UV-LED Color Conversion

Sang Hun LEE[1], *Suk-Rok BAE[1], Yong Gyu CHOI[2], Woon Jin CHUNG[1]*
([1]Kongju National University, Korea, [2]Korea Aerospace University, Korea)

GL-P07

Compositional Effects of Metal Oxides on Reaction Between Sealing Glass and Soda-Lime Glass Substrate

Aram SUNG[1], *Seunggon CHOI[1], Hyungsun KIM[1]*
(Inha University, Korea)

GL-P08

Thermal Expansion of Ternary Ge-Sb-Se Chalcogenide Glasses in Compositional Range for Molded Infrared Lens Applications

Jun Ho LEE[1], *Sang Yeol SHIN[1], Jeong Han YI[1], Woo Hyung LEE[1], Bong Je PARK[2], Yong Gyu CHOI[1]*
([1]Korea Aerospace University, Korea, [2]Electronics and Telecommunications Research Institute(ETRI), Korea)

GL-P10

Raman Spectroscopic Study of the Structure of ZnO-Bi_2O_3-B_2O_3 Glasses

Shun TSUJI[1], *Kohei FUKUMI[2], Naoyuki KITAMURA[2], Hiromitsu KOZUKA[1], Hiroaki*

UCHIYAMA[1]
([1]Kansai University, Japan, [2]National Institute of Advanced Industrial Science and Technology, Japan)

BI-P Biomaterials

BI-P01
Synthesis of Calcium Phosphate Minerals from Biowaste
***Sachin N, BRAMHE*[1]**, *Seon Ae HWANGBO[2], Min Cheol CHU[1,3]*
([1]Korea Research Institute of Standards and Science(KRISS), Korea, [2]Pukyong University, Korea, [3]University of Science and Technology(UST), Korea)

BI-P02
Fabrication and Characteristics of Nano-Structured Hydroxyapatite Coating by Aerosol Deposition Method
Dae-Geun KIM, *Myeong-No LEE, Hyeonu HONG, Sang-hun LEE and Jae-Hyuk PARK*
(IONES Co., Ltd., Korea)

BI-P03
Targeting of Specific Cell using Fluorescent Titanate Nanosheets
Motoko TOKUNAGA, *Kai KAMADA[*], Taro UEDA, Takeo HYODO, Yasuhiro SHIMIZU*
(Nagasaki University, Japan)

BI-P04
Synthesis of Bioglass Ceramic Using Commercial Water Glasses for Plasma Spray Coating on Dental Implants
Jaehui JEON, *Sukyoung KIM*
(Yeungnam University, Korea)

BI-P05
Ti Surface Modification by Hydrothermal Method Using Various Acids Solution
Asywendi RUKINI, *Indu BAJPAI, Sukyoung KIM*
(Yeungnam University, Korea)

PI-P Piezoelectric Device & Application

PI-P01
Fabrication of Piezoelectric Micromachined Ultrasonic Transducer (pMUT) Using Aerosol Deposition Method
***Joontaek JUNG*[1]**, *Ju-Eun KANG[2], Jungho RYU[2], Hyeryung HONG[3], Hongshoo CHOI[1]*
([1]Daegu Gyeongbuk Institute of Science and Technology(DGIST), Korea, [2]Korea Institute of Material Science(KIMS), Korea, [3]Johns Hopkins University, USA)

PI-P02

Driving Characteristics of a θ–Type Piezoelectric Generating Device for Energy Harvesting

Seongsu JEONG, *Taegone PARK*
(Changwon National University, Korea)

PI-P03

Driving Characteristics of Hexadecagon Shaped Ultrasonic Motor

SeongKyu CHEON[1], *SeongSu JEONG*[1], *ByungHa LEE*[1], *YongWoo HA*[1], *MinHo PARK*[2], *HoIk JUN*[3], *TaeGone PARK*[1*]
([1]Changwon National University, Korea, [2]Defense Agency for Technology and Quality, Korea)

PI-P04

High Energy Density Magneto-Mechano-Electric Harvester with Anisotropic Piezoelectric Single Crystal Fiber Composite and Ni Laminates

Ju-Eun KANG[1,2], *Yuan ZHOU*[3], *Dae-Yong JEONG*[*4], *Woon-Ha YOON*[1], *Dong-Soo PARK*[1], *Jong-Jin CHOI*[1], *Byung-Dong HAHN*[1], *Cheol-Woo AHN*[1], *Jong-Woo KIM*[1], *Yang-Do KIM*[2], *Shashank PRIYA*[3], *and Jungho RYU*[1]
([1]Korea Institute of Materials Science (KIMS), Korea, [2]Pusan National University, Korea, [3]Virginia Tech., USA, [4]Inha University, Korea)

PI-P05

Flexible Single Crystalline PMN-PT Thin Film Energy Harvester and Its Application for Self-powered Cardiac Pacemaker

Geon Tae HWANG
(Korea Advanced Institute of Science and Technology(KAIST), Korea)

PI-P06

Piezoelectric and Dielectric Properties of Non-stoichiometry $(Na_{0.53+x}K_{0.47+x})(Nb_{0.55}Ta_{0.45})O_3$ ceramics

S. Y. LIM, *J. S. KIM, T. K. SONG, W. J. KIM, M. H. KIM*
(Changwon National University, Korea)

PI-P07

Enhanced Field-induced Strain Response of Nb-doped $(Bi_{0.5}Na_{0.5})_{0.935}Ba_{0.065}TiO_3$–$SrZrO_3$ Lead-free Piezoceramics

Adnan MAQBOOL, *Ali HUSSAIN, Jamil Ur RAHMAN, Rizwan Ahmed MALIK, Tae Kwon SONG, Won-Jeong KIM and Myong-Ho KIM*
(Changwon National University, Korea)

LD-P LED and Display Materials

LD-P01

Influence of electron-beam irradiation on properties of ITO thin films

Seung-Hong KIM[1], *Jae-Hyun JEON*[1], *Tae-Kyung GONG*[1], *Sun-Kyung KIM*[1], *So-Young KIM*[1],

Dong-Hyuk CHOI[2], Dong-Il SON[2], Daeil KIM[1]
([1]University of Ulsan, Korea, [2]Dongkook Inc., Korea)

LD-P02
Enhanced electrical conductivity in hybrid Ag paste containing Ag nanoparticles
***Kyeong-Seob KWON**, Kyungwon LEE, In Hwan LEE*
(Chonbuk National University, Korea)

LD-P03
TEM and XRD analysis of Thin Film Phosphors on Sapphire
***Ki-Woong CHAE**, Ta-Ryeong PARK, Chae Il CHEON, Jeong Seog KIM*
(Hoseo University, Korea)

LD-P04
Effect of B-doping on Persistent Luminescence in (Sr,Ca)Al_2O_4: Eu^{2+},Dy^3
***Jeong Seog KIM**, Ta-Ryeong PARK, Chae Il CHEON , and Ki-Woong CHAE*
(Hoseo University, Korea)

AD-P Advanced Coating for Gas Turbines

AD-P01
Relation between Na_2SiF_6 Concentration and Mechanical Properties of AZ31 Magnesium Alloy coated by Electrolytic Plasma Processing
***Jeong Yeong SEUNG**, Keun Young PARK, Sung Jae KIM, Jung il SONG, Bon Heun KOO*
(Changwon National University, Korea)

AD-P02
Effect of Time on The Properties of oxide layers of Al7075 aluminum alloy Prepared by Electrolytic Plasma processing
***Keun Young PARK**, Dong Gun LEE, Jung Il SONG, Bon Heun KOO*
(Changwon National University, Korea)

AD-P03
Fabrication of EBC with Eutectic Structure for Silicon Carbide Substrate
*Kyosuke SEYA[1], Byung-Koog Jang[2], **Shunkichi UENO[1]***
([1]Nihon University, Japan, [2]National Institute for Materials Science(NIMS), Japan)

November 28 (Fri), 2014

[Time : 12:00 – 13:30 / Venue : Convention Hall Lobby]

TF-P Thin Films & Layers

TF-P01
Structural and Electrical Properties of Chemical Solution Deposited 0.7$BiFeO_3$-0.3$CaTiO_3$ Solid Solution Thin Film
Jinwon. KIM, *Hinnambedumurugesan RAGHAVAN, J. Y. CHOI, Sangsoo KIM*
(Changwon National University, Korea)

TF-P02
Effects of La Doping on the Structural and Electrical Properties of $Bi_7Fe_3Ti_3O_{21}$ Thin Film
C. M. RAGHAVAN, *J. W. KIM, J. Y. CHOI, S. S. KIM**
(Changwon National University, Korea)

TF-P03
Effects of Seed Layer on the Structural Properties of R.F. Sputtering ZnO Thin Films
Soon-Chul UR and ***Seung-Hwan YI***
(Korea National University of Transportation, Korea)

TF-P04
The influence of Ag interlayer on the electrical and optical properties of ZTO/Ag/ZTO multilayer films
Tae-Kyung GONG[1], *Seung-Hong KIM[1], Jae-Hyun JEON[1], Sun-Kyung KIM[1], SO-Young KIM[1], Dong-Huk CHOI[2], Dong-il SON[2], Daeil KIM[1]**
([1]University of Ulsan, Korea, [2]Dongkook Inc., Korea)

TF-P05
Effect of Ti buffer layer on the optical and electrical property of In_2O_3 thin films
Jae-Hyun JEON[1], *Seung-Hong KIM[1], Tae-Kyung GONG[1], Sun-Kyung KIM[1], So-Young KIM[1], Dong-Huk CHOI[2], Dong-il SON[2], Daeil KIM[1]*
([1]University of Ulsan, Korea, [2]Dongkook Inc., Korea)

TF-P06
Composition-dependent Functional Properties of High Quality PZT Films for Micro-scale Electronic Device Applications
J. S. KIM[1], *S. Y. LEE[1], H. S. SHIN[1], J. H. YEOM[1], S-H. KIM[2]*
([1]KCMC Co., Ltd., Korea, [2]Brown University, USA)

TF-P07

Effect of annealing condition on properties of $SnO_2/Zn/SnO_2$ multilayer thin films deposited by RF sputtering
Sung Jae KIM[1], *Keun Young PARK*[1], *Yeong Seung JEONG*[1], *Tae Kwon SONG*[1], *Hang Joo KO*[2], *Bon Heun KOO*[1]
([1]Changwon National University, Korea, [2]Korea Photonics Technology Institute(KOPTI), Korea)

TF-P08
Optimized Process Conditions of Pt Bottom Electrode for High Quality Piezoelectric Films and Multi-functional MEMS Devices
S. Y. LEE[1*], *J. S. KIM*[1], *H. S. SHIN*[1], *J. H. YEOM*[1], *S-H. KIM*[2]
([1]KCMC Co., Ltd., Korea, [2]Brown University, USA)

TF-P09
Electronic structure and magnetic properties of Mn doped TiO_2 thin films using X-ray absorption spectroscopy
Shalendra KUMAR[1], *Tae Kwon SONG*[1], *M.H. LEE*[1], *J.S. PARK*[1], *D. J. KIM*[1], *M. H. KIM*[1], *W. J. KIM*[1], *K.W. JANG*[1], *K.H. CHAE*[2]
([1]Changwon National University, Korea, [2]Korea Institute of Science and Technology(KIST), Korea)

TF-P10
Development of High Energy Density Capacitors Using Anti-ferroelectric PLZT Thin Films
Don Chan WOO, *Chang Young KOO, You Jeong EUM, Hee Young LEE*
(Yeungnam University, Korea)

TF-P11
Multilayer Coatings for Protecting Carbon Materials at temperatures at 1700°C or higher
Changhun HWANG, *Jondo YUN*
(Kyungnam University, Korea)

TF-P12
Thin film multi layer ceramic capacitors (MLCC) using high-dielectric $Bi_2Mg_{2/3}Nb_{4/3}O_7$ (BMNO)
Ji-hyun PARK[1], *Soon-Gil YOON*[1,2]
(Chungnam National University, Korea)

TF-P13
Simultaneous realization of electromagnetic shielding and antibacterial effect of Al doped ZnO multi-layer thin films
Hyung-Jin CHOI, *Soon-Gil YOON*
(Chungnam National University, Korea)

TF-P14
Sol-Gel Preparation of M^+-Doped CuO ($M^+ = Li^+, Na^+, K^+$) Thin Films and Their

Photocathodic Properties
Kota ISOBE, *Hiroaki UCHIYAMA, Hiromitsu KOZUKA*
(Kansai University, Japan)

TF-P15
Study on surface analysis by solution agitation of the electroless copper plating for flexible devices
Seung-deok BAEK, *Na-young KIM, Hyung-chul KIM, Sa-kyun RA, Yoen-seung LEE*
(Hanbat National University, Korea)

TF-P16
Effects of DMAB in Electrolss Ni-B Plating for F-PCB
Hyung-Chul KIM, *Sa-Kyun RHA, Na-Young KIM, Seong-Duk BAEK, Youn-Seoung LEE*
(Hanbat National University, Korea)

NA-P Nano-particles & Nano-structured Materials

NA-P01
Effect of intrinsic defects on the optical and magnetic properties of Co: ZnO nanoparticles based DMS.
Rezq Naji ALJAWFI
(Ibb University, Yemen)

NA-P02
Separation of H_2/CO_2 mixed gas through porous alumina compact
Kota GOTANDA, *Yoshihiro HIRATA, Soichiro SAMESHIMA, Taro SHIMONOSONO*
(Kagoshima University, Japan)

NA-P03
Effect of time on the growth of flowerlike rutile nanostructures and their application for degradation of organic dyes
Rehan DANISH, *M. S. ANWAR, Bon Heun KOO*
(Changwon National University, Korea)

NA-P04
Carbon Nanotubes Grown on Cobalt Supported Zeolite-Porous Ceramics
Jung Gyu PARK[1], *Wei ZHAO*[2], *Sangram MAZUMDER*[1], *Ik Jin KIM*[1]
([1]Hanseo University, Korea, [2]Yeungnam University, Korea)

NA-P05
Carbon Nanotubes Grown on Cobalt Supported Zeolite-Porous Ceramics
Jung Gyu PARK[1], *Wei ZHAO*[2], *Sangram MAZUMDER*[1], *and Ik Jin KIM*[1]
([1]Hanseo University, Korea, [2]Yeungnam University, Korea)

NA-P06

Visible-light-induced Enzymatic Reaction of Peroxidase Hybridized with Layered Iron-titanate
Daiki ITO, *Kai KAMADA, Taro UEDA, Takeo HYODO, Yasuhiro SHIMIZU*
(Nagasaki University, Japan)

NA-P07
Tube-on-plate structured $BiVO_4/Bi_2WO_6$ heterojunction with highly efficient photocatalytic activities
Wei ZHAO[1], *and Ik Jin KIM*[2], *Sukyoung KIM*[1]
([1] Yeungnam University, Korea, [2] Hanseo University, Korea)

NA-P08
Superhydrophobicity from Nano/Microstructure with Carbon Nanotubes on Silica spheres
Ahrong JEONG, *Sangbo HAN, Hongrim LEE, Jondo YUN*
(Kyungnam University, Korea)

NA-P09
***In Situ* Magnetic Field-Assisted Growth of High Quality GaN Nanowires**
Jun Sik KIM[1], *Bhaskar Chandra MOHANTY*[2], *Chan Su HAN*[1] *and* ***Yong Soo CHO***[1]
([1] Yonsei University, Korea, [2] Thapar University, India)

NA-P10
Flow Rate Effects of CdSe Quantum Dots Synthesized by Microreactor
Da-Woon Jeong[1,2], Song Yi Kim[1], Taek Soo Kim[1], Tae-Yeon Seong[2], **Bum Sung Kim**[1]
(Korea Institute of Industrial Technology, [2] Korea University

ST-P Structual Ceramics & Refractory Materials

ST-P01
Properties of SiC Precursors for the precursor impregnation and pyrolysis (PIP) process
Sea Hoon LEE, *Jie YIN*
(Korea Institute of Materials Science(KIMS), Korea)

ST-P02
Theoretical and Experimental Analyses of Thermal Conductivity of the Alumina-Mullite System
Shota ITOH, *Yoshihiro HIRATA, Taro SHIMONOSONO, Soichiro SAMESHIMA*
(Kagoshima University, Japan)

ST-P03
Effect of ZrO_2 on the mechanical properties of mullite composites
Shielah MAVENGERE *and Bum-Rae CHO*
(Keimyung University, Korea)

ST-P04

Effect of Cell Size on Thermal Conductivity of UO_2 Nuclear Fuel Pellet containing Mo Metallic Micro-cell
***Dong-Joo KIM*[1]**, *Young Woo RHEE[1], Jong Hun KIM[1], Keon Sik KIM[1], Jang Soo OH[1], Jae Ho YANG[1], Yang-Hyun KOO[1], Seung Jae LEE[2]*
([1]Korea Atomic Energy Research Institute(KAERI), Korea, [2]KEPCO Nuclear Fuel Co., Korea)

ST-P05
Thermodynamic Assessment of UO_2 Nuclear Fuel Pellet Oxidation in Air, Steam, and H_2 Mixture Atmosphere
***Dong-Joo KIM**, Jong Hun KIM, Keon Sik KIM, Jae Ho YANG, Sun Ki KIM, Yang Hyun KOO*
(Korea Atomic Energy Research Institute(KAERI), Korea)

ST-P06
TEM Analysis Study on the Microstructure of Oxides Formed on the Surface of FeCrAl Alloy at High Temperature
***Dong Jun PARK**, Hyun Gil KIM, Yang Il Jung, Jung Hwan PARK, Yang Hyun KOO*
(Korea Atomic Energy Research Institute(KAERI), Korea)

EL-P Electronic Ceramics

EL-P01
Effect of process parameters on electrical properties of CSD-derived $Ba(Zr,Ti)O_3$ thin films
***Yutaro ODA*[1]**, *Naonori SAKAMOTO[1], Naoki WAKIYA[1], Tomoya OHNO[2], Takeshi MATSUDA[2], Hisao SUZUKI[1]*
([1]Shizuoka University, Japan, [2]Kitami Institute of Technology, Japan)

EL-P02
Structure Analysis of $12CaO \cdot 7Al_2O_3$ Particles Synthesized by Solution Plasma Processing
***Shiori MANEYAMA*[1]**, *Naonori SAKAMOTO[1], Naoki WAKIYA[1], Tomoya OHNO[2], Takeshi MATSUDA[2], Hisao SUZUKI[1]*
([1]Shizuoka University, Japan, [2]Kitami Institute of Technology, Japan)

EL-P03
Phase transition temperature control of thermochromic vanadium dioxide nano-particles by microemulsion method with molecular-designed precursors
***Takuya OKUDA*[1]**, *Naonori SAKAMOTO[1], Naoki WAKIYA[1], Hidetoshi MIYAZAKI[2], Hisao SUZUKI[1]*
([1]Shizuoka University, Japan, [2]Shimane University, Japan)

EL-P04
Vertically aligned microstructures of PLZT ceramic films produced by Electro-static Spray Deposition (ESD)
***Dongsu SON**, Beak Hyun KIM, Hyun-Jeong BAE, Yumin GOH, Do-Kyun KWON*

(Korea Aerospace University, Korea)

EL-P05

Dielectric properties of PIN-PMN-PT Films Prepared by Aerosol-Deposition Method

Soo-Bin KANG[1], *Min-Geun CHOI[1], Young-Min KONG[2], Jungho RYU[3], Linghang WANG[4] and Dae-Yong JEONG[1]*
([1]Inha University, Korea, [2]University of Ulsan, Korea, [3]Korea Institute of Materials Science(KIMS), Korea, [4]Xi'an Jiaotong University, China)

EL-P06

Magnetocaloric Effect in The $SRFE_xCO_{1-x}O_{3-\delta}$ ($0.4 \leq x \leq 0.6$) Synthesized at Ambient Conditions

Zeeshan ur REHMAN, *Bon Heun KOO, M. S. ANWAR, Bon Heun KOO*
(Changwon National University, Korea)

EL-P07

Energy Storage Properties of Lead Lanthanum Zirconate Titanate Films by Aerosol Deposition Method

Min-Geun CHOI[1], *Soo-Bin KANG[1], Jungho RYU[2], and Dae-Yong JEONG[1]*
([1]Inha University, Korea, [2]Korea Institute of Materials Science(KIMS), Korea)

EL-P08

Characterization of LiF and CuO Codoped $BaTiO_3$ for Embedded Capacitor in LTCC Modules

Kyoungho LEE[1,3], Kwangwon CHOI[1,2]
([1]Soonchunhyang University, Korea, [2]RN2 Technologies, Korea)

EL-P09

Effects of Ca substitution on spontaneous superlattice formation of $SrTiO_3$ thin films prepared using dynamic aurora PLD

Tomoaki KUBOTA[1], *Naonori SAKAMOTO[1], Takanori KIGUCHI[2], Kazuo SHINOZAKI[3], Hisao SUZUKI[1], Naoki WAKIYA[1]*
([1]Shizuoka University, Japan, [2]Tohoku University, Japan, [3]Tokyo Institute of Technology, Japan)

EL-P10

Microwave Dielectric Properties of $(Zn_{1-x}Mg_x)_{1.918}GeO_{3.918}$ Ceramics

Young Jun EOH, *Eung Soo KIM*
(Kyonggi University, Korea)

EL-P11

CuO/V_2O_5 Doped BZN Ceramic for Embedded Capacitor Layer in Integrated LTCC Modules

Seungjin KANG, ***Kyoungho LEE***
(Soonchunhyang University, Korea)

LP-P Lead-free Piezoelectrics

LP-P01

Effect of Sintering Temperature on Piezoelectric and Ferroelectric Properties of $0.99(0.67BiFeO_3$-$0.33BaTiO_3)$-$0.01Bi(Ni_{0.5}Ti_{0.5})O_3$ Ceramics

I. J. HWANG[1], *D. DO*[1*], *M. H. LEE*[2], *J. S. PARK*[2], *D. J. KIM*[2], *T. K. SONG*[2], *M.-H. KIM*[2], *S. W. KIM*[2], *W.-J. KIM*[2]
([1]Keimyung University, Korea, [2]Changwon National University, Korea)

LP-P02

Characterization of Lead-Free $0.75(Bi_{0.5}Na_{0.5})TiO_3$-$0.25SrTiO_3$ Thin Films by Pulsed Laser Deposition for Energy Harvesting Applications

Ki-Su YANG, *Jae-Ryong LIM, Soon-Gil YOON*
(Chungnam National University, Korea)

LP-P03

Reactive Sintering of $(K_{0.5}Bi_{0.5})TiO_3$-$BiFeO_3$ lead-free piezoelectric ceramics.

John G. FISHER[1], *Min-Gu KIM*[1], *Daeung KIM*[1], *Su-Jeong CHA*[1], *Hung VU*[1], *Dieu NGUYEN*[1], *Jee-Hoon KIM*[1], *Su-Hyeon MOON*[1], *Jong-Sook LEE*[1], *Ali HUSSAIN*[2] *and Myong-Ho KIM*[2]
([1]Chonnam National University, Korea, [2]Changwon National University, Korea)

LP-P04

Comparative Study between Conventional and Microwave Sintering of Large Strain Bi-Based Perovskite Ceramics

Jin-Kyu KANG[1], *Thi-Hinh DINH*[1], *Young-Hwan HONG*[1], *Mohammad Reza BAFANDEH*[2], *Chang-Do PARK*[1], *and Jae-Shin LEE*[1*]
([1]University of Ulsan, Korea, [2]University of Kashan, Iran)

LP-P05

Improvement in Strain Properties of Bi-Based Ceramic Composites by High Energy Ball Milling

Young-Hwan HONG[1], *Dae-Jun HEO*[1], *Jin-Kyu KANG*[1], *Thi-Hinh DINH*[1] *Chang-Won AHN*[2], *Ill-Won KIM*[2], *Wook JO*[3], *and Jae-Shin LEE*[1]
([1]University of Ulsan, Korea, [2]University of Ulsan, Korea, [3]Ulsan National Institute of Sience and Technology(UNIST), Korea)

LP-P06

Ferroelectric and piezoelectric properties of $Bi(Zn_{2/3}Ta_{1/3})O_3$ modified $0.67BiFeO_3$-$0.33BaTiO_3$ ceramics

Jinsu PARK, *Myang Hwan LEE, Sang Wook KIM, Sung Jin HAN, Da Jeong KIM, Myong-Ho KIM, Won–Jeong KIM, Shalendra KUMAR, Tae Kwon SONG*
(Chanwon National University, Korea)

LP-P07

The structural and electrical properties of Cr doped $BiFeO_3$-$BaTiO_3$ lead free ce-

ramics
S. W. KIM[1], *M. H. LEE*[1], *J. S. PARK*[1], *S. J. HAN*[1], *D. DO*[2], *M. H. KIM*[1], *T. K. SONG*[1], *W. J. KIM*[1]
([1]Changwon National University, Korea, [2]Keimyung University, Korea)

LP-P08
Low-temperature sintering of the lead-free BNKT-BMT using sintering aids for piezoelectric acoustic actuators
Hee Sung KIM[1], *Won Seok WOO*[1], *Song A CHAE*[1], *Chang Won AHN*[1], *Ill Won KIM*[1*]
Ki Bong JANG[2], *Eung Joo HWANG*[2]
([1]University of Ulsan, Korea, [2]Samjeon Co. Ltd., Korea)

LP-P09
Piezoelectric, Dielectric and Ferroelectric response of Nb^{5+} modified of Lead-free $0.97(Bi_{0.5}Na_{0.5}Ti_{1-x}Nb_x)O_3$-$0.03BaZrO_3$ ceramics
Jamil Ur RAHMAN, *Ali HUSSAIN, Adnan MAQBOOL, Rizwan Ahmed MALIK, Tae Kwon SONG, Won Jeong KIM, Myong Ho KIM*
(Changwon National University, Korea)

LP-P10
Hardening Effects and Associated Lattice Defects in Lead-free $(Na_{0.53}K_{0.47})NbO_3$ Piezoelectric Ceramics
Gyung Hyun RYU, *Myang Hwan LEE, Tae Kwon SONG, Won-Jeong KIM, Myong Ho KIM*
(Changwon National University, Korea)

LP-P11
Effect of quenching temperature on the ferroelectric and piezoelectric properties of $BiFeO_3$-$BaTiO_3$ bulk ceramics
Myang Hwan LEE, ***Dajeong KIM***, *Jinsu PARK, Shalendra KUMAR, Tae Kwon SONG, Myong Ho KIM, Sang wook KIM, Won Jeong KIM, Sang Su KIM*
(Changwon National University, Korea)

LP-P12
Effect of Ta-substitution on the dielectric, ferroelectric and field-induce strain properties of Bi0.5 (Na0.82K0.18)0.5TiO3-SrTiO3 ceramics
Rizwan Ahmed MALIK, *Ali HUSSAIN, Jamil Ur RAHMAN, Adnan MAQBOOL, Tae Kwon SONG, Won-Jeong KIM, and Myong-Ho KIM*
(Changwon National University, Korea)

CO-P Computational Ceramic Science and Engineering

CO-P01
Physical Interpretations of Cap-Related Parameters of the Modified Drucker-Prager Cap Model in Relation to the Deviator Stress Curves of Particulate Materials

Hyunho SHIN[1], *Jong-Bong KIM*[2]
([1]Gangneung-Wonju National University, Korea, [2]Seoul National University of Science and Technology, Korea)

CO-P02
Molecular dynamics simulations of caloric effects in ferroelectrics
Takeshi NISHIMATSU
(Tohoku University, Japan)

CE-P Ceramics Culture and Education

CE-P01
Investigation for Materials of Old Porcelain Wares in Houhoku-town
Natsuki HOSOYA[1], *Akira MIKUNI*[1], *Yoshinori MIYATA*[2]
([1]Yamaguchi Prefectural Industrial Technology Institute, Japan, [2]IKKEI-gama, Japan)

ETC

Unique friendship history between Japan and Korea for 260 years of the Edo period, Grate scale missions exchanged sincerity from Korea Yi dynasty and technological exchange (No.4)
– Trace technological exchange on the Asian-Sea area, and put the Korean Mission with friendship on the Memory of the World! –
Ohsato HITOSHI
(Nagoya Industrial Science Research Institute)

Abstracts

Plenary Presentation ····· 71

Invited Presentation ····· 75

Oral Presentation ····· 176

Poster Presentation ····· 267

Plenary Presentation

PL-01

Silicon Carbide Power Semiconductor and Electronic Devices

Hyeong Joon Kim*
Department of Materials Science and Engineering, Seoul National University, Seoul,151-744, Korea

Keywords: Silicon carbide, Power semiconductor, Power devices

Nowadays there are strong needs for power electronic devices because of two reasons: one is a harsh environment which demands high-frequency and high-temperature electronic devices, the other is an energy saving which requests low-loss electronic devices. Si, the widely used semiconductor, can not satisfy the specifications of power electronic devices, which are capable of low energy consumption in harsh environment. The sole choice to solve such huddle is to adopt the wide band gap semiconductors. Therefore, the wide band gap semiconductors such as SiC, GaN, ZnO and diamond attract great attention as a candidate material for high-frequency, high-temperature and low-loss power devices. Among them SiC is the most promising one because its high voltage blocking capability, high speed switching, high energy efficiency and the availability of large-sized wafers.
The SiC-based power devices have great merits compared to the Si-based devices. The presentation includes the comparison of wide band gap semiconductors in the view-point of their applications for power electronic devices, the main issues in the bulk crystal growth, epitaxial growth of SiC semiconductor and fabrication of electronic devices, and the prospects of SiC power electronic devices.

PL-02

Niobate-based lead-free piezoelectric ceramics: from fundamental towards application

Jing-Feng Li*, Ke Wang, Fang-Zhou Yao, Li-Qian Cheng and Fang-Yuan Zhu
School of Materials Science and Engineering, Tsinghua University, Beijing, China

Keywords: Piezoelectric ceramics, Lead-free, Sodium potassium niobate

Piezoelectric materials have the functionality of producing an electrical potential in response to an applied force or generating mechanical movement when subjected to an electric field. Developing high-performance lead-free piezoelectric ceramics is one of the crucial topics for functional materials research. Sodium potassium niobate (KNN) based ceramics have received much attention as a promising candidate of lead-free piezoelectric materials because of its high piezoelectric properties achieved by chemical modifications. This talk will give a comprehensive review on the latest development of KNN-based piezoelectric ceramics, including the phase structure, property enhancement approaches and sintering processes as well as the status of certain promising applications. At first, we will reexamine the phase structure of KNN and discuss the piezoelectricity enhancement in relation with the effects of chemical modifications and sintering processing. In particular, some recent results based on nano-scale KNN single crystals will be introduced. Additionally, a special focus will be placed on the temperature dependence of piezoelectric properties of KNN-based ceramics, followed by reviewing the recent approaches devoted to the temperature-stability enhancement. We will show one approach by introducing $CaZrO_3$-modified KNN-based ceramics that possess high and temperature-insensitive piezoelectric strains, whose fatigue resistance is also very good. Finally, we will introduce several industrial attempts of traditional piezoceramic products using KNN-based ceramics and the update researches on some promising applications in our laboratory.

References:

[1] J.-F. Li, K. Wang, F.-Y. Zhu, L.-Q. Cheng and F.-Z. Yao, J. Am. Ceram. Soc., 96 (2013) 3677.
[2] K. Wang, F.-Z. Yao, W. Jo, D. Gobeljic, V. V. Shvartsman, D. C. Lupascu, J.-F. Li, J. Rodel, Adv. Funct. Mater., 23 (2013) 4079.
[3] L.-Q. Cheng, K. Wang, Q. Yu and J.-F. Li, J. Mater. Chem. C, 2 (2014) 1519.
[4]F.-Z. Yao, E. A. Patterson, K. Wang, W. Jo, J. Roedel, J.-F. Li, Appl. Phys. Lett., 104 (2014) 242912.
[5] F.-Z. Yao, Q. Yu, K. Wang, Q. Li, J.-F. Li, RSC Advances, 4 (2014) 20062.
[6] F.-Z. Yao, J. Glaum, K. Wang, W. Jo, J. Roedel, J.-F. Li, Appl. Phys. Lett., 103 (2013) 192907.
[7] L.-Q. Cheng, K. Wang, J.-F. Li, Chem. Comm., 49 (2013) 4003.
[8] J.-J. Zhou, K. Wang, F. Li, J.-F. Li, X.-W. Zhang, Q.-M. Wang, J. Am. Ceram. Soc., 96 (2013) 519.
[9] Y. Xu, Q. Yu, J.-F. Li, J. Mater. Chem., 22 (2012) 23221.
[10] K. Wang, J.-F. Li, Adv. Funct. Mater., 20 (2010) 1924.
[11] Z.-Y. Shen, Y. Xu, and J.-F. Li, J. Appl. Phys., 105 (2009) 104103
[12] K. Wang, J.-F. Li and N. Liu, Appl. Phys. Lett., 93 (2008) 092904.
[13] K. Wang, J.-F. Li, Appl. Phys. Lett., 91 (2007) 262902.
[14] Y. H. Zhen, J.-F. Li, J. Am. Ceram. Soc., 89 (2006) 3669.
[15] J.-F. Li, K. Wang, B. P. Zhang, L. M. Zhang, J. Am. Ceram. Soc., 89 (2006) 706.

Acknowledgement:

This work was supported by the National Nature Science Foundation of China (Grants No. 51332002, 51302144, 51221291, 51211140345) and Tsinghua University Initiative Scientific Research Program.

PL-03

Hot Spot Phenomenon of Ceramics and its Application

Masasuke Takata
Japan Fine Ceramics Center (JFCC), Japan

The present authors demonstrated that a local area of a $GdBa_2Cu_3O_{7-\delta}$ (Gd-123) ceramic rod glows orange once a voltage exceeding a certain value is applied to the rod at room temperature [1]. The glowing area was named a hot spot. After the appearance of the hot spot, the current decreases with decreasing oxygen partial pressure (Po_2) in ambient atmosphere, which acts as an oxygen sensor without the need for any heating system [2] .

References:

[1] T. Okamoto, B. Huybrechts and M. Takata, Jpn. J. Appl. Phys., **33** (1994) L1212.
[2] M. Takata, Y. Noguchi, Y. Kurihara, T. Okamoto and B. Huybrechts, Bull. Mater. Sci., **22** (1999) 593.

Invited Presentation

Synthesis, Raw Materials & Advanced powder processing(SY) 76
Thermoelectrics(TH) 79
Thin Films & Layers(TF) 86
Nano-particles & Nano-structured Materials(NA) 91
Fuel cells and Batteries(FU) 96
Electronic Ceramics(EL) 102
Structual Ceramics & Refractory materials(ST) 110
Glass & Opto-Electronic Materials(GL) 114
Biomaterials(BI) 116
Sensor Materials(SE) 118
Electric Field Assisted Sintering(EL) 121
Piezoelectric Device & Application(PI) 127
Lead-free Piezoelectrics(LP) 133
Computational Ceramic Science and Engineering(CO) 147
Ceramics Culture and Education(CE) 151
LED and Display Materials(LD) 160
Advanced Coating for Gas Turbines(AD) 170

SY-I01

Novel Environmentally Friendly (Bi, Ca, Zn, La)VO_4 Yellow Pigments

Toshiyuki MASUI, Wendusu, Taihei HONDA, Nobuhito IMANAKA*
Department of Applied Chemistry, Faculty of Engineering, Osaka University, Suita Osaka, 5650871, Japan

Keywords: Bismuth vanadate, Environmentally friendly, Yellow pigment, Solid solution

Inorganic yellow pigments are applied in a wide range of products, such as porcelains, ceramics, inks, and paints. However, several conventional pigments such as chrome yellow ($PbCrO_4$) and cadmium yellow (CdS·ZnS) contain toxic elements, such as Pb, Cr, and Cd. Because of this fact, we focused on monoclinic bismuth vanadate ($BiVO_4$), which is already known as an environmentally friendly inorganic yellow pigment [1]. The coloring mechanism of monoclinic $BiVO_4$ results from a charge transfer transition from a hybrid orbital of Bi_{6s} and O_{2p} to V_{3d} in the $BiVO_4$ band structure [2]. Therefore, it is expected that the color of $BiVO_4$ can be tuned by introducing other elements into the $BiVO_4$ lattice to control the lattice size, because the extent of the orbital hybridization in the valence band should depend on the interionic distance between Bi^{3+} and O^{2-}.

Based on this concept, we successfully synthesized $Bi_{1-x}La_xVO_4$ ($0 \le x \le 0.15$) [3], $Bi_{1-x-y}Ca_xZn_yVO_{4-(x+y)/2}$ ($0 \le x \le 0.10$; $0 \le y \le 0.10$) [4], and $Bi_{0.90-x}Ca_{0.08}Zn_{0.02}La_xVO_{3.95}$ ($0 \le x \le 0.10$) [5] solid solutions as environmentally friendly inorganic pigments, and the composition was optimized to produce the most vivid yellow hue. All pigments exhibited brilliant yellow colors. The L^* (brightness or darkness), a^* (the red–green axis), and b^* (the yellow–blue axis) chromatic coordinates of the representative pigments are summarized in Table 1. The b^* value corresponding to yellow chromaticity depends on the sample composition. The $Bi_{0.85}Ca_{0.08}Zn_{0.02}La_{0.05}VO_{3.95}$ pigment has the highest b^* value at +93.5, and the most vivid yellow hue was obtained for this sample. Although the yellowness value falls just one step short of that for the toxic $PbCrO_4$ ($b^* = +96.5$) pigment, it is significantly greater than that for the conventional $BiVO_4$ pigment ($b^* = +76.9$). Since $BiVO_4$ is an environmentally friendly inorganic yellow pigment, and Ca, Zn, and La are also nontoxic and safe elements, the $Bi_{0.85}Ca_{0.08}Zn_{0.02}La_{0.05}VO_{3.95}$ pigment could be an effective alternative to conventional toxic yellow pigments.

Table 1 Chromatic coordinates of the pigments

Samples	L^*	a^*	b^*
$Bi_{0.90}La_{0.10}VO_4$ [3]	89.0	−14.6	+86.6
$Bi_{0.90}Ca_{0.08}Zn_{0.02}VO_{3.95}$ [4]	87.7	−4.36	+91.6
$Bi_{0.85}Ca_{0.08}Zn_{0.02}La_{0.05}VO_{3.95}$ [5]	92.8	−6.82	+93.5
Commercially available $BiVO_4$	94.4	−16.7	+76.9
Commercially available $PbCrO_4$	89.9	+1.12	+96.5

References:

[1] E.B. Faulkner and R.J. Schwartz, *High performance pigments*, 2nd ed., Wiley (2009) pp.7–12.
[2] A. Kudo, K. Omori, and H. Kato, J. Am. Chem. Soc. 121 (1999) 11459.
[3] Wendusu, K. Ikawa, T. Masui, and N. Imanaka, Chem. Lett. 40 (2011) 792.
[4] T. Masui, T. Honda, Wendusu, and N. Imanaka, Dyes Pigm. 99 (2013) 636.
[5] Wendusu, T. Honda, T. Masui, and N. Imanaka, RSC Adv. 3 (2013) 24941.

Acknowledgement:

The present work was supported by the Development of Alternative Technology for Hazardous Chemical Substance and Development of Novel Environment and Human-friendly Inorganic Pigments for Three Primary Colors (FY2010-2014) programs of the Ministry of Economy, Trade and Industry, Japan (METI).

SY-I02

Novel Low Temperature Synthesis Method of Ceramic Oxide Materials

Kenji TODA,[1,*] Tatsuro KANEKO,[1] Kazuyoshi UEMATSU,[2] Tadashi ISHIGAKI,[1]
Sun Woog KIM,[1] Mineo SATO,[2] Junko KOIDE,[3] Masako TODA,[3] Yoshiaki KUDO[3]
[1]*Graduate School of Science and Technology, Niigata University, 8050 Ikarashi 2-nocho, Niigata 950-2181, Japan*
[2]*Department of Chemistry and Chemical Engineering, Niigata University, 8050 Ikarashi 2-nocho, Niigata 950-2181, Japan*
[3]*N-Luminescence Corporation, 8867-3 Ikarashi 2-nocho, Niigata 950-2101, Japan*

Keywords: Low Temperature, Nano particles, Water

In generally, ceramic oxide materials were synthesized by a high-temperature solid-state reaction method because of simple and inexpensive preparation techniques. However, the synthesis at high temperature leads to increase in the processing cost and irregular particle morphology of the obtained powders [1]. In order to synthesize the ceramic oxide materials having uniform particle morphology at low temperature, therefore, liquid phase reaction methods, such as co-precipitation method, sol-gel method, reverse micelle process, hydrothermal process, and others, usually used on an industrial scale. In addition, some methods using organic acid as a solvent should be effectively synthesized in a single phase of ceramic oxide materials at room temperature without special equipment. However, the most of liquid phase reaction methods require special washing and separation processes because these method generally use the strong basic and acid or organic acids [2]. The special washing and separation processes also contribute to increase the processing cost.

In contrast, we have proposed the novel synthesis methods to synthesize the ceramic oxide materials in a single phase form at low temperature without after heat treatment and the basic and acids. We found that some compounds can be synthesized at room temperature just by mixing of raw materials and the reaction is promoted by a small amount of water addition [3-5]. We refer to this method as a water assisted room temperature solid state reaction (WASSR) method. Furthermore, we are also demonstrated that the some ceramic oxide materials can be synthesized in a single phase form with keeping the hydrate raw material mixtures in reactor shell at low temperature below 100 ºC, so called solid hydrate thermal processing.

In this study, we presents the effect and availability of the our original novel solid state reaction methods on an industrial application in the ceramic oxide materials synthesis processing as the basis of the results obtained by these method.

References:

[1] J. H. Sharp, G. W. Brindley, and B. N. Narahari Achar, J. Am. Ceram. Soc., 49 (1966) 379.
[2] F. M. Nirwan, T. K. G. Rao, P. K. Gupta, and R. B. Pode, Phys. Stat. Sol. (a), 198 (2003) 447.
[3] K. Toda, M. Sato, K. Uematsu, and T. Ishigaki, Japanese Unexamined Patent Application Publication No. 2011-16670 (2009).
[4] A. Toda, K. Uematsu, T. Ishigaki, K. Toda, and M. Sato, Abstract of 216th ECS Meeting (2009), #3224.
[5] T. Kaneko, K. Uematsu, T. Ishigaki, S. W. Kim, K. Toda, M. Sato, J. Koide, M. Toda, and Y. Kudo, Abstract of Internationals Symposium on the Reactivity of Solids 2014 (ISRS-18) (2014), P258

SY-I03

Novel Oxide Phosphor Materials Synthesized by Melt Synthesis Method

Sun Woog KIM,[1] Takuya HASEGAWA,[1] Yukari KAWANO,[1] Hiroko NAKAGAWA,[1] Tadashi ISHIGAKI,[1] Kenji TODA,[1,*] Kazuyoshi UEMATSU,[2] Mineo SATO[2]
[1]*Graduate School of Science and Technology, Niigata University, 8050 Ikarashi 2-nocho, Niigata 950-2181, Japan*
[2]*Department of Chemistry and Chemical Engineering, Niigata University, 8050 Ikarashi 2-nocho, Niigata 950-2181, Japan*

Keywords: Arc-imaging furnace, Melt Synthesis Method, White LED phosphor

Recent years, the phosphor materials based on nitrides and oxynitrides have been usually used the commercial white LEDs phosphors because of their high chemical and thermal stabilities. In particular, yellow- and red-emitting nitrides phosphors have received much attention for the white LED applications. However, these nitride phosphors require a special high-temperature and high-pressure furnace for synthesis of a single phase form and expensive raw materials, which contribute to increase the cost of white LEDs. Therefore, investigations have been devoted to search for novel phosphors based on oxide materials, which can be synthesized in a single phase form and can show high luminescence efficiency under near-UV and blue light excitation.

We proposed melt synthesis technique using arc-imaging furnace as a new synthesis method to develop novel white LED phosphors. Arc-imaging furnace can be heated rapidly the samples at various atmospheres up to high temperatures even greater than 2000 ºC, and also rapidly cooled by removing the sample stage from the mirror′s focus. In addition, the melt reaction is extremely rapid and homogeneous than that of a conventional solid-state reaction method because of liquid mixing and rapid diffusion in the liquid phase [1,2]. Therefore, the melt synthesis technique using arc-imaging furnace is suitable for rapid screening of novel LED phosphors. Furthermore, we have previously demonstrated that this method is suitable to synthesize the oxide materials having metastable phase in the room temperature and it is also suitable for synthesizing glass materials because this method has rapid cooling process [3-5].

In this study, we present the availability of the melt synthesis technique using arc-imaging furnace and the optical properties of the novel phosphor materials obtained by this method.

References:

[1] T. Ishigaki, N. Matsushita, M. Yoshimura, K. Uematsu, K. Toda, and M. Sato, Phys. Procedia, 2 (2009) 578.
[2] T. Ishigaki, M. Yoshimura, N. Matsushita, K. Uematsu, K. Toda, and M. Sato, J. Eur. Ceram. Soc., 30 (2010) 165.
[3] S. W. Kim, T. Hasegawa, T. Ishigaki, K. Uematsu, K. Toda, and M. Sato, ECS Solid State Lett., 2 (2013) R49.
[4] H. Nakagawa, S. W. Kim, K. Uematsu, T. Ishigaki, K. Toda, H. Takaba, and M. Sato, Abstract of 8th Int. Conf. Sci. Technol. for Advanced Ceramics (2014), 25pHO02.
[5] S. W. Kim, T. Hasegawa, M. Inoue, T. Ishigaki, K. Uematsu, K. Toda, and M. Sato, J. Ceram. Soc. Jpn., 122 (2014) 452.

Acknowledgement:

This work was supported by a project from NEDO, New Energy and Industrial Technology Development Organization (Rare Metal Substitute Materials Development Project Development of Technology for Reducing Tb and Eu Usage in Phosphors for Fluorescent Lamp by High-speed Material Synthesis and Evaluation).

TE-I01

N-type Oxide Thermoelectric Materials Having Spin/Orbital Correlations

Tetsuji Okuda
Graduate School of Science and Engineering, Kagoshima University, Kagoshima, 890-0065, Japan

Keywords: Oxide thermoelectric materials, $SrTiO_3$, $CaMnO_3$, Fe pnictide

Since the good p-type thermoelectric (TE) property was discovered in Co oxides [1], transition metal oxides have been expected to be next generation TE materials, because of abundant natural resources and being nontoxic, environmental benign, and stable at high temperatures. However, good n-type oxide TE material being a counterpart of Co oxide has not been found yet till now.

In this talk, I will show our attempts to improve the TE properties at room temperature for some candidates of n-type oxide TE materials such as $SrTiO_3$ [2,3] and $CaMnO_3$ [4,5] by element substitutions, together with relative good n-type TE property of Fe-pnictide at low temperatures [6,7]. Based on these results, I will discuss about the effects of the spin/orbital correlations of 3d transition metal ions and the associated local lattice distortions on the TE properties of these oxides.

References:

[1] I. Terasaki, Y. Sasago, and K. Uchinokura, Phys. Rev. B **56**, R12685 (1997).
[2] T. Okuda, K. Nakanishi, S. Miyasaka, and Y. Tokura, Phys. Rev. B **63**, 113104 (2001).
[3] J. Fukuyado, K. Narikiyo, M. Akaki, H. Kuwahara, and T. Okuda, Phys. Rev. B **85**, 075112 (2012).
[4] M. Ohtaki, H. Koga, T. Tokunaga, K. Eguchi, and H. Arai, J. Solid State Chem. **120**, 105 (1995).
[5] T. Okuda and Y. Fujii, J. Appl. Phys. **108**, 103702 (2010).
[6] L. Pinsard-Gaudart, D. Bérardan, J. Bobroff, and N. Dragoe: Phys. Status Solidi: Rapid Res. Lett. **2**, 185 (2008).
[7] T. Okuda, W. Hirata, A. Takemori, S. Suzuki, S. Saijo, S. Miyasaka, and S. Tajima, J. Phys. Soc. Jpn. **80**, 044704 (2011).

Acknowledgement:

This work was partially supported by JSPS KAKENHI Grant No. 25400378.

TE-I02

Thermoelectric properties of thick film elements fabricated by aerosol deposition method

Yuichi NAKAMURA*, Mitsuteru INOUE
Department of Electrical and Electronic Engineering, Toyohashi University of Technology, Toyohashi, Aichi 441-8580, JAPAN

Keywords: $Ca_3Co_4O_9$, $CaMnO_3$, aerosol deposition method, thick film, thermoelectric element

Thermoelectric conversion is a promising method to harvest thermal energy even from small heat source. Among the thermoelectric materials, the thermoelectric oxides such as $Ca_3Co_4O_9$ (Co349) and $CaMnO_3$ (Mn113) are expected to be used at high temperature up to 1000 K. For the actual application, -type modules are widely used. Recently, the monolithic multilayer type structures, in which the p- and n-type thick layers were stacked with insulators between them, are proposed for their advantage of small size, high packing density, and high reliability [1]. The aerosol deposition (AD) method is a promising technique to prepare high density ceramic thick film by ejecting aerosol consisting of a mixture of fine ceramic particles and gas from the nozzle to the substrate [2-3]. We reported that Co349 thick films fabricated by AD method showed thermoelectric properties as high as the conventional hot pressed bulk after short annealing at 900 °C for 1h [3]. This suggests that the AD process is effective to fabricate thermoelectric thick films. In this work, the Co349/Mn113 thermoelectric thick film elements were fabricated by AD method, and the thermoelectric properties of the elements were evaluated. The Co349 and Mn113 powders with the composition of 10% Bi substituted for Ca site were prepared. The Mn113 films deposited by AD method were annealed at 900~1100 °C for 1h to improve crystallinity, and their properties were shown in Figure 1 with those of bulk sample. The AD films showed the Seebeck coefficient and electrical conductivity as high as those of bulk sample irrespective of low temperature and short annealing time due to high density of as deposited film. Figure 2 shows the output voltage and generated power properties of the one pair Co349/MgO/Mn113 thermoelectric layered element formed by AD method. The voltage decreased linearly as increasing current, and the output power showed the maximum. Although the output power was not enough high due to the small temperature difference and thin thickness, this property was as high as expected from the properties of Co349 and Mn113 single films. This means that the high density films fabricated by AD method is effective to form thermoelectric monolithic module.

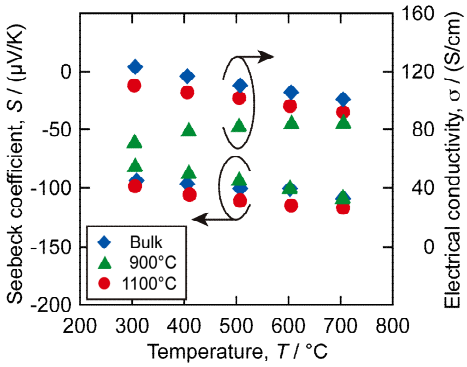

Figure 1 Thermoelectric properties of Mn113 films.

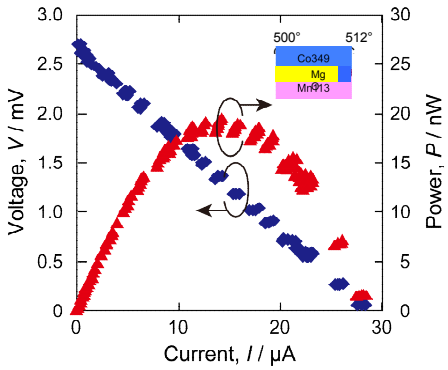

Figure 2 Output voltage and power properties of the Co349/MgO/Mn113 layered element.

References:

[1] S. Funahashi, T. Nakamura, K. Kageyama, H. Ieki, J. Appl. Phys. **109** (2011) 124509.
[2] J. Akedo, M. Lebedev, Jpn. J. Appl. Phys. 38 (1999) 5397.
[3] Y. Nakamura, Y. Matsufuji, M. Inoue, J. Phys.: Conf. Series 352 (2012) 012026.

TE-I03

A study on thermoelectric properties of perovskite-type oxides

Hiroshi Nakatsugawa[1*], Masaki Kubota[1] , Takanori Yamamoto[1], Yosuke Watanabe[1]
[1]*Yokohama National University,79-5 Tokiwadai, Hodogaya, Yokohama 240-8501, Japan*

Keywords: thermoelectric, perovskite-type oxides, 3d transition metal, Heikes formula

Thermoelectric energy conversion technology attracts renewed interest as a new energy resource. Thermoelectric materials can directly convert waste heat from automobiles, facilities, and power plants into electrical energy. Since electrons in solids carry electricity together with thermal entropy, there is a finite coupling between the electrical and heat currents, which is known as the thermoelectric phenomena. The potentiality of the thermoelectric materials is indicated in terms of the dimensionless figure of merit, i.e., $ZT=S^2\sigma T/\kappa$, where S, σ, κ, and T are the Seebeck coefficient, the electric conductivity, the thermal conductivity, and the absolute temperature, respectively. The thermoelectric energy conversion generates energy from the temperature gradient and the heat flow. The thermoelectric energy conversion efficiency η is defined by the ratio between the output electrical power *P* with the heat flux *Q*, i.e., $\eta=P/Q$. By optimizing the efficiency with respect to a load resistance, the maximum efficiency η_{max} is obtained as a monotonically increasing function of ZT. Obviously, a higher temperature with a larger temperature difference and to be a larger ZT gives a larger η_{max}. In this respect, oxides are quite attractive because they are thermally and chemically stable for long time use at high temperatures in air for thermoelectric conversion. Recently, oxides have been studied extensively as a possible candidate for thermoelectric materials at high-temperatures since the discovery of large Seebeck coefficient (S=100μV/K) and low electric resistivity (ρ=0.2*m*Ωcm) at room temperature in the layered cobalt oxide Na_xCoO_2.[1] The misfit-layered cobalt oxide $Ca_3Co_4O_9$ has also been studied as a candidate for p-type thermoelectric materials and typically exhibits S=130μV/K, ρ=15*m*Ωcm, and κ=1.0W/mK at room temperature.[2] For instance, fabrication and power generation of oxide thermoelectric modules consisting of p-type $Ca_{2.7}Bi_{0.3}Co_4O_9$ and n-type $La_{0.9}Bi_{0.1}NiO_3$ bulks have been reported.[3] In face, power charging a portable phone has been successful using this oxide thermoelectric module, however, the maximum efficiency η_{max} was as low as 1.4%.[4] To enhance η_{max}, Urata *et al*.[5] have built thermoelectric modules consisting of p-type $Ca_{2.7}Bi_{0.3}Co_4O_9$ and n-type $CaMn_{0.98}Mo_{0.02}O_3$ bulks and calculated η_{max} to be 2.0% from ZT values. However, the n-type legs were damaged by thermal stress between the alumina substrate. [5] To overcome the lack of oxide thermoelectric materials, we have paid attention to perovskite-type oxides which form both n-type and p-type conductors, since many kinds of metal elements can fit into the perovskite structure with the general formula ABO_3. Perovskite-type oxides such as titanate, manganate, ferrate, and cobaltate phases reveal a large Seebeck coefficient, S, which is one of the essential prerequisites for potential thermoelectric materials. The large S values are caused by a strong interplay between charge, orbital states, electron spin states, and crystal structure. Koshibae *et al*.[6] proposed that the high-temperature limit of S values in 3d transition metal oxides is given by Heikes formula from a localized picture. When both a degeneracy of spin and orbital degrees of freedom of 3d transition metal and the Heikes formula give large values, the large S at room temperature can be expected. Therefore, control of spin and orbital states of 3d transition metal ions would improve the ZT values of thermoelectric oxides. In this paper, the thermoelectric properties S, ρ, and κ, of the perovskite-type oxides, $Pr_{1-x}Sr_xMnO_3$, $Pr_{1-x}Ca_xMnO_3$, and $La_{1-x}Sr_xFeO_3$ will be investigated in order to clarify the possibility of the thermoelectric modules consisting of perovskite-type oxides.

References:

[1] I.Terasaki, Y.Sasago, and K.Uchinokura, *Phys. Rev.* B**56**, R12685 (1997).
[2] Y.Miyazaki, K.Kudo, M.Akoshima, Y.Ono, Y.Koike, and T.Kajitani, *Jpn, J.Appl.Phys*. **39**, L531 (2000).
[3] R.Funahashi, S.Urata, K.Mizuno, T.Kouuchi, and M.Mikami, *Appl.Phys.Lett.* **85**, 1036 (2004).
[4] R.Funahashi, M.Mikami, T.Mihara, S.Urata, and N.Ando, *J.Appl.Phys*. **99**, 066117 (2006).
[5] S.Urata, R.Funahashi, T.Mihara, A.Kosuga, S.Sodeoka, and T.Tanaka, *Int.J.Appl.Ceram.Technol*. **4**, 535 (2007).
[6] W.Koshibae, K.Tsutsui, and S.Maekawa, *Phys.Rev.* B**62**, 6869 (2000).

TE-I04

Oxygen Defect Application for Oxide Thermoelectrics

Soonil LEE
Korea Institute of Ceramic Engineering and Technology, Geumcheon-gu, Seoul 153-801, Korea

Keywords: Thermoelectric, Ferroelectric, Perovskite, Oxygen Defect, Oxides

Perovskite materials have been studied intensively for decades due to their broad applications, most of which are requiring to be insulating for better ferroelectric properties. On the contrary, there is lack of studies on the ferroelectrics with high concentration of electronic charge carriers. This paper demonstrates ferroelectric oxides in the unusual condition where the concentration of electronic carriers is close to a metal-insulator transition; in certain structures and compositions these materials have properties of interest for oxide based thermoelectric applications. To introduce certain amount of electronic carriers in the oxides, oxygen vacancies were generated by reduction process.In the heavily reduced perovskites ($BaTiO_{3-\delta}$, $SrTiO_{3-\delta}$), tungsten bronze structured ($(Sr,Ba)Nb_2O_{6-\delta}$), and perovskite layer structured ($Sr_2Nb_2O_{7-\delta}$) materials, thermopower and electrical conductivity anomalies are observed due to dipole moments, depending on the carrier concentration. The nonstoichiometric *n*-type perovskite $BaTiO_{3-\delta}$ and tungsten bronze $(Sr_{1-x}Ba_x)Nb_2O_{6-\delta}$ shows that metallic-likeconductivity occurs in the paraelectric phase and the onset of ferroelectricity stabilizes semiconducting character. The $(Sr_{1-x}Ba_x)Nb_2O_{6-\delta}$ relaxor ferroelectric single crystals, which have nanopolar regions associated with intrinsic localized phonon modes, have a high thermoelectric power factor along the c-axis, showing a strong crystal anisotropic effect. The charge transport mechanism was controlled by polaron hopping conduction above the *4mm-4/mm* phase transition temperature (T_C), and below T_C the behavior depends on the degree of reduction. The reduced $SrTiO_{3-\delta}$ crystals also show a high thermoelectric power factor at room temperature, which is related with the defect heterogeneity. With this work, the complex nature of the oxygen defect engineered ferroelectrics is discussed in terms of the thermoelectric properties and coupling of ferroelectrics and thermoelectrics.

Acknowledgements:
Clive A. Randall, Gaiying Yang, Rudger H. T. Wilke, Susan Trolier-McKinstry, Shujun Zhang, Sinan Dursun, Cihangir Duran, Takashi Teranishi, Daniel J. Magagnosc, Jonathan A. Bock, Steve Perini, Paul Moses, Jeff Long, Weiguo Qu, Petro Maksymovych, Arthur P. Baddorf

TE-I05

How can we boost thermoelectric properties of oxides by nano?

Yoshiaki KINEMUCHI[1*]
[1] *National Institute of Advanced Industrial Science and Technology (AIST), Nagoya 463-8560, JAPAN*

Keywords: Oxides, Nano particles, Thermoelectricity, Energy filtering, Boundary scattering

Harvesting energy with low exergy, such as wasted heat with low temperature, is fundamentally challenging. As with thermoelectric (TE) energy conversion, "nano" is regarded as one of the key solutions for the challenge. Among the TE materials, oxides provide versatile platform for nanostructuring, which may contributes to the efficiency of energy conversion of TE.
In TE, expected outcomes of nanostructuring are low phonon thermal conductivity, high thermopower and low electric conductivity. The former two effects raise the efficiency, while the last one deteriorates the performance. Thus the tuning or decoupling of the effects is crucial, yet it is not established so far. Here, we will revisit the fundamental idea of nanostructuring and will evaluate the effect independently with examples in oxides.

1. THERMAL CONDUCTIVITY (κ)

Most of oxides possess rigid framework in their crystal structure, thus their tend to be high due to the phonon contribution. For the practical application, less than 1W/(mK), including electron thermal conductivity, is the common limit. Nanostructuring provides the method to control phonon scattering rather than the modification of bonding nature: reducing phonon mean free path (MFP) while maintaining both sound velocity and heat capacity. Practically, this is achieved by rattling or boundary scattering. Nowadays, the boundary scattering is quantitatively evaluated based on Debye-Callaway model and is understood that the strategy can apply any kinds of material. Recent progress in TE efficiency exceeding ZT of 1.5 is mostly owing to this effect. For instance, ZnO of single crystal shows of about 100 W/(mK), while the value largely reduces to 5 W/mK for the crystal size of 30 nm [1].

2. ELECTRICAL CONDUCTIVITY (σ)

Although reduction in phonon thermal conductivity via boundary scattering is rational approach, the drawback of reduction in must be taken in consideration. As a simple picture, it is said that MFP of charged carrier is shorter than that of phonon, and thus the scattering event induced by nanostructuring may be negligible or not seriously influence to. Quantitatively, the influence can be incorporated through Mattisen's rule, and we can understand that a certain size range exists to enhance ZT. Practically, band bending near the boundary, which is caused by band offset or impurity trap, must be solved for a gain in ZT, as seen in In_2O_3 [2].

3. THERMOPOWER (*S*)

Nanostructuring is able to tune the density of state (DOS), which dramatically modify *S*. So far, experimental proof of this idea has been demonstrated mostly in two-dimensional system, namely super lattice approach. On the other hand, practical application of TE power generation requires bulk form; thus realization of the DOS tuning in bulk material is strongly demanded. Recently, we found that surface structure of nano-particles (NPs) of $SrTiO_3$ can be a playground to achieve the DOS tuning of bulk materials. $SrTiO_3$ is non-polar because of its cubic symmetry, while the surface of NPs shows polar caused by the surface relaxation, which leads to obvious first order Raman scattering. By means of chemical pressure, we can modulate the surface relaxation rationally, and thus the potential barrier near the surface vary accordingly. The barrier has the effect to cut the low energy carrier, resulting in apparent DOS tuning, hence we can observe large *S* enhancement [3].

References:

[1] Y. Kinemuchi et al., *J. Appl. Phys.,* 108, 053721 (2010).
[2] Y. Kinemuchi et al., *J. Appl. Phys.*, 110, 12304 (2011).
[3] Y. Kinemuchi et al., *J. Electr. Mater.*, 43, 2011(2014).

TE-I06

Thermoelectric Properties of Doped n-type $Cu_{0.008}Bi_2Te_{2.7}Se_{0.3}$

Kyu Hyoung Lee[1]*, Sung Wng Kim[2,3]
[1]*Department of Nano Applied Engineering, Kangwon National University, Chuncheon, 200-701, Korea*
[2]*Department of Energy Science, Sungkyunkwan University, Suwon, 440-746, Korea*
[3]*IBS Center for Integrated Nanostructure Physics, Institute for Basic Science, Sungkyunkwan University, Suwon, 440-746, Korea*

Keywords: Doping, Seebeck coefficient, Effective mass, DOS engineering

Herein we report that the doping of several transition metal elements is effective in enhancing the Seebeck coefficient of n-type $Cu_{0.008}Bi_2Te_{2.7}Se_{0.3}$. The absolute value of room temperature Seebeck coefficient increases significantly, benefiting from an enhancement of the density of states (DOS) effective mass, due to a DOS engineering effect by resonant state formation and/or chemical potential tuning, which gives rise to higher DOS at the bottom of the conduction band. Enhancement in Seebeck result in the highest thermoelectric figure of merit ZT = 0.85 at 300 K. This compositional tuning approach highlights the possibility of further enhancement of ZT of n-type Bi-Te-based compounds by combination of nanostructuring technologies.

References:

[1] W. Liu, Q. Zhang, Y. Lan, S. Chen, X. Yan, Q. Zhang, H. Wang, D. Wang, G. Chen and Z. Ren, Adv. Energy Mater. 1 (2011) 577.
[2] G. Snyder and E. Toberer, Nat. Mater. 7 (2008) 105.

TE-I07

One alternative way to high thermoelectric performance: the intrinsically low thermal conductivity

Li-Dong Zhao*
School of Materials Science and Engineering, Beihang University, Beijing, 100191, China

Keywords: Thermoelectric, Thermal conductivity, Seebeck coefficient

Thermoelectric materials, capable of converting waste heat into electrical power and vice versa, are currently receiving a significant scientific attention. The efficiency of a thermoelectric device is determined by ZT, $ZT = (S^2\sigma/\kappa)T$, where S, σ, κ and T are the Seebeck coefficient, the electrical conductivity, the thermal conductivity, and the temperature, respectively. S and σ must both be large, while κ must be minimized. However, the high ZT is challenged by the interdependent relationships for these parameters. Several approaches to enhance ZT have emerged in the last decades,[1] including band structure engineering to enhance Seebeck coefficients, nanostructuring and all-scale hierarchical architecturing to reduce thermal conductivity, and band alignment to maintain hole mobility.

Alternatively, one can also seek high thermoelectric performance in pristine materials with intrinsically low thermal conductivity.[2] In this talk, some typical compounds, SnSe,[3] BiCuSeO,[2] BiAgSeS,[4] are presented as promising thermoelectric materials. Their high performances are mainly due to their intrinsically low thermal conductivity, which may arise from a large anharmonicity, lone pair electrons, a large molecular weight, a complex crystal structure, charge density wave distortions, etc.

References:

[1] L.-D. Zhao, *et al. Energy Environ. Sci.* 7 (2014) 251-268.
[2] L.-D. Zhao, *et al. Energy Environ. Sci.* 7 (2014) 2900-2924.
[3] L.-D. Zhao, *et al. Nature* 508 (2014) 373-377.
[4] Y. L. Pei, *et al. Energy Environ. Sci.* 6 (2013) 1750-1755.

Acknowledgement:

This contribution was partly supported by the “zhuoyue” program of Beihang University. I am grateful to Professor Mercouri G. Kanatzidis for fruitful collaborations. Of course most of all, I am grateful to the numerous dedicated collaborators who have contributed to our thermoelectric research efforts, their names appear in this talk.

TF-I01

Domain Structure Change with Temperature in (100)/(001)- oriented Epitaxial $PbTiO_3$ Films Grown on $KTaO_3$ Films

Hiroshi FUNAKUBO[1*], Takaaki NAKASHIMA[1], Daichi ICHINOSE[1],
Yoshitaka EHARA[1], Takao SHIMIZU[1], Takeshi KOBAYASHI[2], and Tomoaki YAMADA[3, 4]
[1]*Department of Innovative and Engineered Materials, Tokyo Institute of Technology, 226-8502, Japan*
[2] *National Institute of Advanced Industrial Science and Technology (AIST), 305-8564, Japan*
[3] *Department of Materials, Physics and Energy Engineering, Nagoya University, 464-8603, Japan*
[4] *PRESTO, Japan Science and Technology Agency, 102-0075, Japan*

Keywords: Domain structure change, $PbTiO_3$, (100)/(001)-oriented epitaxial films

Domain structure of ferroelectric films is widely known to determining ferroelectric and electromechanical properties of these films. We recognize that strain from the substrate is as one of the determine factor of these domain structure[1]. Theoretical prediction has been carried out for $PbTiO_3$[2]. This suggests for (100)/(001)-oriented $PbTiO_3$ films with in-plane tensile strain that the ferroelectric domain structure change from perfect (001) orientation to the mixture one of (100) and (001) under the cooling process below *Tc*. However, this domain structure change with temperature has not been reported experimentally.

In the present study, we grew (100)/(001)-oriented epitaxial $PbTiO_3$ films with in-plane tensile strain and demonstrate this domain structure change with temperature below *Tc*.

Fig.1 shows the XRD reciprocal space mappings (*RSMs*) around (100) $KTaO_3$ *202* measured at (a) 30 ˚C, (b) 500 ˚C, (c) 600 ˚C for 130 nm thick $PbTiO_3$ film grown on (100)$KTaO_3$ substrate. Films showed phase transition between 600 and 500°C because clear (100)-oriented in-plane domain structure was observed at 500°C. Noticeable thing is that this films include (100) orientation at 30°C. This clearly shows that domain structure change between 500 and 30 °C. This domain structure change was in good agreement with the theoretical prediction by Koukhar *et al.*

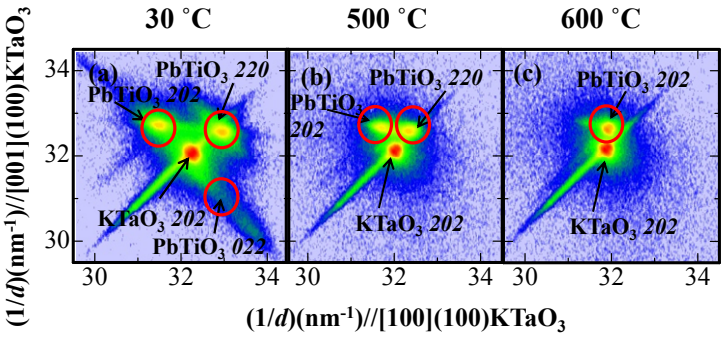

Fig.1 XRD reciprocal space mappings (RSMs) around (100) $KTaO_3$ *202* measured at (a) 30 ˚C, (b) 500 ˚C, (c) 600 ˚C for 130 nm thick $PbTiO_3$ film grown on $KTaO_3$ substrate

References:

[1] A. K. Tagantsev *et al.*,(2009) *Domains in ferroic crystals and thin films*, Sprigner, New York.
[2] V. G. Koukhar. et al., Phys. Rev. B **64**, 214103(2001)

Acknowledgement:

This research was partially supported by JSPS Kakenhi (No. 26220907)

TF-I02

Stress Evolution in Sol-Gel-Derived Thin Films

Hiromitsu KOZUKA*
Faculty of Chemistry, Materials and Bioengineering, Kansai University, Suita, 564-8680, Japan

Keywords: Sol-gel, Thin film, Coating, Stress

The residual stress in sol-gel-derived ceramic thin films greatly affects their properties and functionalities, results in bending of substrates, and hence is an important factor to be controlled. The stress is often thought to develop just as a result of the difference in thermal expansion coefficient between the film and the substrate. However, this is not correct. One should recognize that gel films are densified during heating under constrained conditions, where tensile strain is accumulated in in-plane direction, resulting in the development of in-plane tensile stress. A variety of processing parameters could affect the densification behavior, and hence could affect the evolution of stress during heating as well. During cooling after firing, on the other hand, thermal stress due to the difference in thermal expansion coefficient could be generated. Based on in-plane stress measurements, first we will demonstrate how the stress evolution during heating is affected by processing parameters. Second we will show how the heat treatment temperature could affect the residual in-plane stress. Although the residual stress exhibited a rather complex dependence on heat treatment temperature, the dependence could be understood in terms of film densification, structural relaxation, atomic diffusion, progress of crystallization and thermal strain.

References:

[1] H. Kozuka, *J. Sol-Gel Sci. Techn.*, 40, 287-297 (2006).
[2] H. Kozuka, in Handbook of Sol-Gel Science and Technology: Processing, Characterization and Applications, Volume 1, "Sol-Gel Processing," edited by S. Sakka, Kluwer Academic Publishers, Norwell, U.S.A., 2005, pp. 247-287.
[3] H. Kozuka and T. Iwase, *J. Mater. Res.*, 24, 2511-2519 **(**2009).
[4] T. Kurisu and H. Kozuka, *J. Am. Ceram. Soc.*, 89, 2453-2458 (2006).
[5] Y. Ishikawa and H. Kozuka, *J. Ceram. Soc. Jpn.*, 112, S228-S233 (2004).
[6] H. Kozuka and M. Komeda, *J. Ceram. Soc. Jpn.*, 112, S223-S227 (2004).
[7] K. Ohno, H. Uchiyama, H. Kozuka, *J. Appl. Phys.,*.111, 014901 (2012).

TF-I03

Atomic Layer Deposition of Multicomponent Oxides for Photovoltaic Applications

Jaeyeong HEO*
Department of Materials Science and Engineering, Chonnam National University, Gwangju, 500-757, Republic of Korea

Keywords: Atomic layer deposition, Zinc-tin-oxide, Solar cells

Atomic layer deposition (ALD) is one of the most promising techniques to deposit metal oxide thin films, allowing one to obtain highly conformal layers on planar and three-dimensional structures [1]. I will briefly introduce the ALD technique first and the results on the formation of *n*-type zinc-tin-oxide thin films using diethylzinc and a newly synthesized tin(II) precursor for zinc and tin precursors, respectively [2,3]. 50 wt.% hydrogen peroxide was selected as a common oxidant used for the ALD reaction. Cuprous oxide (Cu_2O) is one of the *p*-type absorber materials under consideration with the potential to reach 20% power conversion efficiency in thin-film solar cells. Zinc oxide has been demonstrated to show the best match with Cu_2O as an *n*-type buffer layer, but its record efficiency still remains low (<1%) among thin-film-based solar cells. By properly controlling the zinc-to-tin ratio in the zinc-tin-oxide buffer layers, the highest efficiency of 2.65% was achieved for Cu_2O-based thin-film solar cells. Detailed analyses on the electrical, structural, and optical properties of the buffer layer will be presented focusing on the tunability of the interface trap states and the conduction band offset.

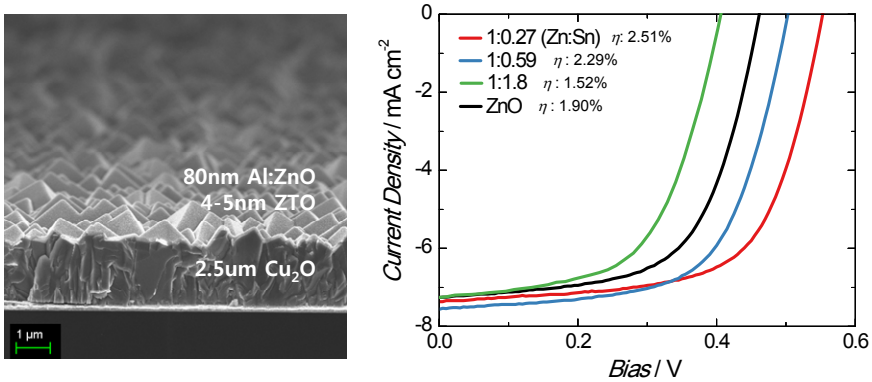

Figure 1 (left) SEM cross-section image of the fabricated Cu_2O-based thin film solar cell, (right) *I-V* characteristics under 1-sun irradiation

References:

[1] S. M. George, Chem. Rev. 110 (2010) 111.
[2] J. Heo, S. B. Kim, and R. G. Gordon, *Appl. Phys. Lett.* 101 (2012) 113507.
[3] Y. S. Lee, J. Heo, S. C. Siah, J. P. Mailoa, R. E. Brandt, S. B. Kim, R. G. Gordon, and T. Buonassisi, *Energy Environ. Sci*. 6 (2013) 2112.

TF-I04

Enhanced transparency, mechanical durability, and antibacterial activity of zinc nanoparticles on glass substrate

Hyung-Jin Choi and Soon-Gil Yoon*
Department of Materials Engineering, Chungnam National University, Daeduk Science Town, 305-764, Daejeon, Korea

***Keywords*:** Zinc NPs; Buffered Ti NPs; Transmittance; Mechanical durability; Antibacterial activity

Homogeneously distributed zinc nanoparticles (NPs) on the glass substrate were investigated for the transmittance, mechanical durability, and antibacterial effect. The buffered Ti NPs between Zn NPs and glass substrate were studied for an enhancement of the transmittance and mechanical endurance. The Ti NPs buffered Zn NPs showed a high transmittance of approximately 91.5% (at a wavelength of 550nm) and a strong antibacterial activity for *Staphylococcus aureus* and *Escherichia coli* bacteria. The buffered Ti NPs are attractive for an excellent mechanical endurance of the Zn NPs. The Zn NPs did not require the protection layer to prevent the degradation of the performance for both the antibacterial effect and the transmittance.

Introduction

The prevention of microbial surface contamination has become most crucial in today's health care system, and in food and pharmaceutical production. Human beings are often infected by microorganisms such as bacteria, viruses, and molds that often infect living environments. Silver nanoparticles or silver ions have been known to have strong inhibitory and bactericidal effects[1-9]. Metallic nanoparticles are most promising as they show good antibacterial properties due to their large surface area to volume ratio, which is coming up as the current interest in the researchers due to the growing microbial resistance against metal ions, antibiotics and the development of resistant strains[7]. However, although the silver NPs showed a good antibacterial effect, they exhibited a strong toxicity to humans and a high cost for mass-production. Recently, transparent electronic devices were widely used as the electronic devices were integrated onto the glass panels. All of electronic devices were required to be applied for the antibacterial function, keeping a high transparency comparable to the glass panels. In addition, the mechanical durability of the glass panels with an antibacterial effect is required for long-term applications.

In the present study, zinc NPs instead of silver were chosen for antibacterial function and their influence on the transmittance was investigated using samples deposited by optimum conditions. Most of the reported results were mainly focused on the zinc oxide nanoparticles for antibacterial effect[10-13]. However, zinc oxide nanoparticles were mainly prepared by solution technique, which resulted in an inhomogeneous antibacterial effect due to the severe agglomeration of the nanoparticles. Zinc oxide nanoparticles are very difficult to establish the comparable transmittance to the glass substrate. To the best of our knowledge, the study to enhance both the transmittance and the antibacterial property using pure zinc NPs has not been reported. For enhanced mechanical endurance of the zinc NPs on glass substrate, the Ti NPs were used as an adhesion layer between zinc NPs and glass. The reason that the Ti NPs deposited via a physical vapor deposition (PVD) process exhibited such a strong adhesion with the glass substrates was intensively investigated in the present study. Morphology, transmittance, antibacterial effect, and mechanical endurance of the zinc NP/glass was investigated for different structures such as Zn NPs/glass, Zn NPs/SiO_2/glass, and Zn NPs/Ti NPs/glass.

References

[1] Song, K. C., Lee, S. M., Park, T. S., Lee, B. S. *Kor. J. Chem. Eng.* 26, 153-155 (2009).
[2] Kang, H. Y., Jung, M. J., Jeong, Y. K. *Kor. J. Biotechnol. Bioeng.* 15, 521-524 (2000).
[3] Burrell, R. E. *Ostomy/Wound Manage.* 49, 19-24 (2003).
[4] Feng, Q. L. et al. *J. Biomed. Mater. Res.* 52, 662-668 (2000).
[5] Hollinger, M. A. *Crit. Rev. Toxicol.* 26, 255-260 (1996).
[6] Ratte, H. T. *Environ. Toxicol. Chem.* 18, 89-108 (1999).
[7] Gong, P. et al. *Nanotechnology*. 18, 285604 (2007).
[8] Navarro, E. et al. *Environ. Sci. Technol*. 42, 8959-8564 (2008).
[9] Loher, S., Schneider, O. D., Maienfisch, T., Bokorny, S., and Stark, W. J. *Small*, 4, 824-832 (2008).
[10] Rosi, N. L., and Mirkin, C. A. *Chemical Review*. 105, 1547-1562 (2005).
[11] Shrivastava, S., Dash, D. *Nanotechnology,* 18, 184702 (2007).
[12] Zhang, Y., Suenaga, K., Collies, C., Iijima, S. *Science* 281, 973-975 (1998).
[13] Vayssieres, L., Keis, K., Hagfeldt, A., Lindquist, S. –E. *Chem. Mater.* 13, 4395- 4398 (2001).

NA-I01

Synthesis and 3D Characterization of Barium-Ferrite Hybrid System with Highly Regulated Structures

Tadachika NAKAYAMA[1*], Hong-Baek CHO[1], Masanao KANNO[1], Shaifulazuar Bin ROZALI[2], Tadafumi ADSCHIRI[3], Hisayuki SUEMATSU[1], Tsuneo SUZUKI[1], Koichi NIIHARA[1]
[1]Nagaoka Univ. of Tech., Nagaoka, Niigata 940-2188, Japan
[2] University Malaya, Kuala Lumpur 50603, MALAYSIA
[3]Tohoku Univ., Sendai, Miyagi 980-8577, Japan

Keywords: Highly Regulated Structures, 3D Structure Analysis, Barium-Ferrite, Hybrid Materials, X-ray CT scan

The organic-inorganic hybrid system with magnetic fillers has been developed for the electomagnetic wave absorber, magnetic sheet and heating element. The texture and micro structure control of the magnetic fillers is one of the important point on these materials The orientation of Barium-Ferrite particles was controlled in polymer-based nanocomposite film using microscopic molds while applying a DC electric field. The Barium-Ferrite particles were dispersed by sonication in a prepolymer mixture of polysiloxane followed by a high speed mixing. The homogeneous suspension was cast on a microscopic mold with different patterns, which is attached to positive electrode during application of electric field before it became cross-linked. Analysis revealed that filament-like linear assembles of Barium-Ferrite particlewere fabricated in polysiloxane/Barium-Ferrite hybrid films, and Barium-Ferrite particles composing filament-like linear assembles were aligned perpendicular to the film plane with high anisotropy. The structure and dimensions of filament-like linear assembles showed direct relation with thermal property of the composite, and could be changed depending on the type of used microscopic molds. The filament-like linear assemblesformation induced by the type of microscopic molds and intensity of applied electric fields are discussed.

Acknowledgement:
This work was supported by JSPS KAKENHI Grant Scientific Research (A), Number 24246108 and 25249108.

NA-I02

Fabrication of a Ni/MgO Nanocomposite Catalyst by Exolution

Yesol LIM,[1] Jong Seol YOON,[1] Haejin HWANG[1*]
[1]*Department of Materials Science and Engineering, Inha University, Incheon, 402-751, Korea*

Keywords: Nanocomposite, Reforming Catalyst, Exolution, Fuel cell, Hydrogen

Methane steam reforming reaction is the most important chemical process to produce hydrogen or synthesis gas. Hydrogen is heavily consumed for ammonia production, the cryogenics industry and methanol production. Recently, the hydrogen demand is expected to increase as fuel cells become more widely accepted and are used more in the near future. For effective production of hydrogen or synthesis gas, the role of the reforming catalyst becomes more significant. Especially, highly active and stable catalyst is necessary for an on-site reformer for fuel cell systems.

In conventional technology, the methane steam reforming reaction is conducted on supported noble metals- (Pt, Pd, Rh, Ru, and Ir) or nickel-based catalysts at temperature up to 700~800°C and steam to methane rations between 2 and 4. However, these catalysts suffer from the deactivation by agglomeration and carbon deposition. Noble metal-based catalysts are less sensitive to carbon deposition than nickel-based catalyst. However, high cost and limited availability are major concern.

In this study, nickel-based nanocomposite catalysts were fabricated by exolution process. The exsolution means the process to precipitate particles from solid solution by means of the heat treatment in a specially-controlled atmosphere. This process is distinguished from the infiltration in which particles are precipitated from solutions by evaporation. First, $Mg_{1-x}Ni_xO$ solid solution powders were synthesized from aqueous magnesium and nickel nitrate solution by precipitation technique and then the powder was heat-treated in reducing atmosphere at 600 to 900°C. SEM and TEM images revealed that the nano-sized nickel particles were homogeneously dispersed in the $Mg_{1-x}Ni_xO$ solid solution matrix and the size and morphology of nano nickel particles can be controlled by the heat-treatment condition. Catalytic activity for the methane steam reforming or methane particle oxidation reaction and durability of the $Ni/Mg_{1-x}Ni_xO$ was investigated in terms of nickel contents and sizes.

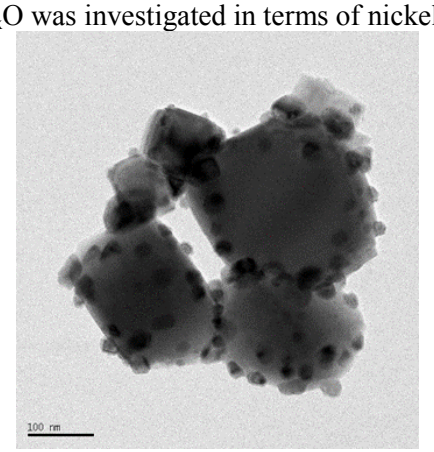

Figure 2. TEM image for Ni/MgO nanocomposites particles

References:
[1] O. Yamazaki, T. Nozaki, K. Omata, K. Fujimoto, Chem. Lett., (1992) 1953.
[2] V. A. Tsipouriari, A. M. Efstathiou, Z. L. Zhang, X. E. Verykios, Catal. Today, 21 (1994) 579.

NA-I03

Synthesis of Magnetite Nanoparticles and Their Surface Modification For Hyperthermia Application

Chang-Yeoul Kim*
Nano-Convergence Intelligence Material Team, Korea Institute of Ceramic Eng. & Tech.
Digital-ro 10 Gil 77 Geumcheon Gu153-801 Seoul Korea

Keywords: magnetite, nanocrystals, hyperthermia, surface modification

Magnetite nanocrystals draw many attractions of their applications for hyperthermia therapy; cancer killing by heating. These days, hyperthermia together with chemotherapy shows improved cancer treatment effects. So, we successfully synthesized magnetite nanoparticles by thermal decomposition method or coprecipitaton method. We try to synthesize magnetite nanoparticles and evaluate the hyperthermia effect by measuring temperature rise under ac inductive magnetic field. We also suggest the method of magnetic nanoparticle's dispersion within phosphor buffer solution and aerogel or silicone matrices. We could present the possibilities of the dispersion of magnetite nanoparticles with molar concentration change by surface modification using PEG within PBS and showed hyperthermia effects; the temperature increased when 689 Oe of magnetic field was applied. PEG coating give two merits: the homogeneous dispersion of the NPs and the hyperthermia effects of the NPs under alternating magnetic field, and the drug delivery because of bio-compatibility.

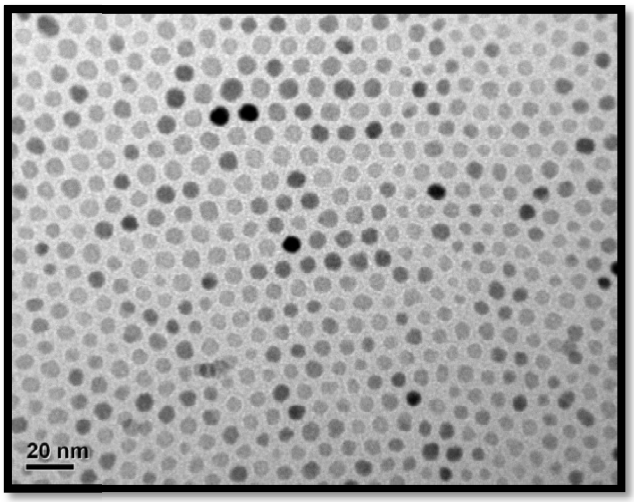

Figure 3 Magnetite nanoparticles synthesized by thermal decomposition

References:

[1] Eun-Hee Lee, Chang-Yeoul Kim, Yong-Ho Choa, Current Applied Physics 12, 2012, P47–52,
[2] CY Kim, L Xu, EH Lee, Journal of the Korean Physical Society 65,2 (2014,), pp 261-266
[3] CY Kim, L Xu, EH Lee, YH Choa, Advances in Polymer Technology, Volume 32, Issue S1, 714–E723, 2013

NA-I04

Eco-fabrication of Metal nanoparticle related Materials by Ultrasonic and Microwave Reactors

Yamato HAYASHI*
Department of Applied Chemistry, School of Engineering, Tohoku University, Sendai, 980-8579, Japan

Keywords: Ecology, Economy, Metal nanoparticle, Ultrasonic, Microwave

Recently, a variety of high-value-added technologies as nanotechnology and the high value-added products as nanomaterials using it can be requested various fields. Ecology and Economy synthesis is one of high-value-added technologies. Nanoparticles is also one of the most important nanomaterials because nanoparticle manufacturing is an essential component of nanotechnology. Also assembling of nanoparticles and related structures is the most generic route to generate nanostructured materials and build-up bulk materials. Nanoparticle were fabricated by various processing. Nano-sized metal related materials have recently attracted considerable interests owing to their potentials in applications. Such particles can be synthesized using physical and chemical methods. We developed a new metal nanoparticle related materials synthesis method that achieved by solid-liquid ultrasonic and micro-wave reactions. This new synthesis method is with the ultrasonic and microwave as non-equilibrium reactor. We have synthesized metal nanoparticle related materials by ultrasound and microwave in liquid-solid slurry and controlled morphology of products. Ultrasound and microwave irradiation in liquid-solid process can be expected as chemical non-equilibrium and nonlinear reactors for metal nanoparticle related materials synthesis. In presentation, we introduce various nano-particle related applications in details.

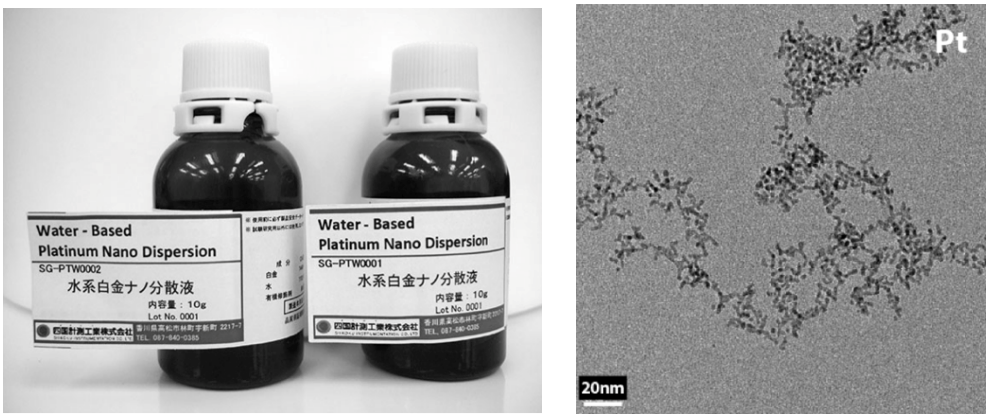

Figure 4 Images of Pt nanoparticle producted by ultrasonic and microwave reactors

References:

[1] Y. Hayashi and H. Takizawa, Catalysis Society of Japan Catalysts and Catalysis. 26 (2014) 41.
[2] H. Koubu, Y. Hayashi, J. Fukushima, H. Takizawa, I. Narita and S. Yoshioka, Mater. Trans. 54 (2013)1496.
[3] Y. Sekiguchi, Y. Hayashi, H. Takizawa, Mater. Trans. 52 (2011)1048.
[4] K. Toisawa, Y. Hayashi, H. Takizawa, Mater. Trans. 51 (2010)1764.
[5] T. Yamada, Y. Hayashi, H. Takizawa, Mater. Trans. 51 (2010)1769.
[6] M. Inoue, Y. Hayashi, H. Takizawa, K. Suganuma, Colloid & Polymer Science. 288 (2010)1061.

NA-I06

The increased optical transmission of the glass substrate coated with SnO_2 nanorod film using nano-aerosol spray pyrolysis deposition

Jeong-Wook Lee[1], Sung-Hwan Park[2], and Doh-Hyung Riu[1,2,*]
[1]*Department of Materials Science and Engineering, College of Engineering, Seoul National University of Science and Technology, 139-743, Seoul, Korea*
[2]*FTO Research Institute, SolarCeramic Co., Venture building 302, KICET, Seoul, Korea*

Nanorod tin oxide film was fabricated using nano aerosol spray pyrolysis deposition (SPD) on aluminosilicate glass. This method is very facile because the film is deposited at relatively low temperatures and at atmospheric pressures. Also, this method enables an easy in-line continuous mass production at a very low costs. Owing to the nano-porous characteristics of the nano-rod film, this type of film can be applied as an optical property modulation layers for OLED and thin film solar cell substrate. In this study, we have examined the formation mechanism of nanorod tin oxide and nanorod fluorine doped tin oxides. The nanorod was formed between the temperatures 500 ~ 600^{o}C when the chamber atmosphere was well maintained using controlled atmospheric gas. The nanorod was formed by self-catalyzed tip growth mechanism. The tip of the nanorod was changed its shape when they were annealed under air atmosphere. This shape change does mean that the equilibrium surface the tip have been changed during air-annealing, which implies that the crystalline nature of the tip was not the same of the nanorod column. Also, we have investigated the optical properties of the nano-rod films deposited using nano-aerosol spray pyrolysis deposition methods. When the nano-rod film thickness was controlled well below several hundred nanometers they showed an increased visible light transmission as compared to the uncoated glass substrates, which encourages us to apply these nanorod films as an optical modulation layers of OLED lightings and photovoltaic cells.

FU-I01

Pure Mg^{2+} Ion Conducting Solid Electrolyte Having NASICON-type Structure

Nobuhito IMANAKA*, Megumi YAMANE, Shinji TAMURA
[1]Department of Applied Chemistry, Faculty of Engineering, Osaka University, Suita, Osaka, 565-0871, Japan

Keywords: Magnesium ion, Solid electrolyte, Ion conduction, NASICON

Divalent Mg^{2+} ion highly-conducting solid electrolytes having the NASICON-type structure, $(Mg_xHf_{1-x})_{4/4-2x}Nb(PO_4)_3$ solids, were developed and their ion conducting properties were studied. Among the samples, the $(Mg_{0.1}Hf_{0.9})_{4/3.8}Nb(PO_4)_3$ solid showed the highest ion conductivity of 1.2×10^{-4} S/cm at 600 °C and the conductivities below 400 °C were higher than those for the Mg^{2+} ion conducting $Mg_{0.7}(Zr_{0.85}Nb_{0.15})_4P_6O_{24}$ solid which has been reported to be the solid showing the highest Mg^{2+} ion conductivity. From dc and ac conductivity measurements in a wide range of oxygen partial pressure region, it was clarified that the present solid possess the cationic transference number over 0.99. Moreover, since the quantitative Mg^{2+} ion migration in the $(Mg_{0.1}Hf_{0.9})_{4/3.8}Nb(PO_4)_3$ solid was successfully demonstrated not only by the dc electrolysis method but also by the modified Tubandt electrolysis method, the present NASICON-type $(Mg_{0.1}Hf_{0.9})_{4/3.8}Nb(PO_4)_3$ solid is demonstrated to be the novel type of pure Mg^{2+} ion conducting solid electrolyte with a reasonably high ion conductivity.

FU-I02

Solid Oxide Electrolysis Cell (SOEC) Technology for Hydrogen Production

Kyung Joong Yoon*, Jongsup Hong, Hyoungchul Kim, Hae-Ryoung Kim,
Ji-Won Son, Jong-Ho Lee, Byung-Kook Kim, Hae-June Je
High Temperature Energy Materials Research Center, Korea Institute of Science and Technology,
Seoul 136-791, Korea

Keywords: Solid Oxide Electrolysis Cell, Hydrogen, Electrolyte, Electrode, Catalyst

Solid oxide electrolysis cells (SOECs) represent one of the most efficient and environmentally clean technologies for conversion of steam into hydrogen, especially when utilizing excess electricity and heat supplied from renewable energy sources, nuclear power plants or high-temperature industrial processes. The overall reaction of SOEC for steam electrolysis is the reverse of solid oxide fuel cell (SOFC) reaction, and, in principle, the identical cell can operate as both SOFC and SOEC. However, two operating modes differ in the electric potential gradient, gas environment and heat requirement, which significantly affect the performance and long-term stability. In general, dedicated SOFCs exhibit inferior performance and stability in electrolysis mode, which emphasizes the importance of material development and microstructural optimization for SOEC operation.

In this research, degradation mechanism of the air electrode was investigated through the electrochemical and microstructural investigations. The main cause of degradation and failure was found to be the cation migration occurring in the perovskite electrode due to oxygen partial pressure change and externally applied electric field. Cation migration was suppressed by employing mixed ionic- and electronic- conducting electrode materials which has no oxygen excess nonstoichiometry in the SOEC operating conditions. The rate limiting process for oxygen evolution reaction was identified to be the chemical surface exchange, and the electrochemical performance of the air electrode was significantly improved by incorporation of nano-catalysts into the porous scaffold. In addition, the performance of an SOEC was strongly influenced by the gas diffusion limitation at the fuel electrode. Transport model was developed to understand the transport phenomena of SOECs, and the hydrogen production rate was improved by a factor of greater than two by increasing the porosity and optimization of the pore distribution. The 200 W-class stack was successfully configured, and stable operation was confirmed at a thermal neutral voltage for over 1000 hours.

FU-I03

Lithium-Excess High-Capacity Electrode Materials with 4d-Transition Metals for Rechargeable Lithium Batteries

Naoaki YABUUCHI[1]
[1]*Department of Green and Sustainable Chemistry, Tokyo 120-8551, Japan*

Keywords: Lithium batteries, 4d-transition metals, oxide ions

In the past three decades, intensive research efforts have been made to explore new positive electrode materials for rechargeable lithium batteries. Lithium-excess manganese oxides, Li_2MnO_3, and their solid solution phases with $LiMeO_2$ (Me = Co, Ni, Mn etc.) have recently attracted interest as high-capacity electrode materials. It has been proposed that the large reversible capacity partly originates from the participation of oxide ions in the crystal lattice in redox reaction.[1,2] The use of analogy is anticipated to be the important strategy to design new high-capacity electrode materials.

In this study, lithium niobium oxide, Li_3NbO_4, which is classified as a cation ordered rocksalt structure with a cubic-close packed (ccp) oxygen array similar to Li_2MnO_3, is targeted as a potential new end-member for high-capacity electrode materials. Framework structure of Li_3NbO_4 consists of Nb_6O_{14} clusters, which further form a body-centered cubic lattice, and lithium ions are located at remaining octahedral sites. Since Li_3NbO_4 is an electrical insulator, transition metals are partly substituted for Li^+ and Nb^{5+}. After several trials, it is found that Co^{2+}, Ni^{2+}, Fe^{3+}, and Mn^{3+} are substituted for Li^+ and Nb^{5+}.[3] Such transition metal substitution is achieved in the series of Li_3NbO_4-MeO (Ni^{2+} and Co^{2+}) and Li_3NbO_4-$LiMeO_2$ (Fe^{3+} and Mn^{3+}) systems with the common ccp oxygen lattice. The metal substitution influences the clustering of niobium in the ccp oxygen array, leading to the formation of cation disordered rocksalt phases. In general, well-crystallized cation disordered rocksalt phases are known to be electrochemically inactive. Nevertheless, a manganese-substituted sample ($0.43Li_3NbO_4$–$0.57LiMnO_2$ or $Li_{1.3}Nb_{0.3}Mn_{0.4}O_2$ as a layered formulation) shows large reversible capacity with small initial irreversible capacity at 60 ^oC.[3] Initial charge/discharge capacity reaches 300 mAh g^{-1}, which is clearly larger than that of the expected capacity (118 mAh g^{-1}) based on the Mn^{3+}/Mn^{4+} redox reaction. Therefore, the charge compensation is expected to be achieved by the contribution of oxide ions in the crystal lattice, similar to Li_2MnO_3-based materials which is further supported by first-principles calculation and hard/soft X-ray absorption spectroscopy.[3]

In addition to Li_3NbO_4, lithium molybdenum (VI) oxide, which is also classified as the cation ordered rocksalt structure with the ccp oxygen array, has been studied as a new host structure for high-capacity positive electrode materials. From these results, we will discuss the possibility of new series of lithium-excess electrode materials containing 4d-transition metal ions with high oxidation states.

References

[1] T. Ohzuku et al., J. Mater. Chem., 21, 10179 (2011).
[2] M. Sathiya et al., Chem. Mater., 25, 1121 (2013).
[3] N. Yabuuchi et al., submitted

Acknowledgement

This study was partly supported by the ALCA project of the Japan Science and Technology Agency.

FU-I04

All-solid-state lithium ion battery by utilizing oxide-based solid electrolyte

Byoungwoo Kang
Department of Materials Science and Engineering at POSTECH, San31, Hyoja-Dong, Pohang, 790-784, Republic of Korea

Our society faces energy challenges which are caused by the burning of fossil fuel. As a result, we face serious climate change. To address these challenges, fossil fuel's energy paradigm should be transformed into sustainable one through further utilizing renewable sources like solar power and wind. However, intermittent property and low quality of renewable sources make their utilization difficult. Energy storage technologies can be a key player for transforming fossil fuels energy paradigm into sustainable energy one by extending the utilization of renewable sources like wind and solar power and by utilizing electric vehicles. Among other technologies, lithium ion batteries are the most promising technology because of their high energy density and wide range of energy spectra coverage. However, the advent of novel applications such as energy storage system for renewable sources and electric vehicles makes present LIB technologies challengeable because these large-scale applications need much demanding requirements than those in portable devices in terms of safety, cost, and cycle life. There are several approaches for solving these demanding requirements of novel applications. One of promising approaches is the change of the electrolyte from liquid electrolyte to solid electrolyte. The change of the electrolyte can bring up several opportunities. For example, solid electrolytes have large stable electrochemical window which can allow us to utilize known materials with high voltage resulting in high energy density without causing any safety problem. In this talk, I will discuss about all solid-state lithium ion battery that is built in the lab.

FU-I05

Preparation and Characterization of Fast Ion Conducting Solid State Electrolytes for the Solid State Li-ion Battery

Inseok Seo[1], Steve W. Martin[2]*
[1]*Research Institute of Industrial Science & Technology, POSCO Global R&D Center 180-1 Songdo-Dong, Yeonsu-Gu, Incheon 406-840, Korea*
[2]*Department of Materials Science and Engineering, Iowa State University 2220 Hoover Hall Ames IA 50011*

In this study, I will describe my research on two types of solid state electrolytes; amorphous lithium thio-germanate thin-films and solid state bulk electrolytes. While the thin film electrolytes, Li_2S + GeS_2, were prepared by RF sputtering deposition, the solid state bulk electrolytes, Li_2S + P_2S_5, were produced by mechanical milling. For the first time, new high quality lithium germanium sulfide thin-films have been successfully made by RF sputtering and synthesized as new solid state electrolytes. The maximum ionic conductivities of the two types solid state electrolytes are over ~10^{-3} (S/cm). The ionic conductivities of the thin-films and bulk electrolytes are ~three order of magnitudes higher than reported values for oxide electrolytes which have been used in commercial products. Although these materials are unstable in air the thin-films and bulk electroyltes were thoroughly characterized by XRD, Raman, SEM, XPS, and impedance spectroscopy using special setups to prevent contamination. In this way, this work may provide a new way for developing new thin-film electrolytes for solid state lithium ion batteries.

FU-I06

Solid Oxide Fuel Cells based on the Low Temperature Ceramic Coating Process

Jong-Jin Choi, Dong-Soo Park
Functional Ceramics Department, Korea Institute of Materials Science, Changwon, Gyeongnam, 642-831, Korea

Keywords: SOFCs, Aerosol Deposition, MSC

Aerosol deposition (AD) is a promising process for preparation of SOFC cells and stacks' component because it has low processing temperature to minimize the adverse interfacial reactions during cell production and flexibility of microstructure modification from gas-tight dense structure to porous structure with nano-scaled composites on various anode structure including porous metal support. Since 2007, our group has been working on development of AD process for SOFC application including nano-structured electrolytes and cathodes coatings [1-3], diffusion barrier layer preparation for large-area cells up to 40 x 25 cm^2 [4], oxidation resistive layer fabrication for metallic interconnects [5,6], and robust and high performance metal-supported SOFCs fabrication on porous FeCr alloy support [7]. This presentation will sum-up those research results and gives our up-to-date results and a prospect.

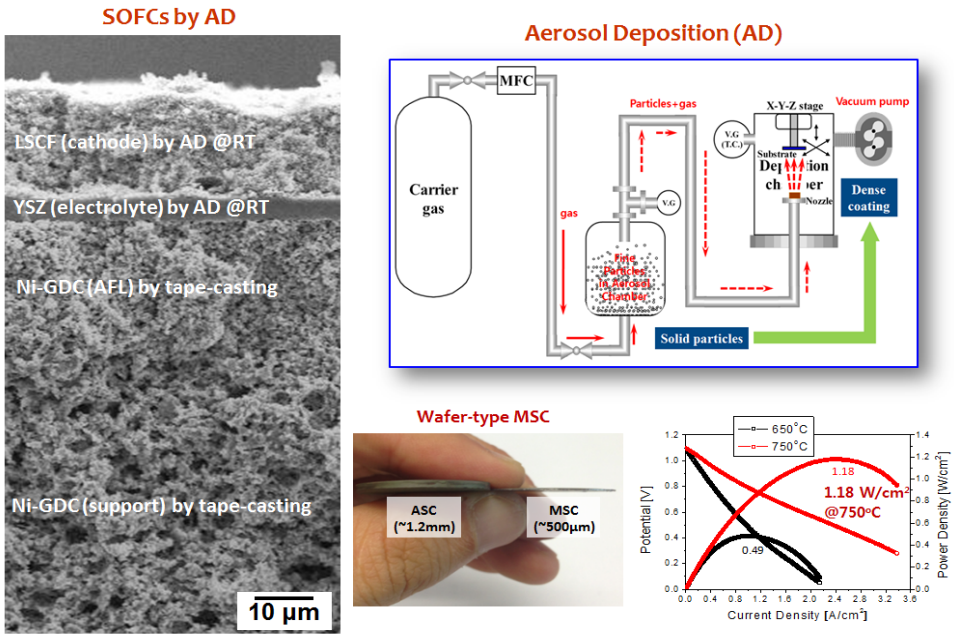

Fig. SEM Microstructure and I-V/I-P plots of SOFCs prepared by AD

References:

[1] J.-J. Choi *et. al. J. Eur. Ceram. Soc.* 2012, 32, 3249.
[2] J.-J. Choi *et. al. Int. J. Hydrogen Energy* 2012, 37 6830.
[3] J.-J. Choi *et. al. J. Alloy. Compd.* 2011, 509, 2627.
[4] J.-J. Choi *et. al. Int. J. Hydrogen Energy* 2012, 37 9809.
[5] J.-J. Choi *et. al. J. Am. Ceram. Soc.* 2007, 90, 1926.
[6] J.-J. Choi *et. al. J. Mater. Sci.* 2009, 44, 843.
[7] J.-J. Choi *et. al. Int. J. Hydrogen Energy* 2014, 39, I2878

EL-I01

Effect of Processing Method on Low-temperature Crystallization of Ion-conductive Cubic $Li_7La_3Zr_2O_{12}$ Nanoparticles

Hisao SUZUKI [1]*, Mamoru SENNA[1, 2], Naonori SAKAMOTO[1], Naoki WAKIYA[1],
[1] *Research Institute of Electronics, Shizuoka University, Hamamatsu, Shizuoka 432-8561, Japan*
[2] *Keio University, Kohoku-ku Hiyoshi 4-1-1, Yokohama, Kanagawa 223-8521, Japan*

Keywords: Cubic $Li_7La_3Zr_2O_{12}$, Nanopowders, Sol-Gel Method, In-situ Precipitation Method., Solid-Liquid Reaction Method

In this study, ion-conductive cubic $Li_7La_3Zr_2O_{12}$ nanoparticles with garnet structure were successfully prepared from molecular-designed precursor at low temperature of 700 ºC. The crystalline phases and the crystallization temperatures for the powders derived from different precursors which were prepared by the solid-liquid reaction method, In-situ precipitation method and sol-gel method, respectively. In addition, we designed the molecular structure of the alkoxide-derived precursors in the sol-gel method. As a result, homogeneity of the precursors was totally different depending on the processing method and the conditions of each preparation method. In the solid-liquid reaction method, zirconia powders were reacted with the liquid phase of ethanol with Li and La acetate. In this case, we need Al addition to obtain cubic $Li_7La_3Zr_2O_{12}$ nanoparticles at 800ºC. On the other hand, homogeneity of the precursor should be high enough to obtain cubic $Li_7La_3Zr_2O_{12}$ nanoparticles without addition of Al at 800ºC because we prepared very fine zirconia sol by the careful hydrolysis of the zirconium-oxychloride. Compared with the above two method, homogeneous precursor at molecular-level could be prepared by the sol-gel method if the partial hydrolysis condition of the zirconium alkoxide were optimized for the low-temperature crystallization. As a result, we concluded that the sol-gel method is the powerful tool to prepare homogeneous precursor for the low-temperature crystallization, in which molecular structure was properly designed.

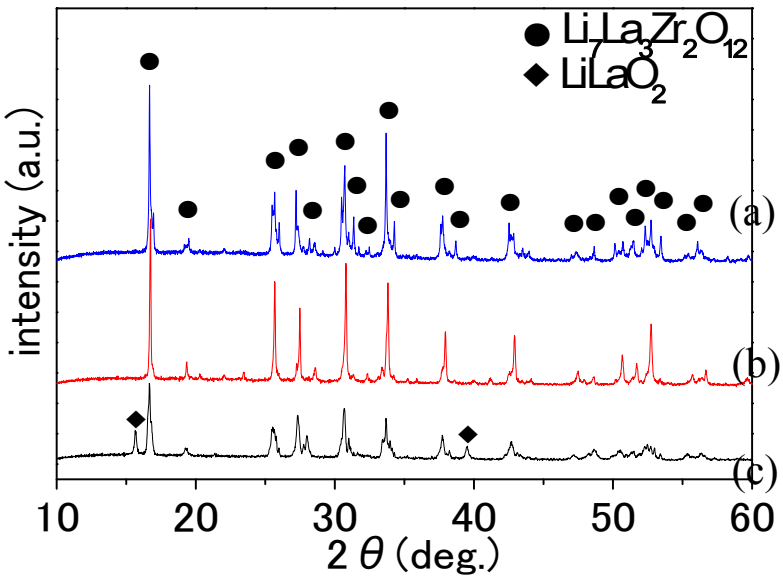

Fig.1 XRD Patterns for calcined powders from (a) molecular-designed precursor at 700 ºC, (b) molecular-designed precursor at 800 ºC, and (c) mixed precursor at 800 ºC, in the sol-gel method.

EL-I02

Dielectric Relaxation in $BiFeO_3$-based Ceramics

Chae Il CHEON[1,2*], Jin Hong CHOI[2], Jeong Seog KIM[2], Wook JO[3*]
[1]*Department of Materials Science & Engineering and* [2]*Department of Semiconductor & Display Engineering, Hoseo University, Asan, Chungnam 336-795 Korea*
[3] *Ulsan National Institute of Science and Technology, Ulsan 689-798, Korea*

Keywords: Dielectric Relaxation, $BiFeO_3$, Relaxor, Ferroelectric, Phase Transition

Bismuth ferrite, $BiFeO_3$ (BF) has attracted many researchers' attention due to its very high Curie temperature (830°C), large polarization (~100 μC/cm^2), and multiferroic properties. However, difficulty in preparation of a single phase by a ceramic process and a large coercive field of above 10 kV/mm restrict its applications. BF-based solid solutions have been proposed for solving these problems. $BaTiO_3$ (BT) and $(Bi,K)TiO_3$ (BKT) with a tetragonal structure (P4mm) could be the proper end-member which makes a solid solution with BF of rhombohedral structure (R3c). It has been reported that the crystal structure of a BF-based solid solution changes from a rhombohedral (R3c) to a pseudocubic with the increase in a BT or BKT content at around 0.3 BT and 0.4 BKT, respectively. BF-BT and BF-BKT ceramics around the phase boundary are known to show outstanding ferroelectric and piezoelectric properties such as a large remanent polarization of about 50 μC/cm^2 and a moderate electro-mechanical coupling factor (k_{33}) of 0.3 ~ 0.35 with temperature stability up to 300°C. However, there is a large variance among temperature-dependent dielectric properties reported in literatures. Relaxor-like dielectric properties, i.e., broad dielectric maximum with frequency dispersion, have been observed in the pseudocubic composition range and claimed to originate from nanosized polar domains. And a Maxwell-Wagner type dielectric relaxation was also observed in a BF-BKT ceramic. These dielectric relaxations due to relaxor ferroelectric phase transitions and extrinsic effects make a definite understanding on the temperature-dependent dielectric behavior difficult in $BiFeO_3$–based ceramics. Therefore, the phase transitions and the related dielectric behaviors are not clearly revealed yet.

In this work, the relaxor-like dielectric behavior was investigated in BF-BKT ceramics with metrically cubic compositions (0.4 ~ 0.8 BKT). Dielectric constant and the corresponding loss factor were measured in the temperature range of RT to 650°C at various frequencies. Two kinds of dielectric relaxations were observed; one at 200 ~ 300°C and the other at 300 ~ 600°C. Impedance spectroscopy was utilized for understanding the origins of the relaxations. The temperature-dependent dielectric properties of BF-BKT ceramics will be compared with the reported results for $BiFeO_3$-based ceramics in literatures.

EL-I03

Investigation of the interaction between the dispersant molecule and the surface of $BaCO_3$ particle

Koichiro TSUZUKU[1], Takeshi YAMANOBE[1]
[1]*Faculty of Science and Technology, Gunma University, Kiryu-shi, Gunma 376-8515, Japan*

Keywords: $BaCO_3$, Poly-carboxylic acid, Solis-state synthesis, ^{1}H-NMR

Introduction

Electro-ceramics synthesized with various methods. Solid-state reaction method is applying widely to not only electro-ceramics but also other fine-ceramics. In the case of preparation of electro-ceramics such as $BaTiO_3$ by solid-state reaction method, quality of resultant products is affected by size of raw materials, homogeneity of dispersion, condition of synthesis process, etc. For example of synthesis of 100nm BaTiO3 by solid-state reaction, several nm $BaCO_3$ and TiO_2 should be dispersed and mixed with uniformly. Normally small size particle are generally formed agglomeration because its higher surface energy. Dispersant such as poly-carboxylic acid is being used to disperse fine raw materials powder. Agglomeration of particles was prevented by electro-chemically and/or physically effects by adsorption of dispersant molecules at surface of each particle. The surface condition of different kind of particles is not same and resultant adsorption condition is also not same. Therefore choice of appropriate dispersant is one of important point to synthesize homogeneous products. However, adsorption state of dispersant molecules at surface of certain particles produced by different manufacturer was not enough investigated.

Result and discussion

Seven kinds of different $BaCO_3$ powder (reagent: R, four products of company S: S-1, S-2, S-3, S-4, two products of company N: N-1, N-2) were used. Ammonium citrate: AC was used as dispersant. Sample slurry was prepared by conventional wet mixing process. Clear parts obtained from centrifuged slurry were analyzed with 300MHz ^{1}H-NMR spectrometer. The interaction between the dispersant molecule and the surface of particle has been estimated from the width of split of -CH_2 quartet peak on ^{1}H-NMR spectra.

Spin coupling constant: J and chemical shift: Δδ calculated from obtained spectra were shown in Fig. 1. J-values obtained from different $BaCO_3$ products were almost same, however Δδ were different. This result is probably indicating that different $BaCO_3$ products have different surface properties. Furthermore, SSA of the samples S-4 and N-2 were almost same, but Δδ of N-2 was larger than S-4. Interaction at the surface of N-2 powder seems to be stronger than that of S-4.

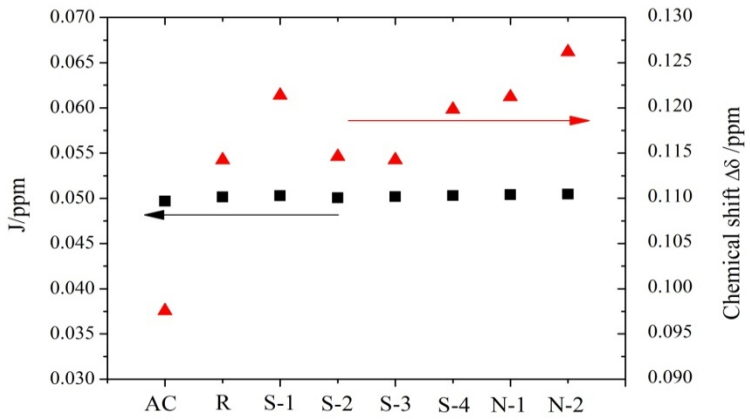

Figure 5 J-values and Δδ calculated from 1H-NMR spectra

EL-I04

Preparation of Bismuth Gallium Iron Garnet on glass substrate by MOD technique

Nobuyasu ADACHI*, Saeko FUJIUCHI, Yusaku KIBA, Toshitaka Ota
Advanced Ceramic Research Center, Nagoya Institute of Technology, Tajimi 507-0071, Japan

Keywords: Magnetic garnet, MO effect, glass substrate, MOD technique

In order to prepare the magneto-optical (MO) devices on glass substrate, the $Bi_3Fe_{5-x}Ga_xO_{12}$ (BIGG) films were prepared on glass substrate by metal organic decomposition (MOD) technique. The MO device on glass substrate has a great advantage for the commercial use of magnetic imaging sensor, waveguide devices with magneto-static waves (MSW) and MO effect and integrated MSW-MO devices. Originally, the $Bi_3Fe_5O_{12}$ (BIG) or BIGG cannot be grown on glass but for single crystal garnet substrate. In order to crystallize on glass substrate, the buffer layers with garnet structure were inserted. For the buffer layer, several composition ratios such as $Bi_1Y_2Fe_5O_{12}$, $Bi_1Nd_2Fe_5O_{12}$ and $Nd_1Y_2Fe_5O_{12}$ were compared each other. The buffer layers were crystallized with garnet structures on glass substrate only by annealing process more than 650 degree C. The metal organic solutions for the BIG and the BIGG were spin-coated on the buffer layer, then dried at 100 degree C and pre-annealed at 400 degree C. These processes were repeated 10 times. Finally, the BIG and BIGG films were crystallized by annealing at 480 degree C. The Faraday rotations of the BIG films with 10 times coating showed the largest values for the case of $Nd_1Y_2Fe_5O_{12}$ buffer layer and this value is almost the same as the film on GGG substrate. The lattice parameter of $Bi_1Nd_2Fe_5O_{12}$ is the most close to the BIG, however the island grain structure was observed for the buffer layer surface. For the case of the $Nd_1Y_2Fe_5O_{12}$, the surface structure was smooth which suggest 2 dimensional crystal growth of the buffer layer. For the optimization of the composition of the buffer layer, both the small lattice mismatch and the smooth surface maybe important in order to achieve the best MO performance of the BIG film. The Ga-substituted BIG films were also prepared by the same procedure. With decreasing the Ga substitution, the Faraday rotation decreased sharply. The substitution on the Fe^{3+} site seemed be biased on the tetragonal Fe^{3+} sites which caused the net magnetization of this system. These behaviors could be also observed for the BIGG films on GGG single crystal substrates [1].

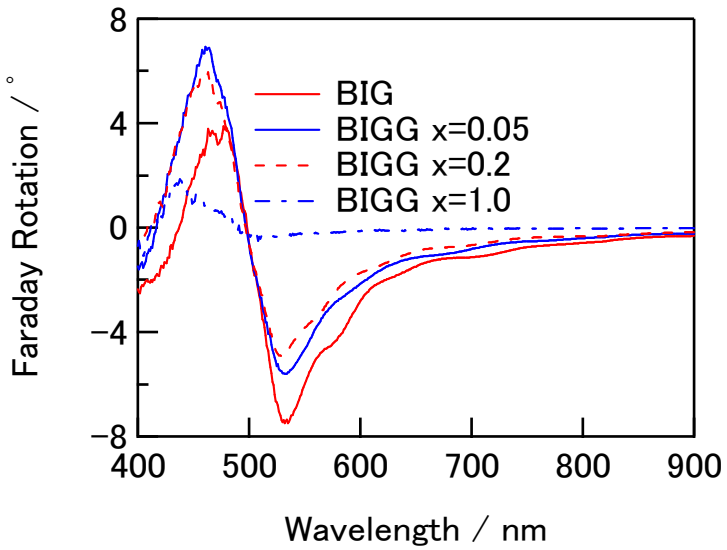

Fig.6 Faraday spectra of BIG and BIGG /NfYIG/ glass substrate

References:

[1] N. Adachi, K. Yogo, T. Ota, M. Takahashi, K. Ishiyama: J. Appl. Phys. 109(7) 07A506 (2011).

EL-I05

Thin film Electrodes for All-solid-state Microbatteries

Ji-Won Choi[1,2] and Haena Yim[1]

[1] *Electronic Materials Research Center, Korea Institute of Science and Technology (KIST), Seoul 136-890, Korea*

[2] *Department of Nanomaterials Science and Technology, University of Science and Technology, Seoul, Korea*

The requirement of advanced thin film lithium batteries have been steady increased as increasing the development of wearable, flexible and soft electronic devices such as smart cards, bio-sensors, various bio-applications, and roll-up displays. Therefore, we have been studying on various types of advanced thin film batteries such as transparent, high-capacity, and flexible batteries. Especially, the cathode electrode thin film play an important role in thin film battery systems in respect that it limits capacity and power density. Thus, we have researched new types of cathode materials, various types of 3D structured cathode thin films, and low temperature annealed cathode thin film which can be applied on flexible substrate.

In this presentation, part 1 focuses on introducing new synthesized cathode thin films and 3D structured cathode thin films such as hemisphere and nano-rod. Part 2 will be presented with subject that fabrication method of flexible all-solid-state thin film lithium battery using low temperature annealed $LiNi_{0.5}Mn_{1.5}O_4$ cathode, LiPON electrolyte, and Li-metal anode thin film on polyimide (PI) substrate. In both parts, the structural properties of the thin films were investigated by X-ray diffraction (XRD) and scanning electron microscopy (SEM). The electrochemical properties were measured using impedance analyzer and WBC3000 battery cycler. The results of this study show the applicability of all-solid-state microbatteries as the promising next-generation miniaturized power source in micro-devices.

EL-I06

Preparation of the Sol-gel derived Metal Oxide Electrode

Tomoya OHNO[1]*, Takeshi MATSUDA[1], Naonori SAKAMOTO[2], Naoki WAKIYA[2], Hisao SUZUKI[2]

[1]*Department of Materials Science and Engineering, Kitami Institute of Technology, Kitami, Hokkaido 090-8507, Japan*

[2]*Graduate School of Science and Technology, Shizuoka University, Hamamatsu, Shizuoka 432-8561, Japan*

Keywords: Metal Oxide Electrode, Chemical Solution Deposition, Thin Film

Metal oxide conductors, such as $LaNiO_3$ (LNO), $La(Sr,Co)O_3$ (LSCO) and $La(Sr,Mn)O_3$ (LSMO) have been studied for the electrode of the fuel cell unit and the various electronic devices. In many cases, the thin films of these conductive materials have been deposited on a substrate by chemical vapor deposition (CVD) such as a sputtering technique [1][2]. For the wide application of these conductive oxide thin films, our research group have attempted to prepare these conductive materials by cost effective chemical solution deposition (CSD) with low processing temperatures.

In the case of CSD, the numerous experimental parameters should be optimized to prepare the materials with excellent properties. In this study, we clarified the effect of the processing parameters such as a starting reagents, experimental conditions, and the substrate on the electrical properties of these conductive materials. For example, lanthanum nitrate, metal strontium and cobalt acetate were selected as starting reagents, and 2-methoxy ethanol and 1,3-butanediol were selected as solvents for LSCO precursor solution.

Figure 1 shows the XRD patterns for the CSD derived LSCO electrode on various substrates. In the case of LSCO layer on a LNO with a-axis preferred orientation, the LSCO layer also exhibited a-axis preferred orientation whereas the randomly orientated LSCO layer was obtained on a Si wafer. The electrical conductivity of the resulting LSCO/LNO layers on a Si wafer increased up to 3.6 x 10^{-2} Ωcm^{-1} depending on the layer thickness.

In addition, we also deposited the piezoelectric materials on the obtained metal oxide electrode, and the electrical properties of the piezoelectric thin film was estimated. As a result, the obtained metal oxide conductive layers were successfully acted as a electrode, and the obtained electrical properties (such as dielectric, ferroelectric and piezoelectric properties) was enhanced compare with that on a conventional metal electrode such as a platinum electrode. Other properties will be exhibited in the presentation.

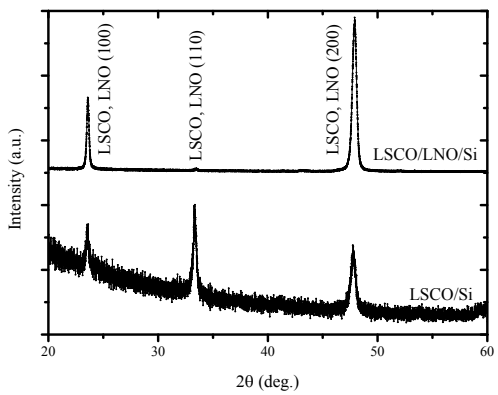

Figure 7 XRD patterns of the LSCO electrode on various substrates

References:

[1] W. Zhang, L. Kang, M. Yuan, Q. Yang and J. Ouyang, J. Alloys and Compounds 580 (2013) 363.
[2] C. B. Samantaray, A. Dhar, D. Bhattacharya, S. K. Ray, Mater. Sci. Eng. B88 (2002) 14.

EL-I07

AC characterization of electroceramics: Issues and way out

Jong-Sook Lee*
School of Materials Science and Engineering, Gwangju, 500-757, Korea

Keywords: parametric analysis, constant phase elements, Cole-Davidson dielectric function

AC characterization technique is an indispensable tool for electroceramic materials, both conducting and dielectric, and for devices comprising them [1-7]. Although the technique is widely applied and getting ever popular, the information therefrom is so far much limited and often disputable. Full parametric analysis based on physical models can provide an unambiguous set of material and device properties. A choice from conventional models such as a brick-layer (Voigt) model and a Debye (Maxwell) model is not generally straightforward, however. Often, the distinction between the ceramic dielectrics and poor (ionic and/or electronic) ceramic conductors is blurred. The electrical roles of the grain boundaries/interfaces and electrodes are multifaceted: constriction, space-charge effects, selectively blocking. Commonly observed dispersive responses are difficult to describe even by employing constant phase elements (CPEs) as generalized capacitors, which arbitrarily adjustable frequency dependence. Frequency-dependent CPEs cannot provide the physical interpretation of capacitance effects. The mono-frequency capacitance analyses typically used for the temperature- or bias-dependence suffer similarly from the frequency-dependent capacitances. In fact, despite strong frequency dispersion in impedance and admittance response, well-defined capacitance effects are indicated in the AC behaviors of a variety of electroceramics. They can be successfully described by employing Cole-Cole or Cole-Davidson dielectric functions, connected in parallel or in ladder network, with the characteristic relaxation times (τ) thermally activated similarly as the bulk conduction and with temperature-independent, constant exponents (γ). The AC response of the electroceramics can be thus simulated as a function of frequency and temperature [1]. It is suggested that "R"-centered impedance spectroscopy should be shifted to "C" spectroscopy with capacitance parameters, which are less affected by the connectivity and inhomogeneity than resistance parameters.

References:

[1] J.-H. Kim et al. Solid State Ionics, 264 (2014) 22
[2] D. T. Nguyen et al. Int. J. Hydrogen Energy (2014) DOI 10.1016/j.ijhydene.2014.07.010
[3] J. Moon et al., Phys. Chem. Chem. Phys. 15 (2013) 9361
[4] E.-C. Shin et al., Solid State Ionics 232 (2013) 80
[5] P.-A. Ahn et al., Fuel Cells 12 (2012) 1070
[6] Y. Kim et al., J. Mater. Chem. 21 (2011) 2940
[7] J.-S. Lee et al., Solid State Ionics 68 (1994) 139; J. Electrochem. Soc. 142 (1995) 1169; Solid State Ionics, 98 (1997) 15; J. Electrochem. Soc., 147, (2000) 2407; J. Mater. Res. 16 (2001) 2739; J. Mater. Res. 19, 864-871 (2004); J. Mater. Res. 20 (2005) 2101; Monat. Chem., 140 (2009) 1113; Appl. Phys. Lett. 96 (2010) 202104

Acknowledgement:

Fundamental R&D Program for Core Technology of Materials funded by the Ministry of Knowledge Economy, Energy Efficiency & Resources Core Technology program (20122010100110 of KETEP granted financial resource from the Ministry of Trade, Industry & Energy, World Class University (WCU) program (R32-2009-000-20074-0) & Fusion Research Program for Green Technologies (2011-0019304), Basic Science Research Program (KRF-2007-412-J02002) through NRF funded by the Ministry of Science, ICT & Future Planning, Republic of Korea, and KIMS Internal Program "Development of Advanced Powder Materials Technology for New Growth Engine and Its Transfer to Industry."

EL-I08

Thermally Stimulated Depolarization Current Analysis for the Dielectric Phenomena of $BaTiO_3$-based Multi Layer Ceramic Capacitor

Seok-Hyun Yoon, Jae-Sung Park, Chang-Hoon Kim, and Doo-Young Kim
LCR R&D Group, LCR Division, Samsung Electro-Mechanics Co. Ltd.
314, Maetan3-Dong, Yeongtong-Gu, Suwon, Gyunggi-Do, 443-743, Korea

Thermally stimulated depolarization current (TSDC) can provide information about defect-related phenomena such as defect dipole, charge trapping/detrapping, and space charge *etc.*. In this study the dielectric aging and I (Current)-V (Voltage) characteristics of $BaTiO_3$-based multi-layer ceramic capacitors were investigated utilizing TSDC analysis. The increase of Mn concentration significantly increased the aging rate. TSDC of low Mn concentration specimen showed one peak, whereas Mn-increased specimen showed two peaks. The first and second peak is supposed to be caused by the phase transition of the undoped core-region and the defect dipole Mn such as Mn_{Ti}''-$V_O^{\bullet\bullet}$ or Mn_{Ti}'-$V_O^{\bullet\bullet}$, respectively. On the other hand, the increase of Dy concentration in the Dy and Mn-codoped $BaTiO_3$ system significantly decreased the aging rate, and caused a disappearance of the thermally stimulated depolarization current (TSDC) peak associated with the defect dipole of Mn such as Mn_{Ti}''-$V_O^{\bullet\bullet}$ or Mn_{Ti}'-$V_O^{\bullet\bullet}$ which was observed in low Dy-concentration specimen. These results experimentally demonstrate that the dielectric aging is controlled by the defect dipoles, and that the rare earth element, Dy, decreases their concentration, and thereby the dielectric aging is reduced. In the I (Current)-V (Voltage) characteristics of Mn-doped $BaTiO_3$ system, the increase of Mn concentration reduced the slope of current increase with increasing dc field, and enhanced the dc field to the abrupt increase of current and thereby breakdown. A peak of thermally stimulated depolarization current (TSDC) beyond 300°C associated with trapped space charges appeared, which increased by the increase of Mn concentration. In addition, the peak intensity increased to a maximum value and then decreased again with increasing polarization dc field in TSDC measurement. Its activation energies were around 1.9 eV for all specimens, which is very close to the energy level for the ionization of Mn^{3+}/Mn^{2+}. These results experimentally demonstrate the role of the variable valence acceptor Mn as trapping center for injected charges, and the occurrence of field enhanced trap charge release, and therefore, the conduction mechanism can be described by the SCL model incorporating the Poole-Frenkel effect.

ST-I01

Effect of Additive Composition on Thermal Conductivity of Liquid-Phase Sintered Silicon Carbide Ceramics

Young-Wook Kim*
Functional Ceramics Laboratory, Department of Materials Science and Engineering, University of Seoul, Seoul 130-743, Republic of Korea

Keywords: SiC, Hot-pressing, Thermal conductivity, Additive composition

Silicon carbide (SiC) is an important structural material due to its excellent wear resistance, corrosion resistance, oxidation resistance, and mechanical properties [1,2]. Various industrial applications of SiC ceramics such as substrate materials for semiconductor devices, heater and heater plates for semiconductor processing, and capsule materials for nuclear fuels take advantage of its excellent thermal conductivity as well as its other excellent properties.

One opportunity for further improvement in the thermal conductivity of SiC ceramics is the judicious selection of sintering additives. The objective of the present study is to investigate new, environmentally benign additive systems for improving the thermal conductivity of liquid-phase sintered (LPS)-SiC ceramics. In this paper, the followings has been investigated and suggested: (1) the influence of additive composition on the thermal conductivity of LPS-SiC using RE_2O_3 additives (RE=Y, La, Nd, Sm, Gd); (2) the effect of initial α-phase content on the thermal conductivity of LPS-SiC ceramics using Y_2O_3-Sc_2O_3 additives; (3) the factors that reduce the thermal conductivity of SiC ceramics; and (4) the potential strategies for achieving high thermal conductivity in LPS-SiC ceramics [3]. Fig. 1 shows typical microstructure of a LPS-SiC ceramic with a thermal conductivity of 234 W/m·K.

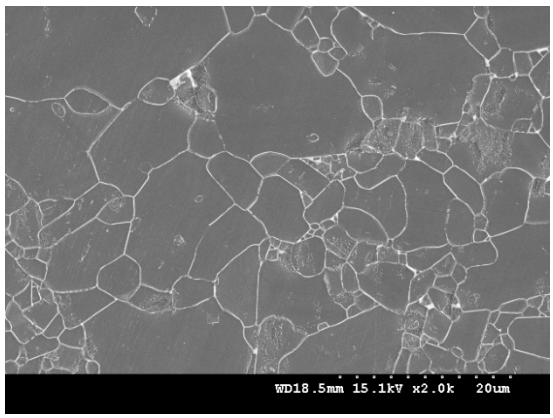

Figure 8. Typical microstructure of the SiC specimen sintered with Y_2O_3-Sc_2O_3 additives

References:

[1] Y.W. Kim, Y.S. Chun, T. Nishimura, M. Mitomo, and Y.H. Lee, Acta Mater. 55 (2007) 727.
[2] K.Y. Lim, Y.W. Kim, T. Nishimura, and W.S. Seo, J. Eur. Ceram. Soc. 33 (2013) 345.
[3] Y.W. Kim, K.Y. Lim, and W.S. Seo, J. Am. Ceram. Soc. 97 (2014) 923.

Acknowledgement:

This research was supported by both a grant from the Fundamental R&D Program for Technology of World Premier Materials (WPM) funded by the Ministry of Trade, Industry and Energy and by the Basic Science Research Program through the National Research Foundation of Korea (NRF) funded by the Ministry of Science, ICT and Future Planning, Republic of Korea (2012R1A2A2A01004284).

ST-I02

Stochastic Model on Granule Collapse during Cold Isostatic Pressing

Kouichi YASUDA[1], Satoshi TANAKA[2], Makio NAITO[1*]
[1]*Department of Metallurgy and Ceramics Science, Tokyo Institute of Technology, Tokyo, 152-8552, Japan*
[2]*Department of Materials Science and Technology, Nagaoka University of Technology, Nagaoka, 940-2188, Japan*

Keywords: Granule, Cold Isostatic Pressing, Stochastic Model, Structural Ceramics

Powder processing with granule is widely used in pharmaceutical, food, and ceramics industries due to its high productivity, and homogeneity of powder compacts has a great influence on its mechanical properties and reliability. As one of effective compaction, cold isostatic pressing (CIP) has been applied to improve the homogeneity of the compacts; however, still there is a change in the local density in the compacts by CIP. The authors proposed a deterministic model in which a concentric multiple shell structure was analyzed by elastic theory to express a stress distribution in the compact during CIP, considering the changes in density and Young's modulus of each shell. In this presentation, the authors step forward to develop a stochastic model on granule collapse during CIP because granule is known to have a stress distribution for collapse. So, we assume that a spherical preform has a continuous distribution of Young's modulus E(r) as a function of radius r, and is compressed by isostatic pressing. The radial displacement $u(r)$ is given by solving the following a derivative equation,

$$\frac{d^2u(r)}{dr^2}+\left\{\frac{2}{r}+\frac{d}{dr}\log E(r)\right\}\frac{du(r)}{dr}-\frac{2}{r}\left\{1-\frac{\upsilon}{1-\upsilon}\frac{d}{dr}\log E(r)\right\}\frac{u(r)}{r}=0 \qquad (1)$$

, where ν is Poisson's ratio. The radial stress $\sigma_r(r)$ is obtained from the displacement as below,

$$\sigma_r(r)=\frac{E(r)}{(1+\nu)(1-2\nu)}\left\{(1-\nu)\frac{du(r)}{dr}+2\nu\frac{u(r)}{r}\right\} \qquad (2)$$

This stress can be normalized by using the applied stress P (viz.CIP pressure) as below,

$$\sigma_r(r)=P\eta(r) \qquad (3)$$

By taking some assumption, the joint probability density function $h(P, r)$ can be expressed by the following equation,

$$h(P,r)=\exp\left[-\left(\frac{V_e}{V_0}\right)\left(\frac{P}{P_0}\right)^m\right]\frac{\partial}{\partial P}\frac{1}{V_0}\left(\frac{P\eta(r)}{P_0}\right)^m \qquad (4)$$

, where m and P_0 are shape and scale parameters of Weibull distribution for granule collapse, and V_e and V_0 are the effective volume and unit volume. The collapse probability can be obtained as a function of applied pressure P and location r by integrating $h(P, r)$ to have a marginal distribution of it.

References:

[1] K.Yasuda et al., *Materials Science and Technology 2006: Processing* (2006) *p*. 495-506.
[2] K.Yasuda, S.Tanaka, and M.Naito, J.Soc.Powder Technol. Japan, 51 (2014) 153-162.

Acknowledgement:

This research was in-part supported by Grant-in-Aid for Scientific Researches (A) (24246108) and (C) (25420706) from Japan Society for the Promotion of Science, and also Joint Research Project of Joining and Welding Research Institute, Osaka University, and also Collaborative Research Project (No.78) of Materials and Structures Laboratory, Tokyo Institute of Technology.

ST-I03

High Temperature Oxidation Kinetics of Ultra-High Temperature Ceramics

Young-Hoon Seong[1, 2], Changyeon Baek[1], and Do Kyung Kim[1, *]
[1] *Department of Materials Science and Engineering, Korea Advanced Institute of Science and Technology (KAIST), 291 Daehak-ro, Yuseong-gu, Daejeon 305-701, Republic of Korea*
[2] *Current address : Korea Institute of Energy Research, Daejeon, 305-343, Republic of Korea*

The oxidation behavior of zirconium boride composites with various SiC contents (0-40 vol%) at 1500 °C in air (pO_2= 10^4 Pa) and under low pO_2 (10^{-8} Pa) was investigated. Due to different oxidation kinetics calculated from the oxidation depths, the oxidized composites exhibited different layered structures. In addition, the composites of ZrB_2-30 vol% SiC (one of the typical compositions) oxidized at 1500 °C for 10 h in air and under low pO_2 conditions were analyzed using TEM (transmission electron microscope). Due to kinetic difference of oxidation behavior, the three layers (surface silica-rich layer, oxide layer, and unreacted layer) were observed over a wide area of specimen in air, while the two layers (oxide layer, and unreacted layer) were observed over a narrow area in specimen under reducing condition. Based on TEM analysis of ZrB_2-SiC composites tested under air and low oxygen partial pressure, the ZrB_2 begin to oxidized preferentially and the SiC was remained without any changes at the interface between oxidized layer and unreacted layer. The high temperature oxidation kinetics of composites also evaluated. In air, the oxidation depth as a function of time indicated a parabolic kinetic behavior, and the ZrB_2-40 vol% SiC composite exhibited the lowest parabolic rate constant (k_P) of 232 m^2/h. Under low pO_2, the oxidation depth as a function of time indicated a parabolic to linear transition kinetic behavior, except for monolithic ZrB_2. The monolithic ZrB_2 exhibited the lowest parabolic rate constant (k_P) of 811m^2/h.

ST-I04

Evaluation of internal defects and their coarsening during sintering in alumina ceramics system

Satoshi TANAKA[1*] Tsuyohi HONDO[1,] Kouichi YASUDA[2]
[1]*Nagaoka Univeristy of Technology, Nagaoka 9402188, Japan*
[2]*Tokyo Institute of Technology, Tokyo 1528552, Japan*

Keywords: Structure, Powder Process, Sintering

The large cracks or coarse defects are present in ceramics if it was prepared by well-controlled processing. By the optical microscopy, coarse defects were observed and their influence was revealed on their characteristics. The size and the number density of coarse defects govern the mechanical properties of ceramics. [1,2] In this study, we examined the development of coarser defects in alumina ceramics by micro-focus x-ray computer tomography (μ-CT) etc.

The origin of coarser defects in ceramics was examined by evaluation of the powder compact. First, we observed the internal structures by the liquid immersion method with the optical microscope. Then we observed the powder compact with μ-CT. There were low packing regions originated from the interstices of granules in the pressed compact. The internal coarse defects in the ceramics were successfully observed. A large number of coarse defects were observed as 3-dimensional image.

The coarser defects formation during sintering was also examined in alumina ceramics by the μ-CT. Using one sample, we repeated the experiment of sintering and observation with μ-CT. The relative density gradually increased with 60% to 96%. With sintering, coarse defects generally grow, and the number of coarse defects with > 5 μm increased. Particularly, a coarser defect with 20 μm in size also grew by incorporating a neighbor coarse defect with ~ 5 μm at the middle stage of sintering. This results shows that the sintering among granules cause the rearrangement of coarse defects. We must focus on inhomogeneous sintering.

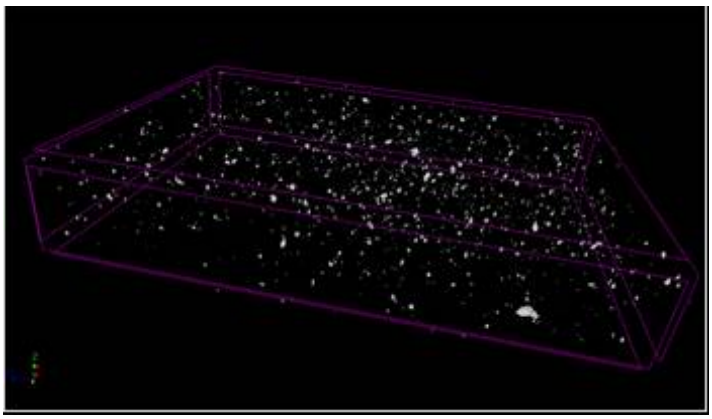

Fig. 9 3D image of large pores in ceramics sintered at 1400°C

Acknowledgement:
This research was in-part supported by Grant-in-Aid for Scientific Researches (C) (25420706) from Japan Society for the Promotion of Science

References:
[1] K. Uematsu et al., J.Ceram.Soc.Japan, 101, 1400 (1993)
[2] S. Nakamura, S.Tanaka et al., J.Am.Ceram.Soc., 92, 688 (2009)

GL-I01

Glass materials for white LED color converters

Woon Jin CHUNG[1*], Hyun-A PARK[1], Karam HAN[1], Sang Hun LEE[1], Won Bin IM[2], Jong HEO[3]
[1]*Division of Advanced Materials Engineering, Kongju National University, Cheonan,Chungnam, 331-717, Republic of Korea*
[2]*School of Materials Science and Engineering, Chonnam National University, Gwangju, 500-757, Republic of Korea*
[3]*Department of Materials Science and Engineering and Division of Advanced Nuclear Engineering, Pohang University of Science and Technology (POSTECH), Pohang, Gyeongbuk 790-784, Republic of Korea*

Keywords: Glass, LED, Phosphors, Luminescence

Conventional light emitting diodes are composed of blue LED chip and yellow phosphors as a color converter which is embedded with organic resins. Due to weak thermal and chemical stability of organic resins which restricts the lifetime of white LEDs, inorganic color converters have been extensively studied recently. Inorganic color converters can be classified as phosphor ceramics (PC), phosphor glass ceramics (PGC), phosphor in glass (PiG) and bulk glass phosphor (BGP). Three of them are glass based materials which shows the importance of glass materials. In this talk, after brief introduction of inorganic color converters for white LED and their recent achievements, various results on PiGs and BGPs will be introduced.
For PiGs, various silicate glass systems were studied to lower the sintering temperature below 600^{o}C to embed red phosphors. SiO2-B2O3-P2O5-RO, SiO2-B2O3-ZnO-R2O and SiO2-Na2O-RO systems were investigated. Glass compositions which can be sintered under 550 ^{o}C were found and successful color tuning was achieved by incorporating additional red phosphors along with the improvement of the color rendering index. Oxyfluoride glasses with LaF_3 nano-crystals were also studied for BGP. Eu^{2+} and Eu^{3+} doped oxyfluoride glass showed some possibility for color conversion when it was heavily crystallized. Silicate glasses with quantum dot were also investigated as a blue LED color converter. CdS, CdSe and CdSSe QDs were formed within glass matrix and CdSe and CdSSe showed possible color converting properties when they were mounted on LED chips.

Acknowledgement:
This research was supported by the Basic Science Research Program through the National Research Foundation of Korea (NRF) funded by the Ministry of Education (NRF-2013R1A1A2005671).

GL-I02

Functional oxide glasses prepared by a levitation technique

Atsunobu MASUNO
Institute of Industrial Science, The University of Tokyo, Tokyo, 153-8505, Japan

Keywords: high refractive index glass, hard glass, containerless processing

Containerless processing is one of the advanced vitrification techniques. A levitated melt is rapidly cooled to obtain spherical bulk glass. Bulk glass formation is due to the absence of both the inhomogeneous nucleation from the container wall and the deeper undercooling in a melt. Recently, we have succeeded in preparing bulk glasses in some binary systems, such as TiO_2-based, Nb_2O_5-based, WO_3-based, and La_2O_3-based glasses without using any network-former oxides by containerless processing.[1-7] These glasses have attracted much attention since they are colorless and transparent, the refractive index n is much high ($n \sim 2.3$), and the wavelength dispersion is rather low in visible range. These excellent optical properties have been desired for advanced optics such as thinner lens for digital camera of smart phones, and solid immersion lens for next-generation optical disk system. The structural analyses by using X-ray and neutron diffraction and reverse Monte-Calro simulation, and molecular dynamics simulation revealed that the glass structures of the high refractive index glasses were quite different from those of the conventional oxide glasses. The high oxygen packing density causing the high refractive index is realized in these new glasses. Furthermore, very recently, we have obtained new glass systems having very high cracking resistance by containerless processing. The details of the new functional oxide glasses will be presented.

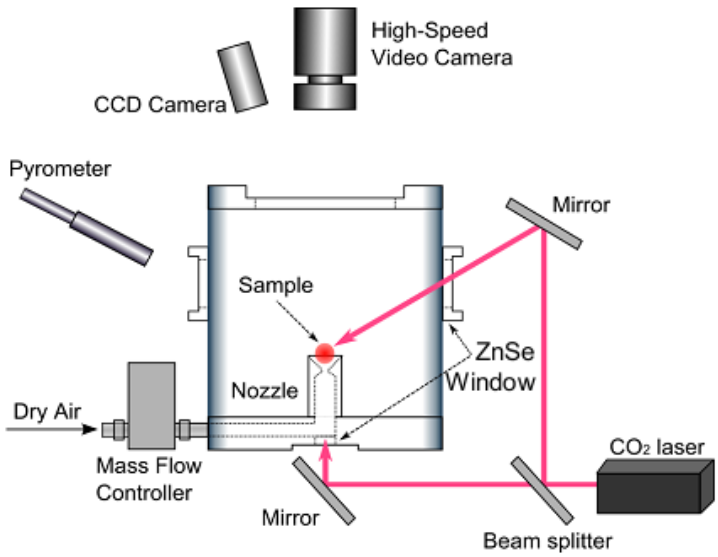

Figure 10 Schematic illustration of glass formation by a levitation technique

References:

[1] J. Yu et al., Chem. Mater. 21 (2009) 259.
[2] A. Masuno et al., J. Appl. Phys. 108 (2010) 063520.
[3] A. Masuno et al., J. Mater. Chem. 21 (2011) 17441.
[4] H. Inoue et al., Opt. Mater. 33 (2011) 1853.
[5] K. Yoshimoto et al., J. Am. Ceram. Soc. 95 (2012) 3501.
[6] A. Masuno et al., Chem. Mater. 25 (2013) 3056.
[7] A. Masuno et al., Opt. Mater. Express 4 (2014) 710.

BI-I01

GRAPE® technology: in vitro and in vivo evaluations

K. Uetsuki[1], T. Kuramoto[1], S. Hayakawa[2], A. Osaka[2]

[1]*Nakashima Medical Co., Joto, Okayama-shi 709-0625, Japan*

[2]*Graduate School of Natural Science and Technology, Okayama University, Tsushima, Okayama-shi 700-0082, Japan*

Dry titanium oxide layer is the last to deposit apatite in vitro, though titanium alloys with such layer have known to be compatible to bone tissue as they form relatively firm bonds with living bone tissue. Applying a narrow and confined space to titanium substrates with dry titania layer derived by heating in air at ~500°C enhanced the ability of apatite deposition under in vitro and in vivo environments. We denoted this as GRAPE® technology after GRoove and ApatitE. The narrow space was derived by groove machining or pits, or by set a pair of titanium substrates with <1mm distance. In vitro apatite deposition will be presented for such specimens in Kokubo solution (SBF) as well as new bone tissue generation. From a series of experiments where the titanium substrates with dry titania layer were exposed to still and flowing SBF, the mechanism will be proposed to explain such apatite depositing behavior.

BI-I02

Development and evaluation of novel hybrid systems of ceramic and polymer for bone tissue regeneration

Byong Taek LEE[1,2]*
[1]*Department of Regenerative Medicine, Soonchunhyang University, Cheonan, South Korea*
[2]*Institute of Tissue Regeneration, Soonchunhyang University, Cheonan, South Korea*

Keywords: Biomaterials, Hydroxyapatite, Gelatin, Hyaluronic acid, Extracellular matrix

Bone tissue regeneration using biomaterials based scaffolds is a very much complex process where both physical stability and biological processes should be considered. Traditional synthetic porous scaffolds, fabricated with either metals or polymers or ceramics, were not able to ensure native structure, strength, degradation of the scaffold and osteoblastic activates simultaneously. Thus strategies for bone tissue engineering and regeneration should rely on bioactive scaffolds to mimic the natural extracellular matrix and act as templates onto which cells attach, multiply, migrate and. Our particular interest is composites and hybrid biomaterials based on selective combinations of biodegradable polymers and bioactive ceramic materials. Herein, I am going to present some novel design of hybrid scaffolds and evaluation of their in vitro and in vivo potentiality in bone regeneration. We focus specifically on hydroxyapatite (HA), biphasic calcium phosphate (BCP) and bioactive glass (BG) in combination with biodegradable gelatin, hyaluronic acid, collagen and decellularized extracelluar matrix. Among our several own hybrid systems, BCP scaffold with gelatin-hyaluronic acid hydrogel; three layered spongy scaffold BCP-Bioglass-Gelatin; silicon doped BCP micro channeled granular bone substitute with collagen and BMP-2; BMP-2 and VGEF loaded BCP-Cellulose composite scaffold. These topics include 3D scaffold design and fabrication, vast physical characterizations, in vitro responses through osteoblast attachment, proliferation and osteogenesis and in vivo performance evaluation by implanting the scaffold in non-union defects segmental. We conclude with a perspective on the future application of novel designed ceramic-polymer hybrid scaffolds for regeneration of hard tissue.

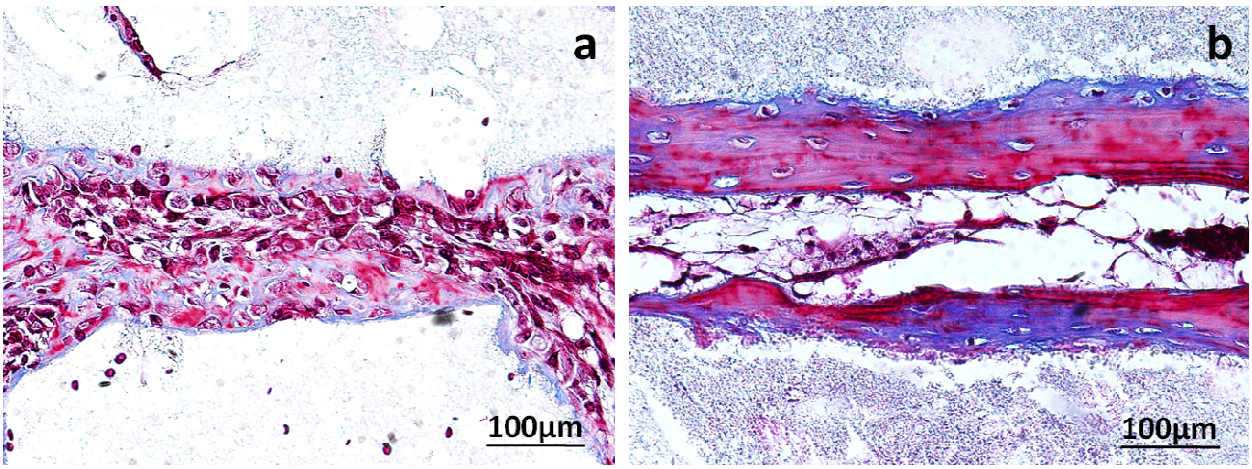

Figure 11 Masson trichrome staining of bone regeneration on the microchannels after 1 week- infiltration of fibroblast cells and osteoblast cells (a). Bone regeneration after 4 weeks- vascularization surrounded by dense collagen to form lamellar bone formation in longitudinal direction (b).

SE-I01

Catalytic combustion type gas sensor of FIGARO engineering

Junji Omori, Kazuya Shinnishi, Tatsuya Tanihira, Kazunari Kaneyasu*
Figaro Engineering , Minoo, Osaka 562-0036, Japan

Keywords: Catalytic combustion type Gas sensor

Gas leak detectors become more important as safety device with the increasing use of gas in every-day life. Among a lot of gas detection technologies, catalytic combustion type gas sensor is superior in terms of high accuracy and is used in many applications with concentration display. While at the same time, it is generally recognized that the disadvantage of catalytic combustion type gas sensor is a deterioration of output signal over time.

Figaro has made a significant improvement on the long-term stability of catalytic combustion type gas sensor. Followings are our countermeasures to suppress the deterioration of output signal:

1) Developed a new filter material for improving the durability against poisoning substances which deteriorate the catalyst activity.
2) Optimized the structure and catalyst quantity of detector element for extending the lifetime
3) Adjusted the proportion of detector element to compensation element for elevating the output signal in fresh air over time.

Fig.1 shows the output voltage behavior of TGS6812, Figaro's catalytic combustion type gas sensor. Gradual increase of output voltage in gas in tandem with output voltage in fresh air enables a fail-safe design of gas detector. With its 10 years life expectancy, TGS6812 is adopted in wide range of gas detectors.

Another disadvantage of catalytic combustion type sensor, compared to other type sensors, is vulnerability against physical impact. It prevents catalytic combustion type sensors from being adopted in portable gas leak detectors.

For such applications, Figaro has been developing a catalytic combustion type MEMS gas sensor with low power consumption and excellent impact durability. It will also be introduced in the presentation.

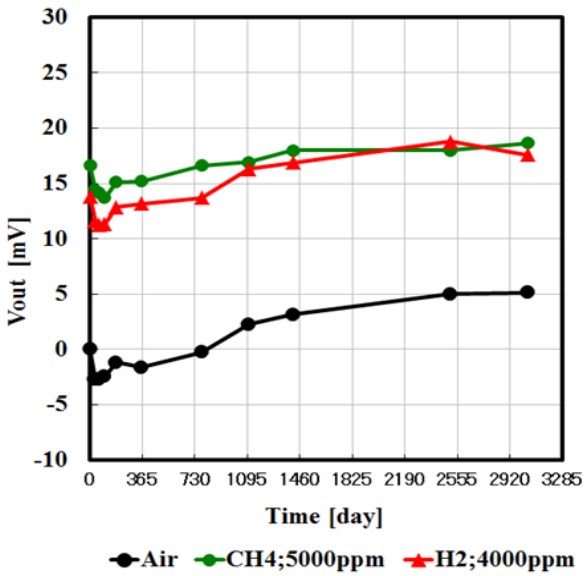

Fig. 12 Behavior of output voltage for long time use

SE-I02

Development of Oxide Semiconductor Gas Sensors for High Sensitivity under Humid Condition

Kengo SHIMANOE[1*], Nan MA[1], Miyuki SASAKI[1], Koichi SUEMATSU[2], Masayoshi YUASA[1]
[1]*Faculty of Engineering Sciences, Kyushu University, Kasuga, Fukuoka 816-8580, Japan*
[2]*Fukuoka Industrial Technology Center, Chikushino, Fukuoka 818-8540, Japan*

Keywords: Gas sensors, Metal oxide, Semiconductor, Humidity, Sensitivity

Semiconductor gas sensors using metal oxides are widely used for various purposes such as alarms of gas leakage and toxic gas, alcohol checker and so on. Recently the strict requirements to gas sensors is increasing, for example lower detection limit in humid atmosphere. So far, we have reported important three factors, receptor and transducer functions and utility factor, for material design of semiconductor gas sensor. Especially the former function is related with the water vapor poisoning deeply. In this presentation, I would like to show the properties of Pd-loaded and Sb-doped SnO_2 as a receptor function.

Neat SnO_2 and antimony-doped tin dioxide powders were prepared by co-precipitation and hydrothermal method. In addition, Pd was loaded on neat SnO_2 by impregnation method using $Pd(NH_3)_2(NO_2)_2$ aqueous solution. The obtained powders were screen-printed on an alumina substrate (9 mm × 13 mm× 0.38 mm) attached with Au electrodes. The resulting devices were heat-treated at 580 °C for 3 h in air to stabilize the sensing layer. The sensor measurements were carried out in a conventional gas flow apparatus equipped with an electric furnace. The sensor response was defined as the ratio of electric resistance in synthetic air (Ra) and hydrogen gas (Rg).

Figure 1 shows the sensor responses to H_2 in different humidity for Pd-loaded and Sb-doped SnO_2. The sensor responses of both devices under humid condition were fairly constant although that of neat SnO_2 was decreased with increasing water vapor concentration. Such a stability to humidity change seems to be due to oxygen adsorption species. From the dependence of electric resistance on oxygen partial pressure under humid condition, O^{2-} was found to be main adsorption species for the Pd-loaded and Sb-doped SnO_2 although neat SnO_2 was related with O^-. Such a difference in adsorption species is known to give a great influence on sensor response[1)]. In addition, it seems that both p-n junction of PdO-SnO_2 and property of Sb on SnO_2 surface are related with suppression of water vapor poisoning. The detail will be explained in the presentation.

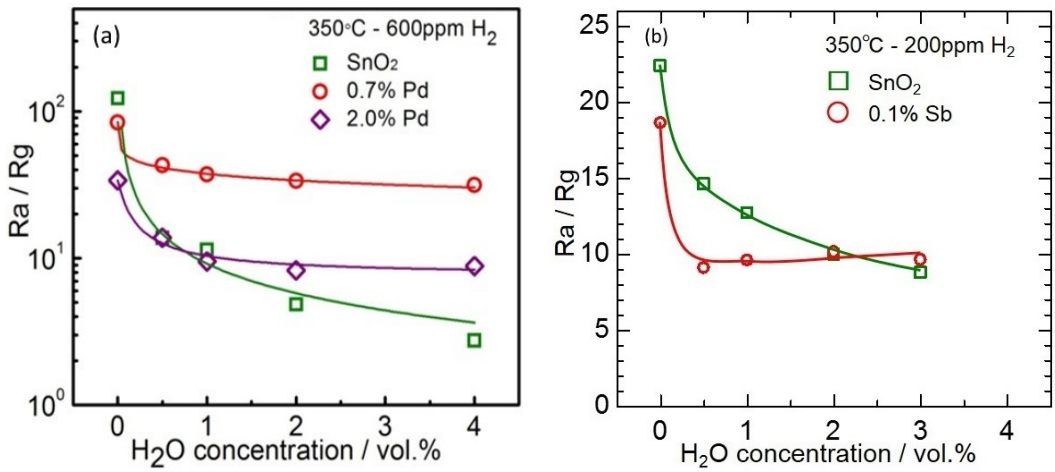

Figure 13 Sensor response to hydrogen under humid condition for Pd-loaded SnO_2 (a) and Sb-doped SnO_2 (b).

Reference:

[1] N. Yamazoe, K. Suematsu, K. Shimanoe, *Sens. Actuators B*, **163**, 128-135 (2012)

SE-I03

Metal oxide thin films with highly ordered nanostructures for high performance gas sensors

Ho Won Jang*
[1]*Department of Materials Science and Engineering, Seoul National University 151-1744, Korea*

Keywords: Gas sensors, metal oxide, nanostructures, synthesis-in-place, nanotubes

Nanostructured oxide thin films can greatly improve the efficiency and performance of many devices including solar cells, secondary batteries, fuel cells, gas sensors, light emitting devices, and photoelectrochemical water splitting systems. However, synthesis-and-place methods which are commonly used to fabricate nanostructured oxide thin films often lack reproducibility, durability, and reliability. In the talk, we will present our approaches to synthesize highly ordered nanostructured oxide thin films on the desired locations using various synthesis-in-place methods such as colloidal templating, glancing angle deposition, anodization, and hydrothermal method [1-3]. We will show the demonstration of high performance gas sensors using the synthesized thin film nanostructures.

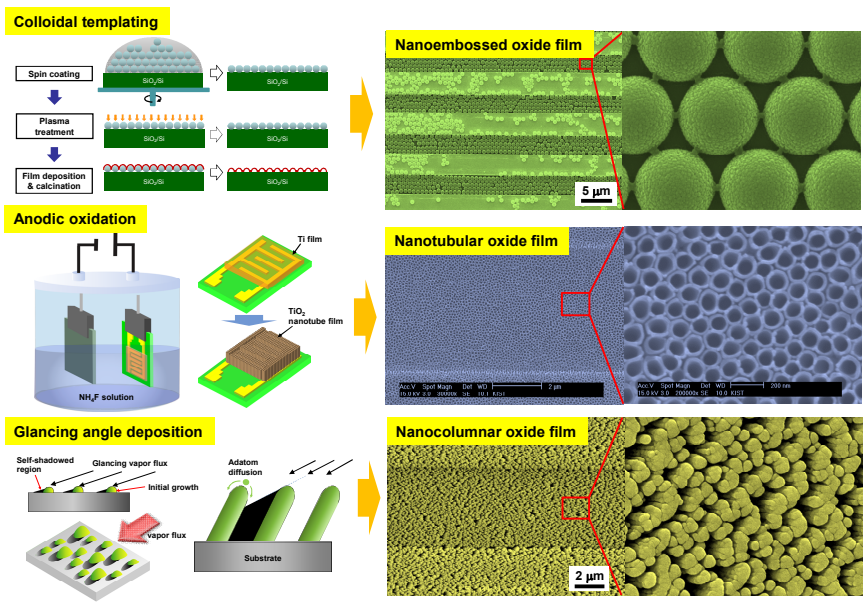

Figure 14. Synthesis-in-place methods to synthesize metal oxide thin films with highly ordered nanostructures

References:

[1] Y. S. Shim et al., Sen. Actuators B 198, 294 (2014).
[2] H. J. Gwon et al., Nano Res. 7, 670 (2014).
[2] D. H. Kim et al., ACS Appl. Mater. Interfaces, DOI: 10.1021/am504156w (2014)

EF-I01

Densification of Undoped Yttria by Means of Flash-sintering

Hidehiro YOSHIDA[1*], Yoshio SAKKA[1], Takahisa YAMAMOTO[2], Jean-Marie LEBRUN[3] Rishi RAJ[3]
[1] *National Institute for Materials Science, Tsukuba, Ibaraki 305-0047, Japan*
[2] *Department of Quantum Engineering, Nagoya University, Nagoya, Aichi 464-8601, Japan*
[3] *Department of Mechanical Engineering, University of Colorado at Boulder, Boulder, CO 80309-0427, United States*

Keywords: Y_2O_3, Flash-sintering, Field-assisted sintering, Electrical conductivity, Microstructure

Yttria (Y_2O_3) ceramics have special chemical and physical properties such as high resistance to halogen-plasma corrosion and thermal stability. At the same time they are difficult to sinter; conventional sintering requires very high temperatures, typically >1400°C, and a vacuum or hydrogen atmosphere. New techniques that use electrical fields have shown that ceramics can be sintered quickly at low temperatures. Collectively these methods are called field-assisted sintering techniques (FAST). Recently, it has been demonstrated that nanocrystalline, yttria stabilized tetragonal zirconia (Y-TZP) can be sintered at 850°C within 5 seconds under an electric field of 120 V/cm [1]. This phenomenon is called FLASH-sintering. The nature of flash-sintering, where densification occurs in just a few seconds under a threshold condition of temperature and applied field, is fundamentally different from FAST [2]. The flash-sintering can also be characterized by nonlinear increase of electric conductivity during sintering experiments. In the present study we demonstrate that undoped Y_2O_3 can be sintered nearly instantaneously to full density under DC applied fields of more than 500 V/cm [3]. For instance, the flash-sintering preceded by gradually accelerated field-assisted sintering occurs at furnace temperature of 1133°C under a DC applied field of 500 V/cm. In the Y_2O_3, FAST is followed by flash-sintering. The microstructure of the flash-sintered specimens indicated that the densification was accompanied by rapid grain growth. The single-phase nature of the flash-sintered Y_2O_3 was confirmed by high resolution transmission electron microscopy (HRTEM). It is postulated that a combination of Joule heating and defect generation triggered by the flash event leads to the higher rates of diffusion and densification.

References:

[1] M. Cologna, B. Rashkova, R. Raj, *J. Am. Ceram. Soc.*, 93 (2010) 3556.
[2] R. Raj, M. Cologna, J.S.C. Francis, *J. Am. Ceram. Soc.*, 94 (2011) 1941.
[3] H. Yoshida, Y. Sakka, T. Yamamoto, J.-M. Lebrun, R. Raj, *J. Eur. Ceram. Soc.*, 34 (2014) 991.

Acknowledgement:

The authors thank Dr. John S.C. Francis for his assistance with the sintering experiments. This work was financially supported by a Grant-in-Aid for Scientific Research on Innovative Areas 2505 from the Ministry of Education, Culture, Sports, Science and Technology of Japan. Lebrun and Raj were supported in this work by the Office of Naval Research under the guidance of Dr. Lawrence Kabacoff, under grant no. N00014-12-1-0710.

EF-I02

Influence of Carbon Nanotubes on Phase Transformation (*t* - *m*) of Spark Plasma Sintered ZrO_2

Young-Hwan Han
School of Materials Science and Engineering, Yeungnam University, Gyeongsan, Republic of Korea

Keywords:ZrO2: phase transformation: spark plasma sintering

A technique of Spark Plasma Sintering (SPS) uses the idea of pressure driven powder consolidation under pulsed direct electric current which is passed through a sample compressed in a graphite die set. In general, the SPS process results in a finer grain size. The reported phase transformation fraction on fractured surface still encountered contradiction and the phase transformation behavior of ZrO_2/CNT composite in indentation range has never been systematically studied. These differences may be resulted from the dispersion state of CNTs, sintering condition and therefore the microstructure and residual stress state of the composites. The densification behavior during SPS, microstructure and mechanical property were examined. Commercial 3YSZ/CNT composite powder (Applied Carbon Nanotechnology Co., LTD, Korea) with a CNT content of 0, 1, 3, 5 and 10 vol.% were used as the starting powders. The ZrO_2/CNT composite powders were produced by a high energy ball milling process. The composite powders underwent SPS (FCT Gmbh, Germany) in a vacuum at 1300°C at a heating rate of 100°C/min and holding time of 3 min. The pressure load was initially 30 MPa and was increased linearly to 60 MPa when the temperature reached 1300°C. The addition of CNTs could also lead to refined grain size, improved fracture toughness while reduced Vickers hardness and nanoindentation. An initially decreasing and then increasing tendency for the tetragonal to monoclinic phase transformation were observed at 5% CNT addition in the indentation of composites by the Raman technique, also characterized by XRD, SEM, TEM, and AFM.

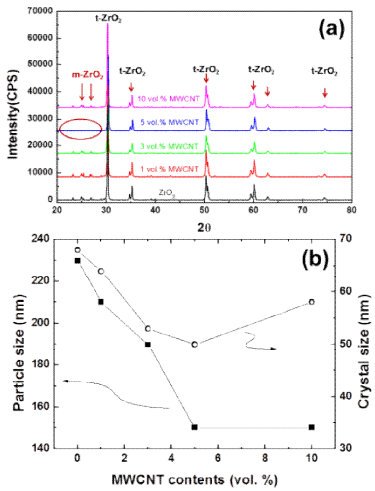

Figure 1 (a) X-ray diffraction patterns of the ZrO_2/MWCNT composites. (b) Apparent particle size measured From SEM and the crystal size estimated from XRD patterns

References :

[1] L. Shen, Y.H. Han, C. Xiang, H. Tang, A. Mukherjee, S. Kim, S.I. Bae, Q. Huang, Scripta Mater. 69(2013) 736.
[2] I. Ahmad, H. Cao, H. Chen, H. Zhao, A. Kennedy, Y.Q. Zhu, J. Eur. Ceram. Soc. 30 (2010) 865.
[3] M. Poorterman, M. Traianidis, G. Bister, F. Cambier, J. Eur. Ceram. Soc. 29 (2009) 669.
[4] N. Garmendia, S. Grandjean, J. Chevalier, L.A. Diaz, R. Torrecillas, I. Obejeta, J. Eur. Ceram. Soc. 31 (2011) 1009.
[5] J.P. Zhou, Q.M. Gong, K.Y. Yuan, J.J. Wu, Y.F. Chen, C.S. Li, Mater. Sci. Eng. A 520 (2009) 153.

EF-I03

Spark-Plasma-Sintering (SPS) of Transparent $MgAl_2O_4$ Spinel

Koji MORITA[1*], Byung-Nam KIM[1], Hidehiro YOSHIDA[1], Keijiro HIRAGA[2], Yoshio SAKKA[1]
[1] *National Institute for Materials Science, 1-2-1 Sengen, Tsukuba, Ibaraki 305-0047, Japan*
[2] *Kitami Institute of Technology, 165 Koencho, Kitami, Hokkaido, 090-8507, Japan*

Keywords: Spark-Plasma-Sintering (SPS), Spinel, Transparency, Carbon Contamination

In order to attain transmission in oxide ceramics, reducing the residual porosity is regarded as a key factors because the pores act as a main light scattering source. Pressure assisted sintering techniques, such as hot pressing (HP) and/or hot isostatic pressing (HIP), has generally been employed for attaining fully dense ceramics. More recently, instead of the HP or HIP techniques, spark-plasma-sintering (SPS) technique has been applied to the fabrication of various transparent oxide ceramics, such as α-Al_2O_3, $MgAl_2O_4$ spinel, MgO, YAG and ZrO_2. The primary reason is that, as compared with the well-known HP or HIP techniques, the SPS technique can utilize high heating rates higher than 50°C/min, and hence, can save the total processing time of powder densification.
The densification, however, is known to be highly sensitive to the SPS conditions, such as heating rate, temperature, holding time and loading schedule. For the fabrication of transparent α-Al_2O_3 and spinel ceramics, for example, a low heating rate of ≤10°C/min is highly effective than the widely used high heating rates of ≥50°C/min. In order to apply the SPS processing to the fabrication of transparent ceramics, optimization of the SPS processing is necessary. For example, the carbon contamination arises from the trace CO_3 impurities pre-existing in the starting powder, irrespective of the SPS conditions. For the higher heating rate, which is the primary advantage of the SPS technique, the additional carbon contamination occurred from the paper/die used in the SPS processing and remained as glassy carbon phases in the matrix. Oxygen vacancies are also introduced into the spinel matrix depending on the SPS condition. In the presentation, we will introduce the recent data of the transparent spinel and will discuss the effect of the SPS conditions on the fabrication of transparent spinel.

EF-I04

Low-Temperature Spark Plasma Sintering of Transparent Alumina and Unusual Grain Growth

Byung-Nam KIM*
National Institute for Materials Science, Tsukuba, Ibaraki 305-0047, Japan

Keywords: Alumina, Transmission, Grain growth, Densification, Grain-boundary sliding

During spark plasma sintering of alumina at low temperatures, the effects of heating rate, pressure and loading schedule on the grain size are examined. When the alumina is densified at low temperatures, high heating rates accelerate grain growth, though the total heating time is reduced. The phenomena is unusual and cannot be explained by the common knowledge. The grain growth rate after full densification is also accelerated for high heating rates. The accelerated grain growth may result from the generation of defects during densification. The densification in the intermediate stage of sintering includes the deformation of powder particles, and the deformation of ceramics occurs mainly by grain-boundary sliding. The defects generated during grain-boundary sliding may enhance the grain-boundary mobility and accelerate the grain growth rate, that is the dynamic grain growth. It is considered, therefore, that the high deformation rate at high heating rates accelerates grain growth. The accelerated grain growth also appears for high-pressure sintering. The grain size after sintering increases with the applied pressure. High pressures lower the deformation temperature and increases the deformation rate. As a result, the higher deformation rate during heating may generate more defects and enhance the grain-boundary mobility. Lastly, the loading schedule during heating also affects the deformation and the grain growth. Applying pressure at lower temperatures may generate more defects and resultantly accelerate the grain growth. All the unusual grain growth observed during low-temperature sintering is explained by the model of grain-boundary sliding.

EF-I05

Spark plasma sintering temperature effects on the microstructure and magnetic properties of carbon nanotube/NiZn ferrite composites

Xiaobing Zhou[a], Young-Hwan Han[b], Jaehyung Lee[b], Qing Huang[a]*
[a] *Ningbo Institute of Materials Technology and Engineering, Chinese Academy of Sciences, Ningbo, 315201, People's Republic of China*
[b] *School of Materials Science and Engineering, Yeungnam University, Gyeongsan, Republic of Korea*

***Keywords*:** spark plasma sintering; carbon nanotube; NiZn ferrite

Carbon nanotube (CNT)-$Ni_{0.5}Zn_{0.5}Fe_2O_4$ composites were synthesized by precipitation-hydrothermal method, and then fabricated by Spark Plasma Sintering (SPS) technique at different temperature. The microstructure and magnetic properties of carbon nanotube/NiZn ferrite composites were investigated by X-Ray Diffraction (XRD), Scanning Electron Microscope (SEM) and physical properties measurement system (PPMS). The results shown that the grain size and saturation magnetization of the carbon nanotube/NiZn ferrite composites were strongly dependent on the SPS temperature. Both the grain size and saturation magnetization increased with the SPS temperature increasing. Ni nanoparticles could be formed by the carbothermal reduction between CNTs and $Ni_{0.5}Zn_{0.5}Fe_2O_4$, and the mass of Ni nanoparticles increased with the SPS temperature increasing.

EF-I06

Milliwave Sintering of Silicon Carbide with Carbon additives

Tetsuo UCHIKOSHI*, Tohru S. SUZUKI*, Hidehiko TANAKA, Toshiyuki NISHIMURA and Yoshio SAKKA
National Institute for Materials Science, Tsukuba, Ibaraki 305-0047, Japan

Keywords: Milliwave, Dielectric loss, Selective sintering, Silicon carbide, Carbon

Microwave heating is one of the new sintering processes in which the materials absorb the electromagnetic energy of microwave and transform it into heat. The use of microwave radiation for sintering of ceramics has been recently proposed as a newly focused scientific approach. Microwave sintering has a lot of advantages, for example, selective heating, self-heating, rapid and volumetric heating. Especially, microwave sintering is one of the effective methods for the sintering of dielectric materials because their loss tangent (tan δ) is quite large. Many researchers have reported the effect of the microwave sintering on the properties in the dielectric ceramics such as PZT and $BaTiO_3$, etc. "Selective heating" is a distinct characteristic that has not been seen in any other heating process: The material with the highest loss tangent is selectively heated if two or more materials with different dielectric losses exist in a compact. In this study, we utilized the milliwave of 28 GHz for densifying hard-to-sinter SiC by coating the SiC particles with high loss tangent carbon additives.

The effect of carbon addition on the densification of SiC specimens sintered by milliwave sintering (M.S.) and conventional sintering (C.S.) is shown in Fig.1. The microstructures of the selected specimens of different sintering conditions are shown in Fig. 2. Dense SiC body with the theoretical density of >97% was obtained by the milliwave sintering at 1800 C. On the other hand, the relative density of the conventionally-sintered body was lower than 80%. It is probable that the carbon surrounding the SiC particles was heated up higher than 1800 C by the selective heating absorbing the milliwave. Consequently, the local heating promote the sintering between the SiC particles. The density of SiC sintered by microwave heating depended on the carbon contents.

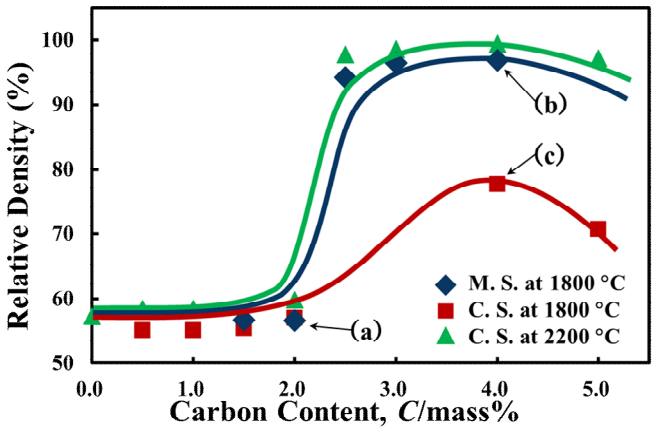

Fig. 1 The effect of carbon addition on the relative density of SiC specimens sintered by milliwave sintering (M.S.) and conventional sintering (C.S.)

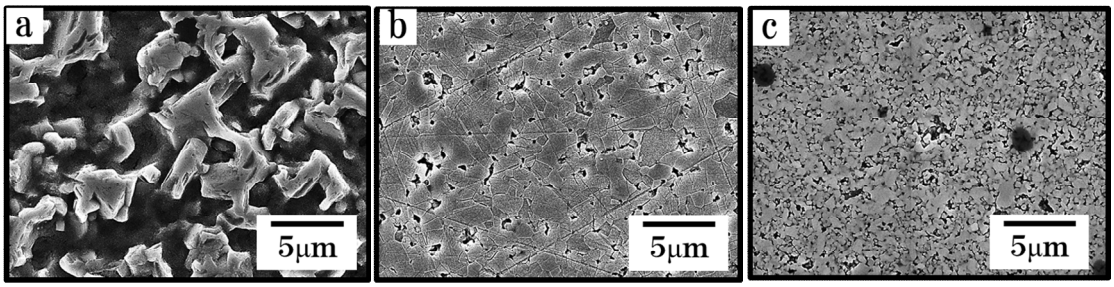

Fig. 2 The microstructure of the SiC specimens: (a) M.S. at 1800 °C with 2.0wt% C, (b) M.S.at 1800 °C with 4.0wt% C, (c) C.S.at 1800 °C with 4.0wt% C

PI-I01

Energy Harvesting Devices by Piezoelectric Ceramics

Toshio OGAWA[1]*, Hiroshi AKAISHI[2]
[1]*Department of Electrical and Electronic Engineering, Shizuoka Institute of Science and Technology, Fukuroi, Shizuoka 437-8555, Japan*
[2]*Plus Comfort Co., Ltd., Shizuoka 420-0876, Japan*

Keywords: Energy harvesting, Piezoelectric buzzer, Resonance vibration, Unimorph

Recently, energy harvesting for energy conversion between electrical energy and mechanical energy in piezoelectric ceramics has been focused on to obtain clean energy. It has various practical uses, such as a floor for electrical generation (electricity-generating floor) at ticket gates in the Tokyo terminal of Japan Railway East Company (JR-East) and LED light illumination for the Metropolitan Expressway generating electricity through the deformation of bridge piers passing through automobiles. We developed new piezoelectric energy harvesting devices utilizing the resonance vibration of piezoelectric ceramics [1]. By applying a piezo-buzzer, new devices such as a night-view footwear [2], a piezo-walker, and so forth could be developed. While an external force was added to a buzzer, a lead zirconate titanate (PZT) unimorph in the buzzer, the ceramic disk diameter, thickness, and capacitance of which were respectively 14 mm, 0.2 mm, and 10 nF, generated resonance vibration. As a result, alternating voltages of around 30 V and a frequency of 5 kHz were observed. When the generated voltages (Figure 1) were applied to a LED lamp, new devices such as a night-view footwear [Figure 2(a)], a piezo-walker [Figure 2(b)] and a display panel composed of a new type of electricity-generation floor were developed. It was confirmed that the piezo-buzzer for energy harvesting utilizing resonance vibration is an effective tool for obtaining clean energy.

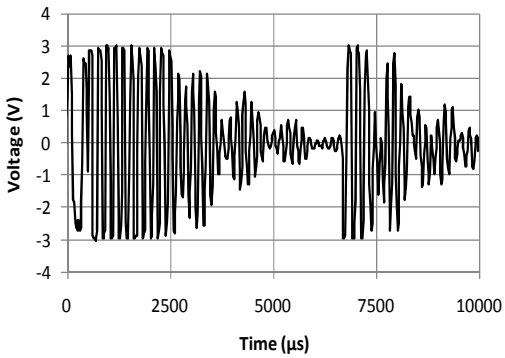

Figure 1. Generated voltage waves in the case of night-view footwear while walking one footstep. There were two types of added force during one footstep: below 5,000 μs and between 7,000 and 10,000 μs

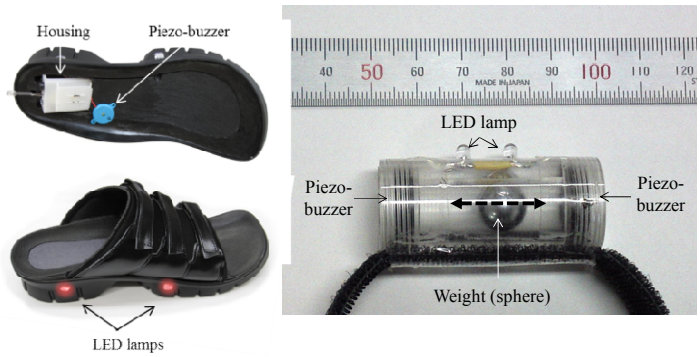

(a) (b)

Figure 2. Energy harvesting devices: (a) night-view footwear (lower photo) included in device housing (upper photo) produced by Plus Comfort Co., Ltd. [2], Shizuoka, Japan and (b) piezo-walker utilizing resonance vibration of PZT unimorph in piezo-buzzer. In the case of night-view footwear, the piezo-buzzer is located inside the housing

References:

[1] T. Ogawa, Footwear: Japanese patent application No. 52623 (2010).
[2] Available online at: http://www.plus-comfort.co.jp

Acknowledgement:

This work was partially supported by Grant 2010 of B-nest at Shizuoka City, Japan, a Grant of Strategic Research Foundation Grant-aided Project for Private Universities 2010-2014 (No. S1001032) from the Ministry of Education, Culture, Sports, Science and Technology, Japan (MEXT), and Research Foundations 2012 and 2013 between Academy and Industry of Fukuroi City, Shizuoka, Japan.

PI-I02

Piezoelectric Energy Harvesting for Wearable and Implantable Applications

Miso Kim[1*]

[1]*Center for Safety Measurement, Korea Research Institute of Standards and Science, Daejoen, 305-34, Republic of Korea*

Keywords: Piezoelectricity, Energy Harvesting, Wearable

As the human body is a tremendous storehouse of energy, the use of power harvesting devices to capture the energy lost during everyday human life is a captivating idea and has been one of the main topics facilitating the rapid growth of the power harvesting field. Piezoelectric materials produce electrical charge or voltage across them when a mechanical stress or strain is applied, or vice versa. Use of such functional materials enables conversion of biomechanical energy from human activities (e.g. walking, muscle stretching, etc.) into useful electrical energy. In order to develop human powered energy harvesting systems, characterization of available harvesting sources, appropriate materials selections, and optical device design are essentially required. In this talk, overview of prior research works and future perspectives are presented from such perspectives to provide design guidelines of highly efficient biomedical energy generators for wearable and implantable applications.

PI-I03

Piezoelectric MEMS devices for artificial cochlea and ultrasonic cell stimulation

Hongshoo Choi[1,2]
[1]*Department of Robotics Engineering, Daegu Gyeongbuk Institute of Science and Technology,*
[2]*DGIST-ETH Microrobot Research Center, Daegu Gyeongbuk Institute of Science and Technology,*
50-1 Sang-ri, Hyeonpung-myeon, Dalseong-gun, Daegu, 711-873, Korea

Keywords: piezoelectric, MEMS, frequency separation, cell stimulation

Piezoelectric thin-film based micro-electro mechanical systems (MEMS) devices have been used for a variety of applications including resonators, ultrasound transducers, micro actuators, micromirror, energy harvesting devices, pressure sensors, and accelerometers. In this presentation, two biomedical applications of the piezoelectric MEMS will be discussed including artificial basilar membrane for a totally implantable artificial cochlea and piezoelectric micromachined ultrasonic transducer (pMUT) for ultrasonic cell stimulation. A prototype of artificial cochlea including artificial basilar membrane array, signal processor with amplifier, pulse width modulator, and intra-cochlear electrode array was used for electrically evoked auditory brainstem response testing. These acoustic sensors have potential for use in next-generation human cochlear implants. A new ultrasonic cell stimulation system was fabricated using two different pMUT arrays with the size of 2.5 by 2.5 mm and 2.27 by 6.84 mm for 10 by 10 and 10 by 29 pMUT arrays, respectively. The measured acoustic intensities were 0.22 MPa and 0.18 MPa for 10 by 10 and 10 by 29 arrays, respectively, at the resonance frequency of 1.494 MHz for both arrays. The proposed system was used to stimulate PC-12 cells to enhance proliferation and differentiation. This system can be used to find the optimized ultrasonic stimulation condition for difference types of cell.

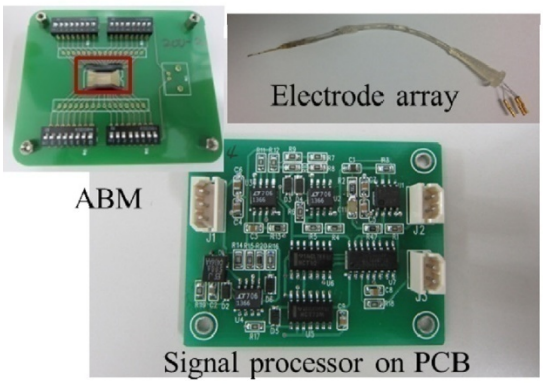

Figure 1: Optical image of the proposed artificial cochlea for animal test

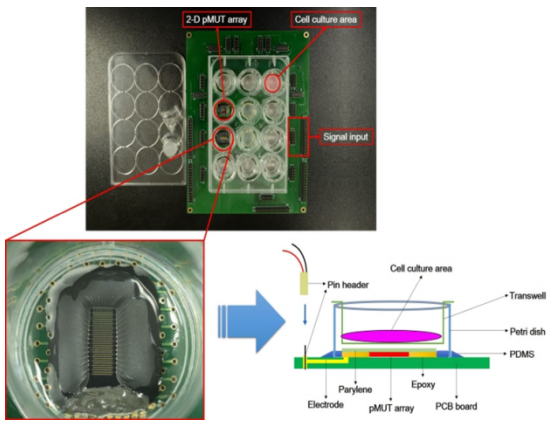

Figure 2: Optical image of the proposed ultrasonic stimulation system

Acknowledgement:
This work was supported by the DGIST MIREBraiN Project and DGIST R&D Program of the Ministry of Science, ICT and Technology of Korea (14-BD-0403).

PI-I04

Piezoelectric thin films and their MEMS applications

Isaku Kanno
Kobe University, Kobe, 657-8501, Japan

Keywords: PZT, thin film, lead-free, MEMS

Micro-electromechanical systems (MEMS) technologies have attracted considerable attention for the development of next-generation functional microdevices. In general MEMS devices, functionality is originated from three-dimensional micro-structures which can be fabricated by Si microfabrication technologies. Recently, functional materials such as piezoelectric materials have gradually been integrated into MEMS to give new functionality in simple micro-structures. For the integration of piezoelectric materials into MEMS, the piezoelectric materials should be prepared in thin-film form. The most popular piezoelectric materials are $Pb(Zr,Ti)O_3$ (PZT) because of its excellent energy conversion efficiency between mechanical and electric domains. The deposition and characterization of PZT thin films have been intensively studied, and recently, some of piezoelectric MEMS composed of PZT films have been developed as commercial products. Fig. 1 shows the images of typical piezoelectric MEMS devices. In addition to these applications, piezoelectric MEMS energy harvesting is one of the promising technologies in the future piezoMEMS.

The technical issues in the development of piezoelectric MEMS devices are

1) Deposition process of high quality piezoelectric thin films
2) Prices measurement of transverse piezoelectric properties of thin films
3) Development of lead-free piezoelectric thin films

In this talk, I will present the deposition process of PZT thin films, especially re-magnetron sputtering from the viewpoint of MEMS applications. In addition, the recent progress of the lead-free piezoelectric thin films is introduced. Among a variety of piezoelectric MEMS, we pick up the piezoelectric MEMS energy harvesters, and the basic characteristics and applications of piezoelectric MEMS energy harvesters will be presented.

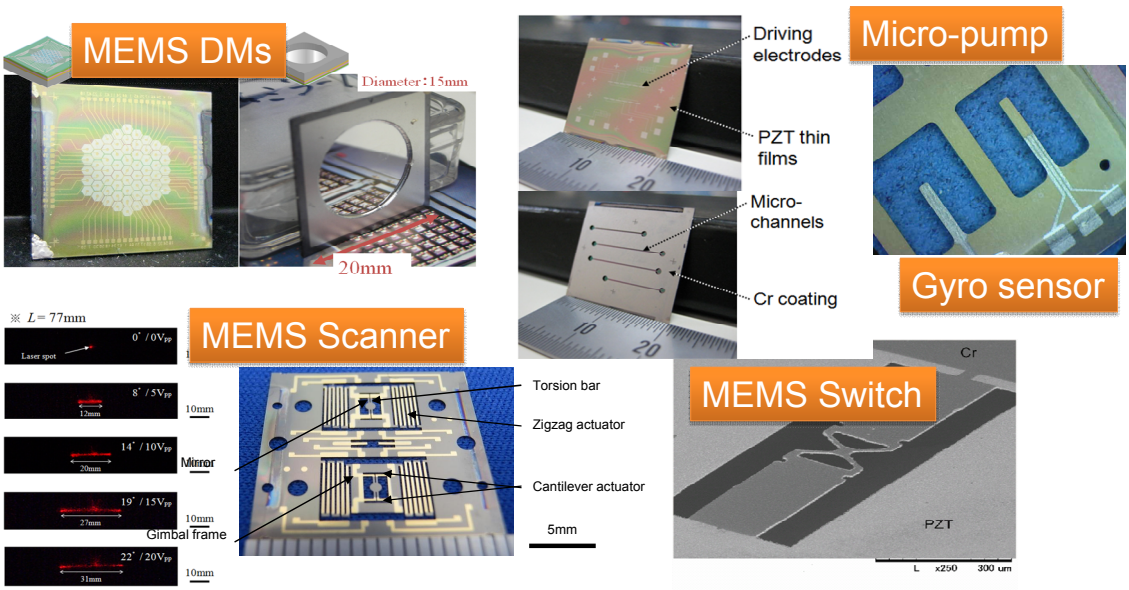

Figure 15 Piezoelectric MEMS applications

PI-I05

Resonant-type Smooth Impact Drive Mechanism (R-SIDM)

Takeshi MORITA
Graduate School of Frontier Sciences, The University of Tokyo
5-1-5 Kashiwanoha, Kashiwa, Chiba 277-8563, Japan

Keywords: piezoelectric linear actuator, stick-slip motion, SIDM, resonant vibration

Smooth impact drive mechanism (SIDM) is one of the stick-slip (or slip-slip) linear actuators, which enables high-speed operation with a simple structure. Previous SIDM actuators have been practically applied in camera modules, cell phones, and blue-ray disc devices[1]. The SIDM actuator is composed of a piezoelectric stator and a slider preloaded to the stator. The stator is driven in two stages: a slow forward motion and a rapid backward motion, namely saw-shaped displacement. Conventional SIDMs were driven at off-resonant frequency; therefore, a large input voltage was indispensable, which caused a heat generation.

In this study, we proposed a resonant-type SIDM (R-SIDM) actuator. This principle utilizes a quasi-saw-shaped displacement obtained by combining two resonant vibrational modes as shown in Fig. 1. The resonant effect enables low input voltage operations, which means small the heat generation. In order to combine two longitudinal vibration modes, the frequency ratio must be 1:2. By using the transfer matrix method and the FEM, we found that one solution is inserting a cupper disk between the piezoelectric part and the CFRP rod. In addition, almost constant velocity was obtained at driving area (CFRP rod). With a preload of 270 mN, the no-load speed was 40 mm/s with 1.6 V as shown in Fig. 2. This input voltage was one-sixth that of previous SIDMs for the same performance and the heat generation was suppressed effectively from 130 to 40 degree C.

Using the same principle, other kinds of the R-SIDMs were examined. One example is a miniaturized R-SIDM actuator, whose stator length was 10 mm. A piezoelectric plate was adhered to the step-shaped metal bar. This step design was important for realizing 1:2 resonant frequency ratio. Other example is a wireguide driven R-SIDM. At the tip of a step-shaped Langevin transducer, an aluminum wireguide (diameter 1mm) was attached. The quasi-saw shaped displacement was propagated from Langevin transducer to the tip of this wireguide for the R-SIDM operation. The length of wireguide was 326 mm at most; however, a longer wireguide, more than 1 m, could be possible.

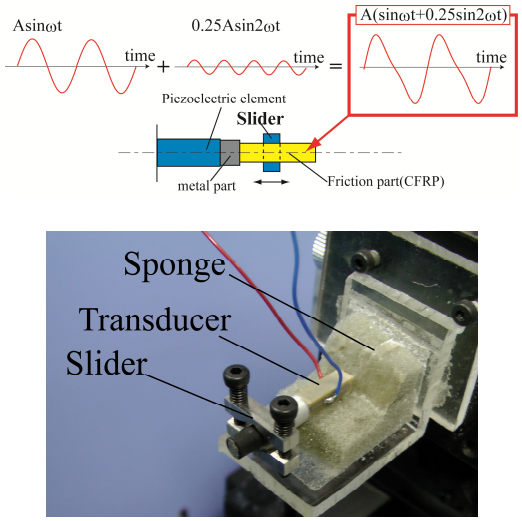

Fig. 16 Principle and photograph for R-SIDM.

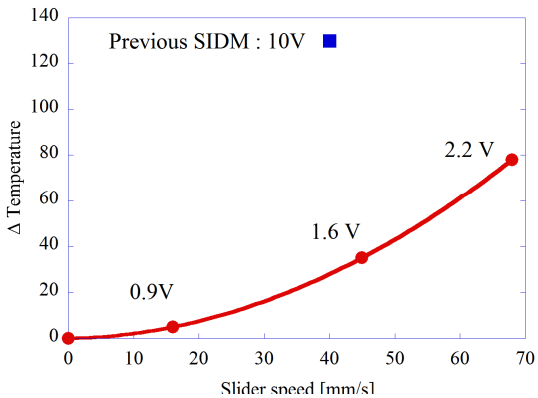

Fig. 2 R-SIDM operation results.

References:

[1] R. Yoshida, Y. Okamoto, T. Higuchi, A. Hamamatsu, , J. Jpn. Soc. Prec. Eng. 65 (1999) 111–115 (in Japanese).

PI-I06

Piezoelectric, ferroelectric and structural properties of $BiFeO_3$-$BaTiO_3$ electroceramics

Myang Hwan Lee, Da Jeong Kim, Jin Su Park, Tae Kwon Song
School of Materials Science and Engineering, Changwon National University, Korea

***Keywords**:* Lead-free piezoceramics, Thermal quenching, Phase diagram

(1-*x*)$BiFeO_3$-*x*$BaTiO_3$ (BF-BT) lead-free piezoelectric systems have potential to be applied at high operation temperature due to their high T_c with good piezoelectric properties. BF (rhombohedral phase) and BT (tetragonal phase) solid solutions were observed in the complete compositional range with rhombohedral (*x*=0.00-0.33), pseudo-cubic (*x*=0.33-0.92), and tetragonal (*x*=0.92-1.00) perovskite crystal structures. Leontsev and Eitel reported Mn-modified BF-BT ceramics exhibit a small-field piezoelectric constant d_{33} of 116 pC/N with high T_c of 619 °C at 0.75BF-0.25BT. However, this report cannot be clearly stated in the electrical properties of pure (unmodified) BF-BT system due to high *dc* conductivity.

Effects of heat-treatment process were investigated in 0.67BF-0.33BT lead-free piezoelectric ceramics. The structure, ferroelectric, and piezoelectric properties of ceramics made by thermal quenching process were investigated and compared to those of furnace cooled ceramics. The lattice constants (*a*) and lattice distortions (rhombohedral 90°- increased and the fraction of Fe^{2+} to Fe^{3+} was reduced in water-quenched ceramics. Ferroelectric and piezoelectric properties were improved with increasing quenching temperature. Small-field and large-field piezoelectric constants d_{33} and d_{33}* were 240 pC/N and 283 pm/V in ceramics water-quenched at the highest temperature 980 °C.

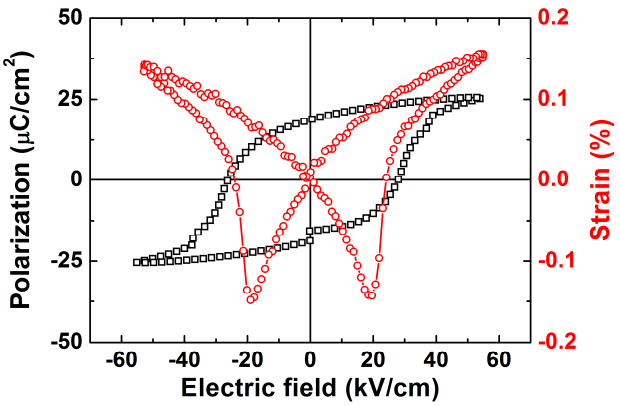

Fig.1 *P-E* hysteresis loop and *S-E* curves of the BF-33BT bulk ceramic.

LP-I02

"Lead-free" Piezoelectric Single Crystals Fabricated by Solid-State Crystal Growth (SSCG) Method:Development and Application

Sung-Min Lee[1], Dong-Ho Kim[1], Jong-Yeb Lee[1], Hyun-Taek Oh[1], Ho-Yong Lee[1,2*]
[1]*Ceracomp Co., Ltd., Cheonan, Chungnam 331-979, Korea*
[2]*Sunmoon University, Asan, Chungnam 336-708, Korea*

Keywords: Piezoelectric, Lead-free, Single Crystal, Growth, Application

Crystallographically engineered Relaxor-PT single crystals, specifically PMN-PT and PZN-PT, offer much higher piezoelectric and electromechanical coupling coefficients (d_{33} > 1,500 pC/N, k_{33} > 0.9), when compared to PZT ceramics. Therefore, the high performance piezoelectric single crystals have been expected to replace polycrystalline PZT ceramics in many application fields such as ultrasound transducers (medical and NDA), SONAR transducer, piezoelectric actuators, piezoelectric sensors, ultrasonic motors and piezoelectric energy harvesting, etc.

Ceracomp Co., Ltd. (South Korea) has developed the solid-state single crystal growth (SSCG) technique for fabricating the high performance "lead(Pb)-based" piezoelectric single crystals such as PMN-PT and PMN-PZT. Since the SSCG process is quite simple and similar to conventional sintering process, compared to conventional single crystal growth methods such as flux and Bridgman methods, it is very cost-effective and suitable to mass production. And recently the SSCG method was successfully applied to growth of "lead(Pb)-free" piezoelectric single crystals of high electromechanical coupling coefficients (k_{33} > 0.85).

In this presentation the recent progress on development and application of "lead-free" piezoelectric single crystals using the "cost-effective" SSCG process will be reviewed.

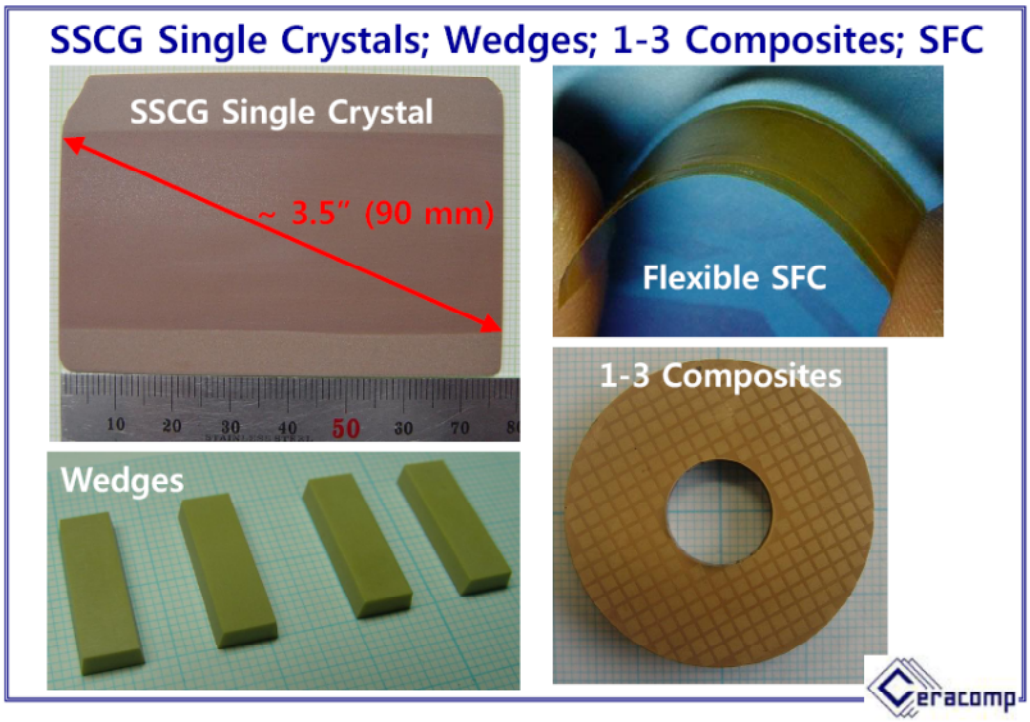

Fig. 17. "Lead-free" and "Lead-based" Piezoelectric Single Crystals and Their Composites

LP-I03

Fabrication and characterization of epitaxial KNN films

Feng Chen[1], Yuanhang Li[1], Wenbin Wu[1], Ke Wang[2], Jing-Feng Li[2], Shunyi Li[3] and Adreas Klein[3]
[1]*High Magnetic Field Laboratory, Chinese Academy of Science, Shushanhu Road 350, Hefei 230031, China*
[2]*State Key Laboratory of New Ceramics and Fine Processing, Department of Materials Science and Engineering, Tsinghua University, Beijing, 100084, China*
[3]*Technische Universität Darmstadt, Institute of Material Sciences, Surface Science, Jovanka-Bontschits-Str. 2, 64287 Darmstadt, Germany*

***Keywords**:* KNN epitaxial film, fatigue

$(K,Na)NbO_3$ was supposed to be one of the most promising substitutes for toxic Pb-based ferroelectrics because of the comparable properties to PZT system.[1] Therefore; tremendous efforts have been devoted to the environment-friendly KNN-based material during the past decade. Modern devices require function materials with low dimension. In this presentation, we report on epitaxial $(1-x)(Na_{0.49}K_{0.49}Li_{0.02})(Nb_{0.8}Ta_{0.2})O_3$-$xCaZrO_3$ [KNN] films grown by pulsed laser deposition on $SrTiO_3$ substrate. The effects of deposition parameters and electrode configurations on their ferroelectric properties were systematically studied. High resolution XRD, Raman scattering and XPS were carried out to characterize the quality of the films. The film made with optimized parameters shows high crystallinity with FWHM at ~ 0.1° and exhibits large remnant and saturated polarization of 13.2 and 27.9 μC/cm^2. Moreover, it is found that KNN epitaxial films show a high fatigue resistance even with Pt metallic electrode, which is dramatically different from PZT films,[2] indicating a higher capability of integration in modern micro-electromechanical systems (MEMS). The XPS results show that KNN/Pt interface is much stable, comparing to PZT/Pt interface, which might be closely related to the fatigue behavior.

References:

[1] Ke, Wang, Fang-Zhou Yao, Wook Jo, Danka Gobeljic, Vladimir V Shvartsman, Doru C Lupascu, Jing-Feng Li,Jürgen Rödel, Adv. Funct. Mater., 23, 33, (2013), 4079-7086
[2] Feng Chen, Qin-Zhuan Liu, Hai-Feng Wang, Fu-Heng Zhang, Wenbin Wu, Appl. Phys. Lett., 90, 19, (2007), 192907-192909

LP-I04

Synthesis of NaNbO3-BaTiO3 Lead-free Piezoelectric Ceramics using Submicron-sized Starting Materials

Rintaro Aoyagi *
Department of Engineering Physics, Electronics and Mechanics, Nagoya Institute of Technology
Nagoya, 466-8555, Japan

Keywords: Sodium niobate, Lead-free material, Piezoelectric property, Ceramics

PZT-based ceramics are widely used in piezoelectric devices such as actuator, ultrasonic generator, and resonator. Recently, it has been a strong demand to develop environmentally friendly lead-free piezoelectric materials. Many researchers have focused on alkaline niobate ($ANbO_3$)-based piezoelectric materials as alternative candidates for lead-based substances. Among of them, sodium niobate $NaNbO_3$ is a well-known anti-ferroelectric material and some NN-based perovskite solid solutions exhibit piezoelectric and ferroelectric properties above room temperature. It is considered that the control of domain size and grain size is one of key techniques for improvement of piezoelectric properties in lead-free material. Especially, the two-step sintering method using fine powder source is very effective to control the grain size for bulk ceramics. In this study, the $(1\text{-}x)NaNbO_3$–$xBaTiO_3$ (NNBTx) solid solution has been synthesized using submicron-sized $BaTiO_3$ and $NaNbO_3$ powders.

The submicron-sized $NaNbO_3$ powder was synthesized by a molten salt method and average particle size of that was 180 nm. The $NaNbO_3$ powder synthesized via molten salt method and commercially available BaTiO3 powder (100 nm: Sakai Chemical Ltd. BT-01) were mixed and the greens were prepared using mixture. The greens were sintered at 500–1220 °C in order to investigate the reaction and grain growth.

In this study, $BaTiO_3$ concentrations of x=0 and 0.1 were prepared. Sintering temperatures of both NNBT0 and NNBT0.1 ceramics prepared using molten salt $NaNbO_3$ powder were 100 °C lower than those prepared by mixed oxide and carbonate route. It was found that the starting materials of $NaNbO_3$ and $BaTiO_3$ reacts to a tetragonal NNBT-type perovskite structure at 1000 °C and to start rapid grain growth and densification at >1100 °C. The piezoelectric constant d_{33} and coupling factor k_p of NNBT0.10 synthesized from fine powders were 145 pC/N and 0.34, respectively, which are larger than those of conventional samples.

LP-I05

Phase Transition and Effect of Poling Temperature on Piezoelectricity of $CaZrO_3$-Modified (K, Na)NbO_3-Based Lead-Free Ceramics

Ke Wang*, Fang-Zhou Yao and Jing-Feng Li
School of Materials Science and Engineering, Tsinghua University, Beijing, China

Keywords: Piezoelectric ceramics, Lead-free, Sodium potassium niobate

(K, Na)NbO_3 (KNN)-based ceramics received incredible attention recently, due to its promising potential as next generation lead-free piezoceramics. The enhanced piezoelectric performance of KNN is recognized and related to the coexistence of polymorphic phases. Recently, we found that the phase constitution of $CaZrO_3$-modified KNN ceramics is not only influenced by chemical doping, but also affected by intergranular stress. In addition, we also noticed that little attention has been paid to the optimization of poling conditions in KNN-based ceramics with a polymorphic phase transition, while electrical poling is indispensable for endowing isotropic ferroelectric polycrystals with a net macroscopic polarization and hence piezoelectricity. This study investigated the electrical properties of $CaZrO_3$-modified KNN-based lead-free piezoceramics as a function of the poling temperature. Peak piezoelectric coefficient d_{33} of 352 $\pm$ 7 pC/N and planar electromechanical coupling factor k_p of 0.47 were obtained at the optimized poling temperature of 120 ^oC, which crosses the polymorphic phase transition regime. In-depth analysis of the asymmetric polarization hysteresis loops and bipolar strain curves uncovered striking analogy between electrical poling and unipolar cycling in the current system, which is attributed to a competition between domain reorientation and space charge accumulation.

References:

[1] J.-F. Li, K. Wang, F.-Y. Zhu, L.-Q. Cheng and F.-Z. Yao, J. Am. Ceram. Soc. 96 (2013) 3677.
[2] K. Wang, F.-Z. Yao, W. Jo, D. Gobeljic, V. V. Shvartsman, D. C. Lupascu, J.-F. Li, J. Rodel, Adv. Funct. Mater. 23(2013) 4079.
[3]F.-Z. Yao, E. A. Patterson, K. Wang, W. Jo, J. Roedel, J.-F. Li, Appl. Phys. Lett., 104 (2014)242912.
[4] F.-Z. Yao, Q. Yu, K. Wang, Q. Li, J.-F. Li, RSC Advances 4(2014)20062.
[5] F.-Z. Yao, J. Glaum, K. Wang, W. Jo, J. Roedel, J.-F. Li, Appl. Phys. Lett., 103 (2013)192907.
[6] K. Wang, J.-F. Li, Adv. Funct. Mater. 20 (2010)1924.
[7] K. Wang, J.-F. Li and N. Liu, Appl. Phys. Lett., 93(2008) 092904.
[8] K. Wang, J.-F. Li, Appl. Phys. Lett., 91(2007) 262902.

Acknowledgement:

This work was supported by National Nature Science Foundation of China (Grants No. 51332002, 51302144) and Tsinghua University Initiative Scientific Research Program.

LP-I06

Piezoelectric Properties Of $(Bi_{0.5}Na_{0.5})TiO_3$-$BaTiO_3$-Based Lead-Free Ceramics And Its Application To Ultrasonic Cleaner

Tonshaku TOU*, Yuki HAMAGUTI, Yuichi MAIDA
Ceramics Division, Electronics Co., Ltd., Toyohashi, Aichi 441-3193, Japan

Keywords: Lead-free, Piezoelectricity, Transducer, Cleaner, Piezoceramics

$Pb(Zr,Ti)O_3$ piezoceramics has been widely used in actuators, sensors, resonators and ultrasonic transducers. However, environmentally friendly piezoelectric materials are required to replace the materials due to the toxicity of lead oxide. $(Bi_{0.5}Na_{0.5})TiO_3$-based ceramics is considered to be a good candidate for lead-free ceramics. We have developed a new lead-free piezoceramics $(Bi_{0.5}Na_{0.5})TiO_3$-$BaTiO_3$-$(Bi_{0.5}Na_{0.5})(Mn_{1/3}Nb_{2/3})O_3$. Here, the high power characteristics of the ceramics were reported. The properties of a bolt-clamped Langevin transducer (BLT) using the ceramics were investigated. The cleaning effect of an ultrasonic cleaner using the BLTs was evaluated. The problem of practical application and the solution was reported.

Commercially available Bi_2O_3, Na_2CO_3, $BaCO_3$, TiO_2, Nb_2O_5 and $MnCO_3$ powders, all with a purity of at least 99.0% were used as raw materials. After the corresponding metal oxides of the prescribed amount being mixed by ball-milling, $(Bi_{0.5}Na_{0.5})TiO_3$-$BaTiO_3$-$(Bi_{0.5}Na_{0.5})(Mn_{1/3}Nb_{2/3})O_3$ was synthesized by heating at 850°C for 2 hours, and then pulverized. The pulverized powder was formed and sintered isothermally at 1100- 1200°C for 2 hours. The piezoelectric properties of the sample were measured after poled. The poled samples were used to fabricate BLT. The BLTs were applied to ultrasonic cleaner.

Various quantities of $(Bi_{0.5}Na_{0.5})(Mn_{1/3}Nb_{2/3})O_3$ were added into $(Bi_{0.5}Na_{0.5})TiO_3$-$BaTiO_3$ ceramics. Optimum composition $0.82(Bi_{0.5}Na_{0.5})TiO_3$-$0.15BaTiO_3$-$0.03(Bi_{0.5}Na_{0.5})(Mn_{1/3}Nb_{2/3})O_3$ ceramicsshows a good piezoelectric behavior of Kt=45%, Qm=500, d_{33}=110 pC/N and high mechanical strength. Figure 1 shows the vibration velocity of the vibration surface of the BLT (28 kHz) as a function of input electric power. The vibration velocity of both BLTs increased with an increase in input electric power. The vibration velocity of BLT using lead-free piezoelectric ceramics was larger than that of hard PZT at the same input power. This suggests that the power loss in lead-free BLT is smaller than that in hard BLT. Figure 2 variation of the intensity of ultrasound of the cleaner (15 BLTs, 600W type) with distance from the bottom. The intensity of ultrasound of cleaner using lead-free ceramics was higher than that of hard PZT. This result was correspondent to the relationship between vibration velocity and input electric power as shown in Fig. 1. Therefore, the ultrasonic cleaner using lead-free ceramics had a high clean effect which was good for commercial application.

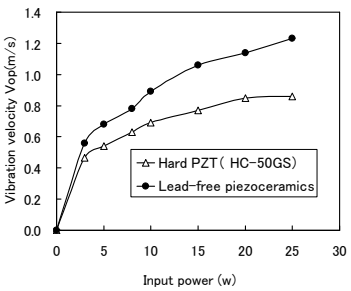

Figure 1. Vibration velocity of the vibration surface of the BLT (28 kHz) as a function of input electric power.

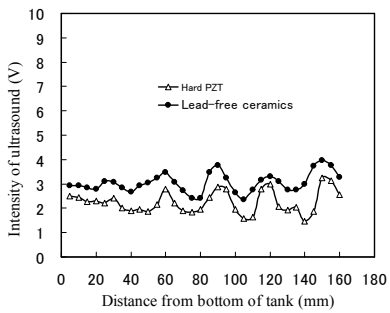

Figure 2. Vibration of the intensity of the ultrasound of the cleaner with the distance from bottom.

LP-I07

Piezoelectric Enhancement of Lead-free Piezoelectrics with Nano/macro Complex-domain Configurations for Piezo-frontier

Satoshi WADA[1*], Ryo IIZUKA[1], Shintaro UENO[1], Kouichi NAKASHIMA[1], Chikako MORIYOSHI[2], Yoshihiro KUROIWA[2]

[1]*Material Science and Technology, University of Yamanashi, 4-4-37 takeda, Kofu, Yamanashi 400-8510, Japan*

[2]*Department of Physical Science, Hiroshima University, 1-3-1 Kagamiyama, Higashi-Hiroshima, Hiroshima 739-8526, Japan*

Keywords: Materials, Process, Property, Structure, Ceramics

It is well known that for the relaxor-based ferroelectrics, the domain configuration is dependent on chemical composition and orientation. This means that if relaxor-based lead-free ferroelectrics are prepared, it can be expected that they might have high piezoelectric performances. Recently, we reported that BT-Bi($Zn_{1/2}Ti_{1/2}$)O_3 (BT-BZT) and BT-Bi($Mg_{1/2}Ti_{1/2}$)O_3 (BT-BMT) were relaxor ferroelectrics with high T_{max} (temperature with maximum dielectric constant) over 250 ˚C. Thus, it is possible to control domain configurations by solid solution system between the above relaxors and normal ferroelectric such as $BiFeO_3$ (BF) with high T_c of 830 ˚C. In this study, the BT-BMT-BF and BT-BZT-BF system ceramics were prepared using a conventional solid–state reaction and their crystal structure and electrical properties were investigated. A single phase of perovskite was prepared for these ceramics with various compositions except for a few. TEM observation revealed that BT-BMT had no domain configuration while BF-rich ceramics had normal rhombohedral domain configurations. Moreover, the ceramic with the intermediate composition between relaxor and BF had nanodomain configuration with domain sizes less than 50 nm. For the ceramics, the temperature dependences of dielectric constants were measured at various frequencies, and the T_{max} was determined. As the results, the T_{max} increased with increasing BF content, while T_{max} decreased with increasing BT content. Finally, their strain vs. electric-field behaviors were measured, and the relaxors showed typical electrostrictive behavior while BF-rich ceramics showed typical butterfly-like ferroelectric strain behavior. For the ceramics with nanodomain configuration, the strain curve with hysteresis was clearly observed and the apparent d_{33}^* ($=S_{max}/E_{max}$) from the slope was over 850 pC/N.

LP-I08

Enhanced Strain Properties of Relaxor Matrix Ferroelectric Composites in Bi-Based Lead-Free Piezoelectric Ceramics

Jae-Shin LEE[1*], Chang-Won AHN[2], Soon-Jong JEONG[3], Jing-Feng LI[4], and Wook JO[5]
[1]*School of Materials Science and Engineering, University of Ulsan, Ulsan 680-749, Korea*
[2]*Department of Physics, University of Ulsan, Ulsan 680-749, Korea*
[3]*Korea Electrotechnology Research Institute, Changwon 642-120, Korea*
[4]*State Key Laboratory of New Ceramics and Fine Processing, School of Materials Science and Engineering, Tsinghua University, Beijing 100084, China*
[5]*School of Materials Science and Engineering, Ulsan National Institute of Science and Technology, Ulsan 689-798, Korea*

Keywords: Lead-free, Piezoelectric, Strain, Relaxor, Ferroelectric, Composites

Recently, Bi-perovskite ceramics have attracted much attention because of their large electric field-induced strains (EFIS) at ferroelectric (FE) – relaxor ferroelectric (RFE) phase boundaries. During the last decade, we found that many modified $Bi_{1/2}Na_{1/2}TiO_3$ - $Bi_{1/2}K_{1/2}TiO_3$ (BNT-BKT or BNKT) solid solutions exhibited abnormally large strain properties when there was a ferroelectric-relaxor (FE-R) crossover with increasing the modifier content [1]. In the case of A- or B-site impurities, the FE-R crossover was observed when the tolerance factor (t) of the perovskite structure was decreased by doping, whereas the FE state of unmodified BNKT remained stable when the dopant increased the t.
Despite the fact that BNKT-based ceramics have shown large normalized strains up to S_{max}/E_{max} = 876 pm/V at RT near the FE-R transition region [2], there still remain critical problems to be resolved for practical applications; large strain-field hysteresis and large electric-field to trigger large strain.
In order to overcome these issues, we attempted to prepare ceramic-ceramic composites by embedding FE particles in a relaxor matrix. The normalized strain S_{max}/E_{max} was remarkably enhanced by lowering the triggering field even though the maximum strain was almost unchanged. The ceramic-ceramic composite is believed to enlighten a new road to large strain lead-free alternatives of Pb-based actuator materials.

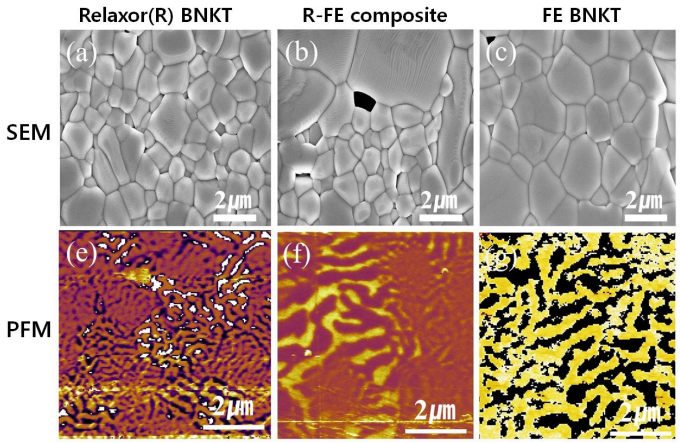

Figure 18. SEM and PFM images of a relaxor-ferroelectric BNKT composite**.**

References:

[1] H. B. Lee, D. J Heo, R. A. Malik, C. H. Yoon, H. S. Han, and J. S Lee, *Ceram. Int.* 39, Suppl. 1, s705 (2013).
[2] R. A. Malik, J. K. Kang, A. Hussain, C. W. Ahn, H. S. Han, and J. S. Lee, *Appl. Phys. Express* 7, 61502 (2014).

LP-I09

Giant Electrostrain in Textured $Bi_{0.5}(Na,K)_{0.5}TiO_3$–based Ceramics

Chang Won AHN[1*], Si-Young CHOI[2], Gang Ho CHOI[1], Aman ULLAH,[1] Dae-Soo LEE[3], Soon-Jong JEONG[3], Ki Bong JANG[4], Jae-Shin LEE[5], and Ill Won KIM[1]
[1]*Department of Physics and EHSRC, University of Ulsan, Ulsan 680-749, S. Korea*
[2]*Advanced Characterization & Analysis Group, KIMS, Changwon 642-831, S. Korea*
[3]*Advanced Materials & Application Research Laboratory, KERI, Changwon 642-120, S. Korea*
[4]*R&D Center, Samjeon Co. Ltd. Ulsan 689-934, S. Korea*
[5]*School of Materials Science and Engineering, University of Ulsan, Ulsan 680-749, S. Korea*

Keywords: Lead-free, Texture, Strain, $Bi_{0.5}Na_{0.5}TiO_3$

Lead-free piezoelectric ceramics exhibited superior electromechanical responses near the morphotropic phase boundary (MPB). Among the lead-free piezoelectric ceramics so far developed, the binary $(1\text{-}x)Bi_{0.5}Na_{0.5}TiO_3$ - $xBi_{0.5}K_{0.5}TiO_3$ class of materials has received considerable attention due to its excellent ferroelectric and piezoelectric properties near the rhombohedral-tetragonal morphotropic phase boundary. Recently, a large electric field induced strain has been reported in $BiAlO_3$-modified $Bi_{0.5}(Na_{0.78}K_{0.22})_{0.5}TiO_3$ lead-free piezoceramics. However, the applied electric field (60kV/cm) for the observed large strain is also high, limiting its applications in actuator devices. On the other hand, it is widely known that textured ceramics showed enhanced piezoelectric properties. In this work, textured $(1\text{-}x)(Bi_{0.5}(Na_{0.78}K_{0.22})_{0.5}TiO_3)$-$xBiAlO_3$ (BNKT-BA-x ; x = 0, 0.015) ceramics were fabricated by templated grain growth (TGG) method using plate-like $Na_{0.5}Bi_{4.5}Ti_4O_{15}$ (NBiT) templates with the viewpoint of improving the strain response and reducing the driving electric field. X-ray diffraction analysis shows pure perovskite phase with tetragonal symmetry. Moreover, it was found that, the textured ceramics show high orientation factor (lotgering's factor) >90%. The textured BNKT-BA-0.015 ceramics exhibited large strain (S = 0.55%) at applied electric field of 40 kV/cm, which corresponds to a normalized strain (S_{max}/E_{max}) of ~1370 pm/V. Furthermore, the strain value is fairly temperature stable up to 110 °C, which is highly promising for actuator applications.

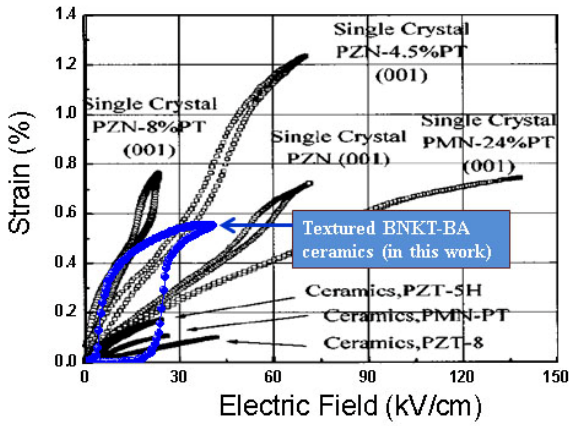

Figure 19 S-E curve of textured BNKT-BA ceramics in comparison to Pb-based materials

References:

[1] S.-E. Park *et al*., J. Appl. Phys. 82, (1997) 1804.

Acknowledgement:

This work was supported by Priority Research Centers Program through the National Research Foundation of Korea(NRF) funded by the Ministry of Education (2009-0093818)

LP-I10

Electric Field Induced Antiferroelectric - Ferroelectric Phase Transition on $NaNbO_3$-Based Lead-Free Ceramics

Hiroyuki SHIMIZU[1,2*], Youichi MIZUNO[1], Clive RANDALL[2]
[1]*Taiyo Yuden Co., Ltd., Material R&D Department 1, Takasaki, Gunma 5607-2, Japan*
[2]*The Pennsylvania State University, Center for Dielectrics and Piezoelectrics, University Park, Pennsylvania 16802, USA*

Keywords: $NaNbO_3$, antiferroelectric, tolerance factor, electric field induced phase transition

Sodium niobate $NaNbO_3$ (NN) has been known structurally to be antiferroelectric (AFE) phase with *Pbma* at room temperature.[1] However, a number of groups have already reported an electric field induced metastable ferroelectric (FE) phase with $P2_1ma$,[2] and the observed electrical properties can be attributed to a metastable FE phase. As for polarization-electric field (*P-E*) characteristics, lead-containing AFE ceramics such as $PbZrO_3$ and La doped PZT95/5 (PLZT) feature double *P-E* loops, marking a reversible AFE↔FE phase transition.[3-5] In contrast, square *P-E* loops, typical characteristic of ferroelectrics, are usually observed in polycrystalline NN ceramics at room temperature once large polarizations are developed. In this work, we stabilized the AFE phase in NN ceramics in terms of designing tolerance factor and electronegativity in the perovskite structure, and thereby demonstrated clear double *P-E* loops under ac field and small capacitance change with dc field. Tolerance factor can be generally categorized into two regions of AFE and FE distortive, as shown in Fig. 1. Considering polarizability in systems that have a tolerance factor decrease, AFE cations such as Zr^{4+} and Hf^{4+} can be expected enough for lowering tolerance factor. In that case, divalent cations such as Sr^{2+} and Ca^{2+} should be needed for charge neutrality. These combinations between 2+ and 4+ ions chemically derive stabilized antiferroelectricity according to increased average-electronegativity-difference in the perovskite structure. From these expectations, $(Na_{1-x}Ca_x)(Nb_{1-x}Zr_x)O_3$ (x=0.00, 0.02, 0.04, 0.05, 0.06 and 0.10, abbreviated as CZNNx) ceramics were prepared by conventional solid state reaction. Figure 2 shows close view of XRD spectra around AFE {1 1 3/4} superlattice peak in the sintered ceramics. The normalized intensity obviously increased comparing to CZNN0.00 ceramic although solid state limitation seems to be around x=0.06. This indicates that antiferroelectricity in NN is enhanced as expected. Figure 3 shows the AFE↔FE phase transition behavior at high temperature. The CZNN0.00 ceramic showed a square *P-E* loop resulting from induced metastable FE phase as mentioned above, on the other hand, the CZNN0.02, CZNN0.04 and CZNN0.05 ceramics showed clear double *P-E* loops. Remarkably, the induced polarization decreased and switching field ($E_{\text{AFE to FE}}$) increased with amount of Ca and Zr. Reflecting this behavior, the CZNN0.05 ceramic showed much smaller capacitance change and loss under dc field below the switching field at high temperature. This work will provide new opportunities for lead-free AFE application like high temperature-voltage capacitors as well as PLZT of lead-containing AFE ceramics.

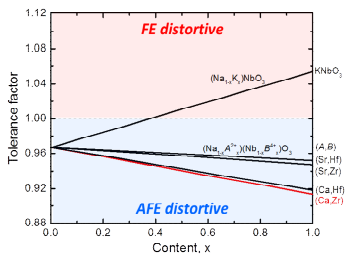

Figure 1 Relation of tolerance factor and dopant content in NN.

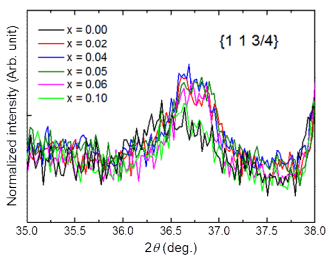

Figure 2 Close view of XRD spectra on the characteristic AFE {1 1 3/4} superlattice peak

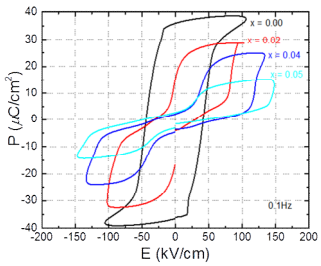

Figure 3 Polarization vs. electric field hysteresis loops observed at high temperature around 120°C.

References:

[1] A. C. Sakowski-Cowley, K. Lukaszewicz, and H. D. Megaw, *Acta Crystallogr.,* 25, 851–65 (1969).
[2] V. A. Shuvaeva, M. Yu. Antipin, R. S. V. Lindeman, O. E. Fesenko, V. G. Smotrakov, and Yu. T. Struchkov, *Ferroelect.,* 141 [1], 307–31 (1993).
[3] Z. Xu, X. Dai, and D. Viehland, *Phys. Rev. B,* 51, 10 (1995).
[4] D. Berlincourt, H. H. A. Krueger, and B. Jaffe, *J. Phys. Chem. Solids.*, 25, 659 (1964).
[5] X. Tan, C. Ma, J. Frederick, S. Beckman, and K. G. Webber, *J. Am. Ceram. Soc.*, 94, 4091 (2011).

LP-I11

Electromechanical Properties of $0.94Bi_{0.5}(Na_{0.75}K_{0.25})_{0.5}TiO_3$-$0.06BiAlO_3$ / $Bi_{0.5}(Na_{0.8}K_{0.2})_{0.5}TiO_3$ ceramic composite

Soon-Jong Jeong[1*], Min-Soo Kim[1], Seok-Myung Jang[1]
[1] *Battery Research center, Korea Electrotechnology Research Institute, Changwon, 641-120,Korea*

Keywords: Lead-free Piezoelectrics, Composites, Process, Property, Structure, Ceramics

We investigated the temperature-dependent polarization and strain of two Bismuth-based perovskite composites. Matrix material was chosen as $0.94Bi_{0.5}(Na_{0.75}K_{0.25})_{0.5}TiO_3$-$0.06BiAlO_3$ (BNKT-BA) which have a transition from relaxor to ferroelectric phase (T_{R-F}). Seed materials were $Bi_{0.5}(Na_{0.8}K_{0.2})_{0.5}TiO_3$ (BNKT) and $0.985Bi_{0.5}(Na_{0.8}K_{0.2})_{0.5}TiO_3 - 0.015BiAlO_3$ (BNKTBA), which possessing different polarization characteristics. Depending on the test temperature, the different polarization and strain behaviors were observed between the BNKT-BA/BNKT and BNKT-BA/BNKT BA composites. At T=25 ^oC, the two composites (BNKT-BA/BNKT and BNKT-BA/BNKTBA) exhibited double-like polarization loops and parabolic strain curves which involve an ergodic relaxor-to-normal ferroelectric phase transition with external electric field and a reverse ferroelectric-to relaxor phase transition with removal of the field. At T= 120 ^oC, two composites have slim polarization and strain curves, which are almost the same as those of the pure BNKT-BA. The high field-induced polarization and strain with respect to temperature for the composites are related to the thermal stability of the ferroelectric seeds, and the nucleation and growth of ferroelectric domain in the relaxor matrix.

LP-I12

Giant Electric-Field-Induced Strain and Coupling Mechanisms of Relaxor-Ferroelectric Lead-Free Ceramic Composites

Haibo Zhang[1*], Qi Zhang[2], Wook Jo[3] Shenglin Jiang[4]

[1]*College of Materials Science and Engineering, State Key Laboratory of Material Processing and Die & Mould Technology, Huazhong University of Science and Technology, Luoyu Road 1037, Wuhan 430074, P. R. China*

[2]*School of Materials Science and Engineering, The University of New South Wales, New South Wales 2052, Australia*

[3]*School of Materials Science and Engineering, Ulsan National Institute of Science and Technology,Ulsan 689-798, South Korea*

[4]*School of Optical and Electronic Information, Huazhong University of Science and Technology, Luoyu Road 1037, Wuhan 43007 , P. R. China*

Keywords: Lead-free piezoceramics, Electric-Field-Induced Strain, Polarization coupling, Strain coupling Structure

A new relaxor(RE)/ferroelectric(FE) 0-3 composite lead-free piezoceramics were developed and the giant strain resulted from the electric-field-induced ergodic relaxor to ferroelectric phase transition could realize at a relatively low field of 4 kV/mm. The composite comprised of 70 vol.% $0.91Bi_{1/2}Na_{1/2}TiO_3$-$0.06BaTiO_3$-$0.03AgNbO_3$ RE matrix and 30 vol.% $0.93Bi_{1/2}Na_{1/2}TiO_3$-$0.07BaTiO_3$ FE seed shows a giant normalized d_{33}^* of 824 pm V^{-1} at room temperature(Figure 1). In order to explore the underlying mechanisms of this composite effect, two multilayer ceramics with alternating RE and FE layers were also prepared, one with the layers parallel (PCM, polarization coupled multilayer) and the other with the layers perpendicular (SCM, strain coupled multilayer) to the electroded surfaces. It was found that additional to the polarization coupling the strain coupling also plays an equally critical role in the reduction of electric field required for RE to FE phase transition.

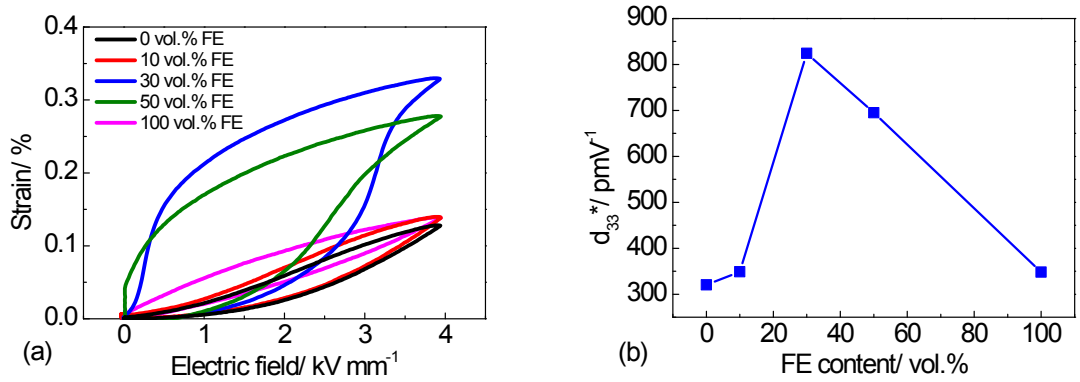

Figure 1. (a) Unipolar strain at 4 kV/mm and (b) the large signal d_{33}^*, S_{max}/E_{max} of bulk composites with various FE content

Acknowledgement:
Helpful discussions with Claudia Groh Dr. Kyle Webber*, and Professor Jürgen Rödel were gratefully acknowledged.

LP-I13

Processing and Characterization of Reduction-Resistant Lead-Free Piezoelectric (Ba,Ca)TiO_3 Ceramics and Their Grain Growth Control

Wataru SAKAMOTO[1*], Hiroki ICHIKAWA[1], Yoshikazu AKIYAMA[2], Toshinobu YOGO[1]
[1]*EcoTopia Science Institute, Nagoya University, Furo-cho, Chikusa-ku, Nagoya 464-8603, Japan*
[2]*Ricoh Co., Ltd., Atsugi, Kanagawa 243-0298, Japan*

Keywords: Barium titanate, Reduction-resistant, Lead-free piezoelectric, Grain-oriented, Electrical properties

$Pb(Zr,Ti)O_3$ (PZT)-based oxides have been widely applied as piezoelectric materials because of their excellent electrical properties. However, these materials contain toxic PbO as a major component. Recently, because of growing concerns about the effects of toxic lead on the global environment, the development of materials which do not contain toxic elements is strongly required. Therefore, the research and development of lead-free piezoelectric materials have been carried out extensively all over the world. Among several ferroelectric alternatives to PZT, $BaTiO_3$ has been receiving much attention as a potential candidate. In $BaTiO_3$-based materials, the phase diagram and the characteristic giant electromechanical response of Ca-substituted $BaTiO_3$ following the application of an electric field have been reported [1].

In this study, processing of reduction-resistant (Ba,Ca)TiO_3 ceramics as lead-free piezoelectric materials was investigated. Nonreducible (Ba,Ca)TiO_3 ceramics were fabricated by appropriately setting the chemical composition, such as the Ba and Mn concentrations in Mn-doped (Ba,Ca)TiO_3 ceramics. Among (Ba,Ca)TiO_3 ceramics with various $CaTiO_3$ contents, the nonreducible $(Ba_{0.85}Ca_{0.15})TiO_3$ exhibited the highest field-induced strain coefficient (estimated from the slope of an unipolar strain loop) of 260 pm/V at room temperature. To improve their electrical properties, (100),(001)-oriented $(Ba_{0.85}Ca_{0.15})TiO_3$ ceramics were fabricated by the reactive templated grain growth (RTGG) method using a mixture of platelike $CaTiO_3$ and $BaTiO_3$ particles. The platelike $CaTiO_3$ and $BaTiO_3$ particles were prepared through a topochemical microcrystal conversion process [2] using $CaBi_4Ti_4O_{15}$ and $BaBi_4Ti_4O_{15}$ plate-like precursor crystals. The {100} orientation degree of the grain-oriented $(Ba_{0.85}Ca_{0.15})TiO_3$ ceramics was 92%, as estimated by Lotgering's equation. In addition, 1 mol% Ba excess and 1 mol% Mn-doped $(Ba_{0.85}Ca_{0.15})TiO_3$ sintered bodies, which were sintered at 1350 ^oC in an Ar flow containing H_2 (0.3%), had sufficient resistivity to allow the characterization of electrical properties utilizing a high applied field. The ferroelectric and field-induced strain properties of the $(Ba_{0.85}Ca_{0.15})TiO_3$ ceramics, sintered in the reducing atmosphere (oxygen partial pressure below 0.1 Pa (10^{-6} atm)), were markedly improved as a result of fabricating grain-oriented samples [3]. The field-induced strain coefficient of the nonreducible (100),(001)-oriented $(Ba_{0.85}Ca_{0.15})TiO_3$ ceramics reached 570 pm/V, which was higher than that of polycrystals (260 pm/V) with no preferential orientation.

Although further enhancements of the piezoelectric properties are still necessary, the reduction-resistant grain-oriented (Ba,Ca)TiO_3-based ceramics are expected to be promising candidates for lead-free ceramic materials for multilayer-type piezoelectric applications.

References:

[1] D. Fu, M. Itoh, S. Koshihara, T. Kosugi, S. Tsuneyuki, Phys. Rev. Lett. 100 (2008) 227601.
[2] Y. Saito, H. Takao, T. Tani, T. Nonoyama, K. Takatori, T. Hommma, T. Nagaya, M. Nakamura, Nature 432 (2004) 84.
[3] H. Ichikawa, W. Sakamoto, Y. Akiyama, H. Maiwa, M. Moriya, T. Yogo, Jpn. J. Appl. Phys. 52 (2013) 09KD08.

LP-I14

Regarding electric-field-induced transition between ferroelectric and relaxor

Wook Jo
Sustainable Functional Materials Lab, School of Materials Science and Engineering,
Ulsan National Institute of Science and Technology, Korea

$(Bi_{1/2}Na_{1/2})TiO_3$ (BNT)-$BaTiO_3$ (BT) solid solution system is one of the most attended lead-free piezoceramic systems over the last decades due to many scientifically intriguing issues such as alleged antiferroelectricity with relaxor features, highly sophisticated temperature-dependent polymorphisms, the presence of morphotropic phase boundary (MPB) similar to that in the market dominating PZT ceramics,, *etc*. In addition, compositional modifications usually result in the birth of so-called 'incipient' piezoelectric strains that are typically about two times as large as those the conventional lead-based piezoceramics can deliver. A key to resolving the existing issues for the system is to identify the phase stability that depends on various thermodynamic variables such as temperature, composition, and electric field. In this talk, we present comprehensive aspects of the phase stability of BNT-BT piezoceramics revealed by temperature-dependent dielectric permittivity measurements, pyroelectric/ferroelectric measurements, as well as in situ diffraction studies. The role of Ba in BNT piezoceramic as well as the intriguing feature of the phase diagram will be discussed in detail.

LP-I15

Fabrication of Textured $Na_{0.5}Bi_{0.5}TiO_3$–$BaZrO_3$ Ceramics by Tape Casting Technique

Ali HUSSAIN[1], Rizwan-Ahmed MALIK[1], Jin-Soo KIM[1], Myong-Ho KIM[1], Tae-Kwon SONG[1] and Won-Jeong KIM[2]

[1]*School of Advanced Materials Engineering, Changwon National University, Gyeongnam 641-773, Republic of Korea*

[2]*Department of Physics, Changwon National University, Gyeongnam 641-773, Republic of Korea*

Keywords: $Na_{0.5}Bi_{0.5}TiO_3$ ceramics, grain orientation, tape casting

Over the past two decades, lead-free piezoelectric ceramics have been focused as alternative materials for the replacement of lead-based ceramics in piezoelectric industry [1]. Nevertheless, most of the lead-free piezoelectric ceramics have substandard properties as compared with lead-based piezoelectric ceramics. Much research works have been conducted to investigate new materials and methods for the improvement of piezoelectric properties of lead-free ceramics. In general, two methods are considered very effective: first, development of new ceramics through compositional modification of the morphotropic boundary (MPB) solid solution, second, fabrication of textured ceramics, i.e., ceramics having a uniform grain orientation.

Grain orientation technique, such as templated grain growth (TGG) method has been largely used to prepare textured ferroelectric and piezoelectric ceramics with perovskite structure [2]. In this work, textured $0.94Na_{0.5}Bi_{0.5}TiO_3$-$0.06BaZrO_3$ (NBT-BZ) ceramics with a preferred {100} grain orientation were fabricated by a tape casting method using plate-like $Na_{0.5}Bi_{0.5}TiO_3$ (NBT) particles and their physical properties were compared with non-textured NBT-BZ ceramics prepared by a conventional method. The experimental results show that textured NBT-BZ ceramics sintered at 1150 ^oC for 15 h have improved dielectric and piezoelectric properties. Both textured and non-textured ceramics exhibit pseudo-cubic crystal structure, however, textured NBT-BZ ceramics have {100} preferred orientation degree of 83% and have large grain growth. The room temperature dielectric constant increased from 1250 for non-textured ceramics to 1580 for the textured NBT-BZ ceramics. The textured ceramics show high piezoelectric constant than non-textured NBT-BZ ceramics. In addition, the field-induced strain response improved from 0.15% for non-textured NBT-BZ to 0.30% for textured NBT-BZ ceramics.

References:

[1] J. Rödel, W. Jo W, K. T. P. Seifert, E-M. Anton, T. Granzow, D. Damjanovic, J. Am. Ceram. Soc. 92 **(**2009)1153.

[2] H. Amorín, A. L. Kholkin, M. E. V. Costa, J. Eur. Ceram. Soc. 25 **(**2005) 2453.

Acknowledgement:

This work is supported by the National Research Foundation of Korea (NRF) grant funded by the Korean government (MOE) (2013R1A1A2058345) and Basic Research program through the National Research Foundation of Korea (NRF) funded by Ministry, Science and Technology (MEST) (2011-0030058).

CO-I01

Multi-scale computational design of active components for Li-ion batteries

Joonhee Kang[1], Hyejin Lee[1], Byoungwoo Kang[2], Habin Chung[2], Byungchan Han[1*]
[1] *Department of Energy Systems Engineering, DGIST, Daegu, 711-873, South Korea*
[2] *Department of Materials Science and Engineering, Pohang, 790-784, Republic of Korea*

Keywords: Materials genome, First principles calculations, Energy materials, Batteries

With advanced computing power and soft engineering first principles computation opened new areas for discovering new materials. If combined with rigorous statistical mechanics this approach becomes even more powerful tool, in particular, for screening promising candidates from wide range of sampling space. This presentation shows two such examples regarding energy materials: solid-state electrolyte and high energy density cathode for Li-ion battery application.

Fundamental diffusion mechanisms of Li-ion in the solid-state NASICON structures were studied using first principles density functional theory (DFT) calculations and validated with experimental measurements. For two materials without ($Li_{1.0}Ge_{2.0}(PO_4)_3$, LGP) and with ($Li_{1.5}Al_{0.5}Ge_{1.5}(PO_4)_3$, LAGP) an Al^{3+}-doped materials to (LGP), thermodynamically the most plausible diffusion path and the activation energy along the way were rigorously evaluated. Based on the calculated results we propose that aliovalent doping can significantly enhance Li-ion conductivity as high as 100 times depending on the doing level. More interestingly, we discovered that the doped Al3+ ions create new diffusion path that allows at least two Li-ions *cooperatively* interact to transport together at the same time with substantially reduced activation barriers compared with other paths. We validated the calculated Li-ion conductivities in the two solid-state materials by experimental measurements ending up with good agreement with the prediction.

As the second example, we studied the electrochemical and thermal stabilities of high-Ni compounds for cathode materials for Li-ion batteries. It was known that incorporating high Ni composition improves energy densities, however, only by scarifying structural integrity. Our studies unveil the underlying mechanisms of the degradation on atomic scale, and propose methodologies ensuring those two materials properties: high energy density and cyclability with a high voltage window.

This presentation sorts out key atomic descriptors in designing energy materials leading to high functionality for engineering-scale systems.

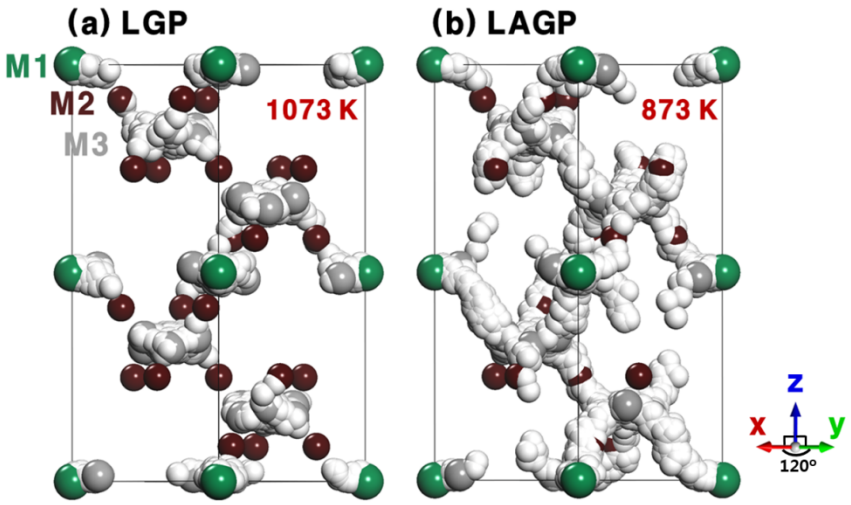

Figure 1. Diffusion paths of Li ions in solid-state LGP and LAGP electrolytes

CO-I02

First-Principles Study of Piezoelectricity in AlN-based Materials

Hiroyoshi MOMIDA[1*], Akihiko TESHIGAHARA[2], Tamio OGUCHI[1]
[1]*Institute of Scientific and Industrial Research, Osaka University, Ibaraki, Osaka 567-0047, Japan*
[2]*Research Laboratories, DENSO CORPORATION, Nisshin, Aichi 470-0111, Japan*

Keywords: Aluminum nitrides, First-principles calculations, piezoelectricity

Piezoelectric materials are now used in numerous ways such as sensors, actuators, and filters in modern electronic devices. In the recent industrial applications, one of the widely used materials is metal oxide ceramics such as lead zirconium titanium oxides which has high piezoelectric constants of about 410 pC/N at temperatures up to about 250°C, and there are growing demands for novel materials that are usable in higher temperature environments such as in automobile engines. AlN is a candidate material for the high temperature applications due to its high Curie temperature of about 1150°C, and recently significant enhancement of piezoelectricity by alloying with Sc has been found experimentally, attracting great interest in technological as well as scientific fields [1].

In the context of such background, we have computationally investigated atomic mechanisms of the piezoelectricity enhancement of $Sc_xAl_{1-x}N$ materials, and our major goal is to provide a guiding principle to design highly piezoelectric materials by using first-principles calculations. AlN is known to have the wurtzite crystal structure, and we generate several $Sc_xAl_{1-x}N$ model structures by substituting Al with Sc for wide composition range of x=0–1. The first-principles calculations are based on the density functional theory within the generalized gradient approximation, and quantitatively reliable calculations of piezoelectric properties are possible on the basis of the Berry phase approach.

Figure 1 shows calculated piezoelectric constants of $Sc_xAl_{1-x}N$ models versus Sc concentrations. The calculated result clearly demonstrates that the piezoelectric responses of $Sc_xAl_{1-x}N$ increase with increasing Sc concentration (x), as reported by the experiments [1] and calculations [2]. Calculated piezoelectric constants are scattered especially in higher x, and this is due to different spatial distributions of Sc atoms in the models. We analyze microscopic origins of the enhanced piezoelectricity by Sc in AlN, and find that the positions of atoms around Sc largely change in response to external strains. We further carry out similar study for Y and La doped in AlN to examine an element dependence on piezoelectricity, though they are found to be less effective than Sc, probably due to their larger atomic sizes. We discuss a general trend of piezoelectricity versus structure parameters on the basis of our results for several materials with the wurtzite structure.

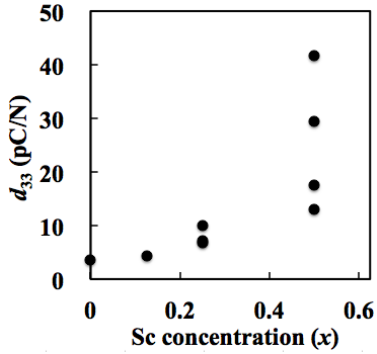

Figure 20 Calculated piezoelectric constants (d_{33}) of $Sc_xAl_{1-x}N$ models vs. Sc concentration (x)

References:

[1] A. Teshigahara *et al.*, *Proc. of Ultrasonics Symposium (IUS), 2012 IEEE International* (2012); M. Akiyama *et al.*, Adv. Mater. 21 (2009) 593.
[2] F. Tasnádi *et al.*, Phys. Rev. Lett. 104 (2010) 137601.

CO-I03

Molecular dynamics simulations of caloric effects in ferroelectrics

Takeshi Nishimatsu
Institute for Materials Research (IMR), Tohoku University, Sendai 980-8577, Japan

Keywords: first-principles effective Hamiltonian, electrocaloric effect, elactocaloric effect

Since 2005, we have been developing our original simulation code named feram specialized for ferroelectric materials[1]. feram is fast molecular dynamics (MD) simulation code for ABO_3 perovskite-type ferroelectrics and distributed as free software from http://loto.sourceforge.net/feram/. The code is based on a first-principles effective Hamiltonian and can be applicable not only bulk ferroelectrics but also ferroelectric thin-film capacitors. Because, in the code, dipole interactions are treated in reciprocal space with fast Fourier transform (FFT), feram is fast enough for simulating ferroelectric materials with a realistic system size up to 100 nm and a realistic time span (> 1000 ns).

Recently, we have developed a direct simulation method of electrocaloric and elastocaloric effects of ferroelectric materials with our feram code[2,3]. The electrocaloric effect is an adiabatic change in the temperature, DT, of a material upon applying an external electric field. In particular, if an electric field is applied to a ferroelectric material at just above its phase transition temperature, T_C, and the field is then removed, a large reduction in temperature is expected. The elastocaloric effect is that of external stress field. It is widely believed that these effects are applicable to solid-state refrigeration technologies.

In Fig. 1, the temperature dependence for the electrocaloric effect DT of $BaTiO_3$, under various initial external electric fields is compared. It can be seen that even with a small initial external electric field (50 kV/cm), $BaTiO_3$ gives a large DT, but the temperature range where this large DT can be obtained is narrow. By increasing the applied fields (>100 kV/cm) the range of applicable temperatures broadens.

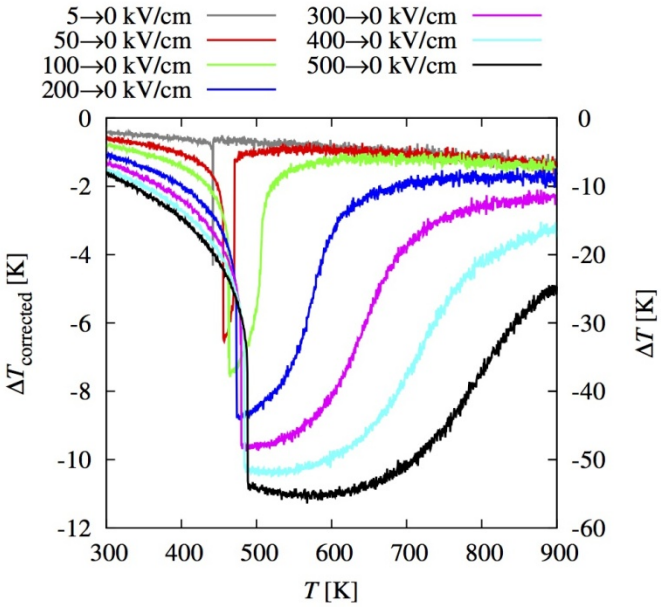

Figure 1 The temperature dependence of DT for various initial external electric fields. The external electric field switches from E_z=5–500 to 0 kV/cm

References:

[1] Takeshi Nishimatsu, Umesh V. Waghmare, Yoshiyuki Kawazoe and David Vanderbilt: Phys. Rev. B 78, 104104 (2008).
[2] T. Nishimatsu, J. A. Barr and S. P. Beckman, J. Phys. Soc. Jpn. 82, 114605 (2013).

CO-I04

Strategy for high-throughput *ab initio* screening of functional ceramic materials

Kanghoon YIM[1], Joohee LEE[1], Kyuhyun LEE[1], Yong YOUN[1], Ho-Hyun NAHM[2,3], Seungwu HAN[1] *

[1] *Department of Materials Science and Engineering, Seoul National University, Seoul, 151-747, South Korea*

[2] *Center for Correlated Electron Systems, Institute for Basic Science (IBS), Seoul, 151-747, South Korea*

[3] *Department of Physics and Astronomy, Seoul National University, Seoul, 151-747, South Korea*

Keywords: High-throughput screening, *ab* initio calculation, functional oxides

Making a perfect handbook for desired properties of all existing materials is always a dream work for materials scientists. Recently, remarkable advances in computing power and first-principles technique present a good opportunity for building a vast theoretical database of material properties. Fast and accurate high-throughput calculations can be achieved by aligning proper computational methods into a sophisticated automatic procedure. In this talk, I will present our recent efforts to identify functional oxides appropriate for specific application targets, utilizing the high-throughput *ab initio* screening. First, we try to find candidate dielectric materials that can be used in next-generation memory (DRAM or FLASH) and logic (CPU) devices, based on the digital database of energy gap, dielectric constant, and defect formation energies for a large collection of binary and ternary oxides available on ICSD. Second, we try to identify ideal dopants for ZnO when the material is used for electronic or energy devices. For these ends, we develop a series of automation codes that can carry out *ab initio* computation of bulk and defect properties of oxides efficiently and reliably. As a result, we calculate ~1,800 oxides for searching new high-k dielectric materials and find new candidate materials shown in Fig 1. We also developed the fully-automated code that can search all possible doping sites for a given dopant in a few days.

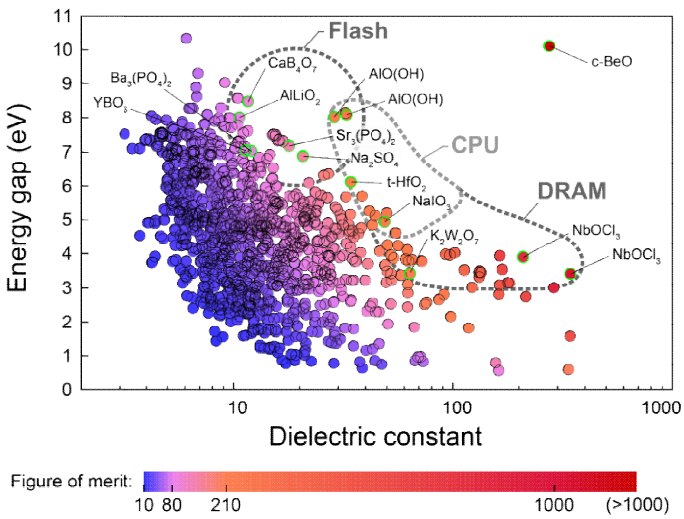

Figure 21. Oxide property map for high-k dielectrics

CE-I01

Technological Innovation in Ceramics : History of Pottery to Ceramic Industries

Junichi HOJO
Faculty of Engineering, Kyushu University, Fukuoka, 812-8581, Japan

Keywords: Pottery, Porcelain, New ceramics, Fine ceramics, Technology

According to progress of human civilization, ceramic products have been developed as fundamental materials supporting our life and industrial activities. Ceramics have been fabricated by using natural resources consisting of silicate compounds including silica and alumina, which are easily mined on the surface of earth crust and consolidated by firing. That is to say, it is a generally-generated technology since human family received fire in hand. Ceramic wares are supposed to have started in Yin dynasty of China (B. C. ca. 1400), and have been developed from clay pot to pottery and then porcelain. The ceramic technologies were transferred from China to Korea and Japan. After then, original technologies have been developed in Japan. The typical one is Arita porcelain. Furthermore, the ceramic technologies were transferred to European countries and progressed to new porcelains, such as hard porcelain in Meissen, Germany and bone china in England. The western technologies were back-transferred to Japan in the early Meiji period (before 1900) and opened ceramic industries. Now, the ceramics have been developed to new ceramics and fine ceramics.

The ceramics technologies have been supported by progress in powder preparation and firing techniques. Potter's wheel contributed to improve the productivity and climbing kiln enabled the high-temperature firing to produce porcelains. Coal-firing furnace was developed in Europe and brought a great contribution to ceramics production. Traditional ceramics, such as table and sanitary wares, refractory etc., have been produced by using natural resources at low temperature and normal pressure. New ceramics mean the use of new raw materials such as synthesized oxide and artificial non-oxides (carbide, nitride, boride). The industrial porcelain is supposed to have started from suspension insulator with high strength and electrical resistance, which was enabled by highly-pure oxide. To produce new ceramics, new fabrication techniques have been developed, ex., high temperature and pressure processes, CVD, PVD, sol-gel and so on. Fine ceramics mean the precise control of composition and microstructure, and shape control like nanoparticle, nanofiber, nanofilm and so on, to create new functions. The history of ceramics from pottery and porcelain will be discussed with emphasis on the relation to new industry innovation.

Table 1 Development of ceramic materials

	Source	**Process**	**Product**	**Production system**
Traditional ceramics	Natural source (silicate)	・low temperature ・normal pressure ・melting	・china ・glass ・cement ・refractory	Large scale production
↓ New ceramics	Artificial source ・oxide ・carbide ・nitride ・boride	・high temperature ・high pressure ・CVD method ・sol-gel method	・high temperature structural materials ・engineering parts ・tool materials ・semiconductor ・dielectric materials ・magnetic materials ・optical materials ・biomaterials	Small scale production
↓ Fine ceramics	Homogeneous composition Fine microstructure Variety of morphology (single crystal, polycrystal, fiber, film, particles)	Material design		

CE-I02

Applying the Social Network Service in Ceramic Culture and Education

Jong Up Chun
Induk University Wolgye 2-dong, Nowon-gu, Seoul, Korea

The term 'SOCIAL NETWORK SERVICE", in short SNS, as we know today signifies the connection between people in other words it is a network for the societal interpreted through text, photographs, moving images and more. The service shares such information while connecting people.
The early 1990s information sites based on WEB 1.0 were somewhat closed with a one-way system but the WEB 2.0 based social network is a more interactive user-friendly system with easy accessing and sharing of information and for this reason it is a more user focused system creating a user based internet environment.
Therefore information consumers no longer require to follow the structures of information set by the data base architecture. They are no longer forced to follow other people's ways but rather individuals can easily search information for reference and transmission.
There are a wide variety of ceramic culture and education related information all around the world. The period requires for us to think about ways of continuously revising sporadic information spread by WEB 1.0. The introduction of Social Network Service has facilitated this issue somewhat therefore it may be easier than we initially thought of resolve the problem.

CE-I03

Johjima roof tile's past, present and future

Naotaka SAKAMOTO
Fukuoka Industrial Technology Center, Chikushino City, Fukuoka, JAPAN

Keywords: Clay roof tile, Mass production, Small quantity, large variety, Custom- made

1. Introduction

There was tile industry in each place of Japan, and the making of product using the local raw materials has been performed in old days. In Jojima area of Fukuoka (Fig.1) located in the lower basin of the relatively big river where high quality clay was provided, roof tile production has been performed from approximately 400 years ago. From superiority in the marine transportation, the Johjima roof tile was exported to the foreign countries from more than 100 years ago, and it was a big production center to line up with Nagoya, Shimane, Ehime in Japan. However, the number of the production companies greatly decreases, and the situation declining remarkably includes it. Even the maintenance as the roof tile production center is difficult now. Therefore the persons concerned with the Johjima roof tile strengthen a sense to confront the impending crisis and start some actions including the development of new products suitable for the present market trend. Then, in this presentation, some current actions in Johjima area for roof tile production are introduced with past process.

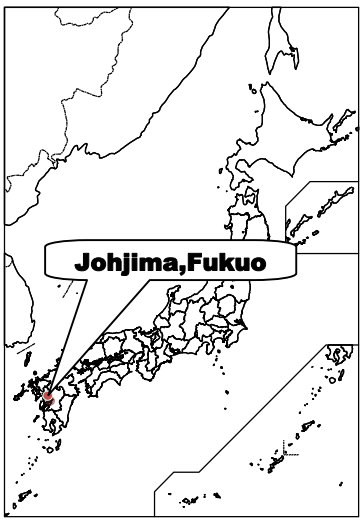

Fig.22 Location of Johjima

2. The decline as the roof tile production center

Just after the end of the World War II, more than 200 companies connected with roof tile were gathered in the Johjima area and the area was well-known as a top 3 roof tile production center in Japan. However, the demand for clay roof tile tended to drop by the changes of the house style recently, and the amount of shipment of clay roof tile was decreased rapidly in all of Japan. The number of the production companies gradually decreases to 5 in the Jojima area now. It is difficult to make a performance as brand-name products "the Jojima roof tile", and it is the crisis of the life and death for the production center "Johjima" anymore.

3. New action for survival

The process of roof tiles production was resolved into technical element and each technique was investigated the possibility to be applied to any production except the roof tile. It was clear that the production technology of the clay roof tile was not good at performing the manufacturing aimed for the individual correspondence to customer needs. However, We judged that the switch that does not have unreasonableness to multikind and small-quantity production is demanded from a conventional market strategy to produce it in large quantities and to scheme mass sale. Some processing techniques with low cost such as the introduction of resin molding die (Fig.2) or the printing with the small laser are worked, and the new line of products which past does not have is constructing now.

Fig.2 Trial product using the resin molding die

Acknowledgement:
I sincerely thank to Johjima clay roof tiles Cooperative for molding and firing samples.

CE-I04

Effect of *Onggi* on Fermentation Characteristics of Korean Traditional Soy Sauce, *Ganjang*

Misook KIM
Department of Food Science and Nutrition, Dankook University, Yongin-si, Gyeonggi-do 448-701, South Korea

Keywords: *Onggi*, *Ganjang*, fermentation profile, salt

Onggi has been traditionally used as a container for Korean traditional fermented foods such as *Doenjang, Gochujang* and *Ganjang*. Among them, *Ganjang* is most vulnerable to the impact of a fermentation container. The fermentation container is one of critical factors including a fermented soybean brick, *meju* and the initial salt concentration to determine the final flavor and salt concentration. *Onggi* varies with region in its size, shape, and porosity. We obtained *Onggi* from five distinct regions such as Gangjin, Jeju, Ulsan, Yeoju and Yesan in Korea, and observed chemical, microbiological, sensory and antioxidant characteristics in *Ganjang* during fermentation in *Onggi*.
Ganjang was fermented for 120 days in *Onggis* obtained from five different regions at the ambient temperature. During the fermentation period, the average temperature was 20.0°C and varied between -4.4 and 42.6°C in *Onggi*. *Bacillus* sp. was solely responsible for the fermentation of *Ganjang* and protease activity was increased in all *Onggi*. *Ganjang* fermented in Gangjin *Onggi* with the widest mouth and highest porosity showed higher water loss (5.8%) and contained larger salt crystals and less salinity compared to other *Onggi*. The contents of total amino acids and glutamic acid were the highest (5,377 mg/100 ml and 1,619 mg/100 ml) in *Ganjang* fermented in Gangjin and the lowest (4,540 mg/100 ml and 1366 mg/100 ml) in *Ganjang* fermented in Yeoju. In the descriptive analysis, *Ganjang* fermented in Gangjin showed lower intensity of salty and biting than others. *Ganjang* fermented in Gangjin contained the highest total phenolic contents, followed by Ulsan, Yeoju, Jeju and Yesan. *Ganjang* in Gangjin also possessed stronger DPPH radical scavenging activity and FRAP ability than others.
Onggi from different regions in Korea significantly affected the fermentation attributes of *Ganjang*. Gangjin *Onggi* with the widest mouth and highest porosity offers opportunities to develop high quality *ganjang* with low sodium.

Acknowledgement:
This work was supported by Korea Institute of Ceramic Engineering and Technology (KICET).

CE-I05

Construction of Ceramic Color Database and its recent improvement

Toyohiko SUGIYAMA*, Masayoshi OHASHI, Keiji KUSUMOTO
Materials Research Institute for Sustainable Development, National Institute of Advanced Industrial Science and Technology, Nagoya, Aichi 463-8560, Japan

Keywords: Glaze, Database, Color, Pottery, Porcelain

The Ceramic Color Database; a database of ceramic glaze has been constructed by organizing the data of more than 300,000 glaze test pieces. The large amount of glaze test pieces was created in the course of more than 80 years of ceramics research. The test pieces are valuable source materials in a sense that research processes and results are preserved in a visible manner. To further promote their use, the systematic organization of the vast amount of the test pieces and construction of the database was started in 1995. The open database on the internet was also constructed using the data from the original database. These databases provide fundamental information of ceramic glaze to the manufacturers and researchers of ceramics. The work of preparing the glaze test piece and improving its recipe is repeated many times on the development of new glaze. The information provided by the glaze database shortens the time required for the testing. The database has been frequently used by many kinds of users, especially after the database was opened on the internet. It was recognized that the database was useful in new R&D on ceramics. The database has been also used in the field of high school education. The database includes the data items such as glaze name, firing temperature, firing atmosphere, color, chemical composition, recipe, physical state, and other related information, as well as images of the glaze pieces. During the construction of the database, we faced many problems, and have received many requests from users. The database has been revised and improved corresponding to such issues. The use of the database, however, largely expanded as the open database was publicized on the Internet. The database has also been used in fields other than ceramics and in unexpected way. The recent communication speed and memory capacity of the Internet and usual computer are very different from those of 20 years ago when the open database was designed. The large reconstruction of the database is planed and now in progress. The database will provide larger amount of data. It will also possess new search function based on the recent developments in computer technology.

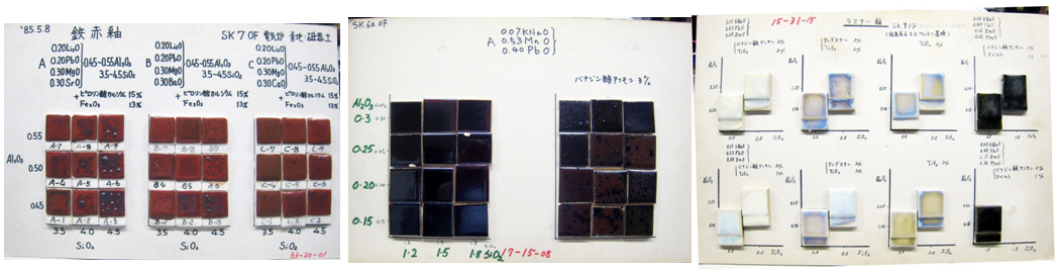

Figure 23 Examples of glaze test piece

References:

[1] T. Sugiyama, Synthesiology, 6 (2013) 84

Acknowledgement:

The authors would like to express our thanks to the members working for the database reconstruction; Ms. T. Mizunoue, Ms. K. Fukuoka, Ms. M. Kato, Ms. Y. Asano, Mr. K. Oshimoto, Ms. J. Kondo, Ms. E. Kuno, Ms. N. Suzuki, and Ms. T. Kumagai of AIST, and Mr. Y. Hyono of Cori company.

CE-I06

Quantitative Phase Analysis of Porcelain Raw Materials Using X-ray Diffraction Method

Seung-Joo KIM[1*], Jaegyeom KIM[1], Jong-Young KIM[2]
[1]*Department of Chemistry, Division of Energy Systems Research, Ajou University, 443-749,Korea*
[2]*Icheon Branch, Korea Institute of Ceramic Engineering and Technology, Icheon 467-843, Korea*

Keywords: X-ray diffraction, Quantitative analysis, Porcelain raw materials

Powder X-ray diffraction (pXRD) is most commonly applied for characterization of polycrystalline samples. pXRD enables a non-destructive determination of the material composition and the determination of the crystalline structure of the components. It can also be used to measure various microstructural properties of these crystalline phases such as strain, grain size, and defect structure. Since H. Rietveld developed a whole pattern fitting structure refinement based on the powder XRD data in 1969, the refinement procedure called "Rielveld refinement" has been widely accepted as an exceptionally valuable method for structural analysis of nearly all classes of crystalline materials. In this presentation, the principle of the Rielveld refinement is introduced and applied for quantitative analysis of porcelain raw materials. Typical porcelain bodies are made from materials collected from selected deposits using different mixing proportions of clay, feldspar and quartz, which are heat-treated to form a mixture of glass and crystalline phases. The phase proportion is very important factor to affect the physical properties of porcelains. The present study investigates the accuracy and reliability of the quantitative Rietveld analysis at various weight fractions of the reference mixtures and several commercial products. For the analysis, a freely distributed program FULLPROF was used in its whole pattern fitting mode with CuKa X-ray data. Micro-strain and preferred orientation effects are also considered.

References:

[1] R.A. Young, *The Rietveld Method* (Oxford Publication, 1993)
[2] R.L. Snyder, J. Fiala and H.J. Bunge, *Defects and Microstructure Analysis by Diffraction* (Oxford Publications, 1999)
[3] W.I.F. David, K. Shankland, L.B. McCusker and Ch Baerlocher, *Structure Determination from Powder Diffraction Data* (Oxford Publications, 2002)

Acknowledgement:

This work was supported by the National Research Foundation of Korea (grant No. 2010-0013089).

CE-I07

Role of Kogaratsu Research and Exchange Association on the Coming Progress of Karatsu Ware

Hiroaki KATSUKI[1]* , Masahito MINAMIMORI[2], Yasumoto KAJIHARA[3]
[1]*Saga Ceramics Research Laboratory, 3037-7, Arita-cho, Saga 844-0022 Japan*
[2]*Ryujin Gama, 3312-1, Hieda, Kitahata, Karatsu-shi, Saga 847-1214 Japan*
[3]*Ohtani Thobou Handou Gama, 3391-11, Sari, Ouchi, Karatsu-shi, Saga 849-3233 Japan*

Keywords: Karatsu ware, Korean ware, Mutual exchange, Potters, Science

1. Introduction

Karatsu ware (Karatsu-yaki) is one of traditional Japanese potteries and has been produced since the late 16th century based on Korean ceramic wares (Punch'ong and Onggi ware) technologies in and around Karatsu-shi, Saga, Japan. Karatsu ware is formed from some sandy clay with high Fe_2O_3 content which are mined in Karatsu area, and fired with ash slip glazes in a traditional climbing kiln. As of now around 70 companies of Karatsu ware produce a traditional tea ceremony bowl, flower vase and some table wares, but the production activity of Karatsu ware has been continuously retarded due to a global recession of the ceramic ware consumption since 1990's.

Kogaratsu Research and Exchange Association was established in 2004 and supported with 50 members from Japan, Korea, France and USA for the coming progress and creation of a new Karatsu ware, and also for the scientific reconfirmation of old Karatsu (Kogaratsu) ware. The Association is organized by local potter, clay and glaze companies, merchant, archaeologist, scientist, collector, and public organizations.

2. Activities of the Association

(1)Study of historical transfer of old Korean pottery technology to old Karatsu ware
(2)Study on what is same or different on old Karatsu ware and old Korean ceramic ware such as Punch'ong(Funsei-saki)
(3)Reconfirmation of the traditional technology of old Karatsu ware
(Raw materials, glazes, forming, firing by climbing kiln, body style, color and painting)
(4)Study of the effect of production technology of old Karatsu ware on old Arita porcelain produced in the early 17th century
(5)Field study of old Karatsu ware shards produced in 1580-1590's
(6)Scientific research of clays produced from sandstone and some weathered sedimentary clay from sandstones and granites in Karatsu area[1,2)]
(7)Scientific and comparative study of raw clays mined in Korea
(8)Organizing some seminars on the related fields (raw materials, production, history and culture)
(9)Support for publication of some books for a global introduction to Karatsu ware[3)]
(10)Study of new design and color decoration of modern Katatsu ware for young Japanese consumer
(11)Exhibition of recent new products produced by younger potters in Karatsu-shi and Korea
(12)Visit old Korean pottery kiln sites located in Jeollanam-do,Jeollabuk-do, Gyeongsangnam-do
(13)Workshop and technology exchange with Korean potters in Karatsu-shi and Korea
(14)Support of understand of the technology and production experience of Karatsu ware for younger generation (schoolchildren) in Karatsu-shi and Saga Pref.

References:

1) H.Katsuki, N.Kamochi, A.Kawahara, Y.Kajihara, J. Ceram. Soc. Japan, 121(9), 863-866(2013). "Some properties of clays for Karatsu ware prepared from sandstone"
2) H.Katsuki, A.Kawahara, N.Kamochi, Jae-Hwan Pee, Woo-Seok Cho, Hyung-Tae Kim, J. Ceram. Soc. Japan, 122(8), 642-644(2014). "Properties of sedimentary clays for Karatsu ware"
3) F.Villemin, "The Golden Age of KARATSU STONEWARE", Schiffer Publishing Ltd., USA(2013).

CE-I08

Trend of Research and Development for Environmentally Benign Ceramic Technology in Gifu Tono Region

Tetsuya KAMEYAMA[1]*, Seizo OBATA[2]
[1]*National Institute of Advanced Industrial Science and Technology, Nagoya, 463-8570, Japan*
[2]*Gifu Prefectural Ceramics Research Institute, Tajimi, 507-0811, Japan*

Keyword: Environmentally Benign ceramic, Porcelain, Ceramic processing

The western Tono area, including the cities of Tajimi, Toki, and Mizunami, possesses excellent mass-production technology for pottery/porcelain and related products, and is one of the largest pottery/porcelain production regions in Japan. The industry, mainly producing the ceramic tableware and ceramic tile, had accounted for about 40%of production output in Japan. However, sales had fallen dramatically in recent years because of a prolonged recession.

In this area, therefore, it was a priority to advance local industries and to encourage sustainable development. The universities and research institutes in this area had achieved outstanding results in terms of manufacturing techniques such as porous ceramics and functional inorganic particles, as well as in the technology required to reduce the environmental load based on catalysts and recycling.

The aims of this project supported by Ministry of Education,Culture,Sports, Science and Technology-Japan was to create a new industry involving environmentally friendly pottery/fine ceramics by fusing the technological seeds of universities and research institutes with the technical capabilities of industries in the area. Using these technologies, we have sought to develop the following materials: 1) materials to counter the heat-island effect, 2) particles effective in shielding from infra-red radiation, 3) ceramics effective in environmental cleanup, and 4) environmentally benign pottery, etc. Figure 1 shows the developments themes and products conducted in this project.

Consequently, the Western Tono Area has successfully developed many new products [1]. As the typical example, new porcelain sintered at fired temperatures lower than 300°C compared with conventional porcelain. This decreasing fired temperature of porcelain contributed to reduce an almost 40% in energy consumption and carbon dioxide emissions. Another invention was a high-temperature superheated steam generator of which main parts utilized new conductive ceramics could be used in various applications, such as the high-efficiency washing of electronic parts and the recycling of carbon fiber in the carbon fiber reinforced plastics. Furthermore, the developed materials in this project would be examined in terms of their potential for commercialization.

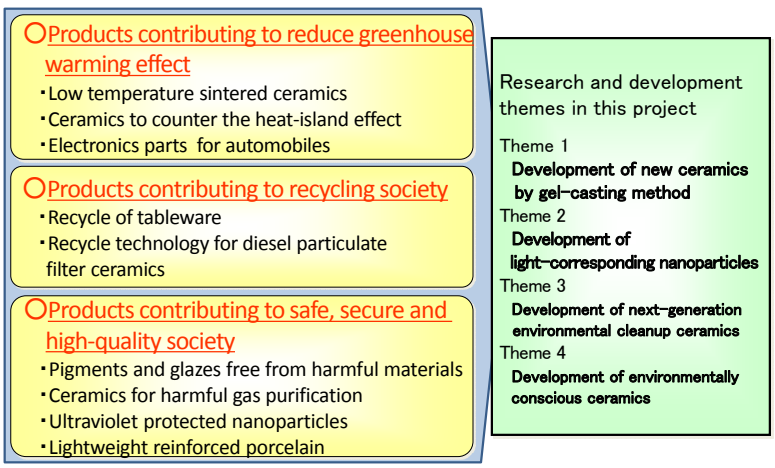

Fig 1 Development products(left side) and development themes(right side)

Reference:

[1] T. Kameyama, Bull. Ceram. Soc. Japan. 49 (2014) 780.

CE-I09

Investigation for Materials of Old Porcelain Wares in Houhoku-town

Natsuki HOSOYA[1*], Akira MIKUNI[1], Yoshinori MIYATA[2]
[1]*Yamaguchi Prefectural Industrial Technology Institute, 4-1-1 Asutopia, Ube-city, Yamaguchi, 755-0195, Japan*
[2]*IKKEI-gama, 112-8 Awano, Houhoku, Shimonoseki-city, Yamaguchi, 759-5101, Japan*

Keywords : Porcelain wares, Houhoku-town, X-ray fluorescence spectroscopy

1. Introduction

Houhoku-town locates in the western part of Yamaguchi prefecture in Japan. From the late 1700's to early 1900's, there were some manufacturing porcelain kilns such as Nakabara-kiln, Sakaige-kiln, Iinoyama-kiln and Hara-kiln in this town. However, none of them exists any longer and there is less information about these porcelain wares.[1] Folklore said these porcelain wares were made by using some raw materials which was reserved and mined in Houhoku-town.[2] In this study, for the purpose of investigating these materials, we analyzed the mineral composition of six raw materials which is possibly used in old porcelain wares in Houhoku-town. Moreover, we compared them with those of old porcelain wares in Houhoku-town.

2. Experimental procedure

Ig. Loss of six raw materials (A, B, C, D, E and F) was measured by taking difference of weight between before and after burning at 1000K. Samples for X-ray fluorescence (XRF) spectroscopy analysis were prepared in 1 : 10 glass beads to analyze the chemical composition of 9 major elements (Si, Al, Fe, Ti, Ca, Mg, Na, K and P). After XRF analysis, the mineral composition was calculated by CIPW norm which assumes clay as $Al_2Si_2O_5(OH)_4$, silica as SiO_2, feldspar as $Na_2Al_2Si_6O_{16}$ and $K_2Al_2Si_6O_{16}$, and iron oxide as Fe_2O_3.

3. Results and Discussion

Figure 1 shows the calculated mineral composition of six raw materials. As shown in figure 1, only material D is rich in feldspar with the content rate of 30 wt%. Since 24~27 wt% feldspar is contained in collected old porcelain wares at Nakabara- and Sakaige-kilns, material D would be possibly used as feldspar. On the other hand, collected porcelain wares in Iinoyama- and Hara-kilns contain 31~37 wt% feldspar. In this case, there is no corresponding material containing more than 30 wt% feldspar. Therefore, these porcelain wares would be produced by using other materials that contains much feldspar.

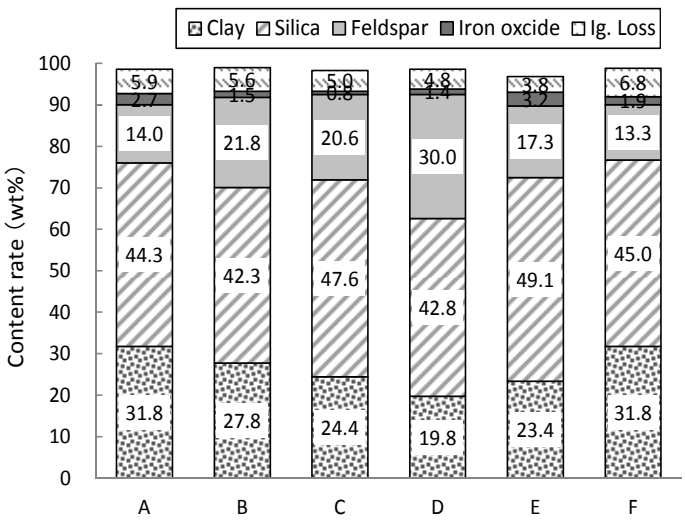

Fig.1 Mineral composition of six raw materials

References:

[1] Implementation Report of Iconotheque Project, p37-49 (1997)
[2] Taisho-kan, UTSUWA, p8-15 (2012)

Acknowledgement:

This work partly supported by the Creation and New Business-Supported for the Yamaguchi Industrial Promotion Foundation, 2011.
Special thanks to Satoshi Kawata (*Doigahama site anthropological museum*) and Asami Sasada (*Houhoku historical folk material museum*) for providing six raw materials.

LD-I01

New Approach to Fabricate Green, Red and IR Light Sources Based on Nitride Semiconductors by DERI Method

Y. Nanishi[1], T.Yamaguchi[2] and T.Araki[1]
[1] Ritsumeikan University, Kusatsu, 525-8577, Japan, [2] Kogakuin University, Hachioji, 192-0015, Japan

More than ten years have already passed since narrow band gap energy of InN around 0.7eV was first reported in 2002. This finding opened up new application field of group III nitride optoelectronic semiconductors to green, red and near IR wavelength region. In contrast to such high potential, however, developments of actual optoelectronic devices based on InN and In-rich InGaN were hindered mainly due to relatively poor quality of these material systems.

Main difficulty for preparing high quality material comes from its low dissociation temperature and high equilibrium nitrogen vapor pressure during growth. In droplets which form on the growing surface give another essential problem for high quality InN growth.

We have developed a new RF-MBE growth method called DERI (Droplet Elimination by Radical Beam Irradiation) for growth of these materials. This growth method is consisted of the two series of growth steps with In-rich growth step (MRGP: Metal Rich Growth Process) and consecutive nitrogen radical beam irradiation step (DEP: Droplet Elimination Process). We found that this growth process can be considered as atomic layer level Liquid Phase Epitaxy from in-situ observation by RHEED and optical reflection. This method enabled us to obtain flat and high quality InN reproducibly without precise control of V/III ratio.

As DERI process is carried out under almost thermal equilibrium condition like conventional LPE, InGaN tends to make phase separation under highly metal rich growth condition. Using this phenomenon positively, we have successfully obtained InN/InGaN, InGaN/InGaN MQW structures, which emitted strong PL at IR and green wavelength range, respectively.

In order to realize InGaN LED covering full wave length between GaN to InN on one specific substrate, we should eliminate electrical or optical adverse effects of generated misfit dislocations due to 11% lattice mismatch. For this purpose, we propose a new way to suppress dislocation effect by using this phase separation phenomenon, growing wider band gap material surrounding dislocation cores.

We have also investigated plasma induced defects in InN by RF-MBE changing plasma power during growth. It was found that even from radical source, in which most of ions are supposed to be eliminated, residual ions are supplied to the growing surface and adversely affect quality of InN with increase in carrier concentration and decrease in mobility as we increase plasma power. Positron annihilation experiments revealed that this is due to point defects generated by plasma damage. It was found that DERI method, has advantage to reduce plasma-induced point defects by a few mono-layer of metal coverage on the surface during growth.

Acknowledgement:
This work is supported by MEXT through grant-in-Aids for Scientific Research #26600090.

LD-I02

GaN Electronic Devices and Their Applications

Jae Kyoung MUN[1,2*], Woojin CHANG[1], Sang Choon KO[1], Eun Soo NAM[3]
[1]*GaN Power Devices R&D Section, ETRI, Daejeon, 305-700, Korea*
[2]*Department of Advanced Device Engineering, Univ. of Sci. & Tech.(UST), Daejeon, 305-343, Korea*
[3]*Components and Materials Lab, ETRI, Daejeon, 305-700, Korea*

Keywords: GaN, Electronic Devices, Microwave Amplifier, Power Switching, Platform

ETRI has a long R&D history over 25 years for device and process technologies of compound semiconductors, such as GaAs, InP and GaN. But I will talk about GaN, next generation compound semiconductor platform in this talk. GaN-based HEMT devices are attractive candidates for high-power amplifier applications such as next-generation microwave communication systems and high power electronic switching devices. We started the R&D of GaN technologies in 2010, and the progress of GaN microwave and power devices technologies will be presented today.[1-3] In the first part, I will briefly introduce the current status of GaN high power microwave devices for radar system applications. In the second half part of the talk, I'd like to mention about some recent R&D results of GaN power electronic switching devices, such as normally-off FETs and Schottky barrier diodes developed using the ETRI's proprietary 4-inch GaN full process. During my talk, backside via-etching and copper plated metal-filling technologies will be also discussed as one of the cost-effective key solutions for the high power GaN technologies. Finally, we would like to talk a little bit more about the importance of commercializing GaN power electronic devices for high efficiency energy transform technology in the future.

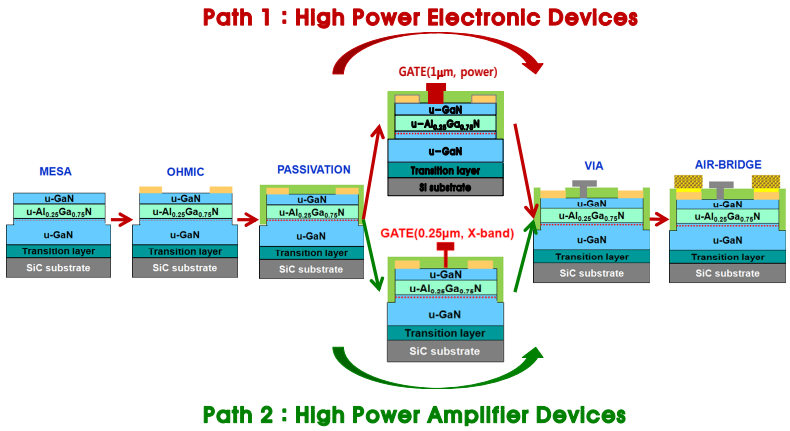

Figure 1. Fabrication process paths for high power amplifier and switching devices

References:

[1] Jae Kyoung Mun, "AlGaN/GaN HEMTs for X-band Radar Applications", RF Integrated Circuit Technology Workshop 2011, pp. 483-495.
[2] Jae Kyoung Mun et. al.,"Current Status of GaN Technologies in ETRI", AWAD 2012.
[3] Youngrak Park et. al., ELECTRONICS LETTERS, Vol. 50 No. 16, pp. 1164–1165(2014).

Acknowledgement:

This work was supported by the 'Energy Efficient Power Semiconductor Technology for Next Generation Data Center' IT R&D project (no. 10038766) and the 'High Efficiency GaN-based Power Module for Harsh Environment Applications' R&D project (no. B551179-13-02-06) of the Korea Ministry of Science, ICT and Future Planning.

LD-I03

Towards Performance Enhancement of InGaN/GaN LED by Exploring Localized Surface Plasmons

In-Hwan Lee [1*]
[1] *School of Advanced Materials Science & Engineering, Engineering College, Chonbuk National University, Jeonju 561-756, Chonbuk, Korea*

Keywords: Localized surface plasmon, optical properties, nanopillar structure.

Surface plasmons (SP) are coherent electron oscillations that exist at a metal-dielectric interface. Specifically, the SP in noble metal nano-particles (NP) embedded in a dielectric matrix is called localized surface plasmons (LSP). These LSP have been studied for applications in sensing, medical imaging, and surface enhanced spectroscopy. Recently, the LSP phenomena have attracted great interest in InGaN/GaN based light-emitting diode (LED) as the luminescence efficiency can be improved by the energy coupling (EC) of LSP with the active quantum well (QW) region of such LED [1]. According to the EC mechanism, when the metal nanostructure forming LSP is deposited in close proximity to the active layer of LED and the emission energy matches the LSP oscillation energy, excitons in the active layer of LED can transfer their energy directly to the LSP mode as well as emitting light at the active layer, rather than decay via radiative and nonradiative recombination channels in the semiconductor structure.

Recently, we reported on the properties of chemically synthesized Ag and Ag/SiO_2 NP and the performance enhancement of LED coated with these NP [2]. The attractive feature of such NP is the possibility to increase and carefully regulate the NP density with consequent increase in the enhancement factor. This is in contrast to metal NP formed by annealing. Moreover, for core/shell Ag/SiO_2 NP a very substantial improvement in performance stability was observed as compared to purely metal NP [3].

In this talk we describe the results of experimental and theoretical studies of optical properties and electric field distribution in Ag and Ag/SiO_2 NP, and report on the EC of their LSP resonance with InGaN/GaN MQW. Also, we proposed the fabrication of NP embedded in InGaN/GaN based nanopillar LEDs.

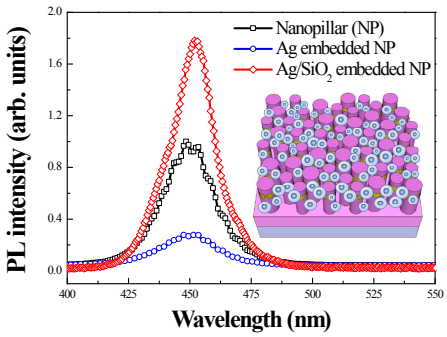

Figure 24 PL spectra from the nanopillar, Ag and Ag/SiO_2 NP embedded sample and its schematic structure (inset)

References:

[1] K. Okamoto, I. Niki, A. Shvartser, Y. Narukawa, T. Mukai, A. Schere: Nat. Mater. 3 (2004) 601.
[2] L. W. Jang, D. W. Jeon, T. Sahoo, D. S. Jo, J. W. Ju, S. J. Lee, J. H. Baek, J. K. Yang, J. H. Song, A. Y. Polyakov, I. H. Lee: Opt. Exp. 20, 3 (2012) 2116.
[3] L. W. Jang, D. W. Jeon, M. Kim, J. W. Jeon, A. Y. Polyakov, J. W. Ju, S. J. Lee, J. H. Baek, J. K. Yang, I. H. Lee: Adv. Func. Mater. 22 (2012) 2728.

Acknowledgement:

This research was supported by National Research Foundation of Korea(NRF) funded by Ministry of Science, ICT & Future Planning (2013R1A2A2A07067688, 2010-0019626)

LD-I04

In situ XRD analysis of GaInN/GaN heterostructure grown on GaN underlying layer with different dislocation density

Motoaki Iwaya[1], Koji Ishihara[1], Taiji Yamamoto[1], Daisuke Iida[1], Yasunari Kondo[1], Hiroyuki Matsubara[1], Tetsuya Takeuchi[1], Satoshi Kamiyama[1], and Isamu Akasaki[1,2]
1Faculty of Science and Technology, Meijo University, Nagoya 468-8502, Japan
2Akasaki Research Center, Nagoya University, Nagoya 464-8603, Japan

A GaInN/GaN heterostructure system is widely used to high-brightness blue and green LEDs and high power violet laser diodes. The application of GaInN films in high-efficiency solar cells is also expected, because the bandgap of GaInN alloys ranges from 0.65 to 3.43 eV. Although there are many reports of the analysis of the relaxation process in GaInN/GaN heterostructure system characterized by TEM and XRD reciprocal space mapping (XRD-map), an understanding of the critical layer thickness at which misfit dislocations (MDs) are introduced in the GaInN/GaN heterostructure is insufficient. For instance, a large fluctuation exists in the reported value of the critical thickness in GaInN/GaN heterostructure system. In this study, we investigated an *in situ* XRD analysis of GaInN/GaN heterostructure grown on GaN underlying layer with different dislocation density. The GaInN layers were grown on GaN template (threading dislocation density: ~3 × 108 cm-2) on sapphire substrate covered with lowtemperature buffer layer and freestanding GaN substrates (threading dislocation density: <3 × 106 cm- 2). We evaluated the GaInN films with symmetric (0002) Bragg diffraction using an *in situ* XRD system. The X-ray was focused on the sample surface using a Johansson curved crystal mirror. By using this method, the incidence angle of the X-rays can be changed without moving the X-ray source. Moreover, the diffracted X-ray was detected by a 1D X-ray CCD. By using this method, the scattered X-ray can be detected without moving the substrate and detector. By using this configuration, this system realized the equivalent of a (0002) 2θ/ω scan without requiring the use of an analyzer crystal in 1 s during the rotation of the wafers. Although the resolution limit decreases slightly, this *in situ* XRD system is able to perform the equivalent of a (0002) 2θ/ω scan at a resolution of 1 arcsec. In this setup, the full width at half maximum (FWHM) is both controlled by the dispersion in the lattice constant *c* and the mosaicity of the crystal. We observed the GaInN surface structure and defects close to the GaInN/GaN heterointerface by SEM, CL, AFM and TEM, respectively. Strain relaxation was also evaluated by a typical *ex situ* XRD-map. By comparing *in situ* XRD measurement results and *ex situ* characterization such as TEM, CL, AFM, SEM, and XRD-map, we found that it is possible to accurately determine the critical thickness of introduced the MDs in the GaInN are introduced by analyzing the FWHM of the *in situ* XRD spectrum from GaInN. In particular, we found that measurement accuracy of the critical thickness by this *in situ* XRD system is higher than that by XRD-maps. Moreover, critical thickness of introduced MDs in GaInN was significant depends on the dislocation density in the GaN underlying layer.

LD-I05

High Mobility and Highly Stable Aluminum-doped Indium Zinc Tin Oxide Thin-Film Transistors Compatible with Back-Channel Etch Process

Sung Haeng Cho[1], Sang-Hee Ko Park[2], Hee-Ok Kim[1], Oh-Sang Kwon[1], Eun-Sook Park[1], Min Ki Ryu[1], Sun Kwon Lim[3] and Chi-Sun Hwang[1]

[1] *Oxide Electronics Research Team, Electronics and Telecommunications Research Institute (ETRI), 138 Gajeong-Ro, Yuseong-Gu, Daejeon 305-350, Korea*

[2] *Dept. of Materials Science and Engineering, Korea Advanced Institute of Science and Technology (KAIST), 291 Daehak-Ro, Yuseong-Gu, Daejeon 305-701, Korea.*

[3] *Heesung Metal Ltd, Gojan-dong, Namdong-gu, Incheon, Korea*

We report highly stable and high mobility aluminum-doped indium zinc tin oxide (AIZTO) thin-film transistors (TFT) with field effect mobility larger than 30 cm^2/Vs of which process is compatible with the current a-Si :H TFT process. Metal oxide semiconductror thin-film transistors (MOS-TFTs) have attracted great attention as a large area electronics such as a backplane for high-resolution TFT-LCD or AMOLED displays due to their excellent performances such as high mobility, current stability and low off current. MOS TFTs have the advantages of good uniformity, low process temperaure, and low fabrication cost compared with LTPS TFTs, but, the convention metal oxide semiconductors such indium gallium zinc oxide (IGZO) or analogues of zinc oxide (ZnO) are vulnerable to strong acidic solutions of metal etchants or dry etchants in plasma which necessarilly need etch stopper (ES) layer on the backchannel to protect it from source/drain (SD) metal etchant in the bottom gate, staggered configuration. It increases the number of mask in TFT process and adds process complexity. Futhermore, ES-TFTs have a limitation to decrease the channel length below the reolution of photolithography due to the design margin for layer-to layer overlap which also increases overlap area between gate and SD which is origin f large parasitic capacitance in ES-TFTs. On the other hand, in back-channel etch (BCE) TFT process, at least 2 masks can be omitted in compared with ES-TFT process if halftone mask is employed and the parasitic capacitance and the channel length can be made as small as possible which will help to realize the low RC delay in bus line and large aperture ratio in high-resolution display. We developed the new metal oxide semiconductor robust against etch-back process and report here that the high mobility oxide TFTs exceeding 30 cm^2/Vs can be fabricated in BCE process without back-channel damage with Molybdenum source/drain metal. For comparitive study, ES-TFT and BCE-TFTs are fabricated using the same oxide semiconductor and their electrical performances and stabilities againt bias and current stress are reported in this study.

LD-I06

Zinc-Tin Oxide Thin Film Transistors based on atmospheric processes

Hye Ji Jeon, Jae Yoon Bae, and Jin-Seong Park*
Division of Materials Science and Engineering, Hanyang University, Seoul, 133-719, Republic of Korea

Keywords: oxide semiconductor, solution process, thin film transistor, ZnSnO

Amorphous ZnSnO channel layer thin film transistors (TFTs) with various dopants (Al, Ga, and N etc) were fabricated using atmospheric processes (solution and mist-chemical vapor deposition (CVD)). Electrical, structural, and optical properties were systematically investigated as dopants. In particular, co-dopants (Ga and N) ZnSnO TFTs exhibited better electrical performances such as mobility and stability, comparing with only ZnSnO TFTs' performances. In terms of mobility and stability in atmospheric oxide TFTs, the impurity and oxygen-related defects may play important roles to improve electrical performances. In this talk, various dopants in ZnSnO and ZnO TFTs will be discussed about their behaviors related to electrical, optical, and chemical properties. Then, it may suggest an idea to design general oxide semiconductor material systems under atmospheric pressures.

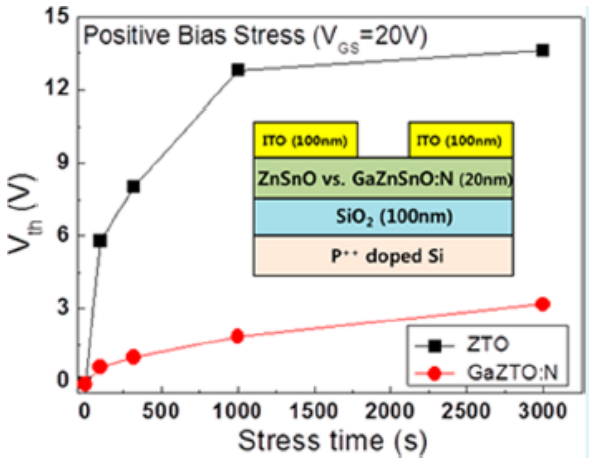

Figure 25 The variation of threshold voltage on ZnSnO and GaZnSnO:N TFTs under positive bias stress (V_{GS}=20V)

References:

[1] H. J. Jeon, W. J. Maeng, and J. S. Park, Ceramics International 40 (2014) 8769.
[2] B. D. Ahn, H. J. Jeon, and J. S. Park, ACS App. Mater. Interface 6 (2014) 9228.
[3] H. J. Jeon, K. B. Chung, and J. S. Park, J. Electroceram. (2014) Doi 10.1007/s10832-014-9902-8
[4] H. J. Jeon, S. G. Lee, K. S. Shin, S. W. Kim and J. S. Park, J. Alloy and Compounds 614 (2014) 244

Acknowledgement:

This work was supported by the National Research Foundation of Korea (NRF) grant funded by the Korea government(MEST) (No. 2012011730)

LD-I07

Electrical stability of multilayer MoS_2 field effect transistor under negative bias stress at various temperatures

Suk Yang[1,2], Solah Park[1,2], Sukjin Jang[1,2], Hojoong Kim[1,2], and Jang-Yeon Kwon[1,2]
[1]School of Integrated Technology, Yonsei University, 406-840 Yeonsu-gu, Incheon, Korea
[2]Yonsei Institute of Convergence Technology, Yonsei University, 406-840 Yeonsu-gu, Incheon, Korea

Transition metal dichalcogenides (TMDCs), which have a layered structure, are promising semiconductor materials for future electronics [1]. TMDCs are a class of materials with formula MX_2, where M is a transition metal element and X is a chalcogen (S, Se, or Te). Among these, MoS_2field effect transistors (FETs) presenting excellent electrical characteristics have been investigated for their potential use in several applications such as logic circuits, memory devices, gas sensors, and phototransistors for future electronics and optoelectronics.

The electrical stability of a transistor is a key requirement for use in a wide range of applications, such as in memory and displays. Specifically, the threshold voltage (V_{th}) shift under gate bias stress is a critical property for stable operation. The gate bias stress effect is commonly described in a variety of transistors: a-Si thin film transistor (TFT) [2], organic transistor [3], and amorphous oxide TFT [4].

In this study, we investigated electrical stability of multilayer MoS_2 FETs under negative gate bias stress at various temperature conditions. The evaluation of the stability was carried out in conditions which minimize artifact due to humidity, light, and electrical stress during transfer curve measurement in order to evaluate inherent properties of MoS_2 FETs. The instability of MoS_2 FETs under negative bias stress was explained to be due to charge trapping at the gate dielectric or at the interface between the gate dielectric and the channel.

References

[1] Q. H. Wang, K. Kalantar-Zadeh, A. Kis, J. N. Coleman, andM. S. Strano, Nature Nanotechnol. 7, 699 (2012).
[2] F. R. Libsch and J. Kanicki, Appl. Phys. Lett. 62, 1286(1993).
[3] S. Mathijssen, M. Clle, H. Gomes, E. Smits, B. deBoer,I. McCulloch, P. Bobbert, and D. deLeeuw, Adv. Mater.19,2785 (2007)
[4] R. B. M. Cross and M. M. De Souza, Appl. Phys. Lett. 89,263513 (2006).

LD-I08

Transparent Display using Quantum Dot LED & Solution-based Oxide TFT

Min Suk OH[1*]
[1]*Display Convergence Research Center, Korea Electronics Technology Institute (KETI), Seongnam, 463-816, Korea*

Keywords: Quantum Dot, Oxide, Solution, Thin Film Transistor

The colloidal quantum dots (QDs) which are composed of the compound semiconductors have been one of the prospective candidates for the new light emitting diodes (LEDs) due to their merits such as the low-cost solution process and the color tunability by controlling the size of quantum dot. But, because of the instability of the organic materials, there have been many research activities about the new charge transport layer. But, it is not easy to find the stable organic layers for QD-LEDs because of many restrictions. So, to solve these problems, several research groups have reported the QD-LED using inorganic charge transport layer. Here, to improve the stability of QD-LEDs, we fabricated the QD-LEDs using the inorganic charge transport layer and the inverted structure. And, for the solution-based process, we tried to apply the inorganic nano-particles to the fabrication process of these devices.

And oxide semiconductors have emerged as potential substitute for organic and silicon semiconductors in thin-film electronics. The high mobility in the amorphous state, and excellent uniformity, have extended their applications to active-matrix electronics, including displays, sensor arrays and X-ray detectors. Moreover, their solution processability and optical transparency have opened new horizons for low-cost printable and transparent electronics on plastic substrates. But metal oxide formation by the sol–gel route requires an annealing step at relatively high temperature, which has prevented the incorporation of these materials with the polymer substrates used in high performance flexible electronics. Here we report a general method for forming high-performance and operationally stable metal-oxide semiconductors at room temperature, by deep-ultraviolet photochemical activation of sol–gel films.

References:

[1] Q. Sun, Y. A. Wang, L. S. Li, D. Wang, T. Zhu, J. Xu, C. Yang and Y. Li, Nature Photon., 1 (2007) 717.
[2] J. M. Caruge, J. E. Halpert, V. Wood, V. Bulovic and M. G. Bawendi, Nat. Photonics, 2 (2008) 247.
[3] V. Wood, M. J. Panzer, J. E. Halpert, J.-M. Caruge, M. G. Bawendi and V. Blovic, ACS Nano, 3(11) (2009) 3581.
[4] Y-H. Kim, J-S. Heo, T-H. Kim, S. Park, M-H. Yoon, J. Kim, M. S. Oh, G-R. Yi, Y-Y. Noh and S. K. Park, Nature, 489 (2012) 128.

Acknowledgement:

This research was supported by Industrial Strategic Technology Development Programs (10045145, Development of high performance (>70 cm^2/Vs) chalcogenide TFT backplane and cadmium-free highly efficient (>30 cd/A) hybrid EL material/devices) & (10049080, Core Technology Development of Low-Energy, Visible-Light-Based Photo-Sintering Equipment for TFT Fabrication Process) funded by the Ministry of Trade, Industry and Energy (MOTIE, Korea).

LD-I09

Feasibility of Large Area Devices Based on Group III Nitrides

H. Fujioka[1,2], K. Ueno[1], A. Kobayashi[1], and J.Ohta[1]
[1] Institute of Industrial Science, the University of Tokyo, Tokyo 153-8505, Japan [2]JST-CREST, Tokyo 102-0075, Japan

It is generally believed that III-V semiconductor devices exhibit high performance but are very expensive because their fabrication process involves low throughput high temperature MOCVD or MBE growth on single crystal wafers. To fabricate large area III-nitride semiconductor devices such as solar cells or displays at a reasonable cost, development of a high throughput low temperature growth technique on low cost substrates is quite important. We have recently found that the use of growth technique called PSD (pulsed sputtering deposition) allows us to obtain device quality III nitrides even at room temperature [1]. PSD has attracted much attention of industry engineers because its productivity is much higher than that of MOCVD. In this technique, surface migration of the film precursors is enhanced and, therefore, the temperature for epitaxial growth is dramatically reduced. This reduction allows us to utilize various large area low cost substrates such as metals and mica that have not been used for growth of semiconductors so far due to their chemical vulnerability. In this presentation, we will discuss the feasibility of future large area flexible nitride devices prepared by PSD on these low cost substrates.

Typical GaN films prepared by PSD is highly resistive or lightly doped n-type but they can be doped into highly doped n-type or p-type by introduction of Si or Mg, respectively. With the use of this doping technique, we can fabricate various optical and electron devices. The most striking advantage in the device application of low temperature PSD process is suppression of phase separation reactions in InGaN, which is crucial for fabrication of long wavelength LEDs and solar cells. In fact, we have found that the use of PSD allows us fabricate a LED with a wavelength of 630 nm at a maximum process temperature of 480°C. We have also fabricated AlGaN/GaN HEMT structure on Si substrates and confirmed its successful transistor operation. This successful operation opens up the possibility for the future low cost integration of GaN devices and Si CMOS devices on Si (110) substrates. We have also fabricated InN MISFETs with the use of PSD process and demonstrated large current and low leakage operation.

We then applied the present PSD technique for fabrication of LEDs on large area and flexible substrates such as metal foils and mica sheet. We have confirmed successful operation of full color RGB LEDs on these substrates. We have also worked on growth of GaN on amorphous SiO_2 substrates. However, growth of crystalline GaN materials on top of amorphous materials is quite difficult. To solve this problem, we introduced graphene layers at the nitride/SiO_2 interface and we succeeded in operation of RGB fill color InGaN LEDs on amorphous SiO_2 substrates with the use of the graphene layers. This success implies that we could possibly fabricate InGaN full color displays on large area glass substrates with the use of the proposed process. These results clearly indicate that combination of the PSD low temperature growth technique and the large area substrate is quite promising for fabrication of future low cost large area nitride devices.

LD-I10

Carrier transport phenomena in sputtered ITO ohmic contacts to *p*-GaN

Joon Seop Kwak
Department of Printed Electronics Engineering, Sunchon National University, Sunchon, Jeonnam 540-742, Korea

Keywords: ITO, *p*-GaN, LEDs

High power LEDs have attracted great attention as light sources for general lightings and back-light unit of LCD displays, as well. One of the main concerns in this area is the fabrication of high-quality ohmic contacts to *p*-GaN with low resistance, and high transparency or reflectivity. Achieving low resistance ohmic contacts to p-GaN has been particularly challenging, because of difficulty in obtaining a hole concentration over 1018 cm-3 and the absence of metals having a work function higher than that of p-GaN. In order to achieve high-quality ohmic contacts to InGaN-based LEDs, carrier transport phenomena at the interface between metal and p-GaN should be elucidated.

This presentation discusses carrier transport phenomena in metal contacts to p-GaN. Especially, based upon the carrier transport phenomena, we will focus on Indium tin oxide (ITO) ohmic contact to p-GaN since ITO is commonly used as a transparent electrode on p-type GaN in LEDs. Because transmittance and specific resistance of ITO film have a significant impact on the efficiency of top emission LEDs, various vacuum deposition methods have been studied to grow a high quality ITO film on p-type GaN. However, due to the plasma damage in ITO sputtering process, e-beam evaporated ITO is widely used to make the top emission LEDs in spite of its relatively low film quality. Although a sputtering process is well known to obtain the best quality of ITO films, it cannot be applied due to the degradation of p-type GaN through the impact of high energy ion or electron in plasma. In this study, the properties of sputtered ITO films grown by plasma damage-free condition will be shown, and the mechanism for forming a low resistance sputtered ITO ohmic contact to p-GaN will also be discussed.

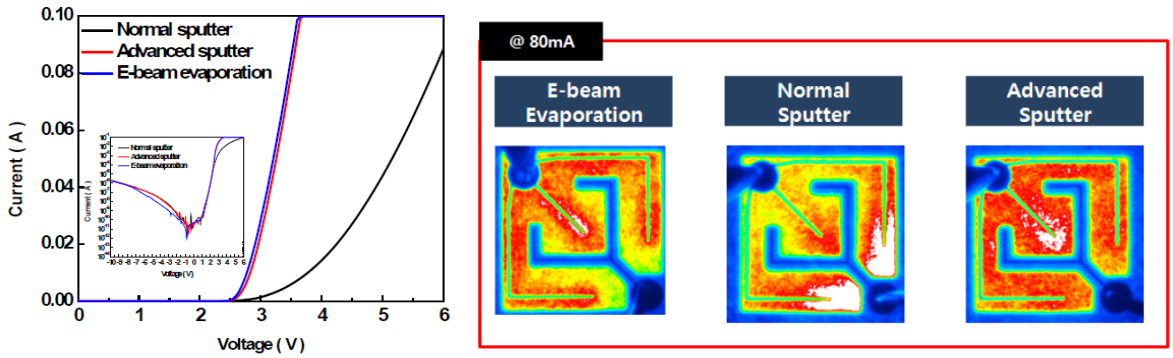

Figure 26. I-V characteristics and emission patterns of ITO contact to p-GaN in LEDs prepared by E-beam evaporation, normal sputter, and advanced sputter

Acknowledgement:
This study is financial supported by Basic Science Research Program through the NRF of Korea funded by the Ministry of Education (NRF-2014R1A6A1030419) and the BK21 PLUS program at SCNU.

AD-I01

Thermal Properties of Y_2O_3 doped ZrO_2, Thermal Barrier Coatings

Byung-Koog JANG [1*], Seongwon KIM [2], Yoon-Suk OH [2], Hyung-Tae KIM [2]
[1]*National Institute for Materials Science, Tsukuba, Ibaraki, 305-0047, Japan*
[2]*Korea Institute of Ceramic Engineering and Technology, Icheon, 467-843, Korea*

Keywords: Thermal barrier coating, ZrO_2, Y_2O_3, EB-PVD, Thermal conductivity

Thermal barrier coatings (TBCs) have received a large attention because they increase the thermal efficiency of gas turbine engines by increasing the gas turbine inlet temperature and reducing the amount of cooling air required for the hot section components. Electron beam-physical vapor deposition (EB-PVD) or plasma spray coatings is a widely used technique for depositing thermal barrier coatings (TBCs) on metal substrates for high temperature applications, such as gas turbines, in order to improve the thermal efficiency. The controlled microstructure of coatings is one of the most important properties for obtaining superior TBCs. To optimize TBCs for integration into gas turbines, characterization of the relationship between microstructure and thermal properties of the coatings is important [1,2]. This work describes the thermal properties of 2~8mol%Y_2O_3-stabilized ZrO_2 (YSZ) coatings by EB-PVD. The thermal conductivity of the coated samples was measured by the pulsed thermal imaging method and the laser flash method. The YSZ coatings consist of porous-columnar grains containing nano pores. Nanosize pores could be observed around feather-like grains as well as inside of columnar grains. The thermal conductivity and thermal diffusivity of the coatings showed decreasing tendency with increasing porosity. In addition, both the thermal conductivity and heat capacity of Y_2O_3-doped ZrO_2 coatings tended to decrease with increasing amounts of Y_2O_3 as shown in Fig.1. The thermal conductivity can be usually reduced by decreasing the mean free path due to the phonon scattering at pores or defects in the coatings.

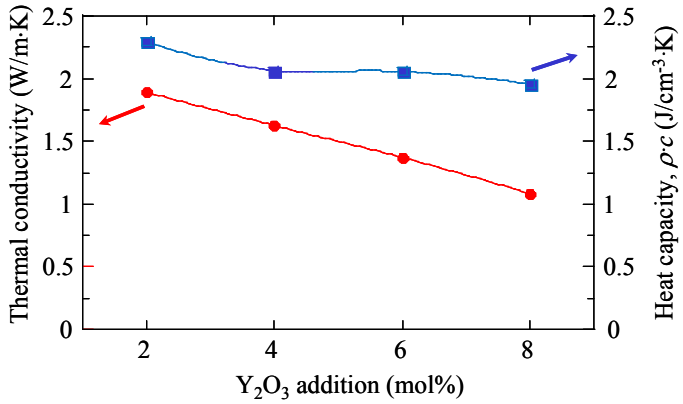

Figure 27 Thermal conductivity and heat capacity of ZrO_2-Y_2O_3 coatings by EB-PVD

References:

[1] B.K.Jang, J.G. Sun, S.W. Kim, Y.S. Oh and H.T. Kim, Surf. Coat. Technol.207 (2012) 177.
[2] U. Schulz, K. Fritscher, A. E. Stahl, Surf. Coat. Technol. 203 (2008) 449.

AD-I02

Mechanical Behavior of Thermal Barrier Coatings after Thermal Shock using Spherical Indentation Analysis

Kee Sung LEE[1*], Dong Heon Lee[2]
[1]*School of Mechanical Systems Engineering, Seoul, 136-702, Korea*

Keywords: Thermal barrier coating, Indentation, Thermal shock

Thermal barrier coating (TBC) is exposed to high temperature from 1100 up to 1600°C during gas turbine operation, by thermal cycling and thermal shock. The thermal expansion coefficient mismatch between ceramic topcoat and metallic bondcoat during thermal shock or cycling causes delamination of coating layer. Sintering of ceramic topcoat during thermal shock or cycling is the other issue to cause the mismatch. Therefore evaluations on the mechanical behavior of thermal barrier coatings after thermal shock are important issue to understand the lifetime of thermal barrier coating.
Mechanical durability are tested in terms of failure modes of thermal barrier coatings. For example, the mode of foreign object damage (FOD) has been studied recently, which can cause cracks at high temperature by particle impact. The other failure mode, erosion, may lead to progressive loss of thickness during operation. Mechanical fatigue by vibration causes damage accumulated failure of thermal barrier coatings.
In this study, materials and structures are designed in the thermal barrier coatings during APS (air plasma spray) and EBPVD (electron beam physical vapor deposition) coatings of YSZ (yttrium stabilized zirconia). Some coatings are conducted using $Gd_2Zr_2O_7$ (gadolinium zirconate) material. Thermal shock tests between 1100°C and room temperature are conducted for 800~1200 cycles in air. Mechanical deteriorations are evaluated by load-displacement behavior from ball-indentation test as shown in Fig. 1. Additionally, the wear tests are conducted and compared in the thermal barrier coatings using the same spherical ball.

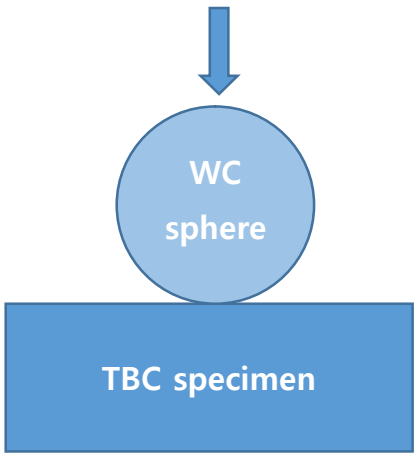

Figure 28 Schematic diagram of spherical indentation on thermal barrier coatings

References:
[1] C. Kim, Y. S. Heo, T. W. Kim and K. S. Lee, J. Korean. Ceram. Soc. 50 (2013) 326.
[2] K. S. Lee, D. H. Lee and T. W. Kim, Yogyo Kyokaishi 122 (2014) 668.

Acknowledgement:
This work was supported by the Korea Evaluation Institute of Industrial Technology (KEIT) gran founded by the Korean government (MOTIE).

AD-I03

Effects of Feedstock Species in Top Coat on Thermal Durability of Thermal Barrier Coatings in Cyclic Thermal Exposure

Sang-Won MYOUNG[1], Zhe LU[1], Qi-Zheng CUI[1], Je-Hyun LEE[1], Yeon-Gil JUNG[1*], Ungyu PAIK[2], Byung-Koog JANG[3]

[1]*School of Advanced Materials Science and Engineering, Changwon National University,Changwon, Gyeongnam 641-773, Republic of Korea*

[2]*Department of Energy Engineering, Hanyang University, Seoul 133-791, Republic of Korea*

[3]*High Temperature Materials Unit, National Institute for Materials Science, Tsukuba, Ibaraki 305-0047, Japan*

Keywords: Thermal barrier coating, Top coat species, Cyclic thermal exposure, Microstructure evolution, Thermal durability

Thermal durability and failure mechanisms of thermal barrier coatings (TBCs) are closely related with its microstructure. Therefore, the effects of feedstock species in a top coat on the thermal durability and/or fracture behavior of TBCs were investigated through thermal fatigue tests. Two kinds of feedstock with different purity in 8YSZ were employed for the top coat, which were prepared by air plasma spray (APS) process [1-2]. The bond coat was formed by high velocity oxygen fuel (HVOF) process using Ni based intermatellic powder. The microstructural evolution and mechanical properties of the designed TBCs were investigated through thermal fatigue tests. The cyclic furnace thermal fatigue (CFTF) tests were performed at 1100 and 1300 °C with a temperature difference of 150 °C between the surface and bottom of TBC sample till 872 cycles in the specially designed furnace. The flame thermal fatigue (FTF) tests were also performed at a surface temperature of 1100°C for a dwell time of 5 min till 872 cycles. The TBC with a high purity showed a better thermal durability than that with a relatively low purity at both temperatures in the CFTF, and the microstructure of TBC after the CFTF was more dramatically changed than that after the FTF, showing a relatively thick TGO layer. The influences of feedstock species on microstructural evolution and interfacial stability was discussed, based on the microstructure observation and comparison before and after cyclic thermal exposure tests.

References:

[1] Y.H. Sohn, E.Y. Lee, B.A. Nagaraj, R.R. Biederman and R.D. Sisson Jr, *Surf. Coat. Technol* 132 (2001) *p*. 146

[2] K. Richardt, K. Bobzin, D. Sporer, T. Schläfer, P. Fiala, *Surf. Coat. Technol* 17 (2008) *p*. 612

AD-I04

Microstructure Design and Thermal Durability of Thermal Barrier Coatings with Layered Structure

Yeon-Gil JUNG[1*]
[1]*School of Advanced Materials Science and Engineering, Changwon National University, Changwon, Gyeongnam 641-773, Republic of Korea*

Keywords: Microstructures, Durability, Thermal Barrier Coating, Structure

Now days the turbine inlet temperature of gas turbines has been increased to 1600°C, which is much higher than the allowed temperature of the superalloy employed. Therefore, the thermal durability and lifetime performance of thermal barrier coating (TBC) system applied to the high-temperature components of gas turbines should be enhanced, and various microstructures have been proposed, such as dense vertical cracked TBC, gradient coating, high porosity coating, and thick thickness coating, etc [1-3]. In this study, the microstructure of TBC was controlled in the top and bond coats to propose the layered TBC and its influence on the thermal durability was investigated through cyclic thermal exposure tests. The results included the number of cycle to failure and a phenomenological description of failure with microstructure species. Several properties for the single and layered TBCs, such as hardness, toughness, damage tolerance, and thermal durability, were determined and compared. The microstructure in TBCs was well controlled, showing layered structure either in the top coat or in the bond coat. Mechanical properties were also well corresponded to the microstructure design in TBCs. The layered TBC showed a better thermal durability than the common TBC (single layered TBC) in cyclic thermal exposure, without or less degradation in properties. Especially, the TBC with the layered structure enhanced the thermal durability, indicating that the structural effectiveness is one of important factors for improving the thermal durability. These observations allows us to design a certain microstructure in TBC to propose an efficient coating to ensure the thermal durability and mechanical properties in the cyclic thermal exposure environments.

References:

[1] N. P. Padture, M. Gell, and E. H. Jordan, *Science* 296 (2002) *p*. 280-
[2] G. Bertrand, P. Bertrand, P. Roy, C. Rio and R. Mevrel, *Surf. Coat. Technol* 202 (2008) *p*. 1994
[3] S.W. Myoung, S.S. Lee, H.S. Kim, M.S. Kim, Y.G. Jung, S.I. Jung, T.K. Woo and U. Paik, *Surf. Coat. Technol* 215 (2013) *p*. 46

AD-I05

Development of Oxides Eutectic EBC for Silicon Nitride Ceramics

Shunkichi UENO
College of Engineering, Nihon University, Koriyama, Fukushima 963-8642, Japan

Keywords: EBC, Lu2Si2O7/mullite, steamjet test, corrosion, recession

In this paper, the corrosion and recession behavior of $Lu_2Si_2O_7/Al_6Si_2O_{13}$ (mullite) eutectic oxide phase that discovered by the authors in the Lu_2O_3-SiO_2-Al_2O_3 ternary system were discussed. The eutectic point was approximately at 1510°C. It was found that the thermal expansion coefficient of eutectic oxide is comparable to those Si-based ceramic materials. Thus, it was surmised that this eutectic oxide could be potential candidate for environmental barrier coating (EBC) system for these Si-based ceramics because of its high eutectic point. The corrosion and recession tests were performed for eutectic bulks at 1300°C under the static water vapor environment and high speed stem jet environment. Results showed that there was little or no corrosion observed after the static state corrosion test. Since no boundary phase exists in this eutectic oxide, no selective corrosion of the boundary phase occurred during the test. The eutectic oxide film was then prepared on silicon nitride surface via the reaction sintering method. The water vapor corrosion test for silicon nitride with the eutectic oxide film was performed at 1300^{o}C for up to 500h. However, mullite phase decomposed and removed after recession test under high speed steam jet test. A silicon nitride with multi-layered environmental barrier coating (EBC) system was prepared and the recession test for this sample was performed at 1300^{o}C for 500 hours using high-speed steam jet equipment, which was employed to simulate the gas turbine engine conditions. Post-test examinations showed that the multi-layered EBC system well sustained during the high-temperature steam jet test. Also, the silicon nitride substrate was protected from the oxidation and corrosion, and thus no material recession was observed.

AD-I06

Growth behavior of YSZ thermal barrier coatings based on the substrate condition and heat treatment by electron beam evaporation method

Chanyoung Park[1,3], Yoonsoo Han[1], Seongwon Kim[1], Sungmin Lee[1], Hyungtae Kim[1], Byungkoog Jang[2], Daesoon Lim[3], and Yoonsuk Oh[1*]

[1]*Korea Institute of Ceramic Engineering and Technology, Icheon, 467-843, Korea*
[2]*Department of High Temperature Materials Unit, National Institute for Materials Science, Tsukuba, Japan*
[3]*Department of Materials Science and Engineering Korea University, Korea*

Keywords: Thermal Barrier Coatings (TBCs), EBPVD, Rotation, Columnar structure.

A thermal barrier coating (TBC) can provide higher durability on alloy metal parts worked in turbine system for power plant or airfoil engines [1]. For this TBC, Yttria stabilized zirconia (YSZ) and plasma sprays are conventionally used as a coating material and coating technology, respectively. Electron beam physical vapor deposition (EBPVD), one of the advanced coating technology, has been attention for its structural stability by increase of strain tolerance at high temperature operation condition [2]. During the deposition, control of column structure and pore distribution is a critical factor to promote optimization of coating structure.

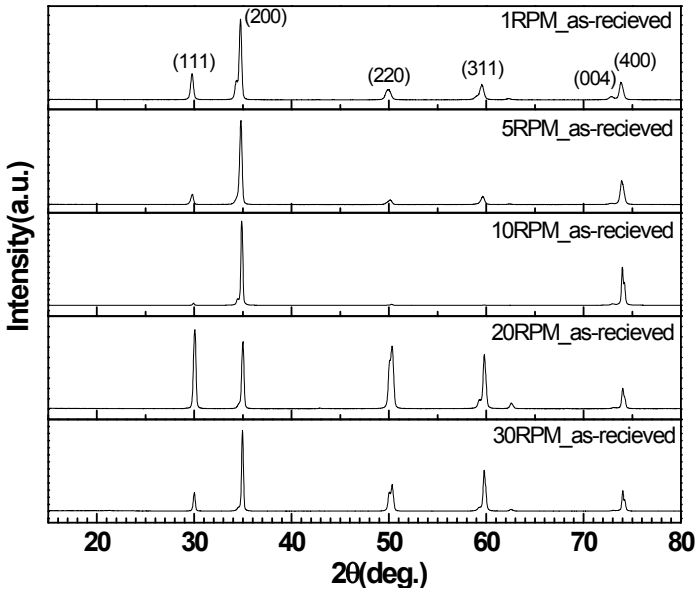

Figure 29 XRD data of 4YSZ coatings with different rotation condition

In this study, YSZ based thermal barrier coatings are fabricated by EBPVD with different substrate rotation condition. Phase formation, microstructures, and interface analysis are examined with the deposited condition and post heat-treatments. Column structure of coating is strongly affected by rotation condition differ from the phase forming behavior.

References:

[1] N. P. Padture et al, Science, 296, 280-284 (2002).
[2] J. Singh and D. E. Wolfe, J. Mater. Sci., 40, 1-26 (2005).

Acknowledgement:

This research was supported by a grant from the Fundamental R&D Program for Strategic Core Technology of Materials funded by the Ministry of Trade, Industry and Energy and by a grant from the Basic and Strategic R&D Program funded by the Korea Institute of Ceramic Engineering and Technology, Republic of Korea.

Oral Presentation

Synthesis, Raw Materials & Advanced powder processing(SY)	……	177
Thermoelectrics(TH)	……	181
Thin Films & Layers(TF)	……	183
Nano-particles & Nano-structured Materials(NA)	……	189
Fuel cells and Batteries(FU)	……	194
Electronic Ceramics(EL)	……	196
Structual Ceramics & Refractory materials(ST)	……	203
Glass & Opto-Electronic Materials(GL)	……	219
Biomaterials(BI)	……	229
Sensor Materials(SE)		239
Piezoelectric Device & Application(PI)	……	240
Lead-free Piezoelectrics(LP)	……	248
Computational Ceramic Science and Engineering(CO)	……	255
Ceramics Culture and Education(CE)	……	256
LED and Display Materials(LD)	……	259
Advanced Coating for Gas Turbines(AD)	……	265

SY-O01

Sintering and Thermal properties of the Glass/Al_2O_3 Composites for the Substrate of Supercapacitor

Tae-Ho Lee[1], Dae-Hyeon Kim[1], In-Tae Seo[1], Sahn Nahm[1*]
[1]*Department of Materials Science and Engineering, Korea University, Seoul, 136-701, South Korea*

Keywords: Glass/Al_2O_3, Sintering, Bending strength, Thermal conductivity, LTCC

In the past decades, low temperature cofired ceramics (LTCC) substrate and related packaging technology have been extensively studied for the miniaturization of the electronic devices. In this study, a new LTCC ceramics consisting of CaO-Al_2O_3-SiO_2-B_2O_3-MgO (MLS-22) and Al_2O_3 were fabricated and their sintering mechanism, mechanical and thermal properties were investigated. When 20wt% Al_2O_3 was added to MLS-22, the LTCC ceramics was well sintered at 900°C for 1 h with a high relative density of 93% of theoretical density. They also showed a high bending strength and a good thermal conductivity of 322.9MPa and 3.75 W/mk, respectively, indicating that these LTCC ceramics can be used to the substrate for supercapacitors. In addition, the detailed investigation on the variation of microstructure with respect to the sintering condition was studied. Moreover, the relation between the microstructure and the mechanical and thermal properties of the specimens were discussed in this work.

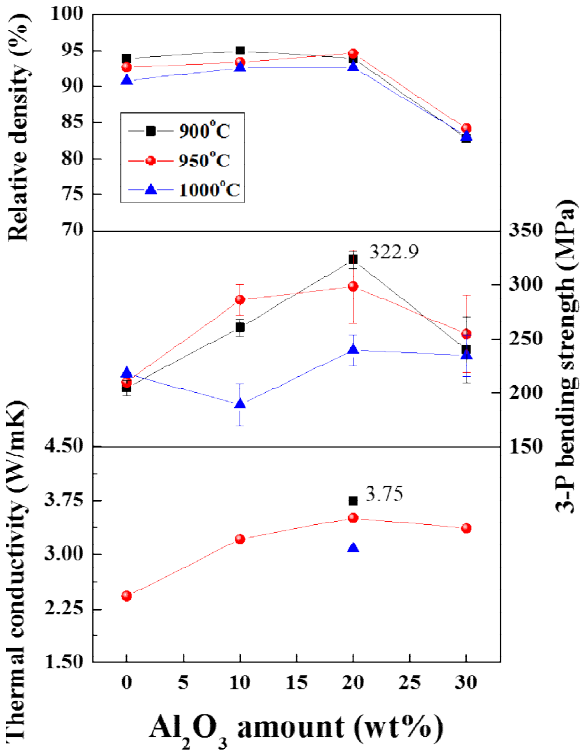

Figure 30 Relative density, bending strength and thermal conductivity of glass/Al_2O_3 with variation Al_2O_3 amount

SY-O02

Electronic Spectra of Tourmaline Treated by Heat and Electron Beam Irradiation

Apichate MANEEWONG [1, 2,3], Beak Seok SEONG[1, 2, *], JeongSeog KIM[4]
[1]*Korean University of Science & Technology, 217 Gujeong-ro, Yuseong-gu, Daejeon, 305-350, Republic of Korea*
[2]*Neutron Science Divisions, Korea Atomic Energy Research Institute,1045 Daedeok-daero, Yuseong-gu, Daejeon, 305-353, Republic of Korea*
[3]*Gems Irradiation Center, Thailand Institute of Nuclear Technology, 9/9 Moo 7, Saimoon, Onkharak, Nakhon-Nayok, 26120, Thailand*
[4]*Department of Digital Display Engineering, Hoseo University, Sechul-ri, BaeBang-eup, Asan, Chungnam-do, 336-795, Republic of Korea*

***Keywords*:** Tourmaline, Heat treatment, Neutron Diffraction, Rietveld refinement, UV-Visible Spectroscopy

Tourmaline is an extremely important mineral. Known as the “Electric Stone”, Tourmaline is the highest-energy crystal in the world. In 1880, lab experiments performed by Pierre and Jacques Curie proved that Tourmaline generates a weak electrical charge. This electrical charge enables Tourmaline to produce far infrared photon energy, negative ions, and alpha waves [1]. Therefore, in this work electronic spectra, chemical compositions and structure behavior of two pink and one green tourmaline from Nigeria and Afghanistan have been investigated by UV–Vis, EDXRF, XRD, HRPD, XPS and SANS. Tourmaline minerals observed in different geologic environment, show significant variations in terms of chemical compositions. All samples were fluor-elbaite with fluorine weight fraction about 2.00%. The origin of color in pink tourmaline can be attributed to the presence of Mn^{2+} and Mn^{3+} which showed a small and broad absorption band at 396 and 520 nm, respectively. The heating completely reduced both the Mn^{3+} and Mn^{2+} which making colorless at 600 °C. The green color in tourmaline is related to the presence of ferrous iron at the octahedral site. Resulting showed the ferrous ions which did not reduce or oxidize upon heating in air. Pink tourmalines with a high Mn content return to original color after irradiation with electron 800 kGy. Both heat treatment and electron irradiation do not produce any significant changed of composition on the cation side of tourmaline

References:

[1] Timothy Winey, “Method and apparatus for the exploitation of piezoelectric and other effects in carbon-based life forms,” U.S. Patent 20070258329 A1, Nov 8, 2007.

SY-O03

Synthesis and Characterization of the Spinel System Inorganic-Pigment by a Reverse Micelle Processing

JEONG HUN SON[1], DONG SIK BAE[1]*
[1]*Department of Advanced Materials Engineering, Changwon National Univ., 20 Changwondaehak-ro Uichang-gu Changwon-si, Gyeongsangnam-do 641-773 KOREA*

Keywords: Spinel, Inorganic – Pigment, Synthesis, Reverse Micelle, Nanoparticle.

The spinel system inorganic pigments have high thermal stability and chemical resistance at high temperature. So Inorganic pigments used in clay, paints, plastic, polymer, color glass and ceramics. Spinel structures have general formula AB_2O_4. In this structure there are four octahedral holes and eight tetrahedral holes per molecule. In normal spinels, A^{2+} ions occupy tetrahedral holes and B^{3+} ions are present in the octahedral holes and the anions are arranged in a cubic close packed array. $CoAl_2O_4$ nanopowders was synthesized by reverse micelle processing the mixed precursor (consisting of A^{2+} ions Cobalt(Ⅱ) nitrate hexahydrate and B^{3+} ions Aluminum nitrate nonhydrate). The $CoAl_2O_4$ was prepared by mixing the aqueous solution at a molar ratio of Co : Al = 1 : 2. The average size and distribution of synthesized powders with heat treat at 900, 1000, 1100 and 1200°C for 2h were in the range of 10-20nm and narrow, respectively. The average size of the synthesized nanoparticles increased with increasing water to surfactant molar ratio. The synthesized CoA_2O_4 powders were characterized by X-ray diffraction analysis (XRD), Field emission scanning electron microscopy (FE-SEM) and Color spectrophotometer. The intensities of X-ray diffraction synthesized $CoAl_2O_4$ powder increased with increasing heating temperature. As increasing of the heating temperature, crystalline size of the synthesized powders is increased. As increasing of the R value(water/surfactant) and heating temperature, color of inorganic pigments is changed dark blue-green to cerulean blue.

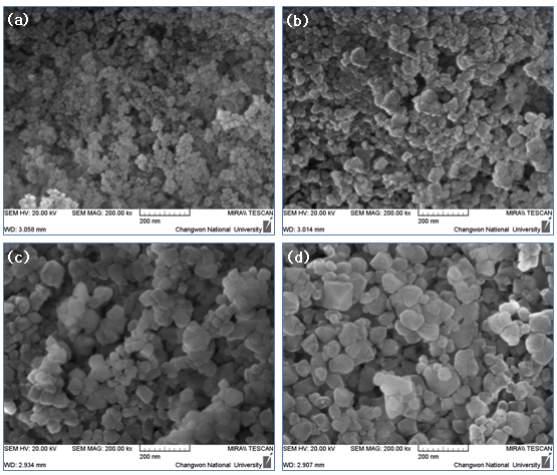

Figure 31 FE-SEM image of $CoAl_2O_4$ nanoparticles synthesized at R=8 and various calcinations temperatures; (a) 900℃, (b)1000℃, (c) 1100℃ and (d) 1200℃

References:

[1] R. K. Sharma and R. Ghose, Ceram. Int. 40 (2014) 3209.

SY-O04

Synthesis and tribological characteristics of silicon carbide-derived carbon layer synthesized from different α- and β-SiC polytypes

Yoon-Soo CHUN[1], Min-Gun JEONG[1], Dae-Soon LIM[1*]
[1]*Department of Materials Science and Engineering, Korea University, Seoul, 136-701, Korea*

Keywords: Carbide, CDC, Tribology, α- and β-SiC, Polytypes

Carbide-derived carbons (CDCs) were synthesized from two different carbide polytypes, which are hexagonal SiC (α-SiC) and cubic SiC (β-SiC) powders, by chlorination at temperatures between 900 and 1200°C. Also, hydrogen content was varied from 0 to 7.5 vol.%. The content of the sp^2- and sp^3-bonded carbon phases and their crystallinity were analyzed by Raman spectroscopy in our proveious report [1]. In this report, the mechanical properties were measured with tribological tests including friction coefficient and wear rate. The morphology of CDCs showed interesting features that varied with the starting SiC polytypes. Diamond nanocrystals were more frequently observed in α-SiC-derived carbon than that in β-SiC-derived carbon, which was investigated by CVD dimond deposition study as shonw in Fig.1. The rate of graphitization of CDCs was affected by not only synthesis temperature and hydrogen content but also SiC polytypes. A possible mechanism responsible for the observed results was also investigated. Tribological properties were measured with pin-on disk type tribometer. The β-SiC-derived carbon shows lower frcition coefficient that that of α-SiC-derived carbon due to higher graphitization of CDC layer. However, the wear rate measurements of both CDCs shows similar values but with different trend, where diamond nanocrystals are only formed on the surface of α-SiC-derived carbon to improve its hardness.

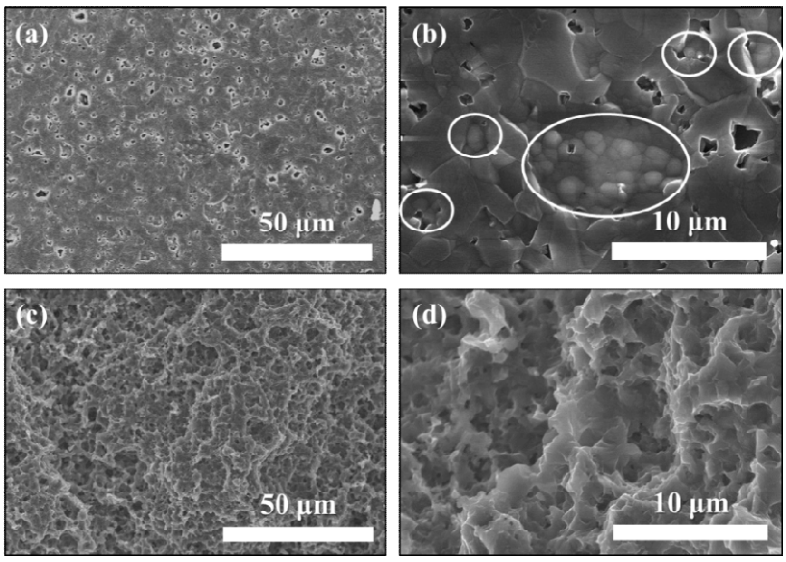

Figure 32 SEM images of the surface of CDCs after the synthesis of CVD diamond: (a, b) are α-SiC-derived carbon, and (c, d) are β-SiC-derived carbon

References:

[1] M.G. Jeong, S.H. Yoon, Y.S. Chun, E.S. Lee and D.S. Lim, Carbon 79 (2014) 19.

TE-O01

Thermoelectric Properties of Titanium Doped Zinc Oxide Thin Films Deposited by Co-Sputtering method

Venkatraju.JELLA[1], Soon-Gil YOON[1]*
[1]*Department of Materials Science and Engineering, Chungnam National University, Daeduk Science Town, 305-764, Daejeon, Korea*

Keywords: Ti-doped ZnO (TZO) thin film, Co-Sputtering, Thermoelectric properties

Thermoelectric energy harvesting is the transformation of waste heat into useful electricity for applications — acquired the great interest for energy sustainability. The main obstacle is the low thermoelectric efficiency of materials for converting heat to electricity, quantified by the thermoelectric figure of merit, ZT. The best available n-type materials for use in mid-temperature (500–900K) thermoelectric generators have a relatively low ZT of 1 or less, and so there is much interest in finding avenues for increasing this figure of merit [1]. Among oxides, ZnO has always been attracted much attention because low-cost, nontoxic, stable thermoelectric material but thermoelectric properties of ZnO thin films have not been sufficiently explored, even if they are relatively easy to prepare [2,3]. The main reason is the practical difficulty in the measurement of thermoelectric properties at high temperature.

In this present study, Titanium doped ZnO (TZO) thin films were grown onto SiO_2(250 nm)/Si substrate by Co-sputtering method with the using of both Titanium and ZnO targets and annealed at various temperatures ranging from 773 to 1073K in argon ambient for various time. Thermoelectric properties of TZO thin films with various thickness investigated by the different annealing conditions. The Crystalline structure, thickness, morphologies and carrier concentration of the deposited TZO thin films were measured by X-ray diffraction (XRD), Scanning electron microscope (SEM) and Hall measurement respectively. The XRD data indicated that all deposited TZO films have polycrystalline nature, showed only peak at $2\theta \sim 34°$ with (002) preferential orientation .This indicating that the films were hexagonal wurtzite structure and showed a good c-axis orientation perpendicular to the substrate. The experimental results showed that the absolute value of Seebeck coefficient of TZO thin film annealed in-between the temperature 873-973K increases stably with increasing of measuring temperature. Also, investigated the dopant different content effect of Titanium in TZO thin films by controlling the deposition powers for better thermoelectric properties.

References:

[1] Snyder, G. J. & Toberer, E. S. Complex thermoelectric materials. Nature Mater. 7,105–114 (2008).
[2] J. Mass, P. Bhattacharya, and R.S. Katiyar, Mater. Sci. Eng. B103, 9 (2003).
[3] B. Singh, Z.A. Khan, I. Khan, and S. Ghosh, Appl. Phys. Lett. 97, 241903 (2010).

TE-O02

Thermoelectric Properties of Bulk $Bi_2Mg_{2/3}Nb_{4/3}O_7$-Bi (BMNO-Bi) Composite and BMNO-Bi Composite Thin Films

Ji-Ho EOM[1], San-Kwon LEE[2], Soon-Gil YOON[1*]
[1]*Department of Materials Science and Engineering, Chungnam National University, Daeduk Science Town, 305-764, Daejeon, Korea*
[2]*Department of Physics, Chung-Ang University, 221 Heukseok-dong, Dongjak-gu, 156-756, Seoul, Korea*

***Keywords*:** Thermoelectric, Pulsed laser deposition, Seebeck coefficient, $Bi_2Mg_{2/3}Nb_{4/3}O_7$ –Bi

Thermoelectric materials have the unique capability to directly convert heat to electricity and provide spot cooling or heating. Thermoelectric devices for energy conversion and temperature control have widely exploited in many industrials field. The primary candidate technology for miniaturizing thermoelectric devices is to apply semiconductor-processing technologies including thin film process. A practical thermoelectric material should have high Seebeck coefficient, high electrical conductivity, and low thermal conductivity.

Bismuth magnesium niobium oxide ($Bi_2Mg_{2/3}Nb_{4/3}O_7$) has low thermal conductivity owing to its pyrochlore structure [1]. Especially, BMNO is easily reduced in the reduced atmosphere, resulting in a self - assembled Bi metal into the BMNO films grown by pulsed laser deposition (PLD) in N_2 atmosphere [2]. Therefore, electric property of BMNO was changed insulator to semiconductor. In the present study, self - assembled Bi metal into the BMNO thin films was compared with bulk type self - assembled Bi metal into the BMNO.

BMNO – Bi composite films were deposited on SiO_2 / Si substrate by pulsed laser deposition with various thicknesses (100, 300, 500, 700, and 1000 nm). The BMNO–Bi thin films were measured for thermoelectric properties using TFTEP – 800 (SEEPEL Co. in Korea) at various temperatures (30 ~ 500 ^oC, 10 points). The BMNO – Bi thin films were measured thermal conductivity at room temperature (measured in Chung – Ang University). Bulk type BMNO specimen was sintered using furnace at air atmosphere. BMNO – Bi specimen was annealed at Ar atmosphere. Bulk type BMNO – Bi specimen was measured thermoelectric properties using ZEM – 2 : M8/L (ULVAC Co. in Japan) at various temperatures (30 ~ 500 ^oC, 10 points). The thermal conductivity of the bulk type BMNO – Bi specimen was measured at room temperature.

Through this study, BMNO can be applied for the thermoelectric property. This study will contribute to find new thermoelectric materials using insulators.

References:

[1] David P. Cann, Clive A. Randall and Thomas R. Shrout, Solid State Communications, Vol. 100, No. 7, pp 529, 1996
[2] J.K Ahn, N.D Cuong, N.J Seong, and S.G Yoon, Journal of The Electrochemical Society, 156 (9) G134-G137 (2009)

TF-O01

Perovskite manganite based hetero-junction structure for cross-point arrays of ReRAM

Hong-Sub LEE, Yoon Kwang LEE, Hyung-Ho PARK*
Department of Materials Science and Engineering, Yonsei University, Seoul 120-749, Korea

Keywords: resistive switching, ReRAM, cross point array, perovskite manganite, heterojunction

Recently, the resistive switching (RS) phenomena of transition metal oxides (TMOs) have received a great deal of attention for next generation non-volatile memory (NVM) application.[1-2] Among the candidates of NVMs, the resistive RAM (ReRAM) using the RS phenomena has distinguishable merits as simple structure of metal/insulator/metal (MIM) and various RS characteristics of most TMOs. We can apply various materials with the RS characteristics to device fabrication with the various RS characteristics, and the MIM structure enables us to realize the highest density integration as a cross-point array (CPA) structure due to MIM simple structure which the CPA integration is operated by only bit line and word line without a cell selection transistor.[3] On the other hand, it has relatively weak point in endurance property because the RS characteristics in TMOs based on a redox. From the relatively fragile endurance property and a possibility of the highest density, the ReRAM is expected to substitute the position of present NAND flash memory. Therefore realization of the CPA structure of the highest density integration is most important issue of ReRAM for competitiveness. But cross-talk of CPA structure by sneak current should be overcome to realize ReRAM of the CPA structure and many studies noted the non-linearity characteristic of RS curve as one of the solutions of the sneak current issue. Figure 1 shows the sneak current of the worst condition in CPA circuit (*N* x *N*) which selected high resistance state (HRS) cell is surrounded by unselected selected low resistance state (LRS) cells. When we read the selected HRS cell (current path A) at V_{read}, the sneak current as much as current at $1/2V_{read}$ of RS element is induced through current path B and the sneak current increases as increasing of the number of '*N*' in *N* x *N* circuit. In that case, the selected resistor and sneak path resistors are connected as parallel series and increasing of the number of '*N*' increases sneak current. The result, sensing margin is reduced according to increasing '*N*'. Therefore the array size '*N*' can be maximized from minimized sneak current which can be achieved from high non-linear characteristic of RS curve.[4] This study fabricated pnp bipolar hetero-structure using perovskite manganite family such as p-type $R_{0.7}A_{0.3}MnO_3$ (*R*: rare-earth, *A*: alkaline-earth) (*RA*MO) and n-type $AMnO_{3-\delta}$ (*A*MO) to obtain non-linear resistive switching (RS) curve. The pnp structure shows not only non-linear characteristic but also tunable characteristic with thickness of *A*MO layer. Basically, the non-linear characteristic could be obtained from potential barrier of *A*MO interlayer in hole transport and its tunable characteristic was induced by resistance change of *A*MO layer. From the results, this study demonstrated the systematically tunable non-linear characteristic.

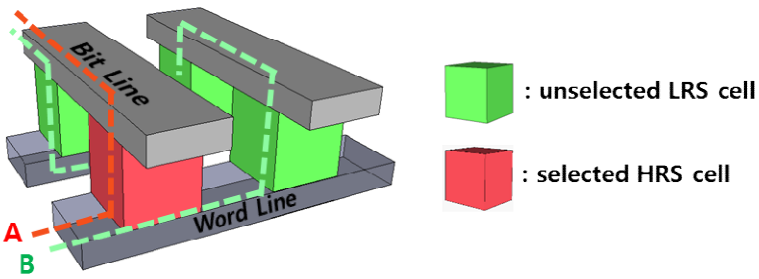

Figure 1 A scheme of sneak current in cross-point array structure

References:
[1] M. J. Rozenberg, Scholarpedia 6(4) (2011) 11414.
[2] H. S. Lee, S. G. Choi, H. H. Park, and M. J. Rozenberg, Sci. Rep. 3 (2013) 1704.
[3] E. Linn, R. Rosezin, C. Kügeler, and R. Waser, Nat. Mater. 9 (2010) 403.
[4] J.-J. Huang, Y.-M. Tseng, C.-W. Hsu, T.-H. Hou, IEEE Electron Device Lett. 32 (2011) 1427.

Acknowledgement:
This work was supported by the Industrial Strategic technology development program (10041926, Development of high density plasma technologies for thin film deposition of nanoscale semiconductor and flexible display processing) funded by the Ministry of Knowledge Economy (MKE, Korea). The experiments at the PLS were supported in part by MEST and POSTECH.

TF-O02

TiO_2 blocking layer grown by nanocluster deposition for improved perovskite solar cell performance

Thanh Tung Duong and Soon-Gil Yoon*,
Department of Materials Science and Engineering, Chungnam National University, 305-764, Daejeon, Korea

Keywords: NCD, blocking layer, Perovskite solar cells.

There have been some very interesting reports dealing with the application of perovskite sensitizer to hybrid organic-inorganic solar cells, since the power conversion efficiency (PCE) of lead halide perovskite (CH3NH3PbX3, X = Cl,Br, I)–based thin film photovoltaic devices has skyrocketed from 3.8% to more than 19% in just 4 years (1–6). In a typical perovskite solar cell, a several-hundred-nanometer-thick absorber layer, either with or without mesoporous scaffold, is sandwiched between the electron and hole transport layers (ETLs and HTLs, respectively). Upon the absorption of incident photons, carriers are created in the absorber that travel through a transport pathway including the ETL or HTL, the electrodes, and each interface in between. To increase the PCE, it is essential to precisely manipulate carriers along the entire pathway from the absorber to both electrodes.

In this study, we demostrate the thickness effect of compact-TiO_2 blocking layer and TiO_2 mesoporous layer to the perovskite sensitizer solar cells perfomance. The TiO_2 blocking layer prepared by nano-cluster deposition (NCD) played an important role in increasing the contact area between TiO_2 thick films and FTO, which helped prevent electron movement back to the electrolyte, and decreased the contact resistance at the TiO_2/FTO interface, whereas mesoporous TiO_2 layer fabricated by spincoating method acts as an electron transportation layer. The photovoltaic performance of perovskite solar cells was enhanced at 80 nm TiO_2 BL and 600 nm TiO_2 mesoporous layer, following parameters were obtained: J_{sc} = 21.0 mAcm^{-2}, V_{oc} = 0.89 V, FF = 62%, and efficiency (η) = 11.5%.

References:

[1] A. Kojima, K. Teshima, Y. Shirai, T. Miyasaka, J. Am. Chem. Soc. 131, 6050–6051 (2009).
[2] www.nrel.gov/ncpv/images/efficiency_chart.jpg.
[3] B. V. Lotsch, Angew. Chem. Int. Ed. 53, 635–637 (2014).
[4] N.-G. Park, J. Phys.Chem. Lett. 4, 2423–2429 (2013).
[5] H. J. Snaith, J. Phys.Chem. Lett. 4, 3623–3630 (2013).
[6] H. Zhou, Q. Chen, G. Li, S. Luo, T.Song, H.Duan, Z. Hong, J. You, Y.Liu, Y. Yang. Science, 345, 542(2014)

TF-O03

Fabrication and field emission properties of nanostructuralized diamond films

Chunyuan Lu[1], Qi Dong[1], Kelimu Tulugan[2], Yeong Min Park[1], Dae Woo Kim[1], Jeong Wan Kim[1], Tae Gyu Kim[3*]

[1]*Department of Nano Fusion Technology, Pusan National University,Miryang,627-706,Korea*
[2]*Department of energy—Mech.Eng, Gyeongsang,National University, Tongyeong,650-160,Korea*
[3]*Department of Nanomechatronics Engineering,Pusan National University,Miryang,627-706,Korea*

Keywords: Pre-seeding, nanostructuralized diamond films, field emission

The excellent properties of diamond as electron emitting materials for its low or negative electron affinity, superior mechanical, inert chemical properties and fine thermal conductivities, is drawing lots of attention. While compared with the fabrication of array sharp tip shaped metals or semiconductors, the deposition of diamond films by microwave plasma enhanced chemical vapor deposition (MPECVD) is much efficient. Seeding substrate is vital process to obtain high nucleation densities for the growth of continuous diamond films. In this research, two types of seeding methods are applied, scratching by diamond particles and ultrasonic bath with nanodiamond suspension as pre-seeding treatment. In the comparison of these two methods, the seeding result indicates that ultrasonic bath with nanodiamond suspension is more satisfying. Afterwards diamond films were deposited on p-type Si (100) substrate by MPECVD. Then diamond films were characterized by Raman spectroscopy, XRD, SEM and AFM. In order to obtain nanostructuralized diamond films, firstly gold, nickel and copper were used as masking material for nanostructuralized of diamond by RF plasma etching process. Applying plasma in a mixtured gas of CF_4/O_2 results in different types of diamond nanostructures, depending on the type of mask material used. This is a simple etching method for obtaining nanostructuralized surfaces of diamond films without complicated lithographic steps. Finally, the field emission properties of obtained nanostructuralized diamond films were investigated. The experiment results indicated that nanostructuralized diamond films showed enhanced field emission properties than non-nanostructure diamond films. The enhanced field emission properties of nanostructuralized diamond films is contributed to the nanostructures of the diamond surface.

TF-O04

Effect of Surface Modification of Boron-doped Diamond Electrode on Electrochemical Degradation of Organic Dyes in Wastewater

Choong-hyun LEE, Ji-yoon BAK, Dae-soon LIM*
Department of Materials Science and Engineering, Korea University, Seoul 136-713, Republic of Korea

Keywords: Diamond electrode, Electrochemistry, Water treatment, Advanced oxidation process

Electrochemical advanced oxidation processes (EAOPs) are being examined by many researchers as a powerful methodology for decontaminating organic dyes in wastewater[1]. Boron-doped diamond (BDD) is a popular material used for the anode in the EAOPs owing to its wide potential window, high durability[2]. However, it still has some difficulties applying to industrial scale water treatment because of low efficiency considering its cost[3]. In order to improve efficiency of water treatment, we prepared modified BDD electrodes having wide surface area and investigated the water treatment efficiency using those electrodes. Modifications were performed in two ways; Pyramid structured electrode and porous electrode were fabricated using alkaline chemical etching and CO_2 activation at high temperature, respectively. Both of BDD electrodes were fabricated by using electrostatic self-assembly (ESA) nano-diamond seeding method and hot filament chemical vapor deposition (HFCVD). The effective surface area of the pyramid structured BDD electrode increased more than twice than that of the non-modified electrode. The increase in the effective surface area affected directly to the improvement of the current efficiency for the dye wastewater treatment (Fig.1). In the case of porous BDD, the surface features of the electrodes were different according to activation temperatures. At the 1000 ^{o}C, more nano-sized pores were formed and effective surface area was slightly larger than that of the electrode etched at 900 ^{o}C. Also, there were some changes in Raman peaks showing some peaks intensified while some diminished. The result for the water treatment using the porous BDD electrode was also better than that of the non-modified electrode. Unlike the pyramid structured electrode, however, the change in film characteristic also affected the current efficiency for the oxidation process as well as the increase in effective surface area. These results indicate that modification of BDD electrodes can improve the efficiency of the electrochemical oxidation process.

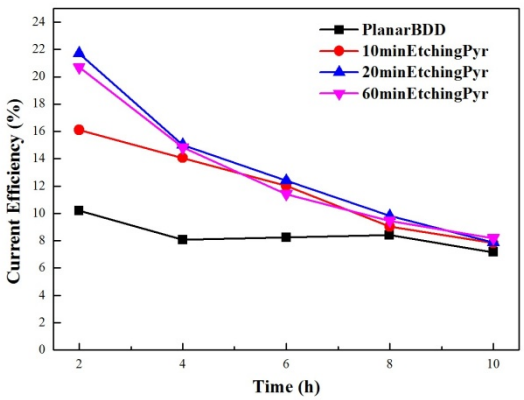

Figure 33. Current efficiency of pyramid structured BDD electrode

References:

[1] Martínez-Huitle, C. A. and Brillas, E. *Applied Catalysis B: Environmental* 87, 105–145 (2009).
[2] Tröster, I. *et al. Diamond and Related Materials* 11, 640–645 (2002).
[3] Luo, D., Wu, L. and Zhi, J. *ACS Nano* 3, 2121–2128 (2009).

TF-O05

Epitaxial growth and the electric/magnetic properties of magneto-electric Cr_2O_3 thin film

Takeshi YOKOTA*, Izuna TSUBOI, Manabu GOMI
[1]*Department of Materials Science and Engineering, Graduate School of Engineering, Nagoya Institute of Technology, Nagoya, Aichi, 466-8555, JAPAN*

Keywords: Epitaxial growth, Magneto-electric Effect, Compressive stress

Magneto-electric (ME) materials have attracted much attention as a new generation of magneto-electronics, because magnetic or ferroelectric properties can be controlled by an external electric or magnetic field. Cr_2O_3 is one of the typical ME material and many researches have been performed. Recently, Iyama et.al reported magnetic and electric order in Cr_2O_3 single crystal under a high electric and magnetic field in room temperature. [1] We focused an epitaxial Cr_2O_3 thin film having epitaxial stress, because we expected the similar ferromagnetic order induced by stress in Cr_2O_3. It is also expected to reduce the external magnetic field for obtaining the electric polarization. In this presentation, we prepared Cr_2O_3 epitaxial film having different epitaxial stress and investigated the magnetic properties.

The Cr_2O_3 thin films were prepared using a radio-frequency (RF) magnetron sputtering method. Cr_2O_3-sintered ceramic was used as the target. A c-cut Al_2O_3 and Nb-doped $SrTiO_3$ 111 single crystal were used as a substrate. Pt was deposited as a bottom electrode for c-Al_2O_3 substrate. A mixture of Ar and O_2 was used as the sputtering gas; the ratio was 32: 1. The RF power was 60 W. The growth temperature was 530 °C. The thickness was fixed at 30 nm. The surface morphology was measured using Atomic Force Microscope. The polarization curves measured using a ferroelectric property measurement system (FCE-1). A compressive stress measured using in/out-of-plane X-ray diffraction (XRD). The magnetic properties were measured using a vibrating sample magnetometer.

The RHEED patterns revealed the films are epitaxially grown on the both Pt/c-Al_2O_3 and $SrTiO_3$ substrates. It is also revealed that the both film has epitaxial compressive stress in the films. The compressive stress estimated using XRD of each film is 0.7 GPa and 3.04 GPa, respectively. Figure 1 showed magnetic hysteresis curves of samples. The magnetization curves of the sample deposited on $SrTiO_3$ is larger than that of Pt/c-Al_2O_3. This results are more likely due to differences in the compressive stress.

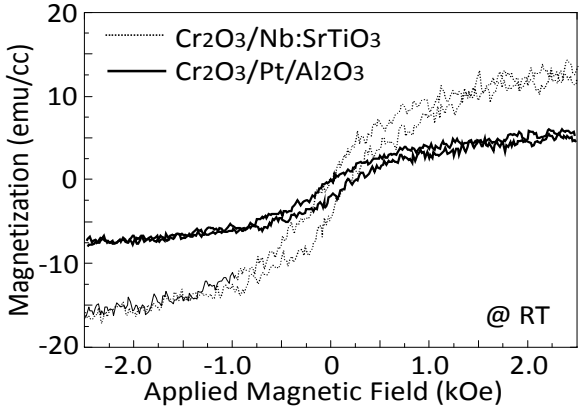

Figure 1 Magnetization curves of Cr_2O_3 film deposited on Pt/Al_2O_3 and $SrTiO_3$ substrate

References:

[1]A. Iyama. et. al, Phys. Rev. B87(2013) pp 180408-1

Acknowledgement:

This research was supported in part by a Grant-in-Aid for Challenging Exploratory Research (26600100) from the Japan Society for the Promotion of Science

NA-O01

The New Methodologies for the Synthesis of Nano Precipitated Calcium Carbonates

THENEPALLI Thriveni[1], CHILAKALA. Ramakrishna[2], Ji-Whan Ahn[3*]
[1,2,3,]*Mineral Processing Division, Korea Institute of Geoscience and Mineral Resources(KIGAM), 124 Gwahagno , Gajeong-dong 30, Yuseong-gu, Daejeon 305-350, South Korea*

Keywords: New Methods, Nano PCC, Applications

Recently the interest for aragonite, the calcium carbonate polymorph is increasing because new fields, like biomaterials, tissue engineering, paper making are developing. We investigated the possibility of synthesis of nano aragonite type precipitated calcium carbonate with uniform particle size by novel carbonation method and solution process. Some recent studies report synthesis of nano aragonite precipitated calcium carbonate is possible with the double jet methods in presence of organic additives [1,2]. The controlled double-jet precipitation method allows the production of colloidal particles with a good control of their monodispersity [3].

The carbonation process can be proceeded by solid – liquid – gas, solid $Ca(OH)_2$ is added to the $MgCl_2$ solution and gaseous CO_2 is injected to the suspension of $MgCl_2$- $Ca(OH)_2$ solution. The solution process is followed by liquid-liquid reaction using double-jet precipitation method using at the fixed temperature of 50ºC, with a flow rate of 1 ml/min.

We reported in this paper, the aspect ratio of aragonite-type PCC was controlled by the reaction temperature and CO_2 (g) flow rate. From the both processes, nano aragonite was obtained with average particle size is from 10~40 nm.

References:

[1] C. D. Mateescu, R. Isopescu, F. Branzoi, M. Mihai and I. Chilibon, J. Optoelectr. Adv. Mat. 10 (2008) 2667.
[2] Irinela Chilibon, 17th International Congress on Sound and Vibration (ICSV17), Cairo, Egypt, 18-22 July (2010)
[3] G. Xu, N.Yao, I.A. Aksay and J.T. Groves, J. Am. Chem. Soc. 120 (1998) 11977.

Acknowledgement:

The authors were highly thankful to Korea Institute of Energy Technology Evaluation and Planning through ETI program (Project No. 2010201010093C) for their financial supporting to this research work

NA-O02

Enzyme-mimetic Activity of Ce-doped Titanate Nanosheets

Kai KAMADA*, Hisanori KOBAYASHI, Taro UEDA, Takeo HYODO, Yasuhiro SHIMIZU
Graduate School of Engineering, Nagasaki University, Nagasaki 852-8521, Japan

Keywords: Biomimetic ceramics, Layered oxide, Radical scavenger, Reactive oxygen species

Cerium-doped titanate nanosheets were fabricated through a hydrolysis reaction of titanium tetraisopropoxide liquid mixed with $Ce(NO_3)_3$, and their reactive oxygen species (ROS) scavenging activity was investigated. The hydrolysis reaction was carried out by an addition of aqueous tetrabutylammonium hydroxide solution to the mixture, followed by aging at 60°C for 2 h. The resultant transparent colloidal solution contained nanoparticles with a tiny size less than 10 nm. XRD and Raman spectroscopy revealed that crystal structure of the nanoparticles is akin to layered tetratitanate ($Ti_4O_9^{2-}$) and the nanoparticles (called below as nanosheets) consist of several tetratitanate layers interstratifying Ce ions.

ROS scavenging activity of the nanosheets was evaluated for superoxide anion radical (O_2^-) as a target. The evaluation was performed by a well-known cytochrome c reduction technique [1]. The dependence of nanosheet concentration on the O_2^- quenching is shown in Figure 1(a), where the 1 mol% Ce-doped titanate nanosheets were employed. The figure clearly indicates dose-dependent O_2^- scavenging behavior, implying that the nanosheets possess superoxide dismutase (SOD) mimetic activity. Figure 1(b) plots 50% inhibitory concentrations (IC_{50}) as a function of Ce-doping amounts. The presence of Ce in the nanosheet drastically reduced the IC_{50} even at a low concentration below 1 mol%.

Typically, an enzyme SOD catalyzes dismutation of O_2^- to O_2 (oxidation) and H_2O_2 (reduction) accompanied by valence fluctuation of transition metal ions (Cu, Mn, etc.) in active centers. Judging from the favorable effect of Ce-doping on IC_{50}, the Ce ions appear to bring about the redox reaction of O_2^-. To clarify an annihilation route of O_2^- in the presence of nanosheets, H_2O_2 produced by the quenching of O_2^- was quantified by means of peroxidase assay [2]. The H_2O_2 concentration after scavenging by the nanosheets was lower than that after spontaneous O_2^- dismutation without the scavengers, suggesting that the oxidation (O_2^-/O_2) is a preferential route. This fact is not conflicted with thermodynamic consideration of redox potentials of $Ce^{3+}/^{4+}$ (E^o = +1.15 V *vs.* NHE at pH 7), O_2^-/H_2O_2 (+0.89 V), and O_2^-/O_2 (-0.33 V). That is, Ce^{4+} ions can oxidize O_2^- to O_2, whereas Ce^{3+} cannot reduce it to H_2O_2. In conclusion, the present study demonstrated that the Ce-doped titanate nanosheets have the scavenging ability of O_2^-, *i.e.*, SOD-mimetic activity, and the O_2^- annihilation is due to the oxidation activity of Ce^{4+} ions.

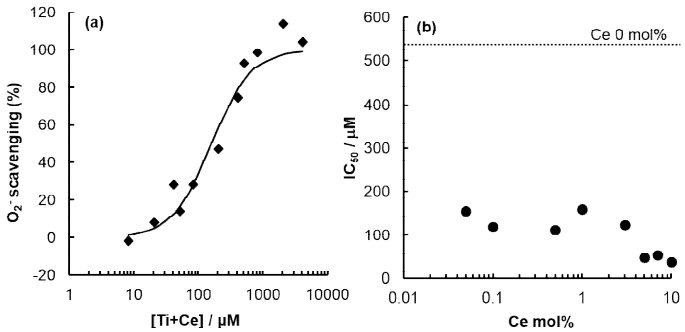

Figure 34 (a) Dose-dependent $\cdot O_2^-$ scavenging activity of 1 mol% Ce-doped titanate nanosheets and (b) influence of doping amounts of Ce on IC_{50}.

References:

[1] C. Korsvik, S. Patil, S. Seal and W.T. Self, Chem. Commun., (2007) 1056.
[2] N. Fujita and K. Kamada, J. Ceram. Soc. Jpn., 122 (2014) 141.

NA-O03

Solid state dye sensitized solar cell using TiO_2 blocking layer deposited by atomic layer deposition

Yun-Jeong KIM, Tung-Duong THANH, Soon-Gil YOON*
Department of Materials Science and Engineering, Chungnam National University,
Dae-Jeon, KS015, Republic of Korea

Keywords: ssDSSC, ALD, NCD, Blocking layer

In these latter days, the declining of the world oil production and increasing global temperature are caused global warming. It means that we need the development of renewable energy source. Solid - state dye sensitized solar cells (ssDSSC) are shown to be the appealing source for economical and effective switch over solar photons to electricity. A typical ssDSSC includes a dye sensitizer in which excitons are induced by light absorption. Generally, ssDSSC is consisted of bottom electrode, a blocking layer, a mesoporous nano crystalline Tin Oxide (TiO_2), monolayer of dye molecules, electrolyte, and the counter electrode. In this study, we are going to produce a thinner cell with a TiO_2 blocking layer using atomic layer deposition (ALD) process with excellent step coverage. The TiO_2 blocking layer can block the electron back reaction effectively, both from Fluorine doped Tin Oxide (FTO) and TiO_2 surface.

First, FTO substrate is deposited by TiO_2 blocking layer using Nano Cluster Deposition (NCD) which the crystallinity at low temperature (140 ~ 160 ℃) is possible. The blocking properties of the TiO_2 deposited using ALD and NCD technique were compared. Then, TiO_2 mesoporous layer, dye ($CH_3NH_3PbI_3$) and hall transition materials (Spiro - MeOTAD) are coated by spin coating techniques. Finally, the Au top electrode is deposited using direct current (DC) sputtering system.

X – Ray diffraction (XRD) was used to investigate whether dye is crystallized or not and scanning electron microscopy (SEM) to verify the correct thickness and image of surface. Also, the optical characteristics are measured for confirming transmittance from bottom electrode to TiO_2 in samples.

Finally, efficiency of the cells was measured using cells in the presence or absence of the blocking layer using ALD and NCD process on FTO substrate by solar simulator at 1.5 Air Mass (AM) and 1000 W/m^2.

References:

[1] J.Pys. Chem. Lett. 2014, 5, 1374-1379
[2] Adv. Mater. 2014, 26, 4309.4312

NA-O04

Three-Dimensional Structural control of insulating BN assembles in Polymer-nanocomposites

Hong-Baek CHO*, Tadachika NAKAYAMA, Hisayuki SUEMATSU, Tsuneo SUZUKI, Weihua JIANG and Koichi NIIHARA
[1]*Extreme Energy-Density Research Institute, Nagaoka University of Technology, Nagaoka , 940-2188, Japan*

Keywords: Polymer-nanocomposites, Boron Nitride, 3-dimensional control, Linear assembly, structural control

Distribution of insulating boron nitride (BN) nanoceramics are 3-dimensionally (3-D) controlled in polymer-nanocomposite films by electric field inducement. BN nanosheets, pretreated by exfoliation and functionalization of the surface were homogeneousely distributed in polysiloxane pre-polymer and they are redistributed by application of switching nanosec pulse electric field until the crosslinking of the prepolymer. A Si-micromold with micro-protrusions on the surface was used as an electrode in order to generate the electric concentration and to control the localization of the BN assembly during the application of electric field. The coordination effects of electric concentration, di-polarization, static energy, surface modification and Columbic attraction are considered as main factors that determine the controlled BN assembly. The application of nanosecond pulse-wise electric field and its' switching was adapted to overcome the electric field limitation, which is generated during application of DC electric field. The hexagonal-BN(*h*-BN), which is famous for its thermal anisotropy; when the *h*-BN are aligned perpendicular to the *c*-axis, their thermal conductivity increases by 20 times to 600 W/mK, compared to 30 W/mK that aligned parallel to the *c*-axis, is used as an insulating fillers. The structural analysis are performed three dimensionally using 3-D X-ray CT scanning. Analysis by scanning electron microscope, transmittance electron microscope and X-ray diffraction are used to evaluate enhancement of anisotropic orientation and structural assembly of BN nanosheets. Thermal conductivity and electric resistivity of the composites are assessed. The controlled fabrication of the 3-D BN assembles may give a way for developing 3-D thermal circuits as thermal interface materials in micro- and nano-electronics, such as, semiconductor, automobile, and aerospace industries. Figure 1 shows BN nanosheets assembly incorporated in polymer-nanocomposites films.

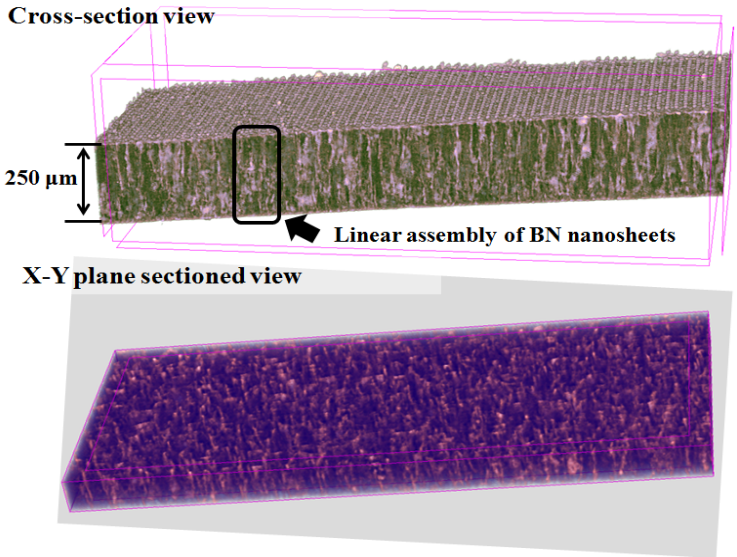

Figure 35. 3-D images of linear assembly of boron nitride nanosheets with columnar structure in polysiloxane matrix (the width of Si-mold;10 μm, type of protrusion; line-type, electric field; switching nanosec pulse electric field)

NA-O05

Synthesis and characterization of novel semiconducting Si-based nanocomposites with slit-like nanopores

Hiroshi Itahara*, Song-Yul Oh, Haruo Imagawa
[1]*Toyota Central Research & Development Labs., Inc., Nagakute, Aichi, 480-1192, Japan*

Keywords: Silicon, Silicide, porous material, semiconductor, direct band gap

Si-based nanostructured materials with a high surface-to-volume ratio (*i.e.*, porous or hollow structure) are promising for various applications, such as Li-ion batteries, photovoltaics and catalyst support. The porous or hollow structured nanomaterials are conventionally prepared by using sacrificing templates [1]: The typical templates are anodized Al_2O_3, polymer fibers and small SiO_2 particles, and they are removed by calcining or chemical etching at the final fabrication process. Despite of usefulness of those nanostructured materials, their synthesis complexity may hinder their mass production.
In contrast, we have developed a template-free fabrication method, a solid-state exfoliation reaction method using layered $CaSi_2$ [2], for the production of Si-based nanocomposites with slit-like nanopores. For example, heating the mixture of layered $CaSi_2$ and $NiCl_2$ provided the composite powders comprised of 'Ni and Ca_xSi_2 (Ca extracted $CaSi_2$)' or 'nickel silicide and Ca_xSi_2'. It was suggested that their formation mechanism is based on a solid-state exfoliation reaction wherein the formation of $CaCl_2$ promotes the extraction of Ca from $CaSi_2$, thereby exfoliating the layered structure (Figure 1). The Ca_xSi_2 particles are the agglomerates comprised of many plate-like particles with thickness of ~ 15 nm. The plate-like particles are stacked with the gap of ~ 4 nm between them.
The prepared nanocomposites of 'Ni and Ca_xSi_2' or 'nickel silicide and Ca_xSi_2' showed a high anode capacity for Li ion batteries [2-3]. The highest initial capacity was 1,020 mAh/g, which is three times higher than that of conventional graphite and twelve times higher than that of the raw $CaSi_2$. Because Ni or nickel silicide does not react with Li, Ca_xSi_2 is considered as Li storable materials. In addition, the plate-like structure of Ca_xSi_2 might facilitate insertion and extraction of Li, thereby leading such high capacity. Furthermore, we found that the Ca_xSi_2 showed direct optical band gap while the layered $CaSi_2$, the raw material, shows metallic property. With changing the synthetic conditions, the band gap was changed from ~ 1.0 eV to ~ 2.0 eV. Because of its simplicity, the solid-state exfoliation reaction using layered $CaSi_2$ would provide a versatile strategy for the Si-based functional nanocomposites with nanopores.

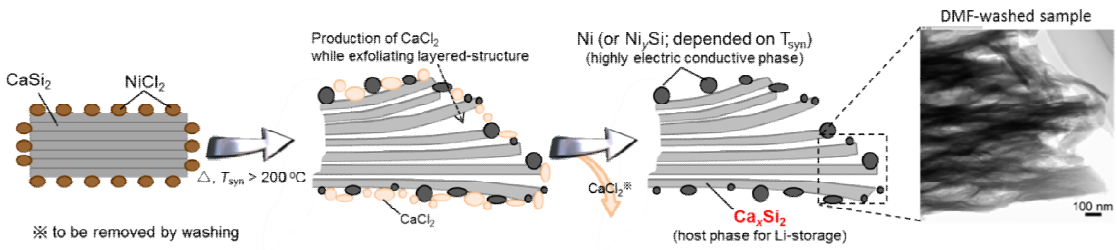

Figure 36 Schematic illustration of a solid-state exfoliation reaction using the layered $CaSi_2$to form nanocomposites containing Ca_xSi_2 (the Ca extracted $CaSi_2$)

References:
[1] X. W. Lou, L. A. Archer, Z. Yang, *Advanced Material*, 20, 3987-4019 (2008).
[2] S.-Y. Oh, H. Imagawa, H. Itahara, *Chemistry, Asian J.,* in press, DOI: 10.1002/asia.201402544.
[3] S.-Y. Oh, H. Imagawa, H. Itahara, *J. Mater. Chem. A*., 2, 12501-12506 (2014).

Acknowledgement:
The authors acknowledge Ms. Akiko Ueki and Mr. Yusuke Akimoto of Toyota CRDL for conducting the microstructural observations.

FU-O01

Decomposition of Carbon Monoxide and Carbon Dioxide Using Cathode-Supported Dense Yttria-Stabilized Zirconia Electrolyte Cell

Taro SHIMONOSONO*, Mana UENO, Yoshihiro HIRATA, Soichiro SAMESHIMA
Department of Chemistry, Biotechnology, and Chemical Engineering, Kagoshima University
1-21-40 Korimoto, Kagoshima 890-0065, Japan

Keywords: Electrochemical decomposition, Carbon monoxide, Carbon dioxide, Yttria-stabilized zirconia, Nickel

The electrochemical decomposition of CO and CO_2 gases was examined using the cell of Ni-YSZ cathode/dense YSZ electrolyte/Ru-YSZ anode (YSZ: 8 mol% Y_2O_3-stabilized ZrO_2) [1]. In the case of the cell with a porous YSZ electrolyte [2], CO gas was decomposed to form solid carbon at the cathode, while the unreacted CO gas was transported to the anode through the porous electrolyte and reacted with the oxide ions to form CO_2 gas (Fig. 1(A)). Such CO_2 formation was avoided by the dense electrolyte and the CO decomposition rate of 67-100% was achieved at the applied voltage of 2-8 V. In the CO_2 decomposition, CO and O_2 gases were formed at the cathode and anode sides, respectively, and the carbon deposition hardly occurred. When the mixture of CO and CO_2 gases was supplied, only a small amount of carbon was observed in the cathode. One of the possible reasons would be the reaction between the deposited carbon and the mixed CO_2 gas ($C + CO_2 \rightarrow 2CO$).

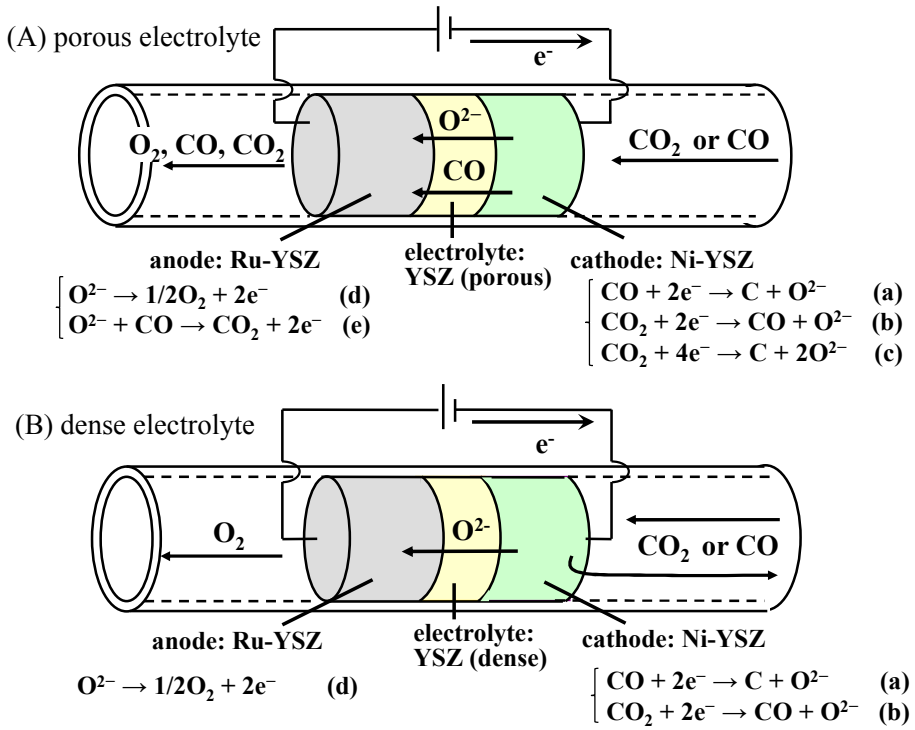

Figure 37 Scheme of electrochemical decomposition of CO and CO_2 gases using (A) porous oxide ion electrolyte and (B) dense oxide ion electrolyte.

References:

[1] T. Shimonosono, M. Ueno, Y. Hirata and S. Sameshima, Ceram. Inter., accepted 2014, DOI: 10.1016/j.ceramint.2014.07.124
[2] Y. Hirata, M. Ando, N. Matsunaga and S. Sameshima, Ceram. Inter., 38 (2012) 6377.

FU-O02

Preparation and electrochemical properties of $Li_{1.3}Ti_{1.7}Al_{0.3}(PO_4)_3$ solid electrolyte for Li ion batteries by sol-gel process

Seoung Soo LEE[1], Hyun Woo KIM[2], Jing LI[1], Yeon-Gil JUNG[1*], Youngsik KIM[2*]*
[1]*School of Nano and Advanced Materials Engineering*
Changwon National University, Changwon, Gyung-Nam, 641-773, Republic of Korea
[2]*UNIST, School of Energy and Chemical Engineering (Build.103-103) UNIST-gil 50, Ulju-gun, Ulsan, 689-798, Republic of Korea*

Keywords: Solid electrolyte, Sol-gel, Li ion batteries, LTAPO

Rechargeable lithium ion batteries are widely used as portable electrochemical energy conversion and storage devices due to their higher energy density than other commercialized rechargeable batteries [1]. However, lithium ion batteries still suffer from a safety issue caused by combustible organic solvents used in their electrolytes [2]. To solve their safety problem, flame retarding solid electrolytes such as $Li_{1.3}Ti_{1.7}Al_{0.3}(PO_4)_3$ (LTAPO) have been considered as the most promising electrolyte [3]. However, the LTAPO has been generally prepared by a solid state reaction with a complex and high temperature process.

The present research reports the synthesis of the LTAPO solid electrolyte by a low temperature method of the sol-gel process and its effects on electrochemical performances. In this study, three types of Li salts were employed as the Li source, which are $LiNO_3$, LiCl, and Li acetate, for investigating the effects of Li salt on the electrochemical properties of solid electrolyte. $Ti(OCH_2(CH_2)2CH_3)_4$, $NH_4H_2PO_4$, and $(AlNO_3)_3{\cdot}9H_2O$ precursors were used for Ti, P, and Al source, respectively. It was shown in our preliminary work that the electrochemical performances of solid electrolyte were affected by the Li source materials. The samples' morphology/microstructure evolution with processing parameter prepared by different Li salt species and their relationship with electrochemical properties will be discussed in this presentation.

References:

[1] G. Ceder, Y. M. Chiang, C. R. Sadoway, M. K. Aydinol, Y. I. Jang, B. Huang, Nature 392 (1998) 694.
[2] X. Xu, X. Wen, J. Wu, X. Yang, Solid State Ionic 178 (2007) 29-34.
[3] T. Abe, M. Ohtsuka, F. Sagane, Y. Iriyama, Z. Ogumi, J. Electrochem. Soc., 151 (2004) A1950.

EL-O01

Fabrication and Characterization of Wrinkle-Free Monolayer Graphene using the Ti/Glass Substrates

Byeong-Ju Park[1] and Soon-Gil Yoon[1]
[1]*Department of Materials Science and Engineering, Chungnam National University, Daeduk Science Town, 305-764, Daejeon, Korea*

Keywords: Graphene, Wrinkle-Free, Ti Adhesion Layer, Monolayer

The graphene films by Chemical Vapor Deposition (CVD) are expected to enable various applications such as graphene Field Effect Transistor (FET) on a wafer scale and transparent conducting films for flexible / stretchable electronics. Although the transfer of the graphene have advantages which make applicable possibility onto various substrates, the CVD-graphene layer control is very difficult when using Cu and Ni film as catalyst and they were transferred on the various substrates, transferred graphene are formed the many wrinkles and / or ripples. The wrinkles and / or ripples cause degradation of the physical and electrical properties of the corresponding electronic devices. In addition, the oxygen atoms that unavoidably contaminate the transferred graphene films may contribute to such degradation.

For fabrication of wrinkle free graphene, we used Ti adhesion layer which is generally used to improve the adhesion between Pt and oxygen-containing or oxygen - philic substrates, such as Si (with native oxide), SiO_2 / Si, glass, and polymers. Ti adhesion layer is deposited by DC sputtering with various thickness and graphene were transferred onto the Ti / glass substrates. The Ti adhesion layer reacted to oxygen within transferred graphene and Ti - C - O phases were formed at interface between Ti adhesion layer and graphene, which was resulted in a smoothing of the graphene on the Ti adhesion layer. Also, for wrinkle free monolayer graphene, we used Ti adhesion layer as another substrates. Through the attaching and detaching process, monolayer wrinkle free graphene separated from multilayer wrinkle free and same process, we can fabricate several wrinkle free monolayer using only one wrinkle free multilayer graphene.

For characterization of wrinkle free monolayer graphene, we measured the transmittance, Raman spectroscopy, AFM and bendability. Also, we fabricated capacitor using BMNO dielectrics and monolayer wrinkle free graphene as electrodes and measured capacitance and dielectric loss for transparent and flexible capacitor.

Acknowledgement:
This work was supported by a National Research Foundation of Korea (NRF) grant funded by the Korean government (MSIP) (No.NRF-2013R1A4A1069528)

EL-O02

Indialite Glass Ceramic Substrates for Millimeterwave Applications

Hitoshi OHSATO[1,2*], Akinori KAN[3], Jeong-Seog KIM[4], Isao. KAGOMIYA[5]
[1] *Dept. of Research, Nagoya Industrial Science Research Institute, Nagoya 464-0819, Japan.*
[2]*Functional Materials Lab., Nagoya Institute of Technology, Nagoya 466-8555, Japan*
[3]*Faculty of Science and Technology, Meijo University, Nagoya 468-8502, Japan*
[4]*Dept. of Material Science and Engineering, Hoseo University, Asan-si, Chungnam 336-795, Korea*
[5]*Dept. of Material Science and Engineering, Nagoya Institute of Technology, Nagoya 466-8555, Japan*

Keywords: Microwave dielectrics, Indialite/cordierite glass ceramics, substrate, direct casting

Millimeterwave dielectric substrates for wireless communications are expected to be developed on the higher quality factor *Q*, low dielectric constant $_r$ and temperature coefficient of resonant frequency *TCf*. Indialite glass ceramics have been developed for candidate of millimeterwave dielectrics, which have high *Qf* of more than 200,000 GHz and low $_r$ of 4.7, and *TCf* of -27 ppm/°C[1]. But, there are big problems of cracking of the ceramics, as the crystal growth of indialite from glass occurs as oriented *c*-axis crystals from the surface [2]. When the crystals with different orientation meet, the cracking occurs.

In this paper, for avoid the cracking of glass ceramics, volume crystallizations on the glass with cordierite composition are applied adding TiO_2 as nucleation material [3]. TiO_2 10 and 20 wt% doped glasses crystallized at 1200, 1250, 1300 and 1350 °C for 20 h were identified as indialite with rutile. Although 0 wt% added one has cracks, and 10 and 20 wt% doped ones have no cracks.

Fig. 1(a), 1(b) and 1(c) show $_r$, *Qf* and *TCf*, respectively, as a function of adding TiO_2 wt%. The $_r$ increase 4.67 to 7.66. *Qf* decreased from 176,000 to 52,700 GHz. And *TCf* increased from -25.8 to +39.4 ppm/°C. *TCf* with near zero ppm/°C ceramics might be obtained among 10 to 20 wt% TiO_2 addition.

Direct casting method for glass ceramics will be presented in the seminal. The glass ceramics fabricated by the direct casting method might be reduced the price because of the short fabricating steps.

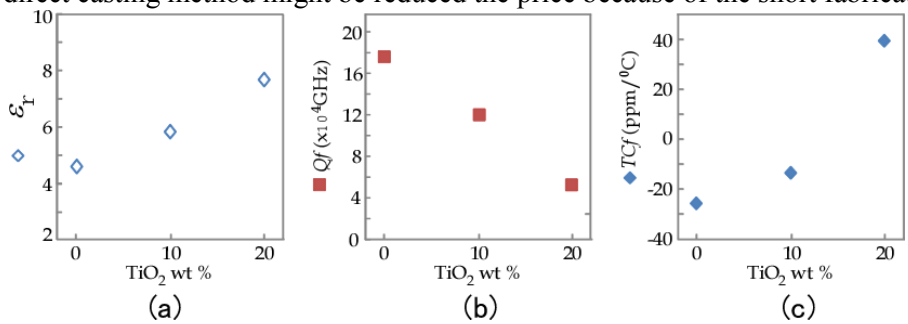

Fig. 1 Millimeterwave dielectric properties of $_r$ (a), *Qf* (b) and *TCf* (c) as a function of TiO_2 addition.

References:

[1] H. Ohsato, J-S. Kim, A-Y. Kim, C-Il Cheon, and K-W. Chae, Jpn. J. Applied Physics, 50, (2011) 09NF01-1-5.
[2] H. Ohsato, J-S. Kim, C.-Il Cheon, I. Kagomiya, J. Ceram. Soc. Japn, 121, 649 (2013).
[3] K. Kagomiya and H. Ohsato, Patent application 2014-164285, (2014,08,12).

Acknowledgement:

The authors thanks to Dr. Chunting Lee and Professors Ken'ichi Kakimoto, Chae-Il Cheon, and Hirotaka Ogawa. A part of this work was supported by a Grant-in Aid for Science Research (C) and Adaptable & Seamless Technology Transfer Program (A-step) by MEXT Japan.

EL-O03

Effects of Mg and/or Ti-site substitution on Microwave Dielectric Properties of $MgTiO_3$-based Ceramics

Hyun Jin JO, Eung Soo KIM*
Department of Materials Engineering, Kyonggi University, Suwon, 443-760, Korea

Keywords: $MgTiO_3$, Microwave dielectric properties, Bond valence, Oxygen octahedral distortion

With the rapid development of wireless communication systems, the high quality factor (*Qf*) of microwave dielectrics is important factor to meet the needs for low dielectric loss. Although $MgTiO_3$-based ceramics are well-known for dielectric materials with high *Qf* value, the dependence of dielectric properties on structural characteristics should be investigated to improve the *Qf* value of $MgTiO_3$-based ceramics. These investigations could be applied to develop the enhanced dielectric properties of materials at microwave frequencies effectively.

In this study, dependence of the microwave dielectric properties on divalent and/or tetravalent cation substitution for Mg and/or Ti-sites of $MgTiO_3$-based ceramics were investigated ($MgTiO_3$ (MT), $(Mg_{0.95}Zn_{0.05})TiO_3$ (MZT), $Mg(Ti_{0.95}Sn_{0.05})O_3$ (MTS), $(Mg_{0.95}Zn_{0.05})(Ti_{0.95}Sn_{0.05})O_3$ (MZTS)). Crystal structural characteristics of $MgTiO_3$-based ceramics were quantitatively evaluated by the Rietveld refinement method from the X-ray diffraction (XRD) data.

Single phase of ilmenite structure was obtained for the $MgTiO_3$-based ceramics sintered at 1400°C for 4h. For the $MgTiO_3$-based ceramics in this study, MZTS ceramics showed the largest unit-cell volume due to the larger ionic radius of Zn^{2+} (0.74 Å) and Sn^{4+} (0.69 Å) than that of Mg^{2+} (0.72 Å) and Ti^{4+} (0.609 Å) at a coordination number of 6, respectively. For the microstructure of MZTS ceramics with substitution of Zn^{2+} and Sn^{4+} for Mg and Ti-sites of $MgTiO_3$ ceramics showed more uniform grain size than that of pure $MgTiO_3$ ceramics, which improved the *Qf* value of MZTS ceramics.

Qf value of $MgTiO_3$-based ceramics significantly depended on the B-site bond valence as well as the average covalency of ABO_3 ilmenite structure. It has been reported that strong bond valence means high bond strength between cation and oxygen ions in oxygen octahedra, which decreased the lattice anharmonicity. MZTS ceramics showed higher *Qf* value than those of other $MgTiO_3$-based ceramics due to both the largest B-site bond valence and average covalency, which was affected by low electronegativity difference. Temperature coefficients of resonant frequency (*TCF*) of $MgTiO_3$-based ceramics were affected by the average oxygen octahedral distortion of ilmenite structure. The *TCF* value of MZTS ceramics was lower than that of other $MgTiO_3$-based ceramics because of lower average oxygen octahedral distortion. Also, the dielectric constants (*K*) of $MgTiO_3$-based ceramics were dependent on the dielectric polarizability of composing ions obtained from the additivity rule. The *K* value of MTS ceramics was lower than that of other $MgTiO_3$-based ceramics due to lower polarizability of Sn^{4+} (2.83 $Å^3$) than that of Ti^{4+} (2.93 $Å^3$).

References:

[1] J. Li, Y. Han, T. Qiu, C. Jin, Mater. Res. Bull. 47 (2012) 2375.

Acknowledgement:

This research was supported by Basic Science Research Program throuth the National Research Foundation of Korea (NRF) funded by the Ministry of Education, Science and Technology.

EL-O04

Microstructure and Electrical Properties of $TiNbO_5$ and Ti_5NbO_{14} Thin Films grown by Electrophoretic Method

Mir Im[1], Sang-Hyo Kweon[2], Sahn Nahm[1,2*]
[1]*KU-KIST Graduate School of Converging Science and Technology, Korea University, Seoul 136-701, South Korea*
[2]*Department of Materials Science and Engineering, Korea University, Seoul 136-701, South Korea*

Keywords: Titano-niobates, Nano-sheets, MLCC, Electophoresis

$TiNbO_5$ and Ti_5NbO_{14} thin films produced by using $KTiNbO_5$ and $K_3Ti_5NbO_{14}$-layered compounds, respectively, have been reported to exhibit a high ε_r with a low leakage current density.[1] Recently, these ultra-thin-films have been actively pursued for the applications in the future multilayer ceramic capacitors. Homogeneous $KTiNbO_5$ and $K_3Ti_5NbO_{14}$ phases were formed at 900°C and the dense $KTiNbO_5$ and $K_3Ti_5NbO_{14}$ oxides were obtained from the specimen sintered at 1150°C and 1125°C, respectively. Liquid-phase-assisted abnormal grain growth occurred in both specimens along the directions perpendicular to <002> during the sintering. A proton exchange process was carried out to synthesize proton-exchanged forms and the stable $[TiNbO_5]^-$ and $[Ti_5NbO_{14}]^-$ nanosheet colloids were formed by reacting intermediate phase powders, tetrabutylammonium hydroxide (TBAOH) solution and DI water. These nanosheet colloids were dispersed into the acetone intermediate, which was used to deposit the thin film by the electrophoresis under 100 V electric source. The $TiNbO_5$ and Ti_5NbO_{14} electrophoretic thin-films have grains along directions perpendicular to <001>. In particular, a high dielectric constant of 48 with a loss of 4.0% at 100 kHz was obtained from the $TiNbO_5$ film annealed at 600°C and this film also showed the low the leakage current density of $2*10^{-7}$ A/cm^2 at 0.25 MV/cm. However, the Ti_5NbO_{14} films anneled at 700°C showed an ε_r of 41 and a dielectric loss of 1.5 % at 100 kHz with the the leakage current density of $1.5*10^{-7}$ A/cm^2 at 0.3 MV/cm.

References:

[1] Osada M, Ebina Y, Funakubo H, Yokoyama S, Kiguchi T, Takada K et al. High-k dielectric nanofilms fabricated from titania nanosheets. Adv Mater. 2006;18:1023-1027.

EL-O05

Effect of oxide electrode and synthesis conditions on electrical properties ofCSD-derived $Pb(Mg_{1/3}Nb_{2/3})O_3$-$PbTiO_3$ thin films

Takashi ARAI[1],Tomoya OHNO[2], Takeshi MATSUDA[2], Naonori SAKAMOTO[3], Naoki WAKIYA[3],and Hisao SUZUKI[3*]

[1] *Graduate School of Science and Technology, Shizuoka University, Hamamatsu, 432-8561,Japan*
[2] *Department of Materials Science, Kitami Institute of Technology, Kitami, 090-8507, Japan*
[3] *Research Institute of Electronics, Shizuoka University, Hamamatsu, 432-8561,Japan*

Keywords: Thin Film, Chemical Solution Deposition, Synthesis condition, relaxor ferroelectrics

1. Introduction

Relaxor ferroelectrics $Pb(Mg_{1/3}Nb_{2/3})O_3$–$PbTiO_3$ (PMN–PT) have attracted considerable attention because of their excellent electrical properties, such as high dielectricity and piezoelectricity.However, many previous papers have been reported the formation of the pyrochlore phase with lower electrical properties because of the similar formationenergies of perovskite and pyrochlore phases.In addition, the reported electrical properties of PMN-PT thin films such as dielectric and piezoelectric properties are significantly lower than those of bulk ceramics and single crystals because processing parameters are still yet optimized for the thin filmscompared with the bulk ceramics and single crystals.In this study,LNO seeding layer was introduced andthe effect of synthesis conditions on the electrical properties of the Chemical Solution Deposition (CSD)-derived PMN-PT thin films have been investigated to prepare single phase perovskite PMN-PT thin film with superior properties on a Si substrate at lower temperatures.

2. Experimental Procedure

PMN-PT and LNO thin films were prepared by CSD. The details of the LNO thin film deposition were described elsewhere. [1] The starting reagents for PMN–PT precursor solution were $Pb(OCOCH_3)_2 \cdot 3H_2O$,$Ti(i\text{-}OC_3H_7)_4$, $Mg(OC_2H_5)_2$, and $Nb(OC_2H_5)_5$. Raw materials for A-site and B-site sourcesof perovskite structure were refluxed separately because Columbite method is effective to suppress the pyrochlore phase formation in bulk process. Then, they were mixed and refluxed. 2-aminoethanol was added to stabilize the obtained precursor solutions.In this process, excess amount of lead with 0 to 30 mol% were added to the precursor solutions. Althoughthe lack of lead by the volatilization will cause the pyrochlore phase, too much addition of excess lead will result in the residual lead oxide or diffusion to the electrode. A concentration and composition of precursor solutions were 0.6M and MPB composition of 0.65PMN-0.35PT, respectively.

PMN–PT layers were depositedon LNO/Si substrate by spin coating. The as-deposited PMN–PT layer was dried at 150 °C, preannealed at 350 or 450 °C, and then annealed at 650 or 750 °C to investigate the effect of synthesis conditions. Synthesis conditions will affect the microstructures, leading to the different electrical properties. Hence, the optimization of the heat treatment and the excess amount of lead are essential.

3. Results and Discussion

As a result, LNO seeding layer was effective to preparethe single phase(100)-oriented PMN-PT perovskite thin films andthe annealing conditionssignificantly affected the electrical properties of the resultant PMN-PT thin films (Figure1). The optimized 0.65PMN-0.35PT thin film exhibited dielectric constant over 4000 (1 kHz, at room temperature) and relatively higher electrostrictive effect.

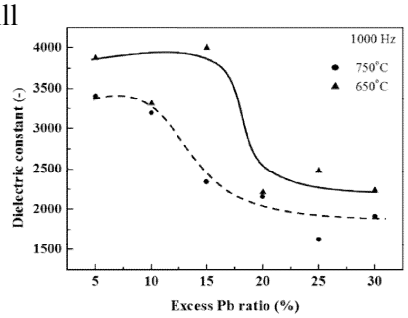

Figure 1 The dielectric constants dependent on excess lead ratios of obtained PMN-PT thin films

References:

[1]H. Suzuki, T. Naoe, H. Miyazaki, and T. Ota, J. Eur. Ceram. Soc. 27 (2007) 3769.

EL-O06

Dielectric Properties and Microstructure Control of $(Ba_{0.7}Sr_{0.25}Ca_{0.05})(Ti_{0.9}Zr_{0.1})O_3$ Ceramics

Young Jun Eoh and Eung Soo Kim*
Department of Materials Science and Engineering, Kyonggi University, Suwon, 443-760, Korea

Keywords: Two-step sintering, Ferroelectrics, Microstructure, Dielectric properties

Modified barium titanate ($BaTiO_3$) ceramics have been of great interest and widely investigated for various applications such as multilayer ceramic capacitors (MLCC), electrostrictive actuators, and electromechanical transducers due to their good ferroelectric properties. The general requirements of ferroelectrics are high dielectric constant (ε_r) and breakdown voltage (V_b) with low dielectric loss ($tan\delta$). To achieve those properties, the dielectric materials should have high relative density and homogeneous microstructure consisting of small grains. It has been reported that the Y_2O_3, c-ZrO_2 and ZnO ceramics sintered by two-step method showed the improved mechanical properties due to their homogeneous microstructure and small grain size. Therefore, the two-step sintering can be effectively applied for improving ε_r and V_b of the modified barium titanate ceramics without large dielectric loss.

In this study, the dielectric properties and microstructure of $(Ba_{0.7}Sr_{0.25}Ca_{0.05})(Ti_{0.9}Zr_{0.1})O_3$ (BSCTZ) ceramics with ZnO ($0 \le x(wt\%) \le 0.15$) were controlled by various two-step sintering condition. Two-step sintering includes two types of steps. First step is the increasing the temperature (T1) to achieve an intermediate density and obtain proper grain size. Second step is the rapid cooling to second temperature (T2) and holding efficient time to obtain high density. To succeed in two-step sintering method, a sufficiently high relative density (more 70%) needs to be achieved at T1 and proper T2 which have high densification rate should be determined. T1 was changed from 1350°C to 1450°C and the T2 was selected as 1300°C which have maximum densification rate.

For the pure BSCTZ ceramics sintered by two-step method, the specimens showed the higher density and homogeneous microstructure with smaller grain size than those of the specimens sintered by single-step method. Therefore, the V_b of the specimens sintered by two-step method was improved. With increase of T1 from 1350°C to 1450°C, the ε_r of the specimens increased while the tanδ of the specimens decreased. However, *P-E* hysteresis loops of the specimens were slightly changed with two-step sintering condition. With increase of ZnO content, the single phase of perovskite structure was observed for all of the specimens. Also, the grain size of the specimens rapidly increased with ZnO addition due to the substitution of Zn^{2+} for B-site ion. The specimens with 0.1wt% ZnO showed the maximum V_b value, while the both of ε_r and tanδ were remarkably decreased. This could be attributed to the eliminations of pore and low conductivity of ZnO, respectively. Any frequency dispersions of the dielectric properties were not observed from 1kHz to 1MHz.

References:

[1] K. Maca, V. Pouchly, P. Zalud,J. Eur. Ceram. Soc. 30 (2010) 583.
[2] Y. Mizuno, H. Kishi, K. Ohnuma, T. Ishikawa, H. Ohsato : J. Eur. Ceram. Soc. 27 (2007) 4017.

Acknowledgement:

This work was supported by Kyonggi University Research Grant 2014.

EL-O07

Microstructure and Microwave Dielectric Properties of $Zn_{1.8}SiO_{3.8}$ Ceramics Prepared by Two-Step Sintering

Hong Jun Ahn, Young Jun Eoh, Eung Soo Kim*
Department of Materials Engineering, Suwon, 443-760, Korea

Keywords: $Zn_{1.8}SiO_{3.8}$, Two-step sintering, Dielectric properties, Willemite

The rapid progress in mobile and communication systems have increased the demand for the development of dielectric materials applicable to various devices working at microwave and millimeter wave. A low dielectric constant (*K*), a high-quality factor (*Qf*) and a near-zero temperature coefficient of resonant frequency (*TCF*) is necessary for these materials. $Zn_{1.8}SiO_{3.8}$ ceramics have been studied as a candidate material for advanced microwave applications because this ceramics prepared by conventional sintering method, exhibited good microwave dielectric properties. However, it is still needed to investigate the relationships between microwave dielectric properties and microstructural characteristics of $Zn_{1.8}SiO_{3.8}$ for the improvement of dielectric properties. Microstructural characteristics of ceramics could be controlled by sintering process.

In this study, the dependence of microwave dielectric properties of $Zn_{1.8}SiO_{3.8}$ ceramics on the two-step sintering was investigated. Single phase of willemite structure was confirmed for the $Zn_{1.8}SiO_{3.8}$ ceramics prepared by single-step and/or two-step sintering. Two-step sintering was composed of first step for grain growth and second step for densification. Densification temperature was selected at 1250°C which showed the maximum densification rate by dilatometry analysis.

The *Qf* value of the specimens with different holding time of densification temperature showed similar tendencies to the relative density of the specimens. For the specimens sintered at 1400°C for 5min and held at 1250°C for 4h to 12h, the *Qf* value showed the lower value than the specimens sintered at 1350°C for 5min and held at 1250°C for 4h to 12h. This result could be attributed to the higher density of specimens with 1350°C for 5min and held at 1250°C for 4h to 12h. Comparing to the specimens prepared by single step sintering, the specimens were prepared by two-step sintering showed the improved *Qf* value. For the specimens sintered at 1350°C for 5min and held at 1250°C for 4h, the *Qf* value showed the higher value (187,600GHz) than the specimens sintered at 1350°C for 4h. This result could be due to the densification of the specimens was successfully achieved. With increasing holding time, the *Qf* was decrease due to the increase of abnormal grain growth. However, similar *K* and *TCF* were obtained for the specimens prepared by single-step and/or two-step sintering.

References:

[1] Yiping Guo, Hitoshi Ohsato and Ken-ichi Kakimoto, J. Eur. Ceram. Soc. 26 (2006) 1827-1830.

Acknowledgement:

This research was supported by Basic Science Research Program through the National Research Foundation of Korea (NRF) funded by the Ministry of Education, Science and Technology.

ST-O01

Fabrication of Si_3N_4 ceramics by post-reaction sintering using Si-Y_2O_3-Al_2O_3 nanocomposite particles prepared by mechanical treatment

Kwangjin JEONG[1], Motoyuki IIJIMA[1], Takuma TAKAHASHI[2] Junichi TATAMI[1*]
[1]*Yokohama National University, Yokohama, Kanagawa 240-8501, Japan*
[2]*Kanagawa Academy of Science and Technology, Kawasaki, Kanagawa 213-0012, Japan*

Keywords: Si_3N_4, Nitridation, Nanocomposite particles, Post-reaction sintering, Mechanical treatment

Silicon nitride (Si_3N_4) ceramics have been attracting attention as advanced materials with excellent mechanical properties and thermal stability at room and high temperatures. The reduction of production cost and the improvement of mechanical reliability are desired to expand an application target of Si_3N_4 ceramics. Post-reaction sintering technique is one of the solutions to reduce the production cost, in which a powder compact of a powder mixture of inexpensive Si and sintering aids is nitrided, followed by densification at higher temperatures[1)]. However, the control of the nitridation of Si is difficult because of its exothermic reaction. Inhomogeneous nitridation sometimes results in the strength degradation of the Si_3N_4 ceramics. One of the ideas is to avoid abnormal heating uniform coating of the sintering aids on the surface of the Si particles. In this research, Si_3N_4 ceramics were fabricated by the post-reaction sintering technique using the Si-Y_2O_3-Al_2O_3 nanocomposite particles prepared by mechanical treatment. Specific surface area of the powder mixtures of Si-Y_2O_3-Al_2O_3 prepared by mechanical treatment decreased with an increase in the applied power due to an increase in joining area between Si and the additives. The prepared nanocomposite particles were molded by uniaxial pressing, followed bycold isostatic pressing. The green body thus obtained was calcined at 1375°C for 2 h in 0.15 MPa, N_2 gas to form Si_3N_4. For comparison, a powder mixture prepared by conventional wet ball milling was used. Nitridation in the green body produced from the nanocomposite particles prepared by mechanical treatment were more uniform and nitridation ratio was higher than that of ball milling process. Furthermore, nitridation ratio was also increased by mechanical treatment with an increase in the applied power. This means that nitridation was enhanced by using the nanocomposite particles while abnormally exothermic reaction between Si and N_2 was inhibited. After densification at 1800°C for 2 h in 0.9 MPa, N_2 gas, the Si_3N_4 ceramics prepared by mechanical treatment had more homogeneous microstructure and higher density than that by ball milling process.

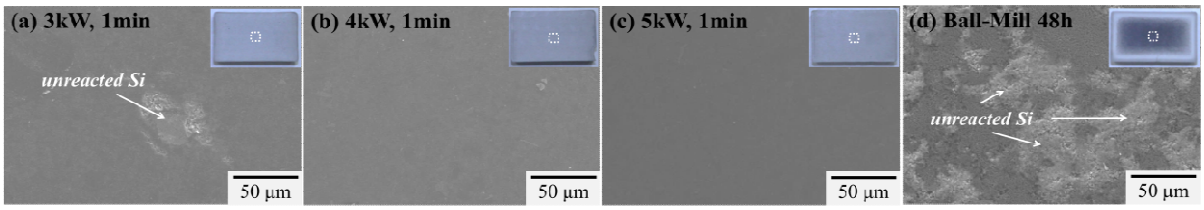

Figure 38 The SEM photographs of the microstructure of RBSN bodies after nitridation (a) 3kW, (b) 4kW, (c) 5kW and (d) Ball-Mill

References:

[1] S. H. Lee, et al., J. Kor. Ceram. Soc., Vol. 50, No. 3, (2013) 218-225.

ST-O02

Analysis of High Temperature Stability of White Amorphous Si–O–C(–H) Ceramics in Terms of Structure Evolution and Photoluminescence Degradation

Masaki NARISAWA[1], Guangyu MA[1], Hiroki HOKAZONO[1], Seiji WATASE[2], Kimihiro MATSUKAWA[2] and Akihiro IWASE[1]

[1]*Graduate School of Engineering, Osaka Prefecture University, 1-1 Gakuen-Cho, Naka-Ku, Sakai, Osaka599-8531, Japan*

[2]*Osaka Municipal Technical Research Institute, 1-6-50, Morinomiya, Joto-ku, Osaka 536-8553, Japan*

Keywords: Silicon oxycarbide, Heat resistance, Thermodynamics, Photoluminescence

Two kinds of white Si−O−C(−H) ceramic powders, named S900 and S1100, were prepared from cross-linked polysiloxane particles with an averaged diameter of 6 m [1, 2]. S900 was the product obtained in a hydrogen gas flow at 900 °C with a holding time of 1h, whereas S1100 was the product obtained at 1100 °C with a holding time of 3h. In an Ar gas flow, heat stability of the powders on graphite boats were examined at a temperature range of 1200−1600 °C. S900 was colored brown and black after the heat treatment at 1200 and 1400 °C. On the other hand, color of S1100 was changed to light grey after the heat treatment at 1400 °C. PL intensity of S900 substantially decreased at 1200°C, whereas that of S1100 decreased at 1400°C (Figure 1). Substantial mass loss of the powders occurred beyond 1500 °C, which was accompanied by fusing of individual particles at the contact points. At 1600 °C, precipitation of cristobalite was observed (Figure 2), and particles were completely fused together. From viewpoints of mass loss, XRD patterns and aggregate formation process, there were no major differences between S900 and S1100, although difference in color and PL was obvious. The white Si−O−C(−H) ceramic would be useful as basic parts of thermal protection systems available at relatively low costs [3], like High-Temperature Reusable Surface Insulation (HRSI) tiles.

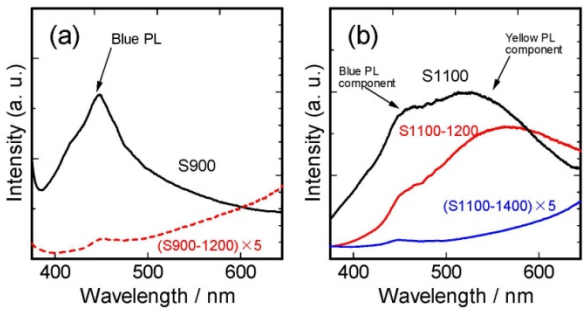

Figure 39 PL spectra of Si-O-C(-H) powders before and after heat treatment; (a)S900, (b) S1100.

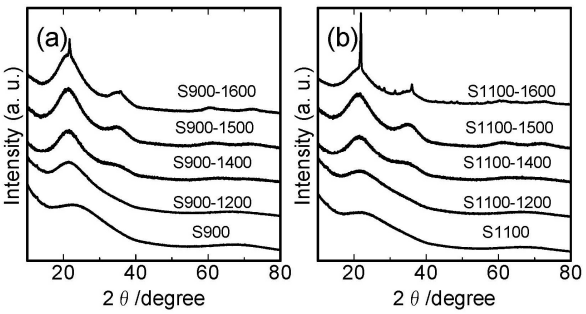

Figure 2 XRD patterns of Si-O-C(-H) powders before and after heat treatment; (a)S900, (b)S1100.

References:

[1] M. Narisawa, S. Watase, K. Matsukawa, T. Dohmaru, K. Okamura, *Bull. Chem. Soc. Japan* 85 (2012) 724.
[2] M. Narisawa, K. Terauds, R. Raj, Y. Kawamoto, T. Matsui, A. Iwase, *Scripta Materialia* 69 (2013) 602.
[3] M. M. Opeka, I. G. Talmy, J. A. Zaykoski, *J. Mater. Sci.*, 39 (2004) 5887.

ST-O03

Carbon Nanotubes Grown on Cobalt Supported Zeolite-Porous Ceramics

Jung Gyu PARK[1], Wei ZHAO[2], Sangram MAZUMDER[1], and Ik Jin KIM[1*]
[1]*Institute of Processing and Application of Inorganic Materials, (PAIM), Department of Materials Science and Engineering, Hanseo University, Hanseo 1 ro, Haemi-myun, Seosan-si, Chungcheongnam-do, 356-706, Korea*
[2]*School of Material Science and Engineering, Yeungnam University, 280, Daehak-ro, Gyeongsan-si, Gyeongsangbut-do, 712-749, Korea*

Keywords: Carbon nanotubes, Porous Ceramic, Direct foaming, Ion-exchange reaction.

Macro porous ceramics are useful in the industrial sphere due to its large surface area with interconnected pores. Also, carbon nanotubes(CNTs) can dramatically increase surface area. With those benefits composite as a nano filter.But normally on porous ceramics CNTs cannot be grown on their surface. In this study, we synthesized CNTs on porous ceramics using ion-exchanged zeolite coating process. Here, we have used cobalt ion for the ion exchange process. Substrate of CNTs consists of inorganic particles (for example Al_2O_3 and SiO_2) were synthesized by direct foaming method using short chain carboxylic amphiphiles such as propyl gallate, with average solid content of 30vol%, average pore size 100~150um.The CNTs were grown by catalytic chemical vapor deposition (CCVD) method. Field Emission Scanning Electron Microscope (FE-SEM) and Transparent Electron Microscope (TEM) images for investigate synthesized CNTs morphology, microstructure and surface. Also CNTs were investigated for characterization byRamanspectroscopic analysis and TGA/DTA study. To compare surface area, BET analysis was done.

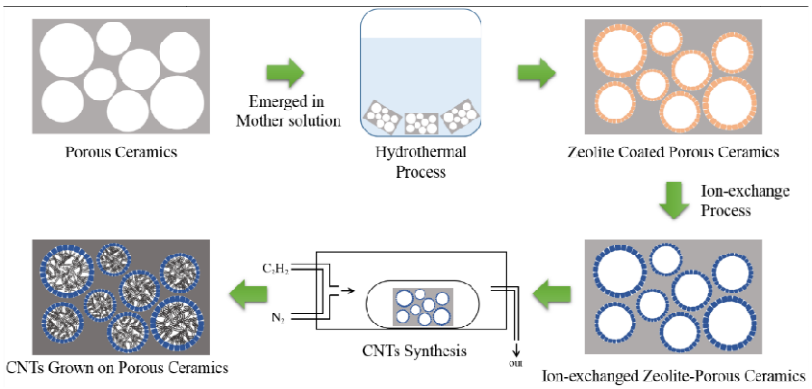

Figure 40 Schematic diagram of CNTs grown on Co-supported zeolite-porous ceramics

References:

[1] W. Zhao, B. Basnet and I. J. Kim, Journal of Advanced Ceramics 1(3) (2004) *p*. 179.
[2] A. Srivastava, O.N. Srivastava, S. Talapatra, R. Vajtai and P. M. Ajayan, Nature (2004) *p*. 610.
[3] A. Pokhrel, J. G. Park, J. S. Nam, D. S. Cheong, and I. J. Kim, Journal of the Korean Ceramic Society 48(5) (2011) *p*. 463.
[4] A. Pokhrel, J. G. Park, G. H. Jho, J. Y. Kim and I. J. Kim, Journal of Korean Ceramics Society 48(6) (2011) *p*.600

Acknowledgement:

I would like to thank Prof. Dr. IkJin Kim for his kind cooperation and continuous follow-up towards my work. Also, I would like to thank Hanseo University for providing a suitable laboratory for the work.

ST-O04

Co-dispersion system of ZrB2-SiC in non-aqueous solvent

Jin Soon HAN[1], Sung Bok WEE[1], Gye Seok AN[1], Jae Seok CHOI[1], Hyun Cheol OH[1], Sung Churl CHOI[1*]

[1]*Department of Materials Science and Engineering, Hanyang university, Seoul, 133-791, Korea*

Keywords: ZrB2, SiC, Co-dispersion system, Non-aqueous solvent

ZrB2 has been studied for several decades. The excellent properties of ZrB2 such as low density, high thermal conductivity, low thermal expansion, good strength and hardness make ZrB2 attractive candidate for Ultra High Temperature Ceramics (UHTC). However ZrB2 is easily oxidized to ZrO2 from its surface which has weak and worse properties than ZrB2. Thus, it is used with SiC as a composite, which oxidizes instead of ZrB2 in oxidizing conditions, forms the sticky oxidation resistance silica layer and prevents ZrB2 from attaching O2 and oxidization, without any negative effect to properties of ZrB2. In spite of the benefits of ZrB2-SiC system, some problems remain in its manufacturing process. Naturally, ZrB2 and SiC are hard to be dispersed and this causes unexpected agglomeration and lager grains during heating process. These larger grains are not covering ZrB2 perfectly which means ZrB2 can be damaged by oxidation due to unequal oxidation resistance. Also, this lager grain Accordingly, the uniform distribution with smaller grain size have been required in the ZrB2-SiC composite system, and this can be achieved with approach about the colloidal dispersion and prevent agglomeration of ZrB2 and SiC nano-particle in non-aqueous solvent by chemical route.

In this study, stable colloidal dispersion system was performed for the wide application of ZrB2-SiC nano particle system. This dispersion system was performed in non-aqueous solvent to prevent oxidation occurred by water which contained in aqueous solution. Especially oleic acid was introduced as dispersant for maximization of steric effect. Also N-Methyl-2-pyrrolidone (NMP) was selected for polar aprotic solvents by Hansen solubility parameter for its high affinity with powder and dispersion, and maximization of polarity. The amount of powder loading was fixed at 40 wt% and the different amount of dispersant (none to 3 wt%) was added. The solutions were analyzed by FT-IR, particle size distribution, Energy Dispersive X-ray Spectroscopy (EDS), Zeta-potential in terms of surface charge of powder, size and co-dispersion.

ST-O05

Slow Crack Growth Behavior of Yttrium Oxide from Static/dynamic Fatigue and Double Torsion Tests

Sung-Min LEE[1,*], Amit SHYAM[2], and Hua-Tay LIN[2]
[1] *Engineering Ceramic Team, Korea Institute of Ceramic Engineering and Technology, Icheon, Gyeonggi-do, 467-843, Korea*
[2]*Material Science Division, Oak Ridge National Laboratory, Oak Ridge, TN 37831-6069, USA*

Keywords: slow crack growth, fatigue, yttria

Yttria has been widely used in the semiconductor industry as a plasma facing material to F-containing plasma. It has been manufactured as sintered bulks or plasma-sprayed coatings. However, ceramic industry has experiences of unexpected failure during the application of the parts made of yttria. Large sintered parts were reported to break randomly during their applications without any determined lifetime. However, causes were not clear and some weakness due to thermal shock was inferred without evidences. In this stduy, we tried to approach this unpredictable failure from the aspects of the slow crack growth. To the authors' knowledge, slow-crack growth behavior of yttria ceramics has not been reported yet. We used various techniques including static and dynamic fatigue and double torsion tests. In dynamic test, Vickers indents were made on the specimens to introduce artificial flaw and compare the results with those from machined specimens. We found very strong sensitivity of yttria ceramics to humidity with stress exponent of around 21 after considering residual stress effect from indentation (Fig 1). From double torsion experiment we obtained quantitative crack growth rate as functions of the stress intensity factor and humidity level. The crack growth rate was effectively zero under mineral oil and very fast inside water with threshold stress intensity factor of around 0.7 $MPam^{0.5}$. The threshold value was around 50% of critical stress intensity factor, showing strong sensitivity of yttria ceramics to humid environment.

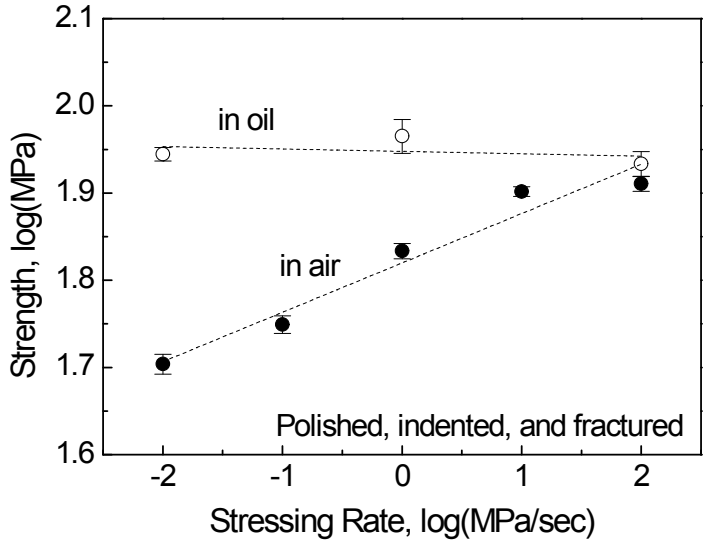

Figure 41 Strength Variation of yttria as a function of stressing rate inside oil or air

References:
[1] A. Shyam and E. Lara-Curzio, J. Mater. Sci., 41 (2006) 4093.

ST-O06

Transparent $MgAl_2O_4$ Spinel Fabricated by Sinter-HIP process

Ha-Neul KIM[1*], Jin-Myung KIM[1], Jae-Woong KO[1], Young-Jo PARK[1], and Hai-Doo KIM[1]
[1]*Engineering Ceramics Research group, Korea Institute of Materials Science*
797 Changwondaero, Changwon, Gyeongsangnam-Do, 642-831, Republic of Korea

Keywords: Transparent, $MgAl_2O_4$, HIP, Spinel

Magnesium aluminate spinel ($MgAl_2O_4$) have been considered as a leading candidate for optical ceramics applications, since it had been developed as translucent bulks by R.J. Bratton[1]. For highly transparent (>80%) $MgAl_2O_4$, total volume porosity should be less than 50ppm, and nano-size pores with 40~70nm (one-tenth of visible wavelength range) also should be minimized according to the Mie-scattering theory[2]. In order to realize that, various different sintering methods have been applied such as hot-press[3], hot-press/hot isostatic press (HIP)[4, 5], spark plasma sintering (SPS)[6,7], and sinter-HIP[8,9]. For the armor application, it is important to make sub-um grained bulks for enhancing the hardness, so that improves the ballistic resistance. Until now, it is reported that only sinter-HIP process can meet both the high transmittance (>80%) and the fabrication of large $MgAl_2O_4$ bulk with sub-um grain.

In this study, highly transparent $MgAl_2O_4$ spinel was fabricated by sinter-HIP process. Commercial $MgAl_2O_4$ nanopowder which has $30m^2/g$ of surface area (primary pariticle size = ~55nm), was effectively disintegrated into nano-dispersed slurry (D_{50}<150nm) via microfluidization method. Uniform compacts with narrow pore size distribution, were made from the slurry via slip-casting process. The compacts were sintered under air atmosphere in the range of 1400°C ~ 1600°C in order to analyze the sintering behavior and remove open pores prior to HIP process. Selected air-sintered samples were HIPed at 1450°C for 5hrs to achieve transparent $MgAl_2O_4$. The in-line transmittance of a fabricated $MgAl_2O_4$ with 1mm of thickness, was close to the theoretical transmittance (~86.9%), 85.1% at 550nm and over 80% even at 300nm (UV wavelength). It is considered that the high in-line transmission is related to the delicate ceramic processing technique (especially microfluidization), and a small amount of Ca impurities from gypsum mold.

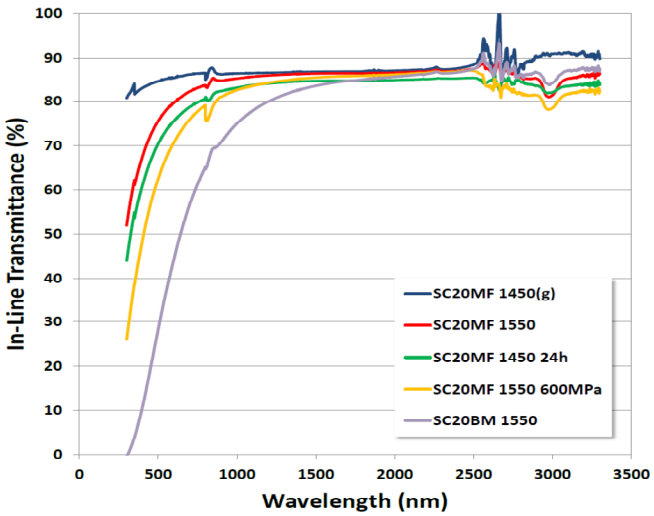

Figure 42 In-line transmittance of sinter-HIPed $MgAl_2O_4$ spinel

References:

[1] R.J. Bratton, J. Am. Ceram. Soc. 57[7] (1974) p.283.
[2] R.Apetz et al., J. Am. Ceram. Soc. 86[3] (2003) p.480
[3] L. Eposito et al., J. Eur. Ceram. Soc. 33 (2013) p.737
[4] A.C. Sutorik et al., J. Am. Ceram. Soc. 95[2] (2012) p.636
[5] http://www.techassess.com
[6] G. Bonnefont et al., Ceram. Int. 38 (2012) p.131
[7] K. Morita et al. J. Am. Ceram. Soc. 92[6] (2009) p.1208
[8] A. Krell et al. J. Am. Ceram. Soc. 93[9] (2010) p.2656
[9] A. Goldstein et al. J. Ceram. Soc. Jpn. 117[11] (2009) p.1281

Acknowledgement:

This work was supported by the MCTD (Materials & Components Technology Development) Program (PN : 10047010, Development of 80% Light-Transmitting Polycrystalline Ceramics for Transparent Armor·Window Applications) funded By the Ministry of Trade, industry & Energy (MI, Korea).

ST-O07

Common Ceramics for Refrigeration: Be Cool Be Environmental Friendly

M. S. ANWAR[1], Bon Heun KOO[1*]
[1]*School of Materials Science and Engineering, Changwon National University, Changwon, Gyeongnam, 641-773, South Korea*

Keywords: Ceramics, Magnetic refrigeration, XRD, Magnetization, Ceramics

Magnetic cooling based on magnetocaloric effect (MCE) has been demonstrated as a promising alternative technology to classical refrigeration (air conditioning, refrigeration, liquefaction of gases, etc.) and has a great potential to compete successfully with compression and relaxation of the gases for refrigeration. In the present work, We report detail study on the structural, magnetic, and magnetocaloric properties of Zn doped manganese-zinc ferrites with different Zn-concentrations. Polycrystalline $Mn_{1-x}Zn_xFe_2O_4$ ($0.0 \leq x \leq 0.7$) ferrite samples were prepared using the conventional solid-state reaction method. The x-ray diffraction result indicates that the ferrite samples have a cubic spinel type structure without any impurity phase. Temperature dependent magnetization measurements and Arrott analysis reveal second order ferromagnetic transition in all samples with Curie temperature decreasing progressively with increasing Zn concentration from ~571 K for x = 0.0 to 240 K for x = 0.7. A decrease in magnetization was observed with Zn doping. A maximum in magnetic entropy change, $|\Delta S_M^{max}|$ (~1.25 $Jkg^{-1}K^{-1}$ at 2.5 T) has been observed in $MnFe_2O_4$ sample. The width of magnetic entropy curve was found to increase with the Zn concentration. Also, the $|\Delta S_M^{max}|$ and relative cooling power were found to increase with increasing the applied magnetic field, which indicates much larger cooling power to expected at higher magnetic field. This investigation suggests that $Mn_{1-x}Zn_xFe_2O_4$ ($0.0 \leq x \leq 0.7$) ferrite samples can be used as a potential magnetic refrigerating material with wide range of temperature.

Acknowledgement:
This research was supported by the Basic Science Research Program through the National Research Foundation of Korea (NRF) funded by the Ministry of Education, Science and Technology (2012-R1A1B3000784) and National Research Foundation of Korea (NRF) grant funded by the Korean government (MEST) (NO.2011-0030058).

ST-O08

Ceramic membrane for water treatment using diatomite based natural materials

In-Hyuck SONG[1*], Jang-Hoon HA[1], Byungseo BAE[1], Young-Wook KIM[2]
[1]*Engineering Ceramics Department, Korea Institute of Materials Science, Changwon, Gyeongnam 641–831, Republic of Korea*
[2]*Department of Materials Science and Engineering, The University of Seoul, Seoul 130–743, Republic of Korea*

Keywords: Porous ceramics, Diatomite, Porosity, Membrane

Ceramic membranes can be applied under extreme operating conditions such as low pH, high pressure and high temperature. Especially, the inherent limitations of conventional polymer membranes can be overcome by adopting ceramic membranes simply to the existing water treatment systems. Moreover, there are a lot of potential applications of ceramic membranes such as distillation, adsorption and extraction in various industrial areas. Therefore, the ceramic membrane technology is not a mere ceramic processing technology, but a highly influential technology to the overall environment technology.
In this study, we focused that the cost-effective membrane manufacturing process by adopting various kinds of natural materials like diatomite or clays. These low-cost materials offer attractive mechanical resistance and can be used as a filter, filler, or a mild abrasive material due to its highly porous structure. Accordingly, a challenging area among the membrane applications of natural materials is how to consolidate them as a bulk structure that retains its unique, inherent properties or how to coat them properly on any suitable substrate. This presentation consists of three parts: (1) Tailoring pore structures of the substrate of ceramic membrane, (2) Functionalizing the coating layer of ceramic membrane, and (3) Extruding the substrate of ceramic membrane. Also, the aim of this study is to clarify whether natural materials such as diatomite and clays can be applied to water treatment area either as a substrate material or a coating material.

References:

[1] N. van Garderen, F.J. Clemens, M. Mezzomo, C. P. Bergmann, T. Graule, *Applied Clay Science,* 2011, 52, 115.
[2] P.V. Vasconcelos, J. A. Labrincha, J. M. F. Ferreira, *Journal of the European Ceramic Society* 2000, 20, 201.

Acknowledgement:

This study was supported financially by the Research Program of the Korea Institute of Materials Science (KIMS) (PNK3680).

ST-O09

Characteristics of Zirconate-based Oxides for Thermal Barrier Coatings (TBCs)

Seongwon KIM[1*], Chang-Sup KWON[1], Yoon-Suk OH[1], Sung-Min LEE[1], Hyung-Tae KIM[1], and Byung-Koog JANG[2]

[1] *Engineering Ceramic Team, Korea Institute of Ceramic Engineering and Technology, Icheon, Gyeonggi-do, 467-843, Korea*

[2]*High Temperature Materials Unit, National Institute of Materials Science, Tsukuba, 305-0047, Japan*

Keywords: Thermal Barrier Coatings (TBCs), Rare-earth Zirconate, Pyrochlore/Fluorite, Thermal Conductivity

Over the past decades, studies of thermal barrier coatings (TBCs) have been conducted to increase the operating temperature of gas turbines for power generation and aircraft. One of the most widely used materials for TBC application is yttria-stabilized zirconia (YSZ), which has low thermal conductivity and a high thermal expansion coefficient. Among candidates for future TBCs, fluorite and pyrochlore oxides are two prevailing materials. Both have analogous cubic structures with a space group of $Fm\bar{3}m$ for the former and $Fd\bar{3}m$ for the latter. The general formula of the fluorite and pyrochlore oxides is AO_2 and $A_2B_2O_7$, respectively. The low thermal conductivities of rare earth oxides with these structures are attributed to the phonon scattering by point defects in the crystallographic structures.
In this study, we characterized the phase structures and thermal conductivities of rare-earth zirconates. Several compositions from $La_2(Zr_{1-x}Ce_x)_2O_7$ or $(La_{1-y}Gd_y)_2Zr_2O_7$ are fabricated using solid-state reaction for this study using La_2O_3(High Purity Chemicals , 99.9% , 11μm), Gd_2O_3(High Purity Chemicals , 99.9% , 11μm), CeO_2(High Purity Chemicals , 99.9% , 5μm), and ZrO_2(Aldrich , 99% , 5μm) oxide powders. The samples were prepared by the solid-state reaction. For heat-treated samples, apparent densities were measured by using the Archimedes Principle. Crystallographic phase of heat-treated samples were identified by X-ray diffractometer with Cu Kα radiation(0.1506nm). The specific heat capacities (C_p) and thermal diffusivities (λ) of the sintered samples were measured by laser flash analysis as a function of the temperature up to 1000℃. The thermal conductivity (K) can be calculated by Eq. (1) with the apparent density (ρ), heat capacity (C_p), and thermal diffusivity (λ).

$$K = \rho \cdot C_p \cdot \lambda \qquad (1)$$

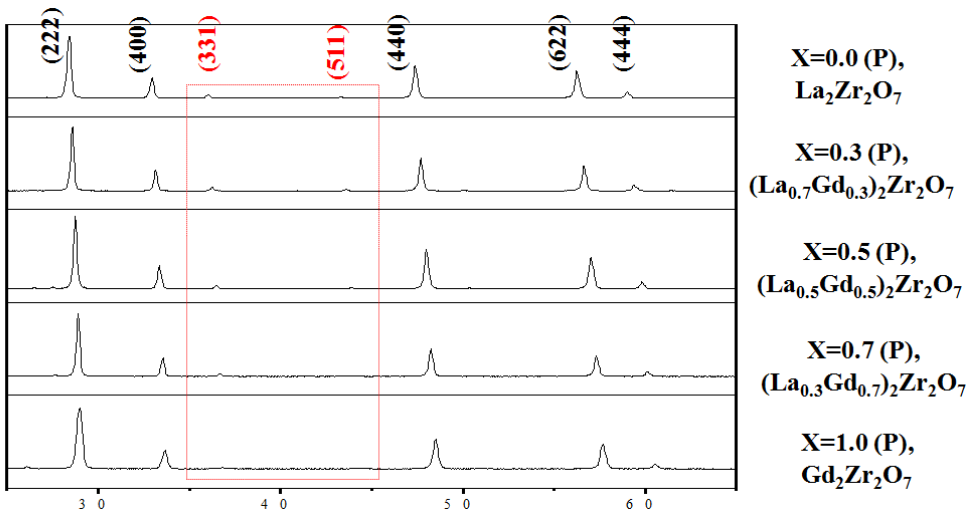

Figure 43 XRD patterns of $(La_{1-x}Gd_x)_2Zr_2O_7$ coatings : (a) as-deposited and (b) after heat treatment at 1400℃.

Figure 1 shows the XRD patterns of sintered $(La_{1-x}Gd_x)_2Zr_2O_7$ samples. Among these XRD patterns, the existence of (331) and (511) peaks of superlattice confirms the presence of pyrochlore phases in this $(La_{1-x}Gd_x)_2Zr_2O_7$ system. The LZ to GZ composition turns out to have a pyrochlore phase through the whole composition range.

References:

[1] D.R. Clarke and C.G. Levi, *Annu. Rev. Mater. Res.,***33** (2003) 383.
[2] C.G. Levi, *Curr. Op. in Sol. Sta. & Mater. Sci.,* **8** (2004) 77.
[3] M.R. Winter and D.R. Clarke, *J. Am. Ceram. Soc.,* **90** (2007) 553.
[4] P.K. Schelling, S.R. Plillpot, and R.W. Grimes, *Philos. Mag. Lett.*, **84** (2004) 127.
[5] J. Wu, X. Wei, N.P. Padture, P.G. Klemens, M. Gell, E. Garcia, P. Miranzo, and M.I. Osendi, , *J. Am. Ceram. Soc.,* **85** (2002) 3331.

Acknowledgement:

This research was supported by a grant from the Fundamental R&D Program for Strategic Core Technology of Materials funded by the Ministry of Trade, Industry and Energy and by a grant from the Basic and Strategic R&D Program funded by the Korea Institute of Ceramic Engineering and Technology, Republic of Korea.

ST-O10

Sintering of transparent polycrystalline Y_2O_3 by using graphite vacuum furnace

Young-Jo PARK, Lin GAN, Mi-Jeung PARK, Jin-Myung KIM, Haneul KIM, Jae-Woong KO, Hai-Doo KIM
Engineering Ceramics Research Group, Korea Institute of Materials Science, Changwon, 642-831, Korea

Keywords: Y_2O_3, transparent, IR, window

Yttria (Y_2O_3) is an indispensable core ingredient in the various material-related fields just like the licorice (甘草, アマクサ) in the Chinese medicine (漢方). Some of the well-known examples include the usages as the sintering additive for some of the hardly sinterable ceramics, the stabilizer for zirconia, and the flame controller for magnesium alloy, and so forth. In addition, monolithic yttria by itself finds an important industrial application due to its excellent halogen plasma resistance. That is, bulk yttria and coated yttria are the key parts of the processing facility for the semiconductor/display industry.

In the current presentation, authors are going to focus on the excellence of yttria as a window material for the mid IR (2-5 μm) range. That is, the transmittance at high temperature regime is higher, while the emissivity at high temperature regime is lower than other window materials. Further, the transmittance of more than 80% is maintained over 5 μm wavelength. Consequently, the S/N (signal to noise) ratio through the yttria window is the highest among the known window materials.

The vigorous research activities have been reported on the sintering of transparent polycrystalline Y_2O_3. Somewhat different approach has been tried at KIMS by the vacuum sintering using the graphite heating element. Graphite furnace is the most widely established infra, therefore it is insisted that research at KIMS has an important industrial implication for the application of transparent ceramics. The mechanism for the development of transparency, transmittance, and strength of yttria sintered by graphite furnace will be provided at the presentation.

ST-O11

Measurement of Local Fracture Toughness of Soda-lime Glass and Si_3N_4 Ceramics Using Microcantilever Beam Specimens

Junichi TATAMI[1]*, Masaki KATAYAMA[1], Motoyuki IIJIMA[1], Tsukaho YAHAGI[2] and Takuma TAKAHASHI[2]
[1] *Yokohama National University, Yokohama, 240-8501,Japan*
[2] *Kanagawa Academy of Science and Technology, Kawasaki, 213-0012, Japan*

Keywords: Fracture toughness, soda-lime glass, Si_3N_4

Local mechanical properties are important to understand the nature of the mechanical properties of bulk ceramics and glass. In this study, the local mechanical properties, in particular fracture toughness, of soda-lime glass and Si_3N_4 ceramics were measured using microcantilever beam specimens prepared by focused ion beam technique.
The size of the sample for strength measurement was 2.5×2×15 m and their section profile was pentagonal. A sharp single notch was also machined along a target to measure the fracture toughness. After bending test, the grain boundary fracture toughness was calculated by displacement method based on finite element analysis.
Table 1 shows the fracture toughness near the surface of soda-lime glass. In this study, the target to measure the fracture toughness is as-received and HF-eched surfaces. The fracture toughness of the HF-eched surface is higher than that of the as-received surface. Since the chemical composition in soda-lime glass changes from the surface toward the inner part, the difference in the fracture toughness between the as-received and the HF-etched surfaces probably resulted from the chemical composition. It has been reported that removal of the surface by HF-etching improved the strength of soda-lime glass. In consideration of the result of the present study, it was shown that removal of the defects by etching has a great effect on the improvement of the strength.
Table 2 shows the fracture toughness of grain and grain boundary of Si_3N_4 ceramics. The fracture toughness of the Si_3N_4 grain was 2.77 $MPam^{1/2}$, which is higher than the estimation by calculation. The difference should result from the dissipative energy other than formation of new fracture surfaces. The grain boundary fracture toughness of Si_3N_4 ceramics depended on the added rare earth oxide, which is higher than the fracture toughness of SiAlON glass. It was suggested that structure of the intergranular glassy film should be different from that of the bulk SiAlON glass. The dependence of the grain boundary fracture toughness on the added rare earth oxide was explained by the difference in the grain boundary structure.

Table 1 Fracture toughness of soda-lime glass

Target	K_{IC}/ $MPam^{1/2}$
As-received surface	0.51±0.06
HF etched surface	0.68±0.03

Table 2 Fracture toughness of Si_3N_4 ceramics

Target		K_{IC}/ $MPam^{1/2}$
Si_3N_4 single grain		2.77±0.54
Grain boundary	Y_2O_3-Al_2O_3 additive	1.73±0.52
	La_2O_3-Al_2O_3 additive	1.63±0.60
	Lu_2O_3-Al_2O_3 additive	2.28±0.37

ST-O12

Synthesis of Meso-Macro Porous β-SiC by a Direct Reaction between Metallic Si and Carbon

Sang Whan PARK[1]*, Mi-Rae YOUM[1], Sung-Il YUN[1]
[1]*Interfacial Control Research Center, Korea Institute of Science and Technology, Seoul, 136-791, Korea*

Keywords: Porous SiC, Direct reaction, Meos-macro porous, carburization

It has been known that porous SiC has many excellent properties such as stability at high temperature, high chemical resistance, and high termal conductivity. Importance of the meso-macro porous SiC with high surface area has been increased for the use of the catalyst support under harsh conditions such as hydro desulfurization as well as high thermal conductive catalyst support for the gas reforming. In this study, meso-macro porous SiC bodies were fabricated by a direct reaction between metallic Si and carbon black in Si-C green body. The β -SiC were synthesized by carburizing Si-C preforms with various C/Si mole ratios at the temperature of 1200 ~ 1300°C under vacuum and/or in Ar atmosphere. In addition, the effects of Ni as a catalyst were studied on the synthesis temperature as well as the pore characteristics of meso-macro porous SiC bodies. The crack free Meso-macro porous SiC bodies were successfully synthesized by a direct Si-C reaction with additional processes to remove residual Si and C. It was found that Ni catalyst reduced the synthesis temperature as shown in Fig. 1. BET surface area of synthesized meso-macro porous SiC were varied from 25 to 60 m^2/g depending on the synthesis temperature and C/Si mole ratios of C/Si preform. The compressive strengths of the synthesized meso-macro porous SiC bodies were found to be dependent on the synthesis temperature and C/Si mole ratios of Si-C green body.

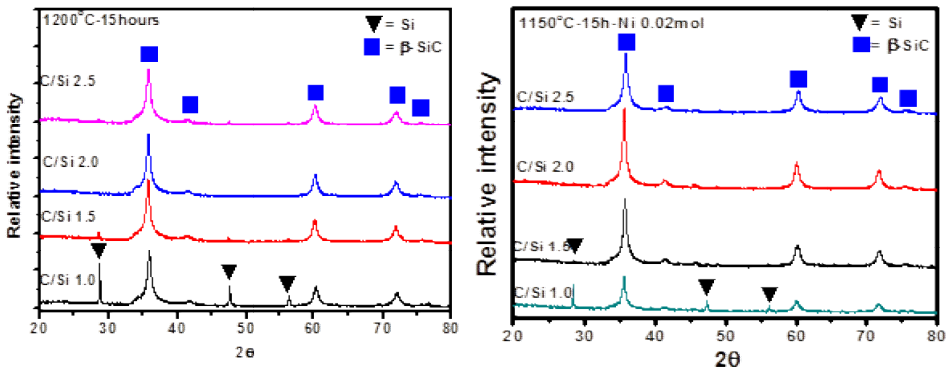

Fig. 1. XRD patterns of meso-macro porous SiC synthesized by a direct reaction between Si and carbon black; (a) without Ni catatyst, (b) with Ni catalyst.

References:

[1] Zhicheng Liu, etal. Microporous and Mesoporous Materials 82(2005) *p.*137
[2] Guo-Qiang Jin, etal. Microporous and Mesoporous Materials 60 (2003) *p*. 207

Acknowledgement:

This study was financially supported by KIST Institute own program.

ST-O13

Effect of grain size on properties of porous alumina for support substrates of permselective ceramic membranes

Sawao HONDA[1*], Gaetan GRABARSKI[2], Yusuke DAIKO[1], Shinobu HASHIMOTO[1],
Benoit NAIT-ALI[2], David S. SMITH[2], Yuji IWAMOTO[1]
[1]*Department of Materials Sciences and Engineering, Nagoya Institute of Technology, Nagoya, 4668555, JAPAN*
[2]*Center Europeen de la Ceramique, Limoges, 87068, FRANCE*

Keywords: Porous alumina, Grain size, Necking size, Fracture strength, Thermal conductivity

Porous alumina has been investigated as support material for the ceramic permselective membranes. This porous structure design is essential for the separation membrane support to maximize the fluid permeability and minimizes the pressure drop of the permeating fluids by increasing pore volume as much as possible. Generally, fracture strength or thermal shock resistance of porous ceramics can be enhanced by decreasing the porosity or pore size. However, there is a fundamental trade-off between the mechanical properties and the permeation property, and the fluid permeability through the porous support decreases consistently with the decrease in the porosity or pore size. To apply porous alumina as a porous support for microporous ceramic membranes, it is important to establish a novel porous structure design concept to harmonize the simultaneous and sufficient fracture resistance and permeability of the porous alumina. In this research, a series of macroporous alumina with different pore size and porosity were fabricated. The permeability of the macroporous alumina was characterized by measuring nitrogen gas permeance, while the mechanical and thermal properties of the macroporous alumina were evaluated. The relations between the parameters which characterizing the porous structure and the thermo-mechanical properties were discussed from a viewpoint to develop macroporous support for microporous ceramic membranes by the tailored macroporous structure controlling. The nitrogen permeability of porous alumina was increased with pore volume remarkably. The gain necking of porous alumina with higher fracture resistance properties was larger than that of the others. In order to estimate the effect of grain size and grain necking on thermal conductivity, porous alumina were fabricated using various grain size alumina powder and pulse electric current sintering without grain growth, as shown Fig.1, and the numerical analysis was performed using interfacial thermal resistance at grain boundary. The high thermal conductivity was due to the large grain size and grain necking. This research clarified that increasing the grain necking size could improve the fracture resistance without lowering the permeability.

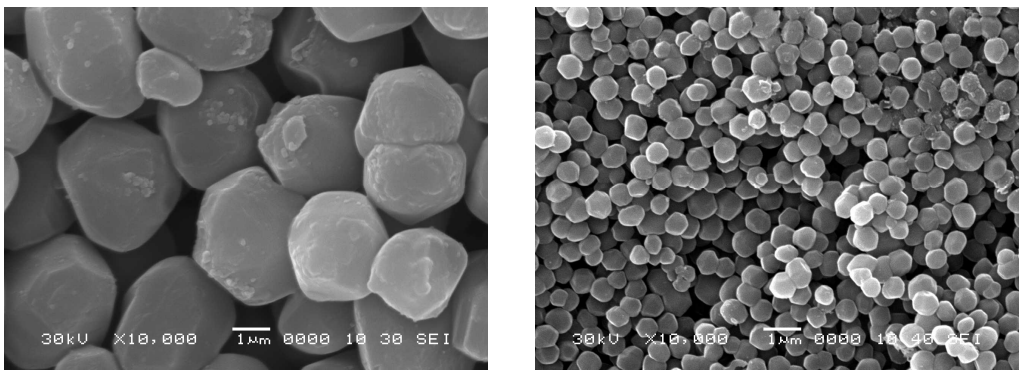

(a) (b)

Fig.1 Microstructure of porous alumina sintered by PECS method. (Grain size of starting powder: (a) 3 μm , (b) 0.7μm)

ST-O14

Erosion Resistance and Degradation of Various SiC/SiC Composites

Min-Soo SUH[1*], Se-Young KIM[1], In-Sub HAN[1], Sang-Kuk WOO
[1]*Korea Institute of Energy Research, Daejeon 305-343, Korea*

Keywords: Ceramic, Silicon carbide (SiC), Composite, Fiber reinforcement, Chemical vapor infiltration, Liquid pressure sintering, Erosion

SiC fiber-reinforced SiC matrix composite is candidate material for utmost severe environment due to their promising mechanical properties under the elevated temperature. Ablation resistant and erosion resistant are of significant importance in the field of aerospace application. Those mechanical characteristics have to be considered to improve the overall performance by developing the fabrication route. This study investigate erosive wear behavior of various SiC/SiC composites manufactured by different fabrication routes, especially for the liquid pressure sintering (LPS) and chemical vapor infiltration (CVI) route. The fabrication characteristics shows that Tyranno SA grade SiC fibers were adopted with the pyrolytic carbon (PyC) interface and laminated as cross-ply fiber structure. For the LPS-P route, the phenolic resin interfaced were applied on Tyranno AG grade fibers, due to the volumetric shrinkage whilst the sintering. After erosive wear test, the material degradation mechanisms are unearthed primarily by the microscopic observation, and illustrated for each of composite material. The results show that the porosity seems to be one of the crucial material property when facing the erosion damage. In case of near-stoichiometric SiC/SiC composite fabricated by CVI (chemical vapor infiltration) route, particle bombardment cause severe fragment and damage. The dominant mechanism was that the high-applied flexural stresses resulted from the macro-sized pores inherent in the CVI composites only brings the partial support to upper layer. In the opposite, relatively low flexural stress was applied that the high densified LPS (liquid pressure sintering) SiC/SiC composite only contains micro-sized pores, and sufficiently gives the full support when the particle bombardment took place. The optimal fabrication conditions were characterized for LPS route, which shows high erosion resistant. The followings have to be concerned for manufacturing high performance SiC/SiC composite under harsh erosive environment: high volume fraction of matrix, high strength of matrix, high bonding strength of each constituent, and the coating of PyC interface.

References:

[1] M.S. Suh, T. Hinoki, and A. Kohyama, Tribol. Lett. 41 (2011) 503-513.
[2] S.R. Choi, J. Am. Ceram. Soc., 91(9) 2963–2968, (2008)

GL-O01

DC voltage application to alkali containing oxide glass

Junji NISHII, T. Misawa and H. Kaiju
Research Institute for Electronic Science, Hokkaido University, Sapporo, Hokkaido 001-0020, Japan

Keywords: DC voltage, Alkali ion, Proton, Oxide glass, Ion conductivity, Ion exchange

Two ways are known for the DC voltage application to glass, i.e., contact electrode and non-contact electrode. The former is a conventional blocking electrode method used for the second order harmonic generation [1] and the anodic bonding [2]. The latter is known as a background technology for static electricity removal or dust removal, which is called as corona discharge [3]. This paper reviews our recent studies on the electrical nanoimprint (contact electrode) and corona discharge treatment (non-contact electrode).

1. Electrical nanoimprint

A two dimensional SiO_2 grating (700 nm period) coated with carbon was contacted to a soda-lime glass (10 mm × 10 mm × 1 mm) with glass transition temperature of 555°C in a N_2 atmosphere at 450°C and 0.02 MPa in pressure. A DC voltage of 200 V was applied to the mold for 60 s. The AFM views of mold and imprinted glass surface are shown in Fig. 1. The ToF-SIMS using C_{60} sputtering revealed the formation of the Na^+ deficient regions of 400 nm depth below the mold contacted area. The chemical etching using a 55 wt% KOH solution (70°C) remove the Na^+ deficient regions selectively (see (c)), because its chemical durability is much lower than that of the non-contacted area. The fine pattern was formed in the whole plate with a convex surface having 80 nm vertical interval, which is much larger than the imprinted structure height. An electrostatic attractive force might cause the perfect contact between mold and glass.

2. Corona discharge

The corona discharge is generated by a high DC voltage application between an anode electrode and a cathode electrode. A soda-lime glass plate coated with a UV curable resin pattern placed on the cathode stage heated at 100°C in air. The protons generated in the corona migrated and penetrated into the glass surface. The resin-patterned area protected the injection of proton. The Na^+ equivalent with the injected proton discharged at the anode side. The Na^+ deficient area was removed by the KOH etching. Fig. 2 shows the surface views of the resin pattern and the glass surface after the corona discharge treatment for 24 h followed by the KOH etching for 24 h. This process is appropriate for the large area patterning under atmospheric pressure and low temperature.

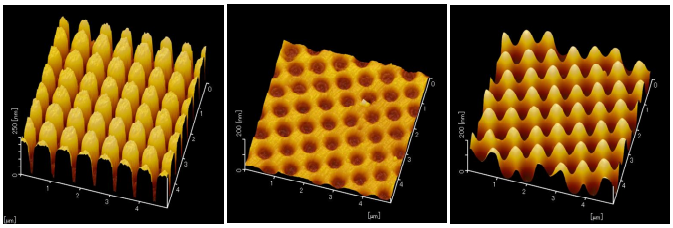

Fig. 1 Surface views of (a) SiO_2 mold, (b) electrically imprinted glass and (c) chemically etched glass (2 h).

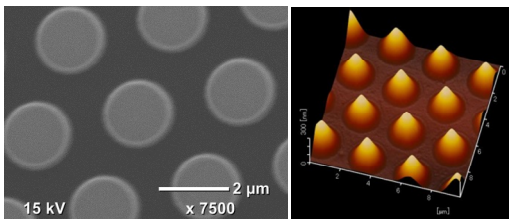

Fig. 2 Surface views of (a) UV curable resin pattern on glass and (b) corona treated glass followed by etching (24h).

References:
[1] R.A. Myers et al., Opt. Lett., 16(1991)732-734.
[2] M. Esashi et al., Sensors and Actuators, A21-A23(1990)931-934.
[3] M. Pavlik at al., Rapid Commun. Mass Spectrom., 11 (1997)1757-1766.

Acknowledgement:
The author thanks profs. D. Sakai, K. Harada of Kitami Int. Tech., H. Ikeda of Kyushu Univ., Dr. K. Yamamoto, Mr. T. Suzuki, Mr. K. Uraji of AGC Co.Ltd., Mr. Nishiura of Maruzen Petrochemical Co., Ltd. for their collaborations.

GL-O02

Potassium ion migration between non-contacted glass plates using corona discharge treatment in H_2 atmosphere

Keiga KAWAGUCHI[1]*, Hideo KAIJU, Junji NISHII
Research Institute for Electronic Science, Hokkaido University, Sapporo, Hokkaido 001-0020, Japan

Keywords: Corona discharge, Alkali, Proton, Silicate glass, Surface modification

1. Introduction

Corona discharge treatment is known as a non-contact surface modification method for glasses [1-2]. We previously reported that the uniform alkali ion migration occurs between the stacked glasses containing different alkali ions during the corona discharge treatment in air and H_2 atmosphere [3]. This report describes the spatial migration of alkali ions between two glass plates with 1 mm gap during the corona discharge treatment.

2. Experimental procedure

Two types of borosilicate glass plates with compositions (mol%) of $20K_2O$-$10B_2O_3$-$70SiO_2$ (KBSi) and $20Na_2O$-$10B_2O_3$-$70SiO_2$ (NaBSi) of 1 mm thickness were used for the corona discharge treatment. Fig. 1 shows the experimental setup for the corona discharge treatment. The KBSi was placed on the NaBSi via an Al_2O_3 spacer with 1 mm thickness. The corona discharge treatment was performed onto KBSi by the application of a DC voltage of 4.5 kV to the anode needle for 12 h at 200°C in an atmosphere of ambient air or 100% H_2. The current was monitored using a data logger. After the treatment, the surface compositions of two glass plates were analyzed using an energy dispersive X-ray spectroscopy (EDS).

3. Results and Discussion

The K^+ injection to NaBSi accompanied with a current of 14 A was observed only by the c orona discharge treatment in H_2 atmosphere. Fig. 2 represents the result of cross-sectional EDS profile of NaBSi after the treatment. A uniform K^+ injected layer of 2 m thickness was formed in the anode side surface of NaBSi, which suggests that the K^+ in the KBSi migrated to NaBSi even if the 1 mm gap exists between two glass plates.

The corona discharge treatment in H_2 atmosphere realized the spatial migration of alkali ion in the gap between two glass plates, which should be used for the glass surface modification containing alkali ions in ambient pressure and low temperature without molten salts.

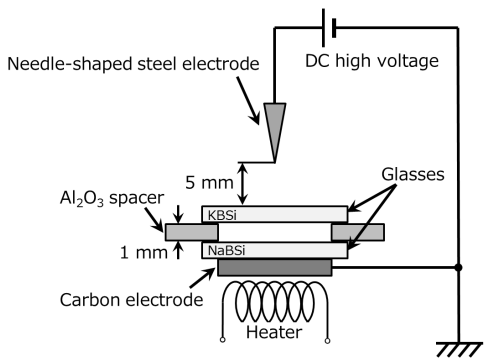

Fig. 1. Experimental setup for corona discharge treatment.

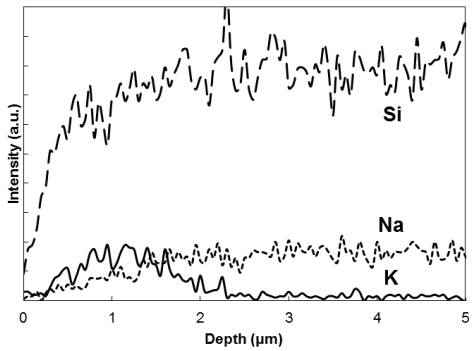

Fig. 2. Cross-sectional EDS profiles of corona discharge treated NaBSi glass plate in H_2, which was placed 1 mm below KBSi glass plate.

References:

[1] D. Sakai et al., Appl. Phys. Lett. **90**, 061102 (2007)
[2] K. Kawaguchi et al., Appl. Surf. Sci. **300**, 149-153 (2014)
[3] K. Kawaguchi et al., *Proc. of the 30th J-K International Seminar on Ceramics* K-01 (2013)

GL-O03

Recent Progress in Laser Patterning of Functional Crystals with High Orientation in Glasses

Takayuki KOMATSU,* Tsuyoshi HONMA, Kenji SHINOZAKI
Department of Materials Science and Technology, Nagaoka University of Technology, Nagaoka 940-2188, Japan

Keywords: Laser Patterning, Single Crystals, Orientation, Morphology, Nanocrystals, Glass

Laser irradiation to glass has been regarded as a process for spatially selected structural modification and/or crystallization in glass, and the laser-induced crystallization method, especially driven by thermal mechanisms, has been applied to pattern optical active crystals [1-3]. In the laser-induced crystallization, only spatially limited region is heated locally. This provides two important points for the crystallization mechanism of glasses: 1) the probability of nucleation in the spatially selected small region during laser irradiations would be very small, 2) a steep temperature gradient is created in the laser irradiated region and such a temperature gradient is moved along laser scanning direction. In particular, the generation and moving of steep temperature gradient would be one of the key points for the laser patterning of crystals with high orientations. In the presentation, we describe the recent progress in the laser pattering of functional crystals with high orientations in glasses.

For instance, -BBO crystals with dot, line, and planar two-dimensional morphologies are patterned in Sm_2O_3-BaO-B_2O_3 glasses by just scanning continuous wave lasers such as Yb:YVO_4 fiber lasers (wavelength: 1080nm). In the patterning of -BBO crystals in the inside of glass fibers (diameter: 450m), the focal position of Yb:YVO_4 lasers (e.g., power: 0.9~1.0 W, scanning speed: 2m/s) was moved from the surface to the inside. It was confirmed that -BBO crystals patterned are highly oriented, i.e., c-axis orientation, along the laser scanning direction. The curved and bending -BBO crystal lines were also patterned by just changing the laser scanning direction (Figs. 1 and 2).

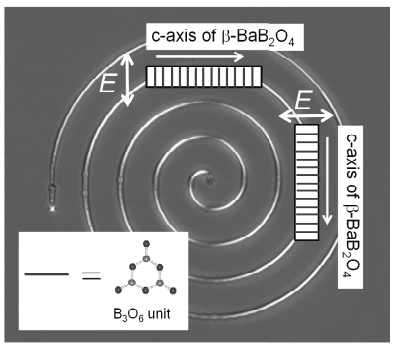

Figure 1 Polarized optical microscope photograph of the bending-BBO line

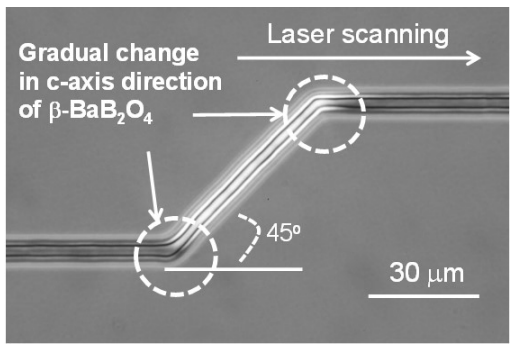

Figure 2 Curved -BBO line patterned by laser-induced crystallization

References:

[1] K. Shinozaki, T. Honma, and T. Komatsu, J. Appl. Phys. 112 (2012) 093506
[2] T. Komatsu and T. Honma, J. Asian Ceram. Soc. 1 (2013) 9.
[3] K. Ogawa, T. Honma, and T. Komatsu, J. Solid State Chem. 207 (2013) 6.

GL-O04

Fabrication of Sn^{2+}-doped Phosphate Glasses for Phosphor Applications

Hirokazu MASAI[1*], Toshiro TANIMOTO[1], Shun OKUMURA[1], Kentaro TERAMURA[2], Syuji MATSUMOTO[3], Takayuki YANAGIDA[4], Yomei TOKUDA[1], Toshinobu YOKO[1]
[1]*Institute for Chemical Research, Kyoto University, Uji, Kyoto 611-0011, Japan*
[2]*Department of Molecular Engineering, Kyoto University, Kyotodaigaku Katsura, Nishikyo-ku, Kyoto 615-8510, Japan*
[3]*Asahi Glass Co., Ltd., 1150, Hazawa-cho, Kanagawa-ku, Yokohama 211-8755, Japan*
[4]*Kyushu Institute of Technology, 2-4, Hibikino, Wakamatsu-ku, Kitakyushu 808-0196, Japan*

Keywords: Tin, Oxide Glass, Photoluminescence

Phosphors have been used in several applications in our daily lives. In contrast to most of trivalent rare earth cations, the emission of the ns^2-type emission center can be widely tailored by tuning the local coordination state because of the electron in the outermost shell. Recently, we have reported Sn^{2+}-doped phosphate glass phosphor that shows high quantum efficiency comparable to conventional crystalline phosphor [1]. The Sn^{2+} emission center appears to be very advantageous from the viewpoint of unique emission mechanisms in a random matrix; the coexistence of high efficiency and broad emission [2]. However, neither the correlation between actual concentration of Sn^{2+} centers and emission properties nor the local coordination states has been fully clarified.

In this paper, we report correlation between preparation conditions and the photoluminescence properties of Sn^{2+} centers in a zinc phosphate glass. When prepared in air, the local coordination state of Sn^{2+} centers depends on the starting material due to oxidation of Sn^{2+} into Sn^{4+}. In contrast, PL properties of Sn^{2+} centers of the glass prepared in inert atmosphere conditions is independent of the starting material because of elimination of the oxidation reaction. ^{119m}Sn Mössbauer and X-ray absorption fine structure analyses indicate that most of Sn^{2+} centers in the glass prepared in the inert atmosphere exists at a SnO-like coordination state. Because most Sn^{2+} centers take on a coordination state similar to that of Sn^{2+} in SnO crystals, it was determined that the coordination state was the origin of the PLE band at lower photon energy that accompanies high quantum efficiency. Since existence of two PLE band is characteristic of Sn^{2+} center in glass material, glass phosphor will be a novel light-emitting material that is quite different from the conventional crystalline phosphor. For future emitting devices, we believe that these oxide glasses will be one of the most industrially favorable inorganic materials possessing transparency and emitting properties.

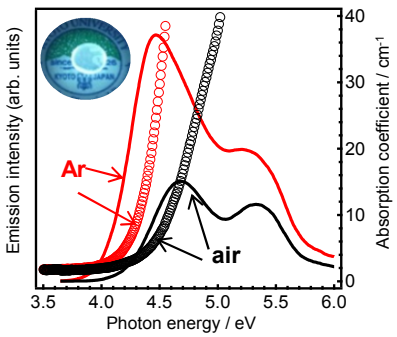

Figure 44 Optical absorption and PLE spectra of SZP glasses prepared in air and in Ar.

References:

[1] H. Masai, Y. Takahashi, T. Fujiwara, S. Matsumoto, and T. Yoko, Appl. Phys. Express, 3 (2010) 082102.
[2] H. Masai, T. Fujiwara, S. Matsumoto, Y. Takahashi, K. Iwasaki, Y. Tokuda, T. Yoko, Opt. Lett. 36, (2011) 2868.

GL-O05

Accumulation of Lanthanide Ions inside the Crystalline Phases in Vitustie Glass-Ceramics Wasteforms

Miae KIM[1*], Jayhyok SONG[2], Jong HEO[1,3]
[1]*Department of Materials Science and Engineering, POSTECH, Pohang, Republic of Korea*
[2]*Energy1 Lab., Samsung SDI, Yongin, Republic of Korea*
[3]*Department of Advanced Nuclear Engineering, POSTECH, Pohang, Republic of Korea*

Keywords: Glass-ceramics, Wasteforms, Pyro-processing, Vitusite, EXAFS

Pyro-processing is being investigated to recover radioactive uranium and trans-uranium elements from the spent fuels of pressurized water reactors [1-2]. We fabricated glass-ceramics containing sodium cerium(neodymium) phosphate [$Na_3Ln(PO_4)_2$] crystals as wasteforms for immobilization of lanthanide ion wastes produced by pyro-processing. We investigated the distributions and local environment of rare-earth ions in the glass-ceramics and evaluated the chemical durability of glass-ceramics wasteforms.

The nominal composition (mol %) of the glass prepared was $47SiO_2$ - $28Na_2O$ - $11B_2O_3$ - $8Li_2O$ - $2CeO_2$ - $1.6Nd_2O_3$ - $5.4P_2O_5$. As-prepared glasses were heat-treated at 500-800°C for 3h to precipitate crystals. The crystals formed was identified as vitusite [$Na_3Ln(PO_4)_2$] based on peaks in the X-ray diffraction (XRD) patterns. Most of the radionuclides appear to reside in the crystalline phases and it was proven by energy dispersive spectroscopy (EDS). In addition, local structure surrounding lanthanide ions were also analyzed by extended X-ray absorption fine structure (EXAFS). All results suggest that glass-ceramics containing sodium phosphate crystals are good candidate wasteforms for immobilization of lanthanide wastes generated by pyro-processing.

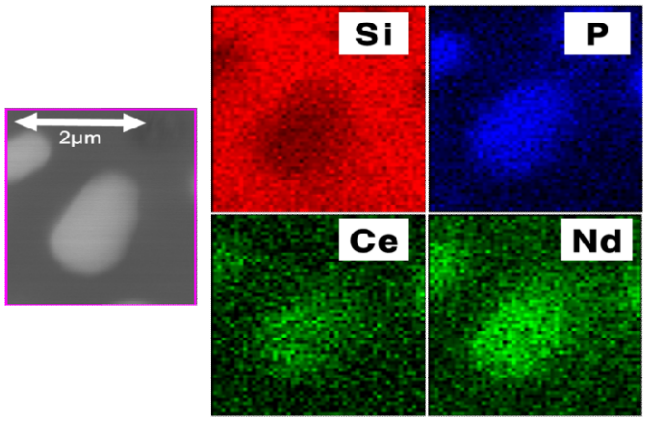

Figure 45 SEM image of one vitusite crystal and elemental mappings of Si, P, Ce and Nd obtained from EDS. Brightness increases with concentration.

References:

[1] T. Inque, L. Koch, Nucl. Eng. Technol., 40 (2008) 183
[2] H.S. Lee, J.M. Hur, J.G. Kim, D.H. Ahn, Y.Z. Cho and S.Y Paek, Energy Procedia, 7(2011) p. 391-395

Acknowledgement:

This research was supported by Priority Research Center (2009-0094036) and BK21+ Program through the National Research Foundation (NRF) of Korea funded by the Ministry of Education.

GL-O06

Kinetics of PbS Quantum Dots Precipitation on Nd^{3+}-O Clusters

J. Heo[1,2*], Won Ji Park[1], Woon Jin Chung[3]
[1]*Department of Materials Science and Engineering, Pohang University of Science and Technology (POSTECH), 77 Cheongam-Ro. Nam-Gu. Pohang. Gyeongbuk, 790-784, Republic of Korea*
[2]*Division of Advanced Nuclear Engineering, Pohang University of Science and Technology (POSTECH), 77 Cheongam-Ro. Nam-Gu. Pohang. Gyeongbuk, 790-784, Republic of Korea*
[3]*Institute for Rare Metals and Division of Advanced Materials Engineering Kongju National University, Cheonan, Chungnam 330-717, Republic of Korea*

Keywords: Quantum dots, rare-earth ions, crystallization kinetics

Quantum dots (QDs) have received attention in the past years due to their unique optical and electronic properties depending on their size. Therefore, precise control on the size of QDs is important for the applications. It was reported that PbS QDs size can be controlled by the changing Er^{3+} , Tm^{3+} and La^{3+} ion content in glasses [1-2]. However, it has been difficult to understand the on the role of rare-earth ions during the crystallization.

Glasses containing different amount of Nd^{3+} ions were prepared by conventional melt-quenching methods and PbS QDs were precipitated following various pre-determined heat treatment. Diameters of QDs were calculated from positions of the absorption bands and were plotted as a function of time at different temperature. It suggested that nucleation and growth of QDs were slower than that during the classical crystallization process. (Fig. 1.) EELS analysis showed that Nd^{3+} ions were preferentially concentrated inside the PbS QDs compared to glass matrix after heat-treatment. EXAFS result indicates that Nd^{3+} ions are surrounded by oxygen ions instead of sulfur even after heat-treatment.

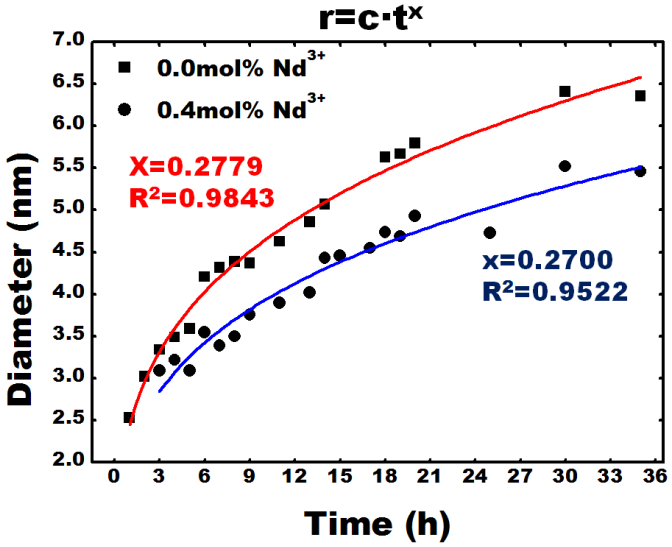

Fig. 1. Growth kinetics of PbS QDs in Nd^{3+}-free and 0.4 mol% Nd^{3+} ions containing glasses. Glass was heat-treated at 500°C for 1-36h.

References:

[1] S. M. Shim, C. Liu, Y. K. Kwon, J. Heo, J. Am. Ceram. Soc., 93 (2010) 3092-3094
[2] M. A. Kim, Y. K. Kwon, C. Liu, J. Heo, J. Non-Cryst. Solids, 383 (2014) 173-175

GL-O07

Luminescence and Absorption Properties of PbS Quantum Dots in Glasses

Won Ji Park, Mi Ae Kim, Jong Heo*
Department of Materials Science and Engineering and Division of Advanced Nuclear Engineering, Pohang University of Science and Technology (POSTECH), 77 Cheongam-Ro. Nam-Gu. Pohang. Gyeongbuk, 790-784, Republic of Korea

Keywords: Quantum dots, rare-earth ions, photoluminescence

It is important to control the size of quantum dots (QDs) precisely because QDs have unique optical and electronic properties depending on their sizes. Previously, it was necessary to carefully control the heat-treatment temperature and duration if one were to design the optical properties of quantum dots size precipitated in glasses. We have investigated the influence of rare-earth ions on the control of nucleation and growth of the semiconductor nanocrystals in silicate glasses.

Glasses containing different concentration of Nd^{3+} ions were prepared through conventional melt-quenching methods, PbS quantum dots (QDs) were precipitated in glasses by heat treatment method. The peak positions of the absorption from PbS QDs moved to short-wavelength side as the concentration of Nd^{3+} ions in glass increased under the same heat-treatment condition. For example, center wavelengths of the absorption bands decreased from 1398 nm for a Nd^{3+}-free glass to 1272 nm at Nd_2O_3 content of 0.6 mol %.(Fig. 1(a)) The center wavelengths of the PL spectra also moved from 1518 nm to 1370 nm as the concentration of Nd^{3+} ions increased.(Fig. 1(b)) It was proposed that Er^{3+} ions act as the nucleation centers for the formation of PbS QDs in glasses.[1-2] In this work, absorption, photoluminescence and TEM analysis were performed to understand of the role of rare-earth ions. Lifetimes of several rare-earths energy levels were measured and extended x-ray absorption fine structure (EXAFS) investigation were also performed to analyse the local environment of rare-earth ions.

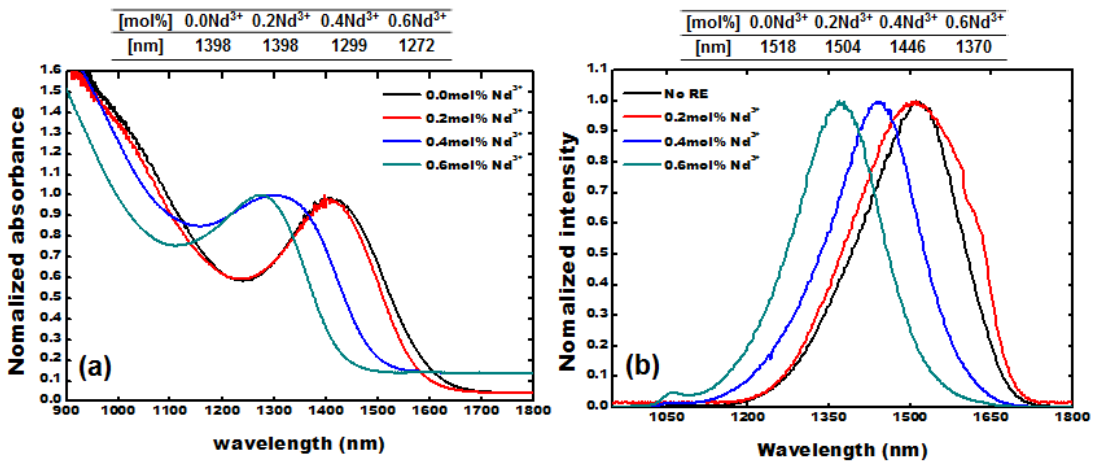

Fig. 1. Normalized (a) absorption and (b) PL spectra of the glasses with different Nd_2O_3 concentrations heat-treated at 500°C for 25h.

References:

[1] S. M. Shim, C. Liu, Y. K. Kwon, J. Heo, J. Am. Ceram. Soc., 93 (2010) 3092-3094
[2] M. A. Kim, Y. K. Kwon, C. Liu, J. Heo, J. Non-Cryst. Solids, 383 (2014) 173-175

GL-O08

Influence of composition on near-infrared luminescence of $BaSn_xO_3$

Yosuke OHYA[1], Yuichiro KUROKI[2], Tomoichiro OKAMOTO[1*], Masasuke TAKATA[3]
[1]*Department of Electrical Engineering, Nagaoka University of Technology, Nagaoka, Niigata 940-2188, Japan*
[2]*Salesian polytechnic, Machida, Tokyo 194-0215, Japan*
[3]*Japan Fine Ceramics Center, Atsuta, Nagoya 456-8587, Japan*

Keywords: Phosphor, Ceramics, Near-infrared

Near-infrared (NIR) phosphors have attracted attention in various fields such as in vivo luminescence imaging[1)] and spectral conversion materials for Si solar cells[2)]. The GaAs and YAG:Er is known as phosphors exhibiting a strong infrared luminescence. They include a rare earth element or toxic element which leads the problems on raw material supply and handling of the synthesis and disposal. Barium stannate ($BaSnO_3$) has cubic perovskite crystal structure without rare earth nor toxic elements. Mizoguchi et al.[3)] reported that strong near-infrared luminescence was observed in $BaSnO_3$. They presumed that the origin of the luminescence related to Sn^{2+}. In this study, the influence of molar ratio of Sn to Ba in $BaSn_xO_3$ on near-infrared luminescence was investigated to increase the luminescent intensity.

The powders of $BaSn_xO_3$ (x = 0.80 – 1.60) were synthesized by solid-state reaction. Powders of SnO_2 and $BaCO_3$ as starting materials were mixed in the molar ratio of Ba : Sn = 1 : x (x = 0.80 – 1.60) in 2 - propanol using an alumina mortar and pestle. The mixture was pressed into pellets under a uniaxial pressure of 70 MPa and sintered at 1350℃ for 3 h in air.

XRD measurements revealed that all the resultant samples had $BaSnO_3$ phase. From the cathodoluminescence measurements, all the samples exhibited near-infrared luminescence with a peak wavelength at 890 nm. Fig.1 shows the dependence of luminescence intensity on starting composition x. The intensity increased with increasing x, and reached the maximum at x = 1.25. Further increasing x resulted in the decrease of the intensity which reflects a concentration quenching. The luminescence intensity of x = 1.25 was 2 times higher than that of x = 1.00. The results imply that the excess Sn plays an important role in the enhancement of the luminescence. Result of XPS measurements will be reported in order to discuss the enhancement.

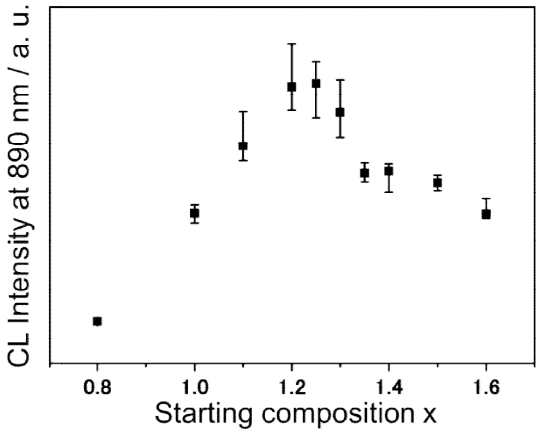

Fig.1. The dependence of near-infrared luminescence intensity on starting composition x of $BaSn_xO_3$.

References:

[1]Michael D. Ward et al., Coordin. Chem. Rev., 251(2007)1663
[2]Ye Li et al., Appl. Phys. Exp., 6(2013) 082301
[3]H. Mizoguchi et al., J. AM. CHEM. SOC., 126(2004) 9796

GL-O09

In-Situ XAFS Study of Amorphous $Ge_{50}Se_{50}$ Film under DC Electric Field

Sang Yeol SHIN[1], Roman GOLOVCHAK[2], Byung-ki CHEONG[3], Himanshu JAIN[4], Yong Gyu CHOI[1,*]

[1]*Department of Materials Science and Engineering, Korea Aerospace University, Gyeonggi 412-791, Republic of Korea*

[2]*Department of Physics and Astronomy, Austin Peay State University, Clarksville, TN 37044, USA*

[3]*Electronic Materials Research Center, Korea Institute of Science and Technology, Seoul 136-791, Republic of Korea*

[4]*Department of Materials Science and Engineering, Lehigh University, Bethlehem, PA 18015, USA*

Keywords: Amorphous chalcogenide film, XAFS spectroscopy, Ovonic threshold switching

Ovonic threshold switching (OTS) of amorphous chalcogenide film is normally more reproducible and durable than that of other amorphous materials. For practical switching devices application, a good amorphous chalcogenide film showing OTS phenomenon should maintain its non-crystalline state during operation without temperature- or current- induced crystallization. In this respect, OTS of amorphous film in binary Ge-Se system is quite attractive thanks to its reasonably high electrical conductivity as well as wide operation temperature range given by crystallization temperature exceeding 300 ^{o}C. Indeed, quite a good performance of OTS device was recently achieved using equiatomic $Ge_{50}Se_{50}$ film [1, 2]. The underlying mechanism of OTS, however, has not been fully resolved despite a number of previous investigations. As such, in an effort to better understand OTS of amorphous chalcogenide film, in this study, we employ in-situ X-ray absorption spectroscopic analysis of $Ge_{50}Se_{50}$ film under DC electric field being applied.

Preliminary EXAFS study of this equiatomic GeSe film with no applied electric field reveals that the local atomic environments of each constituent atom undergo conspicuous changes during the phase change. Specifically, its amorphous structure satisfies the 4(Ge):2(Se) arrangements, which becomes the 3(Ge):3(Se) arrangements after crystallization [3]. This clear structural contrast associated with crystallization would facilitate our in-situ XAFS analysis. Based on this consideration, we have designed a suitable geometry of specimen for obtaining X-ray absorption spectra during electric field being applied. XANES and EXAFS spectra of both Ge K- and Se K-edges are delineated in relation to magnitude of applied DC electric field. Information thus obtained is explained in connection with the non-ohmic I-V characteristics of this equiatomic GeSe film.

References:

[1] S.-D. Kim, H.-W. Ahn, S.Y. Shin, D.S. Jeong, S.H. Son, H. Lee, B.-k. Cheong, D.W. Shin and S. Lee, Electrochem. Solid-State Lett. 2 (2013) Q75.
[2] D.S. Jeong, H. Lim, G.H. Park, C.S. Hwang, S. Lee and B.-k. Cheong, J. Appl. Phys. 111 (2012) 102807.
[3] S.Y. Shin, R. Golovchak, S. Lee, B.-k. Cheong, H. Jain and Y.G. Choi, Scripta Mater. 86 (2014) 56.

Acknowledgement:

This work has been supported by NSF's International Materials Institute for New Functionality in Glass (IMI-NFG) through Grant No. DMR 0844014, and also by Basic Science Research Program of the National Research Foundation of Korea (NRF) funded by the Ministry of Education, Science and Technology (2012R1A1A2003832).

GL-O10

Improved Luminous Efficacy by Enhancing Transmittance of Phosphor-in-Glass

Yurian KIM, Sunil KIM, Hyungsun KIM *
[1]*Department of Materials Engineering, Inha University, Incheon, 402-751, Korea*

Keywords: Phosphor-in-glass, Transmittance, Pores, luminous efficacy, LED packages.

The color converters for phosphor-in-glass (PIG) have been recently researched in order to improve luminous properties of LED packages by changing composition of glass frit, phosphor ratio and thickness of plates. The residual pores of sintered glass plate generally govern the transmittance. It is considered as a factor affecting the luminous properties. In this study, the sintered glass and PIG plates were fabricated in various sintering temperature and time, and the correlation between the pores of the sintered glass and the optical properties of the glass and PIG plates were investigated. The pore features were analyzed using scanning electron microscope, and the transmittance was measured by UV-visible spectrum. The luminous properties of PIG were evaluated using an integrating sphere. The transmittance of sintered glass and PIG plates was calculated as a function of porosity and pore average size with the Mie light scattering theory. The highest value in transmittance of glass plates was 48% at 550 nm and luminous efficacy of PIG is 71.7lm/W. The effective scattering coefficient increased with the increase of porosity in both sintered glass and PIG plates. The luminous properties such as luminous efficacy and emission intensity linearly increased with increasing transmittance of PIG plates. The increase in luminous efficacy of PIG was attributed to decrease in light scattering loss. These results indicate that the high transmittance of PIG can increase the interaction between phosphor and light rays coming from blue LED chip and will cause emission of white light from PIG plate. The CRI remained constant with increase transmittance. On the other hand, the CCT showed the similar trend to luminous efficacy, and the color coordinates of emission light were shifted from blue to yellow region owing to low PIG transmittance.

References:

[1] Y. Lee, J. Lee, J. Heo, W. Im, and W. Chung, Opt. Lett. 37 (2012) 15.
[2] R. Boulesteix, A. Maitre, J. Baumard, Y. Rabinovitch, and F. Reynaud, Opt. Express 18 (2010) 14.
[3] I. Yamashita, H. Nagayama, and K. Tsukuma, J. Am. Ceram. Soc. 91 (2008) 8.

Acknowledgement:

This work was supported by the Technology Innovation Program (10044203, Development of phosphor materials based on Blue/UV LED) funded by the Ministry of Trade, industry & Energy (MI, Korea).

BI-O01

The Relevance of Biological Nutrients to the Prevention and Treatment of Osteoporosis

Garima TRIPATHI[1], Hui Suk YUN[1*]
[1]*Engineering Ceramic Department, Powder & Ceramic Division, KIMS(Korea Institute of Materials Science), 797 Changwondaero, Changwon, Kyungnam, Korea 642-831*

***Keywords**:* Genistein, Calcium Phosphate, 3-D printing, Cell Proliferation

Osteoporosis is a worldwide disease with an excessive prevalence in humans. A number of commercial biomaterials are presently used to treat osteoporotic bone fractures, but most of these have not been precisely designed for the purpose. Calcium Phosphate (CaP) compounds are well accepted by living organism with time, newly formed bone grows onto/into calcium phosphate ceramics and finally leads to stable osteointegration. For the purpose, in the present paper, a novel room temperature process has been reported to produce a 3D porous calcium phosphate scaffold with drug load/release efficacy for use in the treatment of osteoporosis. The developed technique is a combination of a paste extruding deposition (PED) system and cement chemistry. Cementation process has been chosen as opposed to the typical sintering process in ceramic scaffold fabrication which lead to unexpected crystallization, low biodegradability and bioactivity, unstable mechanical properties, high cost, and suppressed biological performance. Flavonoids, commonly known as a nutrient, have been selected as a model drug; it was loaded onto CaP powder to introduce homogeneous distribution in the scaffold. The cytocompatibility of the developed drug loaded scaffolds was validated through cell culture experiment with different types of bone cells which are responsible for bone formation as well as bone resorption. The results showed that the cell proliferation behavior was enhanced on flavonoid loaded 3D CaP scaffold in case of bone forming osteoblast type cells. On the other hand there was decrease in the proliferation rate in case of bone resorbing multinucleated osteoclast cells. In summary it can be reported that preliminary experiments can conclude that the chosen biomolecule can be an emergent candidate for the treatment of osteoporosis.

References:

[1] P. Weiss, L. Obadia, D. Magne, X. Bourges, C. Rau, T. Weitkamp, et al. Biomaterials.24(2003):4591.
[2] L. Qing-Chuan, X. Zhou-Sheng, Q. Yan-Fang, Z. Hong-Hao, Acta Pharmacol Sin. 2007;28(10):1597.

Acknowledgement:

This work was supported by the Mid-Career Researcher Program, through an NRF grant funded by The Korea Ministry of Education, Science, and Technology (MEST) (Number 2011-0017572).

BI-O02

Behaviour of Human Stem Cell on HA-TCP Composites

Indu BAJPAI[1], Duk Yeon KIM[1], Jung Kyong-JIN[2], Soyoung YANG[1], In-Hwan SONG[2], Sukyoung KIM[1]*

[1]*Materials Science and Engineering, Yeungnam University, Gyeongsan, Gyeongbuk 712-749, Korea*
2Department of Anatomy, College of Medicine, Yeungnam University, Namgu, Daegu 705-717, Korea

Keywords: Stem cells, Hydroxyapatite, Tricalcium phosphate

Calcium phosphate ceramics are well accepted as bone substitutes due to their excellent biocompatibility. The most widely used calcium phosphate bioceramics are hydroxyapatite [HA, $Ca_{10}(PO_4)_6(OH)_2$] and tricalcium phosphate [TCP, $Ca_3(PO_4)_2$]. HA is stable in a body fluid and has been used for many years for hard tissue replacement. But, TCP which has two types (α and β) is rather soluble compared to the HA in a body fluid. Therefore, α- or β-TCP materials are not used alone. The biphasic calcium phosphates (BCP) in combination with the various ratio of HA/TCP are commonly used as an artificial bone substitutes to control the biodegradation rate in a body fluid.
The aim of current study is to investigate the behavior of stem cells on HA-TCP samples. For this purpose hydroxyapatite (HA), dicalcium phosphate dehydrate (DCPD) and calcium hydroxide ($Ca(OH)_2$) in the varying composition were mixed, cold compacted and then sintered at 1250 °C in air environment. Quantification of HA and TCP phases was done by XRD, and a surface profilometer was used to measure the surface roughness. Wettability and surface energy of all compositions were measured by a contact angle goniometer. Cell adhesion at HA-TCP surface after incubation for two days was observed by scanning electron microscopy and fluorescence microscopy. Number of cells per unit area and area covered by cells was analyzed by the image J software. Stem cell viability and proliferation of 8 days incubated cells was observed by colorimetric (MTT) assay. The maximum viability was found at HA100D100 sample with the composition equivalent of HA-TCP (60:40) composition. The cell viability was related to the TCP content in BCP disc samples. It is believed that the TCP content above a certain HA-TCP ratio (for example, 60:40) rather reduce the stem cells viability due the fast degradation of TCP, as shown in Fig. 1.

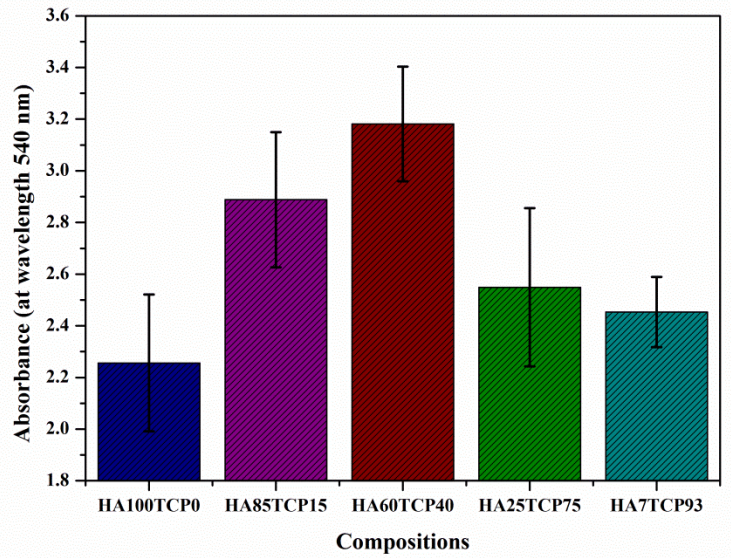

Fig. 1. Viability of stem cells on HA-TCP samples after incubation for 8 days

Reference:

[1] Hassna RR Ramay, M. Zhang, Biomaterials 25(2004)5171.

BI-O03

Fabrication of Core shell scaffolds by simultaneous extrusion of ceramic and hydrogel for bone tissue engineering

Naren RAJA[1, 2], Jongman LEE[2], Hui-suk YUN[1, 2 *]
[1]*Korea University of Science and Technology, Daejeon, South Korea.*
[2]*Korea Institute of Materials Science, Changwon, Kyungnam, 642-831 South Korea.*

Keywords: Calcium phosphate, Alginate, Core-shell designed scaffolds, 3D printing

An ideal scaffold for bone tissue regeneration should have bone-mimicking features such as high porosity and pore structure, biodegradability, bioactivity, biocompatibility and sufficient mechanical properties. Clinically favored materials for bone scaffold are based on bioceramics because of the chemical similarity of these materials to the mineral phase of bone. Scaffolds can be fabricated in a variety of ways including particulate leaching, gas foaming, phase separation, freeze drying, and 3D printing. Regardless of fabrication processes, heterogeneous cell distribution and in-growth into the scaffolds still remain as significant shortcomings in bone tissue engineering because cell seeding is normally performed by pipetting cells after the fabrication of the 3D scaffolds. The purpose of this study is to overcome this problem. Paste extruding deposition process, which is one of 3D printing process, was applied to obtain ideal structural conditions of scaffold and calcium phosphates was selected to satisfy biocompatibility and mechanical properties as well. We designed ceramic-hydrogel core-shell structured scaffold to this end and developed novel process using our original room temperature fabrication process of 3D ceramic scaffolds [1]. By precise control over the system using computer-aided design data we could fabricate calcium deficient hydroxyapatite-alginate core shell structured scaffolds. By using this construction we could not only achieve homogeneous cell distribution throughout the 3D scaffolds but also obtain favorable mechanical properties as bone scaffold. The dimensions of the scaffolds in terms of compressive strength and modulus increased with increasing the size of core. Because the whole process is carried out in a gentle condition for the cells, the incorporated cells in the shell were well distributed and alive throughout the 3D scaffold for the entire cultured period (7 days).

References

[1] Lee, J., Farag, M. M., Park, E. K., Lim, J., & Yun, H. S. (2014). A simultaneous process of 3D magnesium phosphate scaffold fabrication and bioactive substance loading for hard tissue regeneration. Materials Science and Engineering: C, 36, 252-260.

Acknowledgement:

This work was supported by the Mid-Career Researcher Program, through an NRF grant funded by The Korea Ministry of Education, Science, and Technology (MEST) (Number 2011-0017572).

BI-O04

Tissue engineered regeneration of completely transected femur using modified hydroxyapatite porous scaffold

Thuy Ba Linh NGUYEN[1, 3], Dong Woo JANG[1], Young Ki MIN[2] and Byong Taek LEE[*,1,3]
[1]*Department of Regenerative Medicine, Soonchunhyang University, Cheonan, 330-090, Korea*
[2]*Department of Physiology, Soonchunhyang University, Cheonan, 330-090, Korea*
[3]*Institute of Tissue Regeneration, Soonchunhyang University, Cheonan, 330-090, Korea*

Keywords: Hydroxyapatite, Surface modification, BMP-2 coating, bone tissue engineering

In this study, surface of porous Hydroxyapatite (HAp) scaffolds have been modified by collagen treatment and rhBMP-2 conjugation for bone regeneration. The in vitro studies were investigated to evaluate the effective of the modified surface compared to unmodified HAp surface. The rabbit model was prepared by complete removal of a 5-mm length of femur. The aim of the current study was to advance a treatment strategy for regeneration of completely transaction model, a finding that could have significant implantation for clinical application using three-dimension scaffolds HAp and HAp with collagen and BMP-2 surface modification.
Figure 1a & 1b showed an optical image and micro-CT of the HAp scaffold. The outer shell is dense, which gives ideal structural support to the scaffold jointly with the innermost thin shell. Figure 1c & d shows a surface and cross-sectional SEM micrograph of the HAp scaffolds. The fibril formation for collagen was observed by SEM on the surface and fracture surface of HAp-Collagen scaffolds, as shown in Fig.1f.

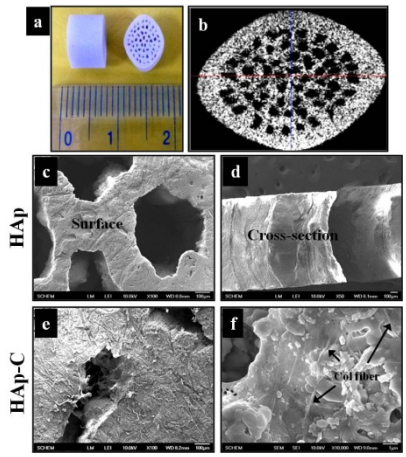

Figure 1. Photograph (a), (b) micro-CT image of HAp, (c) SEM images of surface HAp, (d) cross-section HAp; (e) Collagen coated HAp and (f) enlarge in (e).

References

[1] K. Kang, D. Kim, S. Yoon, J. Lee, B. Lee, J. Kwon, H. Seo, I.Lee, H. Shin, Y. Kim, H.Kim, J. Kim, B. Min, H. Lee and M. Kim. Biomaterials 33 (2012) 4828.
[2] T. Guda, J. Walker, B. Singleton, J. Hernandez, D. Oh, M. Appleford, J. Ong and J. Wenke. J. Biomater. Appl. (2013), online first.
[3] A. Mata, Y. Geng, K. Henrikson, C. Aparicio, S. Stock, R. Satcher and S. Stupp. Biomaterial 31 (2010) 6004.

Acknowledgement:

This work was supported by Mid-career Research Program (NRF) grant number: 2009-0092808, Republic of Korea.

BI-O05

Characterization of Multiwalled Carbon Nanotube-Reinforced Hydroxyapatite Composites Consolidated by Spark Plasma Sintering

Duk-Yeon Kim[1], Young-Hwan Han[1], Sungsil Jung[2], Sukyoung Kim[1]
[1]*School of Materials Science and Engineering, Yeungnam University, Gyeongbuk, Korea*
[2]*Pohang Techno Park 4th Venture-Dong, Pohang, Gyeongbuk 790-834, Korea*

Keywords: Hydroxyapatite, Multiwalled carbon nanotubes, Spark plasma sintering

The Chemistry of the human bone is similar to hydroxyapatite (HA), which is composed of both calcium and phosphate at a ratio of 1:1.67. HA has the excellent biocompatibility with living bone tissue and does not cause defensive body reactions. On the other hand, the poor mechanical properties of HA precludes its use as a replacement with load-bearing applications. Recently, the Multiwalled carbon nanotubes (MWNT) was used as the reinforcement in the ceramic matrix for enhancing the mechanical properties. The MWNT has the many good properties such as the low density, high aspect ratio and remarkable mechanical, thermal and electronic properties.
In this study, the pure HA and 1, 3, 5, 10 vol% MWNT reinforced HA were consolidated using a spark plasma sintering (SPS) technique. The decreasing of the gain size with increasing MWNT amount and pull-out toughening of the MWNT in the composites were observed which can be used to predict the improvement of the mechanical properties. Consequently, the addition of MWNT in HA increased the hardness and fracture toughness by approximately 3 ~ 4 times.

References:

[1] D. Lahiri, V. Singh, A. K. Keshri, S. Seal, and A. Agarwal, *Carbon 48* (2010) *p*. 3103.
[2] C. F. Deng, D. Z. Wang, X. X. Zhang, and A. B. Li, *Materials Science and Enginieering A444* (2007) *p*. 138.
[3] D. Lahiri, S. Ghosh, and A. Agarwal, Materials Science and Enginieering C32 (2012), *p.*1727

BI-O06

Effect of Ag_2O substitution on solubility and structure of CaO-P_2O_5-Nb_2O_5 glasses

Sungho LEE[1], Hirotaka MAEDA[2], Akiko OBATA[1], Kyosuke UEDA[3], Takayuki NARUSHIMA[3], Toshihiro KASUGA[1*]

[1]*Department of Frontier Materials, Nagoya Institute of Technology, Gokiso-cho, Showa-ku, Nagoya 466-8555, Japan*

[2]*Center for Innovative Young Researchers, Nagoya Institute of Technology, Gokiso-cho, Showa-ku, Nagoya 466-8555, Japan*

[3]*Graduate School of Engineering, Tohoku University, 6-6-02 Aoba, Aramaki, Aoba-ku, Sendai 980-8579, Japan*

Keywords: Antibacterial, Glass, Calcium, Phosphate, Structure

Infrequently biomaterial-centered infection occurred and some of case led to revision surgery. Antibiotics are one of method for prophylaxis of infection, but they show low efficacy to adherent bacteria on biomaterials. To increase efficacy of infection prophylaxis around biomaterial surface, antibacterial biomaterials is important. Silver ion is representative antibacterial species and shows antibacterial activity in low concentration. Niobium-containing phosphate invert glasses were developed in our group. They compose Nb-O-P bonds in glass network; it indicates excellent chemical durability and glassification. ALP activity and calcification enhanced due to Nb^{5+} ion dissolved from the glasses [1]. Purpose in this work is to evaluate effect of Ag_2O substitution on solubility and structure of niobium-containing phosphate invert glasses. Silver/Niobium-containing glasses expect to enhance bone-forming ability and antibacterial activity due to dissolved ions.

Niobium-containing phosphate invert glasses substituted with silver oxide or sodium oxide were prepared by melt-quenching method (1500 ^oC, 30 min, composition: $60CaO{\cdot}30P_2O_5{\cdot}(10\text{-}x)Nb_2O_5{\cdot}xAg_2O$ (mol%, x = 0 ~ 5, denoted by xAg), $60CaO{\cdot}30P_2O_5{\cdot}5Nb_2O_5{\cdot}5Na_2O$ (mol%, denoted by 5Na)). The samples structures were evaluated by FT-IR and ^{31}P MAS-NMR and solubility were evaluated by ICP-AES (Tris buffer solution (37 ^oC), 1 ~ 7 days).

FT-IR spectra of the 5Ag and 5Na glasses show no significant differences. This means silver in the glass acts as a network modifier like a sodium. From the ^{31}P MAS-NMR spectra, orthophosphate (Q^0) ratio increased (43% to 46%) and pyrophosphate (Q^1) ratio decreased (57% to 54%) linearly with increasing Ag_2O substitution (1 to 5 mol%). Q^0/Q^1 ratio of 5Ag and 5Na shows no significant difference (0.85 and 0.88). This means silver in the glasses break the phosphate chains, which is a similar role as sodium. M. Bellantone *et al.* reported 1 ~ 10 mM of Ag^+ ion shows antibacterial activity [2]. Silver ion dissolution amounts of 1Ag indicate 3 ~ 11 mM, which expected to show antibacterial activity.

Ag_2O substituted niobium-containing phosphate invert glasses were successfully prepared. Silver in glasses acts as a network modifier, which break the phosphate chains as similar as sodium. 1Ag glass is expected to show antibacterial activity.

References:

[1] A. Obata, Y. Takahashi, T. Miyajima, K. Ueda, T. Narushima, T. Kasuga, *ACS Appl. Mater. Interfaces* 4 (2012) 5684.

[2] M. Bellantone, H.D. Williams, L.L. Hench, *Antimicrob. Agents Chemother.* 46 (2002) 1940.

BI-O07

Synthesis of Bioglass Ceramic Using Commercial Water Glasses for Plasma Spray Coating on Dental Implants

Jaehui JEON, Sukyoung KIM
School of Materials Science and Engineering, Yeungnam University, 280 Daehak-Ro, Gyeongsan, Gyeoungbuk 712-749, Korea

Keywords: Bioglass, Glass ceramic, Dental implant, Water glass, Plasma spraying

Among various bioceramic materials, bioinert hydroxyapatite (HA) was used to coat as a coating material on Ti by a plasma spraying method to provide favorable sites to bone cells/tissue. Nevertheless, the clinical application showed the undesirable results such as the delamination of HA coated layer from the surface of Ti dental implants. However, the HA coating on dental implants is considered a priority considering method because of direct bonding with natural bone. In other manner bioactive glass which was invented by L.L. Hench, bioglass (45S5) has been recently applied for bioactive coating on Ti implants to utilize the excellent bioactivity and biodegradation property. But the bioglass itself has a couple of problems such as a complicate process for bioglass preparation and fast degradation compared to the osseointegration rate.
In this study, the new synthetic method of bioglass ceramics was developed using a commercial water-glass by adding bioglass elements. As a result, the bioglass ceramic materials can be manufactured by relatively simple and inexpensive process. First, the mixed solution of phosphoric acid and distilled water was prepared. Water glass was added into the solution using a high-speed stirrer. Calcium nitrate tetrahydrate and 5N sodium hydroxide solution were added little by little over 1 hour into the solution to adjust the bioglass composition. This entire mixing process with magnetic stirrer was conducted at 80℃. And then, the solution was dried for a single day in a drying oven. The dried powdery sample was heat treated at 1200℃ for 2 hours. A mass of glass-ceramic was crushed with a roller crusher to obtain appropriate size of granules. The glass ceramic granules were milled with 6mm zirconia ball in a HDPE jar for 24 hours to obtain round shape granules by grinding. Prior to the plasma spray coating, the washing and sieving of the ground granules were conducted in an alcohol bath to improve the flowability of powder during a plasma spray coating. The obtained granule size was 30~50 μm with a narrow size distribution.

References:

[1] Larry L. Hench, The story of Bioglass, J Mater Sci: Mater Med (2006) 17:967–978
[2] J.M. Gomez-Vega, E. Saiz, A.P. Tomsia, G.W. Marshall, S.J. Marshall, Bioactive glass coatings with hydroxyapatite and Bioglass particles on Ti-based implants. 1. Processing, Biomaterials 21 (2000) 105-111

BI-O08

The influence of calcium chloride ($CaCl_2$) concentration on apatite precipitation of surface-modified cobalt-chromium (Co-Cr) alloys in a simulated body fluid

Chao LIU[1], Toshiki MIYAZAKI[1*] and Yuki SHIROSAKI[2]
[1]*Graduate School of Life Science and Systems Engineering, Kyushu Institute of Technology, Kyushu Institute of Technology, 2-4 Hibikino, Wakamatsu-ku, Kitakyushu 808-0196, Japan.*
[2]*Frontier Research Academy for Young Researchers, Kyushu Institute of Technology, Kyushu Institute of Technology, 2-4 Hibikino, Wakamatsu-ku, Kitakyushu 808-0196, Japan.*

Keywords: Co-Cr alloys, Apatite, Chemical surface modification

Although there has been an increasingly preferred use of Co-Cr alloys as biomaterials in a variety of biomedical applications such as dentistry, cardiovascular devices and orthopedics, they are poor in bone-bonding ability, i.e. bioactivity [1]. In this research, the bioactivity behavior was investigated through surface chemical modification method by immobilizing cross-linked γ-polyglutamic acid onto Co-Cr alloy by changing the concentration of calcium chloride ($CaCl_2$) pre-treatment before soaking in a simulated body fluid [2]. After soaking in SBF for 4 days, the alloy specimens were characterized by thin-film X-ray diffraction (TF-XRD) and scanning electron microscopy (SEM).

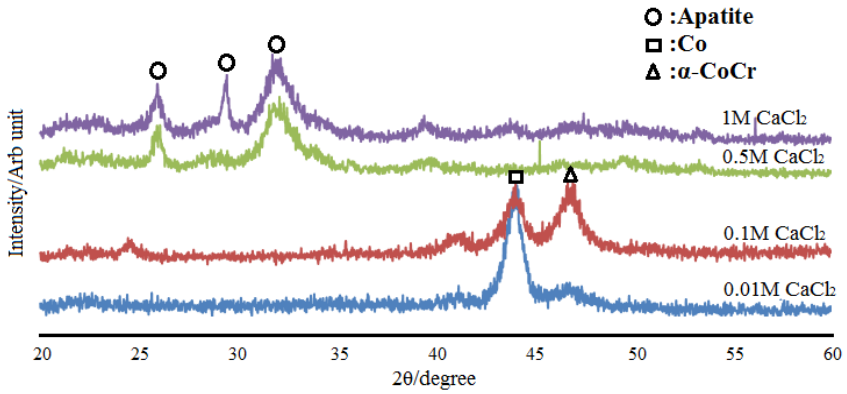

Fig 1. TF-XRD patterns of the surfaces of Co-Cr alloy with different concentration of $CaCl_2$ after soaking in SBF for 4 days

Figure 1 shows TF-XRD patterns of the Co-Cr alloys with different concentration of $CaCl_2$ pre-treatment after soaking in SBF for 4 days. When the Co-Cr alloys were pre-treated with concentration of 0.5 M and 1 M $CaCl_2$ solution, obvious broad peaks at 26° and 32° in 2θ were detected in the diffraction patterns which indicated the apatite were formed on the alloys' surface. However these peaks were not detected from the alloys with treatment of concentration of 0.01 M and 0.1 M $CaCl_2$ solutions. On the other hand, in contrast with low concentration of $CaCl_2$ solution, after pre-treatment with concentration of 0.5 M and 1 M $CaCl_2$ solution, the apatite layer with spherical particles covered were observed on the surfaces from the SEM photographs. The results of this study show that the apatite formation on Co-Cr alloy in SBF could be successfully induced by chemical surface modification with an appropriate concentration of $CaCl_2$ solution, which would lead to the improvement of bioactivity behavior.

References:

[1] R. Bhure, A. Mahapatro, C. Bonner, T.M. Abdel-Fattah, Materials Science and Engineering C(2013)33:2050-2058.
[2] T. Miyazaki, A. Kuramoto, A. Hirakawa, et al. Dental Materials Journal(2013)32: 544–549.

BI-O09

Response of human osteoblast-like cells to different surface modified titanium alloys

J. M. Zhao[1], K. H. Hwang[1*]
[1]*Eng. Res. Inst., Gyeongsang National University, Jinju, 660-701, Korea*

Keywords: Biomaterials, Cell attachment, Cell morphology, Cell proliferation, Osteoblast, Surface modification, Titanium.

Titanium as one kind of biomaterials come in direct contact with the body, making evaluation of biocompatibility an important aspect to biomaterials development. While implants were traditionally allowed to "osseointegrate" over several months without carrying load, clinical and experimental data show that prostheses with roughened surfaces allow successful integration when subject to earlier loading and more challenging implant sites. However, to design implant surfaces for an optimal biological response requires an understanding of the mechanism by which roughened surfaces promote osseointegration.

So our research focus primarily on the response of osteoblastic cells to surface topography in vitro. Our in vitro test used human osteoblast cell MG-63. Cell culture experiments were conducted on surface textures. Titanium samples were chemical treated to produce morphologically similar surfaces with different roughness. Osteoblast attachment and cell viability were conducted by MTT assay and Alamar Blue assay over a different period. In addition, scanning electric microscopy was used to examine cell morphology and cell attachment on each surface, and to visualize specific interactions between cellular structures. The aim of this study was to develop Ti surface modification and to evaluate cell adhesion, proliferation, morphology on modified implant surfaces. NaOH with heat treatment of the samples increased the surface energy and improved its bioactivity further. Also, improved the bioactivity compared to other surface modification.

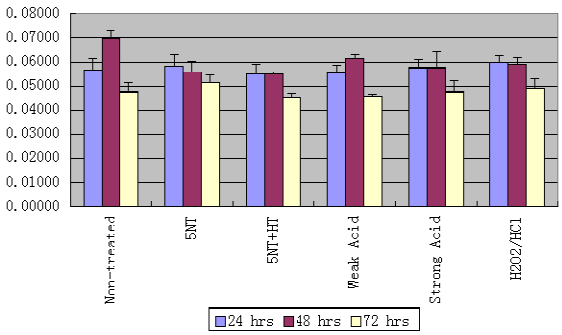

Figure 46 Cell viability after 1day, 2days & 3days culturing

References:

[1] W. Suchanek and M. Yoshimura, J Mater Res, 13 (1998), p. 94–117.
[2] Morra M, Cassinelli C, Bruzzone G, Carpi A, Di Santi G and Giardino R, Int J Oral Maxillofac Implants 18(1), (2003) p. 40–5.

BI-O10

Morphology of hydroxyapatite prepared from single crystals of calcium compounds

Ill Yong KIM*, Koichi KIKUTA, Chikara OHTSUKI
Graduate School of Engineering, Nagoya University, Nagoya 464-8603, Japan

Keywords: Hydrothermal processing, Hydroxyapatite, Single crystal, Solubility

Morphological control on hydroxyapatite (HAp, $Ca_{10}(PO_4)_6(OH)_2$) crystals is one of very important prospects on development of bioactive ceramic materials. Hydrothermal processing has been the subject of much attention for preparation of HAp because it allows formation of HAp crystals with various morphology. HAp morphology formed through the hydrothermal processing depends on the solubility of starting materials because the growth of HAp crystals was decided by dissolution of starting materials [1-3]. In the previous report, the possibility of orientation of HAp crystals was shown [2]. The orientation of HAp crystals could be formed the homogeneous dissolution from single crystal of calcite. The purpose of the present study is to investigate feasibility of well-crystallized HAp crystals with controlled morphology from single crystals of various calcium compounds through a hydrothermal processing. Single crystals of calcium compounds such as calcite ($CaCO_3$), fluorite (CaF_2), calcium tartrate tetrahydrate ($Ca(C_4H_4O_6)\cdot 4H_2O$) were examined in this study. The single crystals were applied to hydrothermal treatment in a phosphate solution for 24 h. Rod-shaped HAp formed on the surface of calcite. Oriented structure of rod-shaped HAp was constructed after hydrothermal treatment of {104} planes on calcite single crystal. Plate-shaped HAp formed on the fluorite while aggregation of nano-sized HAp on the calcium tartrate tetrahydrate was observed after hydrothermal processing. The HAp crystals formed on the single crystals was not morphologically changed with increasing the treatment periods. The difference in the solubility of the starting materials well affected the morphology of HAp formed on their surfaces under the hydrothermal condition, and thus the specific dissolution rate of calcium compound allowed orientation of the rod-shaped HAp crystals.

References:

[1] T. Goto, I. Y. Kim, K. Kikuta and C. Ohtsuki, J. Ceram. Soc. Japan, 120 (2012)131.
[2] I. Y. Kim, K. Kikuta and C. Ohtsuki, Kor, J. Mater. Res. 22 (2012) 397.
[3] I. Y. Kim, K. Kikuta and C. Ohtsuki, Ceram. Int. 40 (2014) 14385.

Acknowledgement:

This work was supported by Grant-in-Aid for Scientific Research on the Innovative Areas: “Fusion Materials (no. 2206)” from the Ministry of Education, Culture, Sports, Science and Technology, Japan (MEXT).

SE-O01

Catalyst-loaded oxide semiconductor yolk-shell nanostructures for gas sensor applications

Ji-Wook YOON[1], Young Jun HONG[2], Yun Chan KANG[1], Jong-Heun LEE[1*]
[1]*Department of Materials Science and Engineering, Korea University, Seoul 136-713, Korea*
[2]*Department of Chemical Engineering, Konkuk University, Seoul 143-701, Korea*

Keywords: Yolk-shell nanostructures, Spray pyrolysis, Gas sensors, Oxide semiconductors

Yolk-shell nanostructures, hollow spheres containing movable cores and multiple thin shells, are attractive nanoarchitectures for various applications in catalysis, batteries, micro-reactors, drug delivery and gas sensors because of high surface-to-volume ratio, rapid mass transfer, and superior tolerance to volume change. In particular, uniform loading of catalyst on yolk-shell nanostructures can enhance the performance of micro-reactors and gas sensors. The template or partial etching of core materials has been used to prepare multiple shelled yolk-shell oxide semiconductors. However, synthetic route requires prolonged multi-step processes, which hampers the application of yolk-shell nanostructures. In this contribution, SnO_2 yolk-shell nanostructures uniformly loaded with Pd or Ag catalysts were prepared by one-pot spray pyrolysis of precursor solution containing noble metal precursors, Sn-oxalate, sucrose and nitric acid and subsequent heat treatment. The catalyst-loaded SnO_2 yolk-shell nanostructures were prepared by the following steps during one-pot spray pyrolysis reaction: (a) the formation of catalyst-carbon-Sn precursor composite spheres by polymerization and carbonization of sucrose, (b) the development of outermost catalyst-loaded SnO_2 shells by the partial oxidation of carbon and decomposition of precursors near the surface, (c) and subsequent oxidation and decomposition of interior portion of precursors. The dense, yolk-shell, and catalyst-loaded yolk shell SnO_2 spheres were prepared and their gas sensing characteristics were compared to investigate the effect of catalyst loading and yolk-shell morphology on the gas sensing characteristics

The Ag-loaded SnO_2 yolk-shell spheres showed ultrahigh and reversible response (R_a/R_g - 1= 613.9, where R_a is the resistance in air and R_g is the resistance in gas) to 5 ppm H_2S with negligible cross-responses (0.6−17.3) to other 8 interference gases at 350°C [1]. In contrast, neither high response/selectivity to H_2S nor reversible H_2S sensing characteristic was observed both in pure SnO_2 spheres with dense inner structures and yolk-shell morphology. The superior H_2S sensing characteristics were attributed to the enhancement of H_2S response via gas accessible yolk-shell morphology, selective and sensitive detection of H_2S via the strong chemical interaction between Ag and H_2S, and Ag-induced suppression of SO_2-related poisoning of SnO_2 surface.

The Pd-loaded SnO_2 yolk-shell spheres showed high response to methyl benzenes (*o*-xylene and toluene) with low cross-responses to C_2H_5OH, HCHO, benzene, H_2, CO, and CH_4 at 350°C and 375°C [2]. In contrast, both dense and pure SnO_2 yolk-shell spheres showed the highest response (R_a/R_g; R_a: resistance in air, R_g: resistance in gas) to C_2H_5OH at 350-450°C. The selective and sensitive detection of methyl benzene in Pd-loaded SnO_2 yolk-shell spheres are attributed to the synergetic combination between the effective in-diffusion of *o*-xylene and toluene through thin and semipermeable shells and their subsequent dissociation into smaller and active species by catalytic Pd particles on yolk or inner part of the shell. This clearly shows that the micro-reactors using catalyst-loaded yolk-shell nanostructures provide promising nanoarchitectures to design high performance gas sensors.

References:

[1] J.-W. Yoon, Y.J. Hong, Y.C. Kang, and J.H. Lee, RSC Advances 4 (2014) 16067.
[2] Y.J. Hong, J.-W. Yoon, Y.C. Kang, and J.H. Lee, Chem. Eur. J. 20 (2014) 2737.

PI-O01

PZT-PZNN Ceramics for Energy Harvesting and Multilayer Actuator Applications

Joon HUR[1], Dae-hyeon KIM[2], In-Tae SEO[2], Sahn NAHN[1, 2*]

[1]*Department of Nano Bio Information Technology, KU-KIST Graduate School of Converging Science and Technology, Anam-dong 5-ga, Seongbuk-gu, Seoul 136-701, Korea*

[2]*Department of Materials Science and Engineering, Korea University, Anam-dong 5-ga, Seongbuk-gu, Seoul 136-701, Korea*

Keywords: Piezoelectric Ceramics, Energy Harvesting, Multilayer, Actuator

Microstructural and piezoelectric properties of the $0.72Pb(Zr_{1-x}Ti_x)$-$0.28Pb(Zn_{0.4}Ni_{0.6})NbO_3$ ($PZ_{1-x}T_x$-PZNN) ceramics with $0.50 \leq x \leq 0.55$ have been investigated for the application to the actuators and energy harvesters, which have multilayer structure. These devices require a large piezoelectric strain constant (d_{33}) and a small dielectric constant ($\varepsilon^T_{33}/\varepsilon_o$). The $PZ_{0.47}T_{0.53}$-PZNN ceramic having a morphotropic phase boundary (MPB) composition shows the large d_{33} and $\varepsilon^T_{33}/\varepsilon_o$ values, which is not a suitable material for such devices. However, the $PZ_{0.48}T_{0.52}$-PZNN ceramic, which has a pseudo-cubic structure, shows a small $\varepsilon^T_{33}/\varepsilon_o$ of 1605 due to a large remnant polarization but still maintains a high d_{33} of 550 pC/N. In addition, although the $\varepsilon^T_{33}/\varepsilon_o$ value slightly increased when the specimen was heated at 150°C for 4 h, the effect of thermal stimulation was not significant. Moreover, the CuO-added $PZ_{0.48}T_{0.52}$-0.28PZNN ceramic was well sintered at low temperature of 900°C. In particular, the 1.0 mol% CuO-added $PZ_{0.48}T_{0.52}$-0.28PZNN ceramic exhibited the large d_{33} value of 554 pC/N and small $\varepsilon^T_{33}/\varepsilon_o$ of 1582, indicating that this material is a good candidate for the multilayer actuators and energy harvesters.

PI-O02

Mechanical Energy Harvesters Utilizing (001) Textured PZT Films on Flexible Metal Foils

Hong Goo YEO[1], Charles B. YEAGER[1], Thomas N. JACKSON[2], Christopher RAHN[3], Xiaokun MA[3], and Susan TROLIER-MCKINSTRY[1]
[1]*Department of Materials Science and Engineering, The Pennsylvania State University, University Park, Pennsylvania, 16802, USA*
[2]*Department of Electrical Engineering, The Pennsylvania State University, University Park, Pennsylvania, 16802, USA*
[3]*Department of Mechanical Engineering, The Pennsylvania State University, University Park, Pennsylvania, 16802, USA*

Keywords: Piezoelectric energy harvester, PZT films, texture, Metal foils

Recently, interest in extracting energy from human activities such as walking, breathing, typing, and so on using piezoelectric energy harvester is growing.[1~3] However, there are unique challenges to self-powering wearable devices from a user's activities such as weak base excitation, potential damage to fragile structure by shock input, and the low vibration frequency (<10Hz). Thus, a high efficiency, flexible, low resonance frequency harvester with a wide bandwidth is needed. Piezoelectric Compliant Mechanism (PCM), suggested by Ma and Rahn, shows a significantly higher efficiency with uniform strain for its 1st mode, than a simple cantilever design with the strain decreases along the length of the PZT beam. So, higher sensitivity, efficiency and larger power are predicted as compared with that of PCM at low frequency mechanical vibration.

This work shows that strongly {001} oriented PZT could be deposited by RF magnetron sputtering and ex situ annealing on (100) oriented $LaNiO_3$ / HfO_2 / Ni foils. Based on this design, the PCM design with PZT films on Ni foil consists of three main structures such as PZT beam, flexible frame used for compliant hinge and rigid frame for support structure by 2.9 mm thick acrylic plate. The performance of PCM with actual device area of 6.34 cm^2 exhibits an average power of 7.5 μW response at a 0.1 G (G=9.8 m/s^2) excitation level at a resonance frequency of 7.8 Hz after hot poling to align the c-domains out-of-plane. Table 1 exhibits the power performance generated with various excitation accelerations and area power density at 7.8Hz.

Table 1. Performance of PCM harvesting devices at various excitation levels.

Acceleration [G] @ 7.8Hz	Output voltage [mV](R_{opt} = 40kΩ)	Max. Power [μW]	Prms [μW]	Power Density (Power/area×G^2) [μW/cm^2×G^2]	FoM = Power density/Res.Freq
0.4	1340	44.89	22.5	22.1	2.83
0.3	1240	38.44	19.2	33.7	4.32
0.2	990	24.5	12.3	48.3	6.19
0.1	775	15.02	7.5	118.5	15.19

References:

[1] P. Pillatsch, E. M Yeatman, A. S. Holmes, Sensors and Actuators A 206, 178 (2014)
[2] J. Yun, S. N. Patel, M. S. Reynolds, G. D. Abowed, Computing 8, 1 (2010).
[3] J. M. Donelan, Q. Li, V. Naing, J. A. Hoffer, D. J. Weber, A. D. Kuo, Science 319, 807 (2008).

Acknowledgement:

This work was supported by a National Security Science and Engineering faculty fellowship and the NSF ASSIST ERC (EEC-1160483).

PI-O03

Exceptionally High Magnetoelectric Characteristics in Laser Annealed PZT Thick Films on Magnetostrictive Metglas Foil

Haribabu PALNEEDI[1,2], Ju-Eun KANG[2], Deepam MAURYA[3], Shashank PRIYA[3], Suk-Joong L. KANG[1*], and Jungho RYU[2]

[1] *Materials Interface Laboratory, Department of Materials Science and Engineering, Korea Advanced Institute of Science and Technology (KAIST), Daejeon, Republic of Korea*

[2] *Functional Ceramics Group, Korea Institute of Materials Science (KIMS), Changwon, Republic of Korea*

[3] *Center for Energy Harvesting Materials and Systems (CEHMS), Virginia Tech, Blacksburg, VA, USA*

Keywords: Thick Film, PZT, Metglas, Laser Annealing, Magnetoelectric

Engineered magnetoelectric (ME) composites or heterostructured films of magnetostrictive–piezoelectric constituents exhibit stronger ME interactions which are mediated by magnetically induced mechanical forces. These ME composites are attractive, for potential applications in sensors, transducers, and energy harvesting devices, because of their unique magnetic-electric transduction. In this work, we report exceptionally high ME output observed in composites of laser annealed lead zirconate titanate (PZT) thick films and Metglas (FeBSiC alloy). Highly dense piezoelectric films of PZT with layer thickness 2-6 μm were deposited onto amorphous magnetostrictive Metglas (25 μm-thick) by aerosol deposition and then annealed using continuous-wave Yb-doped fiber laser irradiation (560 nm wavelength). Laser annealing was employed to induce grain growth in the as-deposited PZT films and to avoid thermal damage of the substrate so that its inherent magnetostrictive characteristics would be intact. X-ray diffraction and scanning electron microscopy results revealed that single phase, well-bonded and crack-free PZT thick films were formed and no interfacial reaction between the PZT and Metglas phases took place. The laser annealed thick films showed largely improved dielectric, ferroelectric properties compared to as-deposited ones. The PZT/Metglas thick film composites were found to exhibit magnetoelectric voltage coefficients in the range of 200-1500 mV/cm.Oe under a very low bias magnetic field of 30 Oe. The results of the present work demonstrate the applicability of laser annealing in the fabrication of thick film magnetoelectric composites with enhanced properties.

PI-O04

High Temperature Nano-grained PbTiO3 Thick Film by Aerosol-Deposition

Jungho RYU[1]*, Si-Young CHOI[1], Susan TROLIER-McKINSTRY[2], Hongsoo CHOI[3], Shashank PRIYA[4], Jong-Woo KIM[1], Woon-Ha YOON[1], Jong-Jin CHOI[1], Dong-Soo PARK[1], Cheol-Woo AHN[1], Byung-Dong HAHN[1], Dae-Yong JEONG[5]

[1]*Functional Ceramics Group, Korea Institute of Materials Science (KIMS), Korea.*
[2]*Materials Research Institute, The Pennsylvania State University, USA*
[3]*Bio-Micro Robot Lab, Daegu Gyeongbuk Institute of Science and Technology (DGIST), Korea*
[4]*Center for Energy HarvestingMaterials and Systems (CEHMS), Virginia Tech, USA*
[5]*School of Materials Engineering, Inha University, Incheon 402-751, Republic of Korea*

Keywords: $PbTiO_3$, thick film, aerosol-deposition, high temperature

In this research, thick polycrystalline $PbTiO_3$ films on Platinized Si wafer with nano size grains (several tens to 200 nm) and high density were successfully deposited by aerosol deposition. Annealed at 700 °C seven micron thick films exhibit well-saturated ferroelectric hysteresis loops with a remanent polarization and coercive field of 35 μC/cm^2 and 94 kV/cm, respectively. A large-signal effective $d_{33,eff}$ value of > 60 pm/V is achieved at room temperature. The measured ferroelectric transition temperature (T_c) of the films ~ 550°C is >50°C higher than the reported values (~490°C) for $PbTiO_3$ ceramics. First principles calculations combined with electron energy loss spectroscopy (EELS) and structural analysis indicate that the film is composed of nano size grains with slightly decreased tetragonality. There is no severe off-stoichiometry, but a high compressive in-plane residual stress was observed in the film along with a high transition temperature and piezoelectric response. The ferroelectric characteristics were sustained above 250°C providing significant advancement towards realizing high temperature piezoelectric materials.

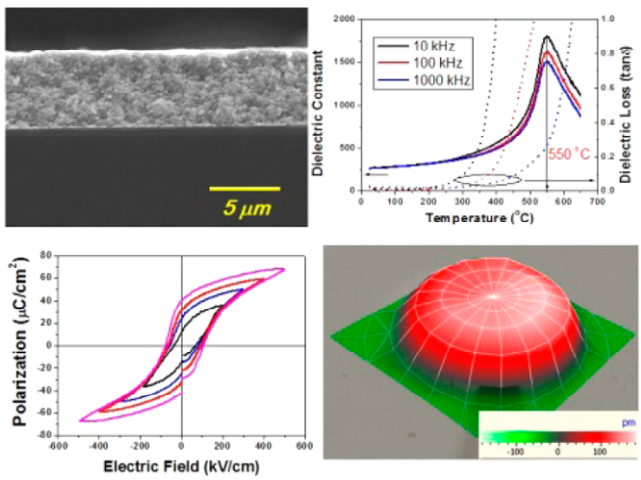

Figure 47 SEM micrograph and electrical properties of $PbTiO_3$ thick film

References:
[1] J. Ryu et al, ACS Applied Materials and Interface, 6, 11980-11987 (2014)

Acknowledgement:
This research was supported by the Basic Science Research Program through the National Research Foundation of Korea (NRF-2012R1A1A2A10041947) and the Global Frontier R&D Program (2013-073298) on Center for Hybrid Interface Materials (HIM) funded by the Ministry of Science, ICT & Future Planning.

PI-O05

Prototype of a Micro Piezoelectric Ultrasonic Motor

Tomoaki MASHIMO[1]
[1]*Electronics-inspired Interdisciplinary Research Institute, Toyohashi University of Technology, Hibarigaoka Tempakucho Toyohashi Aichi 441-8580 Japan*

Keywords: Actuators, Piezoelectricity, micro-robotics.

Piezoelectric ultrasonic motors are expected as the most prominent micromotors for actuating miniature devices that can help minimally invasive diagnoses and treatments, such as endoscopes and catheters. They have two advantages for miniaturization: (1) high energy densities with high torques at low speeds without a gear and (2) simple structures using simple components. In front line of ultrasonic motor miniaturization, prototypes using few millimeter stators have succeeded in generating rotation.

I have proposed a prototype micro ultrasonic motor consisting of a cubic stator with a volume of approximately one cubic millimeter [1]. An advantage of this motor is the use of a vibration mode that generates three waves around the circumference of the hole in the stator. This mode, independent of the length of the stator, can generate a certain magnitude of vibration amplitude, even if the size is reduced to as little as 1 mm. Also, the simple structure of the motor makes the size miniaturized without using any special machining process. In this study, I build and demonstrate the performance of a prototype micro ultrasonic motor. Figure shows the prototype motor: one cubic millimeter stator with four piezoelectric elements at sides and the rotor inserted into the through-hole of the stator.

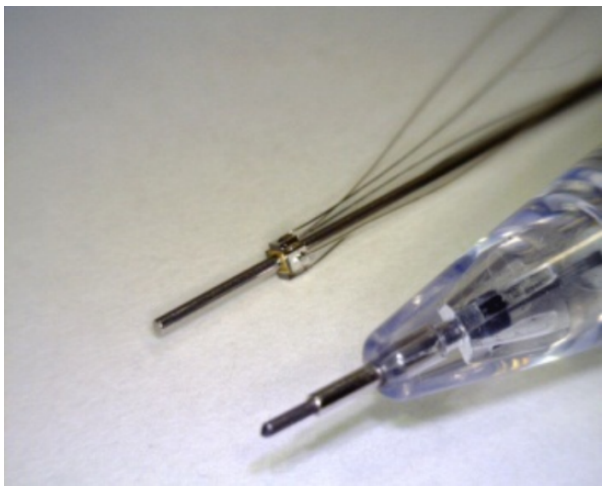

Figure 48 Prototype Micro Ultrasonic Motor

References:

[1] T. Morita, "Miniature piezoelectric motors," Sensors and Actuators A: Physical, vol. 103, pp. 291-300, 2003.
[2] T. Mashimo, "Micro ultrasonic motor using a one cubic millimeter stator," Sensors and Actuators A: Physical, vol. 213, pp. 102-107, 2014.

PI-O06

Piezoelectric Multi-layer Ceramics for Haptic Actuator

In-Tae Seo[1], Joon Hur[2], Jong-Hyun Kim[1], Tae-Ho Lee[1], Sahn Nahm[1,2*]
[1]*Department of Materials Sci. and Eng., Korea University, Seoul, 136-713, Korea*
[2]*KU-KIST Graduate School of Conversing Sci. and Tech., Korea University, Seoul, 136-701, Korea*

Keywords: Piezoelectric, Multi-layer, Actuator, Haptic, Microstructure

For the development of future piezoelectric actuator x mol% CuO added PZT-PZNN [CxPZT-PZNN] ceramics was investigated. The dielectric constant of CxPZT-PZNN ceramics could be controlled by CuO addition and sintering temperature. At the critical size of grain, the ceramic showed minimum dielectric constant. The piezoelectric properties such as d_{33}, k_p and Q_m were independent of grain size. Maximum strain of C0.5PZT-PZNN ceramics was 0.151% at 3kV and it also showed a high strain of 0.014% at 110V which is haptic operation voltage. Moreover, C0.5PZT-PZNN ceramics had excellent fatigue property and their strain behavior was maintained during 10^6 cycle. Therefore, C0.5PZT-PZNN ceramic sintered at 900^{o}C are suitable for piezoelectric vibration actuator because of their high piezoelectric properties and low dielectric constant. The 3-layers C0.5PZT-PZNN MLCs were well fabricated with Ag electrode using tape casting method. And using 3-layers C0.5PZT-PZNN MLC, the piezoelectric vibration actuator was well produced and it showed high vibration acceleration of 2.1G at the resonance frequency of 210 Hz. Moreover, because the capacitance of C0.5PZT-PZNN MLC actuator was very low (20nF) than that of commercial actuator, it is expected that the power consumption of piezoelectric vibration actuator using C0.5PZT-PZNN MLC will be minimized. Therefore, the C0.5PZT-PZNN ceramics is a good candidate for multi-layer piezoelectric actuator and piezoelectric vibration actuator using C0.5PZT-PZNN MLC is suitable for haptic devices for portable components.

PI-O07

Enhancement of Multiferroic Properties in Nanoheterostructured Multilayer Bismuth Ferrite Thin Films

V. Annapu Reddy[1,2,a], and R. Nath[1]

[1]*Functional Ceramics Research Group, Korea Institute of Materials Science (KIMS), Gyeongnam, 641-831, Korea*

[2]*Ferroelectric Materials and Devices Research Laboratory, Department of Physics, Indian Institute of Technology Roorkee, Uttarakhand 247667 India*

Multilayered nano-heterostructured $Bi_{0.9}La_{0.1}Fe_{0.9}Mn_{0.1}O_3$-$BiFeO_3$ (BLFM-BFO) thin films were grown on $Zn_{0.91}Cr_{0.09}O$ buffered Si (100) substrate by chemical solution deposition. Structural analysis indicates that the crystal structure of BLFM film is orthorhombic in contrast to BFO, which is rhombohedral. Reduced leakage current, and increased ferroelectric saturation of multilayer thin films were obtained and compared with those of BFO and BLFM thin films. Improved ferroelectric properties, as well as induced ferromagnetism, were observed for multilayer thin films. The resultant improvements have been attributed to the interface coupling interaction between the thin layers. To better understand the effect of interface coupling on the order of heterojunctions, the order of BFO and BLFM layers in the multilayer thin film has been altered. These nano-hetrostructured thin films have been deposited under the same fabrication conditions and investigated. A significant improvement in the interface coupling and interface constrained effect between the thin multiferroic layers has been observed. These films also exhibit enhancement in ferroelectric fatigue up to 10^8 switching cycles.

PI-O08

Effects of Na excess on dielectric and electrical properties of $(Na_{0.53+x}K_{0.47})$ $(Nb_{0.55}Ta_{0.45})$ O_3 ceramics

M. S. Kim[1], J. S. Kim[1], T. K. Song[1], W. J. Kim[2], M. H. Kim[1*]
[1]*School of Advanced Materials Engineering, Changwon National University, Gyeongnam 641-773, Republic of Korea*
[2]*Department of Physics, Changwon National University, Gyeongnam 641-773, Republic of Korea*

Keywords: Lead-free, Piezoelectric, NKN based ceramics

Lead-based piezoelectric materials, such as lead zirconate titanate (PZT), lead lanthanum zirconate titanate (PLZT) and lead magnesium niobate (PMN) are widely used in filters, resonators, actuators and sensors because of their excellent piezoelectric properties. However, the legislations such as RoHS/WEEE (Restriction of Hazardous Substances / Waste Electrical and Electronic Equipment) demand for lead-free alternatives. Lead-free $Na_{0.5}K_{0.5}NbO_3$ (NKN) based ceramics have been considered as one of the superior lead-free candidate materials to replaced lead-based PZT ceramics because of theirs excellent piezoelectric properties and high curie temperature. However, pure NKN has a poor piezoelectric coefficient and sinterability.[1] Recently, we have investigated that $(Na_{0.545}K_{0.47})$ $(Nb_{0.55}Ta_{0.45})O_3$ ceramic has high piezoelectric coefficient d_{33} = 333 pC/N. It has been reported that Na excess play an important role in enhancement of piezoelectric properties.[2]

During sintering process, due to volatile nature in NKN ceramics, Na and K ion create the alkali-ion vacancies due to their volatility. Furthermore, to retain the charge neutrality, the alkali vacancies make the oxygen vacancy which decrease sample density.[3]

In this work, A-site excessed $(Na_{0.545}K_{0.47+x})(Nb_{0.55}Ta_{0.45})O_3$ (x = -0.01, -0.005, 0, 0.005, 0.01) ceramics were synthesized at various calcination temperatures using Na_2CO_3 and K_2CO_3 as A-site starting materials. It is worth to note that the melting points of Na_2CO_3 and K_2CO_3 are 851 and 891 ^oC, respectively, [4] which can make liquid phases at different temperatures. Calcination temperature effect on piezoelectric properties of the A-site excessed $(Na_{0.545}K_{0.47+x})(Nb_{0.55}Ta_{0.45})$ along with microstructural changes will be discussed in details.

References:

[1] Li at el, J. Am. Ceram. Soc. 96[12], (2013) 3677-3696.
[2] Y. S. Sung et al, Appl. Phys. Lett., 101, 012902 (2012).
[3] N. M. Hagh et al, J. Electroceram. 18 (2007) 339-346
[4] P. Bomlai et al, J. Am. Ceram. Soc. 90[5], (2007), 1650-1655

Acknowledgement:

This work was supported by Basic Science Research Program through the National Research Foundation of Korea (NRF) funded by Ministry of Education, Science and Technology (MEST) (2011-0030058).

LP-O01

Effect of Firing Temperature and DC Poling on Acoustic Wave Velocities in Barium Titanate Piezoelectric Ceramics

Taiki IKEGAYA, Toshio OGAWA*
Department of Electrical and Electronic Engineering, Shizuoka Institute of Science and Technology, Fukuroi, Shizuoka 437-8555, Japan

Keywords: Acoustic wave velocities, Piezoelectric ceramics, Young's modulus, Poisson's ratio

The longitudinal and transverse wave velocities in barium titanate (BT) ceramics made by different firing temperatures were measured using an ultrasonic precision thickness gauge with high-frequency pulse generation to evaluate elastic constants, such as Young's modulus and Poisson's ratio [1, 2]. With increasing firing temperature, the longitudinal and transverse wave velocities increased, as a result, Young's modulus increased because of BT ceramics being mechanical hard (Figure 1). Poisson's ratio after DC poling, however, was almost independent of the firing temperature since Poisson's ratio is an intrinsic materials constant. It was found that there was an important factor for giving piezoelectricity regarding changes in Young's modulus and Poisson's ratio after DC poling in comparison with before poling, that is, lowering Young's modulus and enhancing Poisson's ratio. Furthermore, the increase in modulus of rigidity and bulk modulus increased with firing temperature because of the increase in the ceramic bulk density. The modulus of rigidity decreases and bulk modulus increases after poling because of domain alignment.

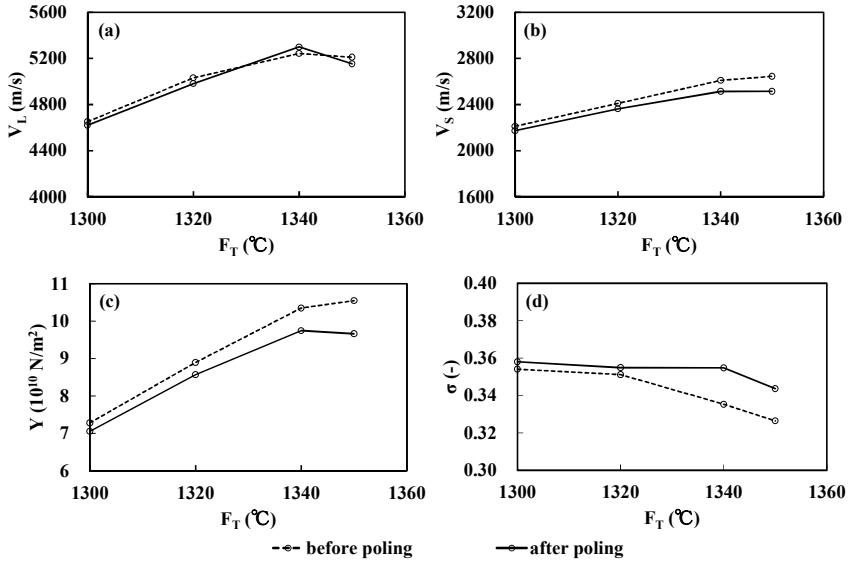

Figure 1 Firing temperature (F_T) vs (a) longitudinal wave velocity (V_L), (b) transverse wave velocity (V_S), (c) Young's modulus (Y) and (d) Poisson's ratio (σ) in BT ceramics before and after DC poling

References:

[1] T. Ogawa and T. Nishina: *Advances and Applications in Electroceramics II*, eds. K. M. Nair and S. Priya (Wiley, Hoboken, 2012) Ceramic Transactions, Vol. 235, p. 105.

[2] T. Ogawa: *Piezoelectric Materials and Devices - Practice and Applications*, ed. F. Ebrahimi (InTech, Rijeka, 2013) p. 35.

Acknowledgement:

This work was partially supported by Grant-in-Aids for Scientific Research C (Nos. 21560340 and 26420282), a Grant of Strategic Research Foundation Grant-aided Project for Private Universities 2010-2014 (No. S1001032) from the Ministry of Education, Culture, Sports, Science and Technology, Japan (MEXT), and a Research Foundation 2014 between Academy and Industry of Fukuroi City, Shizuoka, Japan.

LP-O02

Electric properties of unmodified $BiFeO_3$-$BaTiO_3$ ceramics system by using tape casting method

Dajeong KIM[1], Myanghwan LEE[1], Jinsu PARK[1], Myong-Ho KIM[1], Taekwon SONG[1*], Dalhyun DO[2], Ho-Yong LEE[3]

[1]*School of Mat. Eng., Changwon Nat'l Univ., Gyeongnam 641-773, Korea*
[2]*Department of Advanced Mat. Eng., Keimyung Univ., Daegu 704-701, Korea*
[3]*Ceracomp Co., Ltd., Cheonan-si, Chungcheongnam-do, Korea*

Keywords: MLCC, Tape casting, $BiFeO_3$, $BaTiO_3$,

$BiFeO_3$–$BaTiO_3$ (BF–BTx) solid solution bulk ceramic is presented as potential lead-free piezoelectric ceramic. The phase diagram of BF-BTx material show morphotropic phase boundary (MPB) at x = 33 mol% region, which is coexistence of both rhombohedral ($BiFeO_3$) and tetragonal ($BaTiO_3$) phase, the result of excellent piezoelectric properties in BF-BT33 system can be expected [1,2]. For the piezoelectric application, it is needed for the Multi-layer ceramic capacitor (MLCC) made by using tape casting or screen printing process. Fujii and co-workers reported Mn-modified BF-BT-$Bi(Mg,Ti)O_3$ ternary ceramics, however, unmodified BF-BT based ceramics have not been achieved yet [3]. We have investigated 0.67BF-0.33BT (BF-BT33) ceramic prepared using tape casting method showed high Tc, of ~ 470 °C, and piezoelectric constants d_{33} and d_{33}* were 163 pC/N and 260 pm/V in ceramics quenched at temperature of 960 °C.

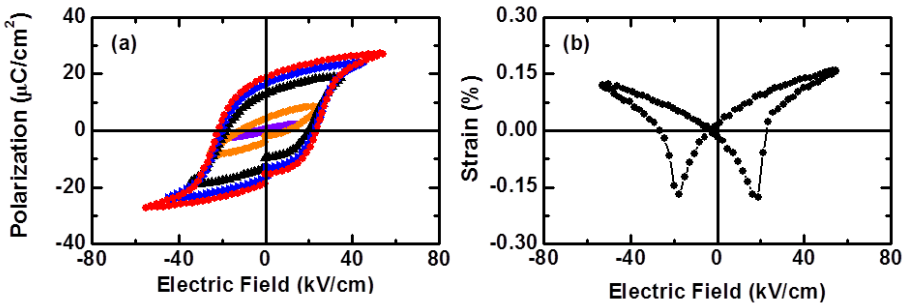

Figure 49 (a) Ferroelectric hysteresis loops and (b) The *S*- *E* curves of unmodified BF-BT ceramic

References:

[1] M. M. Kumar, A. Srinivas, and S. V. Suryanarayana, J. Appl. Phys. 87, 855 (2000).
[2] D. J. Kim, M. H. Lee, J. S. Park, M-H. Kim, T. K. Song, S. W. Kim, W-J. Kim, K. W. Jang, S. S. Kim, D. Do, J. Electrom. online published (2014) DOI: 10.1007/s10832-014-9912-6.
[3**]** I. Fujii, R. Mitsui, K. Nakashima, N. Kumada, M. Shimada, T. Watanabe, J. Hayashi, H. Yabuta, M. Kubota, T. Fukui, and S. Wada, Jpn. Jour. Appl. Phys. 50, 09ND07 (2011)

Acknowledgement:

This work was supported by the National Resarch Foundation of Korea [KRF] grant funded by the Korea government [MSIP] (2012-0007403, and 2012-0009457) and by the Priority Research Centers Program through the National Research Foundation of Korea (NRF) funded by the MEST (2013R1A1A4A01010612, 2012-045424) and by the Technology Innovation Program (10047914, Development of "Lead-free" Piezoelectric Materials of Electromechanical Coupling Factor k33 > 0.85) funded by the Ministry of Trade, Industry and Energy (MOTIE, Korea).

LP-O03

Evaluation of single crystal growth behaviour of $(K_{0.5}Na_{0.5})NbO_3$-$SrTiO_3$ lead free piezoelectric ceramics grown by the solid state crystal growth (SSCG) method

Muhammad Umer FAROOQ and John G. FISHER*
School of Materials Science and Engineering, Chonnam National University, Gwangju 500-757, Republic of Korea

Keywords: lead free piezoelectric material, single crystal growth, microstructure

Lead free piezoelectric ceramics are being developed due to concerns over the health issues of high lead content in conventional lead zirconate titanate piezoelectric ceramics. However, their piezoelectric properties are as yet inferior to those of $Pb(Zr,Ti)O_3$. In order to improve their piezoelectric properties, single crystal growth of lead-free piezoelectric ceramics is being actively studied. Single crystals of $(K_{0.5}Na_{0.5})NbO_3$ (KNN) based ceramics have good piezoelectric properties but conventional crystal growth techniques require specialized furnaces and expensive Pt crucibles. The solid state crystal growth (SSCG) method has been employed to grow single crystals of lead free KNN based ceramics owing to its ease of processing and use of relatively low cost equipment.

In the present work, the single crystal growth by SSCG of $(100\text{-}x)(K_{0.5}Na_{0.5})NbO_3$-$xSrTiO_3$ (KNN-ST), where x= 0,1,2,3 has been examined. Powders are prepared by the conventional mixed oxide method. XRD analysis is performed to verify the single phase perovskite structure of the powders. A <001> $KTaO_3$ seed crystal is buried in the center of the powders and pressed into a pellet. These pellets are then sintered at 1100°C for 1h, 3h, 5h and 10h. A single crystal of the ceramic composition grows onto the seed. Samples are vertically sectioned using a low speed diamond wheel saw, polished, thermally etched and the microstructure examined by Scanning Electron Microscopy. For the KNN sample, both single crystal growth and abnormal grain growth in the matrix begin to take place within one hour. As the amount of $SrTiO_3$ in the KNN-ST solid solution increases, the onset of both single crystal growth and abnormal grain growth are delayed. The effect of $SrTiO_3$ addition on the single crystal and matrix grain growth behavior is explained in terms of the interface reaction-controlled theory of grain growth.

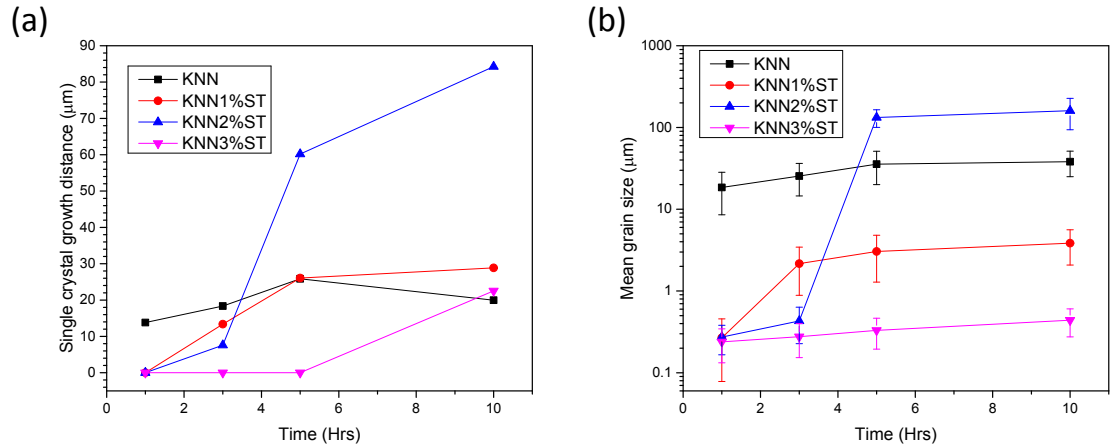

Figure 1 (a) single crystal growth distance and (b) mean matrix grain size of $(100\text{-}x)(K_{0.5}Na_{0.5})NbO_3$-$xSrTiO_3$ (KNN-ST) samples sintered at 1100°C for 1 - 10h.

LP-O04

Piezoelectric properties of Lead-free $0.5Ba(Ti_{0.8}Zr_{0.2})O_3$-$0.5(Ba_{0.7}Ca_{0.3})TiO_3$ epitaxial thin films grown onto Si (001) substrate by Pulsed Laser Deposition for Energy Harvesting Applications

Jae-Ryong LIM[1], TRAN Mhan Trung[2], and Soon-Gil YOON[1,2*]
[1]*Advanced Electronic Circuit Substrate Engineering, Chungnam National University, Daeduk Science Town, Daejeon, 305-764, South Korea*
[2]*Department of Materials Engineering, Chungnam National University, Daeduk Science Town, Daejeon, 305-764, South Korea*

Keywords: Piezoelectric thin films, $0.5Ba(Ti_{0.8}Zr_{0.2})O_3$-$0.5(Ba_{0.7}Ca_{0.3})TiO_3$ (BZT-BCT), Lead-free, Pulsed laser deposition (PLD)

Energy harvesting from irregular mechanical actions in variable and uncontrollable environments is an effective approach for powering wireless mobile electronics to meet a wide range of applications in our daily life. Piezoelectric thin film is robust and can be stimulated by tiny physical motions over a range of frequencies. $PbZrTiO_3$ (P ZT) is most widely used as piezoelectric ceramic, and it is faced on worldwide criticism due to its lead toxicity, so there is need to find a lead free piezoelectric material which is comparable to PZT. There is report that lead free piezoelectric ceramic system $0.5Ba(Ti_{0.8}Zr_{0.2})O_3$-$0.5(Ba_{0.7}Ca_{0.3})TiO_3$ (BZT-BCT) which shows a surprisingly high piezoelectric coefficient of d_{33} = 620 pC/N at optimal composition, it is comparable PZT's piezoelectric coefficient (PZT has d_{33} = 500 - 600 pC/N). So, BZT-BCT is the best candidate of piezoelectric ceramics for energy harvesting applications.

We studied about BZT-BCT thin films grown at high temperature on LSCO/CeO_2/YSZ/p-Si(100) substrates using pulsed laser deposition (PLD) and Pt thin films were prepared as top electrode by DC sputtering. $La_{0.5}Sr_{0.5}CoO_3$ (LSCO) thin films is a bottom electrode and it was deposited at various temperature (450~650℃) and minimum resistivity is $2.2\times10^{-3}\Omega$cm at 550℃. CeO_2 and Yttria Stabilized Zirconia (YSZ) thin films used as buffer layer for epitaxial growth of BZT-BCT thin films. XRD results reveal (100) preferred orientation of BZT-BCT and LSCO thin films and full width at half maximum (FWHM) of rocking curve is 2.63° and 2.19° each. and We can see 4 fold symmetry of all thin films through phi-scan measurement. Also, Polarization Electrical field loop and leakage current of BZT-BCT were measured, Remnant polarization (Pr) is 5.5μC/cm^2 and coercive field (Ec) is 15kV/cm

References:

[1] W. Liu and X. Ren, *Phys. Rev. Lett.* 103, 257602 (2009).

LP-O05

Performance Stabilized Lead-free Piezoelectric Ceramics: (Li, Na, K)(Nb, Ta)O_3 Modified by $BaZrO_3$

Fangyuan ZHU*, Ke Wang and Jing-Feng LI
State Key Laboratory of New Ceramics and Fine Processing, School of Materials Science and Engineering, Tsinghua University, Beijing, 100084, China

Keywords: Lead-free, Sodium Potassium Niobates, Piezoelectric Ceramics

Lead zirconate titanate (PZT) has been dominated commercial manufacturing over several decades to become the market-leading piezoelectric ceramic. Legislation arising from health and environmental concerns has intensified research into finding suitable alternatives to lead-based electroceramics. Solid solutions based on sodium potassium niobates (K, Na)NbO_3 (shorten as KNN) has become one of the global-desired lead-free piezoelectric ceramics in nowadays due to its superior dielectric and piezoelectric properties.

$LiTaO_3$ doped to the perovskite KNN structure (KNNLT) would adjust Na/K ratio, which enhances the piezoelectric properties and significantly lowers the orthorhombic to tetragonal phase transition (T_{O-T}) to the room temperature. Whereas it introduces the coexistence of O/T phase and promotes the piezoelectric response. Also, KNNLT-$BaZrO_3$ (KNNLT-BZ) solid-solution system has been reported to have the optimal piezoelectric charge coefficient about 340-360 pC/N and high level of unipolar strain up to 0.16% at ambient temperature. Most interesting part for the KNNLT-BZ piezoceramics is the temperature stability of field-induced strain under a wide range of temperatures. The effect of $BaZrO_3$ addition on the piezoelectric response has been studied, which piezoelectric properties suggested it could be one of possible candidates for actuator application design purpose.

Acknowledgement:
Authors would like to appreciate the funding and kindly support by the National Nature Science Foundation of China (Grants No. 51332002)

LP-O06

Enhanced Low-Field Strain in Lead-Free Ferroelectric-Relaxor Composite Ceramics

Thi Hinh DINH[1], Chang-Ho YOON[1], Jin-Kyu KANG[1], Young-Hwan HONG[1],Mohammad Reza BAFANDEH[2], and Jae-Shin LEE[1*]

[1]*School of Materials Science and Engineering, University of Ulsan, Nam-Ulsan, 680-749, Republic of Korea*

[2]*Department of Metallurgy, University of Kashan, Ravand Blvd, Kashan, I.R.Iran*

Keywords: Piezoelectric, Composite, Relaxor, Strain, Ceramics

Recently, BNKT ceramics have attracted much attention because of their large electric field-induced strains (EFIS) at ferroelectric (FE) – relaxor ferroelectric (RFE) phase boundaries. However, a critical problem that hinders their practical application to actuators is the fact that large strain in Bi-based lead-free ceramics is obtained only at high electric fields sufficient to induce a FE-RFE phase transition. To lower the critical field (E_{crit}) that can cause the FE-RFE phase transition, FE-RFE composite ceramics were studied in this work. The effects of $0.82(Bi_{1/2}Na_{1/2})TiO_3$-$0.18(Bi_{1/2}K_{1/2})TiO_3$ (BNKT) modification on the dielectric and piezoelectric properties of lead-free $Bi_{0.5}(Na_{0.385}K_{0.09}Li_{0.025})(Ti_{0.975}Ta_{0.025})O_3$ (BNKLTT) ceramics were investigated as a function of BNKT content x in a range of 0, 0.1,0.2, 0.3, and 1. BNKT-modified BNKLTT powders were synthesized using a conventional solid-state reaction method. Ceramic disks were sintered at 1175 ^oC for 2 h in air. As the BNKT content x increased from 0 to 0.3, the relative density of a fired specimen was decreased from 99 % to 95 %. X-ray diffraction analysis revealed that undoped BNKT ceramics correspond to a mixture of tetragonal and rhombohedral symmetry because of reflection at about 40^o and 46^o show the feather of peak splitting, which could be pertained to the (111)/(-111) reflection of the rhombohedral phase and (002)/(200) reflection of tetragonal phase peaks. Interestingly, bipolar strain versus electric field (*S*-*E*) measurement showed that the normalized electric field-induced strain (S_{max}/E_{max}) was increased from 274 pm/V of pure BNKLTT to 756 pm/V for x=0.2 and then decreased with further BNKT modification. More interestingly, unipolar *S*-*E* loop showed a maximum S_{max}/E_{max} of 761 pm/V for x=0.3 at 4 kV/mm (Fig.1) and 833 pm/V for x=2 at 5 kV/mm. BNKLTT-BNKT composite ceramics show large strain under low electric field, which is comparable to that of soft lead zirconate titanate (PZT) ceramics, promising for lead-free actuator applications.

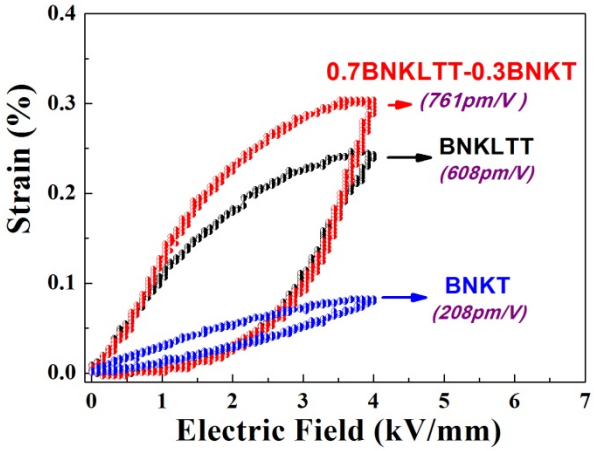

Figure 50 Comparison of unipolar strain between 0.7BNKLTT-0.3BNKT composite, BNKLTT, and BNKT ceramics

LP-O07

Ferroelectric and Piezoelectric response of lead-free $Bi_{0.5}Na_{0.5}TiO_3$-BaTiO-$BaZrO_3$ ceramics

Jamil Ur RAHMAN[1], Ali HUSSAIN[1], Adnan MAQBOOL[1], Rizwan Ahmed MALIK[1], Tae Kwon SONG[1], Won Jong KIM[2], and Myong Ho KIM[1,*]

[1]*School of Advanced Material Engineering, Changwon National University, Gyeongnam 641-773, Republic of Korea*

[2]*Department of Physics, Changwon National University, Gyeongnam 641-773, Republic of Korea*

***Keywords*:** Lead-free, Ceramics, Ferroelectric, Piezoelectric, Strain

The piezoelectric material is a material that can be used the inter conversion between electrical and mechanical. Most of the piezoelectric ceramics devices have been fabricated from lead-based piezoelectric ceramic materials, such as $Pb(Zr_xTi_{1-x})O_3$ (PZT), because of their outstanding piezoelectric properties [1-2]. However, the use of lead-based ceramics causes serious environmental problems because of the high toxicity of lead oxide and its high vapor pressure during sintering. Therefore, there is a great need to develop lead-free piezoelectric ceramics with good piezoelectric properties to replace lead-containing ceramics in various applications

Lead-free piezoelectric ceramics $(0.935\text{-}x)$ $Bi_{0.5}Na_{0.5}TiO_3$–$0.065BaTiO_3$–$xBaZrO_3$ (BNBT-BZ100x) with x = (0-0.05) were synthesis by a conventional solid-state reaction route. The effect of BZ addition on the structure, Dielectric, ferroelectric and electric field induced strain behavior of BNBT was investigated. X-ray diffraction patterns revealed that BZ completely diffused in BNBT lattice in the studied composition range and found that the structural and electrical properties of BNBT ceramics are significantly influenced by the presence of BZ content. A phase transformation from tetragonal to pseudocubic was observed. However, with increasing BZ content, the maximum dielectric constant continuously decreased and the depolarization temperature T_d shifted towards lower temperatures. The polarization and strain hysteresis loops indicate that the addition of BZ significantly disrupts the ferroelectric order. The field induced strain response of BNBT-BZ100x ceramics increases from 0.16% for x = 0 to 0.38% for x = 0.03, at an applied field of 7kV/mm. The corresponding dynamics coefficient for these composition were (S_{max}/E_{max} = 231pm/V) and (S_{max}/E_{max} = 542pm/V) respectively. The results suggest that the BNBT-BZ3 composition can be considered as promising candidate material for piezoelectric application.

References:

[1] B. Jaffe, W.R. Cook, H. Jaffe, Piezoelectric Ceramics, Academic Press, London, 1971.
[2] N. Ichinose, N. Miyamoto, S. Takahashi, J. Eur. Ceram. Soc. 24 (2004) 1681-1685.

Acknowledgement:

This work is supported by the National Research Foundation of Korea (NRF) grant funded by the Korean government (MOE) (2013R1A1A2058345).

CO-O01

Application of CFD Simulation in the SiC-CVD Process

Kyoon CHOI[1*], J.-W. SEO[1,2], Y.-S. Hahn[1], J.-H. Lee[2]
[1]*Icheon Branch, Korea Inst. of Ceramic Eng. & Tech., Gyeonggi-do 467-843, Korea*
[2]*Department of Material Sci. & Eng., Korea Univ., Seoul 136-713, Korea*

Keywords: CFD(computational fluid dynamics), CVD, Silicon carbide, Thickness uniformity

In order to increase the thickness uniformity in chemical vapor depositon of silicon carbide, we have carried out CFD studies for a horizontally-rotated 3-stage susceptor. We deposited silicon carbide films of 3C-SiC phase showing quite uniform thickness between stages but not uniform one in stage. The cause of this nonuniformity is thought to be originated from the high rotational speed. And the uniformity between stages can be further increased with the 120° split type nozzles from CFD results. Through the formation of silicon carbide film on graphite substrates we can make oxidation-resistant and dust-free graphite components with high hardness for the semiconductor applications.

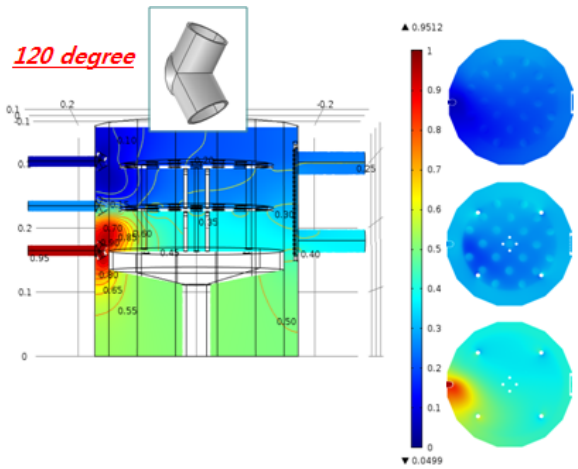

Figure 51 Hydrogen content distribution on cross-section of CVD chamber with 120° nozzles

References:

[1] J.-W. Kim, Y.-S. Hahn, K. Choi and J.-H. Lee, J. Comput. Fluids Eng. 18 (2013) 67.
[2] J.-W. Seo and K. Choi, J. Kor. Ceram. Soc. 50 (2013) 533.

Acknowledgement:

This research was supported by the World Premium Materials (WPM) Program (grant No. 10037913) of the Ministry of Knowledge Economy.

CE-O01

Synthesis and characterization of glazed ceramic ink for ink-jet printing

Kyu-Sung Han*, Ji-Hyeon Lee, Jin-Ho Kim, Kwang-Taek Hwang, Woo-Seok Cho
Icheon Branch, Korea Institute of Ceramic Engineering and Technology, Icheon 467-843, Korea

Keywords: Ceramic ink, Pigment, Inkjet printing, Porcelain product

Ink-jet printing technology has been attractive due to its capability of direct and fine printing onto various substrates. Recent studies have been focused on the expansion of the ink-jet printing application from the purpose of general consumer use and design companies to prototype production of precision parts and parts manufacturing. The use of ink-jet printing technology with ceramic pigment which is a highly stable coloring agent to decorate porcelain products, glass, plastics also has many advantages. There is no direct contact point between the printer and the substrates to be printed, thus the printing process is fast and can be adaptable to various kinds of objects. For the application of ink-jet printing technology to ceramic product decoration, the ink containing highly dispersed inorganic nano-pigments is required. Here, we report the synthesis and characterization of ceramic nano-pigment with thermal and glaze stability for ink-jet printing. Inorganic pigments were synthesized by solid state reaction. Then pigments were grinded using the attrition milling with constant speed of 800 rpm and ball to powder weight ratio was 100:1. The prepared nano-pigments were characterized by X-ray diffraction (XRD), field emission scanning electron microscopy (FE-SEM), transmission electron microscopy (TEM), particle size analyzer (PSA) and CIE L*a*b*. Ceramic ink based on the obtained nano-pigment was prepared by the dissolving pigment particles in the solution with the appropriate viscosity and surface tension for ink-jet printing. The ink solution contains 15 wt% of nano-pigment and CTAB(Cetyltrimethyl ammonium bromide) and SDS(Sodium dodecyl sulfate) as a dispersive agent. The prepared ceramic ink was stably jetted with the formation of sphere-shaped droplet from ink-jet printer.

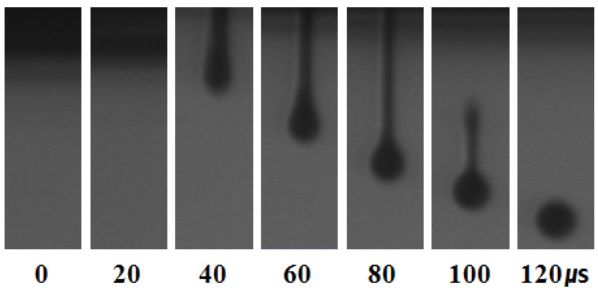

Figure 52 Droplet formation of ceramic ink

Acknowledgement:
This work was supported by Nano-Convergence Foundation (www.nanotech2020.org) funded by the Ministry of Science, ICT and Future Planning(MSIP, Korea)& the Ministry of Trade, Industry and Energy(MOTIE, Korea) [Project Name: Development of glazed nano-ceramic coloring inks for inkjet printing porcelain products]

CE-O02

Comparative Study on the Celadon Color Spectrum between Goryeo and China

Hyunggoo No, Ung Soo Kim, Woo Seok Cho
Ceramicware Team, KICET, Korea

Keywords: Celadon, Glaze, Chemistry, UMF, Color

Goryeo celadon influenced by the Yue ware of 9th century in China is found with similarities in its styles, glaze colors, and manufacture process. In this study chromaticity and chemistry analyses were performed on the 11 shards from Longquan kiln sites in China, and 7 shards from Gangjin and 12 shards from Buan in South Korea for comparison. Glazes of both Korean and Chinese celadons were basically limestone glaze, and composed with potash feldspar as alkali material. SiO_2 content was higher for Chinese celadon than for Goryeo celadon. The chemical compositions of celadon glaze and body were converted based on the UMF approach. According to the results, the value of RO_2/R_2O_3 in glaze was higher for Chinese celadon than for Goryeo celadon, and increased proportionally. The range of RO_2 and $RO+R_2O$ in body was lower for Chinese celadon than for Goryeo celadon, and increased proportionally. The color of celadon was strongly influenced by the concentration of coloring oxides (Fe_2O_3, TiO_2). CIEa* value was negatively increased with Fe_2O_3 for both celadons while it was positively increased with TiO2. This seems to be the result of high-temperature reduction firing. Chinese celadons presented relatively considerable variation in the color. Chinese celadons were generally distributed among grayish dull G, GY, and Y colors while Goryeo celadons were distributed among grayish dull GY colors. The CIEb* value of Chinese celadon was higher compared to that of Goryeo celadon. Gangjin and Buan celadons exhibited the same grayish dull GY colors, but the CIEa* value was higher for Buan celadons.

References:

[1] Min Su Han, *A Scienticfic Provenance Study for Goryeo Celadon Excavated from Seabed*, Chung-Ang University(2006).
[2] Kyung Sin Goh, *Researdch for Re-creation and Further Development of the Korean Traditional Ceramics Technology*, Chung-Ang University(2000).

CE-O03

The skill of Traditional Clay Pot Making in Kgatleng District

Kang Tae-Chun[1], Choi Sung-Jae[1]
[1]Korea National University of Cultural Heritage. KOREA

Keywords: UNESCO, Botwna Kgatleng, manufacturer's standpoint, pottery.

UNESCO registered the method of Africa Botwana Kgatleng district on the list of intangible cultural heritage in need of urgent protection. I would like to investigate the method of this place in the manufacturer's standpoint. This study has its focus on describing general pottery production method, based on the pottery-production images and slides on producing Botswana Kgatleng district pottery production made by UNESCO.

The residents in Bakgatla-ba-Kgafela, which is located to the south-eastern end of Botswana, have been making pottery by using their distinct method. In the stage of gathering clay for making pottery, master-potters ask for the advice of their ancestors by meditating with a view to making the most ideal pottery.

Afterwards, after grinding the gathered sandstone and clayey soil into powder by using a pestle, the powder is mixed and kneaded. Pottery is made by slab-building from the center toward the edge by using hand, fixed by using wooden scoop, and polished.

The method of Kgatleng districe is a good example of the original way of pottery production.

LD-O01

Optical properties of $Ag@SiO_2$ nanoparticles embedded nanopillar LED structures

Kang-Bin Bae[1], Jin-Hyeon Yun[1], Han-Su Cho[1] and In-Hwan Lee[1*]
[1]*School of Advanced Materials Engineering and Research Center of Advanced Materials Development, Chonbuk National University, Jeonju 561-756, Korea*

Keywords: LED, nanopillar, $Ag@SiO_2$ nanoparticles, surface Plasmon

Recent years have seen a growing interest in studying the effects of optical interaction between localized surface plasmons (LSPs) and GaN. The unique optical properties of LSPs have been studied for applications in sensing, imaging, surface enhanced spectroscopy, solar cells, and light-emitting diodes (LEDs). It has been demonstrated that LSPs coupling can also be utilized to enhance the light output of InGaN/GaN multi-quantum well (MQW) LED structure. The LSPs extend its distribution of near field electromagnetic field into the dielectric side for several tens of nanometers. At shorter distances of below 10 nm the Forster resonant energy transfer mechanism based on dipole–dipole interaction is operative. For the LSP enhancement to be efficient, the nanoparticles (NPs) layer should be placed in close proximity to the active MQW region of the device, generally no further than 40-60 nm. But, for very short distances from light-emitting layers, the light emission is generally quenched due to quantum mechanical tunneling effects.[1] In conventional LEDs, the emission efficiency depends on the optical extraction efficiency and internal quantum efficiency. Nanopillar LEDs can effectively increase the optical extraction efficiency, but not necessarily internal quantum efficiency (IQE). In order to try to improve the latter we have synthesized $Ag@SiO_2$ core/shell structures using wet-chemical route and applied them to nanopillar LED structures. Nanopillar LED structures created by top-down method have some etching damage, as a result internal quantum efficiency decreases. To avoid this drawback, nanopillar LED using the bottom-up method have been prepared by molecular beam epitaxy. $Ag@SiO_2$ NPs were deposited on this InGaN/GaN nanopillar LED structure.
In this study, photoluminescence behavior of nanopillar LED structures embedded with $Ag@SiO_2$ NPs and the effect of surface plasmons on InGaN/GaN nanopillar LED with $Ag@SiO_2$ NPs were investigated.

References:
[1] L.W. Jang, D.W Jeon, M. Kim, J.W. Jeon, A.Y. Polyakov, J.W. Ju, S.J. Lee, J.H. Baek, J.K. Yang and I.H. LEE, Adv. Funct. Mater. 22 (2012) 2728.

Acknwoledgement:
This research was supported by National Research Foundation of Korea(NRF) funded by Ministry of Science, ICT & Future Planning (2013R1A2A2A07067688, 2010-0019626).

LD-O02

A Novel technology for fabrication of AlGaN/GaN HFETs using by photo-sensitive polyimide IMD layer

Seung Kyu Oh[1], Hwa Young Ko[2], Taehoon Jang[2], Joon Seop kwak[1*]
[1]*Department of Printed Electronics Engineering, Sunchon National University, Jeonnam 540-742, Korea*
[2]*IGBT Part, System IC R&D, LG Electronics, Seoul 137-724, Korea*

Keywords: Chip shrink, AlGaN/GaN, HFETs, IMD, Polyimide

GaN-based heterostructure field effect transistors (HFETs) are considered a candidate for high-power and high-frequency applications, such as converters and inverters, owing to their high carrier mobility and high breakdown voltage(BV) characteristics[1]. On the other hand, GaN based HFETs for high power applications are expensive compared to Si-based power devices[2]. To achieve lower cost, GaN growth technology with a lower cost substrate and chip shrink technology is needed. This study examined chip shrink technology for lateral-type AlGaN/GaN HFETs fabricated with a bonding pad above the active area (BPAA) structure. The photosensitive polyimide layer was used as inter metal dielectric (IMD) layer, which yielded a very low leakage current of 5.8 nA/mm^2 even at 2kV and a good adhesion property after O_2 plasma treatment. The fabricated AlGaN/GaN HFETs with the BPAA structure exhibited good device characteristics, such as a low leakage current of 7.1 μA at 600 V and a drain current of 24.4 A at V_{DS} 2 V, which has the three times higher value compared to that of the AlGaN/GaN HFETs without the BPAA structure, because the BPAA structure increased the size of active by 300%. This suggests that the BPAA structure is a promising method for reducing the size and cost of the lateral-type AlGaN/GaN HFETs.

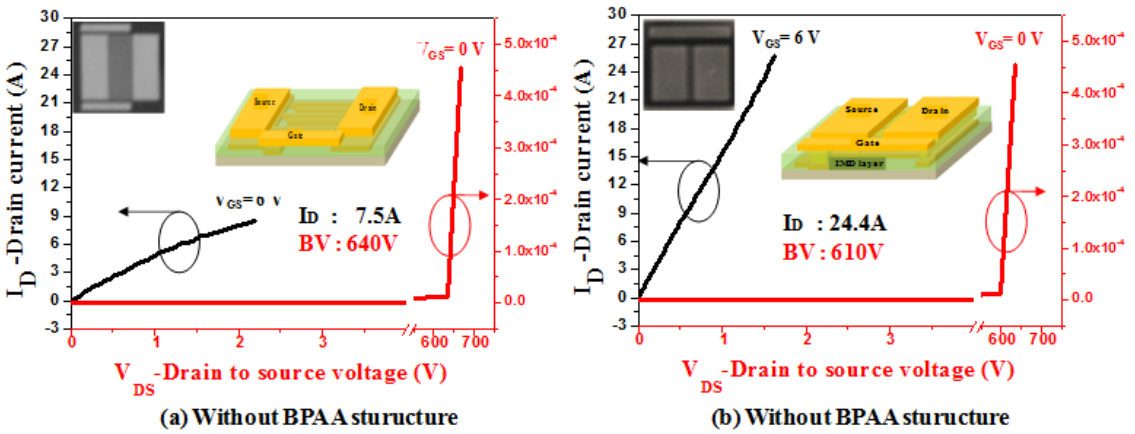

Figure 53 Device characteristics of AlGaN/GaN HFETs (a) without BPAA Structure, (b) with BPAA Structure

References:

[1] J. Baliga, IEEE Trans. Electron Devices. 43 (1996) 1717–1731.
[2] R. Chau, S. Datta, M. Doczy, B. Doyle, B. Jin, J.Kavalieros, A. Majumdar, M. Metz and M. Radosavljevic, IEEE Trans. on Nanotechnology 4 (2005) 1553-158.

Acknowledgement:

This research was supported by Basic Science Research Program through the National Research Foundation of Korea(NRF) fund by the Ministry of Education, Science and Technology(2012R1A1A4A01015373).

LD-O03

Enhanced optical output power of InGaN/GaN blue LED embedded with SiO_2 nanopaticles

Hansu CHO[1], Kyeongseob KWON[1], Myeongji DONG[1], Kangbin BAE[1], Taehoon CHUNG[2], Jonghyeob BAEK[2], Inhwan LEE[1*]
[1]*School of Advanced Materials Engineering and Research Center for Advanced Materials Development, Chonbuk National University, Jeonju, Chonbuk 561-756, Korea*
[2]*Next Generation Device Research Center, Korea Photonics Technology Institute, Gwangju 500-779, Korea*

Keywords: Light-emitting diode, InGaN/GaN, nano-pillar, nano-particles

Light-emitting diodes (LEDs) that are considered as the next generation light source in general lighting applications, are currently being actively studied in order to increase their optical power and efficiency [1]. LEDs on patterned sapphire substrate (PSS) have a reduced threading dislocation (TD) density and improved light extraction efficiency, the latter due to additional scattering on patterned cone shape profile of the PSS substrate. This led to the use of such LEDs in commercial production [2]. In this study, high efficiency InGaN/GaN blue LED embedded with SiO_2 nano-particles was fabricated on PSS. Nano-pillar (NP) GaN was fabricated by a dry etching using a self-assembled Ni nano-dots on a n-GaN layer grown on PSS by a metalorganic chemical vapor deposition (MOCVD). SiO_2 nano-particles (100 nm in diameter) were embedded in the NP GaN template by spin-coating method. InGaN/GaN LED structure was overgrown over this template, as shown in Figure 1. Regrown GaN film could be overgrown only on NP GaN tips because the embedded SiO_2 nano-particles acted as epitaxial lateral overgrowth mask facilitating selective lateral overgrowth, resulting in the formation of the air voids between nano-pillars. Light output powers of overgrown LEDs with SiO_2 embedded in nano-pillar (SiO_2-NP) on PSS have increased by 10 % compared with conventional LEDs on PSS. This result is attributed to the improvement of internal quantum efficiency caused by decreased TD density and relaxed strain due to the NP GaN, also to the increased light extraction efficiency due to additional scattering in the SiO_2-NP structures.

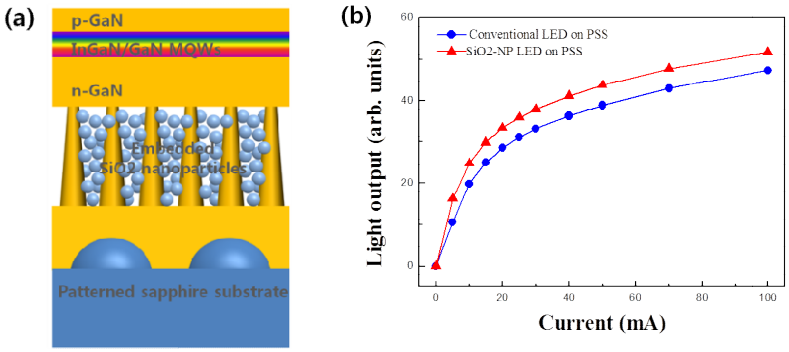

Figure 54 (a) A schematic illustration of the SiO_2-NP LED, (b) L-I characteristics of the conventional LED and SiO_2-NP LED

References:

[1] V. V. Lysak, J. H. Kang, and C. -H. Hong, Appl. Phys. Lett. 102 (2013) 061114.
[2] S. R. Xu, P. X. Li, J. C. Zhang, T. Jiang, J. J. Ma, Z. Y. Lin, and Y. Hao, J. Alloys Comp. 614 (2014) 360.

Acknowledgement:

This research was supported by National Research Foundation of Korea(NRF) funded by Ministry of Science, ICT & Future Planning (2013R1A2A2A07067688, 2010-0019626)

LD-O04

Deposition of nanoparticles on substrate for layer-by-layer assembly

Myeong-Ji DONG[1], In-Hwan LEE[1*]
[1]*School of Advanced Materials Engineering and Research Center of Advanced Materials Development, Chonbuk National University Jeonju, 561-756, Republic of Korea*

Keywords: layer-by-layer, polyelectrolyte assembly, dip coating, spin coating, nanoparticle,

In nanotechnology there exists a serious problem of controllably depositing nanoparticles on the chosen surface. The methods for the assembly of thin films with various degrees of molecular order and stability include: spin coating and solution casting, polyion layer-by-layer self-assembly, chemical self-assembly and Langmuir-Blodgett technique. Layer-by-layer (LbL) assembly has been proven to be a convenient and versatile method to fabricate functional films. This technique makes use of the alternate adsorption of oppositely charged macromolecules to build up multilayered structures. These films have a lower molecular order than Langmuir-Blodgett (LB) films or self-assembled monolayer (SAM) films but they have the advantage of high strength, easy preparation and possibility to be deposited on supports of any shape and dimension. However, using traditional dipping LbL assembly to fabricate micrometer-thick films is time consuming, while the spin-coating electrostatic self-assembly technique has been shown to facilitate the rapid fabrication of polyelectrolyte multilayer assemblies. Films prepared by LbL assembly have been used in a wide range of applications, such as antireflection coatings, super hydrophobic surfaces, electrochromic devices, biosensors, cell adhesion, drug delivery systems, proton exchange membranes, solar-energy conversion, and separation membranes.

In this study, LbL assembly was fabricated using a spin coating technique. Poly (allylamine hydrochloride) (PAH) / poly(sodium 4-styrenesulfonate) (PSS) films were formed by spin-assisted LbL assembly by alternately spinning aqueous solutions of PAH and PSS onto a charged substrate. Subsequently, the particles are coated by the dip coating method on a charged polymer film. In this way, we can coat nanoparticles on various structural templates. Also, it allows to coat the nanoparticles by adjusting their density and then to evaluate the optical properties of the films. In addition, the approach was used to coat a monolayer of quantum dots on charged polymer film. The coated quantum dot films thus prepared were studied to evaluate the optical, electronic and structural properties.

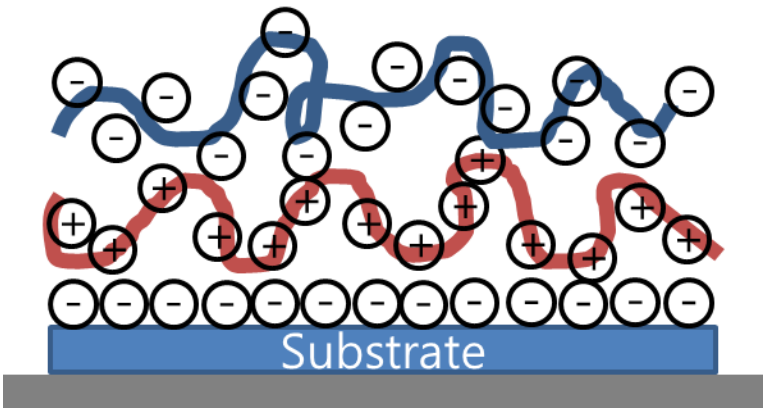

Figure 55. Simplified molecular picture of two adsorption steps

References:

[1] G. Decher, Science 277 (1997) 1232.
[2] Y. Li, X. Wang and J. Sun, Chem. Soc. Rev 41 (2012) 5998-6009.

Acknowledgement:

This research was supported by National Research Foundation of Korea(NRF) funded by Ministry of Science, ICT & Future Planning (2013R1A2A2A07067688, 2010-0019626)

LD-O05

Electrical characteristics of low damage sputtered ITO Ohmic contact to p-GaN

Yu-Jung Cha, Yu Lim Lee, Tae Kyoung Kim, Seung Kyu Oh and Joon Seop Kwak*
[1]*Department of Printed Electronics Engineering, Sunchon National University, Jeonnam 540-742, Korea*

Keywords: Ohmic contact, ITO/GaN

GaN based Light emitting diodes (LEDs) have many applications in daily life. For example, they are used LED traffic lights, full-color display, LCD panels, etc. The construct InGaN-based LEDs with high light-emitting efficiency, the p-type electrodes must have a high transmittance and a low contact resistance. Therefore, much research on p-GaN has involved Indium tin oxide (ITO) electrodes, having high permeability and low contact resistance.

Thin films of ITO thin film are typically deposited by e-Beam evaporation and sputtering. ITO deposition by sputtering achieves lower electrode resistance and higher optical transmittance than deposition by e-Beam evaporation. However, ITO films deposited by Sputtering on the p-GaN have a specific contact resistance higher than that of e-Beam evaporation. This higher resistance is known to be because of damage of the p-GaN layer by plasma generated during the sputtering process.

We report a method to minimize the plasma damage ITO sputtering onto p-GaN by simultaneously using DC power and RF power. By implementing this method, we observe ITO thin films with excellent contact resistance. These improved electrical properties are characterized by measuring IV curves across the RF-DC sputtered ITO on p-GaN Ohmic contact mechanism at temperatures ranging from 200 to 406 K.

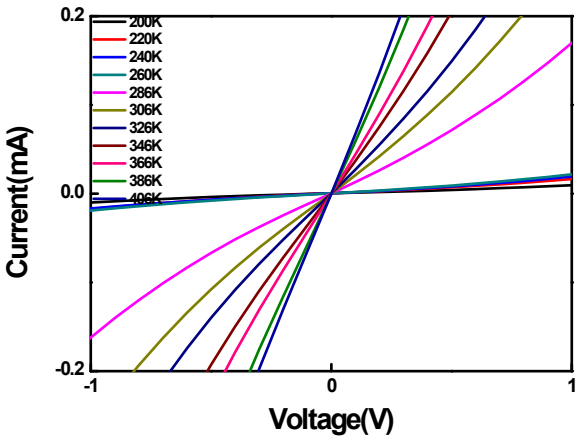

Fig 1. I-V curves with E-beam RF DC power

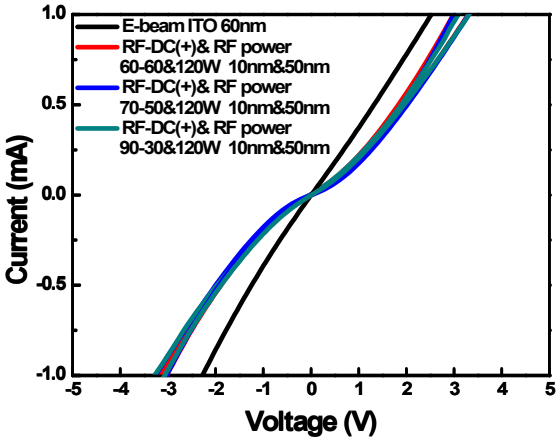

Fig 2. I-V-T characteristics of ITO contacts on p-GaN. (@10um)

Acknowledgement:
This study is financial supported by Basic Science Research Program through the NRF of Korea funded by the Ministry of Education (NRF-2014R1A6A1030419) and the BK21 PLUS program at SCNU.

LD-O06

Optical properties of modified light-emitting diodes structures using localized surface plasmons

Jin-Hyeon Yun[1], Han-Su Cho[1], Kang-Bin Bae[1], Myeong-Ji Dong[1], In-Hwan Lee[1*]
[1] *School of Advanced Materials Engineering and Research Center of Advanced Materials Development and Semiconductor Physics Research Center, Chonbuk National University, Jeonju 561-756, Korea*

Keywords: Light emitting diode, localized surface plasmon, nanostructure, optical properties

Surface plasmons (SPs) are coherent electron oscillations that exist at a metal/dielectric interface. Specifically, the SPs in noble metal nanoparticles (NPs) embedded in a dielectric matrix are called localized surface plasmons (LSPs).[1] These LSPs have been studied for applications in sensing, medical imaging, and surface enhanced spectroscopy. It has been demonstrated that LSP phenomena can also be utilized to enhance the light output of GaN/InGaN multi-quantum well (MQW) structures and GaN/InGaN MQW light emitting diodes (LEDs). For the LSP enhancement to be efficient, the NP layer should be placed in close proximity to the active MQW region of the device, generally no further than ~100 nm.[2] The thickness of the spacer layer between the active region of LED and the LSP region is a serious concern, with the thickness of the p-GaN emitter layer in contemporary LEDs more or less fixed by the spreading resistance and junction performance considerations and difficult to alter. The spacer thickness for effective LSP coupling has been already reported, and the effective distance of the Ag nanostructure from the active layer of LEDs should be within several tens of nanometers. However, in conventional blue LED structures the thickness of the p-type GaN spacer layer is generally greater than 76 nm in order to form a well-behaved p–n junction and to provide reasonably low spreading resistance. Such a GaN thickness is too large for the effective LSP coupling process. As a solution to the problem posed by the high thickness of n-GaN and p-GaN layers of conventional LEDs, we proposed the fabrication of metal NPs embedded in InGaN/GaN nanopillar LEDs and hole-patterned LEDs. In such a structure, the NPs could be placed very close to the active layer of the nanopillar LEDs and hole-patterned LEDs. In this work, photoluminescence behavior of Ag@SiO_2 NPs embedded nanopillar LED structures and hole-patterned LEDs structures and the effect of surface plasmons on InGaN/GaN nanopillar LED and hole-patterned LEDs with Ag@SiO_2 NPs were investigated and discussed. We demonstrate that the approach taken does indeed allow to achieve a strong enhancement of light output as demonstrated in Fig. 1.

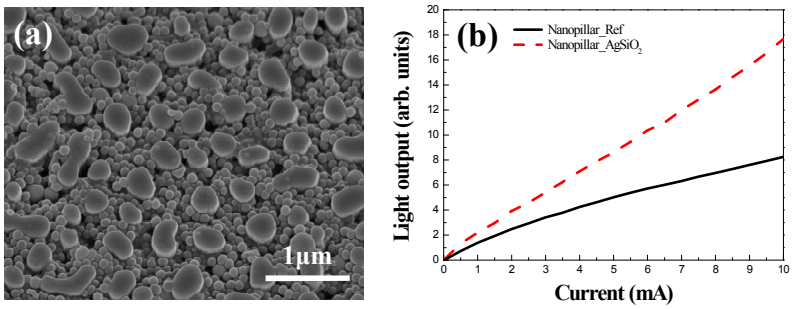

Figure 56 SEM image (a) and light-current curve (b) of Ag@SiO_2 NP-embedded nanopillar LEDs

References:
[1] W. L. Barnes, A. Dereux, and T. W. Ebbesen, Nature, 424 (2003) 824.
[2] K. Okamoto, I. Niki, A. Shvartser, Y. Narukawa, T. Mukai, and A. Scherer, Nature Mater., 3 (2004) 601.

Acknowledgement:
This research was supported by National Research Foundation of Korea(NRF) funded by Ministry of Science, ICT & Future Planning (2013R1A2A2A07067688, 2010-0019626)

AD-O01

Change in Characteristics of $(La_{1-x}Gd_x)_2Zr_2O_7$ TBCs Fabricated by Suspension Plasma Spray after Heat Treatment

Seongwon KIM[1*], Chang-Sup KWON[1], Yoon-Suk OH[1], Sung-Min LEE[1], Hyung-Tae KIM[1], and Byung-Koog JANG[2]

[1] *Engineering Ceramic Team, Korea Institute of Ceramic Engineering and Technology, Icheon, Gyeonggi-do, 467-843, Korea*

[2] *High Temperature Materials Unit, National Institute of Materials Science, Tsukuba, 305-0047, Japan*

Keywords: Thermal Barrier Coatings (TBCs), Lanthanum Gadolinium Zirconate, Suspension Plasma Spray, Thermal Conductivity

Studies on thermal barrier coatings (TBCs) have been conducted over the past decades in order to increase the operating temperature of gas turbines for power generation and aircraft. One of the most commonly used materials for TBC application is yttria-stabilized zirconia (YSZ), which has low thermal conductivity and a high thermal expansion coefficient. Recently, rare-earth zirconate oxides with pyrochlore and/or fluorite have been investigated as candidate materials for future TBCs. Pyrochlore and fluorite have analogous cubic structures with a space group of $Fd\bar{3}m$ for the former and $Fm\bar{3}m$ for the latter. The low thermal conductivities of rare-earth zirconate oxides with these structures are attributed to the phonon scattering by point defects in the crystallographic structures.

In this study, $(La_{1-x}Gd_x)_2Zr_2O_7$ TBCs are fabricated by suspension plasma spray with a variety of suspension preparation conditions, such as conventional or high energy ball milling. Lanthanum/gadolinium zirconate oxides were prepared for this study using La_2O_3(High Purity Chemicals , 99.9% , 11μm), Gd_2O_3(High Purity Chemicals , 99.9% , 11μm), and ZrO_2(Aldrich , 99%, 40nm) oxide powders. The suspension with composition of lanthanum or gadolinium zirconate was prepared by a planetary mill or ball mill. Mixed suspensions were deposited on the superalloy substrate by suspension plasma spray (Axial III, Northwest Mettech Corp., Canada). With deposited or heat-treated coatings, crystallographic phases of samples were identified by X-ray diffractometer (XRD, RIGAKU D/MAX-2500/PC, Japan) with Cu Kα radiation(0.1506nm). The microstructures of polished samples were analyzed by scanning election microscope (SEM, JEOL JSM-6390, Japan).

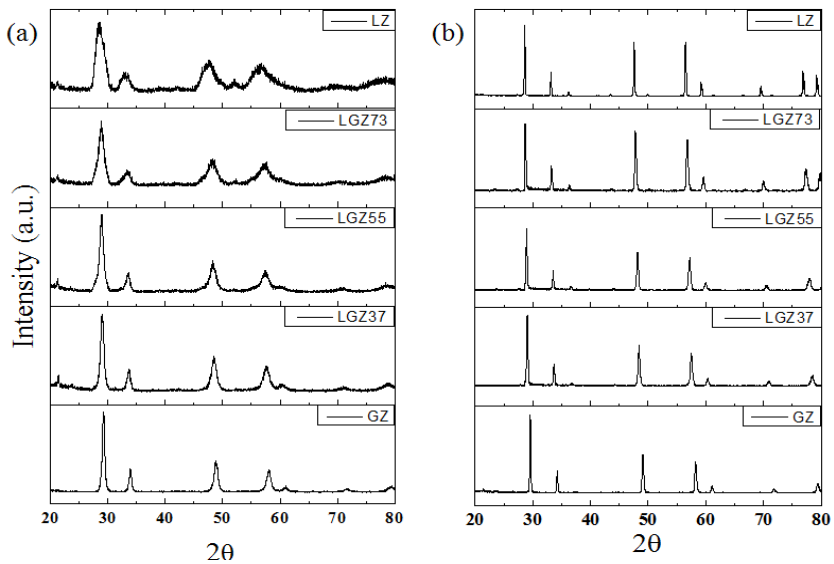

Figure 57 XRD patterns of $(La_{1-x}Gd_x)_2Zr_2O_7$ coatings : (a) as-deposited and (b) after heat treatment at 1400℃

Figure 1 shows the XRD patterns of $(La_{1-x}Gd_x)_2Zr_2O_7$ coatings as deposited as well as after heat treatment. Among these XRD patterns, the existence of (331) and (511) peaks of superlattice confirms the presence of pyrochlore phases in this lanthanum zirconate coatings. The LZ or GZ composition turns out to have a pyrochlore or a fluorite phase, respectively. In addition, both as-deposited coatings have fully developed crystallographic phases with different crystallite sizes.
Phase formation, microstructures, and thermal conductivities are examined with the deposited coatings of $(La_{1-x}Gd_x)_2Zr_2O_7$ compositions. The change in structures and thermal conductivities after heat treatment is investigated as well.

References:

[1] D.R. Clarke and C.G. Levi, *Annu. Rev. Mater. Res.,*33 (2003) 383.
[2] C.G. Levi, *Curr. Op. in Sol. Sta. & Mater. Sci.,* 8 (2004) 77.
[3] M.R. Winter and D.R. Clarke, *J. Am. Ceram. Soc.,* 90 (2007) 553.
[4] P.K. Schelling, S.R. Plillpot, and R.W. Grimes, *Philos. Mag. Lett.*, 84 (2004) 127.
[5] L. Pawlowski, Surf. Coat. Technol., 203 (2009) 2807.

Acknowledgement:

This research was supported by a grant from the Fundamental R&D Program for Strategic Core Technology of Materials funded by the Ministry of Trade, Industry and Energy and by a grant from the Basic and Strategic R&D Program funded by the Korea Institute of Ceramic Engineering and Technology, Republic of Korea.

Poster Presentation

Synthesis, Raw Materials & Advanced powder processing(SY) 268
Thermoelectrics(TH) 273
Thin Films & Layers(TF) 278
Nano-particles & Nano-structured Materials(NA) 294
Fuel cells and Batteries(FU) 304
Electronic Ceramics(EL) 313
Structual Ceramics & Refractory materials(ST) 324
Glass & Opto-Electronic Materials(GL) 330
Biomaterials(BI) 339
Piezoelectric Device & Application(PI) 344
Lead-free Piezoelectrics(LP) 351
Computational Ceramic Science and Engineering(CO) 363
Ceramics Culture and Education(CE) 365
LED and Display Materials(LD) 366
Advanced Coating for Gas Turbines(AD) 370

SY-P01

The Pulsed laser assisted synthesis of Tm^{3+} doped $CaMoO_4$ colloidal nanocrystals and its upconversion luminescence

Jung-Il LEE[1], Joon HWANG[2], Chang Woo HONG[3], Jeong Ho RYU[1*]
[1]*Department of Materials Science and Engineering, Korea National University of Transportation, Chungju, Chungbuk 380-702, Korea*
[2]*Department of Aeronautical and Mechanical Design Engineering, Korea National University of Transportation, Chungju, Chungbuk 380-702, Korea*
[3]*Department of Civil Engineering, Korea National University of Transportation, Chungju, Chungbuk 380-702, Korea*

Keywords: Materials, Process, Property, Structure, Ceramics

In recent years, lanthanide ion doped upconversion (UC) luminescence from near infra-red radiation to visible or UV light has received many attention for their various applications in phosphors, solar cell, flat-panel displays, scintillators, solid state lasers and fluorescent bio-medicals [1]. Especially, lanthanide doped white UC luminescence has been extensively studied, because white luminescent UC phosphors have potentials to replace conventional lighting sources in optical devices and three-dimensional backlighting for colour displays. Also, white UC phosphors are expected to provide more simultaneous detections for bio-medical probes compared to conventional bio-labeling.

Recently, $CaMoO_4$ has been investigated as a potential phosphor because it has high density and more stable physical and chemical properties compared to other oxide materials. Mo^{6+} ions in $CaMoO_4$ matrices have strong polarization induced by large electric charges and small radius, which leads to decrease of symmetries and enhanced stark energy splitting. Therefore, we expect that $CaMoO_4$ can be suitable matrices for UC phosphors with high efficiency for light upconverting applications.

Conventionally, solid state reaction, acid-base, precipitation, hydrothermal and sol-gel methods were used for synthesis of $CaMoO_4$ powders. However, those methods need long processing time and steps for fabrication. Also, chemical additives in procedure may be incorporated to $CaMoO_4$ particles as impurities, which results in bad influence to human body clinically. One novel technique for fabrication of $CaMoO_4$ nanocrystals is pulsed laser ablation (PLA) in liquid medium. PLA of solid target in liquid has been a promising technique for producing nanocrystals for analytical and bioanalytical applications as well as the rapid synthesis of complex materials because the experimental procedure is simple and above all, chemical additive is unnecessary [2]. However, to date, there is little report on the preparation of upconverting $CaMoO_4:Tm^{3+}$ nanocrystals by laser ablation in liquid medium.

In this study, we report a novel synthetic approach to produce $CaMoO_4:Tm^{3+}$ nanocrystals using PLA in liquid medium without any surfactant. The fabricated $CaMoO_4:Tm^{3+}$ nanocrystals were characterized in terms of their crystallinity, microstructure and upconverting property. Moreover, the laser ablation process was discussed by a thermally induced explosive ejection mechanism.

References:

[1]. P. Li, Q. Peng and Y. Li, Adv. Mater. 21 (2009) 1945.
[2] A. Henglein, J. Phys. Chem. 97 (1993) 5457.

SY-P02

Continuous Production of Monodisperse Silica Particles Using Tubular Reactor

Young-Sang CHO[1*]
[1]*Department of Chemical Engineering and Biotechnology, Siheung-si, 429-793, Republic of Korea*

Keywords: Monodisperse particle, Silica, Continuous Process, Tubular Reactor

The synthesis of monodisperse particles have been considered as important research topic in the field of colloid science and technology. Specifically, metal oxide particles with narrow size distribution have been studied for various applications such as building block materials of self-assembly, cosmetics, and chemical mechanical planarization[1-3]. Usually, the synthesis of monodisperse particles has been carried out using laboratory-scale batch-type reactor to study the factors affecting the particle size and distribution. However, batch type reactors have drawback in that it is difficult to establish the scale-up conditions for the large-scale production of the particle suspension. Thus, it is essential to study the continuous production of monodisperse colloids using proper reaction system such as tubular reactor.

In this study, monodisperse silica nanospheres were synthesized by tubular reactor for the continuous production of the particles. For sol-gel reaction, silica precursor such as TEOS (tetraethylorthosilicate) and ammonia/water mixture were separately fed to the T-mixer which connects two input flows of the reactants into one outlet tube composed of Teflon. The mixing of the reactants was performed using static mixer for the complete hydrolysis and condensation reaction of TEOS. For the size control of the particles, retention time of the reactants was adjusted by changing the length of the tubular reactor or feeding rate of the liquid materials. The reactant composition was also changed to study the effect of the particle size and distribution of the silica nanospheres.

Fig. 1 contains the average size of the silica nanospheres as a function of production time. The size of the particle suspension was measured by light scattering method using ZETA PLUS apparatus and retention time was adjusted from 68 to 162 minutes for the tubular reactor with 7.5 m in length. As displayed in the graph in Fig. 1, the particle size fluctuates as a function of production time when the retention time was 68 minutes, which may not be enough for the completion of the reaction. Relatively uniform size of the particles was observed when the retention time becomes longer.

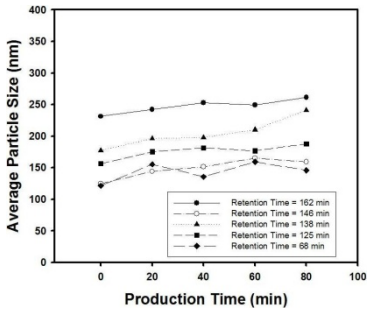

Figure 58. Average size of silica particles as a function of production time

References:

[1] Y.-S. Cho, G.-R. Yi, J.-M. Lim, S.-H. Kim, V. N. Manoharan, D. J. Pine, and S.-M. Yang, J. Am. Chem. Soc. 127 (2005) 15968.
[2] N. S. Kwak and K. H. Youm, Membrane J. 19(2) (2009) 122.
[3] S. Kim, J.-H. So, D.-J. Lee and S.-M. Yang, J. Colloid Interf. Sci., 319 (2008) 48.

Acknowledgement:

This research was financially supported by a grant by Ministry of Land, Infrastructure and Transport (MOLIT) of Korea government and Korea Agency for Infrastructure Technology Advancement (KAIA, 14CTAP-C078865).

SY-P03

Catalytic Liquid-phase Oxidation of Acetaldehyde over a Pt/CeO_2-ZrO_2-SnO_2/γ-Alumina Catalyst

Pil-Gyu CHOI, Takanobu OHNO, Nashito FUKUHARA, Toshiyuki MASUI, Nobuhito IMANAKA*
Department of Applied Chemistry, Faculty of Engineering, Osaka University, 2-1 Yamadaoka, Suita, Osaka 565-0871, Japan

Keywords: Liquid-phase oxidation, Acetaldehyde, Rare earths, Catalyst

Acetaldehyde is a popular organic compound and is often used as a solvent for paints and adhesives. This compound is soluble in water and is identified as a cancer-causing substance. However, acetaldehyde is contained in a high level in industrial liquid waste from synthetic resin plants. To protect our health and the environment, it is important to remove acetaldehyde in wastewater as much as possible. Liquid-phase oxidation of acetaldehyde using a heterogeneous catalyst is one of the effective purification methods. In addition, useful acetic acid can be produced by selective oxidation of acetaldehyde in a liquid phase. In this study, a Pt/CeO_2-ZrO_2-SnO_2/γ-Al_2O_3 catalyst was prepared for the selective oxidation of acetaldehyde to acetic acid. In this catalyst, the main oxidation catalyst is Pt and γ-Al_2O_3 is a catalyst support. The CeO_2-ZrO_2-SnO_2 solid solution works as a promoter to facilitate oxidation by supplying active oxygen from inside the bulk due to the oxygen storage and release properties [1].

The CeO_2-ZrO_2-SnO_2 promoter was supported on γ-Al_2O_3 by a co-precipitation method. The content of the promoter was adjusted to be 16 wt% and the atomic ratio of Ce:Zr:Sn were controlled to be 68:17:15, where the highest oxidation catalysis was obtained for gas-phase oxidation of acetaldehyde [1]. The supported platinum catalyst (Pt/CeO_2-ZrO_2-SnO_2/γ-Al_2O_3) was prepared by impregnating the CeO_2-ZrO_2-SnO_2/γ-Al_2O_3 support with a platinum colloid stabilized with polyvinylpyrrolidone. The amount of Pt in the catalyst was adjusted in the range of 5-10 wt%. After impregnation, the catalyst was dried at 80 °C for 12 h and then calcined at 500 °C for 4 h.

The catalytic liquid phase oxidation of acetaldehyde was carried out in the air atmosphere in batch mode with mechanically stirring. An aqueous solution of 450 ppm acetaldehyde was poured into the flask and the catalyst (0.2 g) was loaded. The reactor was then cooled in an ice bath at 0 °C. After the reaction for 2-8 h, the catalyst was separated by centrifugation and the supernatant liquid was analyzed using gas chromatograph mass spectrometry to evaluate the acetaldehyde conversion to acetic acid. Among the catalysts, 6.4wt%Pt/16wt%$Ce_{0.68}Zr_{0.17}Sn_{0.15}O_2$/γ-$Al_2O_3$ showed the highest acetaldehyde oxidation activity. Figure 1 shows reaction time dependence of residual percentage of acetaldehyde and the selectivity to acetic acid using this catalyst. Acetaldehyde was completely oxidized after the reaction at 0 °C for 8 h, and the selectivity to acetic acid was as high as 97% after the reaction at 0 °C for 6 h.

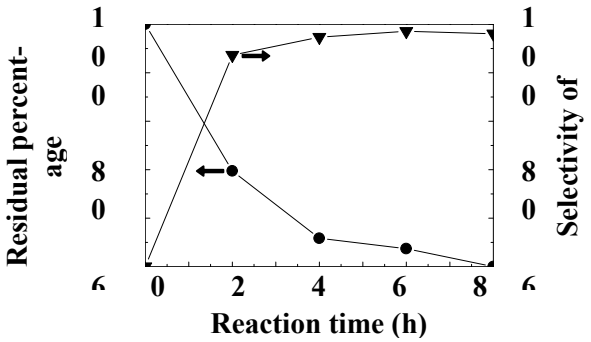

Figure 59 Reaction time dependence of residual percentage of acetaldehyde (●) and the selectivity to acetic acid (▼).

Reference:

[1] K. Yasuda, A. Yoshimura, A. Katsuma, T. Masui, N. Imanaka, Bull. Chem. Soc. Jpn. 85 (2012) 522.

SY-P04

Synthesis of Hydroxyapatite Using Room-temperature Reaction between Egg Shell and Phosphoric Acid

Tae Sung KANG, Mircea Cristian PANTILIMON, Sang-Jin LEE*
Department of Advanced Materials Science and Engineering, Mokpo National University, Muan, 534-729, Korea

Keywords: Hydroxyapatite, Exothermic reaction, Calcium phosphate, Synthesis, Eggshell

Hydroxyapatite and β-tricalcium phosphate are very well known ceramic materials because of their high biocompatibility and they can be used for artificial bones for transplants or even help in regenerating pre-existent bone structures. For the synthesis of these materials the precursors can react with each other in an aqueous solution or they can be combined in solid phase and react during a heating process at high temperatures. In this study, to find the conditions on how to synthesize hydroxyapatite, which is a calcium phosphate based bio-ceramic material, at lower temperature we combined calcined egg shells with various concentrations of phosphoric acid. The very fine CaO powder, made from calcined egg shells that have a high surface area of 31.6 m^2/g, shows a high reactivity with phosphoric acid. The powder was combined with various concentrations of the acid at room temperature and the resulting reaction was highly exothermic. After the reaction the samples showed both CaOH and $CaHPO_4$ crystal phases. In order to observe the changes in crystal phase, the samples were afterwards heat treated at various temperatures. After varying the heating temperature and the concentration of the phosphoric acid, most of the samples had as a major crystal phase the $CaHPO_4$, and only one of the samples displayed the formation of the hydroxyapatite crystal phase.

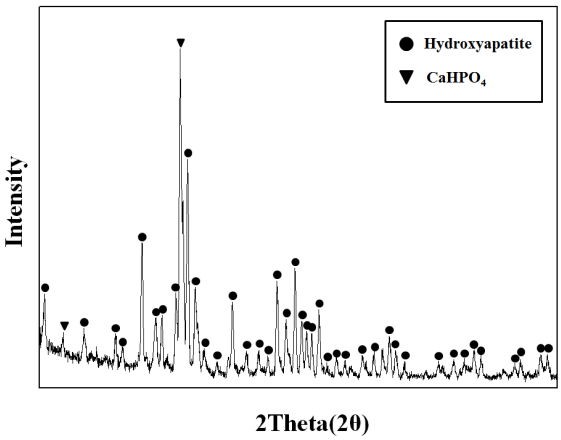

Fig.60 XRD patterns of synthesized calcium phosphate

References:

[1] L.L. Hench, J. Am. Ceram. Soc. 81 (1998) 1705.
[2] S.R. Kim, Y.H. Kim, S.J. Jung and D.H. Riu, J. Kor. Ceram. Soc. 38 (2001) 1132.

SY-P05

Fabrication of WO_3 from UP-Cycled Ammonium ParaTungstate (APT)

Jun-Ki Chung[1]*, Sung-Jin Kim[1], Jin-Ho On[1], Sang-Yeup Park[1,2]**
[1]*Technology Innovation Center for Fine Ceramic, Gangneung-Wonju National University*
Gangneung, 210-702, Rep. of Korea.
[2]*Department of Ceramic Engineering, Gangneung-Wonju National University*
Gangneung, 210-702, Rep. of Korea.

**junki@gwmu.ac.kr, **sypark@gwnu.ac.kr*

Keywords: Ammonium paratungstate, WO_3, Chemical precipitation method

The possibility of chemical precipitation method of up-cycled ammonium paratungstate (APT) has been studied, and compared with thermal decomposition method. WO_3 particles were synthesized by chemical precipitation method using a 1:1.5 weight ratio of ammonium paratungstate hydrate ($H_{42}N_{10}O_{42}W_{12}xH_2O$):($H_2SO_4$). The fabricated products have been characterized by X-ray diffraction (XRD), X-ray Fluorescence Spectrometer (XRF) and scanning electron microscopy (SEM) equipped with energy dispersive spectrometry (EDS).
The formation of monoclinic crystal structure of WO_3 at heating temperatures was confirmed by X-ray diffraction (XRD). Thermogravimetric analysis (TGA) of the sample allowed identification of the sequence of decomposition and reduction reactions occurring during heat treatment. At over 500°C, X-ray diffraction indicates only a major peak of WO_3 (Fig. 1). TGA in air indicated a total weight loss of 10.12 % with the reactions completed by 660 °C. The particle size distribution and morphology of the synthesized WO_3 powders were unaffected by the calcination. WO_3 particle size of 0.67~1.12 ㎛ and apparent density of 6.9 g/cm^3 were obtained by controlling suitable technological parameters.

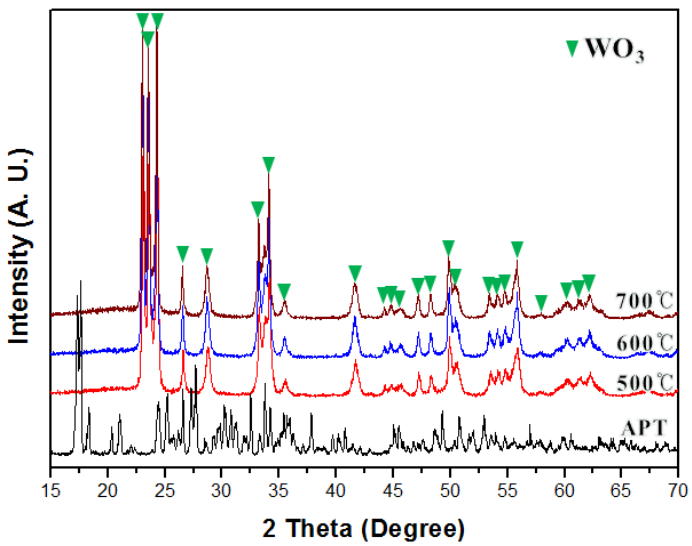

Fig. 61. XRD spectra of the APT powders calcined at different temperatures.

References:

[1]John W. van Put, Willem P.C. Duyvesteyn and Floris G.J. Luger, Hydrometallurgy, 26 (1991) 1.
[2] Jiu-Qing Liu, Zhen-Liang Xu and Kang-Gen Zhou, Journal of Membrane Science, 240 (2004) 1

TE-P01

Thermoelectric Properties of Ceramic Oxide $Sr_{1-x}La_xTiO_3$

Iqbal MAHMUD, Man-Soon YOON, Il-Ho KIM, Dong-Seob KIM, Soo-Young SONG, Moon-Kwan CHOI, Soon-Chul UR*

Department of Materials Science and Engineering/Research Center for Sustainable ECo-Devices and Materials (RIC-ReSEM), Korea National University of Transportation, 50 Daehagno, Chungju 380-702, Korea

Keywords: Thermoelectric properties, XRD, Oxide ceramic, $SrTiO_3$

The ceramic oxide thermoelectric materials have received considerable attention in recent years. These are environmentally-friendly materials comparing to the available materials that consist of toxic heavy elements. Recently, numerous studies of $SrTiO_3$ based materials have been performed, either by modifying fabrication techniques, or by the use of dopants [1, 2]. Some authors showed promising results but the figure of merit is still low compared to other high *ZT* oxide thermoelectric materials. In this work, the effect of lanthanum on the thermoelectric properties of $Sr_{1-x}La_xTiO_3$ (where x = 0.0, 0.04, 0.06, 0.08 and 0.12 mole) have been studied. La-doped $SrTiO_3$ was prepared by conventional mixed-oxide reaction method. Analytical grade raw materials of $SrCO_3$, TiO_2 and La_2O_3 were weighted and ball milled using ethanol. The powders were calcined at 1000° C for 6 hours in air. The calcined powders were then compacted into disks of 15 mm diameter and a rectangular columns of (10 mm × 3 mm × 3 mm), followed by normal sintering in an argon atmosphere (4 vol.% hydrogen in argon). XRD patterns indicated that almost every La atom incorporated into $SrTiO_3$ crystal, providing charge carriers. The lattice parameter increases with increasing La-doping contents. The relative densities of all the samples vary from 89.6% to 94.1%. Temperature dependence of Seebeck coefficient and figure of merit were measured as a function of carrier concentration as well as temperature. The electrical conductivity increased with La doping up to 0.08 mole which then decreased as the content of La increased afterwards. The thermal conductivity decreased with increasing x value and measurement temperature. The largest absolute value of the Seebeck coefficient of 394 μVK^{-1} at 973 K was observed at x = 0.04. $Sr_{0.92}La_{0.08}TiO_3$ sample showed the maximum *ZT* value of 0.20 at 973 K. It can be speculated that La doping would be promising technique to improve the thermoelectric performance.

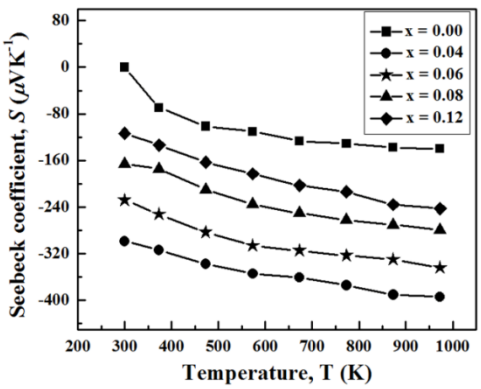

Figure 62. Temperature dependence of the Seebeck coefficient for $Sr_{1-x}La_xTiO_3$ bulk materials

References:

[1] H. Muta, K. Kurosaki and S. Yamanaka, J. of Alloy. Comp. 350 (2003) 292.
[2] N. Wang, H. Chen, H. He, W. Norimatsu, M. Kusunoki and K. Koumoto, Sci. Rep. 3 (2013) 1.

Acknowledgement:

The research was supported by a grant from the Regional Innovation Center (RIC) Program which was conducted by the Ministry of Trade, Industry & Energy of the Korean Govt.

TE-P02

Characterization of stacking faults and thermoelectrical properties of $Mo_{1-x}Ta_xSe_2$

Jaegyeom KIM, Jong-Hyeon PARK, Seung-Joo KIM*
Department of Chemistry, Division of Energy Systems Research, Ajou University, Suwon 443-749, Korea

Keywords: Thermoelectric, Seebeck, Structure

The performance of thermoelectric materials is determined by the material's figure of merit, ZT, as defined in the following equation: $ZT=\alpha^2\sigma T/k$
Where α is the Seebeck coefficient[1], σ is the electrical conductivity, k is the thermal conductivity and T is the absolute temperature. To maximize the ZT value, high power factor ($\alpha^2\sigma$) and low thermal conductivity k are required. These properties are not independent, but determined by the details of the electronic structure and scattering of charge carriers.[2,3] In this study, we report a correlation between the thermoelectric properties and the microstructure in a series of solid solution, $Mo_{1-x}Ta_xSe_2$. From the structural point of view, $MoSe_2$ has hexagonal 2-H type structure, while $TaSe_2$ has rhombohedral 3-R type structure. The solid solution, $Mo_{1-x}Ta_xSe_2$ ($0<x<1$), showed a gradual transition from 2-H to 3-R structure with increasing of Ta content (x). Some samples showed a significant peak broadening effect for (h 0 l) peaks on their XRD patterns. The peak broadening effect was analyzed with a profile simulation based on DIFFaX program, indicating that the $Mo_{0.8}Ta_{0.2}Se_2$ sample contains 60% of 2H structure and 40% of 3R structure. The lowest thermal conductivity for $Mo_{0.8}Ta_{0.2}Se_2$ may be attributed to the disorder enhanced by the stacking mismatch. As amount of tantalum increases, Seebeck coefficient decreases and turns to negative value in the range over 0.6 of tantalum. Maximum power factor and ZT value were obtained for $Mo_{0.8}Ta_{0.2}Se_2$. This methodology can be used to design new thermoelectric material. We also expect to apply the DIFFaX analysis for various studies related with structural disorder in nanostructure and interface.

References:

[1] T. J. Seebeck, *Proc. Prussian Acad. Science*. (1822) 265-373.
[2] D. M. Rowe, *U. K. Patent* No. 87 (1988) 14698
[3] C. M. Bhandari and D. M. Row, ed D. M. Rowe, *CRC Press, Boca Raton, FL* 43 (1995)

TE-P03

Improvement of power-factor deviation in a spark-plasma-sintered poly-crystalline for doped *n*-type $Bi_2Te_{2.7}Se_{0.3}$ thermoelectric materials

Soon-Mok Choi[1*], Kyu Hyoung Lee[2], Young Soo Lim [3], Won-Seon Seo[3], Soonil Lee[3]
[1] School of Energy, Materials and Chemical Engineering, Koreatech, Cheonan 330-708, South Korea
[2] Department of Nano Applied Engineering, Kangwon National University, Chuncheon 200-701, Korea
[3] Energy and Environmental Division, Korea Institute of Ceramic Engineering and Technology, Seoul 153-801, South Korea

Keywords: $Bi_2Te_{2.7}Se_{0.3}$, Polycrystalline, Power factor deviation, Dopants, Thermoelectric

Single-crystal *n*-type $Bi_2Te_{3-x}Se_x$ alloys are susceptible to cleavage perpendicular to the *c* -axis because of their lamellar structure and weak van der Waals bond between layers parallel to a-b plane. For improving the poor mechanical properties of the single-crystal, their polycrystalline is also useful for commercial devices, despite their thermoelectric performance was not better than single crystalline [1]. It has been experimentally confirmed that randomly oriented grains in polycrystalline can improve the mechanical property of *n*-type $Bi_2Te_{3-x}Se_x$ polycrystalline samples, and then nano-engineering for the polycrystalline has been effective approach in enhancing the thermoelectric properties [1]. However, significantly increased carrier concentration in *n*-type $Bi_2Te_{3-x}Se_x$ polycrystalline samples have been reported to cause a serious irreproducibility problem. This increased carrier concentration is probably related to the lattice defects generated during milling process, such as Te vacancies (V_{Te}^{2-}). Then the defects are difficult to control since they are related to the fabrication parameters, such as milling time, milling energy, sintering temperature, etc. In this study, we tried to increase thermoelectric property in *n*-type $Bi_2Te_{3-x}Se_x$ polycrystalline by using combining process of high energy ball-milling and spark-plasma-sintering process as a nano-engineering process. Many kinds of dopants (Sn, In, Mn) are also applied to improve the thermoelectric properties in this system. For improvement of power-factor deviation in a spark-plasma-sintered polycrystalline, Cu dopant are selected in this system and the degree of deviation for Cu doped polycrystalline is compared to other dopant systems.

References:

[1] W. Liu, Q. Zhang, Y. Lan, S. Chen, X. Yan, Q. Zhang, H. Wang, D. Wang, G. Chen, and Z. Ren, *Adv. Energy Mater.,* 1, (2011) *p*. 577.

Acknowledgement:

This work was supported by a Fundamental Research and Development Program for Core Technology of Materials Grant funded by the Ministry of Trade, Industry and Energy, Republic of Korea (10048035). This work was also supported by a research program funded by Koreatech.

TE-P04

Thermoelectric Properties of Chalcogenide based Composite Thin Films

Ji-Eun HONG and Soon-Gil YOON*
Department of Materials Science and Engineering, Chungnam National University, Daejeon, 305-764, Korea

Keywords: Thermoelectric, Thin film, Chalcogenide, Seebeck coefficient, RF-sputtering

Highly efficient thin thermoelectric films have recently gained acceptance for potential applications in the microelectronics industry as sensors, micro coolers and low-power generators.[1, 2]Thermoelectric transport can have a large impact on the performance of semiconductor devices and related nanostructures. [3, 5]The primary candidate technology for miniaturizing thermoelectric devices is to apply semiconductor-processing technologies including thin film process. A practical thermoelectric material should have high Seebeck coefficient, high electrical conductivity and low thermal conductivity. The interrelated Seebeck coefficient, electrical conductivity, and thermal conductivity make it difficult to improve one transport property without affecting the others.[6]The key issue of micro-thermoelectric devices is how to fabricate thin films with high performance by semiconductor-processing technologies.

V-VI-materials, in particular $[Bi,Sb]_2Te_3$ are well known thermoelectric materials with the best thermoelectric properties at room temperature. Similar chalcogenide-materials, which are based mainly on Sb-Te compounds, have shown favorable properties in very different applications namely as optical storage materials.[7]Chalcogenide combined with S, Se and Te, etc. It has a semiconductor property. The chalcogenide-materials are available to control band-gap energy for thermoelectric applications. Therefore, it is one of the best materials as thermoelectric material. So, chalcogenide has been researched actively at first stage of development.

In the present study, chalcogenide-based InSbTe (IST) and GeSbTe (GST) materials were chosen to improve the thermoelectric properties. The InSbTe material was known to show a high electrical conductivity and a low Seebeck coefficient, while GeSbTe material showed a low electrical conductivity and a high Seebeck coefficient. Accordingly, In order to enhance the thermoelectric properties, the advantages of both materials should be utilized using the composite nanostructure. The nanocomposite consists of the IST nanoparticles inserted into the GST matrix.

They were deposited at room temperature by RF-magnetron sputtering. Samples were annealed for crystallization at various temperatures and were investigated their electrical conductivity, Seebeck coefficient, and power factor.

References:

[1] J. P. Fleurial, G. J. Snyder, J. A. Herman, P. H. Giauque, W. M. Phillips, M. A. Ryan, P. Shakkottai, E. A. Kolawa, and M. A. Nicolet. in Proceedings of the 18th International Conference on Thermoelectrics (IEEE, Baltimore, 1999), p. 294.
[2] M. Kishi, H. Nemoto, T. Hamao, M. Yamamoto, S. Sudou, M. Mandai, and S. Yamamoto. in Proceedings of the 18th International Conference on Thermoelectrics (IEEE, Baltimore, 1999), p. 301.
[3] K. L. Grosse, M.-H. Bae, F. Lian, E. Pop, and W. P. King, Nat. Nanotechnol. 6 (2011) 287.
[4] G. Bakan, N. Khan, A. Cywar, K. Cil, M. Akbulut, A. Gokirmak, and H. Silva, J. Mater. Res. 26 (2011) 1061.
[5] D. K. Kim, and Y. Park, IEEE Electron Device Lett. 31 (2010) 120.
[6] K. M. Liou, C. N. Liao. J. Appl. Phys. 108 (2010) 1.
[7] J. Maimon, IEEE Proc. Aerospace Conf. 2001 Vol. 5, p. 2289-2294.

Acknowledgement:

This work was supported by a National Research Foundation of Korea (NRF) grant funded by the Korean government (MSIP) (No.NRF-2013R1A4A1069528).

TE-P05

Thermoelectric Properties of ZnO based composite thin films

Jin-A Kim[1], Soon-Gil Yoon[1]*
[1]*Department of Materials Science and Engineering, Chungnam National University, Daeduk Science Town, 305-764, Daejeon, Korea*

Keywords: Thermoelectric, nanostructure, ZnO, oxide thermoelectric materials

Thermoelectricity has been investigated for approximately 200 years, and it can be used to convert heat to electricity through the Seebeck effect. In the past few decades, materials such as silicon-germanium alloys, [1] metal chalcogenides, [2] boron compounds, [3] and many more have been developed for thermoelectric applications. However, their practical applications have been limited because of low temperature decomposition, oxidation, vaporization, or phase transition. These limitations have stimulated a lot of research on oxides as thermo-electric materials, because they are thermally and electrically stable in air at high temperatures.

ZnO is well known material for thermoelectric. The thermoelectric properties of the ZnO thin films have been reported to show a low electrical conductivity of 25 S/cm approximately and a relatively high Seebeck coefficient of -250 μV/κ. However, the electrical conductivity of the ZnO films is low for thermoelectric devices. New materials with high conductivity should be integrated with ZnO films. The doped-ZnO thin films and Zn metal thin films were known to have a high conductivity. Accordingly, in the present study, doped-ZnO or novel metal particles were integrated into the ZnO films for enhancement of the thermoelectric property. They were grown onto c-Al_2O_3 (0001) single-crystal substrate and p-Si using rf and dc co-sputtering at room temperature. Effect of doping concentration on the structural and electrical properties of ZnO films were studied in details [4]. By means of co-doping with additional low level impurities in ZnO, an enhancement of the figure of merit (ZT) was reported. This is either due to an increase in the phonon scattering at the increased number of interfaces or an enhancement of the electrical transport properties from raising the density of the states which coincides with the addition of carrier electrons [5]. Based on the ZnO nanostructure system, outstanding results such as high power factor and low thermal conductivity will be presented.

References:

[1] N.F. Hinsche, I. Mertig, and P. Zahn, J. Phys. Condens. Matter 24, 275501 (2012).
[2] D. Baoli, Y. Saiga, K. Kajisa, and T. Takabatake, J. Appl. Phys. 111, 013707 (2012).
[3] C. Wood and D. Emin, Phys. Rev. B 29, 4582 (1984).
[4] C. J. Xian and S. G. Yoon, J. Electrochem. Soc. 156, 11, (2009) G180-183
[5] S. Teehan, H. Efstathiadis, P. Haldar, J. Alloys Compd. 509 (2011) 1094

Acknowledgement:

This work was supported by a National Research Foundation of Korea (NRF) grant funded by the Korean government (MSIP) (No.NRF-2013R1A4A1069528)

TF-P01

Structural and Electrical Properties of Chemical Solution Deposited $0.7BiFeO_3$-$0.3CaTiO_3$ Solid Solution Thin Film

J. W. Kim, C. M. Raghavan, J. Y. Choi, S. S. Kim*
Department of Physics, Changwon National University, Changwon, Gyeongnam 641-773, Korea

Keywords: $BiFeO_3$, $CaTiO_3$, Solid solution system, Chemical solution deposition, Ferroelectric properties, Thin film

A $0.7BiFeO_3$-$0.3CaTiO_3$ (7B3C) solid solution thin film was prepared on a Pt(111)/Ti/SiO_2/Si(100) substrate by using a chemical solution deposition method. The microstructure and the surface morphology of the 7B3C solid solution thin film were investigated by an X-ray diffraction pattern, a Raman scattering spectrum and a SEM analysis. For electrical measurements, the upper platinum dot electrodes with areas of 1.54×10^{-4} cm^2 were deposited by an ion sputter through a shadow mask. The improved electrical properties were observed in the 7B3C solid solution thin film compared to the pure $BiFeO_3$ thin film.

Acknowledgement:
This work was supported by the Priority Research Centers Program through the National Research Foundation of Korea (NRF) funded by the Ministry of Education, Science and Technology (2010-0029634).

TF-P02

Effects of La Doping on the Structural and Electrical Properties of $Bi_7Fe_3Ti_3O_{21}$ Thin Film

C. M. Raghavan, J. W. Kim, J. Y. Choi, S. S. Kim*
Department of Physics, Changwon National University, Changwon, Gyeongnam 641-773, Korea

Keywords: $Bi_7Fe_3Ti_3O_{21}$, Bismuth layered structure ferroelectrics, Chemical solution deposition, Ferroelectric properties, Thin film

Pure $Bi_7Fe_3Ti_3O_{21}$ (BFTO21) and La-doped $Bi_7Fe_3Ti_3O_{21}$ ($Bi_{6.4}La_{0.6}Fe_3Ti_3O_{21}$, BLFTO21) thin films were prepared on Pt(111)/Ti/SiO_2/Si(100) substrates by using a chemical solution deposition method. The effects of La doping on the structural and electrical properties of the thin films were investigated. The structures of the thin films were characterized by X-ray diffraction patterns and Raman spectra. Their electrical properties, such as leakage current density, dielectric behavior, remnant polarization and coercive electric field, were systematically investigated and the results were discussed in detail.

Acknowledgement:
This work was supported by the Priority Research Centers Program through the National Research Foundation of Korea (NRF) funded by the Ministry of Education, Science and Technology (2010-0029634).

TF-P03

Effects of Seed Layer on the Structural Properties of R.F. Sputtering ZnO Thin Films

Soon-Chul Ur[1] and Seung-Hwan Yi[2,*]
[1]*Dept. of Material Sci. and Eng./RIC-ReSEM, Korea National University of Transportation, Chungjushi, 380-702, Korea*
[2,*]*Dept. of Mechanical Eng./RIC-ReSEM, Korea National University of Transportation, Chungjushi, 380-702, Korea*

Keywords: sol-gel solution, R.F. sputtered ZnO film, residual stress, precursor concentration, residual stress manipulation

Radio frequency (R.F.) sputtered deposition combined with sol-gel spin coating methods has been applied to achieve a high quality, c-axis oriented ZnO film. The deposited ZnO films show only c-axis oriented ZnO (002) peak. The morphology, structure, and residual stress of deposited ZnO films are found to be strongly dependent on the concentration of the precursor. As the concentration of the precursor is increased from 0.1 M to 0.6 M, the residual stress of the ZnO films changes from compressive (-415 MPa) to mild tensile (+90 MPa) mode. The deposited ZnO film interestingly shows (hexagonal) facets when the concentration of the precursor is 0.6 M. It is suggested that the residual stress manipulation in sputter deposited ZnO film can be controlled by precursor concentration. This technique is believed to be the first time observation, and can be applied for controlling uniformity in micro speaker fabrication.

TF-P04

The influence of Ag interlayer on the electrical and optical properties of ZTO/Ag/ZTO multilayer films

Tae-Kyung GONG[1], Seung-Hong KIM[1], Jae-Hyun JEON[1], Sun-Kyung KIM[1], SO-Young KIM[1], Dong-Huk CHOI[2], Dong-il SON[2], Daeil KIM[1*]

[1]*School of Materials Science and Engineering, University of Ulsan, Ulsan, 680-749 Republic of Korea*

[2]*Dongkook Inc, Ulsan, 683-370 Republic of Korea*

Keywords: ZTO, Ag, Magnetron sputter, Optical transmittance, Resistivity

Silver (Ag) intermediated ZTO (ZTO/Ag/ZTO ; ZAZ) films were deposited with RF and DC magnetron sputtering on a glass substrate. The thickness of Ag interlayer was set at 5, 10 and 15 nm, respectively. The electrical and optical properties of the films were investigated with the Hall effect measurement and the UV-visible spectroscopy[1, 2].

The observed electrical and optical properties were dependent on the thickness of the Ag interlayer. The resistivity of the films with 15 nm thick Ag interlayer decreased as low as 8.5×10^{-5} Ω cm and the highest optical transmittance of 83.2 % was also observed in that films. The ZAZ films with a 15 nm thick Ag interlayer showed a higher optical and electrical performance than another ZAZ films prepared in this study.

Table 63. The compared optical and electrical properties of ZTO and ZAZ films

Thickness of film (nm)	Transmittance (%)	Carrier concentration [$\times 10^{21}$/cm^3]	Hall mobility [cm^2/Vs]	Resistivity [$\times 10^{-3}$Ω cm]	Figure of Merit[Ω^{-1}]
ZTO 100	77.2	0.0000275	4.0	0.00566	1.33×10^{-7}
ZAZ (50/5/50)	64.5	0.69	2.3	3.8	3.44×10^{-5}
ZAZ (50/10/50)	72.9	1.36	12.0	36.5	1.28×10^{-3}
ZAZ (50/15/50)	83.2	2.87	25.0	583	0.2×10^{-1}

References:

[1] Y. S. Kim, J. H. Park, D. H. Choi, H. S. Jang, J. H. Lee, H. J. Park, J. I. Choi, D. H. Ju, J. Y. Lee and Daeil Kim, Applied Surface Science, 254 (2007) 1524

[2] Daeil Kim, Materials Letters 64 (2010) 668

Acknowledgement:

This research was financially supported by the Ministry of Education (MOE) and National Research Foundation of Korea(NRF) through the Human Resource Training Project for Regional Innovation (NO. NRF-2013H1B8A2032122).

TF-P05

Effect of Ti buffer layer on the optical and electrical property of In_2O_3 thin films

Jae-Hyun JEON[1], Seung-Hong KIM[1], Tae-Kyung GONG[1], Sun-Kyung KIM[1],
So-Young KIM[1], Dong-Huk CHOI[2], Dong-il SON[2], Daeil KIM[1*]
[1]*School of Materials Science and Engineering University of Ulsan, Ulsan, 680-749, Republic of Korea*
[2]*Dongkook Inc, Ulsan, 683-370, Republic of Korea*

Keywords: In_2O_3, Ti, FOM, Buffer layer, Magnetron sputtering

Indium Oxide (In_2O_3) films and In_2O_3/Titanium (Ti) bi-layered films were prepared on glass substrates by DC and RF magnetron sputtering without intentional substrate heating. In order to consider the influence of Ti buffer layer on the structural, optical and electrical properties of the films, the thickness of the layer was varied from 5 to 20 nm.

As deposited In_2O_3 films had an optical transmittance of 76% in visible range and an electrical resistivity of 6.5×10^{-3} Ω cm, while In_2O_3/Ti films had different optical and electrical properties that were influenced by the thickness of the Ti buffer layer. The lowest resistivity of 2.6×10^{-3} Ω cm was observed at In_2O_3 90 nm/Ti 10 nm films and the highest optical transmittance of 71%, was obtained at the In_2O_3 95 nm/Ti 5 nm films.

In this study, it can be concluded that the effective thickness of Ti buffer layer is 10 nm in In_2O_3/Ti bi-layered films [1,2].

Table 64. A Comparison of Figure of merit of films

Thickness of In_2O_3/Ti film (nm)	Sheet resistance [Ω/sq]	Transmittance [%]	Figure of merit [$10^{-6}\times\Omega^{-1}$]
100/0	650	76.1	99
95/5	380	71.0	85
90/10	260	70.4	120
85/15	290	52.6	5.6
80/20	340	46.1	1.3

References:

[1] G. Haacke, J. Appl. Phys., 147 (1976) 4086
[2] J.H. Chae and Daeil Kim, Renewable Energy, 35 (2010) 314

Acknowledgement:

This research was financially supported by the Ministry of Education (MOE) and National Research Foundation of Korea(NRF) through the Human Resource Training Project for Regional Innovation (No. NRF-2013H1B8A2032122).

TF-P06

Composition-dependent Functional Properties of High Quality PZT Films for Micro-scale Electronic Device Applications

J. S. KIM[1], S. Y. LEE[1], H. S. SHIN[1], J. H. YEOM[1], S-H. KIM[2]
[1]*R&D Center, KCMC Co., Ltd. Yongin, Gyeonggi, 446-908, Korea*
[2]*School of Engineering, Brown University, Providenece, RI02912, USA*

Keywords: PZT Film, Chemical Solution, Pyroelectric, Piezoelectric, Dielectric

The wide range of functional properties available in ferroelectric materials, including polarization, pyroelectric, dielectric and piezoelectric responses has received significant attention in current micro-scale electronic device applications. Among ferroelectric family, $Pb(Zr,Ti)O_3$ [PZT] films are considered as most promising candidates for infrared sensors, high-k capacitors, piezoelectric sensors and actuators since they can produce the highest pyroelectric current, dielectric constant and mechanical strain under the stringent control of several key parameters. To develop PZT films and to optimize their properties for these applications, it is necessary to have a comprehensive knowledge regarding the mechanisms and the parameters contributing to the optimized electrical properties. As known from bulk ceramics, the piezoelectric and the dielectric properties vary substantially with composition (Zr to Ti ratio). While the bulk PZT ceramics have been well investigated, there is still a lack of understanding for the film properties, particularly as a function of the film composition and the thickness. To make a reliable property map and to find an appropriate application of PZT films, a systematic investigation on the films with various film composition and thickness is extensively performed using KCMC's high quality PZT chemical solution.

Here, we describe the relationships between the effects of film composition and thickness on the pyroelectric, the piezoelectric and the dielectric properties, and also introduce a new chemical solution with unique properties for high quality film preparation in detail.

TF-P07

Effect of annealing condition on properties of $SnO_2/Zn/SnO_2$ multilayer thin films deposited by RF sputtering

Sung Jae Kim[1], Keun Young Park[1], Yeong Seung Jeong[1], Tae Kwon Song[1], Hang Joo Ko[2], Bon Heun Koo[1*]

[1]*School of Materials Science & Engineering, Changwon National University, Changwon, 641-773, South Korea*

[2]*Photovoltaic and Optoelectronic device center, Korea Photonics Technology Institute(KOPTI),* Gwangju, 500-779, South Korea

Keywords: TCO, Multi-layer films, Transmittance, Resistivity, Annealing

Transparent conducting oxides (TCOs) have been extensively studied for a long time due to the variety of their applications; for example, flat-panel displays, light-emitting diodes, touch panels. Recently, some researchers proposed TCO/metal/TCO multilayer structures with much lower resistance as good candidate for electrode devices. Several advantages of TCO/metal/TCO multilayer structures have been reported, which have include low resistance, high optical properties in the visible light range and relatively better chemical stability than single layered metal films.[1-3]

In this study, the $SnO_2/Zn/SnO_2$ multilayer thin films deposited on quartz substrate have been prepared by RF sputtering method using SnO_2 (99.99%) and Zn (99.99%) targets. In order to study the effect of thermal diffusing temperature and time on the structural, electrical and optical performances of $SnO_2/Zn/SnO_2$ multilayer films, the deposited films were annealed at different temperatures for different durations. Structural properties of $SnO_2/Zn/SnO_2$ thin films were studied by X-ray Diffraction (XRD) patterns. The optical and electrical properties were investigated by UV-Vis spectrometer and Hall effect measurement.

References:

[1] Oh D, No YS, Kim SY, Cho WJ, Kwack KD, Kim TW. J Alloys Compd (2011) p.2176
[2] Guille´n C, Herrero J. Thin Solid Films. (2011) p.17.
[3] Hong CH, Jo YJ, Kim HA, Lee IH, Kwak JS. Thin Solid Films. (2011) p.6829

Acknowledgement:

This research was financially supported by the Ministry of Education, Science Technology (MEST) and National Research Foundation of Korea(NRF) through the Human Resource Training Project for Regional Innovation (2012H1B8A2026212), This research was supported by the MSIP(Ministry of Science, ICT&Future Planning), Korea, under the ITRC(Information Technology Research Center) support program supervised by the NIPA(National IT Industry Promotion Agency)(NIPA-2014-H0301-14-1016)

TF-P08

Optimized Process Conditions of Pt Bottom Electrode for High Quality Piezoelectric Films and Multi-functional MEMS Devices

S. Y. LEE[1*], J. S. KIM[1], H. S. SHIN[1], J. H. YEOM[1], S-H. KIM[2]
[1]*R&D Center, KCMC Co., Ltd. Yongin, Gyeonggi, 446-908, Korea*
[2]*School of Engineering, Brown University, Providenece, RI02912, USA*

Keywords: MEMS, Platinum electrode, Sputtering, PZT

High quality piezoelectric thin films have been employed in micro-electro-mechanical systems (MEMS) with a broad spectrum of applications, including energy harvesters, micro-actuators, ultrasonic transducers, ink-jet print-heads and piezoelectric sensors etc. Many of these applications require the films to be supported by non-brittle and stable substrates with specific electrodes. Although a number of experimental and theoretical contributions have been made concerning the performance enhancement of piezoelectric films in MEMS devices, no clear consensus has emerged regarding the effects of bottom electrodes on the properties of these films. Generally, the physical and the electrical properties of these films are critically dependent on the quality of the bottom electrode on the substrate. Among many noble metal electrodes, Pt has been extensively used for most piezoelectric films and devices due to its low resistivity, and excellent corrosion and oxidation resistance.

The objective of this research is to optimize the process conditions for the preparation of high quality Pt bottom electrodes for reliable MEMS devices since the understanding and the control of the Pt electrode are critically important to obtain the maximized property enhancement of the piezoelectric films and the multi-functional devices.

To address these issues, we perform extensive series of experiments with stringent process control parameters such as substrate temperature, pulsed DC power, and bias voltage using our unique DC pulse magnetron sputtering system. Based on our systematic experimental results, we optimize the process parameters for highly textured orientation, excellent adhesion property, dense microstructure, and low resistivity of the Pt electrodes. In parallel, we demonstrate the property improvement of piezoelectric PZT films on our optimized Pt bottom electrodes for successful fabrication of multi-functional MEMS devices.

Detailed experimental results and related mechanisms will be discussed.

TF-P09

Electronic structure and magnetic properties of Mn doped TiO_2 thin films using X-ray absorption spectroscopy

Shalendra Kumar[1], Tae Kwon Song[1*], M.H. Lee[1], J.S. Park[1], D. J. Kim[1], M. H. Kim[1], W. J. Kim[2], K.W. Jang[2], K.H. Chae[3]

[1]School of Materials Science and Engineering, Changwon National University, Changwon, Gyeongnam, 641-773, Republic of Korea

[2]Department of Physics, Changwon National University, Changwon-641-773, S. Korea

[3]*Advanced Analysis Center, Korea Institute of Science and Technology, Seoul 136-791, Republic of Korea*

Keywords: Electronic material; thin film; PLD; NEXAFS; magnetic properties

After the discovery of room temperature ferromagnetism in Co doped anatase and rutile TiO_2 by Matsumoto et al., a lot of efforts have been made to develop RT-FM in TM doped TiO_2. Among several wide band gap semiconductors, TiO_2 is a significant material due to their outstanding properties such as excellent optical transmittance in the visible and near infrared wavelength range, high dielectric constant and low loss tangent and high index of refraction etc. Besides these potential applications, TiO_2 is an ideal system for the room temperature magnetic semiconductors. In this work, we have grown the thin film of Mn doped TiO_2 on $LaAlO_3$ (001) substrate using pulsed laser deposition method. X-ray diffraction (XRD), near-edge x-ray absorption fine structure spectroscopy (NEXAFS), and magnetic hysteresis loop measurements were used to understand the origin of ferromagnetism in pristine and O_2 annealed film. Our structural analysis reveals a single phase nature of the film and excludes the presence of any secondary phase. The NEXAFS spectra collected at Ti $L_{3,2}$, and Mn $L_{3,2}$ edge infers that Mn and Ti ions are in +2 and +4 valence state, respectively. DC magnetization hysteresis measurements reflect that of Mn doped TiO_2 film exhibit ferromagnetic ordering at room temperature.

References:

[1] Y. Matsumoto, M. Murakami, T. Shono, T. Hasegawa, T. Fukumura, M. Kawasaki, et al., Room-Temperature Ferromagnetism in Transparent Transition Metal-Doped Titanium Dioxide, Science 80 291 (2001) 854–856.

Acknowledgement:

This work was supported by the Priority Research Centers Program through the National Research Foundation of Korea (NRF) funded by the Ministry of Education, Science and Technology (MEST;2012-045424) and by the National Research Foundation of Korea (NRF) Grant funded by the Korea government (MSIP) (2011-0030058).

TF-P10

Development of High Energy Density Capacitors Using Anti-ferroelectric PLZT Thin Films

Don Chan Woo[1], Chang Young Koo[1], You Jeong Eum[1], Hee Young Lee[1*]
[1] *School of Materials Science and Engineering, Yeungnam University, Gyeongsan, 712-749, Korea*

Keywords: Anti-ferroelectric, PLZT, Capacitor

This work is for the demonstration of a new approach to power electronic film capacitors for large energy storage density using cost effective chemical solution-derived anti-ferroelectric thin film material systems. It provides an advanced processing platform to dramatically expand the functionality and capability of high power energy storage systems.

A critical issue of all energy storage devices is the need to reduce size and weight so that power conditioning systems of increasing capacity and functionality can be incorporated into a greater range of applications. The main limitation to improving these systems, particularly on mobile platforms, is the capacity, the size and the reliability of the energy storage capacitors. Of all the components used to make power conditioning systems, capacitors usually occupy the largest volume and weight.

Tantalizing tastes of success of the scaling potential have been reported, but no devices without degradations or failures such as electrical or mechanical fatigue and breakdown have yet been scaled to achieve clearly superior energy storage density to existing large size bulk or multi-layer capacitors. Moreover, non-linear dielectrics that are normally utilized in oxide capacitors display decreasing dielectric displacement at the high fields desired for high energy density applications.

In contrast, the dielectric displacements of anti-ferroelectrics are maximized at the field-induced transition between ferroelectric and anti-ferroelectric phases. A key focus of the research is on understanding the switching behavior and tailoring the switching to the key demands of high energy density capacitors operating at high fields. In addition, this work focuses on addressing key questions and solutions about the scaling and the reliability of cost-effective high density energy storage capacitors using anti-ferroelectric thin films, thereby making a major advance towards determining the wide range of utility of proposed materials and device structures.

TF-P11

Multilayer Coatings for Protecting Carbon Materials at temperatures at 1700 C or higher

Changhun Hwang[1], Jondo Yun[2]
[1] *Department of Election Microscopy Laboratory, Insitute for Instrumental Analysis, Kyungnam Univerity, Changwon, 631-701, korea*
[2] *Department of Nano Materials Engineering, Kyungnam University, Changwon, 631-701, Korea*

Keywords: Multilayer, Ceramics, carbon/carbon composite, Oxitation Resistance, CVD

Carbon materials like graphite, or carbon fiber reinforced carbon matrix composites have excellent properties at high temperatures in an inert atmosphere, but are degraded rapidly by oxidation above 400^{o}C in air. Silicon carbide multilayer coating was designed for protecting carbon materials from oxidation. The coating was prepared by consecutive process of chemical vapor deposition (CVD) and solution method. The SiC and buffer layers were prepared by CVD at 1100-1150^{o}C under vaccum using methyltrichlorosilane, methane, and hydrogen as source and carrier gases. Functional layer having SiOC glassy materials was prepared by dip-coating and decomposition of inorganic polymers. The functional layer had self-healing capability by which cracks formed in refractory ceramic layer were healed at high temperature. Oxidation test for carbon/carbon composites with multilayer coating showed excellent oxidation resistance at 1700^{o}C. The microstructure and chemical composition were examined before and after the test with scanning electron microscopy.

TF-P12

Thin film multi layer ceramic capacitors (MLCC) using high-dielectric $Bi_2Mg_{2/3}Nb_{4/3}O_7$ (BMNO)

Ji-hyun Park[1], and Soon-Gil Yoon[1,2*]
[1]*Advanced Electronic Circuit Substrate Engineering, Chungnam National University, Daeduk Science Town, Daejeon, 305-764, South Korea*
[2]*Department of Materials Engineering, Chungnam National University, Daeduk Science Town, Daejeon, 305-764, South Korea*

Keywords: MLCC, Materials, Structure, Dielectric, Capacitor, Thin film

BMNO dielectric materials with a pyrochlore structure have been chosen and they have quite high dielectric constants about 210 for the bulk material. In the case of thin films, 200-nm-thick BMNO films deposited at room temperature by Radio-Frequency magnetron Sputter (RF Sputter) showed a low leakage current density of about 10^{-8} A/cm^2 at 5 V and a dielectric constant of about 20 at 100 kHz. High dielectric constant BMNO thin films grown at room temperature have many applications for capacitor.

A ceramic capacitor is a fixed value capacitor in which ceramic material acts as the dielectric. It is constructed of two or more alternating layers of ceramic and a metal layer acting as the electrodes. Ceramic capacitors, especially the multilayer style (MLCC), are the most produced and used capacitors in electronic equipment.

MLCC should be thinner due to its miniaturization, so there is need to thin film dielectric material which have good electrical characteristic.

It is necessary to minimize the thickness of dielectric layer to improve the capacitance, for the purpose of developing the thin film multi layered ceramic capacitor (MLCC). In this work, the relationship between dielectric properties of MLCC and thickness of dielectric such as dielectric thickness is under 200 nm. In addition, properties of annealed MLCC were compared with MLCC manufactured by room temperature. It was found that annealed MLCC showed a low leakage current density. In this work we present the MLCC structure composed BMNO dielectric by RF Sputter. Also when we using MLCC, capacitance of MLCC is superior to capacitor.

It is expected that this report will help MLCC miniaturization.

TF-P13

Simultaneous realization of electromagnetic shielding and antibacterial effect of Al doped ZnO multi-layer thin films

Hyung-Jin Choi and Soon-Gil Yoon*
Department of Materiasl Science and Engineering Chungnam National University, Daeduk Science Town, Daejeon 305-764, Korea

Keywords: Electromagnetic shielding, Antibacterial effect, Al doped ZnO, Sputtering

With the increasing use of electronic products, their electromagnetic radiation could cause problem, if these high-density electromagnetic waves are not screened effectively. Therefore, electromagnetic interference is becoming a serious global problem. In general, high conductive metal materials are the best shielding materials for reflecting and absorbing electromagnetic waves. However, there is an essential difficulty in satisfying both the electromagnetic shielding performance and the high transparency. Especially, because the touch-panel of the smart device is operated by hand, they are contaminated by the bacteria during use, resulting in the damaged fatal health by these bacteria. Therefore, the simultaneous implementations of the antibacterial properties and electromagnetic wave shield in order to protect us from these hazards were required. In the present study, we intended to achieve both antibacterial properties and electromagnetic shielding using the Al-doped ZnO multi-layer films.

FTS (Facial Target Sputtering) magnetron sputtering was used for the Al doped ZnO thin films instead of the conventional RF sputtering because the FTS sputtering could avoid the damage for the plasma as well as fabrication of thin films with a high quality. The 300-nm thick AZO thin films grown on glass substrate showed a resistivity of about 7×10^{-4} Ω-cm and a transmittance of about 90% at a wavelength of 550 nm. However, the conductivity of the crystallized AZO thin films are deteriorated by absorbing moisture in the air, indicating a long-term stability problem. Therefore, it is intended to ensure long-term stability and an increase of the electrical conductivity by inserting the Ag layer between the AZO thin films. The AZO/Ag/AZO multilayer thin films on glass substrate showed a resistivity of about 7×10^{-5} Ω-cm and a transmittance of about 90% at a wavelength of 550 nm. AZO multi-layer thin films were investigated for the electromagnetic shielding effectiveness measured by 2-port network method at 1.5 ~ 3GHz. An antibacterial effect (Staphylococcus aureus and Escherichia coli) was measured by the film attachment method (JIS Z 2801).

References:

[1] Takahiro Yamada, Tetsuya Yamamoto etc, *Thin Solid Films*. 517, 1027, (2008).
[2] Mingjun Hu, Robert Kwok-Yiu Li etc., *Langmuir*. 28, 7101, (2012)

TF-P14

Sol-Gel Preparation of M^+-Doped CuO ($M^+ = Li^+, Na^+, K^+$) Thin Films and Their Photocathodic Properties

Kota ISOBE[1], Hiroaki UCHIYAMA[2*] and Hiromitsu KOZUKA[2]
[1]*Graduate School of Science and Engineering, Kansai University, Suita, 564-8680, Japan*
[2]*Department of Chemistry, Materials and Bioengineering, Kansai University, Suita, 564-8680, Japan*

Keywords: Sol-gel method, CuO, Photoelectrode

Wet-type solar cells using semiconductor photoelectrodes have been widely investigated since the discovery of the Honda-Fujishima effect in 1972 [1]. CuO, a p-type semiconductor, is receiving much attention as a candidate of an photocathode, because CuO has a relatively small band gap of ca. 1.4 eV that provides photoresponse to the visible light. However, CuO normally shows low energy conversion efficiency, and thus the improvement of the photocathodic performance is required. In this work, we prepared M^+-doped porous CuO films ($M^+ = Li^+, Na^+, K^+$) by sol-gel method, and investigated the effect of the porous structure and the doping with M^+ ions on the photocathodic performance.

CuO films were prepared by dip-coating from the solutions consisting of $Cu(NO_3)_2$, $LiNO_3$, NaCl, KNO_3, H_2O and poly(vinylpyrrolidone) (PVP, viscosity average molecular weight of 960,000) ($[Cu(NO_3)_2]$ = 0.45–0.50 M, $[LiNO_3]$, [NaCl] or $[KNO_3]$ = 0–0.05 M, and [PVP] = 0.05–0.40 M). Precursor films were deposited on silica glass substrates coated with FTO at a withdrawal speed of 3 cm min^{-1}. The films thus obtained were heated at 600 ºC for 30 min in air. The dip-coating and the heat treatment were repeated 2–10 times so that the resultant film thickness was ca. 220 nm. The photocathodic properties were studied in a three-electrode cell with an aqueous buffer solution of pH = 7 as the supporting electrolyte.

Pure CuO films were prepared from the solutions of $[Cu(NO_3)_2]$ = 0.50 M and [PVP] = 0.05–0.40 M. The diffraction peaks attributed to CuO were detected in the XRD patterns for all the films. The CuO films prepared at [PVP] = 0.05–0.25 M had porous structure, and the porosity increased with increasing [PVP] (Figure 1 (a) - (c)). On the other hand, homogeneous films were not obtained at [PVP] = 0.40 M (Figure 1 (d)). The CuO films exhibited photocathodic response under UV and visible light. The photocathodic performance was enhanced with increasing [PVP] from 0.05 M to 0.25 M, and the CuO film prepared at [PVP] = 0.25 M exhibited the maximum IPCE (incident photon-to-current efficiency) of 8.7 % and 4.9 % at the wavelengths of 300 and 500 nm, respectively (Figure 2). On the other hand, IPCE decreased with increasing [PVP] from 0.25 M to 0.40 M (Figure 2).

M^+-doped porous CuO films ($M^+ = Li^+, Na^+, K^+$) were prepared from the solutions of $[Cu(NO_3)_2]$ = 0.45 M, $[LiNO_3]$, [NaCl] or $[KNO_3]$ = 0.05 M and [PVP] = 0.25 M. The M^+-doped CuO films exhibited photocathodic response under UV and visible light, while IPCE decreased by the doping with M^+ ions.

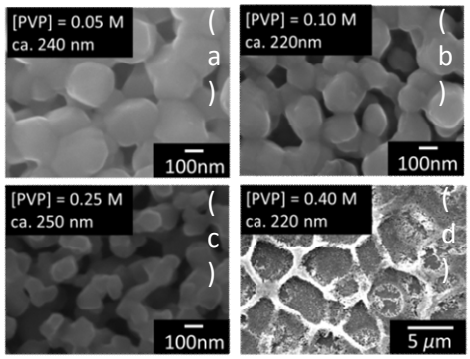

Figure 1. FE-SEM images of the CuO films prepared at [PVP] = 0.05–0.40 M.

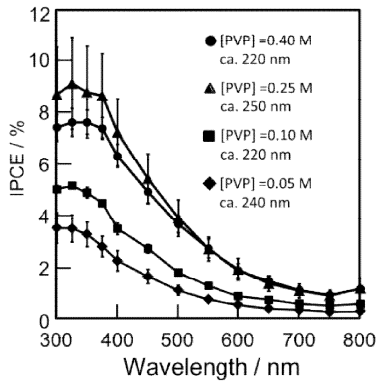

Figure 2. Action spectra of the CuO films prepared at [PVP] = 0.05–0.40 M.

References:

[1] A. Fujishima and K. Honda, *Nature*, **238**, 37 (1971)

TF-P15

Study on surface analysis by solution agitation of the electroless copper plating for flexible devices

Seung-deok Baek[1], Na-young Kim[1], Hyung-chul Kim[2], Sa-kyun Ra[2], Yoen-seung Lee[1*]
[1]*Department of Information&Communication Engineering, Dongseo-daero,125,Yuseong-gu Daejeon,Korea*
[2]*Department of Material Engineering, Dongseo-daero, 125, Yuseong-gu, Daejeon, Korea*

Keywords: Electroless Cu plating, Flexible devices, Agitation

Because the present study, a flexible device recently appeared, thereby forming a Silver paste pattern using a screen printing method to the wiring selective on PET. The enhanced mechanical bonding force between Silver paste the PET by the atmospheric pressure plasma treatment on the PET substrate prior to screen printing. After producing a copper thin film using an electroless plating method and the next, and analyzed with respect to the surface of the copper thin film by changing the stirring speed.

The hydrogen ion concentration(pH) during the electroless copper plating was neutral condition is 7. When plating is performed to give a variation from 0rpm to 1000rpm and the stirring rate of the solution. PET is used as the substrate. Copper film grown by electroless plating, and analyzed the characteristics by using XRD(X-ray Diffraction), FE-SEM(Field Emission Scanning Electron Microscope), AFM(Atomic Force Microscope), and XPS(X-ray Photoelectron Spectroscopy).

References:

[1] Yang-Rae Cho, Youn-Seung Lee, Sa-Kyun Ra, Korean Journal of Materials Research, Vol.23, No.11, pp. 661-665, 2013
[2] Joo-Yul Lee, Man Kim, Deok-Jin Kim, J. Kor. Inst. Surf. Eng, Vol. 41, No. 1, 2008.

TF-P16

Effects of DMAB in Electrolss Ni-B Plating for F-PCB

Hyung-Chul Kim[1], *Sa-Kyun Rha[1], Na-Young Kim[2], Seong-Duk Baek[2] and Youn-Seoung Lee[2]
[1] *Dept. of Materials Engineering, Hanbat National University, Daejeon, 305-719, Korea* [a]
[2] *Dept. of Information and Communications Engineering, Hanbat National University , Daejeon, 305-719, Korea* [a]

Keywords: DMAB, Amorphous, Electroless plating, Nickel-Boron

Flexible and portable electronic products are the most popular because of further miniaturization accompanying more functionality per device and low costs.[1] Flexible substrate such as Polyimide(PI) and Polyethylene terephthalate(PET) is used for Flexible Printed Circuit Board(F-PCB) because of lightness, thin thickness, and superior flexibility. So, F-PCB will become more important To metalize PET substrate.

In this study, we were plating the Nickel-Boron(Ni-B) film on printed Silver(Ag) on PET by electroless plaitng in neutral solution at low temperature for reducing the substrate damage. Ni–B alloy film is one of the functional coatings and is applied in aerospace, automotive, chemical and electrical industries due to their high hardness, high wear and corrosion resistances and good solderability.[2] We investigated the amount of Dimethylamine Borane(DMAB) effect as a reducing agent for electroless Ni-B.

X-ray diffraction (XRD), Field-Emission Scanning Electron Microscopy (FE-SEM), X-ray Photoelectron Spectroscopy (XPS), Extended X-ray Absorption Fine Structure (EXAFS) were used for analysis of Ni-B films. As a result of XRD, increasing the amount of DMAB made a amorphization of Ni-B film and EXAFS data agree with the result of the XRD also. As a result of OM, the Ni-B film grew selectively on only patterned Ag paste surface.

References:

[1] S. H. Park and D. N. Lee, Journal of Materials Science, 23(5), 1643–1654 (1988)
[2] H, Ogihara, K. Udagawa and T. Saji, Surface & Coatings Technology, 206, 2933 (2012)

NA-P01

Effect of intrinsic defects on the optical and magnetic properties of Co: ZnO nanoparticles based DMS

Rezq Naji Aljawfi[1]
[1]*Department of Physics, Ibb University, Ibb, Yemen Arab*

Keywords: Native Defects, ZnO, Nanopartecles, Optical, Ferromagnetism

The optical and ferromagnetism in pure ZnO and Co doped ZnO nanoparticles (NPs) have been reported, The NPs were synthesized through citric-gel process. The single phase nature and the incorporation of Co^{2+} ions into the lattice structure of ZnO have been revealed via X-ray diffraction (XRD) analysis, energy dispersive X-ray spectroscopy (EDS) and Raman spectroscopy. Calculation based on the XRD data shows that the average crystallite sizes of pure ZnO and Co doped ZnO NPs were 19.5 and 14.6 nm respectively. The substitution of Co^{2+} ions affects on the PL spectrum by shifting the energy states, and significantly decreases the band gap energy. The energy deep levels (EDLs), which are created by native defects like oxygen vacancy (V_O), zinc vacancy (V_{Zn}), zinc interstitial (Zn_i), have been estimated through PL and micro-Raman spectroscopic studies. The samples exhibit ferromagnetic (FM) hysteresis loop at 300 K, which has been discussed based on the spin-spilt conduction band model. In this model, the defects of V_O and Zn_i intermediate the interactions between the magnetic moments of the localized electrons in highly state ($3d^7$) of Co^{2+} ions. The week FM can be attributed to present a insolated ions of Co, which is paramagnetic.

NA-P02

Separation of H_2/CO_2 mixed gas through porous alumina compact

Kota GOTANDA, Yoshihiro HIRATA*, Soichiro SAMESHIMA, Taro SHIMONOSONO
Department of Chemistry, Biotechnology, and Chemical Engineering, Kagoshima University
1-21-40 Korimoto, Kagoshima 890-0056, Japan

Keywords: Alumina, Gas separation, Hydrogen, Carbon dioxide

In our previous paper[1], a relatively high flux of permeated H_2 gas was measured in a porous Al_2O_3 compact with average pore size 60 nm at near zero MPa of the pressure gradient between inlet and outlet gases. However, the permeation of N_2 and CO_2 gases occurred above a critical pressure gradient. In this work, the separation of H_2/N_2 and H_2/CO_2 mixed gas through a porous alumina compact was carried out at room temperature. Figure 1 shows the ratio of gas permeability (α mol/msPa) of H_2 to CO_2 gases as a function of the pressure gradient. The ratio increased with decreasing pressure gradient. This trend was more significant at a higher CO_2 composition of the inlet gas. In Fig. 1 the separation ratios for ideal Poiseuille flow (viscous flow) and Knudsen flow of CO_2 and H_2 gas were also presented. The measured result for 20%H_2-80%CO_2 mixed gas indicates the high separation ability when compared with the prediction from the α value for single gas.

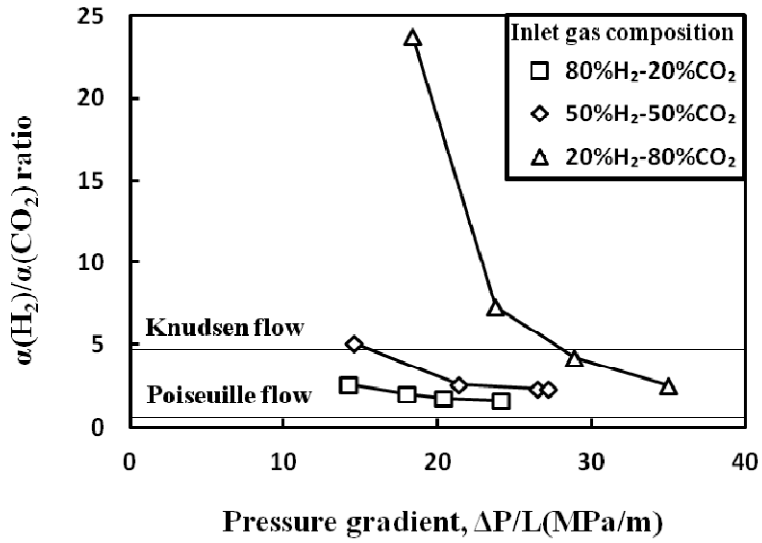

Figure 1 Pressure gradient dependence of the permeability coefficient ratio for H_2 and CO_2 mixed gas

Reference:

[1]H.Shirasaka, T.Shimonosono, Y.Hirata, S.Sameshima, J. Asian Ceram. Soc, 1(2013) 368-373.

NA-P03

Effect of time on the growth of flowerlike rutile nanostructures and their application for degradation of organic dyes

Rehan DANISH, M. S. Anwar, Bon Heun Koo*
School of Nano and Advanced Materials Engineering, Changwon National University, Changwon, Gyeongnam, 641-773, South Korea

Keywords: Rutile, Flower morphology, XRD, organic pollutant, UV

Since the discovery of photocatalytic water splitting by Honda and Fujishima there has been many efforts to utilize this property of TiO2 nanostructures for other applications. One of the major applications of the TiO2 nanostructures is their ability to degrade the organic pollutants in the presence of UV light. Several research groups have been working to find a more efficient nanostructure which takes less time and is much economical to synthesize. Aspect ratio of a nanostructure plays a vital role in enhancing the photocatalytic degrading efficiency of a nanostructure. As the aspect ratio of the nanostructure increases the possibility of the charge carrier combination decreases and hence the efficiency increases. In this study we demonstrate an easy and scalable technique to synthesize high aspect ratio nanostructures and we analyze the effect of varying time on the properties of the nanostructures. The obtained nanostructures were characterized using X- ray diffraction spectrometry for the structural properties and the morphological evolution was analyzed using FESEM. The optical properties were analyzed using UV-Visible spectrometry and the photocatalytic efficiency was analyzed by degradation of Methylene Blue under the presence of UV light. The 96% degradation of MB took place in ~ 3 hrs that is much better than earlier reports making the obtained nanostructures much efficient for the degradation of organic pollutants.

Acknowledgement:
(No.2011-0030058)(2012H1B8A2026212)

NA-P04

Carbon Nanotubes Grown on Cobalt Supported Zeolite-Porous Ceramics

Jung Gyu PARK[1], Wei ZHAO[2], Sangram MAZUMDER[1], and Ik Jin KIM[1]*
[1]*Institute of Processing and Application of Inorganic Materials, (PAIM), Department of Materials Science and Engineering, Hanseo University, Hanseo 1 ro, Haemi-myun, Seosan-si, Chungcheongnam-do, 356-706, Korea*
[2]*School of Material Science and Engineering, Yeungnam University, 280, Daehak-ro, Gyeongsan-si, Gyeongsangbuk-do, 712-749, Korea*

Keywords: Carbon nanotubes, Porous Ceramic, Direct foaming, Ion-exchange reaction.

Macro porous ceramics are useful in the industrial sphere due to its large surface area with interconnected pores. Also, carbon nanotubes(CNTs) can dramatically increase surface area. With those benefits composite as a nano filter. But normally on porous ceramics CNTs cannot be grown on their surface. In this study, we synthesized CNTs on porous ceramics using ion-exchanged zeolite coating process. Here, we have used cobalt ion for the ion exchange process. Substrate of CNTs consists of inorganic particles (for example Al_2O_3 and SiO_2) were synthesized by direct foaming method using short chain carboxylic amphiphiles such as propyl gallate, with average solid content of 30vol%, average pore size 100~150um. The CNTs were grown by catalytic chemical vapor deposition (CCVD) method. Field Emission Scanning Electron Microscope (FE-SEM) and Transparent Electron Microscope (TEM) images for investigate synthesized CNTs morphology, microstructure and surface. Also CNTs were investigated for characterization by Raman spectroscopic analysis and TGA/DTA study. To compare surface area, BET analysis was done.

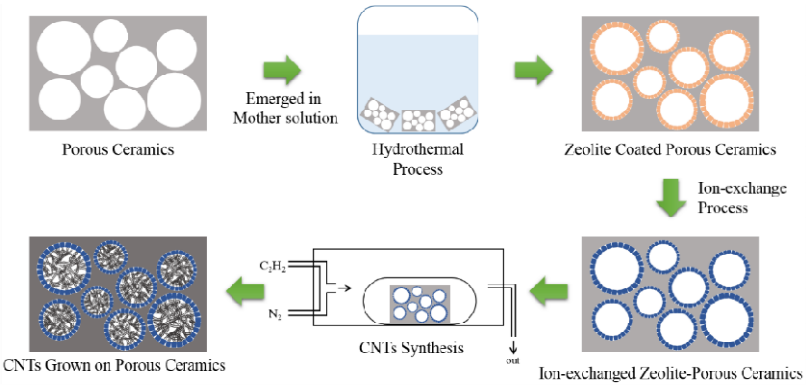

Figure 65 Schematic diagram of CNTs grown on Co-supported zeolite-porous ceramics

References:

[1] W. Zhao, B. Basnet and I. J. Kim, Journal of Advanced Ceramics 1(3) (2004) *p*. 179.
[2] A. Srivastava, O.N. Srivastava, S. Talapatra, R. Vajtai and P. M. Ajayan, Nature (2004) *p*. 610.
[3] A. Pokhrel, J. G. Park, J. S. Nam, D. S. Cheong, and I. J. Kim, Journal of the Korean Ceramic Society 48(5) (2011) *p*. 463.
[4] A. Pokhrel, J. G. Park, G. H. Jho, J. Y. Kim and I. J. Kim, Journal of Korean Ceramics Society 48(6) (2011) *p*.600

Acknowledgement:

I would like to thank Prof. Dr. Ik Jin Kim for his kind cooperation and continuous follow-up towards my work. Also, I would like to thank Hanseo University for providing a suitable laboratory for the work.

NA-P05

Carbon nanotubes synthesized on Fe ion loaded porous ceramics used as a CNT Nano-filter

Sangram MAZUMDER[1], Jung Gyu PARK[1], Wei ZHAO[2], Naboneeta SARKAR[1] and Ik Jin KIM
[1]*Institute of Processing and Application of Inorganic Materials, (PAIM), Department of Materials Science and Engineering, Hanseo University, Hanseo 1 ro, Haemi-myun, Seosan-si, Chungcheongnam-do, 356-706, Korea*
[2]*School of Material Science and Engineering, Yeungnam University, 280, Daehak-ro, Gyeongsan-si, Gyeongsangbut-do, 712-749, Korea*

Keywords: Carbon nanotubes, chemical vapor deposition, CNTs nano-filter, porous ceramics.

Here, we report a novel filter, named as the "CNT nano-filter", composed of carbon nanotubes (CNTs) grown on an ion-exchanged zeolite coated porous ceramic substrate. Porous ceramic matrix mainly consisting of Al_2O_3 and SiO_2 with an average solid content of 30% were processed by direct foaming method for this study. Zeolite NaA crystals were coated on the porous ceramic matrix and was ion exchanged with metal ions (Fe) for its catalytic activity in the synthesis of CNTs. The carbon nanotubes were grown directly upon the porous ceramic substrate using the Chemical Vapor Deposition (CVD) method. The Field Emission Scanning Electron Microscope (FESEM) and Transparent Electron Microscope (TEM) images of the synthesized CNTs on the porous ceramic substrate were observed for morphology, surface quality and structure analysis. This is here the basis for filtration. Crystallinity and defects of the CNTs were studied by Raman spectroscopy and thermo gravimetric analysis (TGA). The CNTs were seen to have grown as bush-like structures creating a close network inside the pores of the ceramic substrate, which shall owe to its filtration ability.

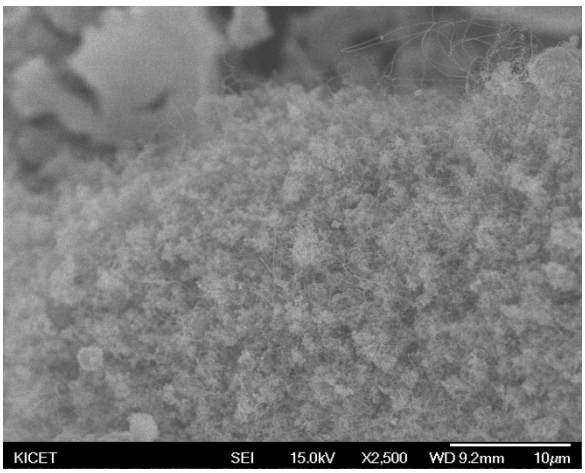

Figure 1 FESEM images of CNTs grown on porous ceramics

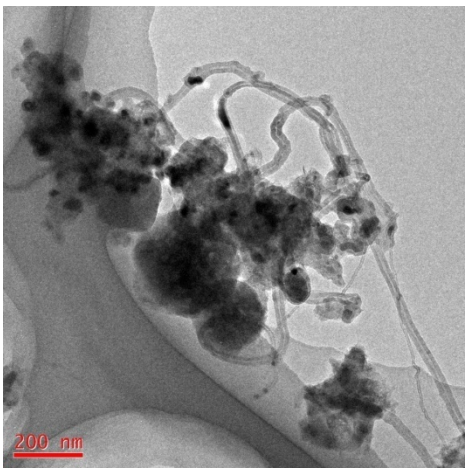

Figure 2 TEM image of CNTs grown on porous ceramics

References:
[1] W. Zhao, B. Basnet, and I. J. Kim, Journal of Adcanced Ceramics 1(3), 179-193, (2014).
[2] A. Srivastava, O. N. Sricastava, S. Talapatra, R. Vajtai and P. M. Ajayan, nature, 3, 610-614, (2014)

Acknowledgement:
I would like to thank Prof. Dr. Ik Jin Kim for his kind cooperation and continuous follow-up towards my work. Also, I would like to thank Hanseo University for providing a suitable laboratory for the work.

NA-P06

Visible-light-induced Enzymatic Reaction of Peroxidase Hybridized with Layered Iron-titanate

Daiki ITO, Kai KAMADA*, Taro UEDA, Takeo HYODO, Yasuhiro SHIMIZU
Graduate School of Engineering, Nagasaki University, Nagasaki 852-8521, Japan

Keywords: Enzymatic reaction, Titanate nanosheets, Photocatalytic reaction

Recently, several groups have reported that photochemical control of enzymatic activity succeeds by ultraviolet (UV) light irradiation to inorganic nanoparticles adsorbing redox enzymes [1]. In these researches, the reaction process consists of photo-excitation of the inorganic nanoparticles, followed by transfer of thermal energy, excited charge carriers, or evolved radicals to the enzymes. The present study proposes a novel photo-induced enzymatic reaction technique operated by irradiating visible light with more moderate energy than UV light. More specifically, horseradish peroxidase (HRP) is adsorbed to semiconducting layered iron-titanate (FTO) with a narrow band gap, and then the HRP/FTO is exposed to visible light for triggering of enzymatic oxidation.

An aqueous colloidal solution of FTO was fabricated via a solution route according to a literature [2]. A buffered solution of HRP (pH = 4) was mixed with the colloidal solution to hybridize with the FTO (HRP/FTO) through electrostatic interaction. In the present study, Amplex Ultrared (AUR) was selected as a model substrate. A mixed solution of HRP/FTO and AUR was injected to a well of 96-well black microplate. To initiate a photo-enzymatic reaction, the well was exposed to blue light (410 nm). Enzymatic oxidation of non-fluorescent AUR under the presence of peroxide causes the formation of a bright fluorescent product. Therefore, the reaction rate was evaluated by measuring relative fluorescence unit (RFU, Ex. 528/20 nm, Em. 590/35 nm) as a function of irradiation time.

Figure 1 shows a schematic model of the proposed photoenzymatic reaction. HRP is transformed into an activated state as a result of oxidation with holes generated in the valence band of the irradiated FTO that can absorb visible light with a wavelength shorter than ca. 430 nm. The excited HRP leads to enzymatic conversion of AUR. Figure 2 indicates variations of relative fluorescence unit (RFU) during the blue light irradiation to the solutions. No rise in RFU in the AUR solution containing only FTO was confirmed, indicating that the photocatalytic oxidation of AUR by FTO did not occur under the visible light. RFU in the HRP/FTO solution were linearly increased with the irradiation time, and were larger than that of free HRP. In addition, the titanate nanosheets excluding Fe (TNS) with a wide band gap did cause little enhancement of RFU. These results indicate that the visible light irradiation to the FTO adsorbing HRP triggers the enzymatic conversion of organic substrates.

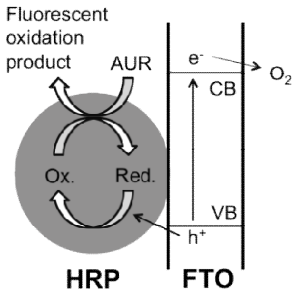

Figure 66 Schematic model of visible-light-induced enzymatic reaction of HRP/FTO

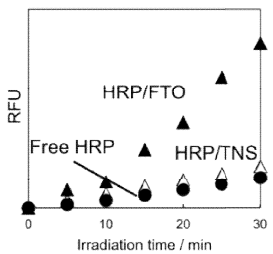

Figure 2 Enhancements of RFU of AUR including free HRP, HRP/FTO, or HRP/TNS during blue light irradiation at room temperature.

References:

[1] L. Fruk, V. Rajendran, M. Spengler, M. Niemeyer, ChemBioChem, 8 (2007) 2195.
[2] T. Ohya, A. Nakayama, T. Ban, Y. Ohya, Y. Takahashi, Chem. Mater., 14 (2002) 3082.

NA-P07

Tube-on-plate structured $BiVO_4/Bi_2WO_6$ heterojunction with highly efficient photocatalytic activities

Wei Zhao[1], and Ik Jin Kim[2], Sukyoung Kim[1]

[1]*School of Materials Science and Engineering, Yeungnam University, Gyeongbuk 712-749, Korea*
[2]*Department of Materials Science and Engineering, Hanseo University, Chungnam, Korea.*

Keywords: Heterojunction, $BiVO_4$, Bi_2WO_6, Photocatalytic activity, Charge transfer

As a potential solution to the global energy problem and environmental pollution, the design and synthesis of artificial photocatalysts with high activities have attracted great scientific interest worldwide [1]. In the past few decades, the conventional TiO_2 photocatalyst with high photoactivity and stability has been extensively investigated, but it is limited for practical applications due to its large band gap. Therefore, the development of visible-light-driven photocatalysts has attracted much attention.
According to the knowledge of authors, there are two main strategies to develop new visible photocatalysts. The first one is the doping of TiO_2 to extend its absorption to visible range. TiO_2 doped with carbon, nitrogen, or sulfur has shown in some cases a photocatalytic activity in the visible range. However, the methods used for the doping element introduction are not fully controlled. And the low thermal stability of these compounds limits their applications. Moreover, these dopants act as recombination centers between photogenerated electrons and holes and consequently decrease the photocatalyst efficiency. In contrast, the second strategy is to use other materials which are absorbing in the visible range. Interestingly, bismuth-based compounds, such as bismuth vanadate ($BiVO_4$) and bismuth tungstate (Bi_2WO_6), are important photocatalysts to replace cadmium-based material due to their low environmental toxicity. They have also inspired a great deal of research interest because of their high thermal stability, wide solar response, and excellent photocatalytic activity under visible-light irradiation [2-3]. It was reported that the composited semiconductor photocatalysts with the formation heterojunctions are photocatalytically more active than the individual components due to the significant recombination reduction of photogenerated charge carriers.
In this study, considering the great photocatalytic activity of both $BiVO_4$ and Bi_2WO_6, we tried to couple them into a composite. A one-pot hydrothermal method was adapted to obtain a novel tube-on-plate composite structure. The photocatalytic performance of the composite was evaluated by the degradation of rhodamine B (Rh.B) under solar light irradiation.

References:

[1] X.Han, Q. Kuang, M. Jin, Z. Xie, and L. Zheng, J. Am. Chem. Soc. 131 (2009) 3152.
[2] J. Q. Yu and A. Kudo, Adv. Funct. Mater. 16 (2006) 2163.
[3] F. Amano, K. Nogami, R. Abe, and B. Ohtani, J. Phys. Chem. C 112 (2008) 9320.

NA-P08

Superhydrophobicity from Nano/Microstructure with Carbon Nanotubes on Silica spheres

Ahrong Jeong[1], Sangbo Han[2], Hongrim Lee[3], and Jondo Yun[1,3]
1 Department of Advanced Engineering, Graduate School, Kyungnam University, Changwon, 631-701, Korea
2 Department of Electrical Engineering, Kyungnam University, Changwon, 631-701, Korea
3 Department of Nano Materials Science and Engineering, Kyungnam University, Changwon, 631-701, Korea

Keywords: Superhydrophobicity, CNTs, Silica spheres, Nanotubes

Recently nanoscience and nanotechnology have been studied intensively, and many plants, insects, and animals in nature have been found to have nanostructures in their bodies. Among them, lotus leaves have a unique nanostructure and microstructure in combination and show superhydrophobicity and a self-cleaning function to wipe and clean impurities on their surfaces. Coating films with combined nanostructures and microstructures resembling those of lotus leaves may also have superhydrophobicity and self-cleaning functions; as a result, they could be used in various applications, such as in outfits, tents, building walls, or exterior surfaces of transportation vehicles like cars, ships, or airplanes.

In this study, the coating films based on silica balls were fabricated by the self-assembly of silica using sol-gel method. And then, we grew carbon nanotubes (CNTs) on coating films by plasma-enhanced chemical vapor deposition (PECVD) method. The coating films of nano/microstructure with CNTs on silica balls were prepared. It was found that carbon nanotubes of about 20 nm lengths were formed on silica balls of 500-600 nm size. The obtained contact angle of coating film was 147°, showing superhydrophobicity.

NA-P09

In Situ Magnetic Field-Assisted Growth of High Quality GaN Nanowires

Jun Sik Kim[1], Bhaskar Chandra Mohanty[2], Chan Su Han[1] and Yong Soo Cho[1]
[1]*Department of Materials Science & Engineering, Yonsei University, Seoul 120-749, Korea*
[2] *School of Physics & Materials Science, Thapar University, Patiala, 147004, India.*

Growth of GaN nanowires at a low temperature of 750 ^{o}C and at atmospheric pressure via the vapor-liquid-solid mechanism is reported with remarkable control of directionality and growth behavior by using an *in situ* magnetic field. The nanowires are severely twisted and kinked, and exhibit a high density of planer stacking defects under typical growth conditions without any magnetic field,. The defects are found to decrease progressively with increasing *in situ* magnetic field strength. Near-vertical aligned straight and several micrometers long nanowires of average diameter of ~40 nm are produced at an applied magnetic field strength of 0.80 T. According to photoluminescence measurements, the relative intensity of the defect-related peaks in the visible region with respect to the near-band-edge emission continuously decreases with increase in the applied magnetic field strength. The degree of agglomerative Ni droplet on Si is critically influenced by the surface tension driven by the magnetic force, which in turn determines the eventual properties of the nanowires.

NA-P10

Flow Rate Effects of CdSe Quantum Dots Synthesized by Microreactor

Da-Woon Jeong[1,2], Song Yi Kim[1], Taek Soo Kim[1], Tae-Yeon Seong[2], Bum Sung Kim[1]*
[1]*Korea Institute for Rare Metals, Korea Institute of Industrial Technology, Incheon, Korea*
[2]*Department of Materials Science and Engineering, Korea University, Seoul, Korea*

Keywords: CdSe, Quantum dot, Phosphor, Flow Rate, Microreactor

The size controlled Quantum dots are capable of controlling the typical emission wavelength and the absorption wavelength by particle size of a few nanometers. Recently, researches that applied these properties are in progress in various fields. Because electrical-, optical-properties are depend on the size of the quantum dots, the synthesizing condition such as flow rate of suspension is one of important process parameter. Continuous process of real-time microreactor is possible to control in-situ process parameters such as temperature, reaction time related flow rates each precursors.
The $Cd(CH_3COO)\cdot 2H_2O$(Cadmium acetate dihydrate, 98%, Aldrich) was dissolved by Oleic acid(90%, Aldrich) and 1-Octadecene(O.D.E, 90%, Aldrich) mixture at 160℃ under argon flow. The Se power (99.99%, Aldrich) was dissolved in Trioctylphosphine(T.O.P, 97%, Aldrich) at room temperature. The CdSe quantum dots synthesized on various flow rates, and characterized photo-luminescence, band-gap behaviors and microstructures.
The luminescence wavelength increased from 503 to 609 nm with decreasing flow rate of the Se precursor from 0.15 to 0.03 ml/min. The bad-gap energy decreased from 2.31 to 2.03 eV in the flow rate range.

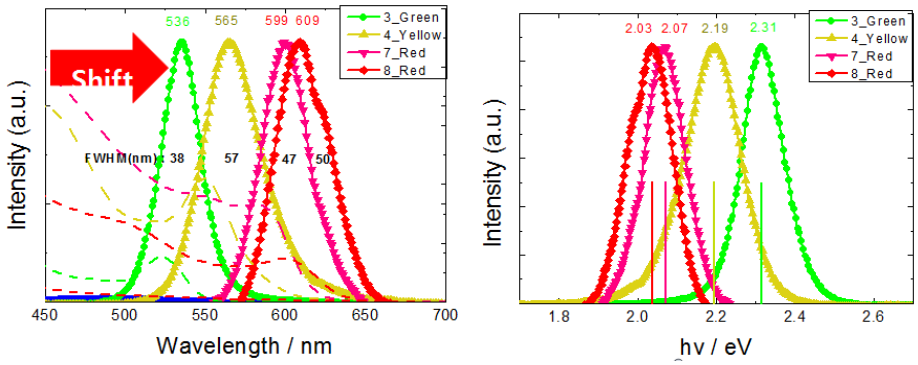

(a) (b)

Figure 67 (a) Photo-luminescence and (b) band-gap behaviors of CdSe QDs synthesized on 0.15 to 0.03 ml/min of Se precursors

FU-P01

$Er_{0.4}Bi_{1.6}O_3$ Electrolyte for Intermediate-Temperature Solid Oxide Fuel Cell

Ji-Na JEUNG[1], Soon-Gil YOON[1*]
[1]*Department of Advanced Electronic Circuit Substrate Engineering, Chungnam National University, Daejeon, KS015, S.Korea*

Keywords: SOFC, ESB, RF-Sputter

A Solid Oxide Fuel Cell (SOFC) is eco-friendly device which converts fossil fuels to electrical energy. SOFC consists of nonporous metal oxide electrolyte which allows ionic conductivity, cathode, and anode. When the supply of air and fuel to the electrodes of the unit cell, the reduction reaction of oxygen produce oxygen ions, oxygen ions moves to the anode through the electrolyte and the oxygen ions react with hydrogen, which supplied anode, produce water. In this case, the cathode generates electrons and the anode consumed the electrons, so when the two electrodes are connected to each other, the electricity flow. This is the reason for the how can dramatically lower emission of CO_2 and NO_2. Also SOFC has simple structure and the less worry about loss of supplements or corrosion problems of electrolytes has been promising a future energy system. SOFC operates at high temperature of about 800 ~ 1000℃ has high power conversion efficiency of the conventional fuel cell. High - temperature solid oxide fuel cells often used as the electrolyte Yittria stabilized zirconia (YSZ) mainly, and SOFC to be used as the electrolyte YSZ is operated near the 1000℃. To withstand at the high temperature like 1000℃, a production price is rise because of the using expensive high temperature resistant material and components. As a result practical application has been delayed. Therefore, it is required the development of Intermediate Temperature-SOFC (IT-SOFC). Trivalent cation doped ceria and bismuth oxide is effective as a material for IT-SOFC because it has high ionic conductivity at intermediate temperature range (500~700℃), so we choose the trivalent cation for Erbium oxide (Er_2O_3). Erbia stabilized bismuth oxide ($Er_{0.4}Bi_{1.6}O_3$, ESB) has been reported to have high ionic conductivity than the YSZ in the range of intermediate temperature. In this experiment, we make ESB 2inch target for Radio frequency-sputtering (RF-sputtering), using bismuth oxide (Bi_2O_3) and erbium oxide (Er_2O_3). By using RF-sputtering system, ESB is deposited on substrate at room temperature and annealed at various temperatures. After that, we confirmed physical characteristics through X-ray diffraction (XRD) and Scanning electron microscope (SEM), and the electrical properties through I-V curves were investigated.

References:

[1] Jun-Young Park, H.Yoon, E.d.Wachsman, J. Am. Ceram. Soc. 88 [9] 2402-2408 (2005)
[2] Kang Taek Lee, D.W.Jung, M.A.Camaratta, H.S.Yoon, J.S.Ahn, E.D,Wachsman, Journal of Power souces 205 (2012) 122-128
[3] J.Li, S.Wang, Z.Wang, R.Liu, T.Wen, Z.Wen, Journal of Power sources 194 (2009) 625-630

FU-P02

Fabrication and characterization of spherical $Li_3V_2(PO_4)_3$/C cathode material by hydrothermal method

Jung-In Moon[1], Eun-Young Kim[2], Chang-Sam Kim[2], Jeong-Hwan Song[1,*]
[1]*Department of Materials Engineering, Graduate School of PaiChai University, Daejeon 302-735, Republic of Korea*
[2]*Battery Research Center, Korea Institute of Science and Technology, Seoul 136-791, Republic of Korea*

Keywords: $Li_3V_2(PO_4)_3$, Hydrothermal, Carbon-coating, Cathode material, Li-ion battery

The Li-ion batteries have been widely used for portable electronic devices and hybrid electric vehicles because of their high energy densities. Among the known cathode materials, most commercial Li-ion secondary batteries use either $LiCoO_2$ or $LiMnO_2$ with layered structure. These materials are industry standard, but appear short lifetime, low energy density, expensive, and possible safety hazards. Therefore, the above mentions and the low thermal stability of Li metal oxides hinder large-scale application in electric vehicles. Currently, the monoclinic $Li_3V_2(PO_4)_3$ (LVP) material is of particular interest because it has good ion mobility, high operate voltage, high theoretical capacity (197 mAh g^{-1}) and good thermal stability. However, the LVP has lower ionic conductivity due to the polarization of V–O bond, which greatly restricts its practical application for Li-ion batteries. Its lower conductance has been better solved to some extent by doping metal and coating the material with a carbon layer.
Spherical $Li_3V_2(PO_4)_3$ (LVP) and carbon-coated LVP (LVP/C) with a monoclinic phase for the cathode materials are synthesized by a hydrothermal method using N_2H_4 as the reducer and saccharose as the carbon source. The structure, composition, morphology, and electro-chemical performance were compared between carbon-coated LVP and pure LVP. The results show that single phase LVP without impurity phases such as $LiV(P_2O_7)$, $Li(VO)(PO_4)$ and $Li_3(PO_4)$ can be obtained after calcination at 800 ^oC for 4 h. SEM and TEM images show that the particle sizes are 0.5–2 μm and the thickness of the amorphous carbon layer is approximately 3–4 nm. The CV curves for the test cell are recorded in the potential ranges 3.0–4.3 V and 3.0–4.8 V at a scan rate of 0.01 mV s^{-1} and at room temperature. At potentials between 3.0 and 4.8 V, the third Li^+ ions from the LVP can be completely extracted, at voltages close to 4.51 V. Cycling tests are carried out at charge-discharge rates of 0.2 to 5 C between 3.0 and 4.3 V.

FU-P03

Sintering Behavior and Electrical Properties of Gd-doped Ceria with the Addition of Li Salt

Jung-A LEE, Joon-Hyung LEE, Young-Woo HEO and Jeong-Joo KIM *
School of Materials Science and Engineering, Kyungpook National University, Daegu, 702-701,Korea

Keywords: Gd-doped CeO_2, Li-dopant, Densification, SOFC

Gd-doped CeO_2(GDC) has high ionic conductivities in the electrolytes at SOFC intermediate temperatures of 500~700^oC. However, GDC required the high sintering temperature above 1300^oC to get the high sintering density of 95%. So many researches were studied the use of dopants and nano-sized powder processing to lower sintering temperature. Transition metal such as Co, Mn, Cu, Ni, Fe and others such as Li, K, Ca, Zn, Al, Bi et al., introduced to GDC as sintering additives. It was reported that Co, Cu, Mn, Fe and Li reduce the sintering temperature, while Ca and Mg has little effect, and Al and K increase the sintering temperature. In particular, Co and Li lowered the sintering temperature by formation of liquid phase. Also, lithium salt, such as $LiNO_3$, Li_2CO_3 and LiF improved the densification and lowered the sintering temperature in the SDC, $BaZr_{0.8}Y_{0.2}O_{3-\delta}$, YSZ, $BaTiO_3$ and complex perovskite materials such as BZT, BMT and BZN. In this study, we investigated the effect of different kinds of Li salt on sintering behavior and electrical property in the GDC.
GDC($Gd_{0.1}Ce_{0.9}O_{1.95}$), Li_2CO_3 and $LiNO_3$ were used as starting materials The samples were sintered with 5^oC/min heating rate at from 800^oC to 1400^oC for 2hrs. The density was determined using the Archimedes method and the dilatometer was used for monitoring the shrinkage. Phase identification was used by x-ray diffraction analysis and the microstructures were determined using a FE-SEM.

References:

[1] B. C. H. Steele and A. Heinzel, Nature 414 (2001) 345.
[2] J. D. Nicholas and L. De Jonghe, Solid State Ionics 178 (2007) 1187.

FU-P04

Degradation Study of Yttria Doped Barium Cerate (BCY) Electrolyte in Protonic Ceramic Fuel Cells under Various Test Conditions

Mi Young Park, Myung Geun Jung, Young Jin Kim, Hyung-Tae Lim*
School of Materials Science and Engineering, Changwon National University,
20 Changwondaehak-ro, Uichang-gu 641-773, Changwon, Gyeongnam, Korea

Keywords: Protonic Ceramic Fuel Cells, Proton conductor, BCY

Acceptor-doped barium cerate has been considered as a potential electrolyte material in solid oxide fuel cell because of its high proton conductivity at temperatures below 700^0C. However, despite its superior transport property, barium cerate cannot be practically used in fuel cell due to its poor chemical stability in the atmosphere of water vapor and carbon dioxide. In the present work, we fabricated two kinds of BCY based anode supported cells, 1) BCY single layer cell and 2) BCY/BZY bi-layer cell, and their stability and degradation mechanism were investigated and compared, especially under severe operating conditions such as a negative voltage and low air flow rate. Constant current (CC) tests were conducted on the cells under various operating conditions such as positive vs. negative cell voltage and high vs. low fuel/air flow rate. Constant current (CC) tests were conducted on the BCY single layer and BCY/BZY bi-layer cells under a negative well as well a positive cell voltage as a function of air flow rate. Before and after the CC tests, I-V curve and impedance spectra were measured and compared to trace any increase in ohmic and/or non-ohmic resistance of the cells. Post-material analyses were conducted using scanning electron microscopy (SEM), X-ray diffraction (XRD) and energy dispersive spectroscopy (EDS) to find out any change in microstructure and phase after severe operations.

FU-P05

Performance of sulfide based all-solid-state lithium secondary batteries with Li-Si alloy anode

Joo Sung Jin, Hye Won Park, Hyung-Tae Lim*
School of Materials Science and Engineering, Changwon National University,
20 Changwondaehak-ro, Uichang-gu 641-773, Changwon, Gyeongnam, Korea

Keywords: Lithium secondary batteries, All-solid-state batteries, Li-Si alloy, Sulfide electrolyte

$Li_{22}Si_5$ alloy powder was synthesized by mechanical alloying and its electrochemical performance was investigated for use in solid-state battery anodes. Using these anode materials, all-solid-state lithium batteries were assembled with $Li_4Ti_5O_{12}$ (LTO) or titanium disulfide (TiS2) as cathode and Li_2S-P_2S_5 as electrolyte. Galvanostatic charge/discharge tests were also performed, and capacity was increased about two times by the additional powder milling process as shown in Figure 1; which is consistent with the impedance results. Thus, the results from the present work indicate that using the secondary milling process to refine the electrode powder is an effective way to increase the kinetics of alloying and de-alloying with higher utilization of anode active material in all-solid-state lithium secondary batteries.

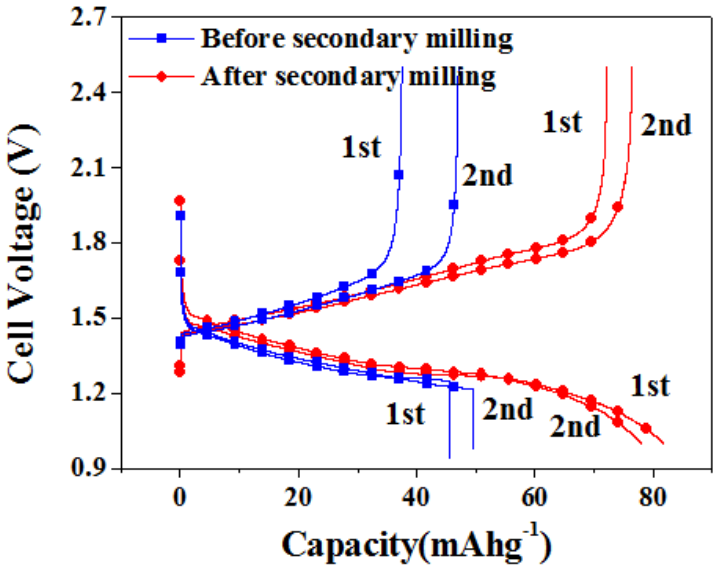

Figure 1. Galvanostatic charge/discharge voltage curves of the solid electrolyte cell with a Li-Si alloy ($Li_{22}Si_5$) anode; before and after the secondary milling process

FU-P06

Fabrication of reduced graphene oxide single layer coated TiO_2 nanorod/FTO electrode for solar hydrogen evolution

Hyun Kim[1], Sang Won Park[1], Gi Wook Lee[1], Bee Lyong Yang[1*]
[1]*School of Advanced Materials and System Engineering, Gyeongsangbukdo, Gumi, 730-701, South Korea*

Keywords: Reduced graphene oxide, TiO_2 nanorod, Hydrogen

The Hydrogen production from solar water splitting has been considered as a solution to the energy and environmental issues. Splitting water into hydrogen and oxygen has been occured by stages, i) absorption of light, ii) electron-hole excitation, iii) charge transfer to reactive sites, iv) redox reaction. Among these stages, charge transfer stage is most important to lead the redox reaction of water. Graphene has been considered a new approach to improve the charge transfer rate without direct or indirect recombination [1]. In this work, graphene sheets were chemically synthesized by improved Hummer's method. TiO_2 nanorods were grown on graphene/FTO glass by hydrothermal method and then directly immersed into solution involving graphene oxide. After several minutes in immersed state, the graphene oxide on TiO_2 nanorods were chemically reduced by adding hydrazine solution as a reducing agent. The microstructural features of TiO_2 nanorods/graphene/FTO photoanode were investigated by FE-SEM, TEM, XRD, Raman spectroscopy. Furthermore solar hydrogen production test was characterized in the PEC cells.

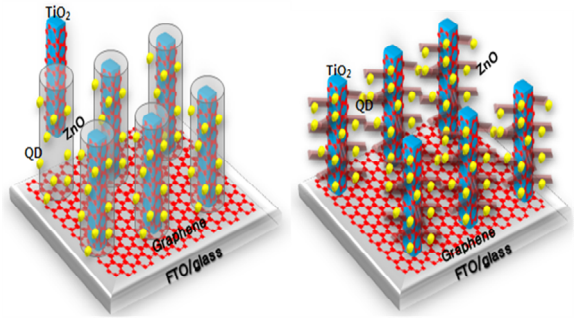

Figure 68 Schematic of hybrid hetero-structures consisting of NR shell and branched shape

References:

[1] D. C. Marcano and J. M. Tour, ACS NANO, 4 (2010) *p*. 4806.

Acknowledgement:

This research was supported by Basic Science Research Program through the National Research Foundation of Korea (NRF) funded by the Ministry of Science, ICT and future Planning (Grant No. 2014005324)

FU-P07

Effects of graphene single layer on TiO_2 nanorod/FTO electrode for solar hydrogen evolution

Hyun Kim[1], Jin Seok Choi[1], Sang Won Park[1], Gi Wook Lee[1], Sung Jin An[1], Bee Lyong Yang[1*]
[1]*School of Advanced Materials and System Engineering, Gyeongsangbukdo, Gumi, 730-701, South Korea*

Keywords: Graphene, TiO_2 nanorod, Hydrogen

The Hydrogen production from solar water splitting has been considered as a solution to the energy and environmental issues. Splitting water into hydrogen and oxygen has been occured by stages, i) absorption of light, ii) electron-hole excitation, iii) charge transfer to reactive sites, iv) redox reaction. Among these stages, charge transfer stage is most important to lead the redox reaction of water. Graphene has been considered a new approach to improve the charge transfer rate without direct or indirect recombination [1]. In this work, graphene sheets were synthesized by chemical vapor deposition using methan source and then the sheets were directly transfered on the FTO glass. TiO_2 nanorods were grown on graphene/FTO glass by hydrothermal method. The microstructural features of TiO_2 nanorods/graphene/FTO photoanode were investigated by FE-SEM, TEM, XRD, Raman spectroscopy. Furthermore solar hydrogen production test was characterized in the PEC cells. In the results of those analysises, recombination of photo-excited electrons and holes was decreased by inserting graphene sheet between TiO_2 nanorods and FTO substrates.

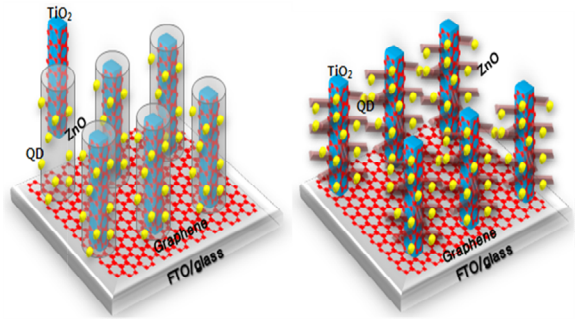

Figure 69 Schematic of hybrid hetero-structures consisting of NR shell and branched shape.

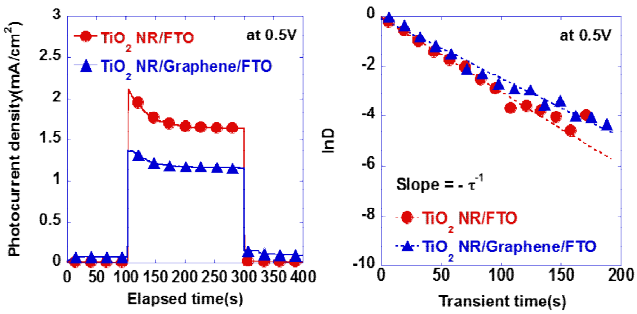

Figure 2 Recombination rates of photo-generated electron and hole pairs

References:
[1] G. Xie and J. R. Gong, Adv. Mater, 25 (2013) *p*. 3820.

Acknowledgement:
This research was supported by Basic Science Research Program through the National Research Foundation of Korea (NRF) funded by the Ministry of Science, ICT and future Planning (Grant No. 2014005324)

FU-P08

A Study of photo-corrosion free CuO photo-catalyst by passivation layers for solar hydrogen evolution

Hyun Kim[1], Sang Won Park[1], Gi Wook Lee[1], Bee Lyong Yang[1*]
[1]*School of Advanced Materials and System Engineering, Gyeongsangbukdo, Gumi, 730-701, South Korea*

Keywords: Photo-corrosion, CuO, passivation layer

The Hydrogen evolution via water splitting in the photo-electrochemical cells is a clean technology. Recently a few groups have been studied dual photo-electrode system which is consisted of the n-type semiconductor photo-anode for water oxidation reaction and the p-type semiconductor photocathode for water reduction reaction. This system is having several advantages such as a without external bias for effective operation, a reducing on-set potential, a selectivity of reaction, a replacing counter electrode instead of Pt metal can reduce a cost compared with formal system which is semiconductor/metal which is specifically Pt [1-2]. The CuO can be used as a p-type semiconductor due to its narrow band gap. However, it shows highly self-oxidation reaction by photo-excited electrons due to its reducing standard potential is located within its band gap. Ultimately self-oxidation of CuO reduce a faradaic efficiency of system. In this work, we demonstrate fabrication and analysis of TiO_2 and ZnO as a passivation layer coated CuO nanosheets on FTO glass substrate as a p-type photo-electrode. Morphology and microstructural properties of the TiO_2/ZnO/CuO electrode was investigated by FE-SEM, XRD and HRTEM analysis. Photo-electrochemical properties were characterized by measuring photocurrents responses under both white and visible light illumination. The effects of passivation layer were also examined by measuring pulsed photocurrent versus elapsed time curve. By increasing thickness of TiO_2, ZnO and TiO_2/ZnO films, stability of CuO electrode were also increased. Furthermore, hydrogen evolution tests will be confirmed by using PEC cell with passivation layer coated CuO and as prepared TiO_2 that can generate hydrogen and oxygen gases without external bias.

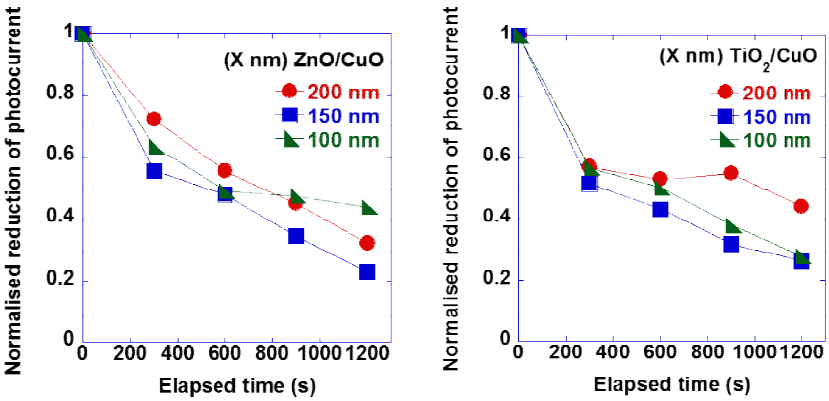

Figure 70 Normalised reduction of photocurrent density

References:

[1] A. Paracchino and E. Thimsen, Nature Materials, 10 (2011) *p*. 456.
[2] S. Ida and T. Ishihara, J. Am. Chem. Soc, 132 (2010) *p*. 17343.

Acknowledgement:

This research was supported by Basic Science Research Program through the National Research Foundation of Korea (NRF) funded by the Ministry of Science, ICT and future Planning (Grant No. 2014005324)

FU-P09

Preparation and Characterization of Fast Ion Conducting Solid State Electrolytes for the Solid State Li-ion Battery

Inseok Seo[1], Steve W. Martin[2]*
[1]Research Institute of Industrial Science & Technology, POSCO Global R&D Center 180-1 Songdo-Dong, Yeonsu-Gu, Incheon 406-840, Korea
[2]Department of Materials Science and Engineering, Iowa State University 2220 Hoover Hall Ames IA 50011, USA.

In this study, I will describe my research on two types of solid state electrolytes; amorphous lithium thio-germanate thin-films and solid state bulk electrolytes. While the thin film electrolytes, Li_2S + GeS_2, were prepared by RF sputtering deposition, the solid state bulk electrolytes, Li_2S + P_2S_5, were produced by mechanical milling. For the first time, new high quality lithium germanium sulfide thin-films have been successfully made by RF sputtering and synthesized as new solid state electrolytes. The maximum ionic conductivities of the two types solid state electrolytes are over ~10^{-3} (S/cm). The ionic conductivities of the thin-films and bulk electrolytes are ~three order of magnitudes higher than reported values for oxide electrolytes which have been used in commercial products. Although these materials are unstable in air the thin-films and bulk electroyltes were thoroughly characterized by XRD, Raman, SEM, XPS, and impedance spectroscopy using special setups to prevent contamination. In this way, this work may provide a new way for developing new thin-film electrolytes for solid state lithium ion batteries.

EL-P01

Effect of process parameters on electrical properties of CSD-derived $Ba(Zr,Ti)O_3$ thin films

Yutaro Oda[1], Naonori Sakamoto [1, 2], Naoki Wakiya [1, 2], Tomoya Ohno [3], Takeshi Matsuda [3], Hisao Suzuki [2*]

[1] *Graduate school of Engineering, Shizuoka University, Hamamatsu, Japan*
[2] *Reseach Institute of Electronics, Shizuoka University, Hamamatsu, Japan*
[3] *Department of Materials Science, Kitami Institute of Technology, Kitami, Hokkaido, Japan*

Keywords: BZT, thin film, LNO, seeding layer, residual stress

1. Introduction

Ba(Zr, Ti)O_3 (BZT) thin films are expected to apply as lead-free piezoelectrics and tunable capacitors because of their excellent dielectricity, piezoelectricity and tunability, if the curie temperatures can be controlled. In this study, we introduced (100)-oriented LNO buffer layer by CSD method in which molecular structure of precursor solution or nanostructure of the resulting thin film was controlled to relax the tensile stress from Si wafer, leading to the compressive residual stress in BZT thin films. As a resalt, (100)-predominant BZT thin films have been successfully deposited on $LaNiO_3$(LNO)/Pt/Si and LSCO/LNO/Pt/Si substrates, and therefore, we can expect the enhancement of the electrical properties of the BZT thin films. Furthermore, we investigate the effect of process parameters in preparation of BZT thin films to obtain the dense nano-structure and/or larger compressive stress.

2. Experimental procedure

Precursor solutions of BZT were prepared by a partial hydrolysis method with different concentrations, and spin-coated on LNO/Pt/Si or LSCO/LNO/Pt/Si substrates. Precursor films of BZT were dried at 150ºC for 10min, followed by the pre-annealing at 500 ºC or 600ºC for 10min under the oxygen atmosphere to reduce the residual organics. Finally, films were annealed up to 900ºC for 5min under the oxygen atmosphere. The morphology of the resulting BZT thin films were observed using FE-SEM. The grain sizes of the BZT thin films were determined from AFM images. Then, we investigated the effect of process parameters on electrical properties of the resultant BZT thin films.

3. Result

(100)-predominant BZT thin films were successfully deposited on LNO/Pt/Si and LSCO/LNO/Pt/Si substrates. As a result, grain size, dielectric constant and ferroelectricity, 2Pr, were increased for the films calcined at 600ºC, as shown in table 1. For the films deposited from precursor solution of 0.1 M, the morphology of BZT thin films showed columnar structure to increase the grain sizes and 2Pr of the BZT thin films and the ferroelectricity were increased with decreasing the mole concentrations of the precursor solutions, as shown in figures 2. Finally, dienectric constant and remanent polarization, 2Pr, of BZT thin films have been successfully increased more than1900 and 7.0 μC/cm^2.

Table 1 Grain size and electrical properties of 0.3 M BZT thin films with different calcining temperature

	500 ºC	600 ºC
grain size [nm]	71	96
dielectric constant	1552	1932
2Pr [μC/cm^2]	2.0	5.5

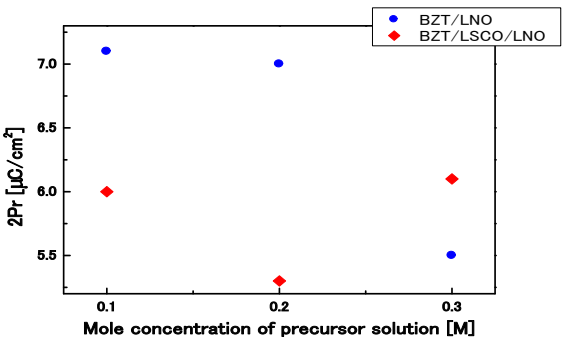

Figure 2 2Pr of BZT thin films with different mole concentrations of precursor solution

EL-P02

Structure Analysis of $12CaO \cdot 7Al_2O_3$ Particles Synthesized by Solution Plasma Processing

Shiori MANEYAMA[1*], Naonori SAKAMOTO[1, 2], Naoki WAKIYA[1, 2], Tomoya OHNO[3], Takeshi MATSUDA[3], Hisao SUZUKI[2]
[1]*Department of Electronics and Materials Science, Shizuoka University, Hamamatsu, 432-8561, Japan*
[2]*Research Institute of Electronics, Shizuoka University, Hamamatsu, 432-8561, Japan*
[3]*Department of Materials Science, Kitami Institute of Technology, Kitami, 090-8517, Japan*

Keywords: $12CaO \cdot 7Al_2O_3$, Solution Plasma Processing, Low-temperature synthesis

[Introduction] $12CaO \cdot 7Al_2O_3$ (C12A7) crystal structure has 12 cages in the unit cell, and two free oxygen ions are encaged in the cages. These ions can be replaced with various anions by the appropriate processing, to show various characteristics [1], [2]. Solution plasma processing is a method of synthesizing the material by vaporization of the liquid with a electric discharge, to be a plasma, as a reaction field [3]. This method has advantage of rapid reaction at lower temperatures over conventional powder preparation methods because of the high density reaction field localized at the interface between liquid and gaseous phases [4]. However, this method has been started to study in the recent years, therefore, there are many issues to be solved to apply it as a powder preparation method. In this study, C12A7 particles were synthesized from alkoxide-derived precursor solution by solution plasma processing for the low-temperature synthesis. As a result, we have identified metastable C12A7 phase and analyzed in detail the structure of the obtained metastable particles.

[Experimental] Aluminum isopropoxide, calcium, ethanolamine and 2-Butanol were mixed and reacted to form precursor solution. The precursor solution was treated with solution plasma processing. As a result, we obtained precipitate on the electrode, and it was dried at 150 ºC. Then the precipitates were characterized by XRD, TEM, and so on.

[Results] From XRD pattern shown in figure1, the crystal structure of the obtained particles was C12A7 single phase substantially. A temperature of 1300 ºC or more was necessary in the conventional solid state reaction to obtain C12A7 single phase, whereas the dried solution plasma processed powder was identified as a C12A7 single phase at room temperature. In addition, C12A7 particles exhibited same crystal symmetry with different lattice parameters. The difference in the lattice parameters may be ascribed to the smaller particle size. From the results, it was concluded that the crystalline phase of the resultant C12A7 exhibited 2 types, depending on the crystallization processes, and solution plasma processing will be a powerful tool to obtain interesting nanopowders at low-temperatures.

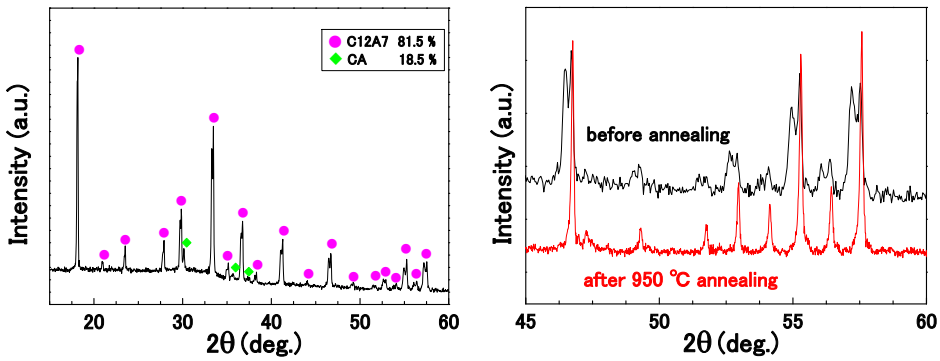

Figure 71 XRD patterns of C12A7 particles synthesized by solution plasma processing

References:

[1] K.Hayashi et al. J.Am.Chem.Soc.124(2002) 738-739.
[2] S.Matsuishi et al.Science 301 (2003) 626-629.
[3] Hirofumi Nameki Aisanken Nyu-su, 91 (2009) 3.
[4] Osamu Takai, Funsai, 51 (2008) 30-36.

EL-P03

Phase transition temperature control of thermochromic vanadium dioxide nanoparticles by microemulsion method with molecular-designed precursors

Takuya OKUDA[1], Naonori SAKAMOTO[1,2], Naoki WAKIYA[1,2], Hidetoshi MIYAZAKI[3], Hisao SUZUKI[2*]

[1] *Graduate School of Engineering, Department of Electronics and Materials Science, Shizuoka University, 3-5-1 Johoku Naka-ku, Hamamatsu, 432-8561, Japan*

[2] *Research Institute of Electronics, Shizuoka University, 3-5-1 Johoku Naka-ku, Hamamatsu, 432-8561, Japan*

[3] *Interdisciplinary Faculty of Science and Engineering, Department of Materials Science, Chemistry, Shimane University, 1060 Nishikawatsu Matsue, 690-8504, Japan*

Keywords: Microemulsion, VO_2, Thermochromic, Smart window

[Introduction] Vanadium dioxide, VO_2, undergoes the phase transition from monoclinic to tetragonal with property change from semiconductor to metal at about 68°C. Metallic tetragonal structure reflects infrared light, and semiconducting monoclinic structure transmits it, leading to the thermochromic smart window. On the other hand, the phase transition temperature is slightly higher than the room temperature, however it can be lowered by tungsten or the other metal cation doping. Furthermore, particle size less than 100 nm is essential for the smart window because the light scattering can be dramatically suppressed by reducing the particle size to obtain a high transparency. In this study, we tried to control the phase transition temperature of VO_2 nanoparticles by the microemulsion method using molecular-designed precursors.

[Experimental] Tungsten pentaethoxide($W(OC_2H_5)_5$) and acetic acid were mixed in cyclohexane, and added vanadium oxyisopropoxide($VO(O\text{-}i\text{-}Pr)_3$) into the solution. Microemulsion was prepared by mixing Triton X-100, cyclohexane and water as surfactant, oil phase and aqueous phase, respectively. Precursor solution was added into the microemulsion, and stirred for 24 hr. Precursor sols were washed with acetone, centrifuged, and dried at 150ºC. Dried gel were annealed at 400ºC for 1hr under the reducing atmosphere of $Ar:H_2$=9:1, then annealed again at 600ºC for 1hr under the inert atmosphere of N_2. Doping amount of tungsten was fixed at 2at.% for all samples and the ratio of acetic acid, R_A(=[Acetic acid]/[W]) was fixed at 3. The resultant VO_2 particle was characterized by XRD, DSC, SEM and TEM.

[Result & Discussion] Primary particle size of the resulting VO_2 nanoparticles was estimated to be 25 nm with average agglomeration size of about 300 nm. The phase transition temperature of W doped VO_2 was lowered to 28 to 40°C by the W-doping. Therefore, microemulsion method from the molecular-designed precursors was expected to control the phase transition temperature to around room temperature and application of VO_2 to the thermochromic smart window.

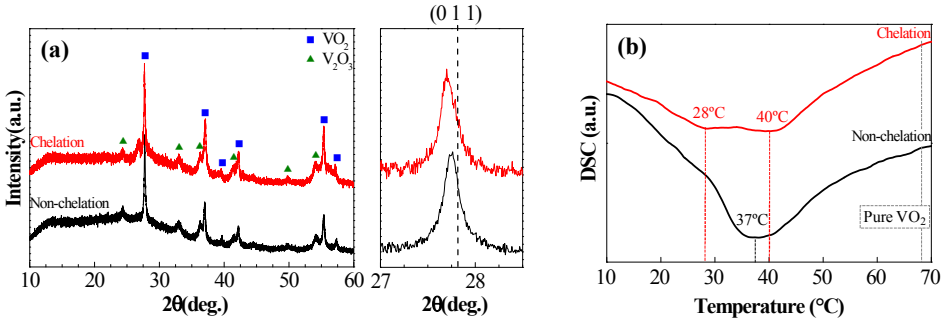

Figure 72 (a)XRD patterns for W-doped VO_2, (b)DSC curves for W-doped VO_2.

EL-P04

Vertically aligned microstructures of PLZT ceramic films produced by Electrostatic Spray Deposition (ESD)

Dongsu SON[1], Beak Hyun KIM[1], Hyun-Jeong BAE[1], Yumin GOH[1], Do-Kyun KWON[1]*
[1]*Department of Materials Engineering, Korea Aerospace University, Go-yang, Gyeonggi-do, 421-791, Korea*

Keywords: Template-free, Vertical aligned, nano-rods, Preferential landing, ESD

The vertically aligned arrays of PLZT perovskite nano-grains on the substrate are considered to be useful for commercial applications in many fields, due to their properties such as large surface areas, specified electron transport path, optical excitations, enhancement in the piezoelectric response etc. So, The distinctive properties of the ceramic films with oriented microstructures has been attracting attention for applications in several fields such as electronics, photonics, sensors, energy harvesting, information storage, and energy converters.

The synthesis methods for the specific nanostructures can be mostly divided into template-assisted synthesis method and template-free synthesis method. The most widely used synthesis method to produce nanostructures is a template-assisted synthesis method. Although template-assisted synthesis method for synthesizing the nanostructures has many advantages, such as precisely controlled physical dimensions, mono-disperse nanostructures, there are a number of synthetic disadvantages, which include the need for template stable to chemical and thermal, the trouble for release of the nanostructures from the template channels, etc. Also, in case of their high volume production, the increased template price makes the cost-efficiency worse.

Therefore, in this work, we produced the vertically aligned PLZT nano-grains without template-assisted ways. It demonstrated a new method and process for synthesis of one-dimensionally well aligned microstructures of the PLZT films by using a preferential landing phenomenon; unique phenomenon of ESD. Also, the deposition mechanism of the aligned ceramic films produced by ESD was described by analyzing with sol concentration and effect of additives. The maximum aspect ratio of the PLZT arrays produced in this work was higher than 1:16. The XRD analysis proved that the PLZT arrays produced by ESD have preferred orientations of (111) and scaled up as those orientations.

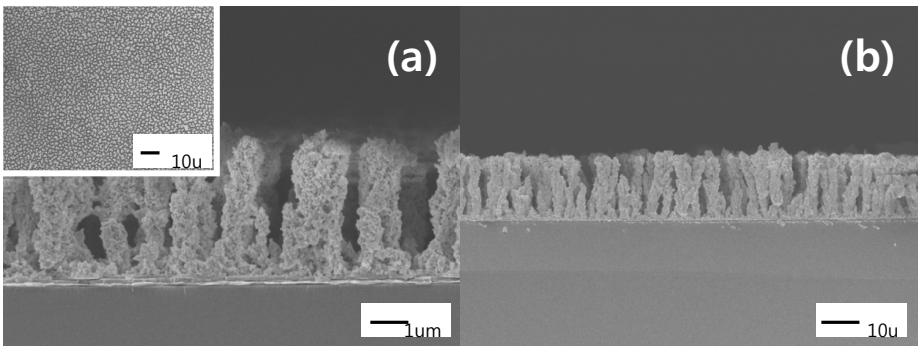

Figure 73 SEM images of the vertical aligned PLZT nano-rods. (a) 0.05M, (b) 0.1M.

References:

[1] Per Martin Rørvik and Tor Grande, Adv. Mater. 23 (2011), 4007-4034.
[2] Dongyang Sun and Sophie A. Rocks, J. Europ. Ceram. Soc. 28 (2008), 3131-3139.
[3] Xiaoxia Jiang and Fei Chen, Sol. Energy Mater. Sol. Cells. 94 (2010), 338-344.
[4] Zhong Lin Wang, Adv. Mater. 24 (2012), 280-285.
[5] By Younan Xia and Peidong Yang, Adv. Mater. 15 (2003), 353-389.
[6] Justin Varghese, Roger W. Whatmore and Justin D. Holmes, J. Mater. Chem. C. 1 (2013), 2618-2638.

Acknowledgement:

This work was supported by the National Research Foundation of Korea(NRF) grant funded by the Korean Government (Grant #: NRF-2013R1A1A2061760)

EL-P05

Dielectric properties of PIN-PMN-PT Films Prepared by Aerosol-Deposition Method

Soo-Bin KANG[1], Min-Geun CHOI[1], Young-Min KONG[2], Jungho RYU[3], Linghang WANG[4] and Dae-Yong JEONG[1*]

[1]*School of Materials Sci. & Eng., Inha University, Incheon, 402-751, Korea.*
2Department of Materials Sci. & Eng., University of Ulsan, Ulsan, 680-749, Korea
[3] *Functional Ceramics Group, Korea Institute of Materials Science, Changwon, 641–831, Korea*
[4]*Electronic Materials Research Laboratory, Xi'an Jiaotong University, Xi'an 710049, People's Republic of China*

Keywords: PIN-PMN-PT, aerosol-deposition, dielectric, relaxor

PIN-PMN-PT($Pb(In_{1/2}Nb_{1/2})O_3$-$Pb(Mg_{1/3}Nb_{2/3})O_3$-$PbTiO_3$) is one of the relaxor-PT based single crystals. As the relaxor-PT based single crystals revealed high piezoelectric and electromechanical properties, the research of these materials was widely carried out. However, their low Curie temperature (Tc~130-170^oC) restrict the application to device due to depoling at low temperature [1]. To overcome this problem, the binary relaxor solid solution system was studied such like PIN-PT, PYN-PT, and PSN-PT. But the crystal growth and the composition controlling of these binary system were very difficult. So lately, the new relaxor based ternary system PIN-PMN-PT was studied. The ternary PIN-PMN-PT could be applied for capacitors in electronic, transducers, MEMS and etc due to the high rhombohedral–tetragonal phase transition temperature. In this study, We fabricated the PIN-PMN-PT films by aerosol-deposition (AD) method. By using the AD method, the films revealed nano-sized grain and dense structure at the room temperature. The AD method can fabricate film through the collision of fine ceramic powder particles onto substrate. The (sub-)micrometer sized particles are crushed nano size, and have strong adhesion between films and substrate. The AD films revealed the slim polarization-electric field hysteresis loop due to the nano-grain like a nano-domain of relaxor ferroelectric [2]. Through the post annealing process, grain size and crystallinity can be controlled, resulting in the improvement of the electrical properties of the AD films. We compared dielectric and ferroelectric properties of the single crystal with the aerosol deposited films. The crystallographic phases of the PIN-PMN-PT films were analyzed through a high resolution X-ray diffraction. The microstructures of the surfaces and fracture sections were observed by field emission scanning electron microscopy. The ferroelectric properties, the dielectric constant by change of the frequency were measured using an impedance analyzer. The polarization-electric field (P-E) hysteresis loops were examined using a standard ferroelectric test system.

References:

[1] S. Zhang , T. Shrout., IEEE. Trans. Ultrason. Ferroelect. Freq. Contr. 57 (2010) *pp*.2138–46.
[2] J. Ryu, J. Choi, B. Hahn, D. Park, W. Yoon, K. Kim, Appl. Phys. Lett. 90 (2007) *pp*.152901(1)-152901(3)

Acknowledgement:

This research was supported by Agency for Defense Development(ADD-12-02-04-01).

EL-P06

Magnetocaloric Effect in the $SRFE_xCO_{1-x}O_{3-\delta}$ ($0.4 \leq x \leq 0.6$) Synthesized at Ambient Conditions

Zeeshan ur Rehman[1], Bon Heun Koo[1,*], M. S. Anwar[1]
[1]*School Of Material Science And Engineering Changwon National University, Changwon Gyeongnam,641-773,Korea*

Keywords: Magnetocaloric effect, Cobaltates, RCP, Magnetic Entrophy

The magnetocaloric effect (MCE) has been a research focus during the past several decades which is ascribed to the fact that magnetic refrigeration based on it has been regarded as a promising alternative technique for its high efficiency and environmental friendliness.
In this work, Effects of Fe doping in $SrCoO_{3-\delta}$ which were prepared through conventional Solid state method have been investigated. SrCoO3 is ferromagnetic with low magnetization while SrFeO3 is an Antiferromagnetic material. By varying the Fe earth on the cobalt site microstructural effects on saturation magnetization and eventually on the curie temperature T_c has been elucidated. To calibrate the magneto caloric properties of the specimen, Magnetic entropy with respect to temperature and Relative cooling Power of the whole series was gauged.(No.2011-0030058), (2012-R1A1B3000784)

EL-P07

Energy Storage Properties of Lead Lanthanum Zirconate Titanate Films by Aerosol Deposition Method

Min-Geun CHOI[1], Soo-Bin KANG[1], Jungho RYU[2], and Dae-Yong JEONG[1*]
[1]*School of Materials Sci. & Eng., Inha University, Incheon, 402-751, Korea.*
[2]*Functional Ceramics Group, Korea Institute of Materials Science, Changwon, 641–831, Korea*

Keywords: Lead Lanthanum Zirconate Titanate, Aerosol Deposition, Tin doping, Relaxor

The rapid development of the electric vehicle industry is requiring the high energy density discharge device [1]. In general, the ceramic based capacitor was used for high energy discharge while short time, but, the lower breakdown voltage of than polymer based capacitor decreased the energy density of device. As the breakdown voltage is proportional to density of ceramics, the high density film is required for the improvement of the energy density. Another method for increasing stored energy is the using of high dielectric constant material such like ferroelectric. However, ferroelectric reveals the large dielectric loss due to the high value of remnant polarization and this dielectric loss induce the temperature rise of devices [2]. Therefore, the anti-ferroelectric which has low remnant polarization is suitable as the material of energy device. Lead Lanthanum Zirconate-Titanate (PLZT) is noted anti-ferroelectric material and has been widely researched for various applications such as actuators, sensors and transducers in the micro electro mechanical systems (MEMS) [2,3]. A-site (Pb-site) of PZT is substituted with the La ion. The differences of ion size and valence electron number between Pb ion and La ion have caused defects in PZT structure. This phenomenon induces the phase change and the dielectric characters become from ferroelectric to anti-ferroelectric [3]. Also, the substitution of Sn into B-site modifies the dielectric properties of the material in the perovskite structure. In this present study, the Aerosol Deposition (AD) method was used to deposit $Pb_{0.97}La_{0.02}(Zr,Sn,Ti)O_3$ films on $Pt/Ti/SiO_2/Si$ substrate modifying the Sn doping concentrations. As AD method can fabricate the dense structure films, the breakdown voltage of films can be easily increased. Also, the film has nano-sized grain and that would conduct like the nano domain of relaxor ferroelectric. The phases of films were identified by X-ray diffraction system (XRD) and the microstructures of films were observed by field emission scanning electron microscopy (FESEM). And, the polarization–electric field hysteresis loops were measured by using a standard ferroelectric test system.

References:

[1] B. Ma, D.-K. Kwon, M. Narayanan, U. (Balu) Balachandran, Materials Letters 62 (2008) 3573.
[2] C.K. Campbell, J.D.V. Wyk, R. Chen, IEEE Transactions on Components and Packaging Technologies 25 (2002) 211.
[3] B. Xu, Y. Ye, Q.-M. Wang, and L. Eric, J. Appl. Phys. 85 (1999) 3753.

Acknowledgement:

This research was supported by Agency for Defense Development(ADD-12-02-04-01).

EL-P08

Characterization of LiF and CuO Codoped $BaTiO_3$ for Embedded Capacitor in LTCC Modules

KYOUNGHO LEE[1,3] and KWANGWON CHOI[1,2]
[1]Department of Display Materials Engineering, Soonchunhyang University, Asan 336-745, Republic of Korea, [2]RN2 Technologies, Pyeongtaek 451-862, Republic of Korea

Keywords: Embedded capacitor, 3D printing module, $BaTiO_3$, sintering additive, CuO/LiF codoping, Compatibility between heterogeneous layers

Sintering additives for $BaTiO_3$ were studied in order to facilitate the use of $BaTiO_3$ as an embedded decoupling capacitor in high density multilayered LTCC modules for mobile communication systems and 3D printing modules. Among the studied additives, the CuO/LiF mixture was the most promising sintering additive for co-firing $BaTiO_3$ with a commercial low permittivity (ε_r) LTCC sheet (MLS-22, NEG Co.). The temperature dependence of the dielectric properties of $BaTiO_3$ was successfully controlled by adjusting the CuO/LiF amount and ratio and the sintering temperature. 10 wt% LiF/CuO (1:1 ratio) codoped $BaTiO_3$ sintered at 860°C for 30 min showed 95% sintering density. The room temperature permittivity (ε_r) of LiF/CuO doped $BaTiO_3$ was 1620 at 1 MHz, and the temperature coefficient of capacitance satisfied the X5R specification. After co-firing this LiF/CuO doped $BaTiO_3$ ceramic with a MLS-22 sheet at 860°C, there were no crack formations at the layer boundary. Also a chemical compatibility test revealed that there were no severe reactions between the LiF/CuO doped $BaTiO_3$ and an Ag electrode.

EL-P09

Effects of Ca substitution on spontaneous superlattice formation of $SrTiO_3$ thin films prepared using dynamic aurora PLD

Tomoaki KUBOTA [1], Naonori SAKAMOTO [1,2], Takanori KIGUCHI[3], Kazuo SHINOZAKI[4], Hisao SUZUKI[2,1] and Naoki WAKIYA [1,2*]

[1]*Department of Electronics and Materials Science, and* [2]*Research Institute of Electronics, Shizuoka University, 3-5-1 Johoku, Nakaku, Hamamatu 432-8561, Japan*

[3]*Institute for Materials Research, Tohoku University, 2-1-1 Katahira, Aoba-ku, Sendai 980-8577, Japan*

[4]*Department of Metallurgy and Ceramics Science, Tokyo Institute of Technology, 2-12-1 O-okayama, Meguro-ku, Tokyo 152-8550, Japan*

Keywords: spontaneous superlattice formation, PLD, $SrTiO_3$

1. Introduction

We have investigated that superlattice structures are spontaneously formed in epitaxially grown $SrTiO_3$, Nb-$SrTiO_3$ and (La,Sr)MnO_3 thin films prepared using a dynamic aurora pulse laser deposition (PLD) on $SrTiO_3$(001) single crystal substrate. We considered that spinodal decomposition is a possible mechanism for the spontaneous superlattice formation. We found some necessary conditions for it. However, the effects of substitution of cations have not been considered yet. The objective of this work is to clarify this problem.

2. Experimental procedure

$(Ca_xSr_{1-x})_{1.4}TiO_y$ (x=0, 0.1, 0.2, 0.5)(CST) thin films were deposited on Nb-$SrTiO_3$ single crystal substrates using a PLD in the magnetic field (aurora PLD). The magnitude of magnetic field during deposition was 2000 G. Crystal structure of the thin films was analyzed using a precise x-ray diffraction (ATX-G). To determine the composition, the thin films were also deposited on Si(001) substrates under same deposition conditions as a control. The composition and thickness of the thin film was analyzed using an x-ray fluorescence analysis (XRF).

3. Result

Clear satellite peaks were observed for all samples. This suggests the spontaneous superlattice formation from the point of XRD. Cross sectional TEM observation for the sample with x=0.5 confirmed the superlattice formation. It was also found that in-plane lattice parameter of the films coincides with that of the substrates, suggesting a coherent growth. Figures 1(a), (b) and (c) show the changes of strain, c/a and 2Pr with the amount of Ca substitution, respectively. Figure 1(a) indicates that in-plane strain increases linearly with composition. On the other hand, out-of-plane lattice parameter increased up to x=0.2 and decreased at x=0.5. The axis ratio c/a monotonically decreased with composition x. Figure 2(c) indicates that the substitution of Sr with Ca drastically lowers the ferroelectricity. These facts suggest that spontaneous superlattice formation occurs irrespective of Sr substitution with Ca. However, the substitution brings about structural change of the thin film that brings about the suppression of ferroelectricity along out-of-plane direction. The effect of detailed substitution and the possibility of ferroelectricity along in-plane direction will be considered.

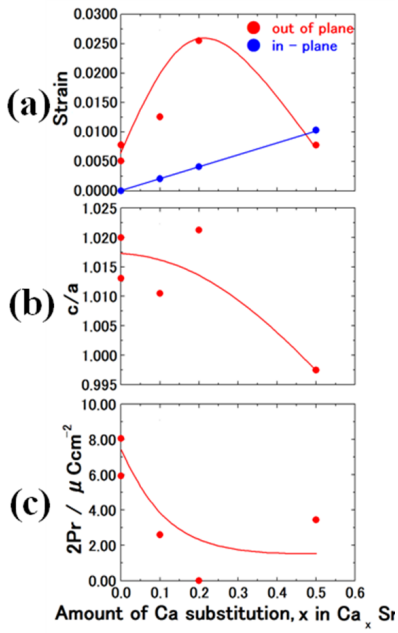

Fig. 74. Change of (a) strain, (b) c/a and (c) 2Pr with the amount of Ca substitution

EL-P10

Microwave Dielectric Properties of $(Zn_{1-x}Mg_x)_{1.918}GeO_{3.918}$ Ceramics

Young Jun Eoh and Eung Soo Kim*
Department of Materials Science and Engineering, Kyonggi University, Suwon, 443-760, Korea

Keywords: Microwave dielectrics, Crystal structural characteristics, Quality factor

Recently many interests have been paid to the dielectric materials applicable to the several types of microwave and millimeter-wave systems. For these applications, the dielectric materials should have a low dielectric constant (*K*) to minimize the cross-coupling effect with conductors, a high quality factor (*Qf*) to increase their selectivity, and a near-zero temperature coefficient of resonant frequency (*TCF*) to ensure the stability of the frequency against temperature changes.

Zn_2SiO_4 ceramics have been widely investigated as the typical candidates for microwave integrated circuits and advanced ceramic substrate materials due to their low *K* (6.6) and high *Qf* value (219,000GHz). However, they show a large negative *TCF* (-61ppm/^oC), which force the addition of material with large positive *TCF* value such as TiO_2. Therefore, the zero *TCF* was obtained while the *Qf* of the specimens rapidly decreased due to the TiO_2 with poor *Qf* value.

In this study, the microwave dielectric properties and crystal structural characteristics of new microwave dielectrics $(Zn_{1-x}Mg_x)_{1.918}GeO_{3.918}$ ($0.2 \leqq x \leqq 0.6$) were investigated as alternative microwave dielectric material of Zn_2SiO_4.

With increasing of Mg^{2+} substitution, the average grain size of the specimens continuously decreased while the single rhombohedral Zn_2GeO_4 phase was observed with Mg^{2+} substitution up to $x = 0.4$. For the specimens with $x = 0.5$ and 0.6, the secondary phase of Mg_2GeO_4 with orthorhombic symmetry was observed due to the phase transition. Generally, *Qf* value of the microwave dielectric ceramics was affected by microstructure and/or cation ordering of crystal structure. In this case, the microwave dielectric properties of $(Zn_{1-x}Mg_x)_{1.918}GeO_{3.918}$ ceramics was significantly dependent on the crystal structural characteristics. Raman spectroscopy and Rietveld refinement were used to evaluate specific crystal structural characteristics such as bond valence and tetrahedral distortion of $(Zn,Mg)O_4$ and GeO_4 tetrahedron. Maximum value of *Qf*(280,000GHz) was observed for the specimens with $x = 0.4$. This result could be attributed to the cation ordering of crystal structure due to the phase transition from low symmetry (rhombohedral) to high symmetry (orthorhombic). From the Rietveld refinement of crystal structure, the specimens with $x = 0.4$ showed equilateral hexagonal ring composed of GeO_4 and $(Zn,Mg)GeO_4$ tetrahedra, which showed the lowest value of tetrahedral distortion. Also, the cation ordering of the specimens could be evaluated by Raman spectroscopy. With increase of Mg^{2+} substitution up to $x = 0.4$, the relative intensity ratio (I_{779}/I_{748}) of Raman spectra increased, which indicated the increase of cation ordering. The *K* of the specimens decreased with Mg^{2+} substitution due to the small polarizability of Mg^{2+} than Zn^{2+}. The *TCF* of the specimens increased slightly to $x = 0.4$, while those of $x = 0.5$ and 0.6 specimens were changed remarkably due to the secondary phase of Mg_2GeO_4.

References:

[1] S. Wu, Q. Ma, J. Alloys Compd. 567 (2013) 40.

Acknowledgement:

This research was supported by Basic Science Research Program through the National Research Foundation of Korea (NRF) funded by the Ministry of Education, Science and Technology.

EL-P11

CuO/V_2O_5 Doped BZN Ceramic for Embedded Capacitor Layer in Integrated LTCC Modules

Seungjin KANG[1] and Kyoungho LEE[1,*]
[1] *Department of Display Materials Engineering, Soonchunhyang University, Asan 336-745, Republic of Korea*

Sintering additives for $Bi_{3/2}ZnNb_{3/2}O_7$ (BZN) ceramic were studied in order to facilitate the use of BZN as an integrated decoupling capacitor in high density multilayer LTCC modules for mobile communication systems. Among the additives, CuO/V_2O_5 mixture was the most promising sintering additive for co-firing BZN ceramic with a commercial LTCC sheet (MLS-22, NEG Co., Japan) and Ag electrode. 0.5 wt% CuO/V_2O_5 doped BZN was successfully densified at 860°C due to a reactive liquid phase sintering. During the liquid phase sintering, $ZnNb_2O_6$ and $BiVO_4$ phases were formed as minor phases but the resulted dielectric properties were acceptable for using the CuO/V_2O_5 doped BZN as the embedded capacitor; permittivity (ε_r) at 1 MHz was 148 and C/C_{25} was less than ± 5%.

The physical and chemical compatibilities of the CuO/V_2O_5 doped BZN with heterogeneous layers in LTCC modules (low ε_r LTCC layer and Ag electrode layer) were also examined. Co-firing test of the doped BZN ceramic with the MLS-22 LTCC sheet revealed that symmetric piling configuration was much safer than asymmetric configuration for avoiding the warpage during co-firing process. It was also revealed that the thickness control of two heterogeneous layers was the critical factor to avoid crack formations during co-firing. The optimum thickness ratio of the doped BZN and MLS-22 layers was less than 0.1. Chemical compatibility test revealed that there was no severe reaction between both the doped BZN/MLS-22 and the doped BZN/Ag electrode. After co-fired at 860°C for 20 min, ~15 μm of reaction layer was formed at the interface of BZN/MLS-22 layers, and the main diffused ions were Al, Nb, and Bi. The co-firing test of the BZN/Ag electrode revealed that BZN was very stable to the Ag electrode.

ST-P01

Properties of SiC Precursors for the precursor impregnation and pyrolysis (PIP) process

Sea Hoon Lee, Jie Yin
Division of powder/Ceramics Research, Korea Institute of Materials Science, Changwon, 641-831, Republic of Korea

Keywords: PIP, precursor, polycarbosilane, CMC

Seven polycarbosilane (PCS)-based precursors provided by American, Chinese and Korean companies were evaluated for the fabrication of SiC/SiC composites by precursor-impregnation and pyrolysis (PIP) process. Tyrano-SA grade 3 woven fabrics with PyC coating were used for the fabrication of the ceramic matrix composites (CMC). The ceramic yields of the American PCS were higher (67 - 80%) than those of the Chinese and Korean ones (50 - 63%). The softening of the solid type precursors mostly occurred at 280-320^{o}C except the American product (175^{o}C). The relative density of the CMC made with the Chinese precursor was the highest among the tested systems after 7 PIP cycles (90%). The CMCs from the American and the Korean precursors showed elegant fracture behavior with relatively low strength (200 - 240 MPa), while those from the Chinese precursor were more brittle and strong (310 MPa). The CMCs made with the Chinese precursor suffered from strong deterioration at 1500^{o}C although the Si/C ratio of the precursor-derived ceramics (PDC, 0.864) was more close to the stoichiometric value than those of the other PDCs (0.475-0.823). Thanks to the fiber pull-out mechanism during fracture, the stress-strain curves displayed a jagged failure behavior. Maximum flexural strength of 305 MPa was obtained from the CMC made with the NaBond precursor, but this CMC showed rather brittle fracture behavior. Several evidences were given to reveal the high temperature strength deterioration of the NaBond-CMC material at 1500^{o}C in Ar atmosphere. For gaining a deeper understanding of the strength degradation of NaBnond-CMC at 1500^{o}C, the high temperature thermal behavior as well as the corresponding phase characterization of NaBond precursor after pyrolysis was further analyzed. Although a major mass loss was completed before 1400^{o}C, a further mass loss in the temperature range of 1400^{o}C to 1500^{o}C was still detected (from 63.6% to 63.0%, as seen in the inset figure). This mass loss may possibly induce voids and cracks, which acted as a negative role as described above. The comparison of crystallization degree for NaBond pyrolyzed at different temperatures indicated that ongoing crystallization after 1400^{o}C occurred and density increase with accompanying the generation of cracks, which would therefore decrease the bending strength.

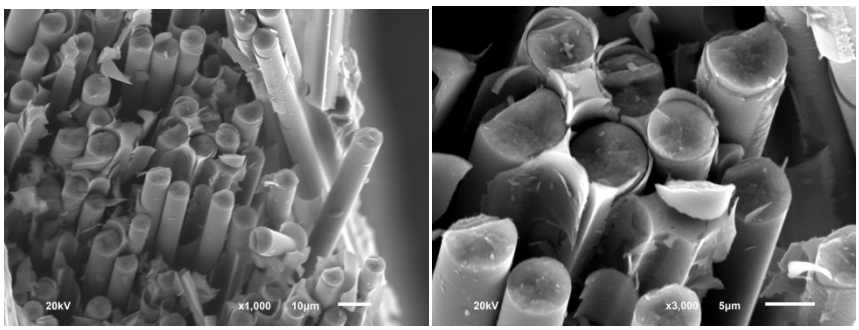

Figure 75 Fractured surfaces of the SiC_f/SiC composite materials using SMP-730 precursors

ST-P02

Theoretical and Experimental Analyses of Thermal Conductivity of the Alumina-Mullite System

Shota ITOH, Yoshihiro HIRATA*, Taro SHIMONOSONO, Soichiro SAMESHIMA
Department of Chemistry, Biotechnology, and Chemical Engineering, Kagoshima University
1-21-40 Korimoto, Kagoshima 890-0065, Japan

Keywords: Thermal conductivity, Alumina, Mullite, Particle size

The thermal conductivity of the three phase system of alumina-mullite-pore was calculated by a theoretical equation developed [1,2] in this research group, and compared with the experimental results. The pores in the sintered composite were treated as one phase. A theoretical thermal conductivity of alumina-mullite-pore system was calculated for two cases : mullite continuous phase and alumina continuous phase. Figure 1 shows the measured and calculated thermal conductivities for the alumina-mullite-pore system. The measured conductivity of the composite with 0.5-25 % porosity was in accordance with the calculated value for the mullite continuous phase. No grain size effect of mullite particles on the thermal conductivity was measured in the range of 1-50 μm. This result is also explained by the developed model.

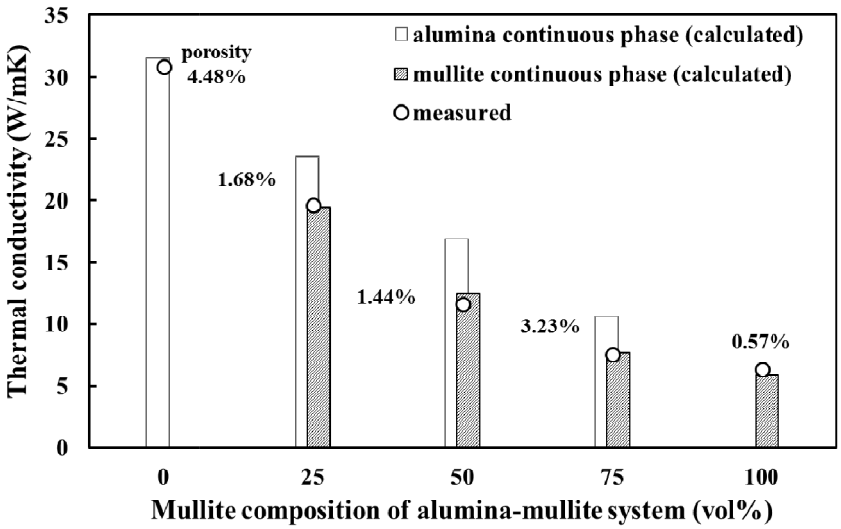

Figure 76 Comparison of thermal conductivities between the measurement and the calculation for the alumina-mullite-pore system.

References:

[1] Y. Hirata, Ceram. Inter., 35, 2921-2926 (2009)
[2] Y. Hirata, N. Matsunaga, J. Yoshitomi. T. Kayama J. Tech. Assoc. Refract. Japan, 31, 156-163 (2011)

ST-P03

Effect of ZrO_2 on the mechanical properties of mullite composites

Shielah MAVENGERE and Bum-Rae CHO*,
Department of Advanced Materials Engineering, Keimyung University, Daegu 704-701, Korea

***Keywords*:** mullite, zirconia composite, reaction-sintering

Mullite interlocking needle-like microstructures offer an efficient filtering effect. The properties of such need-like microstructures include high thermal and chemical stability. However, mullite ceramics processed by ordinary sintering conditions yield alumina-rich and silica-rich phases in the grain boundaries which lead to degradation of mechanical properties. The aim of this study is to produce a needle-like mullite matrix with silica free grain boundaries using a two-step sintering procedure. Mullite composite samples were prepared from high purity $Al(OH)_3$, SiO_2, AlF_3 and yttria stabilized ZrO_2 powders by a two step sintering procedure between 900 ˚C and 1450 ˚C. Effect of ZrO_2 on mechanical properties of mullite was explained in terms of SEM images of the fractured SEM microstructures and phases obtained on XRD patterns. Equi-axed needle-like microstructures with bending strengths of 10.8 MPa to 12.7 MPa were obtained in 5 wt% samples. However, irregular microstructures and bending strengths which ranged from 4.4 MPa to 8.7 MPa were obtained in 10 wt% and 15 wt% samples. At low sintering temperatures mullite and zircon were detected as the major phases, but with increase in sintering temperatures zirconia and mullite phases were dominant. Apparent porosities of up to 62% make these mullite-zirconia composites suitable candidates in filtering applications.

References:

[1] A. J. Pyzik, C. S. Todd and C. Han, J. Eur. Ceram. Soc. 28 (2008) 383.
[2] B. R. Cho and D. H. Heo, Key. Eng. Mat. 105 (2006) 317.
[3] G. Orange, G. Fantozzi, J. Ceram. Mat. Scie. 20 (1985) 2533.
[4] H. S. Tripathi, J. Mater. Sci., 35(4) (2012) 639.
[5] X. Miao, J. Mat. Let. *38* (1999) 167.
[6] W. Yan, N. Li and B. Han, J. Ceram. Proc. Res. 11(3), (2010) 388.

ST-P04

Effect of Cell Size on Thermal Conductivity of UO_2 Nuclear Fuel Pellet containing Mo Metallic Micro-cell

Dong-Joo Kim[1], Young Woo Rhee[1], Jong Hun Kim[1], Keon Sik Kim[1], Jang Soo Oh[1], Jae Ho Yang[1], Yang-Hyun Koo[1], Seung Jae Lee[2]
[1] *Korea Atomic Energy Research Institute, Daejeon, 305-353, South Korea*
[2] *KEPCO Nuclear Fuel Co., Daejeon, 305-353, South Korea*

Keywords: Nuclear fuel pellet, UO_2, Molybdenum, Micro-cell pellet, Thermal conductivity

In the nuclear fuel performance of an LWR (Light Water Reactor), the thermal conductivity of a UO_2 fuel pellet is one of the most important properties. The steep temperature gradient and high centerline temperature in the fuel pellet results from a low thermal conductivity of UO_2, which is a typical ceramic material. The in-reactor performance, integrity, safety and accident tolerance of the nuclear fuel can be significantly affected by the thermal conductivity of the UO_2 fuel pellet.
The improvement in the thermal conductivity of the UO_2 fuel pellet can enhance the fuel performance in various ways – decreased fuel centerline temperature, increased fission gas retention capability, increased pellet dimensional stability, enhanced accident tolerance, etc.
To enhance the thermal conductivity of a UO_2 fuel pellet, we are developing a UO_2-based Mo metallic micro-cell pellet. The UO_2-Mo micro-cell pellet with high density as well as a continuous channel of the Mo metallic phase could be successfully fabricated. Above all, the verification of thermal conductivity of the developed pellet is very important. In this work, the effect of the cell size on the thermal conductivity of the UO_2-Mo micro-cell pellet was measured and verified.

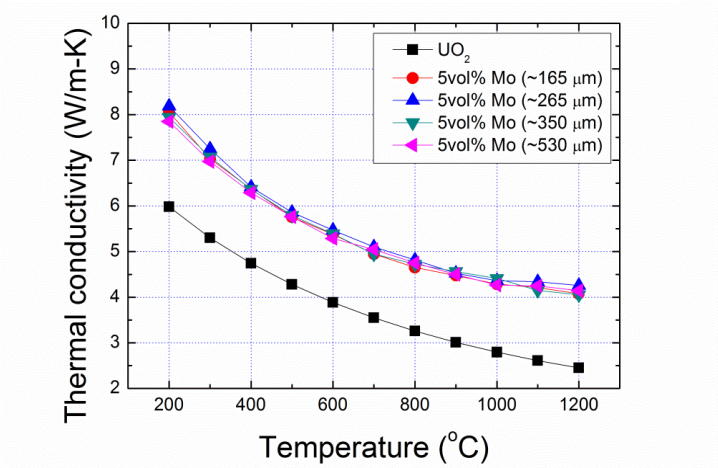

Figure 77 Measured thermal conductivity of UO_2-5 vol% Mo pellet with various cell sizes

References:

[1] J.H. Yang, K.W. Song, K.S. Kim, Y.H. Jung, J. Nucl. Mater. 353 (2006) 202.
[2] S.H. Kim, C.Y. Joung, H.S. Kim, Y.W. Lee, H.J. Ryu, D.S. Sohn, D.J. Kim, J. Nucl. Mater. 352 (2006) 151.
[3] K.H. Sarma, J. Fourcade, S-G. Lee, A.A. Solomon, J. Nucl. Mater., 352 (2006) 324.

Acknowledgement:

This work was supported by the National Research Foundation of Korea (NRF) grant funded by the Korea government (MSIP) (No. 2013000720).

ST-P05

Thermodynamic Assessment of UO_2 Nuclear Fuel Pellet Oxidation in Air, Steam, and H_2 Mixture Atmosphere

Dong-Joo Kim, Jong Hun Kim, Keon Sik Kim, Jae Ho Yang, Sun Ki Kim, Yang Hyun Koo
Korea Atomic Energy Research Institute, Daejeon, 305-353, South Korea

Keywords: Nuclear fuel pellet, UO_2, Oxidation, Oxygen partial pressure

If a loss-of-coolant accident in a spent nuclear fuel pool occurs, it can bring about a massive failure owing to a drastic increase in the temperature of the spent nuclear fuel. In addition, the possibility of an external leakage of a significant amount of radioactive materials can increase. Under a loss-of-coolant accident, an air and/or steam oxidation reaction of the spent nuclear fuel leads to a failure of the fuel cladding, and an air and/or steam oxidation of the spent fuel pellet will follow. The oxidized spent fuel pellet will be expanded and pulverized, and a failure of the fuel cladding can additionally take place.
In this work, to predict the oxidation behavior of a UO_2 nuclear fuel pellet under a loss-of-coolant accident in a spent nuclear fuel pool of an LWR, thermodynamic assessments of UO_2 oxidation were carried out. To simulate the accident scenario, an assessment of UO_2 pellet oxidation under various atmospheres (air, steam, H_2, and a mixture) is required. In an air and steam mixture atmosphere, the UO_2 oxidation was dominantly affected by the air volumetric fraction, because of the relatively higher oxygen partial pressure of air. In addition, the critical value of the hydrogen volumetric fraction affecting the reduction of UO_2 oxidation was calculated.

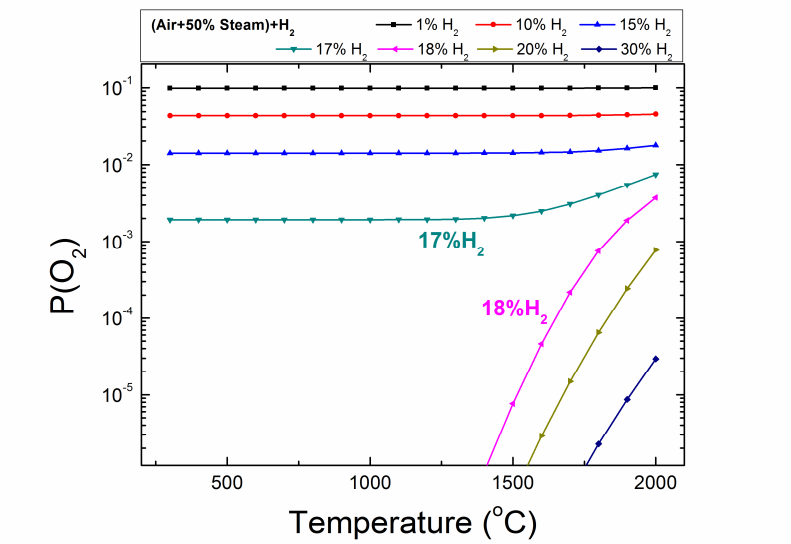

Figure 78 Calculated oxygen partial pressure under air+50%Steam with various H_2 contents

References:
[1] Y.H. Koo, Y.S. Yang, K.W. Song, Progress in Nuclear Energy 74 (2014) 61.
[2] P.D.W. Bottomley et al., Annals of Nuclear Energy 65 (2014) 345.

Acknowledgement:
This work was supported by the National Research Foundation of Korea (NRF) grant funded by the Korea government (MSIP) (No. 2013000720).

ST-P06

TEM Analysis Study on the Microstructure of Oxides Formed on the Surface of FeCrAl Alloy at High Temperature

Dong Jun PARK[1*], Hyun Gil KIM[1], Yang Il Jung[1], Jung Hwan PARK[1], Yang Hyun KOO[1]
[1]*Department LWR Fuel Technology Division, Korea Atomic Energy Research Institute, 989-111 Daedeok-daero, Yuseong-gu, Daejeon, 305-353, Korea*

Keywords: FeCrAl Alloy, Oxide, TEM, Microstructure

Recently, interest in using FeCrAl alloy as the nuclear fuel cladding material in conventional light water reactors (LWRs) has increased considerably. This is because its superior oxidation resistance at high temperatures could significantly reduce the risk of explosions caused by hydrogen gas, as was the case in the Fukushima nuclear reactor accident. Other superior properties of FeCrAl alloy are excellent formability and very good high strength at high temperature. For these reasons, Fe-based alloy is considered as one of the most promising candidates for accident tolerant fuel material.

The integrity of the fuel cladding should be maintained not only during normal operation but also in a postulated design-based accident. Therefore, it is necessary to understand clearly the oxidation behavior of candidate materials under both normal operation and loss-of-coolant accident (LOCA) condition for their application to the fuel cladding material in LWRs.

In this study, long-term corrosion and high temperature oxidation behaviors were investigated in a corrosion environment simulating pressurized water reactor and simulated LOCA condition. In the first test, the alloy was corroded in pressurized 360℃ water representing normal operation conditions for periods up to 400 days, with the aim of studying the long-term corrosion behavior of FeCrAl alloy. In the second one, alloy specimen was exposed to flowing water vapor at 1200℃ for 3000 s to simulated LOCA condition. To study high temperature oxidation behavior of FeCrAl alloy under steam environment, thermo-gravimetric analyzer was used and weight change of the samples was measured in real time. For all the specimens, the effect of oxidation environment was evaluated in terms of weight gain for unit area.

It was observed that oxides grown during the test show differences in their chemical properties and micro structure depending on their test conditions. As shown below image, Fe_2O_3 oxide was grown in water static test at 360ºC while Al_2O_3 layer was observed in high temperature oxidation test at 1200ºC. The detailed analysis study for oxide layers was carried out by using High resolution TEM, XRD, and XPS.

Acknowledgement:
This work was supported by the National Research Foundation of Korea (NRF) grant funded by the Korea government (MSIP) (No. 2012M2A8A5000702)

GL-P01

Synthesis and luminescence property of $Li_{1.11}Ta_{0.89}Ti_{0.11}O_3$: Eu^{3+}, Sm^{3+} red phosphor

Hiromi Nakano[1*], Syohei Furuya[1], Suzuya Yamada[2]
[1] *Department of Environmental and Life Sciences, Toyohashi University of Technology, Toyohashi 441-8580, Japan*
[2] *Central Research Institute, Denki Kagaku Kogyo K.K., Machida 194-8560, Japan*

Keywords: solid solution, luminescence, X-ray diffraction, phosphors, energy transfer

The ternary Li_2O-Ta_2O_5-TiO_2 system compounds have been applied to the host materials of new phosphors [1]. The *RE* (=Eu^{3+}, Sm^{3+}, Er^{3+}, Dy^{3+} or Tm^{3+}) doped $Li_{1+x}Ta_{1-x}Ti_xO_3$ (LTT, $0 \le x \le 0.25$) phosphors, showing various emission colors, have been synthesized to compared their PL properties to those of the LNT phosphors [2]. In the LTT host materials, the most effective activator was Eu^{3+}. The internal quantum efficiency attained the value of over 84 % for the host composition of $Li_{1.11}Ta_{0.89}Ti_{0.11}O_3$ (x = 0.11) [2]. In this work, we have tried to enhance the emission intensities of the LTT phosphors by co-doping of Eu^{3+} and Sm^{3+} because the Sm^{3+} ions have been reported to act as sensitizers for various types of Eu-doped phosphors [3]. The starting powders were mixed and pressed in air at 1423 K for 15 h in a conventional electric furnace. Characterizations were carried out by X-ray diffraction (XRD) and a scanning electron microscope. Excitation and emission spectra of the obtained samples were measured by a spectrometer (model FP-6500, JASCO). Quantum efficiency was measured by a spectral radiometer (MCPD-7000, Otsuka Electronics Co. LTD.,) In order to clarify the effect of Sm^{3+}-ion doping on the photoluminescence properties, the Sm_2O_3 content was varied from 0 to 0.25 wt%, with a fixed Eu_2O_3 concentration of 2.5 wt%. We determined the internal quantum efficiency (Fig. 1). The results show that the co-doped phosphor with Sm_2O_3 at 0.1wt% showed the highest PL intensity, with the internal quantum efficiency being 98 %. The PL intensity of this phosphor, doped with Eu_2O_3 at 0.25 wt% and Sm_2O_3 at 0.1 %, was *ca*. 1.4 times higher than that of the 0.25 wt% Eu^{3+}-doped $Li_{1.11}Ta_{0.89}Ti_{0.11}O_3$ phosphor, indicating that the small amount of Sm^{3+} acted as an effective sensitizer. The external quantum efficiency was slightly improved up to *ca*. 20%, although the improvement degree was still unsatisfactorily low, which must be caused by the low absorptivity due to the forbidden 4*f*-4*f* transition of the Eu^{3+} ion. No emission peak of the co-doped phosphor was observed at around 607 and 650 nm by the transition of the Sm^{3+} ion. The Sm^{3+} transfers energy to the ^5D_J state of Eu^{3+} without any red-light emission. Hence, the highly efficient red-light emission due to Eu^{3+} would occur through the $^5D_0$-^7F_J transition, without the emission due to Sm^{3+}.

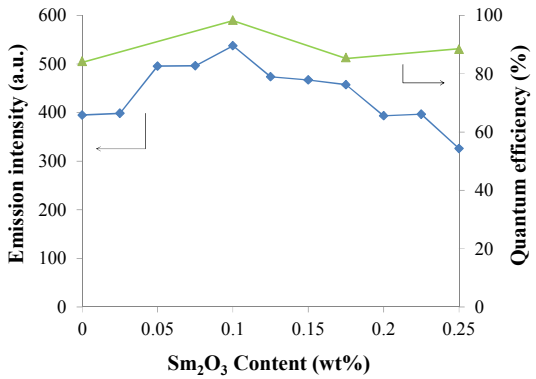

Fig. 1 Changes in emission intensity and internal quantum efficiency against Sm_2O_3 content

References:
[1] H. Nakano, K. Ozono, H. Hayashi, S. Fujihara, J. Am. Ceram. Soc. 95(9) (2012) 2795.
[2]H. Nakano, S. Suehiro, S. Furuya, H. Hayashi, S. Fujihara, Mater. 6 (2013) 2768.
[3] G.-H. Lee, T.-H. Kim, C. Yoon, S. Kang, J. Lumin. 128 (2008) 1922 -1926.

Acknowledgement:
This work (H. N.) was partially supported by a Grant-in-Aid for Scientific Research (c) No. 25420709 by the Japan Society for the Promotion of Science.

GL-P02

Synthesis and luminescence property of RE^{3+}doped $Li_{1.11}(Ta_{1-z}Nb_z)_{0.89}Ti_{0.11}O_3$ ($0 \le z \le 1.0$, *RE*: Sm, Dy, Tm or Er) phosphor

Syohei Furuya[1], Hiromi Nakano[1*], Hiroyuki Hayashi[2], Suzuya Yamada[3]
[1] *Department of Environmental and Life Sciences, Toyohashi University of Technology, Toyohashi 441-8580, Japan*
[2] *KRI, Inc., Chudoji Minami-machi, Shimogyo-ku, Kyoto 600-8813, Japan*
[3] *Central Research Institute, Denki Kagaku Kogyo K.K., Machida 194-8560, Japan*

Keywords: oxide, solid solution, luminescence, X-ray diffraction, phosphors

Recently, we have succeeded in synthesizing new phosphors based on the ternary Li_2O-M_2O_5-TiO_2 (M = Nb or Ta) solid solution system as the host materials. [1-3]. Eu^{3+}doped $Li_{1.11}Ta_{0.89}Ti_{0.11}O_3$ phosphor showed strong red emission in the quaternary $Li_{1+x}(Ta_{1-z}Nb_z)_{1-x}Ti_xO_3$ solid solutions [4].

In this work, we synthesized the phosphors based on the quaternary $Li_{1.11}(Ta_{1-z}Nb_z)_{0.89}Ti_{0.11}O_3$ (LTNT, $0 \le z \le 1.0$) solid solutions as the host materials. In order to highest PL intensity for *RE* (= Sm^{3+}, Er^{3+}, Dy^{3+} or Tm^{3+}) doped LTNT phosphor, the optimal composition was determined. The starting powders were mixed and pressed in air at 1393 K~1423 K for 15 h in a conventional electric furnace. Characterizations were carried out by X-ray diffraction (XRD) and a scanning electron microscope. Excitation and emission spectra of the obtained samples were measured by a spectrometer (model FP-6500, JASCO). Quantum efficiency was measured by a spectral radiometer (MCPD-7000, Otsuka Electronics Co. LTD.,)

Figure 1 shows the relationship between PL intensity and z value in rare-earth doped $Li_{1.11}(Ta_{1-z}Nb_z)_{0.89}Ti_{0.11}O_3$ phosphor ($0 \le z \le 1.0$).The result showed that the optimal composition of the host material were various ratios of Ta/Nb for rare earth ions. Red emission was observed for the Sm^{3+}-doped LTNT upon excitation at around 411 nm due to the $^6H_{5/2}$-$^6P_{3/2}$ transition. Upon excitation at 411 nm, the photoluminescence spectra showed emission peaks at 568 ($^4G_{5/2}$ - $^6H_{5/2}$), 607 nm ($^4G_{5/2}$-$^6H_{7/2}$), and 651 nm ($^4G_{5/2}$-$^6H_{9/2}$). Therefore it seems that the peak intensity ratio of Li-Ta-Ti-O phosphor at 607nm/650nm is larger than that of Li-Nb-Ti-O phosphor. This would be caused by the difference in the overlapping of orbitals with the adjacent anions (Ta/Nb). The green emission peak around 527 nm ($^4S_{3/2}$ -$^4I_{15/2}$) was observed for LTNT:Er^{3+} upon excitation at 551 nm ($^4I_{15/2}$- $^2H_{11/2}$). Blue emission was observed around 363 nm ($^1D_2$-$^3F_4$ transition) for the LTNT:Tm^{3+} phosphor upon excitation at 461 nm ($^3H_6$-$^1D_2$). The yellow emission peak around 581 nm ($^4F_{9/2}$ - $^6H_{13/2}$) was observed for LNT:Dy^{3+} upon excitation at 355 nm ($^6H_{15/2}$ -$^4M_{15/2}$). We have concluded that the small differences in environment of the dopant sites between the host materials of LTNT eventually affect the emission energy of the RE^{3+} ions.

References:
[1] H. Nakano K. Ozono, T. Saji, S. Miyake, H. Hiroyuki, Opt. Mater. 35 (2013) 2045.
[2] H. Nakano, S. Suehrio, T. Saji, S. Miyake, J. Alloys. Compd. 552 (2013) 475.
[3] H. Nakano, S. Suehiro, S. Furuya, H. Hayashi, S. Fujihara, Mater. 6 (2013) 2768.
[4] H. Nakano, K. Ozono, H. Hayashi, S. Fujihara, J. Am. Ceram. Soc. 95(9) (2012) 2795.

Acknowledgement:
This work (H. N.) was partially supported by a Grant-in-Aid for Scientific Research (c) No. 25420709 by the Japan Society for the Promotion of Science.

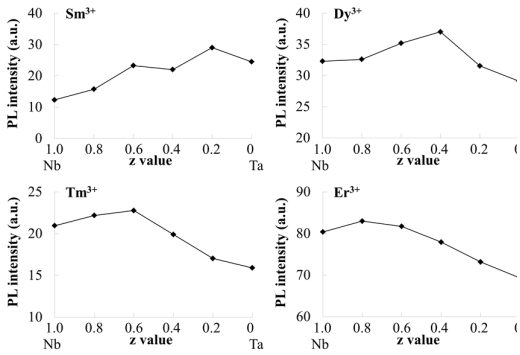

Fig.1 Relationship between PL intensity and z value in $Li_{1.11}(Ta_{1-z}Nb_z)_{0.89}Ti_{0.11}O_3$:$RE^{3+}$ Phosphors.

GL-P03

The contributions of flaw healing effect and ion-exchange to the strength improvement of glass-infiltrated alumina

Dong-Hwan Kim[1,3], Jee-hun Maeng[1], Seong-Jai Cho[2], Sung-Churl Choi[3], Hyeong-Jun Kim[1,*]
[1]*Korea Institute of Ceramic Engineering & Technology, Icheon 467-843, Gyeonggi, Republic of Korea*
[2]*Division of Advanced Technology, Korea Research Institute of Standards and Science, Yuseong, Daejeon 305-340, Republic of Korea*
[3]*Division of Materials Science and Engineering, Hanyang University, Seongdong-gu, Seoul 133-791, Republic of Korea*

Keywords: Ion exchange; Ceramics strengthening; Glass penetration; Glass infiltration

It is well-known that the classic ceramics, as porcelain, are strengthened with thermal expansion mismatch between body and glaze and reduction of the defects on body using glaze coating. Several researchers shows that a low thermal expansion glass penetrated into the surface of dense alumina and zirconia ceramics produced a compressive stress at surface due to the thermal expansion mismatch on cooling thereby strengthening the ceramics remarkably[1,2]. However, it is little-known how much is the difference between the contribution of the flaw healing and thermal expansion mismatching for strengthening the ceramics.

In order to exclude thermal expansion mismatching and only contribute the defect healing effect, we selected the glasses with thermal expansion coefficient similar to ceramic body for infiltration. Meanwhile, it was checked whether the ion exchange method could work to strengthen its glass-infiltrated ceramics or not.

High-density alumina and porous alumina were penetrated by Na_2O-Al_2O_3-SiO_2 and Na_2O-CaO-SiO_2 system glasses, which respectively have similar or larger coefficients of thermal expansion than alumina. Flexural strength of high-density alumina was improved by up to 24 % due to only flaw healing of glass-infiltration without compressive stress generation caused by the difference in the coefficient of thermal expansion. The combination of glass-infiltration and an ion-exchange process enhanced the mechanical properties of the alumina/glass composite by more than 60 %.

References:

[1] Chu. M. C, Panigrahi. B. B, Balakrishnan. A, Cho. S. J, Yoon. K. J, Kim. T. N and Lee. K. H, Mat. Sci and Eng A 452-453 (2007) 110-115
[2] H. Inada, "Change in the properties of glaze through firing and its effect on the stress in glaze(in Jpn)," *J. Ceram. Soc. Jpn*., 86 [3] 107-114 (1978)

GL-P04

Micro-crack Healing on Glass Using Chemically Strengthening

Dong-Hwan Kim[1,2], Jee-hun Maeng[1], Sung-Min Lee[1], Sung-Churl Choi[2], Hyeong-Jun Kim[1,*]
[1]*Korea Institute of Ceramic Engineering & Technology, Icheon-si 467-843, Gyeonggi-do, Republic of Korea*
[2]*Division of Materials Science and Engineering, Hanyang University, Seongdong-gu, Seoul, Republic of Korea*

Keywords: Ion exchange; Chemically strengthening; Indentation; Crack healing

We studied whether the chemically strengthening could heal the flaw on soda-lime silicate glass. The artificial surface cracks were introduced in the glass by sharp indentation with various loads at 2, 10 and 20N. Then the glasses with flaws were treated by ion-exchanging in KNO_3 melt. The dimensional change of the crack on glass was measured by digital microscope and scanning electron microscope.

After treatment, the strength of glass with flaw was enhanced. Chemical strengthening by ion-exchange made the glass surface to develop the compressive stress, which could induce the crack healing effect at crack tip region. The strength was maintained constant until 18 μm size of crack. However, when glass had the crack with over 30 μm, the crack healing effect was rapidly decreased.

GL-P05

Improved Thermal Stability of Phosphor in Glass Varying Glass to Phosphor Mixing Ratio

Hyun-A Park[1], Sang Heon Lee[1], Won Bin Im[2], and Woon Jin Chung[1]
[1]*Division of Advanced Materials Engineering, Kongju National University, Cheonan, Republic of Korea*
[2]*School of Materials Science and Engineering, Chonnam National University, Gwangju, Republic of Korea*

Keywords: Phosphor in glass, LED, Thermal quenching

Recently, inorganic color converter has been studied to replace organic binders which have weak thermal and chemical durability in order to increase lifetime of high power WLED. Phosphor in glass can be fabricated by a simple mixture of glass frit and phosphor. However, conventional PiG with SiO_2-B_2O_3-RO glass has a high sintering temperature at 750 ^oC[1] and thus it is difficult to use various phosphor and control chromaticity of WLED.
In this study, we synthesized a low sintering temperature silicate glasses based on SiO_2-P_2O_5-B_2O_3-ZnO and SiO_2-B_2O_3-ZnO-Na_2O which can be sintered at 500 ^oC and 550 ^oC, respectively the glass were mixed with various ratio of glass to $Y_3Al_5O_{12}$: Ce^{3+} (YAG) yellow and $CaAlSiN_3$:Eu^{2+} (CASN) red phosphors. CIE chromaticity of PiGs were varied by phosphor content. It was showed that the thermal properties of PiG was enhanced when compared to silicon resin. Thermal conductivity of PiG was measured to discuss on the improved thermal stability with the phosphor content.

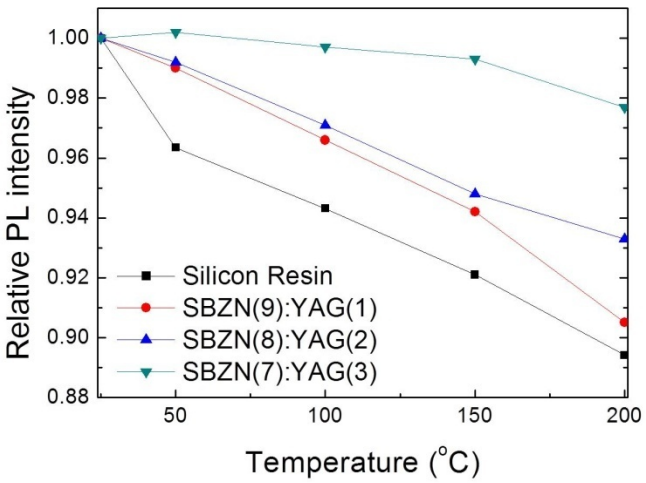

Fig. Thermal quenching property of PiG compared to silicon resin

References

[1] Y.K. Lee, J.S. Lee, J. Heo, W. B. Im, and W.J. Chung, "Phosphor in glasses with Pb-free silicate glass powders as robust color-converting materials for white LED applications", Opt. Lett., 37 (2012) 3276-3278 .

GL-P06

Oxyfluoride glass ceramic doped with Eu^{2+}/Eu^{3+} for 400nm UV-LED Color Conversion

Sang Hun Lee[a], Suk-Rok Bae[a], Yong Gyu Choi[b], Woon Jin Chung[a]
[a] *Div. of Advanced Materials Eng., Kongju National University, Cheonan, Republic of Korea*
[b] *Dept. of Materials Sci. and Eng., Korea Aerospace University.,Goyang, Republic of Korea*

Oxyfluoride glass ceramics have been widely studied due to their high chemical and thermal stability of matrix as well as low phonon energy of fluoride nano-crystals. The low phonon energy around the rare earth ions can improve quantum efficiency of the excited state, thus improve emission. In this paper, we fabricated SiO_2-Na_2O-Al_2O_3-LaF_3 glasses doped with various rare earth ions. Based on absorption and PL spectra, Eu^{2+} and Eu^{3+} were selected as active ions for 400 nm LED color conversion. Concentration of carbon and EuF_3 was varied to control the Eu^{2+}/Eu^{3+} ratio. It was possible to obtain white color coordination under 400 nm LED excitation when 1 mol% of EuF_3 with 18 wt% of carbon was added. Emission intensity was increased as the doped glass was heat treated due to nano-crystal formation. Heavy crystallization of Eu^{3+}/Eu^{2+} doped glass was examined to improve absorption of the UV source and enhance color conversion efficiency when actually mounted on 400 nm LED chips.

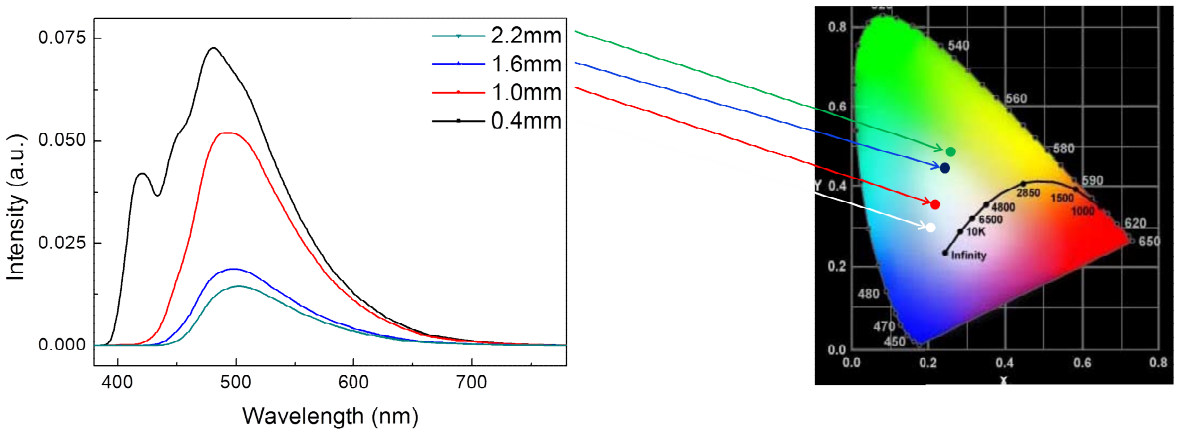

Fig. 1. PL spectra and CIE color coordinates of 400nm LED mounted with heavily crystallized oxyfluoride glass ceramic varying their thickness

GL-P07

Compositional Effects of Metal Oxides on Reaction Between Sealing Glass and Soda-Lime Glass Substrate

Aram SUNG[1], Seunggon CHOI[1], Hyungsun KIM[1*]
[1]*School of Materials Science Engineering, Inha University, 253 Yonghyun-don, Incheon 402-751, Korea*

Keywords: hermetic sealing, Pb-free, sealing glass, adhesive strength

Packaging needs to be hermetic for the manufacturing electornic deives because they are easily damaged by water vapor. Epoxy or metal is widely used as sealing materials, but they have poor strength, short lifetime and high coefficient of thermal expansion which cause the electrical malfunctions by crack generations. On the other hand, glass sealing has high strength and excellent reliability, and it can make hermetic sealing easily. Although the glass frits containing PbO is well known as a low temperature sealing glass, the recent environmental regulation restricts the use of the PbO. Thus, Pb-free sealing glass systems which have low thermal properties and high adhesive strength are being developed. In this study, we have investigated the glass forming region of V_2O_5-P_2O_5-ZnO system and the effects of the addition of metal oxides on the glass transition temperature and coefficient of thermal expansion. Thermal properties and viscous flows of frits were measured via differential scanning calorimeter, dilatometer and hot stage microscope. Interfacial reactions between glass frit and substrates were observed by scanning electron microscope after firing. These frits had a low softening point($\leq 400^oC$) and proper CTE($\approx 75x10^{-7}/K$) to the soda-lime glass substrate. It was also found that metal oxides induce the diffusion of the mobile ions from the glass substrates to the glass sealant and the crystallization near the interface. This indicates that thermal diffusion of ions and the area ratio of the crystal is related with the adhesive strength between sealant and glass substrate.

References:

[1] R.Knechtel, *Microsyst. Tech*, 12 (2005)
[2] T.Sugawara, Y.Kuroki, T.Yano, *Inform.Media Tech.* 59(116) (2005) *p*.41

Acknowledgement:

This work was supported by the Energy Efficiency & Resources of the Korea Instiute of Energy Technology Evaluation and Planning(KETEP) grant funded by the Korea government Ministry of Knowledge Economy (No.20132020101460)

GL-P08

Thermal Expansion of Ternary Ge-Sb-Se Chalcogenide Glasses in Compositional Range for Molded Infrared Lens Applications

Jun Ho LEE[1], Sang Yeol SHIN[1], Jeong Han YI[1], Woo Hyung LEE[1], Bong Je PARK[2], Yong Gyu CHOI[1,*]

[1]*Department of Materials Science and Engineering, Korea Aerospace University, Gyeonggi 412-791, Republic of Korea*

[2]*Transparent Transducer and UX Creative Research Center, Electronics and Telecommunications Research Institute, Daejeon 305-700, Republic of Korea*

Keywords: Chalcogenide glass, Thermal expansion, Molded infrared lens, Infrared camera

With the increasing demand upon the night vision system (infrared camera, for example) for use in transportation and surveillance, in addition to its existing military applications, cost effectiveness of IR transmitting lens becomes rapidly critical. As such, inorganic glasses that can be molded into lenses are certainly competitive against their crystalline counterparts such as Ge and ZnSe. Se-based chalcogenide glasses are being considered as the material of choice for optical-grade lenses operating at mid-infrared wavelength region around ~10 m. Among several selenide glass systems, ternary Ge-Sb-Se system is very promising as a moldable glass material owing to its thermal and mechanical stability [1, 2].

Glass formation out of this ternary system has been known, and various aspects of this unique glass have been studied so far. Compositional dependence of properties related to such a molding process needs to be investigated in order to optimize suitable compositions [3]. As for such composition-dependent properties, thermal expansion coefficient is definitely one of important parameters that should be taken into consideration. We recognize, however, that thermal expansion behavior of ternary Ge-Sb-Se glass in the compositional range targeting the molding process has not been studied systematically. Based on this consideration, we have aimed to evaluate its compositional dependence of thermal expansion coefficient. The measured thermal expansion data are analyzed as a function of content of each constituent atom, and then correlated with structural parameters such as mean coordination number and average bond energy.

References:

[1] X.H. Zhang, Y. Guimond and Y. Bellec, J. Non-Cryst. Solids 326&327 (2003) 519.
[2] D.H. Cha, H.J. Kim, H.S. Park, Y.H. Hwang, J.H. Kim, J.H. Hong and K.S. Lee, Appl. Opt. 49 (2010) 1607.
[3] J.K. Park, J.H. Lee, S.Y. Shin, J.H. Yi, W.H. Lee, N.Y. Kim and Y.G. Choi, Arch. Metall. Mater. (2014) accepted.

Acknowledgement:

This work was supported by the Technology Innovation Program funded by the Ministry of Trade, Industry and Energy (Grant No. 10043803).

GL-P10

Raman Spectroscopic Study of the Structure of $ZnO-Bi_2O_3-B_2O_3$ Glasses

Shun TSUJI[1], Kohei FUKUMI[2], Naoyuki KITAMURA[2], Hiromitsu KOZUKA[3] and Hiroaki UCHIYAMA[3]

[1]*Graduate School of Science and Engineering, Kansai University, Suita, Osaka 564-8680, Japan*
[2]*National Institute of Advanced Industrial Science and Technology, Ikeda, Osaka 563-8577, Japan*
[3]*Faculty of Chemistry, Materials and Bioengineering, Kansai University, Suita, Osaka 564-8680, Japan*

Keywords: glass structure, Raman spectra, bismuth, zinc, borate glass

Bismuth containing glasses are known to be high-refractive-index glasses for precision molding. These glasses, however, show yellow color due to the electronic transition from 6*s* to 6*p* of Bi^{3+} ions depending on their composition. Therefore, it is important to study the structure around Bi^{3+} ions which would affect the color of the glasses. In the present study, the structure around Bi^{3+} ions has been investigated in $ZnO-Bi_2O_3-B_2O_3$ glasses.

Raman spectra of xZnO-$y$$Bi_2O_3$-(100-$x$-$y$)$B_2O_3$ glasses were measured with a Raman spectrometer by the backscattering arrangement. The sample position was adjusted to obtain the maximum Raman scattering intensity. The measured intensity was corrected for the effect of sample thicknesses, the effect of the solid angle of collected light and the effect of the surface reflection. The corrected intensity was reduced to the intensity per one-mole Bi atoms by dividing by the Bi atomic density.

A Raman band due to Bi^{3+} cation vibrations [1,2] was observed at ca. 150 cm^{-1}, as shown in fig.1. The reduced intensity of the 150 cm^{-1} band increased with an increase in Bi_2O_3 content, as shown in fig.2. It was deduced that the 150 cm^{-1} band was related to Bi-O-Bi bond, since the probability of the formation of Bi-O-Bi bonds should increase with increasing Bi_2O_3 content. The peak position of the 150 cm^{-1} band shifted toward low wavenumbers with an increase in ZnO/B_2O_3 molar ratio. In bismuth borate binary crystals, the 150 cm^{-1} band shifts toward low wavenumbers with increasing number of Bi atoms which bond with an O atom [3-5]. The increase of the number of Bi atoms bonding to an oxygen atom implies the increase of the probability that the Bi-O-Bi linkages extend. Therefore it was deduced that the Bi-O-Bi linkages extend with increasing ZnO/B_2O_3. The extent of the peak shift in zinc bismuth borate glasses was smaller than that in lithium bismuth borate glasses, indicating that the ability of ZnO to extend Bi-O-Bi linkages was lower than that of Li_2O.

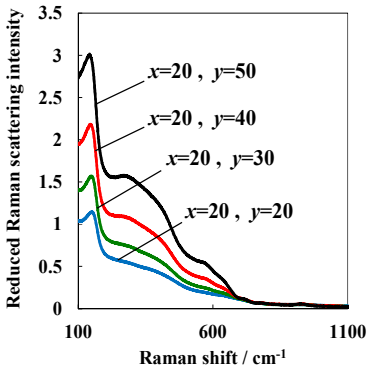

Fig. 1. Raman spectra of xZnO-$y$$Bi_2O_3$-(100-$x$-$y$)$B_2O_3$ glasses.

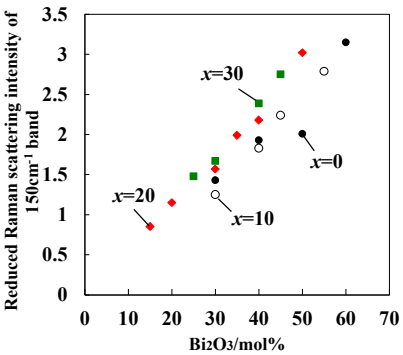

Fig. 2. Relationship between reduced Raman intensity of 150 cm^{-1} band and Bi_2O_3 content in xZnO-$y$$Bi_2O_3$-(100-$x$-$y$)$B_2O_3$ glasses.

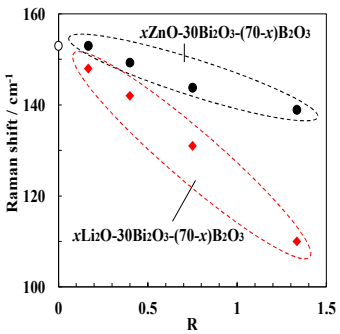

Fig. 3. Relationship between peak position of 150 cm^{-1} band and ZnO/B_2O_3 or Li_2O/B_2O_3 molar ratio, R.

References:

[1] A.E.Miller et al., J.Non-Cryst.Solids 99(1988) 289. [2] A.A.Kharlamov et al., J.Non-Cryst.Solids 202(1996)233. [3] A.A.Kaminskii et al.,Optics Commun. 206(2002)179. [4] A.V.Egorysheva et al.,Fizika Tverdogo Tela 43(2001)1590. [5] A.V.Egorysheva et al., Kristallografiya 50(2005) 127.

BI-P01

Synthesis of Calcium Phosphate Minerals from Biowaste

Sachin N, BRAMHE[1], Seon Ae HWANGBO[2], Min Cheol CHU[1,3*]
[1]*Center for New Functional Materials Metrology, Korea Research Institute of Standards and Science, Daejeon 305-340, South Korea*
[2]*Department of Material Science and Technology, Pukyong University, Busan, South Korea*
[3]*University of Science and Technology, Daejeon 305-340, South Korea*

Keywords: Hydroxyapatite, Tricalcium phosphate, Biowaste, Hydrothermal

Calcium phosphate minerals like hydroxyapatite and tri calcium phosphate have been widely used for applications such as bone materials, chromatography, fertilizers, nutritional supplement and sensors. Variety of chemical methods such as precipitation, solid-state synthesis, hydrolysis, sol-gel and hydrothermal have been implemented for the synthesis of hydroxyapatite and tri-calcium phosphate. Impetus has been on developing economic route for synthesis of these minerals. Clams which are eaten widely throughout South Korea have external shells that are thrown as waste, which represent almost 70% of its total weight. 63,000 tonnes of the clam shells are produced throughout the world annually. These biowaste clam shells are good source of calcium. In the present study we have used these biowaste clam shells for the synthesis of calcium phosphate mineral by hydrothermal route. By changing the Ca:P we can manipulate the final mineral that is formed. Here we have synthesized hydroxyapatite and tri calcium phosphate from calm shells by hydrothermal method. We have checked the effect of temperature and time on formation of these minerals. The phase purity of the sample was analyzed by X-ray diffraction and Fourier transform infrared spectroscopy. The morphology and size of the synthesized calcium phosphate mineral were determined by scanning electron microscopy and transmission electron microscopy.

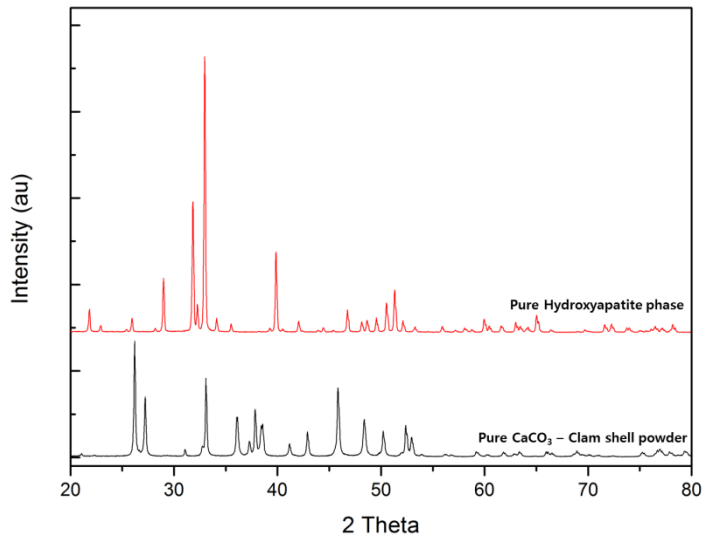

Figure 79 XRD analysis of clam shell powder showing pure CaCO3 phase and the synthesized pure phased hydroxyapatite

References:

[1] Wang J., Wang Q., Xinqing L., Haiqing L., RSC Adv. 3 (2013) 11132-9.
[2] Sanosh K.P., Chu M.C., Balakrishnan A., Kim T.N., Cho S.J., Mat Lett 63 (2009) 2100–2.

BI-P02

Fabrication and Characteristics of Nano-Structured Hydroxyapatite Coating by Aerosol Deposition Method

Dae-Geun Kim, Myeong-No Lee, Hyeonu Hong, Sang-hun Lee and Jae-Hyuk Park *
Division of Nano Coating, R&D center, IONES Co., Ltd., Hwaseong-Si, Gyeonggi-do, Korea

Keywords: Hydroxyapatite, Aerosol Deposition, Nano, Coating, Medical

Bio-ceramic hydroxyapatite (HA) has a good candidate material for medical applications including dentistry and orthopedics. However, it is well-known that it is not easy to apply the HA coating prepared by conventional plasma spraying method since it has a low mechanical reliability and a weak adhesion strength. In this study, highly transparent nano-structured hydroxyapatite (HA) films were fabricated by using aerosol deposition (AD) process [1, 2] at a room temperature. The HA film deposited on a glass substrate shows highly transparent properties with more than 70% at 400 nm to 700nm wavelength (Fig. 1(a)). This value is almost similar to that of bulk HA prepared by spark plasma sintering. This transparency strongly indicate that the HA film has highly dense structures without any pores as well as nanostructured grains of less than 50nm. Also, the HA films deposited on a titanium substrate acquire a strong adhesion strength of more than 35 MPa as well as a mechanical hardness of more than 4.5 GPa. Crystal structure of pure HA retained in the layer, All the XRD peaks were in accordance with the JCPDS data of HA (JCPDS card no. 9-432). We will specially report the coating processes including a rotation speed and a nozzle angle for fabricating the dense and thick films with deep rough surfaces of network structures on the titanium implant fixture (Fig.2. (b, c)).

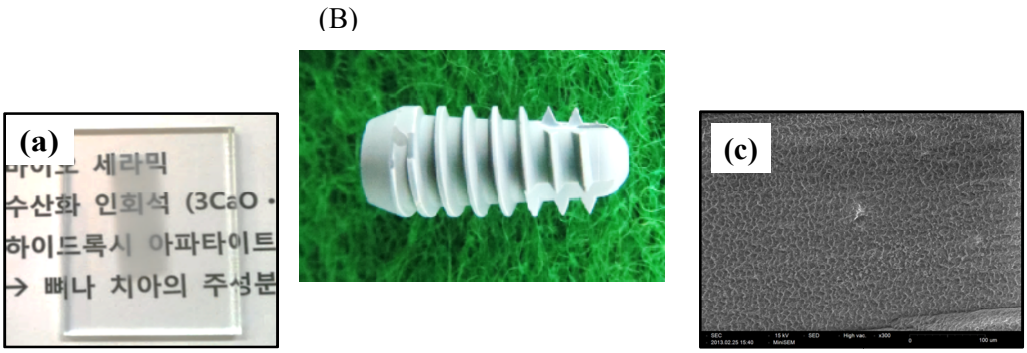

Figure1. Photography of (a) transparent HA film deposited on the glass substrate, (b) titanium implant fixture with thick HA films of more than 10 um, and (c) SEM surface image of (b) implant fixture

References:

[1] T. Fujihara, M. Tsukamoto, N. Abe, S. Miyake, T. Ohji, J. Akedo, Vacuum 73, 629-633 (2004)
[2] B.D. Hahn et al., J. App. Sur. Sci 257, 7792-7799 (2011).

BI-P03

Targeting of Specific Cell using Fluorescent Titanate Nanosheets

Motoko TOKUNAGA, Kai KAMADA*, Taro UEDA, Takeo HYODO, Yasuhiro SHIMIZU
Graduate School of Engineering, Nagasaki University, Nagasaki 852-8521, Japan

Keywords: Biorecognition, Titanate nanosheets, Bioaffinity, Lectin, Human red blood cell

Recently, fluorescent inorganic nanomaterials have been utilized for biochemical application. In this case, surface modification with appropriate biomolecules is required to give biocompatibility and biorecognition ability. Inorganic nanosheets are expected as potential host materials due to high dispersibility in aqueous media and excellent bioaffinity. In the present study, fluorescent titanate nanosheets (TNS) doped with a rare earth element (Eu) were modified with glycoprotein (lectin) recognizing glycans bound to cell surface, and then detection of specific cell using the modified TNS was performed using fluorescence measurements.

Colorless and transparent colloidal solution of Eu-doped TNS (ETNS, $Eu_{0.2}Ti_{3.8}O_9^{2.2-}$, mean diameter < 10 nm) was prepared through a simple hydrolysis reaction of $EuCl_3$-containing titanium(IV) tetraisopropoxide (TTIP) with an aqueous solution of tetrabutylammonium hydroxide [1]. It was confirmed that the produced ETNS showed red fluorescence based on the dopant Eu^{3+} under UV light irradiation (Ex. 395 nm, Em. 615 nm). For surface modification, lectin originated from glycine max was added to the colloidal solution at pH = 4.5. Since isoelectric point (p*I*) of the ETNS and the lectin was ca. 2 and 5, respectively, the lectin spontaneously adsorbed on the ETNS surface through an electrostatic interaction. Biorecognition activity of the surface modified ETNS was investigated for A-type human erythrocytes with N-acetyl-D-galactosamine (D-AclNAc) as a surface glycan (Fig. 1) [2]. As a result of interaction between the lectins on the ETNS and the erythrocytes, red fluorescence was increased as compared with unmodified ETNS along with control (Fig. 2). Hence, it was demonstrated that the ETNS is useful as a fluorescent platform to detect a specific cell.

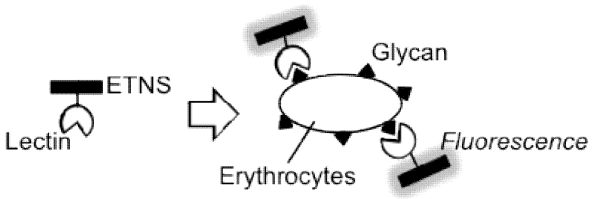

Figure 80 Schematic illustration of erythrocytes detection using ETNS

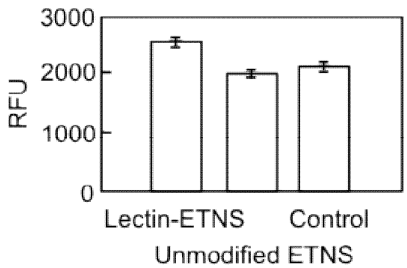

Figure 2 Relative fluorescence unit (RFU, Ex: 420/50 nm, Em: 590/35 nm) of A-type human erythrocytes treated with lectin-ETNS or unmodified ETNS

References:

[1] K. Kamada, RSC Adv., in press.
[2] H. Zhang, L. Zhang, R.-P. Liang, J. Huang, J.-D. Qiu, Anal. Chem., 85 (2013) 10969.

BI-P04

Synthesis of Bioglass Ceramic Using Commercial Water Glasses for Plasma Spray Coating on Dental Implants

Jaehui JEON, Sukyoung KIM
School of Materials Science and Engineering, Yeungnam University, 280 Daehak-Ro, Gyeongsan, Gyeoungbuk 712-749, Korea

Keywords: Bioglass, Glass ceramic, Dental implant, Water glass, Plasma spraying

Among various bioceramic materials, bioinert hydroxyapatite (HA) was used to coat as a coating material on Ti by a plasma spraying method to provide favorable sites to bone cells/tissue. Nevertheless, the clinical application showed the undesirable results such as the delamination of HA coated layer from the surface of Ti dental implants. However, the HA coating on dental implants is considered a priority considering method because of direct bonding with natural bone. In other manner bioactive glass which was invented by L.L. Hench, bioglass (45S5) has been recently applied for bioactive coating on Ti implants to utilize the excellent bioactivity and biodegradation property. But the bioglass itself has a couple of problems such as a complicate process for bioglass preparation and fast degradation compared to the osseointegration rate.
In this study, the new synthetic method of bioglass ceramics was developed using a commercial water-glass by adding bioglass elements. As a result, the bioglass ceramic materials can be manufactured by relatively simple and inexpensive process. First, the mixed solution of phosphoric acid and distilled water was prepared. Water glass was added into the solution using a high-speed stirrer. Calcium nitrate tetrahydrate and 5N sodium hydroxide solution were added little by little over 1 hour into the solution to adjust the bioglass composition. This entire mixing process with magnetic stirrer was conducted at 80℃. And then, the solution was dried for a single day in a drying oven. The dried powdery sample was heat treated at 1200℃ for 2 hours. A mass of glass-ceramic was crushed with a roller crusher to obtain appropriate size of granules. The glass ceramic granules were milled with 6mm zirconia ball in a HDPE jar for 24 hours to obtain round shape granules by grinding. Prior to the plasma spray coating, the washing and sieving of the ground granules were conducted in an alcohol bath to improve the flowability of powder during a plasma spray coating. The obtained granule size was 30~50 μm with a narrow size distribution.

References:

[1] Larry L. Hench, The story of Bioglass, J Mater Sci: Mater Med (2006) 17:967–978
[2] J.M. Gomez-Vega, E. Saiz, A.P. Tomsia, G.W. Marshall, S.J. Marshall, Bioactive glass coatings with hydroxyapatite and Bioglass particles on Ti-based implants. 1. Processing, Biomaterials 21 (2000) 105-111

BI-P05

Ti Surface Modification by Hydrothermal Method Using Various Acids Solution

Asywendi RUKINI[1], Indu BAJPAI[1], and Sukyoung KIM[1*]
[1]*Department of Materials Science and Engineering, Yeungnam University, GyeongsanBuk-do, Daegu, South Korea*

Keywords: Hydrothermal, surface modification

High surface area is found to be more favorable to increase bone – implant contact, where high surface roughness is positively increase the area of implant surface [1]. Combination of surface roughness and porosity making a beneficial interlocking effect on macroscopic scale and porosity itself can also promote bone ingrowth activity[2,3]. A group of study found that certain amount of porous surface (35-40%) with range size of porous about 50-400 μm is an optimum number to improve cell responses[4]. In the present study three different acids solutions are utilized on hydrothermal treatment to increase surface roughness and create porosity in order to improve cell adhesion. Polished c.p Ti disks was ultrasonicated in acetone, ethanol, and distilled water for 20 minutes each then hydrothermally immersed in three different solutions: HCl, H_2SO_4, and H_3PO_4 with various temperature, time, and concentration. SEM observation was conducted to observe morphology evaluation. Chemical compound on the surface of the samples was examined by EDX spectroscopy and X-Ray Diffractometer. Implant was incubated for two days in rat stem cells and then observes under fluorescent spectroscopy to check the adhesion on each morphologies. Macro size crater with various pit-porous size appeared on Ti surface treated in three different acids where pit size grow bigger and went irregular as temperature, acid concentration and immersion time increase. EDX and XRD results confirm that titanium hydride and titanium oxide phase exist on sample surface. Cell adhesion test also displayed positive result on pit-porous structure.

References:

[1] Buser D. et. al. J. Biomed Mater. Res. 25 (1991) pp. 889-902.
[2] Jasty M. et.al. J. Biomed Mater. Res. 27 (1993) pp. 639-644.
[3] Y. Oshida and A. Hashem. Bio-Medical Material and Engineering, Vol. 4, No.5 (1994) pp. 397-407. [4] Y.J. Lim et.al. Int. J. Oral and Maxillofacial Implants 16 (2001) pp. 333-340.
[4] Muddugangadhar BC et.al. Int J Oral Implantology Clin Res Vol. 2, No.1 (2011) pp.13-24.

PI-P01

Fabrication of Piezoelectric Micromachined Ultrasonic Transducer (pMUT) Using Aerosol Deposition Method

Joontaek Jung[1,2], Ju-Eun Kang[3], Jungho Ryu[3], Hyeryung Hong[4], and Hongshoo Choi[1,2*]
[1]*Department of Robotics Engineering, Daegu Gyeongbuk Institute of Science and Technology, 50-1, Sang-ri, Hyeonpung-myeon, Dalseong-gun, Daegu, 711-873, Korea*
[2]*DGIST-ETH Microrobot Research Center, Daegu Gyeongbuk Institute of Science and Technology, 50-1 Sang-ri, Hyeonpung-myeon, Dalseong-gun, Daegu, 711-873, Korea*
[3]*Funtional Ceramics Group, Korea Institute of Material Science, 66 Sangnam-Dong, Changwon, 641-831, Korea*
[4]*Department of Electrical and Computer Engineering, Johns Hopkins University, 3400 N Charles St. Barton 105 Baltimore, MD 21218, USA*

Keywords: ultrasonic transducer, piezoelectric, aerosol deposition

Sol-gel method is widely adapted for the fabrication of piezoelectric micromachined ultrasonic transducer (pMUT) to deposit piezoelectric thin-film, mostly lead zirconate titanate (PZT). However, sol-gel process requires enormous time and efforts for solution preparation and film deposition. Also, the thickness of PZT layer deposited by sol-gel method is limited to few microns in a wafer scale, which may limit the actuation power of the pMUT. To overcome these shortcomings, aerosol deposition (AD) method is introduced to deposit PZT layer for pMUT. This paper presents the fabrication process using aerosol deposition method of pMUT and characterizes the performance of device. The fabrication process for aerosol deposition was conducted at room temperature with high deposition rate of ~5 m/min. The fabrication process starts from the 5 m PECVD SiO_2 deposition process on the 6 inch Si wafer, which works as an insulating and etching stop layer for deep reactive ion etching (DRIE) process. Titanium and Platinum was deposited as an adhesion layer and bottom electrode, respectively. SU-8 2010 photoresist was used for lift-off process for AD PZT patterning. Platinum was deposited as a top electrode and patterned using SU-8. After patterning, annealing was processed at 650 degree Celsius during 1 hour for grain growth. Aluminum masking and back DRIE process was done for the last fabrication step. The fabricated 7 x 7 pMUT array is shown in figure 1. The performance of the device was represented by its hysteresis curve and impedance peaks. pMUT using AD PZT is expected to present comparable coupling coefficient with the sol-gel based pMUT while enormously reducing the fabrication efforts. The advantages and difficulties of pMUT using AD method are discussed.μ

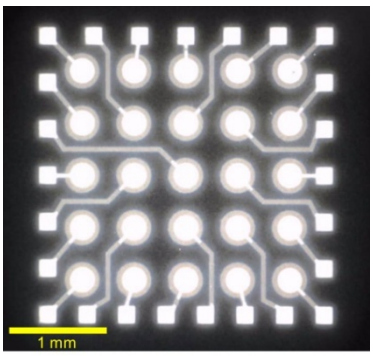

Figure 81 Fabricated 7 x 7 pMUT array

Acknowledgement:
This work was supported by a Ministry of Science, ICT and Future Planning of Korea grant funded by the Korea government (No. PNK3771) and Office of Naval Research.

PI-P02

Driving Characteristics of a θ–Type Piezoelectric Generating Device for Energy Harvesting

Seongsu Jeong[1], Taegone Park[1*]
[1]*Department of Electrical Engineering, Changwon National University, Changwon, 641-773, Korea*

Keywords: θ-type, Theta-type, Cymbal-type, Piezoelectric, Energy harvesting

A newly θ-type piezoelectric generating device that improved from existing cymbal-type piezoelectric generating device was proposed. Generating device was designed by clamping the both ends of plate ceramic using elastic bodies and it convert the vibrations or pressure to horizontal displacement. θ-type generating device has advantages of cymbal-type generating device that have low influence on resonance frequency and high durability. And also it improved generating efficiency and high sensibility despite light vibrations. Optimized model was selected by simulating the proposed device using FEM and the results was confirmed through the fabrication and experiments. In this paper, the characteristics of the generating device were determined by setting the parameters such as size and angles of ceramics and elastic bodies.

References:

[1] H. I. Jun, J. Korean Inst. Elect. Electron. Mat. Engin. 9, 315 (2008).
[2] T. G. Park, M. H. Kim and H. H. Chong, J. Electroceram. 17, 561 (2006).
[3] J. H. Lim, S. S. Jeong, and T. G. Park, Ceramics Inter. 39, S641 (2013).

Acknowledgement:

This work was supported by the National Research Foundation of Korea(NRF) grant funded by the Korea government (MEST) (No. 2011-0030058). This research was financially supported by the Ministry of Education (MOE) and National Research Foundation of Korea(NRF) through the Human Resource Training Project for Regional Innovation (No. 2013H1B8A2032206).

PI-P03

Driving Characteristics of Hexadecagon Shaped Ultrasonic Motor

SeongKyu Cheon[1], SeongSu Jeong[1], ByungHa Lee[1], YongWoo Ha[1], MinHo Park[2], HoIk Jun[3], TaeGone Park[1*]
[1]*Department of Electrical Engineering, Changwon-si, 641-773, Korea*
[2]*Defense Agency for Technology and Quality, Changwon-si, 642-180, Korea*
[3]*Mattron Corp, Changwon-si, 630-724, Korea*

Keywords: Hexadecagon ring stator, Piezoelectric ultrasonic motor, PZT4, ATILA

Novel hexadecagon shaped ultrasonic motor was proposed. It is easy to fabricate the stator because of the simple structure of the stator. Stator of the hexadecagon ultrasonic motor is composed of an elastic ring and ceramics. The elastic ring has sixteen sides and angles. The eight ceramics are attached on outer surface of eight sides of the ring.
When rotor of cylindrical shaft is inserted inside of the ring stator, central lines of sixteen sides of stator hold the shaft by slight pressures. This slight pressure is a preload of the motor and it could be controlled by radius and thickness of the ring. When two AC voltages which have 90 degree phase difference are applied to the eight ceramics, elliptical displacements of inner surface of the ring are obtained. These elliptical displacements of inner surface rotated the shaft rotor through frictions. The proposed hexadecagon ultrasonic motor was designed and analyzed by using finite element analysis (ATILA), depending on the number of piezoelectric ceramic and hexadecagon mode. As a result, the stator was optimally designed by defining the output displacement characteristics depending on change in the chosen parameter. Figure 1 shows structure of hexadecagon shaped ultrasonic motor.

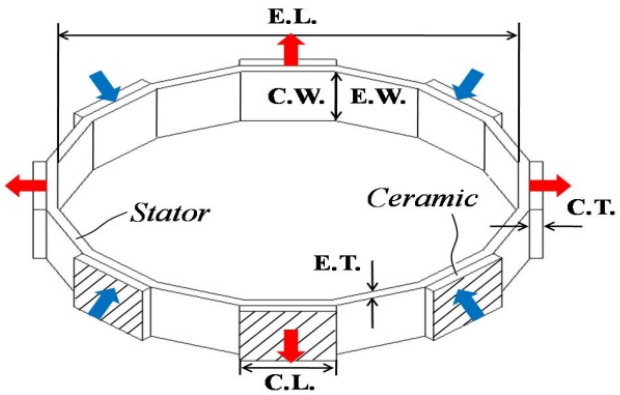

Figure 82 Structure of the stator of the motor

References:

[1] S.S. Jeong, T.G. Park, M.H. Kim, T.K. Song. Characteristics of a V-type ultrasonic rotary motor. Current Applied Physics. 11 (2011) *p*. S364-S367
[2] T.G. Park, H.H. Chong, S.S. Jeong, K. Uchino. Motional characteristics of thin piezoelectric rotary motor using cross shaped stator. Journal of Electroceramics. 23 (2008) *p*. 317-321

Acknowledgement:

Following are results of a study on the "Leaders INdustry-university Cooperation" Project, supported by the Ministry of Education(MOE). This work was supported by the National Research Foundation of Korea(NRF) grant funded by the Korea government (MEST) (No. 2011-0030058).

PI-P04

High Energy Density Magneto-Mechano-Electric Harvester with Anisotropic Piezoelectric Single Crystal Fiber Composite and Ni Laminates

Ju-Eun Kang[1,2], Yuan Zhou[3], Dae-Yong Jeong*[4], Woon-Ha Yoon[1], Dong-Soo Park[1], Jong-Jin Choi[1], Byung-Dong Hahn[1], Cheol-Woo Ahn[1], Jong-Woo Kim[1], Yang-Do Kim[2], Shashank Priya[3], and Jungho Ryu[1]*

[1]*Functional Ceramics Group, Korea Institute of Materials Science (KIMS), Changwon, Gyeongnam 641–831, Republic of Korea*

[2]*School of Materials Science and Engineering, Pusan National University, Busan 609-735, Republic of Korea*

[3]*Bio-inspired Materials and Devices Laboratory (BMDL), Center for Energy Harvesting Materials and Systems (CEHMS), Virginia Tech, Virginia 24061, USA*

[4]*School of Materials Engineering, Inha University, Incheon 402-751, Republic of Korea*

Keywords: Magnetoelectric, Magneto-mechano-electric, piezoelectric single crystal, harvester, composite

We introduce novel Magneto-Mechano-Electric (MME) harvesters with colossal energy density can turn on 20 LEDs under miserably weak magnetic field at low frequency. The MME harvesters are magnetoelectric (ME) laminates composed of (011) oriented anisotropic single crystal fiber composite (SFC) bonded on Ni plate and Nd permanent magnet proof mass. The ME laminate has strong ME coupling (α_{ME} ~160 V/cmOe) at zero magnetic bias. It is also found that the MME harvester of ME laminate with permanent magnet proof mass generates colossal output power density of 47 mW/cm^3Oe^2 under weak magnetic field of 1.6 x 10^{-4} T at 60 Hz. This MME harvester can be potential ubiquitous power source for sensor networks by harvesting tiny parasitic magnetic energy induced from electric power cables.

PI-P05

Flexible Single Crystalline PMN-PT Thin Film Energy Harvester and Its Application for Self-powered Cardiac Pacemaker

Geon Tae Hwang
Korea Advanced Institute of Science & Technology(KAIST), 291 Daehak-ro (373-1 Guseong-dong), Yuseong-gu, Daejeon 305-701, Korea

Artificial cardiac pacemaker is widely used to maintain an adequate heart rate. The repetitive surgery are required to replace the pacemakers due to limited lifespan of batteries. Recharging battery in a human body and adopting self-powered nerve stimulation are reasonable solution for solving the problem. This paper describes flexible single crystal PMN-PT thin film nanogenerator (NG) as a high-performance flexible energy harvester for application of self-powered cardiac pacemaker. The NG device generates open-circuit voltage of 8.2 V and short-circuit current of 0.22 mA which is the highest output current among previously reported piezoelectric ceramic-based flexible NGs. We successfully drive 50 LEDs and charge batteries by electric energy harvested from the thin film NG. Finally, the flexible PMN-PT NG is utilized to make direct stimulation of cardiac nerve for artificial heartbeat without external power source.

PI-P06

Piezoelectric and Dielectric Properties of Non-stoichiometry $(Na_{0.53+x}K_{0.47+x})(Nb_{0.55}Ta_{0.45})O_3$ ceramics

S. Y. Lim, J. S. Kim[1], T. K. Song[1], W. J. Kim[2], M. H. Kim[1*]
[1]*School of Advanced Materials Engineering, Changwon National University, Gyeongnam 641-773, Republic of Korea*
[2]*Department of Physics, Changwon National University, Gyeongnam 641-773, Republic of Korea*

Keywords: Lead-free, Piezoelectric, NKN based ceramics

In the past two decades, to replace lead-based piezoelectric materials, many lead-free candidate materials were studied. Among these alternatives, (Na,K)NbO_3(NKN)–based ceramics have been proposed as possible lead-free candidate materials because of their good piezoelectric constant (about 100 pC/N) and high Curie temperature (above 400 °C). High piezoelectric properties can be obtained by controlling the phase coexistence region formed at the transition temperature between the orthorhombic and the tetragonal phase [1-3]. Numerous studies investigated the effects of the substitution of Li, Sb, Ta, Ag on the piezoelectric properties of the NKN ceramic [4, 5]. Ta substitution in (Na,K)(Nb,Ta)O_3 affects the dielectric behavior and the piezoelectric properties, making this ceramic a possible candidate for practical applications [6, 7]. In this study, we investigated the effect of Na/K excess on the structural and electrical properties of Ta-modified $(Na_{0.53+x}K_{0.47+x})(Nb_{0.55}Ta_{0.45})O_3$ ceramics (NKNT, x = - 0.01, - 0.005, 0, 0.005 and 0.01).

References:

[1] G. H. Haertling, Properties of hot-pressed ferroelectric alkali niobate ceramics, J. Am. Ceram. Soc 50, 329–330 (1967).
[2] R. E. Jaeger, L. Egerton, Hot pressing of potassium–sodium niobates, *J. Am. Ceram. Soc*, 45, 209–213 (1962).
[3] P. Kumar, M. Pattanaik, Sonia, Synthesis and characterizations of KNN ferroelectric ceramics near 50/50 MPB, Ceram. Int. 39, pp 65-69 (2013).
[4] Dunmin Lin, K. W Kwok, K. H. Lam, and H. L. W Chan, Structure, piezoelectric and ferroelectric properties of Li- and Sb-modified $K_{0.5}Na_{0.5}NbO_3$ lead-free ceramics, Appl. Phys, 40 3500-3505 (2007).
[5] Y. Guo, K. Kakimoto, H.Ohsato, Phase transitional behavior and piezoelectric properties of $(Na_{0.5}K_{0.5})NbO_3$-$LiNbO_3$ ceramics, Appl. Phys. 85-18 (2004).
[6] Y. S. Sung, S. Baik, J. H. Lee, G. H. Ryu, D. Do, T. K. Song, M. H. Kim, and W. J. Kim,
Enhanced piezoelectric properties of $(Na_{0.5+y+z}K_{0.5-y})(Nb_{1-x}Ta_x)O_3$ ceramics, Appl. Phys. Lett. 101, 012902 (2012).
[7] Y.S. Sung, J.H. Lee, S.W. Kim, T.H. Lee, J.M. Kim, J.H. Cho, T. K. Song, M.H. Kim, T. G. Park et al. *Ceram. Int*, 38S S301-S304, (2012).

Acknowledgement:

This work was supported by Basic Science Research Program through the National Research Foundation of Korea (NRF) funded by Ministry of Education, Science and Technology (MEST) (2011-0030058).

PI-P07

Enhanced Field-induced Strain Response of Nb-doped $(Bi_{0.5}Na_{0.5})_{0.935}Ba_{0.065}TiO_3$–$SrZrO_3$ Lead-free Piezoceramics

Adnan MAQBOOL[1], Ali HUSSAIN[1], Jamil Ur RAHMAN[1], Rizwan Ahmed MALIK[1], Tae Kwon SONG[1], Won-Jeong KIM[2] and and Myong-Ho KIM[1,*]

[1]*Engineering Research Center for Integrated Mechatronics Materials and Components, Changwon National University, Gyeongnam 641-773, Republic of Korea*

[2]*Department of Physics, Changwon National University, Gyeongnam 641-773, Republic of Korea*

Keywords: lead-free ceramics, dielectric, relaxor behavior, Electric field-induced strain

Field-induced strain of piezoelectric materials is widely utilized in numerous electromechanical devices. The crystal structure, dielectric properties, electric field-induced strain (EFIS), and polarization response of lead-free $(Bi_{0.5}Na_{0.5})_{0.935}Ba_{0.065}Ti_{(1-x)}Nb_xO_3$–$0.01SrZO_3$ (BNBTNb100*x*–SZ, with x = 0–1) ceramics were investigated. X-ray diffraction analysis revealed that all compositions had a pure perovskite structure with tetragonal symmetry.

The depolarization temperature (T_d) shifted toward lower temperatures and the dielectric curves became more diffuse with increased Nb doping, producing a significant disruption of the long-range ferroelectric order. A giant EFIS of 0.33% was achieved at an optimized composition of Nb1.0 (BNBTNb1.0–SZ), corresponding to a normalized strain (S_{max}/E_{max}) of 825 pm/V at a low applied field of 4 kV/mm. Moreover, at a low applied field of 3 kV/mm, the Nb0.75 and Nb1.0 samples displayed a high EFIS response of 0.25%, corresponding to a S_{max}/E_{max} of 833 pm/V. These results suggest that BNBTNb–SZ ceramics are promising candidate materials for lead-free actuator applications.

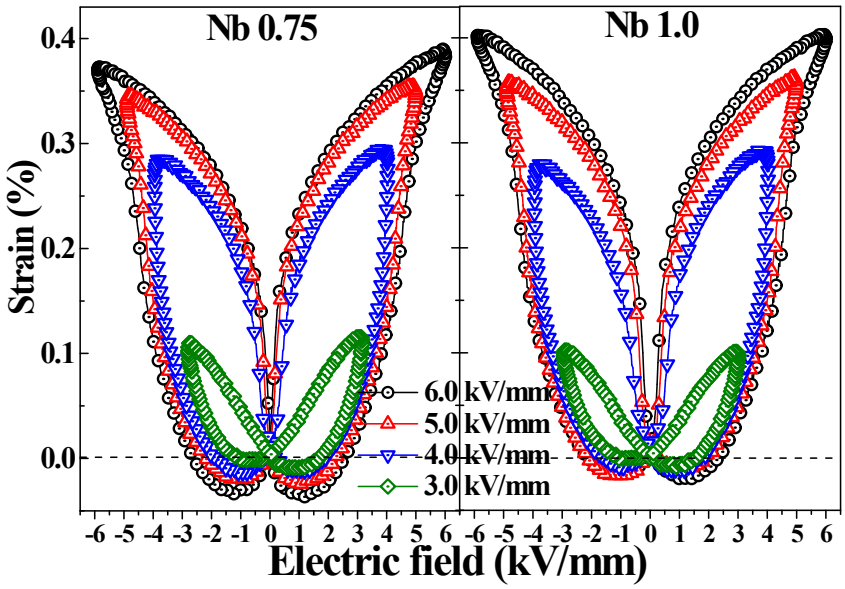

Figure 1 Electric field-induced bipolar (*S*–*E*) loops of BNBTNb–SZ ceramics under different applied electric fields

Acknowledgements:
This work is supported by the Basic Research Program through the National Research Foundation of Korea (NRF) funded by the Ministry, Science and Technology (MEST) (2011-0030058).

LP-P01

Effect of Sintering Temperature on Piezoelectric and Ferroelectric Properties of $0.99(0.67BiFeO_3$-$0.33BaTiO_3)$-$0.01Bi(Ni_{0.5}Ti_{0.5})O_3$ Ceramics

I. J. HWANG[1], D. DO[1*], M. H. LEE[2], J. S. PARK[2], D. J. KIM[2], T. K. SONG[2], M.-H. KIM[2], S. W. KIM[3], W.-J. KIM[3]

[1]*Department of Advanced Materials Engineering, Keimyung University, Daegu 704-701, Korea*
[2]*School of Materials Science and Engineering, Changwon National University, Changwon 641-773, Korea*
[3]*Department of Physics, Changwon National University, Changwon 641-773, Korea*

Keywords: High T_c, Lead-free, Piezoelectric property, $BiFeO_3$-$BaTiO_3$, $Bi(Ni_{0.5}Ti_{0.5})O_3$

In order to replace lead-based piezoelectric ceramics such as $Pb(Zr,Ti)O_3$ (PZT), a lot of efforts have been done to develop lead-free piezoelectric materials including the $(Bi,Na)TiO_3$, $(Bi,K)TiO_3$, $(K,Na)NbO_3$ systems. Although remarkable improvement in piezoelectric properties of some complex systems was achieved, it is still unsuitable for high temperature applications. Recently, lead-free $(1-x)BiFeO_3$-$xBaTiO_3$ (BF-BT) ceramics have been introduced and exhibited Curie temperature (T_c) close to 600℃ [1]. BF-BT has a morphotrophic phase boundary (MPB) with the coexistence of both rhombohedral and cubic phases near 67 mol% of $BiFeO_3$. It can be expected a large piezoelectric coefficient near a MPB region in the BF-BT system, such as PZT. In this study, $0.99(0.67BiFeO_3$-$0.33BaTiO_3)$-$0.01Bi(Ni_{0.5}Ti_{0.5})O_3$ (BF-BT-BNT) ceramics were studied. The BF-BT-BNT ceramics were prepared by a water quenching method after sintering instead of a traditional solid-reaction process. Sintering temperature dependences of crystal structure, piezoelectricity, and ferroelectricity of the ceramics were investigated. There was no significant change in the crystal structure depending on sintering temperature from 970 to 1020℃. The average grain size increased with increasing sintering temperature. It was found that the BF-BT-BNT ceramics sintered at 980, 990, and 1000℃ showed better piezoelectric and ferroelectric properties than those of the BNT ceramics sintered at 970, 1010, and 1020℃. The piezoelectric coefficient (d_{33}) and remnant polarization ($2P_r$) of the BF-BT-BNT ceramics sintered at 980, 990, and 1000℃ were about 165 pC/N and over 50 μC/cm^2, respectively. Also typical butterfly shaped strain-electric field loops were observed in the BF-BT-BNT ceramics. The T_c of the BF-BT-BNT ceramics was over 400℃. These results indicate that $0.99(0.67BiFeO_3$-$0.33BaTiO_3)$-$0.01Bi(Ni_{0.5}Ti_{0.5})O_3$ ceramics can be a promising candidate for a high T_c lead-free piezoelectric material.

References:

[1] S. O. Leontsev and R. E. Eitel, Sci. Technol. Adv. Matter. 11 (2010) 044302.

LP-P02

Characterization of Lead-Free $0.75(Bi_{0.5}Na_{0.5})TiO_3$-$0.25SrTiO_3$ Thin Films by Pulsed Laser Deposition for Energy Harvesting Applications

Ki-Su YANG[1], Jae-Ryong LIM[2] and Soon-Gil YOON[1]*
Nano Thin Film Research Laboratory, [1]Department of Material Science and Engineering, Chungnam National University, Daeduk Science Town, Daejeon, 305-764, Korea
[2]Advanced Circuit Interconnection, Chungnam National University, Daeduk Science Town, Daejeon, 305-764, Korea

Keywords: $0.75(Bi_{0.5}Na_{0.5})TiO_3$-$0.25SrTiO_3$, thin film, PLD

Energy harvesting from irregular mechanical actions in variable and uncontrollable environments is an effective approach for powering wireless mobile electronics to meet a wide range of applications in our daily life. Piezoelectric thin film is strong and can be stimulated by tiny physical motions over a range of frequencies.

Generally, $PbZrTiO_3$ (PZT) is most widely using a piezoelectric ceramic. But PZT is well-known material which has toxic element like Pb. Therefore, there is need to find lead free piezoelectric material which is comparable to PZT. Among them, sodium bismuth titanate $Bi_{0.5}Na_{0.5}TiO_3$ (BNT) is considered to be one promising candidate ascribed to the high piezoelectric properties around the morphotropic phase boundary (MPB). So many studies related to Bi-based materials are proceeding.

There is a lead free piezoelectric ceramic system $0.75(Bi_{0.5}Na_{0.5})TiO_3$-$0.25SrTiO_3$ (0.75BNT-0.25ST) which shows a surprisingly high piezoelectric coefficient of d_{33} = 600 pm/V. $SrTiO_3$ is able to reduce effectively the electric field needed to obtain high strains in the BNT. Because of this $SrTiO_3$'s characteristic, piezoelectric property of 0.75BNT-0.25ST structure can be enhanced. Therefore, in this study, BNT-ST material which was only evaluated at a bulk state was grown as a thin film at high temperature using pulsed laser deposition (PLD) .

We used yttria stabilized zirconia (YSZ) and cerium oxide (CeO_2) thin film as a buffer layer, for epitaxial growth of 0.75BNT-0.25ST thin film. Also, we used $La_{0.5}Sr_{0.5}CoO_3$ (LSCO) that can maintain its property at high temperature as a bottom electrode and Pt as a top electrode which was deposited by dc sputtering.

X-ray diffraction (XRD) θ-2θ, ω-, and ϕ-scan was used to investigate the epitaxial growth morphology. The morphologies of the films were investigated using scanning electron microscope (SEM) and atomic force microscope (AFM). Also, Polarization electric field curve (PE curve) and piezoelectric constant of 0.75BNT-0.25ST thin film were measured.

References:

[1] Matias Acosta, Wook Jo* and Jürgen Rödel J. Am. Ceram. Soc., 97 [6] 1937–1943 (2014)

LP-P03

Reactive Sintering of $(K_{0.5}Bi_{0.5})TiO_3$-$BiFeO_3$ lead-free piezoelectric ceramics.

John G. FISHER[1*], Min-Gu KIM[1], Daeung KIM[1], Su-Jeong CHA[1], Hung VU[1], Dieu NGUYEN[1], Jee-Hoon KIM[1], Su-Hyeon MOON[1], Jong-Sook LEE[1], Ali HUSSAIN[2] and Myong-Ho KIM[2]
[1]*School of Materials Science and Engineering, Chonnam National University, Gwangju 500-757, Republic of Korea.*
[2]*Engineering Research Center for Integrated Mechatronics Materials and Components, Changwon National University, Changwon, Gyeongnam 641-773, Korea.*

Keywords: lead-free piezoelectric, reactive sintering, $BiFeO_3$, dielectric properties, piezoelectric properties

Ceramics based on $BiFeO_3$ are potential lead-free replacements for $Pb(Zr,Ti)O_3$ in a variety of applications such as sensors, transducers and actuators. Recently, ceramics in the $(K_{0.5}Bi_{0.5})TiO_3$-$BiFeO_3$ system were developed which have excellent piezoelectric properties (d_{33} = 225 pm/V, k_{33} = 0.36) [1] However, these ceramics are difficult to sinter to high density. The present work studies the use of reactive sintering to prepare $0.4(K_{0.5}Bi_{0.5})TiO_3$-$0.6BiFeO_3$ ceramics. Undoped and MnO-doped powders are prepared by ball milling K_2CO_3, $(BiO)_2CO_3$, TiO_2, α-FeO(OH) and $MnCO_3$ in ethanol with zirconia milling media. Samples are sintered in the temperature range 1000-1075°C and their structure and microstructure examined by X-ray diffraction, micro-Raman scattering and scanning electron microscopy. The dielectric, ferroelectric and piezoelectric properties of undoped and MnO-doped samples are measured.

Both undoped and MnO-doped samples sintered at 1050°C for 1 hour have a maximum density of 91 % theoretical density. X-ray diffraction and micro-Raman scattering show that undoped samples have a rhombohedral unit cell and that MnO doping reduces the rhombohedral distortion. Undoped samples show relaxor behavior and high conductivity and loss tangent. MnO doping reduces both conductivity and loss tangent. The undoped samples have Polarization vs. Electric field loops of a lossy ferroelectric material whereas MnO doping causes the loops to become very narrow. The undoped samples have Strain vs. Electric field loops of a normal ferroelectric material. A strain of 0.13% is measured at an electric field of 9 kV/mm, corresponding to a high field d^*_{33} =144 pm/V. For the KBT-BFO-Mn sample, no strain response could be measured for electric fields below 5 kV/mm. For fields > 5 kV/mm, electrical breakdown occurred.

References:

[1] H. Matsuo, Y. Noguchi, M. Miyayama, M. Suzuki, A. Watanabe, S. Sasabe, T. Ozaki, S. Mori, S. Torii, T. Kamiyama, *J Appl Phys* 108, 104103 (2010).

LP-P04

Comparative Study between Conventional and Microwave Sintering of Large Strain Bi-Based Perovskite Ceramics

Jin-Kyu KANG[1], Thi-Hinh DINH[1], Young-Hwan HONG[1], Mohammad Reza BAFANDEH[2], Chang-Do PARK[1], and Jae-Shin LEE[1*]

[1]*School of Materials Science and Engineering, University of Ulsan, Nam-Ulsan, 680-749, Republic of Korea*

[2]*Department of Metallurgy, University of Kashan, Ravand Blvd, Kashan, I.R.Iran*

Keywords: Piezoelectric, Microwave, Sintering, Strain, Lead-free

A comparative study has been attempted for microwave and conventional sintering of lead-free $0.96Bi_{1/2}(Na_{0.82}K_{0.18})_{1/2}TiO_3 - 0.04BaZrO_3$ (BNKT–BZ) ceramics. It was found that microwave sintering (MWS) that was 10 times faster than conventional sintering as can be seen in Fig. 1 could be successfully applied to the fabrication of the large strain Bi-perovskite ceramics with electric field-induced strains comparable to those obtained using conventional sintering (CFS). Although MWS resulted in smaller grained microstructures than CFS, the ferroelectric properties were stronger in MWS-derived specimens. As given in Fig. 2, the piezoelectric strain constant d_{33}^* of CFS-derived specimen reached a maximum value of 372 pm/V after sintering at 1100°C while that of MWS-derived specimen peaked at 950°C with d_{33}^* =324 pm/V.

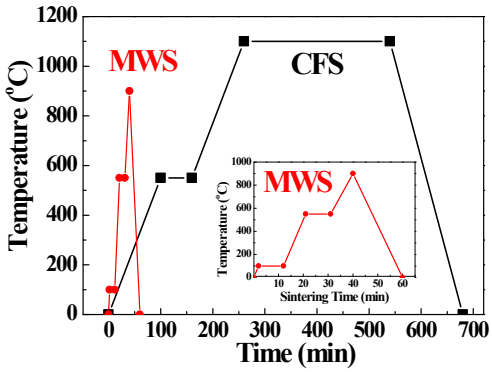

Figure 1. Comparison of firing cycles between conventional furnace sintering and microwave sintering attempted in this work.

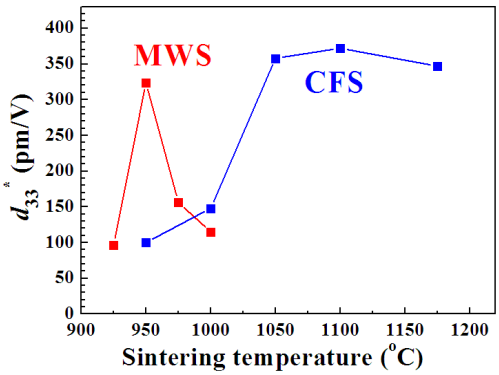

Figure 2. Normalized strain, S_{max}/E_{max}, of BNKT-BZ ceramics as a function of sintering temperature.

LP-P05

Improvement in Strain Properties of Bi-Based Ceramic Composites by High Energy Ball Milling

Young-Hwan HONG[1], Dae-Jun HEO[1], Jin-Kyu KANG[1], Thi-Hinh DINH[1] Chang-Won AHN[2], Ill-Won KIM[2], Wook JO[3], and Jae-Shin LEE[1*]

[1]*School of Materials Science and Engineering, University of Ulsan, Nam-Ulsan, 680-749, Republic of Korea*

[2]*School of Department of Physics, University of Ulsan, Ulsan 680-749, Republic of Korea*

[3]*School of Materials Science and Engineering, UNIST, Ulsan 689-798, Republic of Korea*

Keywords: Lead-free, Piezoelectric, High energy ball milling, Bi-perovskite

Recently, BNKT ceramics and their solid solutions with other perovskites attract great attention because of their large electric field-induced strains (EFIS). However, a critical problem that hinders their practical application to actuators is the fact that large stains in Bi-based lead-free ceramics are obtained only at high electric fields. To lower the critical field (E_{crit}) that can cause giant strain by a phase transition from relaxor to ferroelectric state in incipient piezoelectric materials, ferroelectric-relaxor composite ceramics were investigated in this study. In this work, $0.98[Bi_{0.5}(Na_{0.82}K_{0.18})_{0.5}TiO_3]$-$0.02LaFeO_3$ (BNKT2LF) and $Bi_{0.5}(Na_{0.82}K_{0.18})_{0.5}TiO_3$(BNKT) were selected as a relaxor matrix and ferroelectric filler compositions, respectively.

BNKT2LF powders were synthesized using a conventional solid-state reaction method and then further treated using a planetary ball-mill with different treatment durations of 0 to 60 min. The powder was mixed with BNKT powder preapared by a conventional solid state reaction route, and then sintered at 1175°C for 2 h. The effect of HEBM on the field-induced strain behaviors were analyzd using a linear variable differential transducer.

Interestingly, it was found that HEBM treatment enhanced the converse piezoelectric constant d_{33}^* from 513 pm/V for t=0 to 617 pm/V at 30 min.

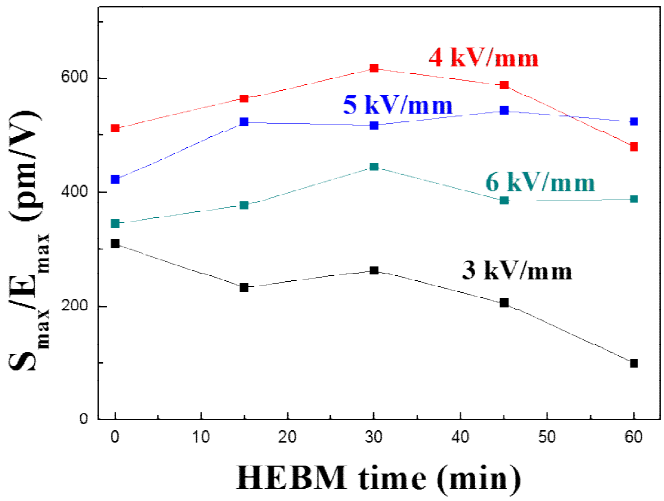

Figure 1. Normalized strain of BNKT/BNKT-LF compsites as a function of HEBM treatment time

LP-P06

Ferroelectric and piezoelectric properties of $Bi(Zn_{2/3}Ta_{1/3})O_3$ modified $0.67BiFeO_3$-$0.33BaTiO_3$ ceramics

Jinsu Park[1] Myang Hwan Lee[1], Sang Wook Kim[2], Sung Jin Han[2], Da Jeong Kim[1], Myong-Ho Kim[1], Won–Jeong Kim[2], Shalendra Kumar[3] and Tae Kwon Song1[*]

[1]*School of Materials Science and Eng., Changwon Nat,I Univ., Gyeongnam 641-773, Korea*
[2]*Deparment of Physics, Changwon Nat,I Univ., Gyeongnam 641-773, Korea*
[3]*Instisute of Basic Sciences, Changwon Nat,I Univ., Gyeongnam 641-773, Korea*

Keywords: Ferroelectric, Piezoelectric, $BiFeO_3$-$BaTiO_3$, $Bi(Zn_{2/3}Ta_{1/3})O_3$

Lead-based piezoelectric ceramics with a perovskite structure, such as $Pb(Zr,Ti)O_3$, are widely used for actuators, sensors and microelectronic devices because of their excellent piezoelectric properties. However, the toxicity of lead and its high vapor pressure during processing have led to a demand for alternative lead-free piezoelectric materials that are environmentally benign from the viewpoint of sustainable development. $BiFeO_3$-$BaTiO_3$ materials have been developed as a promising lead-free piezoelectric material for their potential applications piezoelectric devices [1-2]. Lead-free ceramics with compositions of 1-x[$0.67BiFeO_3$-$0.33BaTiO_3$]-$x$$Bi(Zn_{2/3}Ta_{1/3})O_3$ (x = 0.00, 0.01, 0.02, 0.03, 0.04, and 0.05) [BF-BT-BZTx] have been prepared through by a conventional solid state reaction method. The effect of BZT addition on BF-BT have been investigated in terms of X-ray diffraction, micro-structure, piezoelectric, and electrical properties. Based on the XRD studies, BZT modified BF-BT ceramics were found to be a pseudo-cubic perovskite structure without any secondary phases. The BF-BT-BZT 0.02 ceramic exhibited good ferroelectric, and piezoelectric properties. The remnant polarization ($2P_r$) and the coercive field ($2E_c$) for BF-BT-BZT 0.02 ceramic were observed to be 46 μC/cm^2 and 52.19 kV/cm, respectively, whereas the piezoelectric constants d_{33} and d_{33}* were 55 pC/N and 310 pm/V, respectively.

References:

[1] M. H. Lee, J. S. Park, D. J. Kim, R. C. Kambale, M -H. Kim, T. K. Song, H. J. Jung, S. W. Kim, H. I. Choi, W –j. Kim, S. S. Kim, K. W. Jang, and D. Do, Ferroelectrics, 452 (2013) 7.
[2] S O. Leontsev and E. Eitel, J. Am. Ceram. Soc., 92 (2009) 2957

Acknowledgement:

This research was supported by Basic Science Research Program through the National Research Foundation of Korea(NRF) funded by the Ministry of Education (2013R1A1A4A01010612) and by the National Research Foundation of Korea(NRF) grant funded by the Korea government(MSIP) (2011-0030058) and by the Priority Research Centers Program through the National Research Foundation of Korea (NRF) funded by the Ministry of Education, Science and Technology (MEST; 2012-045424)

LP-P07

The structural and electrical properties of Cr doped $BiFeO_3$-$BaTiO_3$ lead free ceramics

S. W. Kim[1], M. H. Lee[2], J. S. Park[2], S. J. Han[1], D. Do[3], M. H. Kim[2], T. K. Song[2], W. J. Kim[1*]
[1]*Department of Physics, Changwon National University, Changwon 641-773, Republic of Korea*
[2]*School of Nano and Advanced Materials Engineering, Changwon National University, Changwon 641-773, Republic of Korea*
[3]*Department of Advanced Materials Engineering, Keimyung University, Dalseo-gu, Taegu 704-710, Republic of Korea*

Keywords: Lead-free, Quenching, $BiFeO_3$-$BaTiO_3$, Structure refinement

Lead based piezoelectric bulk ceramics are used for various devices because of their excellent piezoelectric properties. Due to the toxic lead in lead-free piezoelectric, it is important to fine other lead-free piezoelectric metals for device applications. Recently, $BiFeO_3$-$BaTiO_3$ ceramics is consider as a replacement lead based piezoelectric metals, because $BiFeO_3$-$BaTiO_3$ has a high Curie temperature [1]. However, $BiFeO_3$-$BaTiO_3$ ceramics do not exhibit enough piezoelectric properties to replace for replacement lead based piezoelectric metals.

In this study, Cr doped $BiFeO_3$-$BaTiO_3$ bulk ceramics were formed using a solid state reaction. The crystal structures were investigated using x-ray diffractometer and Rietveld analysis. The piezoelectric property was increased with comparing to pure $BiFeO_3$-$BaTiO_3$ ceramics. More detailed electrical and structural properties, including correlation between piezoelectric and structural properties, will be discussed in presentation.

References:

[1] M. Mahesh Kumar, J. Appl. Phys. 87 (2000) 855.

Acknowledgement:

This research was supported by Basic Science Research Program through the National Research Foundation of Korea(NRF) funded by the Ministry of Education (2013R1A1A4A01010612) and by the National Research Foundation of Korea(NRF) grant funded by the Korea government(MSIP) (2011-0030058)

LP-P08

Low-temperature sintering of the lead-free BNKT-BMT using sintering aids for piezoelectric acoustic actuators

Hee Sung Kim[1], Won Seok Woo[1], Song A Chae[1], Chang Won Ahn[1], Ill Won Kim[1*]
Ki Bong Jang[2], Eung Joo Hwang[2]
[1] Dept. of Physics and Energy Harvest-Storage Research Center, Univ. of Ulsan, Korea
[2] R&D Center, Samjeon Co., Ltd, Ulsan, 689-934

Keywords: Lead-free, Low temperature sintering, Multilayer ceramic actuators, $Bi_{0.5}Na_{0.5}TiO_3$

In general, BNKT-based ceramics should be sintered at high temperatures range of 1150℃-1180℃ in order to obtain complete densification. Multilayer ceramics actuators device requires co-firing with Ag/Pd internal electrode. The ratio of expensive Pd in Ag/Pd internal electrode must be increased when multilayer structured piezoelectric ceramics are co-fired with internal electrode since the sintering temperature of BNKT system ceramics is higher than 1150^{o}C. And also, high sintering temperature can deteriorate the stability of the piezoelectric properties due to the formation of interfacial micro-defects and internal electrode loss. Therefore, the decreasing sintering temperature of piezoelectric ceramics is important process for development of multilayer ceramics actuators. In this study, we have studied low-temperature sintering behaviors of $0.96Bi_{0.5}(Na_{0.78}K_{0.22})_{0.5}TiO_3$-$0.04Bi(Mg_{0.5}Ti_{0.5})O_3$ (BNKT-BMT) ceramics, which shows high normalized strain (S_{max}/E_{max}) of 540 pm/V at an low applied electric field of 35 kV/cm,[1] using CuO (0 – 2 mol%) as sintering aids in range of sintering temperatures of 900 – 1000 ^{o}C and investigated dielectric, piezoelectric and ferroelectric properties.

References:

[1] Aman Ullah, Chang Won Ahn, Amir Ullah, and Ill Won Kim, Appl. Phys. Lett. 103, 022906 (2013).

Acknowledgement

This work was supported by the development program of local science park funded by the ULSAN Metropolitan City and the MSIP(Ministry of Science, ICT and Future Planning)

LP-P09

Piezoelectric, Dielectric and Ferroelectric response of Nb^{5+} modified of Lead-free $0.97(Bi_{0.5}Na_{0.5}Ti_{1-x}Nb_x)O_3$-$0.03BaZrO_3$ ceramics

Jamil Ur RAHMAN[1], Ali HUSSAIN[1], Adnan MAQBOOL[1], Rizwan Ahmed MALIK[1], Tae Kwon SONG[1], Won Jeong KIM[2], and Myong Ho KIM[1,*]

[1]*School of Advanced Material Engineering, Changwon National University, Gyeongnam 641-773, Republic of Korea*

[2]*Department of Physics, Changwon National University, Gyeongnam 641-773, Republic of Korea*

***Keywords*:** Perovskite, Dielectric, Ferroelectric, Piezoelectric

The piezoelectric material is a material that can be used the inter conversion between electrical and mechanical energy. Most of the piezoelectric ceramics devices have been fabricated from lead-based piezoelectric ceramic materials, such as $Pb(Zr_xTi_{1-x})O_3$ (PZT), because of their outstanding piezoelectric properties [1-2]. However, the use of lead-based ceramics causes serious environmental problems because of the high toxicity of lead oxide and its high vapor pressure during sintering. Therefore, there is a great need to develop lead-free piezoelectric ceramics with good piezoelectric properties to replace lead-containing ceramics in various applications.

In this work we have prepared $0.97(Bi_{0.5}Na_{0.5}Ti_{1-x}Nb_x)O_3$-$0.03BaZrO_3$ lead-free ceramics (with x = 0~0.03), by a conventional solid-state reaction method. Crystal structure, microstructure, dielectric, ferroelectric and piezoelectric properties of Nb-modified BNT-BZ3 ceramics were studied. X-ray diffraction patterns revealed the formation of single phase perovskite structure with $x \leq 0.015$. The depolarization temperature and dielectric constant were decreasing with increasing Nb-contents. The remanent polarization (P_r) and piezoelectric constant (d_{33}) increased from 28 μC/cm^2 and 98 pC/N for x = 0 to 31 μC/cm^2 and 128 pC/N for x = 0.005, respectively. In addition, electric field-induced strain was enhanced to form a maximum value (S_{max} = 0.17%) with normalized piezoelectric coefficient (d^*_{33} = 283 pm/V) at an applied electric field 6kV/mm for x = 0.015.

References:

[1] B. Jaffe, W.R. Cook, H. Jaffe, Piezoelectric Ceramics, Academic Press, London, 1971.
[2] N. Ichinose, N. Miyamoto, S. Takahashi, J. Eur. Ceram. Soc. 24 (2004) 1681-1685.

Acknowledgement:

This work is supported by the National Research Foundation of Korea (NRF) grant funded by the Korean government (MOE) (2013R1A1A2058345).

LP-P10

Hardening Effects and Associated Lattice Defects in Lead-free $(Na_{0.53}K_{0.47})NbO_3$ Piezoelectric Ceramics

Gyung Hyun Ryu[1], Myang Hwan Lee[1], Tae Kwon Song[1], Won-Jeong Kim[2], and Myong Ho Kim[1,*]
[1]*School of Advanced Materials Engineering, Changwon National University, Gyeongnam, 641-773, Korea*
[2]*Department of Physics, Changwon National University, Gyeongnam, 641-773, Korea*

Keywords: lead-free, perovskite, defect, oxygen vacancy, internal bias field

$(Na,K)NbO_3$ (NKN)-based ceramics are considered a most promising candidate for lead-free piezoceramics due to their high Curie temperature (T_C), low coercive electric field (E_C), and large piezoelectric coefficient (d_{33}). Recently, many studies for enhancing piezoelectric properties of NKN-based ceramics have been made progress by controlling polymorphic phase transition (PPT), and morphotropic phase boundary (MPB). In spite of these efforts, NKN-based materials still have a potential problem, high leakage current. Reason for the high conductivity is highly related with the formation of lattice defects during sintering process at high temperature. It is well accepted that oxygen vacancies are main defects as charge carriers which make the ceramic leaky. In addition, oxygen vacancies cause the ferroelectricity degradations, such as fatigue, imprint, and retention loss. In this study, we studied influences of lattice defects on ferroelectric and piezoelectric properties of undoped $(Na_{0.53}K_{0.47})NbO_3$ (NKN) ceramic. Change of polarization and bipolar strain values as a function of bipolar cycling suggests interesting phenomena, charge migration and hardening effects with internal bias field. Possible defects in NKN ceramic were investigated using electrical conductivity versus oxygen partial pressure at various temperatures. Room temperature current density and its hysteresis showed bipolar cycling dependence.

Acknowledgement:
This work was supported by a National Research Foundation of Korea Grant funded by the Korea Government (2011-0030058).

LP-P11

Effect of quenching temperature on the ferroelectric and piezoelectric properties of $BiFeO_3$-$BaTiO_3$ bulk ceramics

Myang Hwan Lee[1], Dajeong Kim[1], Jinsu Park[1], Shalendra Kumar[1], Tae Kwon Song[1,*],
Myong Ho Kim[1], Sang wook Kim[2], Won Jeong Kim[2], and, Sang Su Kim[2]
[1]*School of Advanced Materials Engineering, Changwon National University,Gyeongnam, 641-773, Korea*
[2]*Department of Physics, Changwon National University,Gyeongnam, 641-773, Korea*

Keywords: lead-free, perovskite, $BiFeO_3$, $BiFeO_3$, quenching

Recently, (1-x)$BiFeO_3$-$x$$BaTiO_3$ (BF-BT) lead-free piezoelectric systems have potential to be applied at a high operation temperature due to their high T_c and high depolarization temperature (T_d). BF (rhombohedral phase) and BT (tetragonal phase) solid solutions were observed in the complete compositional range with rhombohedral (x=0.00-0.33), pseudo-cubic (x=0.33-0.92), and tetragonal (x=0.92-1.00) perovskite crystal structures. Leontsev and Eite reported Mn-modified BF-BT ceramics exhibit a small-field piezoelectric constant d_{33} of 116 pC/N with high T_c of 619 ^oC at 0.75BF-0.25BT. However, this report cannot be clearly stated in the electrical properties of pure (unmodified) BF-BT system due to high *dc* conductivity.

In this work, the effects of heat-treatment process were investigated in 0.67BF-0.33BT lead-free piezoelectric ceramics. The structure, ferroelectric, and piezoelectric properties of ceramics made by thermal quenching process were investigated and compared to those of furnace cooled ceramics. The lattice constants (a) and lattice distortions (rhombohedral 90^o- increased and the fraction of Fe^{2+} to Fe^{3+} was reduced in water-quenched ceramics. Ferroelectric and piezoelectric properties were improved with increasing quenching temperature. Small and large-field piezoelectric constants d_{33} and d_{33}* were 240 pC/N and 283 pm/V in ceramics water quenched at the highest temperature 980 ^oC.

Acknowledgement:
This work was supported by the National Resarch Foundation of Korea [KRF] grant funded by the Korea government [MSIP] (2012-0007403, and 2012-0009457) and by the Priority Research Centers Program through the National Research Foundation of Korea (NRF) funded by the MEST (2013R1A1A4A01010612, 2012-045424)

LP-P12

Effect of Ta-substitution on the dielectric, ferroelectric and field-induce strain properties of $Bi_{0.5}(Na_{0.82}K_{0.18})_{0.5}TiO_3$-$SrTiO_3$ ceramics

Rizwan Ahmed MALIK,[1] Ali HUSSAIN,[1] Jamil Ur RAHMAN,[1] Adnan MAQBOOL,[1] Tae Kwon SONG,[1] Won-Jeong KIM,[2] and Myong-Ho KIM,[1*]

[1]*School of Advanced Materials Engineering, Changwon National University, Gyeongnam 641-773, Republic of Korea*

[2]*Department of Physics, Changwon National University, Gyeongnam 641-773, Republic of Korea*

Keywords: Piezoelectricity, Ferroelectricity, Lead-free, Field-induced strain

The effect of Ta substitution on the crystal structure, electromechanical, dielectric, and piezoelectric properties of BNKTT-ST ($0.96Bi_{0.5}(Na_{0.84}K_{0.16})_{0.5}Ti_{1-x}Ta_xO_3$]–$0.04SrTiO_3$ where x = 0.00 – 0.030) ceramics has been investigated. X-ray diffraction patterns revealed that Ta doping resulted in a transition from coexistence of rhombohedral and tetragonal phases to a pseudocubic phase. Both the dielectric constant and depolarization temperature decreased with an increase in Ta-content. The polarization and strain hysteresis loops indicate that the ferroelectric order of the BNKT-ST ceramics was significantly disrupted by the addition of Ta content, leading to degradation in the remnant polarization and coercive field.

However, the destabilization of the ferroelectric order is accompanied by significant enhancements in the bipolar and unipolar strains. A large electric field-induced strain (S = 0.38%) and a corresponding normalized strain (S_{max}/E_{max} = 633 pm/V) were observed under 6 kV/mm when 2% Ta was substituted on Ti sites. This significant strain enhancement may be attributed to a reversible field-induced ergodic relaxor to ferroelectric phase transformation.

Acknowledgement:
This work is supported by the Basic Research program through the National Research Foundation of Korea (NRF) funded by Ministry, Science and Technology (MEST) (2011-0030058).

CO-P01

Physical Interpretations of Cap-Related Parameters of the Modified Drucker-Prager Cap Model in Relation to the Deviator Stress Curves of Particulate Materials

Hyunho SHIN[1*], Jong-Bong KIM[2]
[1]*Department of Materials Engineering, Gangneung-Wonju National University, 7 Jugheon-gil,Gangneung, Gangnwon-do 210-702, Republic of Korea*
[2]*Department of Mechanical and Automotive Engineering, Seoul National University of Science and Technology, 232 Gongneung-ro,Nowon-gu, Seoul 139-743, Republic of Korea*

Keywords: Modified Drucker-Prager model, Cap aspect ratio, Transition radius parameter

The physical meanings of cap aspect ratio (R) and transition surface parameter ( ) of the modified Drucker-Prager cap (MDPC) model in relation to the deviator stress curves of particulate materials generated by the conventional traixial test have been uncovered by simulating the curves using varying R and based on the finite element analysis. The yield surfaces of the model are shown in Figure 1. R controls the rate of the stress rise with the increase of the strain; the smaller the R, the faster the rise of the deviator stress. This phenomenon results because, in $J_{2D}^{1/2}$ –p space (J_{2D} is the second deviatoric stress invariant and p is the mean stress), the cap with a smaller R needs to move a less distance on the p axis to maintain the current stress state according to the hardening law. As for the influence of , it artificially lowers the true failure surface by the amount that is proportional to so that a fictitious ultimate failure state is achieved. Therefore, it is desirable to set the value of as small as possible unless the numerical analysis using the MDPC model results in a converged solution. An analytical expression to calculate the maximum deviator stress that can be predicted by the MDPC model is provided in terms of and the parameters of the true failure surface.

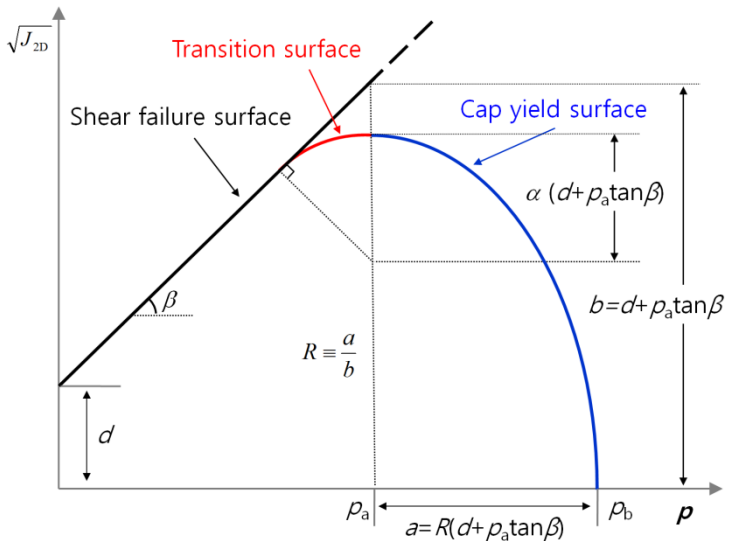

Figure 83 Yield surfaces of the modified Drucker-Prager model for particulate materials

Acknowledgement:
This study was financially supported by the Ministry of Education, Science, and Technology through the National Research Foundation (NRF) of Korea under contract No. 2013R1A1A2007455.

CO-P02

Molecular dynamics simulations of caloric effects in ferroelectrics

Takeshi Nishimatsu
Institute for Materials Research (IMR), Tohoku University, Sendai 980-8577, Japan

Keywords: first-principles effective Hamiltonian, electrocaloric effect, elactocaloric effect

Since 2005, we have been developing our original simulation code named feram specialized for ferroelectric materials[1]. feram is fast molecular dynamics (MD) simulation code for ABO_3 perovskite-type ferroelectrics and distributed as free software from http://loto.sourceforge.net/feram/. The code is based on a first-principles effective Hamiltonian and can be applicable not only bulk ferroelectrics but also ferroelectric thin-film capacitors. Because, in the code, dipole interactions are treated in reciprocal space with fast Fourier transform (FFT), feram is fast enough for simulating ferroelectric materials with a realistic system size up to 100 nm and a realistic time span (> 1000 ns).
Recently, we have developed a direct simulation method of electrocaloric and elastocaloric effects of ferroelectric materials with our feram code[2,3]. The electrocaloric effect is an adiabatic change in the temperature, DT, of a material upon applying an external electric field. In particular, if an electric field is applied to a ferroelectric material at just above its phase transition temperature, T_C, and the field is then removed, a large reduction in temperature is expected. The elastocaloric effect is that of external stress field. It is widely believed that these effects are applicable to solid-state refrigeration technologies.
In Fig. 1, the temperature dependence for the electrocaloric effect DT of $BaTiO_3$, under various initial external electric fields is compared. It can be seen that even with a small initial external electric field (50 kV/cm), $BaTiO_3$ gives a large DT, but the temperature range where this large DT can be obtained is narrow. By increasing the applied fields (>100 kV/cm) the range of applicable temperatures broadens.

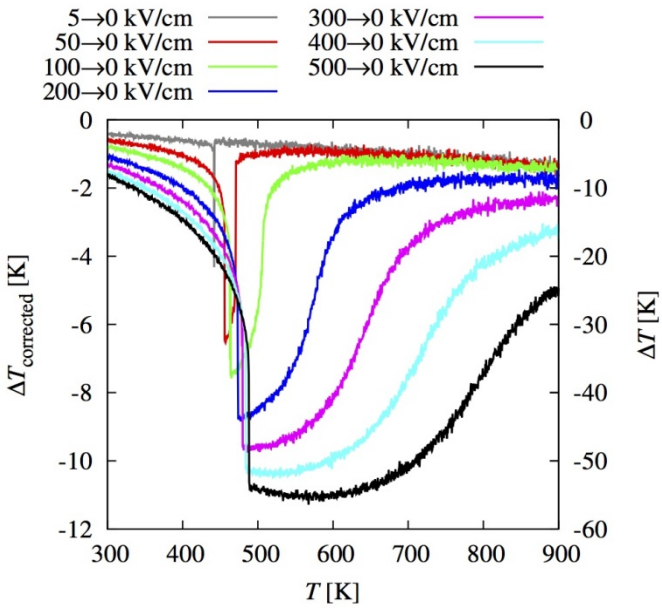

Figure 1 The temperature dependence of DT for various initial external electric fields. The external electric field switches from E_z=5–500 to 0 kV/cm.

References:

[1] Takeshi Nishimatsu, Umesh V. Waghmare, Yoshiyuki Kawazoe and David Vanderbilt: Phys. Rev. B 78, 104104 (2008).
[2] T. Nishimatsu, J. A. Barr and S. P. Beckman, J. Phys. Soc. Jpn. 82, 114605 (2013).

CE-P01

Investigation for Materials of Old Porcelain Wares in Houhoku-town

Natsuki HOSOYA[1*], Akira MIKUNI[1], Yoshinori MIYATA[2]
[1]*Yamaguchi Prefectural Industrial Technology Institute, 4-1-1 Asutopia, Ube-city, Yamaguchi, 755-0195, Japan*
[2]*IKKEI-gama, 112-8 Awano, Houhoku, Shimonoseki-city, Yamaguchi, 759-5101, Japan*

Keywords: Porcelain wares, Houhoku-town, X-ray fluorescence spectroscopy

1. Introduction

Houhoku-town locates in the western part of Yamaguchi prefecture in Japan. From the late 1700's to early 1900's, there were some manufacturing porcelain kilns such as Nakabara-kiln, Sakaige-kiln, Iinoyama-kiln and Hara-kiln in this town. However, none of them exists any longer and there is less information about these porcelain wares.[1] Folklore said these porcelain wares were made by using some raw materials which was reserved and mined in Houhoku-town.[2] In this study, for the purpose of investigating these materials, we analyzed the mineral composition of six raw materials which is possibly used in old porcelain wares in Houhoku-town. Moreover, we compared them with those of old porcelain wares in Houhoku-town.

2. Experimental procedure

Ig. Loss of six raw materials (A, B, C, D, E and F) was measured by taking difference of weight between before and after burning at 1000K. Samples for X-ray fluorescence (XRF) spectroscopy analysis were prepared in 1 : 10 glass beads to analyze the chemical composition of 9 major elements (Si, Al, Fe, Ti, Ca, Mg, Na, K and P). After XRF analysis, the mineral composition was calculated by CIPW norm which assumes clay as $Al_2Si_2O_5(OH)_4$, silica as SiO_2, feldspar as $Na_2Al_2Si_6O_{16}$ and $K_2Al_2Si_6O_{16}$, and iron oxide as Fe_2O_3.

3. Results and Discussion

Figure 1 shows the calculated mineral composition of six raw materials. As shown in figure 1, only material D is rich in feldspar with the content rate of 30 wt%. Since 24~27 wt% feldspar is contained in collected old porcelain wares at Nakabara- and Sakaige-kilns, material D would be possibly used as feldspar. On the other hand, collected porcelain wares in Iinoyama- and Hara-kilns contain 31~37 wt% feldspar. In this case, there is no corresponding material containing more than 30 wt% feldspar. Therefore, these porcelain wares would be produced by using other materials that contains much feldspar.

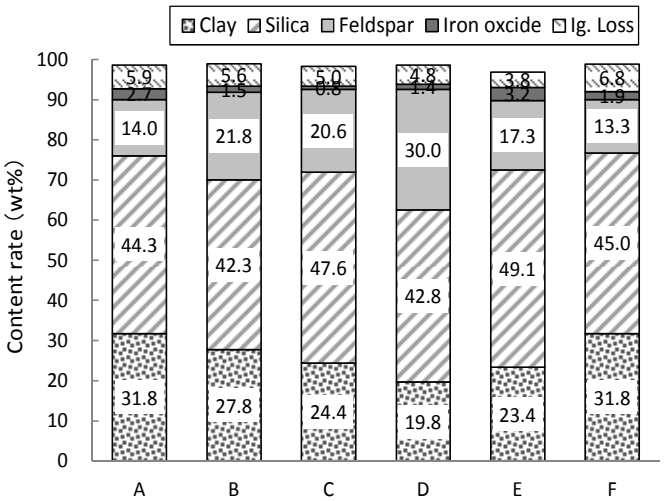

Fig.1 Mineral composition of six raw materials

References:

[1] Implementation Report of Iconotheque Project, p37-49 (1997)
[2] Taisho-kan, UTSUWA, p8-15 (2012)

Acknowledgement:

This work partly supported by the Creation and New Business-Supported for the Yamaguchi Industrial Promotion Foundation, 2011.
Special thanks to Satoshi Kawata (*Doigahama site anthropological museum*) and Asami Sasada (*Houhoku historical folk material museum*) for providing six raw materials.

LD-P01

Influence of electron-beam irradiation on properties of ITO thin films

Seung-Hong KIM[1], Jae-Hyun JEON[1], Tae-Kyung GONG[1], Sun-Kyung KIM[1,]
So-Young KIM[1], Dong-Hyuk CHOI[2], Dong-Il SON[2], Daeil KIM[1*]
[1]*School of Materials Science and Engineering, University of Ulsan, Ulsan, 680-749, Republic of Korea*
[2]*Dongkook Inc., Ulsan, 683-370, Republic of Korea*

Keywords: ITO, Thin film, Electron-beam, Flexible electrode

Sn doped In_2O_3 (ITO) films have been studied in the optoelectronic industry because it contains unique optical and electrical properties. However, conventional ITO film prepared on flexible substrate shows the high resistivity and it is difficult to activate Sn dopant into In_2O_3 matrix due to limitations of process temperature [1]. Thus, low temperature process is essentially required to activate of dopant for flexible device.

In this study, to develop a good quality of ITO thin film (100 nm). It has been deposited on polycarbonate (PC) substrate by RF magnetron sputtering and in addition, electron-beam irradiation on the surface also conducted with optimized e-beam incident energy. The resistivity and transmittance of the e-beam irradiated films were measured by the Hall-effect measurement and the UV-visible spectrometer. The structural and morphological characterization was performed by X-ray diffraction (XRD) and atomic force microscopy (AFM), respectively.

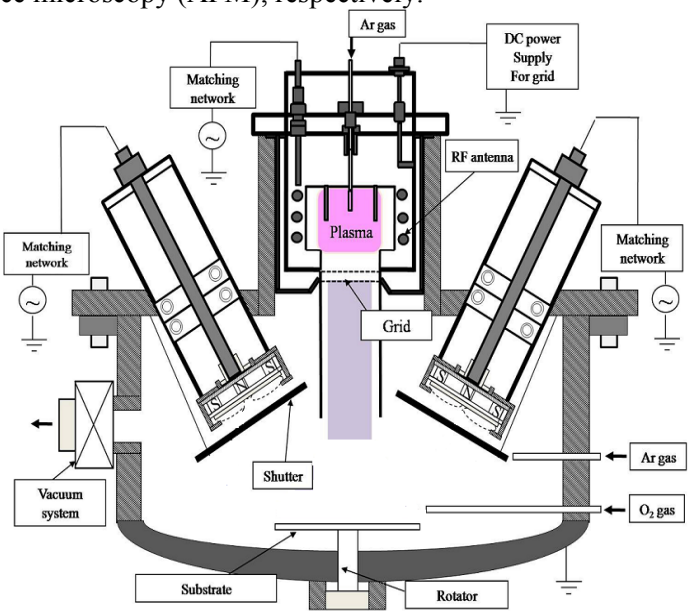

Figure 84. A schematic diagram of the RF magnetron sputtering and electron-beam irradiation system.

References:

[1] S.H Choa, C.K Cho, W.J Hwang, K.T Eun and H.K Kim, SOLMAT. 95 (2011) 3442.

Acknowledgement:

This research was financially supported by the Ministry of Education (MOE) and National Research Foundation of Korea(NRF) through the Human Resource Training Project for Regional Innovation (No. NRF-2013H1B8A2032122)

LD-P02

Enhanced electrical conductivity in hybrid Ag paste containing Ag nano-particles

Kyeong-Seob Kwon[1], Kyungwon Lee[1], In Hwan Lee[1*]
[1]*School of Advanced Materials Engineering and Research Center of Advanced Materials Development, Chonbuk National University, Jeonju 561-756, Korea*

Keywords: Hybrid paste, Ag nanoparticles, Ag paste, Electrical conductivity

Silver (Ag) paste has been widely used in solar cell, display (OLED, LCD, PDP), EMI-related products as an electrode material in a variety of applications with high reliability and low resistance. Ag paste which is the universal filler to micro-sized flakes, shows characteristics of a good electrical conductivity [1]. However, there is a limit to improve the electrical conductivity because the Ag filler with a micro size does not provide a continuous film within the filler, which results in the existence of multiple voids and increased sheet resistance. Recently, there have been reported attempts of using the Ag ink in order to effectively reduce the impact of such voids, but the problems of oxide nanoparticles aggregation phenomena and as high cost have emerged.[2] Hybrid paste obtained by mixing the nano-sized particle and micro-sized particle to circumvent these problems have been previously reported [3].
In this study, we develop hybrid Ag paste by mixing the nano-sized Ag particles in the Ag paste, which is composed of micro-sized Ag flakes in order to improve the electrical properties of the conductive adhesive. The mixture of nano-sized Ag particles in diluent agent was thus fabricated. The hybrid Ag paste was deposited on a slide glass using a 3M tape to form the test pattern. The electrical properties were evaluated after sintering. It was found that the electrical conductivity was greatly improved when the size of the nanoparticles was about 500 nm. This is due to the effective filling of the voids between the flakes and the nano-sized Ag particles.

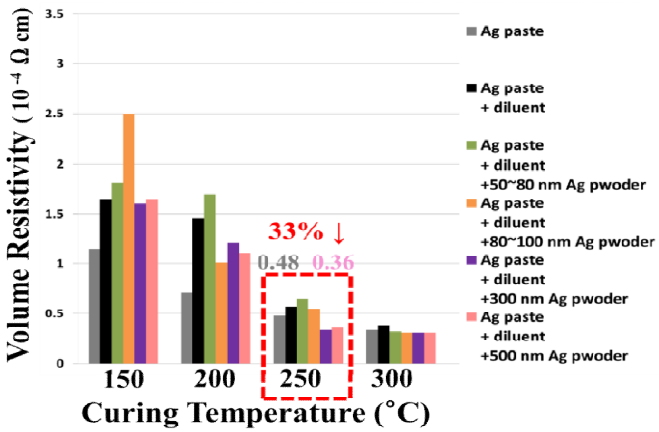

Figure 85. Changes in the electrical properties of the hybrid Ag paste in accordance with the size of the Ag nano-particles used

References:

[1] S. Rane, V. Puri, and D. Amalnerkar, J. Mater. Sci.: Mater. Electron., 11 (2000) 677.
[2] D. Russev, D. Raclev, and S. Kava, J. Met. Finish. 81 (1983) 27-30.
[3] A. Slistan-Grijalvaa, R. Herrera-Urbinab, J.F. Rivas-Silvac, M. Ávalos-Borjad, F.F. Castillón-Barrazad, and A. Posada-Amarillase, Mater. Res. Bull., 43 (2008) 96.

Acknowledgement:

This research was supported by National Research Foundation of Korea(NRF) funded by Ministry of Science, ICT & Future Planning (2013R1A2A2A07067688, 2010-0019626).

LD-P03

TEM and XRD analysis of Thin Film Phosphors on Sapphire

Ki-Woong CHAE[1], Ta-Ryeong PARK[2], Chae Il CHEON[1], and Jeong Seog KIM[2]
[1]*Dept. of Materials Science and Engineering, Hoseo University, Asan, Chungnam 336-795, Korea*
[2]*Dept. of Display Engineering, Hoseo University, Asan, Chungnam 336-795, Korea*

Keywords: Thin film, phosphors, TEM, XRD, sapphire, Eu-oxide

Transparent thin film phosphors can have potential applications in display devices and LED packagings. However, the transparency and the luminescence intensity are directly opposed properties that it can be hardly attained simultaneously. We recently reported that both properties can be achieved simultaneously when Eu-oxide is deposited on the sapphire substrate. Ihe deposited phases were so complicated that we could not draw any conclusion which phase contribute to the luminescence.
In this study we performed TEM and XRD analyses to identify the crystal phase on the substrate. The figure shows that TEM image of the thin film sample cross-sectioned across the sapphire substrate. We could confirmed the stacking faults by the Eu-diffusion through the sapphire substrate. The PL characteristics and transparency will be discussed in terms of the phase analysis results.

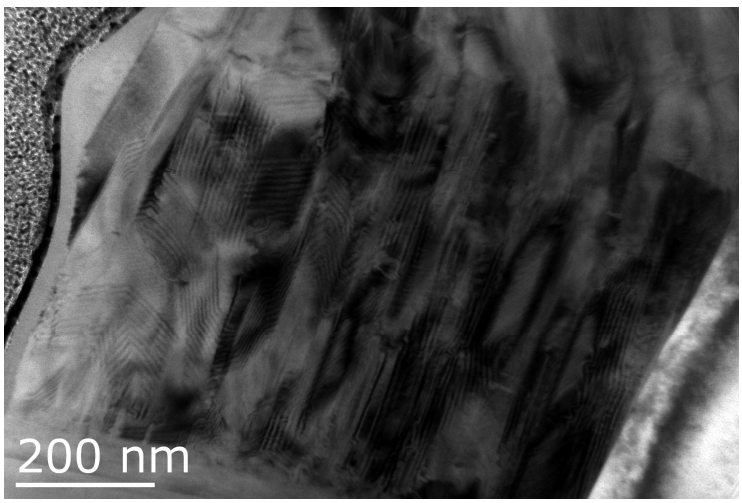

Figure 86. TEM image of thin film phosphor (left-top: Pt layer, middle: thin film EuO phosophor, Right-bottom: sapphire substrate)

References:

[1] Ki-Woong Chae, Ta-Ryeong Park,Chae Il Cheon, Nam In Cho, and Jeong Seog Kim, Electron. Mater. Lett., 9(S) (2013) 59-63
[2] J. Y. Cho, Y.-D. Huh, Y. R. Do, *Appl. Phys. Lett*. 89 (2006) 131915.
[3] S. Yi, J. S. Bae, B. K. Moon, J. H. Jeong, and J. H. Kim, Appl. Phys. Lett. 86, 1 (2005) 07192

LD-P04

Effect of B-doping on Persistent Luminescence in (Sr,Ca)Al_2O_4: Eu^{2+},Dy^3

Jeong Seog Kim[1], Ta-Ryeong Park[1], Chae Il Cheon [2], and Ki-Woong Chae[2]
[1]*Dept. of Display Engineering, Hoseo University, Asan, Chungnam 336-795, Korea*
[2]*Dept. of Materials Science and Engineering, Hoseo University, Asan, Chungnam 336-795, Korea*

Keywords: oxide phosphors, B-doping, persistent, life-time, decay, phase analysis

Persistent phosphors have much longer decay-life time than a second. Some persistent phosphors show the decay time over several hours after dosing excitation energy such as UV- and VIS-light. Hence long persistent phosphor materials can have various applications such as night-vision surveillance, safety signage, energy harvesting, and optical data storage. However, bottle neck in this field is how to increase the luminescence intensity during the decaying time and to fine-tune the excitation energy to visible light range. In this study we investigated the effect of B-addition in (Sr,Ca)Al_2O_4: Eu^{2+},Dy^3 on the luminescence intensity and the decay-life. We analyzed phase formation by the addition of B of the phosphors.

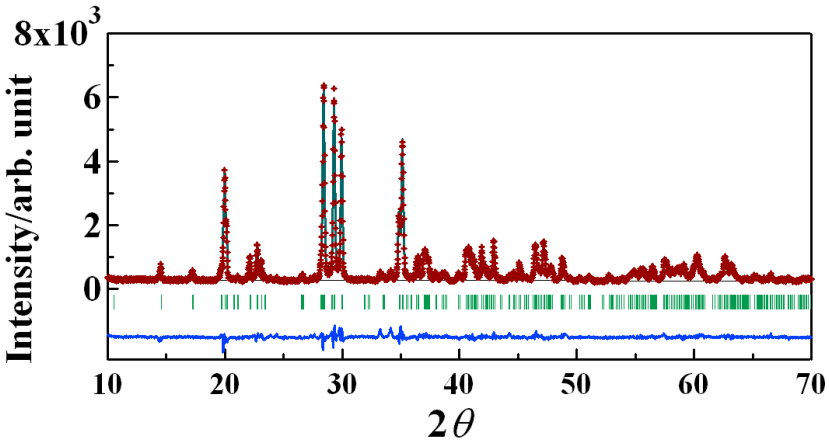

Figure 87. Rietveld refinement profiles of $SrAl_2O_4$:Eu^{2+},Dy^{3+} annealed at 1320 °C under reduction atmosphere. (Lattice parameters : a= 8.4455(3), b= 8.8274(2) , c= 5.1593(1) Å, β= 93.398(1)°, Rwp = 7.76, Rp = 5.62, Re = 4.64, S = 1.6721, RI = 4.45, RF = 2.61)

References:

[1] Matsuzawa, T.; Aoki, Y.; Takeuchi, N.; Murayama, Y. A new long phosphorescent phosphor with high brightness, SrAl2O4:Eu2+,Dy3+. J. Electrochem. Soc., 143(1996) 2670–2673
[2] Clabau, F.; Rocquefelte, X.; Le Mercier, T.; Deniard, P.; Jobic, S.; Whangbo, M.H. Formulation of phosphorescence mechanisms in inorganic solids based on a new model of defect conglomeration. Chem. Mater. 18(2006) 3212–3220.

AD-P01

Relation between Na_2SiF_6 Concentration and Mechanical Properties of AZ31 Magnesium Alloy coated by Electrolytic Plasma Processing

Jeong Yeong Seung, Park Keun Young[1],Kim Sung Jae[1] ,Song Jung il[2], Koo Bon Heun[1*]
[1]*School of Materials Science & Engineering, Changwon National University, Changwon,641-773, Korea*
[2]*Department of Mechanical Engineering, Changwon National University, Changwon ,641-773,Korea*

Keywords:AZ31,electrolytic plasma processing, coating, Magnesium alloy

Electrolytic Plasma Processing (EPP) is an electro chemical and physical surface treatment process for generating oxide coatings on metals. It is used to grow thick and dense ceramic oxide coatings on metals such as aluminum, magnesium and titanium. Earlier researches showed that the EPP ceramic coatings could offer attractive combination properties of wear resistance, corrosion resistance, mechanical strength, interfacial adhesion, thermal resistance and so on. According to these researches, coating performances are determined by such complex EPP experimental parameters as substrate material, electrolyte composition, applied voltage, current, frequency, process time, and so on.[1,2]

The effect of Na_2SiF_6 concentration on the ceramic oxide coatings prepared on AZ31 magnesium alloy through electrolytic plasma processing in a Na_2SiO_3 -NaOH electrolytic solution, have been investigated. The x-ray diffraction (XRD) results show that the coating formed in silicate electrolyte is mainly composed of MgO, Mg_2SiO_4. Scanning electron microscopy (SEM) micrographs reveals that the number of pores on coating surface decreases by increasing concentration of Na_2SiF_6 and all coatings have similar surface morphologies. The observed micro-hardness of coating layers is over 1000 Hv, which is much higher than that of the uncoated AZ31 magnesium alloy. The wear-loss of the coatings formed in electrolyte of 0.3 g/L Na_2SiF_6 shows better properties than the other two electrolytes. Because the coated specimen (in 0.3 g/L Na_2SiF_6) has the higher density, than the coatings formed with the other electrolytes.

References:

[1] J. Liang, B.G. Guo, J. Tian, H.W. Liu, J.F. Zhou, T. Xu, Appl. Surf. Sci. 252 (2005) 345.
[2] H.F. Guo, M.Z. An, Appl. Surf. Sci. 246 (2005) 229.

Acknowledgement:

This work was supported by the National Research Foundation of Korea(NRF) grant funded by the Korea government(MSIP) (No.2011-0030058). This research was financially supported by the Ministry of Education, Science Technology (MEST) and National Research Foundation of Korea(NRF) through the Human Resource Training Project for Regional Innovation (2012H1B8A2026212)

AD-P02

Effect of Time on The Properties of oxide layers of Al7075 aluminum alloyPrepared by Electrolytic Plasma processing

Keun Young Park[1], Dong Gun Lee[1], Jung Il Song[2], Bon Heun Koo[1,*]
[1]*School of materials science & engineering, Changwon National University,Changwon 641-773, korea*
[2]*Department of Mechanical Engineering, Changwon National University,Changwon 641-773, Korea*

Keywords: EPP, Coating, Al7075, Alloys

Electrolytic plasma processing (EPP) is a novel electrochemical and physical surface treatment process for generating protective coatings on light metals. Because these coatings can present high hardness and continuous barriers, it can offers good protection against abrasion, in this work corrosion and heat as well as electrical insulation. The EPP treatments were carried out under a hybrid voltage of AC 200V (50Hz) combined with DC 260V power supply. Micro-hardness of coatings is measured by Vickers hardness test. A combined composition and structure analysis of surface and cross-sectional layer was carried out by X-ray diffractometer (XRD), scanning electron microscopy (SEM), and energy dispersive spectrometer (EDS). The results of XRD show that the ceramic coatings mainly consist of mullite, α-Al2O3 and γ-Al2O3 phase. The ceramic coatings prepared in 30 min have highest value (1794 Hv) of micro-hardnes. (2012H1B8A2026212), (No.2011-0030058)

References:

[1] Tokio Nakada, Electron. Mater. Lett. 8 (2012) 179.
[2] W. S. Choi, Electron. Mater. Lett. 8 (2012) 87

Acknowledgement:

This work was supported by the National Research Foundation of Korea(NRF) grant funded by the Korea government(MSIP) (No.2011-0030058). This research was financially supported by the Ministry of Education, Science Technology (MEST) and National Research Foundation of Korea(NRF) through the Human Resource Training Project for Regional Innovation (2012H1B8A2026212)

AD-P03

Fabrication of EBC with Eutectic Structure for Silicon Carbide Substrate

Kyosuke SEYA[1], Byung-Koog Jang[2], Shunkichi UENO[1]
1 *College of Engineering, Nihon University, Koriyama, Fukushima 963-8642, Japan*
2 *National Institute for Materials Science, Tsukuba, Ibaraki 305-0047, Japan*

Keywords: Al_2O_3/HfO_2 Eutectic EBC, FGM layer, solidification

A silicon carbide ceramics with Al_2O_3/HfO_2 eutectic layer was successfully prepared by optical zone melting method. The EBC film is consisted with thin HfC/HfO_2 functional graded Material (FGM) layer and eutectic structure layer. These two layers were formed together during the optical zone melting process. At this process, the mixture of oxides with Al_2O_3/HfO_2 eutectic composition was melt down on the SiC substrate. The surface of SiC substrate is slightly decomposed and the liquid phase on the substrate was reduced. The alumina component in the liquid phase sublimated in to atmosphere and the composition of the liquid phase become hafnia rich composition. The excess hafnia component reacts with free carbon and hafnium carbide phase was solidified on the SiC substrate. Then, solidification of the liquid phase produced the Al_2O_3/HfO_2 eutectic layer on the HfC intermediate layer.

ETC

世界に希有な 260 年続いた友好な歴史　江戸時代の朝鮮通信使と技術交流（その 4）
アジア海域の技術交流を辿り、朝鮮通信使をユネスコ記憶遺産に！
Unique friendship history between Japan and Korea for 260 years of the Edo period, Grate scale missions exchanged sincerity from Korea Yi dynasty and technological exchange (No.4) – Trace technological exchange on the Asian-Sea area, and put the Korean Mission with friendship on the Memory of the World! –

要旨：岡山で開催された第 28 回日韓セミナーで“江戸時代の朝鮮通信使と技術交流”の特別ポスターを編集委員会のご厚意で出させて頂き、今回で 4 回目である。岡山の牛窓が朝鮮通信使の“迎接所”として通信使一行を“おもてなし”して、文化交流を行った歴史的地であることを、日韓のセミナーの参加者に江戸時代の友好な歴史として共有して頂きたく、僭越ながら始めた。一昨年は、大邱で開催され、その 2 として、茶碗戦争と呼ばれる文禄・慶長の役（壬辰・丁酉再乱：イムジン・チョンユジュラン）で諸大名によって拉致されてきた陶工によってもたらされた磁器のルーツを辿った。昨年は、信長・秀吉の大名茶湯で高麗茶碗がもてはやされ、茶碗戦争に繋がり、家康による国交回復後、対馬藩による日朝貿易の拠点“倭館”での“釜山窯（1639～1718）”をめぐるもう一つの日朝友好の歴史を辿った。今年は、朝鮮通信使をユネスコ記憶遺産に登録のうごきとアジア海域の技術交流に触れたい。

- 文責：名古屋産業科学研究所・上席研究員・大里
Senior Researcher, Department of Research, Nagoya Industrial Science Research Institute

세계에서도 희유한 260 년간 계속된 우호의 역사 에도(江戸) 시대의 조선 통신사와 기술교류 (그 4 번째)
아시아 해역의 기술교류를 돌아보며 조선통신사를 세계기록유산으로!

요지：오카야마에서 개최된 제 28 회 일한 세미나에서 “에도시대의 조선통신사와 기술교류”의 특별 포스터를 편집 위원회의 후의로 내게 되어 이번으로 4 회째가 되었다. 오카야마의 우시마도가 조선통신사의 “영접소”로서 통신사일행을 “환대”하여, 문화교류를 행한 역사적 땅인 것을, 일한의 세미나 참가자들에게 에도 시대의 우호의 역사로서 공유하기를 바라며 외람되지만 시작했다. 재작년, 대구에서 개최된 두 번째세미나에서, 도자기전쟁이라고 불리는 분로쿠·케이쵸의 역(임진·정유 재란)때에 여러 다이묘들이 납치해 온 도공들에 의해 시작된 자기의 루트를 되돌아봤다. 작년에는 노부나가·히데요시의 다이묘들의 다도에서 고려 시대찻잔이 극구 찬양되어, 도자기전쟁으로 이어지고, 이에야스에 의한 국교회복 후, 쓰시마 번에 의한 일한 무역의 거점인 “왜관”의 “부산가마(1639～1718)”를 둘러싼 또 하나의 일한 우호의 역사를 되돌아봤다. 금년에는 조선통신사를 세계기록유산으로 등재하기 위한 움직임과 아시아 해역의 기술교류에 대해 언급하고자 한다.

- 문장 책임: 나고야산업과학연구소/상석연구원/오사토 히토시

Author Index

A

Wendusu		Osaka Univ.	SY-I01
Nobuyasu	ADACHI	Nagoya Inst. of Tech.	EL-I04
Tadafumi	ADSCHIRI	Tohoku Univ.	NA-I01
Chang-Won	AHN	Univ. of Ulsan	LP-I08, LP-I09, LP-P05, LP-P08
Cheol-Woo	AHN	KIMS	PI-O04, PI-P04
Hong Jun	AHN	Kyonggi Univ.	EL-O07
Ji-Whan	AHN	KIGAM	NA-O01
Hiroshi	AKAISHI	Plus Comfort Co., Ltd	PI-I01
Isamu	AKASAKI	Meijo Univ. & Nagoya Univ.	LD-I04
Yoshikazu	AKIYAMA	Ricoh Co., Ltd.	LP-I13
Rezq Naji	ALJAWFI	Ibb Univ.	NA-P01
Gye Seok	AN	Hanyang Univ.	ST-O04
Sung Jin	AN	Kumoh Nat'l Inst. of Tech.	FU-P07
M. S.	ANWAR	Changwon Nat'l Univ.	NA-P03, EL-P06, ST-O07
Rintaro	AOYAGI	Nagoya Inst. of Tech.	LP-I04
Takashi	ARAI	Shizuoka Univ.	EL-O05
T.	ARAKI	Ritsumeikan Univ.	LD-I01

B

Byungseo	BAE	KIMS	ST-O08
Dong Sik	BAE	Changwon Nat'l Univ.	SY-O03
Hyun-Jeong	BAE	Korea Aerospace Univ.	EL-P04
Jae Yoon	BAE	Hanyang Univ.	LD-I06
Kang-Bin	BAE	Chonbuk Nat'l Univ.	LD-O01, LD-O03, LD-O06
Suk-Rok	BAE	Kongju Nat'l Univ.	GL-P06
Changyeon	BAEK	KAIST	ST-I03
Jonghyeob	BAEK	KOPTI	LD-O03
Seung-deok	BAEK	Hanbat Nat'l Univ.	TF-P15, TF-P16
Mohammad Reza	BAFANDEH	Univ. of Kashan	LP-O06, LP-P04
Indu	BAJPAI	Yeungnam Univ.	BI-O02, BI-P05
Ji-yoon	BAK	Korea Univ.	TF-O04
Sachin N.	BRAMHE	KRISS	BI-P01

C

Yu-Jung	CHA	Sunchon Nat'l Univ.	LD-O05
K. H.	CHAE	KIST	TF-P09
Ki-Woong	CHAE	Hoseo Univ.	LD-P03, LD-P04
Song A	CHAE	Univ. of Ulsan	LP-P08
Su-Jeong	CHAE	Chonnam Nat'l Univ.	LP-P03
Woojin	CHANG	ETRI	LD-I02
Feng	CHEN	Chinese Academy of Sci.	LP-I03
Li-Qian	CHENG	Tsinghua Univ.	PL-02

Chae Il	CHEON	Hoseo Univ.	EL-I02, LD-P03, LD-P04
SeongKyu	CHEON	Changwon Nat'l Univ.	PI-P03
Byung-ki	CHEONG	KIST	GL-O09
Bum-Rae	CHO	Keimyung Univ.	ST-P03
Han-Su	CHO	Chonbuk Nat'l Univ.	LD-O01, LD-O03, LD-O06
Hong-Baek	CHO	Nagaoka Univ. of Tech.	NA-I01, NA-O04
Seong-Jai	CHO	KRISS	GL-P03
Sung Haeng	CHO	ETRI	LD-I05
Woo Seok	CHO	KICET	CE-O01, CE-O02
Yong Soo	CHO	Yonsei Univ.	NA-P09
Young-Sang	CHO	Korea Polytechnic Univ.	SY-P02
Dong-Huk	CHOI	Dongkook Inc.	TF-P04, TF-P05
Dong-Hyuk	CHOI	Dongkook Inc.	LD-P01
Gang Ho	CHOI	Univ. of Ulsan	LP-I09
Hongshoo	CHOI	DGIST	PI-I03, PI-P01
Hongsoo	CHOI	DGIST	PI-O04
Hyung-Jin	CHOI	Chungnam Nat'l Univ.	TF-I04, TF-P13
J. Y.	CHOI	Changwon Nat'l Univ.	TF-P01, TF-P02
Jae Seok	CHOI	Hanyang Univ.	ST-O04
Jin Hong	CHOI	Hoseo Univ.	EL-I02
Jin Seok	CHOI	Kumoh Nat'l Inst. of Tech.	FU-P07
Ji-Won	CHOI	KIST & UST	EL-I05
Jong-Jin	CHOI	KIMS	FU-I06, PI-O04, PI-P04
Kwangwon	CHOI	Soonchunhyang Univ. & RN2 Technologies	EL-P08
Kyoon	CHOI	KICET	CO-O01
Min-Geun	CHOI	Inha Univ.	EL-P05, EL-P07
Moon-Kwan	CHOI	Korea Nat'l Univ. of Transportation	TE-P01
Pil-Gyu	CHOI	Osaka Univ.	SY-P03
Seunggon	CHOI	Inha Univ.	GL-P07
Si-Young	CHOI	KIMS	PI-O04, LP-I09
Soon-Mok	CHOI	Koreatech Co.	TE-P03
Sung Churl	CHOI	Hanyang Univ.	ST-O04, GL-P03, GL-P04
Sung-Jae	CHOI	Korea Nat'l Univ. of Cultural Heritage	CE-O03
Yong Gyu	CHOI	Korea Aerospace Univ.	GL-O09, GL-P06, GL-P08
Min Cheol	CHU	KRISS & UST	BI-P01
Jongup	CHUN	Induk Univ.	CE-I02
Yoon-Soo	CHUN	Korea Univ.	SY-O04
Habin	CHUNG	POSTECH	CO-I01
Jun-Ki	CHUNG	Gangneung-Wonju Nat'l Univ.	SY-P05
Taehoon	CHUNG	KOPTI	LD-O03
Woon Jin	CHUNG	Kongju Nat'l Univ.	GL-I01, GL-O06, GL-P05, GL-P06
Qi-Zheng	CUI	Changwon Nat'l Univ.	AD-I03

D

Yusuke	DAIKO	Nagoya Inst. of Tech.	ST-O13
Rehan	DANISH	Changwon Nat'l Univ.	NA-P03
Thi Hinh	DINH	Univ. of Ulsan	LP-O06, LP-P04, LP-P05
D.	DO	Keimyung Univ.	LP-P01, LP-P07
Dalhyun	DO	Keimyung Univ	LP-O02
Myeong-Ji	DONG	Chonbuk Nat'l Univ.	LD-O03, LD-O04, LD-O06
Qi	DONG	Pusan Nat'l Univ.	TF-O03
Thanh Tung	DUONG	Chungnam Nat'l Univ.	TF-O02

E

Yoshitaka	EHARA	Tokyo Inst. of Tech.	TF-I01
Young Jun	EOH	Kyonggi Univ.	EL-O06, EL-O07, EL-P10
Ji-Ho	EOM	Chungnam Nat'l Univ.	TE-O02
You Jeong	EUM	Yeungnam Univ.	TF-P10

F

Muhammad Umer	FAROOQ	Chonnam Nat'l Univ.	LP-O03
John G.	FISHER	Chonnam Nat'l Univ.	LP-O03, LP-P03
H.	FUJIOKA	Univ. of Tokyo & JST-CREST	LD-I09
Saeko	FUJIUCHI	Nagoya Inst. of Tech.	EL-I04
Nashito	FUKUHARA	Osaka Univ.	SY-P03
Kohei	FUKUMI	AIST	GL-P10
Hiroshi	FUNAKUBO	Tokyo Inst. of Tech.	TF-I01
Syohei	FURUYA	Toyohashi Univ. of Tech.	GL-P01, GL-P02

G

Lin	GAN	KIMS	ST-O10
Yumin	GOH	Korea Aerospace Univ.	EL-P04
Roman	GOLOVCHAK	Austin Peay State Univ.	GL-O09
Manabu	GOMI	Nagoya Inst. of Tech.	TF-O05
Tae-Kyung	GONG	Univ. of Ulsan	TF-P04, TF-P05, LD-P01
Kota	GOTANDA	Kagoshima Univ.	NA-P02
Gaetan	GRABARSKI	Center Europeen de la Ceramique	ST-O13

H

Jang-Hoon	HA	KIMS	ST-O08
YongWoo	HA	Changwon Nat'l Univ.	PI-P03
Byung-Dong	HAHN	KIMS	PI-O04, PI-P04
Y.-S.	HAHN	KICET	CO-O01
Yuki	HAMAGUTI	Electronics Co., Ltd.	LP-I06

Byungchan	HAN	DGIST	CO-I01
Chan Su	HAN	Yonsei Univ.	NA-P09
In-Sub	HAN	KIER	ST-O14
Jin Soon	HAN	Hanyang Univ.	ST-O04
Karam	HAN	Kongju Nat'l Univ.	GL-I01
Kyu-Sung	HAN	KICET	CE-O01
S. J.	HAN	Changwon Nat'l Univ.	LP-P07
Sangbo	HAN	Kyungnam Univ.	NA-P08
Seungwu	HAN	Seoul Nat'l Univ.	CO-I04
Sung Jin	HAN	Changwon Nat'l Univ.	LP-P06
Yoonsoo	HAN	KICET	AD-I06
Young-Hwan	HAN	Yeungnam Univ.	BI-O05, EF-I02, EF-I05
Takuya	HASEGAWA	Niigata Univ.	SY-I03
Shinobu	HASHIMOTO	Nagoya Inst. of Tech.	ST-O13
S.	HAYAKAWA	Okayama Univ.	BI-I01
Hiroyuki	HAYASHI	KRI, Inc.	GL-P02
Yamato	HAYASHI	Tohoku Univ.	NA-I04
Dae-Jun	HEO	Univ. of Ulsan	LP-P05
J.	HEO	POSTECH	GL-O06
Jaeyeong	HEO	Chonnam Nat'l Univ.	TF-I03
Jong	HEO	POSTECH	GL-I01, GL-O05, GL-O07
Young-Woo	HEO	Kyungpook Nat'l Univ.	FU-P03
Keijiro	HIRAGA	Kitami Inst. of Tech.	EF-I03
Yoshihiro	HIRATA	Kagoshima Univ.	NA-P02, FU-O01, ST-P02
Ohsato	HITOSHI	Nagoya Industrial Sci. Research Inst.	ETC
Junichi	HOJO	Kyushu Univ.	CE-I01
Hiroki	HOKAZONO	Osaka Prefecture Univ.	ST-O02
Sawao	HONDA	Nagoya Inst. of Tech.	ST-O13
Taihei	HONDA	Osaka Univ.	SY-I01
Tsuyohi	HONDO	Nagaoka Univ. of Tech.	ST-I04
Chang Woo	HONG	Korea Nat'l Univ. of Transportation	SY-P01
Hyeonu	HONG	IONES Co., Ltd.	BI-P02
Hyeryung	HONG	Johns Hopkins Univ.	PI-P01
Ji-Eun	HONG	Chungnam Nat'l Univ.	TE-P04
Jongsup	HONG	KIST	FU-I02
Young Jun	HONG	Konkuk Univ.	SE-O01
Young-Hwan	HONG	Univ. of Ulsan	LP-O06, LP-P04, LP-P05
Tsuyoshi	HONMA	Nagaoka Univ. of Tech.	GL-O03
Natsuki	HOSOYA	Yamaguchi Prefectural Industrial Tech. Inst.	CE-I09, CE-P01
Qing	HUANG	Ningbo Inst. of Materials Tech. and Eng.	EF-I05
Joon	HUR	Korea Univ.	PI-O01, PI-O06
Ali	HUSSAIN	Changwon Nat'l Univ.	PI-P07, LP-I15, LP-O07, LP-P03, LP-P09, LP-P12
Changhun	HWANG	Kyungnam Univ.	TF-P11
Chi-Sun	HWANG	ETRI	LD-I05

Eung Joo	HWANG	Samjeon Co., Ltd.	LP-P08
Geon Tae	HWANG	KAIST	PI-P05
Haejin	HWANG	Inha Univ.	NA-I02
I. J.	HWANG	Keimyung Univ.	LP-P01
Joon	HWANG	Korea Nat'l Univ. of Transportation	SY-P01
K. H.	HWANG	Gyeongsang Nat'l Univ.	BI-O09
Kwang-Taek	HWANG	KICET	CE-O01
Seon Ae	HWANGBO	Pukyong Univ.	BI-P01
Takeo	HYODO	Nagasaki Univ.	NA-P06, NA-O02, BI-P03

I

Hiroki	ICHIKAWA	Nagoya Univ.	LP-I13
Daichi	ICHINOSE	Tokyo Inst. of Tech.	TF-I01
Daisuke	IIDA	Meijo Univ.	LD-I04
Motoyuki	IIJIMA	Yokohama Nat'l Univ.	ST-O01, ST-O11
Ryo	IIZUKA	Univ. of Yamanashi	LP-I07
Taiki	IKEGAYA	Shizuoka Inst. of Sci. & Tech.	LP-O01
Mir	IM	Korea Univ.	EL-O04
Won Bin	IM	Chonnam Nat'l Univ.	GL-I01, GL-P05
Haruo	IMAGAWA	Toyota Central Research & Development Labs.	NA-O05
Nobuhito	IMANAKA	Osaka Univ.	SY-I01, SY-P03, FU-I01
Mitsuteru	INOUE	Toyohashi Univ. of Tech.	TE-I02
Tadashi	ISHIGAKI	Niigata Univ.	SY-I02, SY-I03
Koji	ISHIHARA	Meijo Univ.	LD-I04
Kota	ISOBE	Kansai Univ.	TF-P14
Hiroshi	ITAHARA	Toyota Central Research & Development Labs.	NA-O05
Daiki	ITO	Nagasaki Univ.	NA-P06
Shota	ITOH	Kagoshima Univ.	ST-P02
Yuji	IWAMOTO	Nagoya Inst. of Tech.	ST-O13
Akihiro	IWASE	Osaka Prefecture Univ.	ST-O02
Motoaki	IWAYA	Meijo Univ.	LD-I04

J

Thomas N.	JACKSON	The Pennsylvania State Univ.	PI-O02
Himanshu	JAIN	Lehigh Univ.	GL-O09
Byung-Koog	JANG	NIMS	ST-O09, AD-I01, AD-I03, AD-I06, AD-O01, AD-P03
Dong Woo	JANG	Soonchunhyang Univ.	BI-O04
Ho Won	JANG	Seoul Nat'l Univ.	SE-I03
K. W.	JANG	Changwon Nat'l Univ.	TF-P09
Ki Bong	JANG	Samjeon Co. Ltd.	LP-I09, LP-P08
Seok-Myung	JANG	KERI	LP-I11
Sukjin	JANG	Yonsei Univ.	LD-I07

Taehoon	JANG	LG Electronics	LD-O02
Hae-June	JE	KIST	FU-I02
Venkatraju	JELLA	Chungnam Nat'l Univ.	TE-O01
Hye Ji	JEON	Hanyang Univ.	LD-I06
Jaehui	JEON	Yeungnam Univ.	BI-O07, BI-P04
Jae-Hyun	JEON	Univ. of Ulsan	LD-P01, TF-P04, TF-P05
Ahrong	JEONG	Kyungnam Univ.	NA-P08
Dae-Yong	JEONG	Inha Univ.	EL-P05, EL-P07, PI-O04, PI-P04
Da-Woon	JEONG	KITECH & Korea Univ.	NA-P10
Kwangjin	JEONG	Yokohama Nat'l Univ.	ST-O01
Min-Gun	JEONG	Korea Univ.	SY-O04
Seongsu	JEONG	Changwon Nat'l Univ.	PI-P02, PI-P03
Soon-Jong	JEONG	KERI	LP-I08, LP-I09, LP-I11
Yeong Seung	JEONG	Changwon Nat'l Univ.	TF-P07, AD-P01
Ji-Na	JEUNG	Chungnam Nat'l Univ.	FU-P01
Shenglin	JIANG	Huazhong Univ. of Sci. and Tech.	LP-I12
Weihua	JIANG	Nagaoka Univ. of Tech.	NA-O04
Joo Sung	JIN	Changwon Nat'l Univ.	FU-P05
Jung Kyong	JIN	Yeungnam Univ.	BI-O02
Hyun Jin	JO	Kyonggi Univ.	EL-O03
Wook	JO	UNIST	EL-I02, LP-I08, LP-I12, LP-I14, LP-P05
Ho Ik	JUN	Mattron Corp.	PI-P03
Joontaek	JUNG	DGIST	PI-P01
Myung Geun	JUNG	Changwon Nat'l Univ.	FU-P04
Sungsil	JUNG	Pohang Techno Park	BI-O05
Yang Il	JUNG	KAERI	ST-P06
Yeon-Gil	JUNG	Changwon Nat'l Univ.	FU-O02, AD-I03, AD-I04

K

Isao	KAGOMIYA	Nagoya Inst. of Tech.	EL-O02
H.	KAIJU	Hokkaido Univ.	GL-O01
Hideo	KAIJU	Hokkaido Univ.	GL-O02
Yasumoto	KAJIHARA	Ohtani Thobou Handou Gama	CE-I07
Kai	KAMADA	Nagasaki Univ.	NA-P06, NA-O02, BI-P03
Tetsuya	KAMEYAMA	AIST	CE-I08
Satoshi	KAMIYAMA	Meijo Univ.	LD-I04
Akinori	KAN	Meijo Univ.	EL-O02
Tatsuro	KANEKO	Niigata Univ.	SY-I02
Kazunari	KANEYASU	Figaro Eng.	SE-I01
Byoungwoo	KANG	POSTECH	FU-I04, CO-I01
Jin-Kyu	KANG	Univ. of Ulsan	LP-O06, LP-P04, LP-P05
Joonhee	KANG	DGIST	CO-I01
Ju-Eun	KANG	KIMS & Pusan Nat'l Univ.	PI-O03, PI-P01, PI-P04
Seungjin	KANG	Soonchunhyang Univ.	EL-P11

Soo-Bin	KANG	Inha Univ.	EL-P05, EL-P07
Suk-Joong L.	KANG	KAIST	PI-O03
Tae Sung	KANG	Mokpo Nat'l Univ.	SY-P04
Tae-Chun	KANG	Korea Nat'l Univ. of Cultural Heritage	CE-O03
Yun Chan	KANG	Korea Univ.	SE-O01
Isaku	KANNO	Kobe Univ.	PI-I04
Masanao	KANNO	Nagaoka Univ. of Tech.	NA-I01
Toshihiro	KASUGA	Nagoya Inst. of Tech.	BI-O06
Masaki	KATAYAMA	Yokohama Nat'l Univ.	ST-O11
Hiroaki	KATSUKI	Saga Ceramics Research Lab.	CE-I07
Keiga	KAWAGUCHI	Hokkaido Univ.	GL-O02
Yukari	KAWANO	Niigata Univ.	SY-I03
Yusaku	KIBA	Nagoya Inst. of Tech.	EL-I04
Takanori	KIGUCHI	Tohoku Univ.	EL-P09
Koichi	KIKUTA	Nagoya Univ.	BI-O10
Beak Hyun	KIM	Korea Aerospace Univ.	EL-P04
Bum Sung	KIM	KITECH	NA-P10
Byung-Kook	KIM	KIST	FU-I02
Byung-Nam	KIM	NIMS	EF-I03, EF-I04
Chang-Hoon	KIM	Samsung Electro-Mechanics Co. Ltd	EL-I08
Chang-Sam	KIM	KIST	FU-P02
Chang-Yeoul	KIM	KICET	NA-I03
D. J.	KIM	Changwon Nat'l Univ.	TF-P09, LP-P01
Da Jeong	KIM	Changwon Nat'l Univ.	PI-I06, LP-P06
Dae Woo	KIM	Pusan Nat'l Univ.	TF-O03
Dae-Geun	KIM	IONES Co., Ltd.	BI-P02
Dae-Hyeon	KIM	Korea Univ.	SY-O01, PI-O01
Daeil	KIM	Univ. of Ulsan	TF-P04, TF-P05, LD-P01
Daeung	KIM	Chonnam Nat'l Univ.	LP-P03
Dajeong	KIM	Changwon Nat'l Univ.	LP-O02, LP-P11
Do Kyung	KIM	KAIST	ST-I03
Dong-Ho	KIM	Ceracomp Co., Ltd	LP-I02
Dong-Hwan	KIM	KICET & Hanyang Univ.	GL-P03, GL-P04
Dong-Joo	KIM	KAERI	ST-P04, ST-P05
Dong-Seob	KIM	Korea Nat'l Univ. of Transportation	TE-P01
Doo-Young	KIM	Samsung Electro-Mechanics Co. Ltd	EL-I08
Duk-Yeon	KIM	Yeungnam Univ.	BI-O02, BI-O05
Eung Soo	KIM	Kyonggi Univ.	EL-O03, EL-O06, EL-O07, EL-P10
Eun-Young	KIM	KIST	FU-P02
Hae-Ryoung	KIM	KIST	FU-I02
Hai-Doo	KIM	KIMS	ST-O06, ST-O10
Ha-Neul	KIM	KIMS	ST-O06, ST-O10
Hee Sung	KIM	Univ. of Ulsan	LP-P08
Hee-Ok	KIM	ETRI	LD-I05

Hojoong	KIM	Yonsei Univ.	LD-I07
Hyeong Joon	KIM	Seoul Nat'l Univ.	PL-01
Hyeong-Jun	KIM	KICET	GL-P03, GL-P04
Hyoungchul	KIM	KIST	FU-I02
Hyun	KIM	Kumoh Nat'l Inst. of Tech.	FU-P06, FU-P07, FU-P08
Hyun Gil	KIM	KAERI	ST-P06
Hyun Woo	KIM	UNIST	FU-O02
Hyung-chul	KIM	Hanbat Nat'l Univ.	TF-P15, TF-P16
Hyungsun	KIM	Inha Univ.	GL-O10, GL-P07
Hyung-Tae	KIM	KICET	ST-O09, AD-I01, AD-I06, AD-O01
Ik Jin	KIM	Hanseo Univ.	NA-P04, NA-P05, NA-P07, ST-O03
Il-Ho	KIM	Korea Nat'l Univ. of Transportation	TE-P01
Ill Won	KIM	Univ. of Ulsan	LP-I09, LP-P05, LP-P08
Ill Yong	KIM	Nagoya Univ.	BI-O10
J. S.	KIM	Changwon Nat'l Univ.	PI-O08, PI-P06
J. S.	KIM	KCMC Co., Ltd.	TF-P06, TF-P08
J. W.	KIM	Changwon Nat'l Univ.	TF-P01, TF-P02
Jaegyeom	KIM	Ajou Univ.	TE-P02, CE-I06
Jee-Hoon	KIM	Chonnam Nat'l Univ.	LP-P03
Jeong Seog	KIM	Hoseo Univ.	SY-O02, EL-I02, EL-O02, LD-P03, LD-P04
Jeong Wan	KIM	Pusan Nat'l Univ.	TF-O03
Jeong-Joo	KIM	Kyungpook Nat'l Univ.	FU-P03
Jin-A	KIM	Chungnam Nat'l Univ.	TE-P05
Jin-Ho	KIM	KICET	CE-O01
Jin-Myung	KIM	KIMS	ST-O06, ST-O10
Jin-Soo	KIM	Changwon Nat'l Univ.	LP-I15
Jong Hun	KIM	KAERI	ST-P04, ST-P05
Jong-Bong	KIM	Seoul Nat'l Univ. of Sci. and Tech.	CO-P01
Jong-Hyun	KIM	Korea Univ.	PI-O06
Jong-Woo	KIM	KIMS	PI-O04, PI-P04
Jong-Young	KIM	KICET	CE-I06
Jun Sik	KIM	Yonsei Univ.	NA-P09
Keon Sik	KIM	KAERI	ST-P04, ST-P05
M. H.	KIM	Changwon Nat'l Univ.	TF-P09, PI-O08, PI-P06, LP-P01, LP-P07
M. S.	KIM	Changwon Nat'l Univ.	PI-O08
Mi Ae	KIM	POSTECH	GL-O05, GL-O07
Min-Gu	KIM	Chonnam Nat'l Univ.	LP-P03
Min-Soo	KIM	KERI	LP-I11
Miso	KIM	KRISS	PI-I02
Misook	KIM	Dankook Univ.	CE-I04
Myong Ho	KIM	Changwon Nat'l Univ.	PI-P07, LP-I15, LP-O02, LP-O07, LP-P03, LP-P06, LP-P09, LP-P10, LP-P11, LP-P12

Na-young	KIM	Hanbat Nat'l Univ.	TF-P15, TF-P16
S. S.	KIM	Changwon Nat'l Univ.	TF-P01, TF-P02
S. W.	KIM	Changwon Nat'l Univ.	LP-P01, LP-P07
Sang Su	KIM	Changwon Nat'l Univ.	LP-P11
Sang Wook	KIM	Changwon Nat'l Univ.	LP-P06, LP-P11
Seongwon	KIM	KICET	ST-O09, AD-I01, AD-I06, AD-O01
Seung-Hong	KIM	Univ. of Ulsan	TF-P04, TF-P05, LD-P01
Seung-Joo	KIM	Ajou Univ.	TE-P02, CE-I06
Se-Young	KIM	KIER	ST-O14
S-H.	KIM	Brown Univ.	TF-P06, TF-P08
Song Yi	KIM	KITECH	NA-P10
So-Young	KIM	Univ. of Ulsan	TF-P04, TF-P05, LD-P01
Sukyoung	KIM	Yeungnam Univ.	NA-P07, BI-O02, BI-O05, BI-O07, BI-P04, BI-P05
Sun Ki	KIM	KAERI	ST-P05
Sun Woog	KIM	Niigata Univ.	SY-I02, SY-I03
Sung Jae	KIM	Changwon Nat'l Univ.	TF-P07, AD-P01
Sung-Jin	KIM	Gangneung-Wonju Nat'l Univ.	SY-P05
Sung Wng	KIM	Sungkyunkwan Univ.	TE-I06
Sunil	KIM	Inha Univ.	GL-O10
Sun-Kyung	KIM	Univ. of Ulsan	TF-P04, TF-P05, LD-P01
Tae Gyu	KIM	Pusan Nat'l Univ.	TF-O03
Tae Kyoung	KIM	Sunchon Nat'l Univ.	LD-O05
Taek Soo	KIM	KITECH	NA-P10
Ung Soo	KIM	KICET	CE-O02
W. J.	KIM	Changwon Nat'l Univ.	TF-P09, PI-O08, PI-P06, LP-P01, LP-P07
Won Jeong	KIM	Changwon Nat'l Univ.	PI-P07, LP-P06, LP-P09, LP-P10, LP-P11, LP-P12, LP-I15
Won Jong	KIM	Changwon Nat'l Univ.	LP-O07
Yang-Do	KIM	Pusan Nat'l Univ.	PI-P04
Young Jin	KIM	Changwon Nat'l Univ.	FU-P04
Youngsik	KIM	UNIST	FU-O02
Young-Wook	KIM	Univ. of Seoul	ST-I01, ST-O08
Yun-Jeong	KIM	Chungnam Nat'l Univ.	NA-O03
Yurian	KIM	Inha Univ.	GL-O10
Yoshiaki	KINEMUCHI	AIST	TE-I05
Naoyuki	KITAMURA	AIST	GL-P10
Adreas	KLEIN	Technische Universität Darm-stadt	LP-I03
Hang Joo	KO	KOPTI	TF-P07
Hwa Young	KO	LG Electronics	LD-O02
Jae-Woong	KO	KIMS	ST-O06, ST-O10
Sang Choon	KO	ETRI	LD-I02
A.	KOBAYASHI	Univ. of Tokyo	LD-I09
Hisanori	KOBAYASHI	Nagasaki Univ.	NA-O02
Takeshi	KOBAYASHI	AIST	TF-I01
Junko	KOIDE	N-Luminescence Corp.	SY-I02

Takayuki	KOMATSU	Nagaoka Univ. of Tech.	GL-O03
Yasunari	KONDO	Meijo Univ.	LD-I04
Young-Min	KONG	Univ. of Ulsan	EL-P05
Bon Heun	KOO	Changwon Nat'l Univ.	TF-P07, NA-P03, ST-O07, EL-P06, AD-P01, AD-P02
Chang Young	KOO	Yeungnam Univ.	TF-P10
Yang-Hyun	KOO	KAERI	ST-P04, ST-P05, ST-P06
Hiromitsu	KOZUKA	Kansai Univ.	TF-I02, TF-P14, GL-P10
Masaki	KUBOTA	Yokohama Nat'l Univ.	TE-I03
Tomoaki	KUBOTA	Shizuoka Univ.	EL-P09
Yoshiaki	KUDO	N-Luminescence Corp.	SY-I02
Shalendra	KUMAR	Changwon Nat'l Univ.	TF-P09, LP-P06, LP-P11
T.	KURAMOTO	Nakashima Medical Co.	BI-I01
Yoshihiro	KUROIWA	Hiroshima Univ.	LP-I07
Yuichiro	KUROKI	Salesian Polytechnic	GL-O08
Keiji	KUSUMOTO	AIST	CE-I05
Joon Seop	KWAK	Sunchon Nat'l Univ.	LD-I10, LD-O02, LD-O05
Sang-Hyo	KWEON	Korea Univ.	EL-O04
Chang-Sup	KWON	KICET	AD-O01
Chang-Sup	KWON	KICET	ST-O09
Jang-Yeon	KWON	Yonsei Univ.	LD-I07
Kyeong-Seob	KWON	Chonbuk Nat'l Univ.	LD-O03, LD-P02
Oh-Sang	KWON	ETRI	LD-I05
Do-Kyun	KWON	Korea Aerospace Univ.	EL-P04

L

Jean-Marie	LEBRUN	Univ. of Colorado at Boulder	EF-I01
Byong Taek	LEE	Soonchunhyang Univ.	BI-I02, BI-O04
Byung Ha	LEE	Changwon Nat'l Univ.	PI-P03
Choong-hyun	LEE	Korea Univ.	TF-O04
Dae-Soo	LEE	KERI	LP-I09
Dong Gun	LEE	Changwon Nat'l Univ.	AD-P02
Dong Heon	LEE	Kookmin Univ.	AD-I02
Gi Wook	LEE	Kumoh Nat'l Inst. of Tech.	FU-P06, FU-P07, FU-P08
Hee Young	LEE	Yeungnam Univ.	TF-P10
Hongrim	LEE	Kyungnam Univ.	NA-P08
Hong-Sub	LEE	Yonsei Univ.	TF-O01
Ho-Yong	LEE	Ceracomp Co., Ltd. & Sunmoon Univ.	LP-I02, LP-O02
Hyejin	LEE	DGIST	CO-I01
In-Hwan	LEE	Chonbuk Nat'l Univ.	LD-I03, LD-O01, LD-O03, LD-O04, LD-O06, LD-P02
J.-H.	LEE	Korea Univ.	CO-O01
Jaehyung	LEE	Yeungnam Univ.	EF-I05
Jae-Shin	LEE	Univ. of Ulsan	LP-I08, LP-I09, LP-O06, LP-P04, LP-P05
Je-Hyun	LEE	Changwon Nat'l Univ.	AD-I03

Jeong-Wook	LEE	Seoul Nat'l Univ. of Sci. and Tech.	NA-I06
Ji-Hyeon	LEE	KICET	CE-O01
Jong-Heun	LEE	Korea Univ.	SE-O01
Jong-Ho	LEE	KIST	FU-I02
Jongman	LEE	KIMS	BI-O03
Jong-Sook	LEE	Chonnam Nat'l Univ.	EL-I07, LP-P03
Jong-Yeb	LEE	Ceracomp Co., Ltd	LP-I02
Joohee	LEE	Seoul Nat'l Univ.	CO-I04
Joon-Hyung	LEE	Kyungpook Nat'l Univ.	FU-P03
Jun Ho	LEE	Korea Aerospace Univ.	GL-P08
Jung-A	LEE	Kyungpook Nat'l Univ.	FU-P03
Jung-Il	LEE	Korea Nat'l Univ. of Transportation	SY-P01
Kee Sung	LEE	Kookmin Univ.	AD-I02
Kyoungho	LEE	Soonchunhyang Univ.	EL-P08, EL-P11
Kyu Hyoung	LEE	Kangwon Nat'l Univ.	TE-I06, TE-P03
Kyuhyun	LEE	Seoul Nat'l Univ.	CO-I04
Kyungwon	LEE	Chonbuk Nat'l Univ.	LD-P02
M. H.	LEE	Changwon Nat'l Univ.	TF-P09, LP-P01, LP-P07
Myang Hwan	LEE	Changwon Nat'l Univ.	PI-I06, LP-O02, LP-P06, LP-P10, LP-P11
Myeong-No	LEE	IONES Co., Ltd.	BI-P02
S. Y.	LEE	KCMC Co., Ltd.	TF-P06, TF-P08
Sang Heon	LEE	Kongju Nat'l Univ.	GL-P05
Sang Hun	LEE	Kongju Nat'l Univ.	GL-I01, GL-P06
Sang-hun	LEE	IONES Co., Ltd.	BI-P02
Sang-Jin	LEE	Mokpo Nat'l Univ.	SY-P04
San-Kwon	LEE	Chung-Ang Univ.	TE-O02
Sea Hoon	LEE	KIMS	ST-P01
Seoung Soo	LEE	Changwon Nat'l Univ.	FU-O02
Seung Jae	LEE	KEPCO Nuclear Fuel Co.	ST-P04
Soonil	LEE	KICET	TE-I04, TE-P03
Sungho	LEE	Nagoya Inst. of Tech.	BI-O06
Sung-Min	LEE	KICET	ST-O05, ST-O09, GL-P04, AD-I06, AD-O01
Sung-Min	LEE	Ceracomp Co., Ltd	LP-I02
Tae-Ho	LEE	Korea Univ.	SY-O01, PI-O06
Woo Hyung	LEE	Korea Aerospace Univ.	GL-P08
Yoen-seung	LEE	Hanbat Nat'l Univ.	TF-P15, TF-P16
Yoon Kwang	LEE	Yonsei Univ.	TF-O01
Yu Lim	LEE	Sunchon Nat'l Univ.	LD-O05
Jing	LI	Changwon Nat'l Univ.	FU-O02
Jing-Feng	LI	Tsinghua Univ.	PL-02, LP-I03, LP-I05, LP-I08, LP-O05
Shunyi	LI	Technische Universität Darmstadt	LP-I03
Yuanhang	LI	Chinese Academy of Sci.	LP-I03
Daesoon	LIM	Korea Univ.	SY-O04, TF-O04, AD-I06

Hyung-Tae	LIM	Changwon Nat'l Univ.	FU-P04, FU-P05
Jae-Ryong	LIM	Chungnam Nat'l Univ.	LP-O04, LP-P02
S. Y.	LIM	Changwon Nat'l Univ.	PI-P06
Sun Kwon	LIM	Heesung Metal Ltd.	LD-I05
Yesol	LIM	Inha Univ.	NA-I02
Young Soo	LIM	KICET	TE-P03
Hua-Tay	LIN	Oak Ridge Nat'l Lab.	ST-O05
Chao	LIU	Kyushu Inst. of Tech.	BI-O08
Chunyuan	LU	Pusan Nat'l Univ.	TF-O03
Zhe	LU	Changwon Nat'l Univ.	AD-I03

M

Guangyu	MA	Osaka Prefecture Univ.	ST-O02
Nan	MA	Kyushu Univ.	SE-I02
Xiaokun	MA	The Pennsylvania State Univ.	PI-O02
Hirotaka	MAEDA	Nagoya Inst. of Tech.	BI-O06
Jee-hun	MAENG	KICET	GL-P03, GL-P04
Iqbal	MAHMUD	Korea Nat'l Univ. of Transportation	TE-P01
Yuichi	MAIDA	Electronics Co., Ltd.	LP-I06
Rizwan Ahmed	MALIK	Changwon Nat'l Univ.	PI-P07, LP-O07, LP-P09, LP-P12, LP-I15
Apichate	MANEEWONG	UST & KAERI & Thailand Inst. of Nuclear Tech.	SY-O02
Shiori	MANEYAMA	Shizuoka Univ.	EL-P02
Adnan	MAQBOOL	Changwon Nat'l Univ.	PI-P07, LP-O07, LP-P09, LP-P12
Steve W.	MARTIN	Iowa State Univ.	FU-I05, FU-P09
Hirokazu	MASAI	Kyoto Univ.	GL-O04
Tomoaki	MASHIMO	Toyohashi Univ. of Tech.	PI-O05
Toshiyuki	MASUI	Osaka Univ.	SY-I01, SY-P03
Atsunobu	MASUNO	The Univ. of Tokyo	GL-I02
Hiroyuki	MATSUBARA	Meijo Univ.	LD-I04
Takeshi	MATSUDA	Kitami Inst. of Tech.	EL-I06, EL-O05, EL-P01, EL-P02
Kimihiro	MATSUKAWA	Osaka Municipal Technical Research Inst.	ST-O02
Syuji	MATSUMOTO	Asahi Glass Co., Ltd.	GL-O04
Deepam	MAURYA	Virginia Tech.	PI-O03
Shielah	MAVENGERE	Keimyung Univ.	ST-P03
Sangram	MAZUMDER	Hanseo Univ.	NA-P04, NA-P05, ST-O03
Akira	MIKUNI	Yamaguchi Prefectural Industrial Tech. Inst.	CE-I09, CE-P01
Young Ki	MIN	Soonchunhyang Univ.	BI-O04
Masahito	MINAMIMORI	Ryujin Gama	CE-I07
T.	MISAWA	Hokkaido Univ.	GL-O01
Yoshinori	MIYATA	IKKEI-gama	CE-I09, CE-P01
Hidetoshi	MIYAZAKI	Shimane Univ.	EL-P03

Toshiki	MIYAZAKI	Kyushu Inst. of Tech.	BI-O08
Youichi	MIZUNO	Taiyo Yuden Co. Ltd.	LP-I10
Bhaskar Chandra	MOHANTY	Thapar Univ.	NA-P09
Hiroyoshi	MOMIDA	Osaka Univ.	CO-I02
Jung-In	MOON	PaiChai Univ.	FU-P02
Su-Hyeon	MOON	Chonnam Nat'l Univ.	LP-P03
Koji	MORITA	NIMS	EF-I03
Takeshi	MORITA	The Univ. of Tokyo	PI-I05
Chikako	MORIYOSHI	Hiroshima Univ.	LP-I07
Jae Kyoung	MUN	ETRI & UST	LD-I02
Sang-Won	MYOUNG	Changwon Nat'l Univ.	AD-I03

N

Ho-Hyun	NAHM	Seoul Nat'l Univ. & Inst. for Basic Sci.	CO-I04
Sahn	NAHM	Korea Univ.	SY-O01, EL-O04, PI-O01, PI-O06
Benoit	NAIT-ALI	Center Europeen de la Ceramique	ST-O13
Makio	NAITO	Tokyo Inst. of Tech.	ST-I02
Hiroko	NAKAGAWA	Niigata Univ.	SY-I03
Yuichi	NAKAMURA	Toyohashi Univ. of Tech.	TE-I02
Hiromi	NAKANO	Toyohashi Univ. of Tech.	GL-P01, GL-P02
Kouichi	NAKASHIMA	Univ. of Yamanashi	LP-I07
Takaaki	NAKASHIMA	Tokyo Inst. of Tech.	TF-I01
Hiroshi	NAKATSUGAWA	Yokohama Nat'l Univ.	TE-I03
Tadachika	NAKAYAMA	Nagaoka Univ. of Tech.	NA-I01, NA-O04
Eun Soo	NAM	ETRI	LD-I02
Y.	NANISHI	Ritsumeikan Univ.	LD-I01
Masaki	NARISAWA	Osaka Prefecture Univ.	ST-O02
Takayuki	NARUSHIMA	Tohoku Univ.	BI-O06
R.	NATH	KIMS	PI-O07
Dieu	NGUYEN	Chonnam Nat'l Univ.	LP-P03
Thuy Ba Linh	NGUYEN	Soonchunhyang Univ.	BI-O04
Koichi	NIIHARA	Nagaoka Univ. of Tech.	NA-I01, NA-O04
Junji	NISHII	Hokkaido Univ.	GL-O01, GL-O02
Takeshi	NISHIMATSU	Tohoku Univ.	CO-I03, CO-P02
Toshiyuki	NISHIMURA	NIMS	EF-I06
Hyunggoo	NO	KICET	CE-O02

O

Akiko	OBATA	Nagoya Inst. of Tech.	BI-O06
Seizo	OBATA	Gifu Prefectural Ceramics Research Inst.	CE-I08
Yutaro	ODA	Shizuoka Univ.	EL-P01

Toshio	OGAWA	Shizuoka Inst. of Sci. & Tech.	PI-I01, LP-O01
Tamio	OGUCHI	Osaka Univ.	CO-I02
Hyun Cheol	OH	Hanyang Univ.	ST-O04
Hyun-Taek	OH	Ceracomp Co., Ltd	LP-I02
Jang Soo	OH	KAERI	ST-P04
Min Suk	OH	KETI	LD-I08
Seung Kyu	OH	Sunchon Nat'l Univ.	LD-O02, LD-O05
Song-Yul	OH	Toyota Central Research & Development Labs.	NA-O05
Yoon-Suk	OH	KICET	ST-O09, AD-I01, AD-I06, AD-O01
Masayoshi	OHASHI	AIST	CE-I05
Takanobu	OHNO	Osaka Univ.	SY-P03
Tomoya	OHNO	Kitami Inst. of Tech.	EL-P01, EL-P02, EL-I06, EL-O05
Hitoshi	OHSATO	Nagoya Industrial Sci. Research Inst. & Nagoya Inst. of Tech.	EL-O02
J.	OHTA	Univ. of Tokyo	LD-I09
Chikara	OHTSUKI	Nagoya Univ.	BI-O10
Yosuke	OHYA	Nagaoka Univ. of Tech.	GL-O08
Tomoichiro	OKAMOTO	Nagaoka Univ. of Tech.	GL-O08
Takuya	OKUDA	Shizuoka Univ.	EL-P03
Tetsuji	OKUDA	Kagoshima Univ.	TE-I01
Shun	OKUMURA	Kyoto Univ.	GL-O04
Junji	OMORI	Figaro Eng.	SE-I01
A.	OSAKA	Okayama Univ.	BI-I01
Toshitaka	OTA	Nagoya Inst. of Tech.	EL-I04

P

Ungyu	PAIK	Hanyang Univ.	AD-I03
Haribabu	PALNEEDI	KAIST & KIMS	PI-O03
Mircea Cristian	PANTILIMON	Mokpo Nat'l Univ.	SY-P04
Bong Je	PARK	ETRI	GL-P08
Byeong-Ju	PARK	Chungnam Nat'l Univ.	EL-O01
Chang-Do	PARK	Univ. of Ulsan	LP-P04
Chanyoung	PARK	KICET & Korea Univ.	AD-I06
Dong Jun	PARK	KAERI	ST-P06
Dong-Soo	PARK	KIMS	FU-I06, PI-O04, PI-P04
Eun-Sook	PARK	ETRI	LD-I05
Hye Won	PARK	Changwon Nat'l Univ.	FU-P05
Hyun-A	PARK	Kongju Nat'l Univ.	GL-I01, GL-P05
Hyung-Ho	PARK	Yonsei Univ.	TF-O01
J. S.	PARK	Changwon Nat'l Univ.	TF-P09, LP-P01, LP-P07
Jae-Hyuk	PARK	IONES Co., Ltd.	BI-P02
Jae-Sung	PARK	Samsung Electro-Mechanics Co. Ltd	EL-I08

Ji-hyun	PARK	Chungnam Nat'l Univ.	TF-P12
Jin Su	PARK	Changwon Nat'l Univ.	PI-I06
Jin-Seong	PARK	Hanyang Univ.	LD-I06
Jinsu	PARK	Changwon Nat'l Univ.	LP-O02, LP-P06, LP-P11
Jong-Hyeon	PARK	Ajou Univ.	TE-P02
Jung Gyu	PARK	Hanseo Univ.	NA-P04, NA-P05, ST-O03
Jung Hwan	PARK	KAERI	ST-P06
Keun Young	PARK	Changwon Nat'l Univ.	AD-P01, AD-P02, TF-P07
Mi Young	PARK	Changwon Nat'l Univ.	FU-P04
Mi-Jeung	PARK	KIMS	ST-O10
MinHo	PARK	Defense Agency for Technology and Quality	PI-P03
Sang-Yeup	PARK	Gangneung-Wonju Nat'l Univ.	SY-P05
Sang Whan	PARK	KIST	ST-O12
Sang Won	PARK	Kumoh Nat'l Inst. of Tech.	FU-P06, FU-P07, FU-P08
Sang-Hee Ko	PARK	KAIST	LD-I05
Solah	PARK	Yonsei Univ.	LD-I07
Sung-Hwan	PARK	Solar Ceramic Co.	NA-I06
Taegone	PARK	Changwon Nat'l Univ.	PI-P02, PI-P03
Ta-Ryeong	PARK	Hoseo Univ.	LD-P03, LD-P04
Won Ji	PARK	POSTECH	GL-O06, GL-O07
Yeong Min	PARK	Pusan Nat'l Univ.	TF-O03
Young-Jo	PARK	KIMS	ST-O06, ST-O10
Shashank	PRIYA	Virginia Tech.	PI-O03, PI-O04, PI-P04

R

C. M.	RAGHAVAN	Changwon Nat'l Univ.	TF-P01, TF-P02
Jamil Ur	RAHMAN	Changwon Nat'l Univ.	PI-P07, LP-O07, LP-P09, LP-P12
Christopher	RAHN	The Pennsylvania State Univ.	PI-O02
Rishi	RAJ	Univ. of Colorado at Boulder	EF-I01
Naren	RAJA	UST & KIMS	BI-O03
Chilakala	RAMAKRISHNA	KIGAM	NA-O01
Clive	RANDALL	The Pennsylvania State Univ.	LP-I10
V. Annapu	REDDY	KIMS & Indian Inst. of Tech. Roorkee	PI-O07
Zeeshan Ur	REHMAN	Changwon Nat'l Univ.	EL-P06
Sa-kyun	RHA	Hanbat Nat'l Univ.	TF-P15, TF-P16
Young Woo	RHEE	KAERI	ST-P04
Doh-Hyung	RIU	Seoul Nat'l Univ. of Science and Technology & Solar Ceramic Co.	NA-I06
Shaifulazuar Bin	ROZALI	University of Malaya	NA-I01
Asywendi	RUKINI	Yeungnam Univ.	BI-P05
Gyung Hyun	RYU	Changwon Nat'l Univ.	LP-P10

Jeong Ho	RYU	Korea Nat'l Univ. of Transportation	SY-P01
Jungho	RYU	KIMS	PI-O03, PI-O04, PI-P01, PI-P04, EL-P05, EL-P07
Min Ki	RYU	ETRI	LD-I05

S

Naonori	SAKAMOTO	Shizuoka Univ.	EL-I01, EL-I06, EL-O05, EL-P01, EL-P02, EL-P03, EL-P09
Naotaka	SAKAMOTO	Fukuoka Industrial Tech. Center	CE-I03
Wataru	SAKAMOTO	Nagoya Univ.	LP-I13
Yoshio	SAKKA	NIMS	EF-I01, EF-I03, EF-I06
Soichiro	SAMESHIMA	Kagoshima Univ.	FU-O01, NA-P02, ST-P02
Naboneeta	SARKAR	Hanseo Univ.	NA-P05
Miyuki	SASAKI	Kyushu Univ.	SE-I02
Mineo	SATO	Niigata Univ.	SY-I02, SY-I03
Mamoru	SENNA	Shizuoka Univ. & Keio Univ.	EL-I01
Inseok	SEO	POSCO Global R&D Center	FU-I05, FU-P09
In-Tae	SEO	Korea Univ.	PI-O01, PI-O06, SY-O01
J.-W.	SEO	KICET & Korea Univ.	CO-O01
Won-Seon	SEO	KICET	TE-P03
Beak Seok	SEONG	UST & KAERI	SY-O02
Tae-Yeon	SEONG	Korea Univ.	NA-P10
Young-Hoon	SEONG	KAIST & KIER	ST-I03
Kyosuke	SEYA	Nihon Univ.	AD-P03
Kengo	SHIMANOE	Kyushu Univ.	SE-I02
Hiroyuki	SHIMIZU	Taiyo Yuden Co. Ltd. & The Pennsylvania State Univ.	LP-I10
Takao	SHIMIZU	Tokyo Inst. of Tech.	TF-I01
Yasuhiro	SHIMIZU	Nagasaki Univ.	NA-P06, NA-O02, BI-P03
Taro	SHIMONOSONO	Kagoshima Univ.	NA-P02, ST-P02, FU-O01
H. S.	SHIN	KCMC Co., Ltd.	TF-P06, TF-P08
Hyunho	SHIN	Gangneung-Wonju Nat'l Univ.	CO-P01
Sang Yeol	SHIN	Korea Aerospace Univ.	GL-P08, GL-O09
Kazuya	SHINNISHI	Figaro Eng.	SE-I01
Kazuo	SHINOZAKI	Tokyo Inst. of Tech.	EL-P09
Kenji	SHINOZAKI	Nagaoka Univ. of Tech.	GL-O03
Yuki	SHIROSAKI	Kyushu Inst. of Tech.	BI-O08
Amit	SHYAM	Oak Ridge Nat'l Lab.	ST-O05
David S.	SMITH	Center Europeen de la Ceramique	ST-O13
Dong-Il	SON	Dongkook Inc.	TF-P04, TF-P05, LD-P01
Dongsu	SON	Korea Aerospace Univ.	EL-P04
Jeong Hun	SON	Changwon Nat'l Univ.	SY-O03

Ji-Won	SON	KIST	FU-I02
In-Hwan	SONG	Yeungnam Univ.	BI-O02
In-Hyuck	SONG	KIMS	ST-O08
Jayhyok	SONG	Samsung SDI	GL-O05
Jeong-Hwan	SONG	PaiChai Univ.	FU-P02
Jung il	SONG	Changwon Nat'l Univ.	AD-P01, AD-P02
Soo-Young	SONG	Korea Nat'l Univ. of Trans-portation	TE-P01
T. K.	SONG	Changwon Nat'l Univ.	PI-O08, PI-P06, LP-P01, LP-P07
Tae Kwon	SONG	Changwon Nat'l Univ.	TF-P07, TF-P09, PI-I06, PI-P07, LP-O07, LP-P06, LP-P09, LP-P10, LP-O02, LP-P11, LP-P12, LP-I15
Hisayuki	SUEMATSU	Nagaoka Univ. of Tech.	NA-O04, NA-I01
Koichi	SUEMATSU	Fukuoka Industrial Tech. Center	SE-I02
Toyohiko	SUGIYAMA	AIST	CE-I05
Min-Soo	SUH	KIER	ST-O14
Aram	SUNG	Inha Univ.	GL-P07
Hisao	SUZUKI	Shizuoka Univ.	EL-P01, EL-P02, EL-I01, EL-I06, EL-O05, EL-P03, EL-P09
Tohru S.	SUZUKI	NIMS	EF-I06
Tsuneo	SUZUKI	Nagaoka Univ. of Tech.	NA-O04, NA-I01

T

Takuma	TAKAHASHI	Kanagawa Academy of Sci. and Tech.	ST-O01, ST-O11
Masasuke	TAKATA	Japan Fine Ceramics Center	GL-O08, PL-03
Tetsuya	TAKEUCHI	Meijo Univ.	LD-I04
Shinji	TAMURA	Osaka Univ.	FU-I01
Hidehiko	TANAKA	NIMS	EF-I06
Satoshi	TANAKA	Nagaoka Univ. of Tech.	ST-I02, ST-I04
Tatsuya	TANIHIRA	Figaro Eng.	SE-I01
Toshiro	TANIMOTO	Kyoto Univ.	GL-O04
Junichi	TATAMI	Yokohama Nat'l Univ.	ST-O01, ST-O11
Kentaro	TERAMURA	Kyoto Univ.	GL-O04
Akihiko	TESHIGAHARA	DENSO Corp.	CO-I02
Tung-Duong	THANH	Chungnam Nat'l Univ.	NA-O03
Thenepalli	THRIVENI	KIGAM	NA-O01
Kenji	TODA	Niigata Univ.	SY-I02, SY-I03
Masako	TODA	N-Luminescence Corp.	SY-I02
Yomei	TOKUDA	Kyoto Univ.	GL-O04
Motoko	TOKUNAGA	Nagasaki Univ.	BI-P03
Tonshaku	TOU	Electronics Co., Ltd.	LP-I06
Garima	TRIPATHI	KIMS	BI-O01
Susan	TROLIER-	The Pennsylvania State	PI-O02, PI-O04

	MCKINSTRY	Univ.	
Tran Mhan	TRUNG	Chungnam Nat'l Univ.	LP-O04
Izuna	TSUBOI	Nagoya Inst. of Tech.	TF-O05
Shun	TSUJI	Kansai Univ.	GL-P10
Koichiro	TSUZUKU	Gunma Univ.	EL-I03
Kelimu	TULUGAN	Gyeongsang Nat'l Univ.	TF-O03

U

Tetsuo	UCHIKOSHI	NIMS	EF-I06
Hiroaki	UCHIYAMA	Kansai Univ.	TF-P14, GL-P10
Kyosuke	UEDA	Tohoku Univ.	BI-O06
Taro	UEDA	Nagasaki Univ.	BI-P03, NA-P06, NA-O02
Kazuyoshi	UEMATSU	Niigata Univ.	SY-I02, SY-I03
K.	UENO	Univ. of Tokyo	LD-I09
Mana	UENO	Kagoshima Univ.	FU-O01
Shintaro	UENO	Univ. of Yamanashi	LP-I07
Shunkichi	UENO	Nihon Univ.	AD-I05, AD-P03
K.	UETSUKI	Nakashima Medical Co.	BI-I01
Aman	ULLAH	Univ. of Ulsan	LP-I09
Soon-Chul	UR	Korea Nat'l Univ. of Transportation	TE-P01, TF-P03

V,W

Hung	VU	Chonnam Nat'l Univ.	LP-P03
Satoshi	WADA	Univ. of Yamanashi	LP-I07
Naoki	WAKIYA	Shizuoka Univ.	EL-I01, EL-I06, EL-P01, EL-P02, EL-P03, EL-P09, EL-O05
Ke	WANG	Tsinghua Univ.	PL-02, LP-I03, LP-I05, LP-O05
Linghang	WANG	Xi'an Jiaotong Univ.	EL-P05
Yosuke	WATANABE	Yokohama Nat'l Univ.	TE-I03
Seiji	WATASE	Osaka Municipal Technical Research Inst.	ST-O02
Sung Bok	WEE	Hanyang Univ.	ST-O04
Don Chan	WOO	Yeungnam Univ.	TF-P10
Sang-Kuk	WOO	KIER	ST-O14
Won Seok	WOO	Univ. of Ulsan	LP-P08
Wenbin	WU	Chinese Academy of Sci.	LP-I03

Y

Naoaki	YABUUCHI	Tokyo Denki Univ.	FU-I03
Tsukaho	YAHAGI	Kanagawa Academy of Sci. and Tech.	ST-O11
Suzuya	YAMADA	Denki Kagaku Kogyo K.K.	GL-P01, GL-P02
Tomoaki	YAMADA	Nagoya Univ. & Japan Sci. and Tech. Agency	TF-I01

T.	YAMAGUCHI	Kogakuin Univ.	LD-I01
Taiji	YAMAMOTO	Meijo Univ.	LD-I04
Takahisa	YAMAMOTO	Nagoya Univ.	EF-I01
Takanori	YAMAMOTO	Yokohama Nat'l Univ.	TE-I03
Megumi	YAMANE	Osaka Univ.	FU-I01
Takeshi	YAMANOBE	Gunma Univ.	EL-I03
Takayuki	YANAGIDA	Kyushu Inst. of Tech.	GL-O04
Bee Lyong	YANG	Kumoh Nat'l Inst. of Tech.	FU-P06, FU-P07, FU-P08
Jae Ho	YANG	KAERI	ST-P04, ST-P05
Ki-Su	YANG	Chungnam Nat'l Univ.	LP-P02
Soyoung	YANG	Yeungnam Univ.	BI-O02
Suk	YANG	Yonsei Univ.	LD-I07
Fang-Zhou	YAO	Tsinghua Univ.	PL-02, LP-I05
Kouichi	YASUDA	Tokyo Inst. of Tech.	ST-I02, ST-I04
Charles B.	YEAGER	The Pennsylvania State Univ.	PI-O02
Hong Goo	YEO	The Pennsylvania State Univ.	PI-O02
J. H.	YEOM	KCMC Co., Ltd.	TF-P06, TF-P08
Jeong Han	YI	Korea Aerospace Univ.	GL-P08
Seung-Hwan	YI	Korea Nat'l Univ. of Transportation	TF-P03
Haena	YIM	KIST	EL-I05
Kanghoon	YIM	Seoul Nat'l Univ.	CO-I04
Jie	YIN	KIMS	ST-P01
Toshinobu	YOGO	Nagoya Univ.	LP-I13
Toshinobu	YOKO	Kyoto Univ.	GL-O04
Takeshi	YOKOTA	Nagoya Inst. of Tech.	TF-O05
Chang-Ho	YOON	Univ. of Ulsan	LP-O06
Ji-Wook	YOON	Korea Univ.	SE-O01
Jong Seol	YOON	Inha Univ.	NA-I02
Kyung Joong	YOON	KIST	FU-I02
Man-Soon	YOON	Korea Nat'l Univ. of Transportation	TE-P01
Seok-Hyun	YOON	Samsung Electro-Mechanics Co. Ltd	EL-I08
Soon-Gil	YOON	Chungnam Nat'l Univ.	TE-O01, TE-O02, TE-P04, TE-P05, TF-I04, TF-O02, TF-P12, TF-P13, NA-O03, FU-P01, EL-O01, LP-O04, LP-P02
Woon-Ha	YOON	KIMS	PI-O04, PI-P04
Hidehiro	YOSHIDA	NIMS	EF-I01, EF-I03
Mi-Rae	YOUM	KIST	ST-O12
Yong	YOUN	Seoul Nat'l Univ.	CO-I04
Masayoshi	YUASA	Kyushu Univ.	SE-I02
Hui Suk	YUN	KIMS	BI-O01, BI-O03
Jin-Hyeon	YUN	Chonbuk Nat'l Univ.	LD-O01, LD-O06
Jondo	YUN	Kyungnam Univ.	TF-P11, NA-P08
Sung-Il	YUN	KIST	ST-O12

Z

Haibo	ZHANG	Huazhong Univ. of Sci. and Tech.	LP-I12
Qi Zhang	ZHANG	The Univ. of New South Wales	LP-I12
J. M.	ZHAO	Gyeongsang Nat'l Univ.	BI-O09
Li-Dong	ZHAO	Beihang Univ.	TE-I07
Wei	ZHAO	Yeungnam Univ.	ST-O03
Wei	ZHAO	Yeungnam Univ	NA-P04, NA-P05, NA-P07
Xiaobing	ZHOU	Ningbo Inst. of Materials Tech. and Eng.	EF-I05
Yuan	ZHOU	Virginia Tech.	PI-P04
Fangyuan	ZHU	Tsinghua Univ.	LP-O05, PL-02

The 31st International Korea-Japan Seminar on Ceramics